Instytut Chemii Organicznej
Polskiej Akademii Nauk

Diketopyrrolopyrrole-based fluorescent probes for cations

G. Dinesh Kumar M.Sc.

A monothematic series of publications with a commentary presented to the Scientific Council of the Institute of Organic Chemistry of the Polish Academy of Sciences in order to obtain a doctorate in chemical sciences

Promotor: prof. dr hab. Daniel T. Gryko

Warszawa 2022

Praca doktorska wykonana w ramach projektu:

"New generation of fluorescent probes for stimulated emission depletion microscopy"

Realizowanego w ramach programu **TEAM**

Fundacji na rzecz Nauki Polskiej

Numer grantu: POIR.04.04.00-00-3CF4/16-00-TEAM/2016-3/22

Acknowledgements:

First and foremost, I would like to express my sincerest thanks to my supervisor Prof. Daniel T. Gryko, who I'm so grateful for giving me the opportunity to work in his research group. I'm incredibly grateful to have had such an understanding, kind and supportive supervisor throughout my PhD, from whom I've learnt so much. Again, I thank him for his guidance, encouragement, support, and patience throughout the years.

Secondly, I would like to thank all current and past members of the Daniel Gryko group for their support, friendly working environment, comments, and friendship. Special thanks to Dr. Olena Vakuliuk, Dr. Mariusz Tasior, Dr. David Young, and Kateryna Vygranenko for their invaluable support. In particular, I would like to thank Olena Vakuliuk once more for her friendship, guidance and company in the lab for over the years.

Again, I would like to give special thanks to Dr. David Young for the proofreading of this thesis.

I also thank all my collaborators, especially Dr. Marzena Banasiewicz for photophysical characterization of many compounds and Dr. Antoni Wrzosek for great support and guidance in bio-imaging studies.

Additionally, I would like to thank the FNP-TEAM for funding my PhD.

I want to thank my close friends Lakshmi Kantha, Girish, Sudheendra Rao, and G. Santhosh Kumar who have supported and encouraged me throughout the years. I also thank Prof. Satish Patil (IISc, Bangalore), Dr. Madhusudhana Reddy, and Dr. Puttaraju for their kind support, advices, and encouragement.

Finally, I dedicate this thesis to my family, whose love and strength I'm forever grateful for. To my parents, my sister and my wife, I thank them for their encouragement, support and love, which without them, this dissertation would not be possible.

Again, I sincerely thank you all.

Abstract in English

In the past decade, there has been a considerable growth in applying fluorescence technique to cellular imaging. This technique provides unique advantages such as high sensitivity, low cytotoxicity, low cost and non-invasiveness, and makes it a promising tool. Among the wide range of applications of fluorescence technique, sensing of various cations is one of the most important and active areas.

The main objective of my PhD dissertation was the design and synthesis of new generation of fluorescent probes and investigation of their optical properties and bioimaging applications. I have started with extending the novel synthetic methodology for the synthesis of fully asymmetrical diketopyrrolopyrroles developed in our laboratory. Condensation between aromatic nitriles and pyrrolidin-2-one leads to 1,4-diketopyrrolo[4,3-*c*]pyrrole (DPP) derivatives possessing two different C-aryl substituents. The first part of this Thesis explored how the direct linkage of molecular recognition unit to DPP core can affect the optical properties. Taking advantage of the new methodology, I have designed and synthesized new class of diketopyrrolopyrrole sensors directly from nitriles possessing (aza)crown ethers leading to macrocycle-dye hybrids. Their strong interaction with cations possessing Lewis acid character such as Li^+, Mg^{2+} and Zn^{2+} leads to significant changes of optical properties, hence to the new fluorescent probes.

In the second part of my work, I synthesized novel highly sensitive potassium probes with the strategic placement of a recognition crown ether unit at most conjugated position of the second aryl substituent of diketopyrrolopyrrole core. These D-A-D' hybrid fluorophores exhibits very high fluorescence quantum yields (Φ_{fl} = 0.8-0.9%) even in CH_3CN. An additional lariat alkoxy group at *ortho* position to aza-18-crown-6 induces strong coordination to K^+ with 80 nm blue-shift of fluorescence. The incorporation of PPh_3^+ group enables the probe to be selectively accumulated in mitochondria of cardiac H9C2 cells and it makes it possible to observe the fast efflux/influx of mitochondrial K^+ upon stimulation with nigericin.

In the final part of my thesis, I designed and synthesized diketopyrrolopyrrole-based novel highly sensitive fluorescent zinc sensors directly from pyridine-derived nitriles

possessing dipicolylamine as a zinc recognition unit. The obtained DPP sensors showed favorable photophysical properties including strong bathochromic shifts (≈80nm) of fluorescence upon complexation with Zn^{2+} and high fluorescence quantum yields. The probes decorating with PPh_3^+ and morpholine units are selectively localized in mitochondria and lysosomes of cardiac H9C2 cells respectively.

Abstract in Polish

W ostatniej dekadzie nastąpił znaczny wzrost zainteresowania technikami fluorescencyjnymi w obrazowaniu komórkowym. Oferują one wiele korzyści, takich jak wysoka czułość, niska cytotoksyczność, niski koszt i nieinwazyjność, co czyni je obiecującym narzędziem w biologii molekularnej i medycynie. Wśród szerokiego zakresu ich zastosowań jednym z najważniejszych i najbardziej aktywnych obszarów jest wykrywanie różnych kationów.

Głównym celem mojej rozprawy doktorskiej było zaprojektowanie i synteza nowej generacji sond fluorescencyjnych, a także badanie ich właściwości optycznych oraz zastosowanie praktyczne otrzymanych barwników w bioobrazowaniu. Pracę rozpocząłem od rozszerzenia zakresu stosowalności opracowanej w naszym laboratorium nowatorskiej metodologii syntezy asymetrycznych diketopirolopiroli. Kondensacja nitryli aromatycznych i pirolidyn-2-onu prowadzi do pochodnych 1,4-diketopirolo[4,3-*c*]pirolu (DPP) posiadających dwa różne podstawniki C-arylowe. W pierwszej części pracy zbadałem, w jaki sposób bezpośrednie połączenie jednostki rozpoznania molekularnego z rdzeniem DPP może wpływać na właściwości optyczne. Wykorzystując nową metodologię, zaprojektowałem i zsyntetyzowałem nową klasę sond opartych o rdzeń diketopirolopirolu bezpośrednio z nitryli zawierających (aza)etery koronowe. Silne oddziaływanie otrzymanych hybryd makrocykl-barwnik z kationami o charakterze kwasowym, takimi jak Li^+, Mg^{2+} i Zn^{2+} ma znaczący wpływ na właściwości optyczne barwników, a więc potwierdza możliwość ich stosowania jako sond fluorescencyjnych.

W drugiej części mojej pracy zsyntetyzowałem nowe, wysoce czułe sondy potasowe umieszczając jednostkę rozpoznania molekularnego kationów w najbardziej sprzężonej z chromoforem pozycji podstawnika arylowego. Otrzymane hybrydowe fluorofory typu D-A-D' wykazują bardzo wysokie wydajności kwantowe fluorescencji (Φ_{fl} = 0,8-0,9%), nawet w acetonitrylu. Dodatkowa grupa alkoksylowa w pozycji *orto*- do aza-18-korony-6 indukuje silną koordynację K^+ z przesunięciem fluorescencji o 80 nm w kierunku hipsochromowym. Przyłączenie grupy PPh_3^+ umożliwia selektywną akumulację sondy w mitochondriach komórek sercowych H9C2 oraz obserwację szybkiego wypływu/napływu mitochondrialnego K^+ po stymulacji nigerycyną.

W końcowej części pracy zaprojektowałem i zsyntetyzowałem oparte na diketopirolopirolu nowatorskie, wysoce czułe, fluorescencyjne sondy na kationy cynku, wychodząc bezpośrednio z nitrylowych pochodnych pirydyny posiadających dipikoliloaminę jako jednostkę rozpoznawania. Uzyskane sondy oparte o rdzeń DPP wykazywały korzystne właściwości fotofizyczne, w tym silne przesunięcia batochromowe fluorescencji (≈80nm) po kompleksowaniu z Zn^{2+} oraz wysokie wydajności kwantowe fluorescencji. Sondy udekorowane jednostkami PPh_3^+ i morfoliną są selektywnie zlokalizowane odpowiednio w mitochondriach i lizosomach komórek sercowych H9C2.

Table of Contents:

List of Publications for the Doctoral Dissertation:

1. **G. Dinesh Kumar**, M. Banasiewicz, D. Jacquemin, D. T. Gryko, *Chem. Asian J.* **2021**, *16*, 355–362, DOI: 10.1002/asia.202001376. *„Switch-on Diketopyrrolopyrrole-Based Chemosensors for Cations Possessing Lewis Acid Character”* IF_{2022}= 4.839

2. **G. Dinesh Kumar**, M. Banasiewicz, A. Wrzosek, R. P. Kampa, M. H. E. Bousquet, D. Kusy, D. Jacquemin, A. Szewczyk, D. T. Gryko, *Chem. Commun.,* **2022**, *58*, 4500–4503, DOI: 10.1039/d2cc00324d. *„Probing the flux of mitochondrial potassium using an azacrown-diketopyrrolopyrrole based highly sensitive probe”* IF_{2022}= 6.065

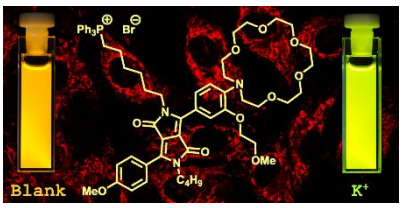

3. **G. Dinesh Kumar**, M. Banasiewicz, A. Wrzosek, O. O'Mari, M. Zochowska, V. I. Vullev, D. Jacquemin, A. Szewczyk, D. T. Gryko, *Org. Biomol. Chem.,* **2022**, *20*, 7439–7447, DOI: https://doi.org/10.1039/D2OB01296K. *„A sensitive zinc probe operating via enhancement of excited-state intramolecular charge transfer”* IF_{2022}= 3.890

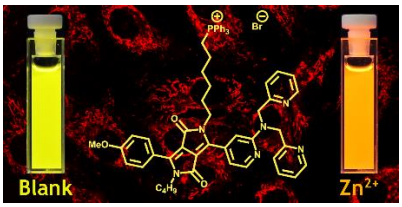

Participation in conferences and seminars

1. 19th International Symposium on Novel Aromatic Compounds (ISNA 2022), 3–8 July, 2022, Warsaw, Poland. Poster title: “A highly sensitive mitochondria-targeting potassium probe based on azacrown-diketopyrrolopyrrole.”
2. 9th MITOCHONDRION on-line conference, 27th January, 2021, Warsaw, Poland. Title of talk “A Diketopyrrolopyrrole-based Fluorescent Potassium Sensors for Mitochondria Targeting.”

Short CV:

I was born on 15th March 1989, in Chimakalahalli, Karnataka, India. In 2006, I started my Bachelor's Degree at the University of Bangalore, India and at the same University I completed a Master's Degree in organic chemistry in 2014. After working in a pharmaceutical company for one year as a research chemist, I joined Prof. Satish Patil's organic electronics research group at the Indian Institute of Science, Bangalore as a research assistant. There I worked on the "design and synthesis of donor-acceptor π-conjugated-based aggregation induced emission materials for OLED applications."

In 2018, I joined Prof. Daniel Gryko's group at the Institute of Organic Chemistry, Polish Academy of Sciences working towards the Foundation for Polish Science grant "New generation of fluorescent probes for stimulated emission depletion microscopy", Grant Agreement nr: POIR.04.04.00-00-3CF4/16-00-TEAM/2016-3/22. Towards this end, I researched diketopyrrolopyrrole based fluorescent probes for the detection of metal cations and their bio-imaging applications. This has culminated in the publication of three papers, a poster presentation and an oral presentation.

1. Introduction

1.1. Introduction to fluorescence

Over the past several decades the phenomenon of photoluminescence has received much attention in the field of biological science. Photoluminescence is the emission of light from excited electronic states of a molecule, first created by the absorption of light. Based on the nature of the excited state, photoluminescence is divided into fluorescence and phosphorescence. Fluorescence is the photoluminescence from a singlet electronic excited state to the ground state where the spin state of the electron does not change. The fluorescence lifetime, the time between excitation and emission, is in the order of nanoseconds. Phosphorescence differs in the fact that emission is from a triplet electronic excited state and relaxation involves the change of electron spin. Due to this spin change, phosphorescence lifetimes are typically in milliseconds or seconds.

In 1845, John Frederick William Herschel reported the first observation of fluorescence from a quinine sulfate solution when it was exposed to a UV light source or the sun.[1] Later, in 1852, George Gabriel Stokes named this phenomenon as “fluorescence” in honor of the fluorescent mineral fluorspar. Stokes also discovered that emission occurs at
longer wavelengths than absorption. This relationship now bears his name and the ‘Stokes Shift’ is counted as one of the most positive characteristics of fluorescent molecular sensors.[2] In 1935, Alexander Jablonski illustrated the processes that occur between the absorption and emission of light using a diagram, now known as a Jablonski diagram (Figure-1).[3]

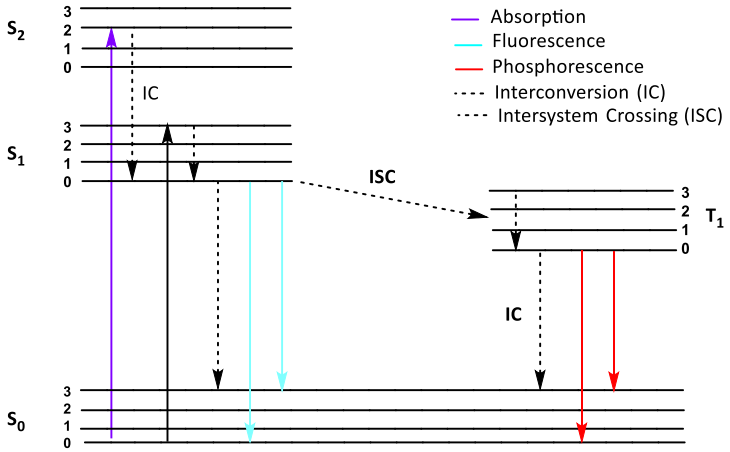

Figure-1: Jablonski diagram showing photon absorption and emission processes. The straight arrows indicate radiative processes and dotted arrows indicate nonradiative processes.

These diagrams often depict the ground state S_0, the first and second singlet excited electronic states S_1 and S_2 as well as the first triplet excited electronic state T_1. Each state can exist in various vibrational energy levels, due to the variety of nuclear geometries, represented by the numbers 0, 1, 2 and 3. According to the Frank-Condon principle, the transitions of electrons between states occurs in a much shorter time (10^{-}

^{15} s) than the displacement of the nuclei (10^{-12} s) and therefore can be represented as vertical lines. Jablonski diagrams provide a theoretical basis for the development of fluorescence and are often used as the starting point for discussing light absorption and emission. As the mechanism of fluorescence became more widely understood, it has received more and more attention and developed into a field of study in its own right.

In recent decades, advances in fluorescent technology has made great strides, and has yielded increasingly fascinating discoveries for diverse fields in biological sciences. Fluorescence spectroscopy is considered to be one of the most important research tools in biochemistry and biophysics. Presently, fluorescence is a dominant methodology widely used in a great number of research domains, including biotechnology, medical diagnostics, genetic analysis, DNA sequencing, flow cytometry, and forensic analysis among others. Due to the high sensitivity of fluorescence detection, there has been a remarkable growth in the use of fluorescence for cellular imaging, which renders fluorescence techniques promising tools to replace radioactive tracers for most biochemical measurements, avoiding the high expense and difficulties of handling such unstable isotopes. Moreover, fluorescence imaging has the resolution to effectively reveal the localization of intracellular molecules.

1.2. Fluorescence sensing

Fluorescence sensing of chemical and biological analytes is an active research field.[4-8] The efforts devoted to this subject were initially driven by the desire to eliminate the use of radioactive tracers, which are costly to use and dispose of. Nowadays, the high sensitivity of fluorescence sensing techniques is another important reason for the increased attention. Fluorescence sensing also meets the need for rapid and low-cost determination methods for a wide range of chemical, biochemical, clinical, and environmental processes.

Fluorescence sensing requires a change in a spectral property, such as fluorescence intensity, emission spectrum, excitation spectrum, fluorescence lifetime, anisotropy, or Φ_{fl} with concominant environmental changes around the fluorophore through a binding event to an analyte. The most popular fluorescence sensing approach is the fluorescence intensity-based strategy, that is, the fluorescence intensity of the probe changes in response to an analyte. A great number of this type of sensor have been developed for pH, cations, anions, DNA, RNA, ATP, enzymes, amino acids, glucose, etc.[9-16] An additional advantage of fluorescence sensing is that detection of analytes can be performed *via* time resolved measurements.

As illustrated in Figure-2, fluorescent probe design strategies mostly include three main features; (1) a recognition moiety with high selectivity for the analyte of interest; (2) a fluorophore with sufficient brightness and spectral properties in some form; (3) a suitable linker that connects the two former moieties allowing for signal transduction.[9, 15, 17] There are generally four types of reaction mechanisms between fluorescent probes

and the corresponding analytes: (1) complexation; (2) formation or cleavage of a covalent bond; (3) redox reaction; and (4) protonation-deprotonation.[15]

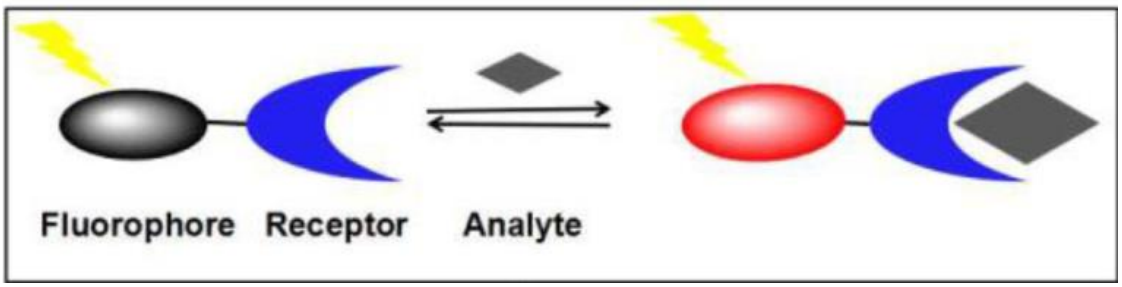

Figure-2: Schematic representation of the mechanism of fluorescent probe. Fluorescence emission is turned-on upon binding with analyte.

1.3. Metal cation sensing

Metal cations are essential for sustaining every form of life because they play a vital role in many chemical, biological, and environmental processes. Based on a physiological viewpoint, metal cations can be broadly classified into two pools: (1) essential metal cations (Li^+, Na^+, K^+, Mg^{2+}, Ca^{2+}, Zn^{2+}, $Fe^{2+/3+}$, etc.) which play an key role in many biological processes, including intra- and intercellular communication, in the regulation of DNA transcription, proper functioning of nerve cells, the transport of oxygen, in photosynthesis and electron transfer processes; and (2) nonessential or toxic metal cations (Hg^{2+}, Cd^{2+}, As^{3+}, Pb^{2+}, $Cr^{3+/6+}$, Ni^{2+}, Co^{2+}, etc.) which have a serious impact on the environment and health. In medicine, it is important to control the serum levels of lithium in patients under treatment for manic depression, and potassium in the case of high blood pressure. Due to their importance in many areas, the chemistry of cation complexation has played an important role in the origin of the field of molecular sensors.

Great efforts have been dedicated towards the development of fluorescent probes for various metal cations. The research on metal cation sensing has come a long way since Pederson's pioneering discovery of crown ethers and their ability to form complexes with metal cations.[18] After Pedersen's first report on the cation-complexation of crown ethers in 1967, a tremendous amount of subsequent work was performed to create more complex structures to bind a variety of metal cations.[19] Among various metal cations, alkali and alkaline earth metal cations, especially Li^+, Na^+, K^+, Mg^{2+}, and Ca^{2+} have attracted significant attention because of their well-known biological significance.[19-25] With the discovery of the important roles of transition metal cations play in a diverse array of biological and environmental processes, more recent attention has been focused on developing sensors for transition metal cations, such as Cr^{3+},[26] Fe^{3+},[27] Co^{2+},[28] Ni^{2+},[29] Cu^{2+},[30] Zn^{2+},[31-32] Cd^{2+},[33] and Hg^{2+}.[33]

Complexation is the most widely used strategy for the development of fluorescent sensors for various metal cations by virtue of their strong binding affinities with electronegative heteroatoms such as N, O, and S.[34] There are some general principles

for probes based on this strategy: (1) an appropriate ring/cavity size for a given metal cation, e.g., crown ethers with different ring sizes bind different alkali metal cations; (2) suitable ligands forming five- or six-membered chelate ring complexes with metal cations, such as probes with an DPA (dipicolylamine) unit complexing Zn^{2+}; and (3) soft-hard acid-base principle, for instance, soft sulfur-containing receptors exhibit high affinities for soft metal cations such as Ag^{+} and Hg^{2+}.

1.4. Mechanism of signal transduction

The signaling moiety acts as signal transducer and is responsible for the conversion of the recognition event into a change in the photophysical properties of the fluorescent probe. This happens because the chemical and structural properties of the excited state are very different from the ones of the ground state and various processes such as fluorescence resonance energy transfer (FRET), photo-induced electron transfer (PET), internal charge transfer (ICT), energy transfer (ET), aggregation induced emission (AIE), excimer and exciplex formation can occur in the excited state.

1.4.1 Fluorescence resonance energy transfer (FRET)

A non-radiative process results from interaction between different fluorophore couples wherein the transfer of resonance energy occurs from a donor fluorophore (D-F) excited state to an acceptor fluorophore (A-F) ground state and emission may subsequently arise from the acceptor centre through non-radiative “dipole–dipole coupling” (Figure-3).[35] The basic necessity for the FRET process is an appropriate overlap of the emission spectrum of donor (D) with the absorption spectrum of acceptor (A). A higher spectral overlap leads to a better FRET depending on the distance between donor and acceptor which should lie between 10 to 100 Å for an efficient process. FRET also depends on the virtual orientation of dipole moments of the donor absorption and acceptor emission.[36] The FRET mechanism is generally used to design fluorescent ratiometric sensors capable of displaying large pseudo Stokes shifts. In metal-complex based FRET fluorescent probes, both the donor-fluorophore (D-F) and acceptor-fluorophore (A-F) are linked to the metal ion bound receptor/ionophore. However, the possibility of another receptor site for metal ion binding enables the entire metal-complex to serve as a FRET probe (Figure-3). It is worth mentioning that usually charge transfer inactive Zn(II) and Cd(II) are pre-bound metal ions in complex based probes so that a non-radiative FRET can be observed. However, occasionally other metal ion (d^1–d^9) based complexes are also fluorescent and can serve as FRET sensors.

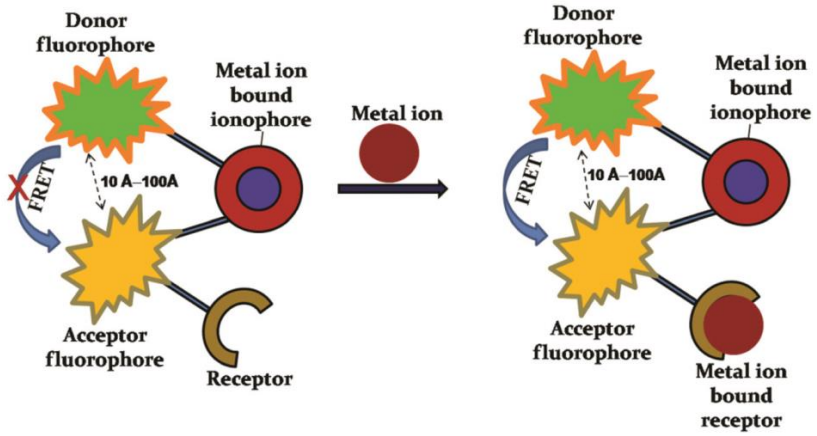

Figure-3: Metal-complex based fluorescent probes for metal ion sensing *via* FRET mechanism.

Scheme-1 shows FRET-based fluorescent probe CPBT for Zn^{2+}, which is a combination of a coumarin moiety acting as the fluorescence donor and 4-amine-7-sulfamoylbenzo[*c*][1,2,5]-oxadiazole (ASBD) as the acceptor.[37] The emission spectrum of coumarin overlaps well with the absorption spectrum of ASBD with strong emission at 560 nm and weak emission at 480 nm. After Zn^{2+} binding, the absorption spectrum of ASBD moiety shows a large blue-shift due to the decreased Intramolecular charge transfer (ICT) effect, which leads to a dramatic decrease in the spatial-overlap and FRET efficiency. Consequently, by increasing the concentration of Zn^{2+}, the emission intensity at 560 nm significantly decreased and fluorescence emission at 480 nm increased.

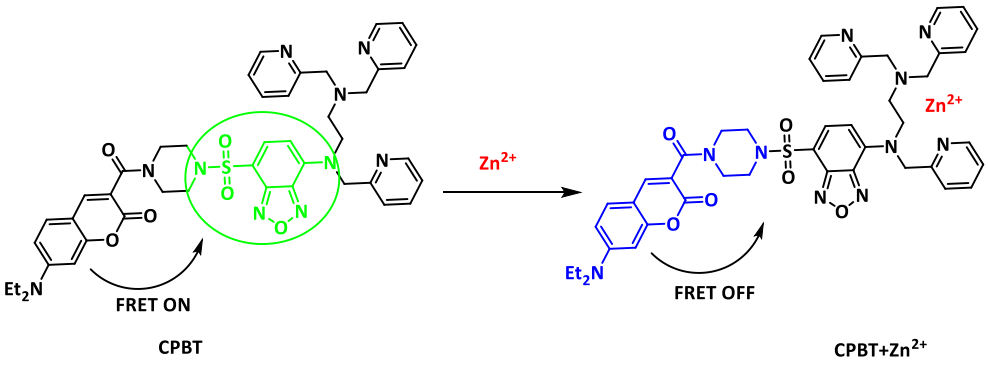

Scheme-1: Schematic illustration of mechanism of FRET probe CPBT.

1.4.2 Photo-induced Intramolecular Charge Transfer (ICT)

ICT processes from a donor to an acceptor in a single molecule have also been used as the basis of the sensing mechanism for macrocyclic fluorescent probes for cations. In this process, fluorescence effects depend on the combination of electron-donating groups and electron-accepting groups in a conjugated π-system that combines the fluorophore and the acceptor. After light excitation, the redistribution of electron cloud density from the electron donor to the electron acceptor produces a dipole moment in the molecule. When an analyte is added, the dipole distance can be increased or

decreased depending on the property of the analyte and the electronic relationship between the acceptor and the fluorophore. The reduced dipole moment will cause a blue-shift in the fluorescence emission spectrum (ICT) pathway to be suppressed, which makes the excited state more unstable than the ground state when reacting with the analyte. Conversely, the increased dipole distance will cause a red-shift in the emission spectrum and the strength of the ICT process is enhanced, which results in the excited state being more stable relative to the ground state after analyte binding (Figure-4).[38]

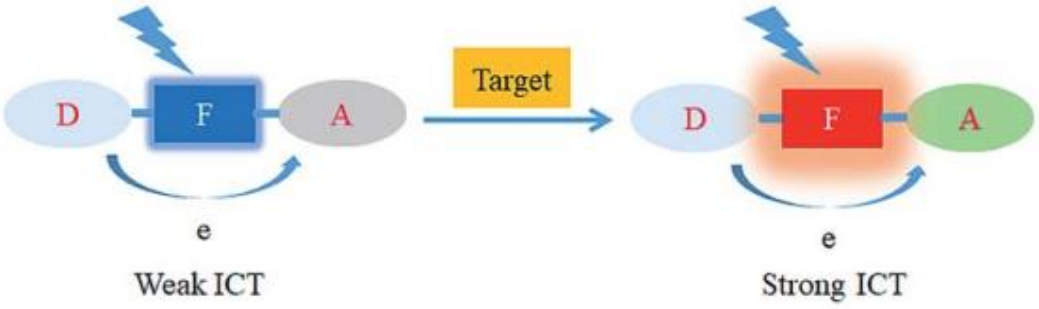

Figure-4: Metal-complex based fluorescent probes for metal ion sensing *via* an ICT mechanism.

To date, many fluorophores have been designed and reported utilizing the ICT mechanism. Scheme-2 shows a typical example of an ICT-based probe, Fura 2.[39] Upon complexing with Ca^{2+}, Fura 2 exhibits a remarkable blue-shifted fluorescence and increased fluorescence intensity.

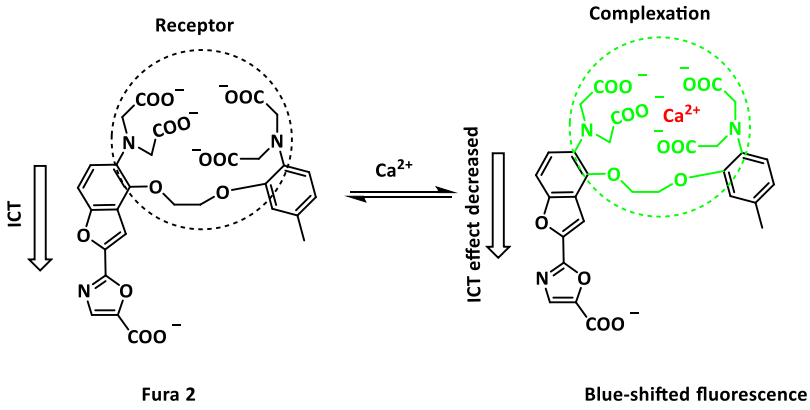

Scheme-2: Schematic illustration of mechanism of ICT probe Fura 2.

1.4.3 Photo-induced Electron Transfer (PET)

In PET probes, the analyte recognition moiety (the receptor) is often connected to a fluorophore *via* a spacer, rendering the receptor and the fluorophore electronically isolated, which essentially differs from ICT-based probes. The electronegative element, usually a nitrogen atom, embraced in the receptor moiety has a high-energy lone pair of electrons, which can transfer an electron to the fluorophore in the excited state, resulting in fluorescence quenching. Upon complexing metal cations, the reduction potential of the receptor is enhanced and, thus, the HOMO of the receptor becomes lower in energy than that of the fluorophore. As a result, the PET process from the

receptor to the fluorophore is restricted, and consequently fluorescence quenching of the fluorophore is reduced, leading to increased fluorescence intensity of the fluorophore.[9,40] Therefore, the PET mechanism has potential to be explored to develop fluorescence "turn-on" sensors.

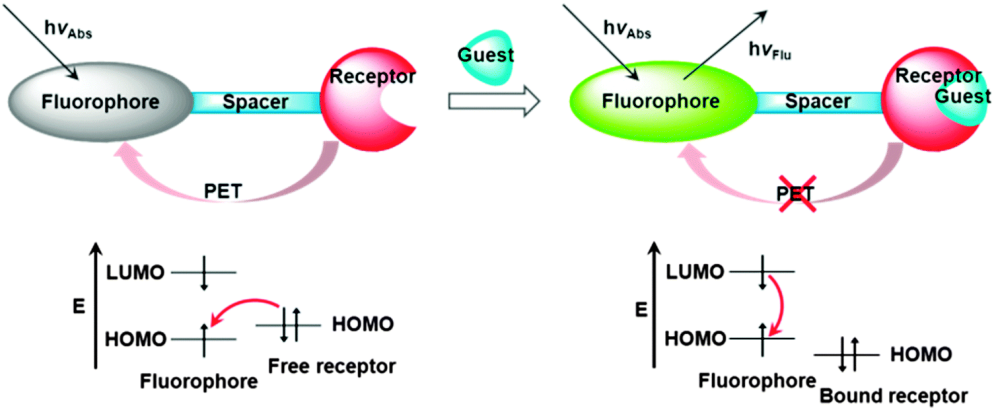

Figure-5: Metal-complex based fluorescent probes for metal ion sensing *via* PET mechanism.

Scheme-3 shows a typical example of a PET probe, in this case a BODIPY based K^+ sensor.[41] In the absence of K^+, KS-6 fluorescence emission is relatively weak because of the PET process from the receptor moiety to the BODIPY fluorophore. However, upon binding with K^+ ions, the fluorescence of the fluorophore is increased 130-fold at 572 nm due to prohibition of the PET process and shows strong transduction to K^+ concentrations ranging from 30 to 500 mM. KS-6 has been applied for selective imaging of the K^+ efflux/influx in mitochondria living cells.[41, 42] Due to the advantages of fluorescence "turn-on" sensors in cell imaging applications, probes utilizing the PET mechanism have become more numerous than others and have been attracting more and more attention in developing various fluorescent probes for metal cations.

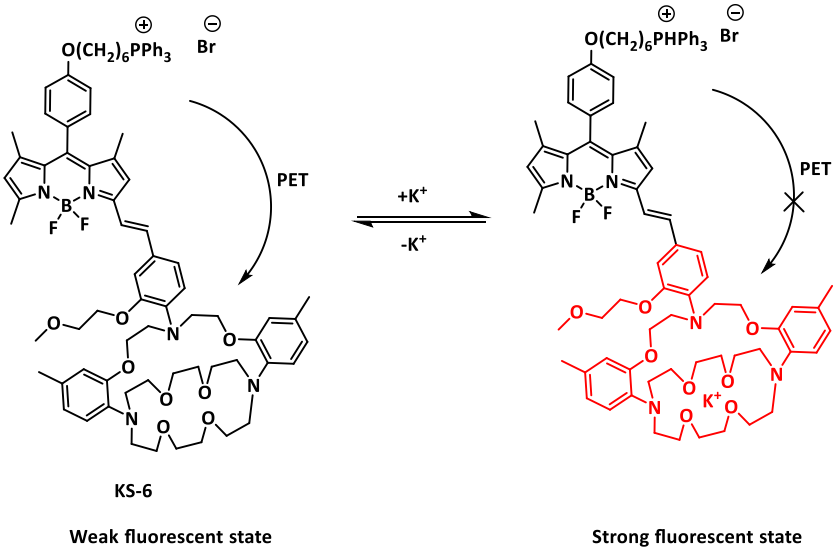

Scheme-3: Schematic illustration of PET probe, BODIPY KS-6.

2. Diketopyrrolopyrroles (DPPs)

In the past two decades, a wide variety of fluorescent probes with different recognition moieties have been designed and synthesized, which were based on the most versatile fluorophores, including fluorescein, coumarin, cyanine, boron-dipyrromethene (BODIPY), rhodamine, and 1,8-naphthalimide, etc., which are applied in many applications including cation, anion and biological relevant molecules detection, food analysis, medical diagnosis, environmental monitoring, and many other applications.

Diketopyrrolopyrroles (DPPs) were first discovered by Farmum *et al.* in 1974 as a by-product of the classical Reformatsky reaction between benzonitrile and ethyl bromoacetate (Figure-6).[43] Due to poor yields, the discovery of DPPs went largely unnoticed until 1983, when Iqbal *et al* [44] reported the synthesis of DPP *via* a new one-step route, using benzonitrile and diethyl succinate in the presence of base. This revised synthesis increased the yield to 60-70%, encouraging the commercialization of DPPs for use as a pigment in inks, varnishes and paints due to their easy functionalization, bright red color, high thermal stability, and excellent photophysical properties.[45] Since expiration of the key patent in 2003, they underwent transformation from high-quality pigments to the most popular dyes for optoelectronic applications including organic field-effect transistors (OFETs), organic photovoltaics (OPVs), organic light emitting diodes (OLEDs), dye sensitized solar cells (DSSCs) and perovskite solar cells.[46] Further striking innovations include the development of DPP-based singlet fission,[47] organic sensorimotor synapse,[48] and circularly polarized luminescence.[49]

DPP

Figure-6: Structure of diketopyrrolopyrrole (DPP) where Ar represents aryl groups.

The synthesis of the DPP core generally occurs *via* a condensation reaction between one equivalent of diethyl succinate and two equivalents of an aromatic nitrile, under basic conditions.[45] The DPP core is electron deficient due to the two amide groups present in the ring and, through incorporation of electron rich moieties such as benzene or thiophene, as flanking groups on either side of the DPP core, the absorption and emission able to be tuned in the bathochromic direction. It is well known that unsubstituted DPPs are highly insoluble due to intermolecular hydrogen bonding between N-H and O atoms. In order to improve the solubility, it is necessary to functionalize the lactam N-H position, usually by means of alkylation (Scheme-4).

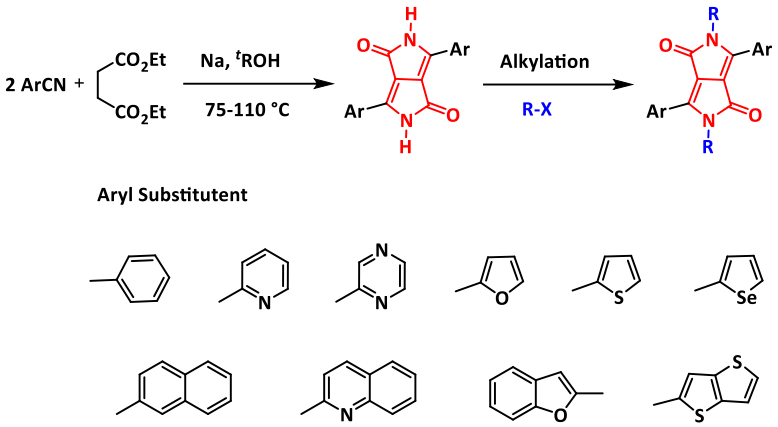

Scheme-4: Classical nitrile-succinate method for the synthesis of DPP *via* condensation.

3. New developments

In recent years there has been a growing interest in the synthesis of asymmetrically substituted DPPs, in which the DPP core is flanked by two different aryl groups and two various substituents on the nitrogen atoms. This breaks the symmetry of final molecule and improves solubility in non-chlorinated solvents. There have been various reported examples of asymmetrical DPPs possessing a wide variety of aryl substituents, mostly relying on the use of analogs of 4,5-dihydro-5-oxo-2-arylpyrrole-3-carboxylate developed in Ciba-Geigy laboratories.[50] Although this synthetic method allows for the formation of free-NH DPPs, which can be mono-alkylated non-selectively, the yields of such transformations are low which limits the substrate scope especially for highly electron-rich and sterically bulky nitriles. To overcome this problem, in 2020, Gryko and co-workers developed an efficient method for the programmed synthesis of asymmetrical DPPs (Scheme-5).[51] In order to increase the stability and solubility of the intermediate pyrrolidone in *t*-AmOH, a trimethylsilane (TMS) protected hydroxyl group was introduced in pyrrolidone **1** which could then be used in condensation reactions with nitriles providing asymmetrical DPPs incorporating two different aryl groups and selective incorporation of a single alkylated lactam product in good yields.

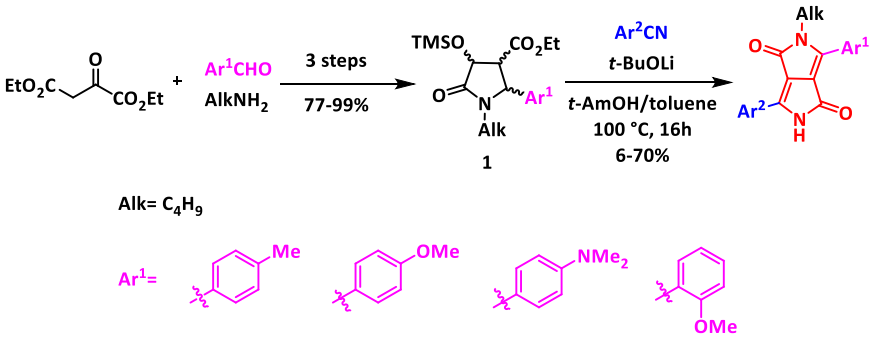

Scheme-5: The method for synthesis of asymmetrical DPPs developed by Gryko and co-workers.[51]

With this new methodology authors have been able to transform nitriles, which failed to produce diketopyrrolopyrroles in classical succinate method, into asymmetrical DPPs. This is especially true for electron-rich nitriles derived from benzene, carbazole,

naphtho[2,3-*b*]furan and sterically hindered nitriles such as 2-bromobenzonitrile, 2-methoxybenzonitrile, 8-methoxy-4-cyanoquinoline, and 9-cyanoacridine. Furthermore, electron-donating substituents such as 4-dimethyl-aminophenyl, 3-indolyl, and even 2-methoxyphenyl, which are both electron-donating and sterically hindered moieties can be easily incorporated into DPPs with good yields. This programmed method for the synthesis of diketopyrrolopyrroles enables freedom to incorporate an almost unrestricted variety of substituents around the heterocyclic core.

During the past decade, DPP dyes have shown incredible potential as fluorescent probes for applications in biological systems. So far, many research groups have designed and synthesized DPP based fluorescent probes for the detection of metal cations and anions.[45, 52] Among various anions, fluoride ions have the highest affinity to protons and are capable of deprotonating hydrogen-containing polar moieties, such as O-H and N-H groups. In 2010, Tian and co-workers developed the first DPP based fluorescent probes for the detection of fluoride ions.[53] They synthesized mono-N-alkylated DPP chemosensor **2** (Figure-7) for the detection of fluoride ions through colorimetric and ratiometric fluorescence signalling. Upon addition of F^- ions, the color of the solution showed significant change from orange to red and a fluorescence change from yellow to red was observed due to deprotonation of the N-unsubstituted amide group of DPP. In 2013, Wang and co-workers reported the first DPP based fluorescent Zn^{2+} chemosensor **3** (Figure-7) by attaching zinc chelator *N,N*-di(pyridine-2-ylmethyl)amine (DPA) to the phenyl rings at positions 3 and 6 of the DPP core. This moiety shows strong Zn^{2+} complexation with a concurrent large emission enhancement and 70 nm blue-shift response appearing through PeT and ICT mechanisms. Those probes were used for detecting Zn^{2+} ions inside living cells.[54] More recently, Wang, Sessler and co-workers reported DPP-based Zn^{2+} sensors **4** and **5** (Figure-7) by functionalizing the N2 position with a zinc-sensing unit comprised of a methoxy derivative of N,N-di-(-2-picolyl)ethylenediamine (MeO-DPEN) and a mitochondria targeting PPh_3^+ or lysosome-targeting morpholine group at the N5 position, respectively. In these cases, signaling was based on PeT processes.[55] They proved that changing the position of zinc chelator unit to the N-position of the lactam induces a 77-fold fluorescence enhancement upon the addition of Zn^{2+} and were applied to imaging lysosomal Zn^{2+} in prostate cancer cells.

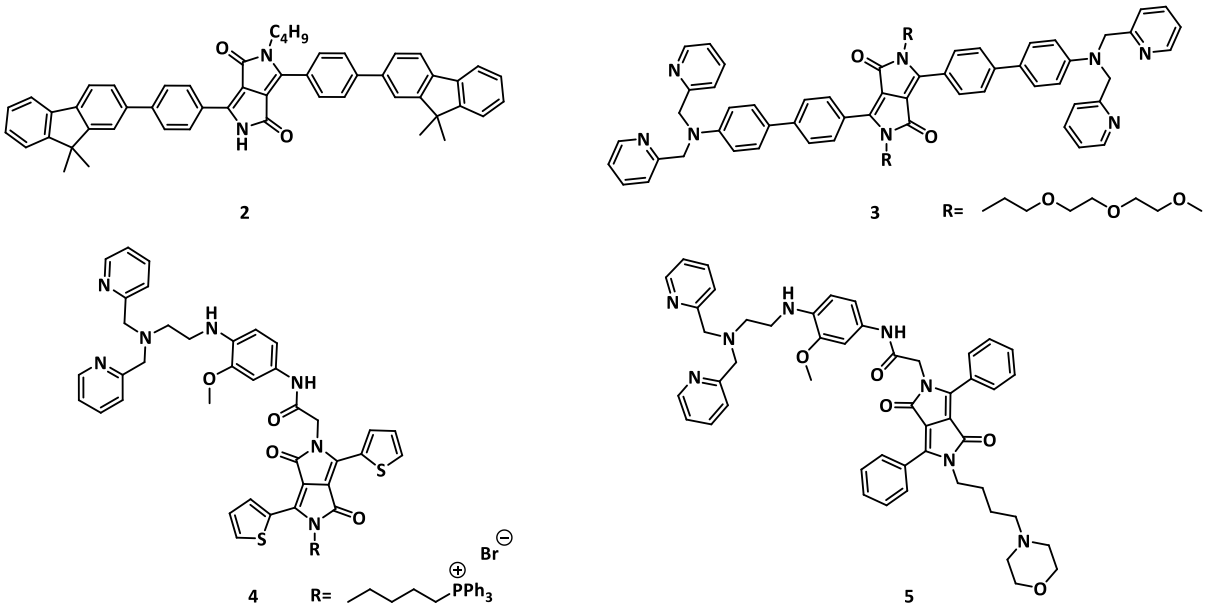

Figure-7: Reported DPP-based fluorescent sensors.

4. Aims and Objectives

Until now, there has only been limited research focused on DPPs designed for detection of metal cations especially for biologically important alkali metal ions including lithium (Li^+), sodium (Na^+), potassium (K^+) and alkaline earth metal ions magnesium (Mg^{2+}) and calcium (Ca^{2+}). Although there have been reports of DPPs designed for zinc (Zn^{2+}) detection, the vast majority of them are based on the photo-induced electron transfer (PET) mechanism. These reported DPP zinc probes have absorption and emission maxima below 600 nm, however, which limits their biological applications in the therapeutic window. Moreover, these probes exhibited low fluorescence quantum yields, even after zinc complexation, and were not organelle-specific, which often results in the detection of the subcellular Zn^{2+} decreasing resolution. While a large number of DPP-based fluorescent probes have been developed for detection of metal cations, the vast majority of them possess poor water solubility and biocompatibility combined with a low Φ_{fl} and low photostability. Therefore, when designing the next generation of fluorescent probes for imaging metal ions in living cellular systems they must meet the above mentioned key properties along with high optical brightness values which can lower the amount of dye needed for cellular applications, minimizing the potential for altering endogenous cellular distribution, and have visible-light excitation in order to minimize sample damage and reduce autofluorescence.

The aim of my project was to investigate ways of overcoming the above limitations by designing and synthesizing new diketopyrrolopyrrole-based fluorescent probes which are not only highly selective and sensitive for the detection of metal cations such as Li^+, K^+ and Zn^{2+}, but also have good solubility in polar solvents, bathochromically shifted emission, high fluorescence quantum yield, hydrophilicity and cell permeability.

The rationale behind the use of diketopyrrolopyrrole as a fluorophore was two-fold. First of all they have appreciable photophysical properties to start with (see above) which can be modulated by alteration of C-aryl substituents. Moreover I would like to exploit the newly developed programmed method for the synthesis of fully asymmetrical diketopyrrolopyrroles[51] which gives full freedom to incorporate an unrestricted variety of substituents regulating all essential features i.e., cation recognition unit, solubility, functional targeting group for a specific organelle in biological systems and modulation of the fluorescence by donor-acceptor architecture. Therefore, I decided to construct highly sensitive and selective probes comprised of two different electron-donating or electron-withdrawing peripheral aryl groups, only one of which would contain the cation recognition unit, and strong electron-accepting DPP core in the middle. Given that the rationale behind my PhD-Thesis was to design and synthesize the targeted fluorescent probes, biological targeting groups will also play an important role to accumulate in specific organelles and increase the solubility in polar solvents for molecular biology cell studies. Finally, all the novel DPP probes may induce better compatibility with the cells to detect changes in concentrations of metal cations (K^+, Zn^{2+}) in specific localization in living cells.

5. Result and discussion

5.1 Diketopyrrolopyrrole-based Chemosensors Possessing Macrocyclic Units

Crown ethers are flexible macrocyclic compounds consisting of multiple oligo-ethylene oxides in a cyclic array and were first discovered by Pedersen in 1967.[18] These crown ethers and their aza-crown analogues have been a popular receptors for alkali and alkaline earth metal cations owing to their strong binding ability between metal ions and electron rich donor atoms through electrostatic ion-dipole interactions. The most common types of crown ethers are 15-crown-5, 18-crown-6 and 1-aza-18-crown-6 which are widely used in the design of fluorescence based sensor systems.[56] The predominant design of such probes is based on photo-induced electron transfer (PET) and the probes typically comprise both a fluorophore and a recognition unit linked *via* a methylene group or longer electronically isolating bridge. However, a limited number of studies have been conducted on the photophysical consequences of directly linking the fluorophore core with a molecular recognition unit. Such fluorescent sensors operate *via* intramolecular charge transfer (ICT) which leads to a strong push-pull electron system. If the dye is polarized, the cation binding to electron-donating group affects the push-pull electronic character of the fluorophore, weakens or strengthens the ICT and leads to changes in emission such as blue- or red-shifts.[57] On the other hand, DPPs have rarely been used as fluorophores to study the recognition of metal cations and to the best of my knowledge, there is no single example on DPP-based fluorescent probe for detection of alkali metal ions such as Li^+, Na^+, K^+ and all existing examples designed for Zn^{2+} detection rely on the PET mechanism. Therefore, I decided to explore the direct linkage of intramolecular charge transfer (ICT) mechanism to construct more

efficient probes based on the DPP chromophore directly from nitriles possessing macrocyclic units.

In the first part of my study (Paper 1), I prepared a series of nitriles bearing crown ether moieties directly fused to a peripheral aryl group of DPP of different ring sizes including 18-crown-6, 15-crown-5 and 21-crown-7 (chosen as Na^+/K^+ ionophores). Initially I attempted condensation of these nitriles under classical DPP synthesis conditions in presence of diethyl succinate. Unfortunately, these reactions were unsuccessful and did not produce the desired symmetrical DPPs. Taking advantage of the recently developed new methodology for synthesis of fully asymmetrical DPPs to overcome the problem of low reactivity of nitrile which relies on the condensation of nitrile with key intermediate pyrrolidin-2-one **1**.[51] I decided to apply these conditions for condensation of nitrile **6** bearing benzo-18-crown-6 scaffold, with pyrrolidin-2-one **1**. This reaction was successful and produced the first ever macrocyclic hybrid dye DPP **7** possessing crown ether unit in low yield (Scheme-6).

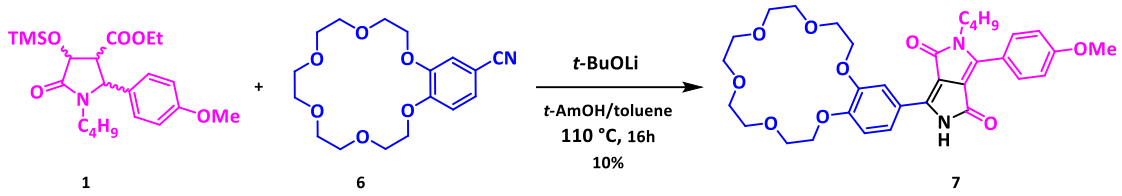

Scheme-6: Synthesis of asymmetrical benzo-crown DPP **7**

After confirming the molecular structure of DPP **7** by ^{1}H-NMR and HR-MS, the methodology was extended to synthesize a library of DPPs possessing benzo crown ethers differing in crown size. The optical studies performed at the Institute of Physics, PAS (Warsaw), revealed that fluorescence quantum yields are in the range of 0.8-0.96 but disappointingly fluorescence titration studies displayed weak selectivity for Na^+ and K^+ even in large excess. Although the size of these crown ethers are known to be compatible for complexation with the radii of Na^+ and K^+ ions, no significant changes in the emission were observed.

Previously, our group had developed a rare example of a non-fluorescent DPP dye possessing 2-dialkylaminopyridine substituents on both sides of the DPP core. I decided to utilize this finding to look for a highly prized "switch-on" fluorescent sensor. For this purpose, suitable nitriles were prepared by attaching azacrown ethers *via* nucleophilic aromatic substitution at position 2 of a 4-cyano pyridine. The resulting nitriles were subsequently used for DPP synthesis *via* condensation of nitrile using same conditions to Scheme-6. The incorporation of pyridine containing crown ethers on DPP core leads to A'-A-D architectures with improved yields of up to 30%. In contrast to the typical DPPs, which are known to be highly fluorescent, these new pyridine DPPs (**8**-**10**, Figure-8) bearing azacrown ether units at the *meta* position turned out to be very weak emissive (Φ_{fl} =0.01-0.03%) compared to benzocrown DPP **7**. The quantum chemical calculations performed by Prof. Denis Jacquemin (Nantes, France) revealed that the triplet T_2 state is located very close in energy to the S_1 with a small energy gap which

leads to efficient intersystem crossing (ISC). Thus, the presence of an accessible triplet state quenches the emission in **8**-**10**.

As predicted, the addition of sodium and potassium salts (1000 eq.) to DPPs **8**, **9** and **10** (Figure-8) possessing 2-dialkylaminopyridin-4-yl (where alkyl is a crown ether) showed moderate fluorescence enhancement with a range of 0.06-0.14% fluorescence quantum yields in acetonitrile and the emission is bathochromically shifted by 9 nm. The photophysical studies of all three DPPs **8**, **9** & **10** displayed significant bathochromic shift of both absorption and emission compared to benzo crown DPP **7** when coordinated to cations possessing Lewis acid character such as Li^+, Mg^{2+} and Zn^{2+} with strong fluorescence enhancement ≈20 to 30 times in presence 1000 eq. of each salt . Both probes **8** and **10** possessed Φ_{fl} of ≈0.2-0.3% in acetonitrile in the presence of 1000 eq. of Li^+, Mg^{2+} and Zn^{2+}, while the emissions were red-shifted from 550 to 630 nm (≈80 nm) going beyond the 600 nm into IR to NIR region.

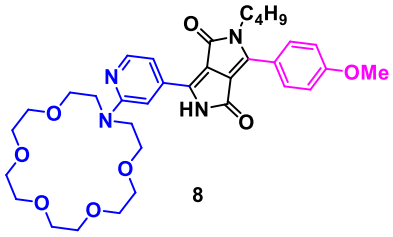

λ_{abs} = 498 nm, λ_{em} = 549, 588 nm
Φ_{fl} = 0.01
$\Phi_{fl}[K^+]$ = 0.14, $\Phi_{fl}[Na^+]$ = 0.06
$\Phi_{fl}[Li^+]$ = 0.28, $\Phi_{fl}[Mg^{2+}]$ = 0.43
$\Phi_{fl}[Zn^{2+}]$ = 0.30, $\Phi_{fl}[H^+]$ = 0.37

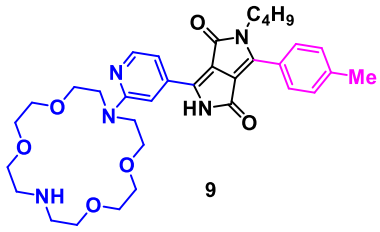

λ_{abs} = 494 nm, λ_{em} = 542, 641 nm
Φ_{fl} = 0.03
$\Phi_{fl}[K^+]$ = 0.05, $\Phi_{fl}[Na^+]$ = 0.07
$\Phi_{fl}[Li^+]$ = 0.94, $\Phi_{fl}[Mg^{2+}]$ = 0.22
$\Phi_{fl}[Zn^{2+}]$ = 0.76, $\Phi_{fl}[H^+]$ = 0.75

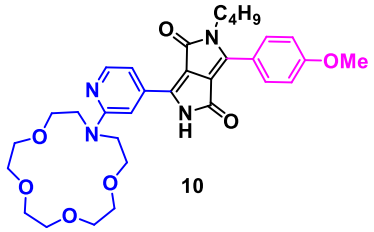

λ_{abs} = 496 nm, λ_{em} = 548, 585 nm
Φ_{fl} = 0.014
$\Phi_{fl}[K^+]$ = 0.08, $\Phi_{fl}[Na^+]$ = 0.14
$\Phi_{fl}[Li^+]$ = 0.16, $\Phi_{fl}[Mg^{2+}]$ = 0.32
$\Phi_{fl}[Zn^{2+}]$ = 0.30, $\Phi_{fl}[H^+]$ = 0.25

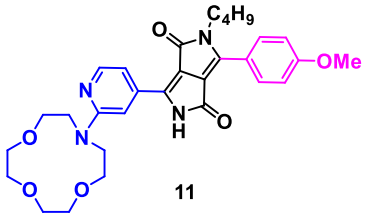

λ_{abs} = 499 nm, λ_{em} = 549, 587 nm
Φ_{fl} = 0.016, $\Phi_{fl}[Li^+]$ = 0.31

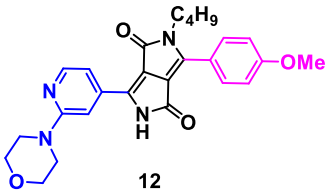

λ_{abs} = 496 nm, λ_{em} = 553, 585 nm
Φ_{fl} = 0.008
$\Phi_{fl}[Li^+]$ = 0.22, $\Phi_{fl}[Mg^{2+}]$ = 0.035
$\Phi_{fl}[Zn^{2+}]$ = 0.14, $\Phi_{fl}[H^+]$ = 0.23

Figure-8: Structures, optical properties of new fluorescent chemosensors (**8-12**) in acetonitrile.

The same trend was observed for protonation with benzenesulfonic acid. Probe **9** displayed very high emission quantum yield upon Li^+ binding (Φ_{fl}= 0.94 & 34 times) and Zn^{2+} (Φ_{fl}= 0.76 & 25 times). Finally, probe **12** (Figure-8) which lacks a macrocyclic ring, showed 30-fold fluorescence enhancement with large bathochromic shift of 120 nm in the presence of 1000 eq. of Li^+. This clearly indicates that interaction of lithium with the 2-dialkylaminopyridine unit is responsible for the striking effect.

In conclusion, by using new, efficient, programmed method for the synthesis of DPPs,[51] it is possible to obtain D-A-D and A'-A-D type DPP based fluorescent chemosensors bearing macrocyclic units directly from nitriles. As I hoped, this new class of chemosensors showed strong fluorescence intensity and bathochromic shift of emission upon complexation with metal cations especially for Li^+, Mg^{2+} and Zn^{2+}. Also, experimental results indicate that these macrocyclic hybrid dyes exhibit moderate fluorescence enhancement in the presence of Na^+ and K^+. These results open the door for me to design and synthesize highly selective and sensitive fluorescent probes for bioimaging applications in living cells as "turn-on" sensors.

5.2 DPP-based K^+ sensitive probes

Potassium ions play diverse roles in a number of biological functions especially in mitochondrial metabolic processes. Moreover, the significance of potassium channels in mitochondria plays indispensable functions in cell proliferation, cell growth, muscle contraction and nerve transmission. On the other hand, an unbalance in the potassium levels in the human body leads to many diseases. Hence, considering the importance of an intracellular and extracellular potassium concentration changes in living cells and taking into consideration of the results of my first project, I aimed to prepare highly sensitive mitochondria targeting potassium probes directly linked to a DPP fluorophore operating *via* the intramolecular charge transfer (ICT) mechanism. The obvious consequence of this fact is that the direct linking an amine-bearing recognition unit with a chromophore leads to a strongly polarized dye. Changing the electron-donating or electron-withdrawing properties in push-pull donor-acceptor systems influences the intramolecular charge transfer (ICT) and leads to increasing or decreasing of HOMO-LUMO gap.[38] To the best of my knowledge, there are no examples of DPP based fluorophores used to study K^+ concentration changes in mitochondria. For this reason in my second project I planned to synthesize K^+ probes possessing phenylaza-18-crown-6 as a key receptor due to its high selectivity and sensitivity for K^+ over Na^+ in biologically relevant conditions. Consequently, I chose an asymmetrical DPP in my molecular design strategy so that I decided to place the basic nitrogen atom at the most conjugated position of the aryl substituent, so that the fluorescence will be sensitive to the binding event. The efficient stepwise DPP synthesis allowed me to prepare 4-bromo-phenyl asymmetrical DPP derivatives bearing additional alkoxy group at an *ortho* position to bromine. The resulting dyes were used for Buchwald-Hartwig amination with 1-aza-18-crown-6 to obtain K^+-probes **13**, **14** and **15** (Figure-9). In order to increase the K^+ binding constant an additional lariat ether at a position adjacent to the aza-18-crown-6 moiety was added in probe **15**. This new programmed method for DPP synthesis selectively gives mono-alkylation at N2-position with NH-free at N5-position. This NH-free position is crucial for my design since I planned to attach the mitochondria targeting lipophilic triphenylphosphonium group which was done by means of alkylation with long alkyl chain 1, 6-dibromohexane which was subsequently reacted to form a triphenylphosphonium salt to give mitochondria probe **16** in 25% yield (Figure-9). Probe **16** represents the first DPP-based mitochondria targeting potassium probe to date. As expected, all four probes displayed good solubility in both polar and non-polar solvents.

The photophysical studies of the new fluorescent probes were broadly investigated at the Institute of Physics, PAS. Simultaneously the bioimaging experiments were performed in Nencki Institute of Experimental Biology, PAS (Warsaw).

Photophysical studies of the new D-A-D' hybrid fluorophores displayed a good combination of favorable properties including strong absorption of green light (500-530 nm) and strong emission of yellow light (560-590 nm), and very high fluorescence quantum yields (0.8-0.9%) in both CH_3CN and toluene. The probes **13**-**16** (Figure-9) bearing additional alkoxy substituents adjacent to crown ether moiety are very sensitive to K^+ which leads to hypsochromic shifts of emission from 580 to 520 nm in the presence of just 1 equivalent of K^+. Discouragingly, all four probes failed to give fluorescence changes in water and in HEPES buffer. In the absence of additional alkoxy group probe **13** displayed no essential changes in the emission even in presence of huge excess of K^+. Probe **16** displayed the highest fluorescence enhancement in the presence of 5 eq. of K^+ in CH_3CN.

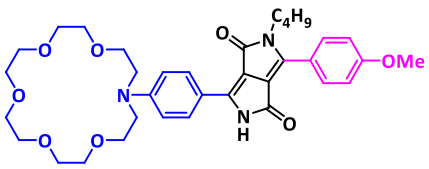

13

λ_{abs} = 525 nm, λ_{em} = 563 nm
Φ_{fl} = 0.87, FEF [K^+] = 0.99
No shift in emission after K^+ binding

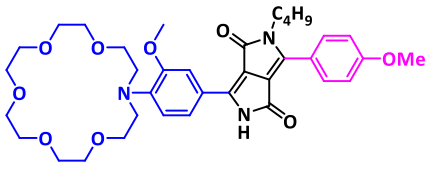

14

λ_{abs} = 506 nm, λ_{em} = 581 nm
Φ_{fl} = 0.84, FEF [K^+] = 0.80
70 nm blue shift in emission after K^+ binding

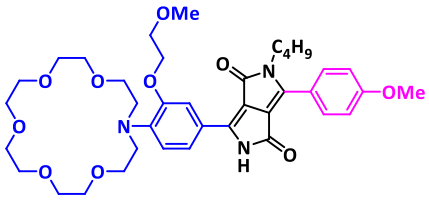

15

λ_{abs} = 514 nm, λ_{em} = 583 nm
Φ_{fl} = 0.81, FEF [K^+] = 0.81
70 nm blue shift in emission after K^+ binding

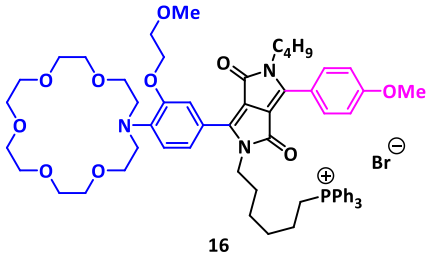

16

λ_{abs} = 499 nm, λ_{em} = 591 nm
Φ_{fl} = 0.48, FEF [K^+] = 1.39
70 nm blue shift in emission after K^+ binding

Figure-9: Structures, optical properties of new fluorescent K^+ probes **13**-**16** in acetonitrile.

As a result, probe **16** was selected for bioimaging studies and investigated by myself together with Dr. Antoni Wrzosek in the group of Prof. Adam Szewczyk (Nencki Institute of Experimental Biology, Warsaw). The conducted fluorescence microscopy experiments showed probe **16** localized selectively in mitochondria of cardiac H9C2 cells which was confirmed by co-localization with MitoTracker™ Green. As probe **16** possesses a lipophilic cation, it accumulated in the mitochondria at very low concentrations (150-500 nM) after incubation with cardiac H9C2 cells. Also, modulation in the mitochondrial K^+ concentration under stimulation in the presence of potassium

ionophore valinomycin and nigericin were visible *via* changes of fluorescence. Importantly, this sensing of mitochondrial K^+ flux in live cells could be observed at two different excitation wavelengths (green and red emission channels). With these results I have demonstrated that probe comprising of the DPP chromophore bridged with phenylaza-18-crown-6 lariat ether and quaternary phosphonium moiety is a promising K^+ sensor for intracellular imaging studies in mitochondria. To the best of my knowledge, probe **16** represents the first ever DPP-based mitochondria-targeting fluorescent K^+ sensor to date.

5.3 DPP-based Zn^{2+} sensitive probes

In the final part of my experimental work I decided on an approach to design, synthesize and study the photophysical properties as well as the intracellular imaging of diketopyrrolopyrrole-based zinc sensors directly obtained from nitriles possessing zinc chelator units. As described for the potassium probe, the development of a probe that is specific for the zinc cation is challenging as it needs to be sensitive and selective. Since zinc's biological significance has led to its intense study and its involvement in important roles in a wide range of biological processes, it is becoming increasingly important to determine zinc in living organisms.

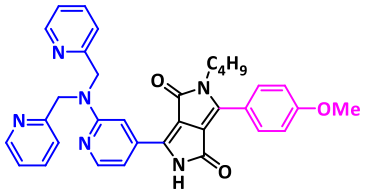

17

λ_{abs} = 499 nm, λ_{em} = 552 nm
Φ_{fl} = 0.40, $\Phi_{fl}[Zn^{2+}]$ = 0.64
FEF $[Zn^{2+}]$ = 1.6, λ_{em} = 629 nm
77 nm red shifted emission after Zn^{2+} binding

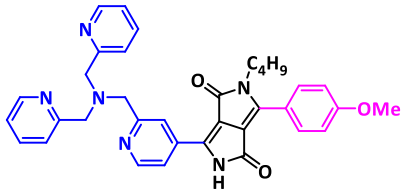

18

λ_{abs} = 497 nm, λ_{em} = 559 nm
Φ_{fl} = 0.56, $\Phi_{fl}[Zn^{2+}]$ = 0.67
FEF $[Zn^{2+}]$ = 1.2, λ_{em} = 637 nm
78 nm red shifted emission after Zn^{2+} binding

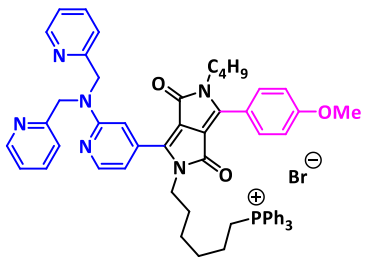

19

λ_{abs} = 474 nm, λ_{em} = 554 nm
Φ_{fl} = 0.33, $\Phi_{fl}[Zn^{2+}]$ = 0.69
FEF $[Zn^{2+}]$ = 2.1, λ_{em} = 622 nm
68 nm red shifted emission after Zn^{2+} binding

Figure-10: Structures, optical properties of new fluorescent Zn^{2+} probes **17**-**19** in acetonitrile.

Although DPP and a large number of different fluorophore-based zinc chemosensors have been extensively investigated and studied, [54-55&58-59] limited attention has been dedicated to direct linking of the DPP fluorophore with the recognition unit for the zinc cation. Since di-(2-picolyl)amine (DPA) is the most commonly used zinc chelator as its strong binding affinity over other metal cations, I decided to attach DPA unit at position 2 of a peripheral pyridine ring, so that the basic nitrogen of the pyridine also actively participates in the binding event along with DPA. Knowing from my first project that hydrophilic nitriles are compatible with DPP synthesis, I prepared two starting materials possessing a DPA unit either directly attached or *via* a methylene spacer at the 2-position of a pyridine-4-carbonitrile and they were used for the final condensation with pyrrolidin-2-one **1** using the developed methodology leading to A'-A-D architecture zinc probes **17** and **18** (Figure-10). Subsequently, I modified the structure of these probes to include triphenylphosphine cation (PPh_3^+), with the idea to transform them into mitochondrial probe **19** (Figure-10) in overall 27% yield.

In addition, a propylmorpholine group was chosen to be present at the N2 position of the final molecule as a lysosome targeting group as, due to its basic nature, it easily accumulates in acidic lysosomes. Hence, I synthesized the key intermediate pyrrolidin-2-one **20** using the previously developed method by multicomponent reaction of 4-methoxybenzaldehyde with 3-aminopropylmorpholine and diethyl oxaloacetate followed by reduction and TMS protection in overall 43% yield.[51] In analogy to the previous probes **17** and **18**, I prepared two lysosome targeting probes **21** and **22** *via* condensation of nitrile with pyrrolidin-2-one **20** using the developed conditions (Scheme-7 & Figure-11).

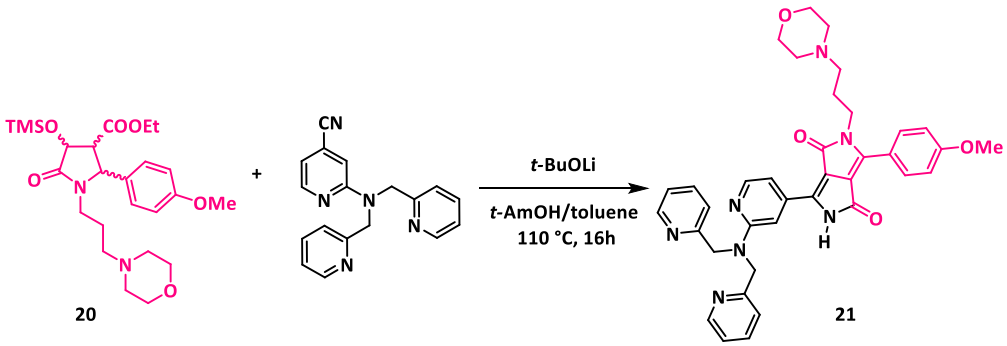

Scheme-7: Exemplary synthesis of asymmetrical, lysosome-targeting DPP **21**

Altogether, a set of five zinc probes have been prepared and the optical properties and bioimaging studies of all five probes were extensively studied in Institute of Physics, PAS and Nencki Institute of Experimental Biology, PAS (Warsaw).

All probes except **19** absorb at ≈500 nm and emit at 550-560 nm. Probes **17** and **18** display moderate fluorescence quantum yields (0.4 & 0.6%) in CH_3CN and obviously the fluorescence quantum yields are usually not too high for lysosomal probes, although probes **21** & **22** have Φ_{fl} = 0.09 and 0.12% respectively. Interestingly, a strong hypsochromic shift of absorption was observed for probe **19** with Φ_{fl} = 0.33%. As

predicted, electronically conjugated polarized DPPs **17**, **18** & **19** are very sensitive to the zinc cation and display strong ≈80 nm red-shifts of emission (yellow to orange-red) upon addition of 1 equivalent of zinc (Figure-10). It is worth mentioning that upon zinc complexation the emission of these probes shifts beyond 600 nm which is almost invisible to the naked-eye.

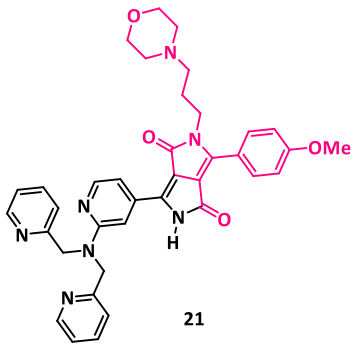

λ_{abs} = 500 nm, λ_{em} = 551 nm
Φ_{fl} = 0.09, $\Phi_{fl}[Zn^{2+}]$ = 0.59
FEF $[Zn^{2+}]$ = 6.6 fold, λ_{em} = 612 nm
61 nm red shifted emission after Zn^{2+} binding

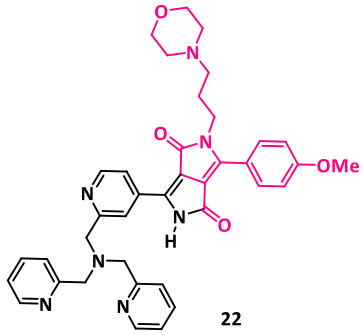

λ_{abs} = 500 nm, λ_{em} = 559 nm
Φ_{fl} = 0.12, $\Phi_{fl}[Zn^{2+}]$ = 0.78
FEF $[Zn^{2+}]$ = 6.5, λ_{em} = 622 nm
63 nm red shifted emission after Zn^{2+} binding

Figure-11: Structures, optical properties of new fluorescent Zn^{2+} probes (**21**-**22**) in acetonitrile.

As shown in the Figure-11 probes **21** and **22** bearing morpholine units displayed the highest fluorescence intensity increase (6-fold) with concurrent 50-60 nm red-shift of emission after zinc complexation with high fluorescence quantum yields in CH_3CN (≈ 0.6-0.8%). The other notable findings are as follows; (a) these probes also react with Cd^{2+} but they are silent to other divalent cations of biological importance such as Mg^{2+} and Ca^{2+}; (b) protonation of these probes with Brønsted acid shifts the emission beyond 700 nm.

Cell studies were conducted by Dr. Antoni Wrzosek and myself in the group of Prof. Adam Szewczyk (Nencki Institute of Experimental Biology, Warsaw). As predicted the staining experiments of probe **19** bearing PPh_3^+ revealed that it was selectively accumulated in mitochondria (confirmed co-localization with MitoTracker™ Green). On the other hand the probe **22** selectively localized in lysosomes which was confirmed by co-localization with LysoTracker ™. The observed photophysical response of studied DPPs and their ability to act as probes were possible due to the installing vital substituents implementing all important features, i.e., cation recognition unit, functional targeting group, solubility and donor-acceptor architecture. This in turn was only possible, thanks to the previously developed programmed synthesis of diketopyrrolopyrroles.[51]

6. Comparison and Conclusions

At the beginning of my PhD I designed and synthesized library of quadrupolar (D'-A-D) and dipolar (A'-A-D) type diketopyrrolopyrrole-based chemosensors for cations possessing Lewis acid character and their optical properties were investigated. Detailed literature studies revealed that there are not too many chemosensors possessing DPP as fluorophore. Therefore, I decided to cross-compare my compounds with other chemosensors possessing either crown ethers or 2-aminopyridine moieties. The structures and key optical properties of chemosensors **23**-**27** are presented on Figure-12. The comparison of cation sensitivity and fluorescence enhancement of dyes **8**-**12** with known probes **23**-**27** revealed that my compounds possess more beneficial properties. Diketopyrrolopyrroles (DPPs) are known to be used as organic dyes but have now, for the first time been successfully applied for detection of cations possessing Lewis acid character such as Li^+, Mg^{2+} and Zn^{2+}. In particular the comparison with 3,6-dibutylbenzodipyrido[3,2-*a*:2'3'-*c*]phenazine **23** which has a low Φ_{fl} and emits in the green region with slight red-shift of emission upon addition of Li^+ is interesting.[60] On the other hand chemosensors possessing a crown ether directly fused with a coumarin fluorophore (**24**) showed emission in the blue region with hypsochromic shift of fluorescence upon Li^+ complexation.[61] Merugu and co-workers reported a zinc chemosensor based on an aminopyridine Schiff base (**25**) which has a weak fluorescence enhancement with 30 nm red-shifted emission upon binding with zinc.[62] Wang and Yu developed a BINOL-based fluorescent sensor **26** for Zn^{2+} which showed weak 7.6-fold fluorescent intensity enhancement and bathochromically shifted emission by 50 nm.[63] One of the classical compounds from the point of Li^+ sensors is **27**, bearing an azacrown ether and possessing emission maximum beyond 600 nm after binding to Li^+ ions, but its fluorescence enhancement is low (15-fold).[64]

In conclusion, my probes **8**-**12** possessing 2-dialkylaminopyridine are more sensitive to Li^+, Mg^{2+} and Zn^{2+} with higher fluorescence quantum yields and displayed strong fluorescence enhancements of up to 45 fold. They also have bathochromically shifted both absorption and emission upon complexation with both acid and cations possessing Lewis acid character. Since the DPP core has never been utilized before to construct chemosensors, especially for Li^+, it is impossible to directly compare the optical behavior of compounds **8**-**12** with data for analogous compounds. Still, they are very favorable compared with chemosensors of similar sensing units and these findings brings DPP to the fore in the design of new generations of sensors.

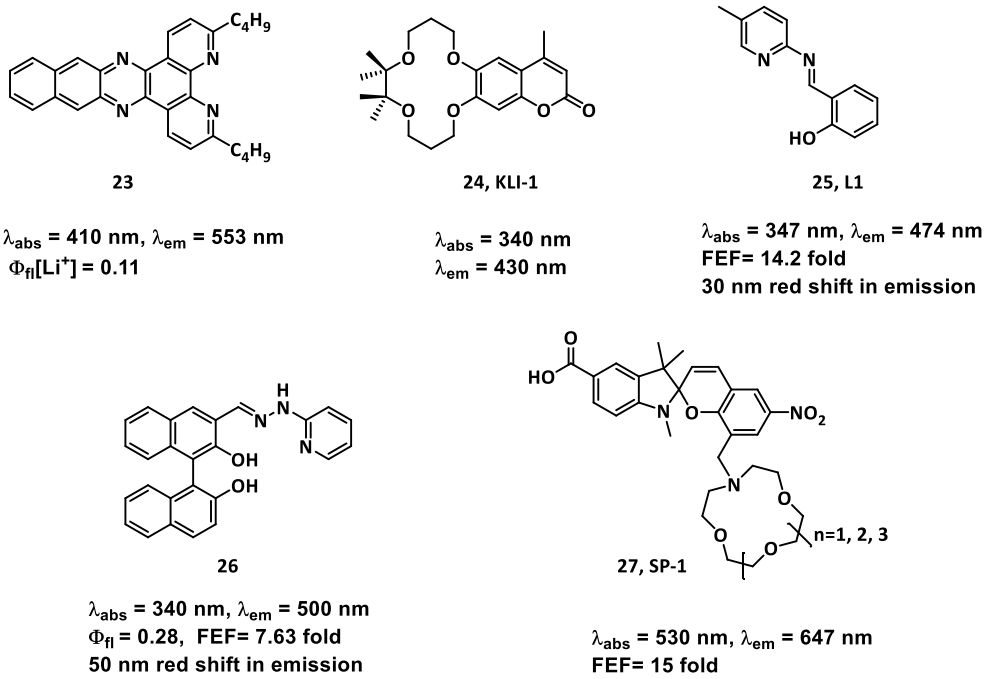

Figure-12: Photophysical results for structurally related chemosensors for Li^+, Mg^{2+} and Zn^{2+}.

In the main part of my work I designed and synthesized a set of DPP-based fluorescent K^+ sensors and their optical properties and biological applications were investigated. Fluorescent K^+ sensors **28**-**32**, well known from literature[22e, 23q,j,o,m] were compared with my new DPP K^+ sensors **13**-**16**. Holdt and co-workers synthesized **28** and proved that the presence of an additional 2-methoxyethoxy lariat group at the *ortho* position of the crown ether moiety is crucial to increase the binding constant. Probe **28** had low fluorescence quantum yields with weak fluorescence enhancement after complexation with K^+.[22] Furthermore, Borisov and co-workers developed set of BODIPY based red- to NIR emitting K^+ sensors with moderate quantum yields.[23j] Recently, Tian and co-workers reported a library of K^+ sensors **29**, **31**, **32** (Figure-13) and they have displayed blue-shift of absorption and very low Φ_{fl} upon K^+ complexation. Moreover, they have comparable changes in fluorescence properties upon addition of K^+ and probe **32** was used for monitoring the K^+ fluxes in mitochondria under stimulations by adding nigericin ionophore.

In summary I have synthesized set of DPP-based K^+ sensors possessing high fluorescence quantum yields (0.8-0.90%). I have shown that there is the possibility to fine tune the photophysical properties of DPP-based K^+ sensors and an addition of just 1 equivalent of potassium salt leads to hypsochromic shift of emission from 580 nm to 520 nm. The incorporation of mitochondria targeting group PPh_3^+ allowed to study changes in concentration of mitochondrial K^+ by adding nigericin and valinomycin at two different excitation wavelengths with increase and decrease in emission intensity. The dual excitation wavelength of the probe **16** is advantageous.

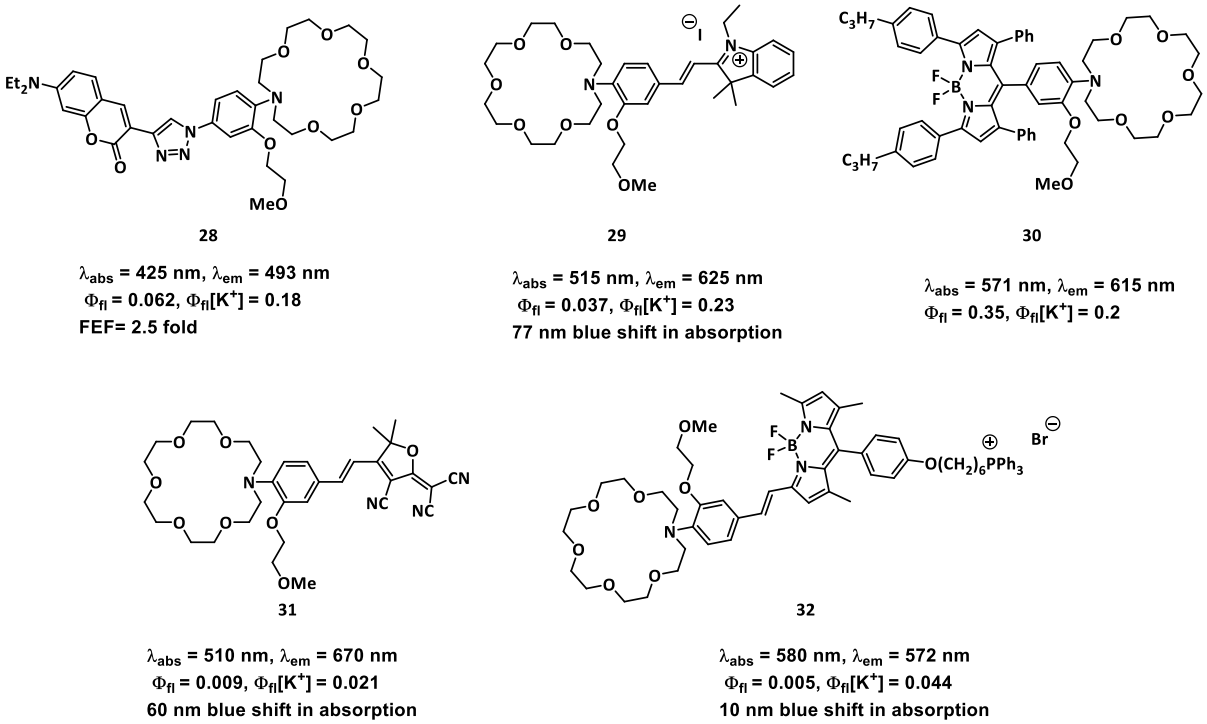

Figure-13: Photophysical results for structurally related fluorescent K^+ sensors.

Finally, I designed and synthesized DPP-based zinc sensors directly from nitriles possessing zinc recognition DPA unit and their photophysical properties and bioimaging studies were investigated. A few DPP-based fluorescent zinc sensors **33**-**35** (Figure-14) are well known from literature[54,55]. Therefore, I decided to cross compare these known sensors **33**-**35** with my zinc probes **17**-**19** and **20**-**21**. Wang and co-workers reported the first DPP based fluorescent Zn^{2+} chemosensor **33** and proved a strong Zn^{2+} complexation with 25-fold fluorescent enhancement and 70 nm blue-shift of emission.[54] Recently, Du *et al.* synthesized mitochondrial zinc probe **34** by changing the zinc chelator to the N2 position and it possessed low fluorescence quantum yield and 77-fold fluorescence enhancement in zinc complexation form, but mitochondrial targeting group PPh_3^+ exhibited a negligible effect on the optical properties of the DPP fluorophore.[55a] Very recently, the Wang and Sessler groups reported a series of lysosomal zinc probes by attaching alkyl morpholine group at N5 position and these probes display rather low quantum yields and moderate fluorescence enhancement after bound with zinc.[55b] In all the above probes authors were not able to shift the emission bathochromically to biological window beyond 600 nm.

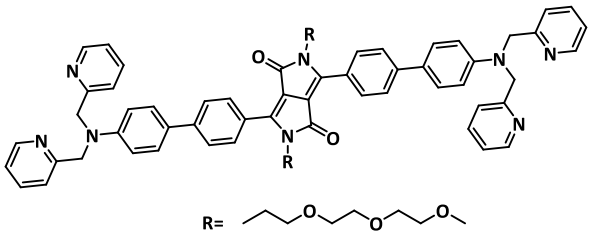

33

λ_{abs} = 490 nm, λ_{em} = 630 nm
Φ_{fl} = 0.07, $\Phi_{fl}[Zn^{2+}]$ = 0.85
FEF= 25 fold

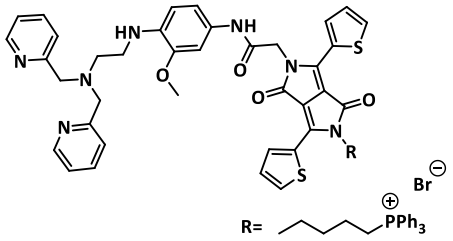

34

λ_{abs} = 520 nm, λ_{em} = 560 nm
Φ_{fl} = 0.0086, $\Phi_{fl}[Zn^{2+}]$ = 0.15
FEF= 77 fold

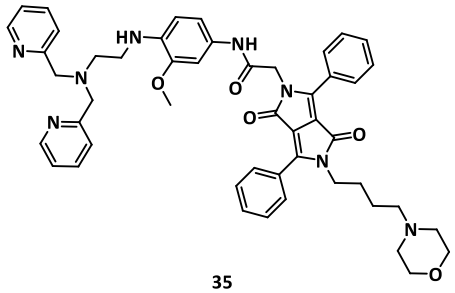

35

λ_{abs} = 453 nm, λ_{em} = 512 nm
Φ_{fl} = 0.008, $\Phi_{fl}[Zn^{2+}]$ = 0.32
FEF= 75 fold

Figure-14: Photophysical results for structurally related fluorescent Zn^{2+} sensors.

In conclusion, I have shown that my probes which contain sensing moieties directly conjugated to fluorophore cores display strong bathochromic shifts of fluorescence moving beyond 600 nm with large fluorescence quantum yields and high emission intensity when they bind to zinc. Addition of just 1 equivalent of zinc changes the fluorescence from yellow to orange-red color. Moreover, in the absence of zinc my compounds possessed nearly 200 fold higher fluorescence quantum yields than previously reported analogous lysoDPP probes. I also proved that direct linking of a zinc chelator to DPP fluorophore in a dipolar architecture opens the pathway towards modulating intramolecular charge transfer *via* increase in the electron-withdrawing properties of pyridyl substituent upon zinc coordination, which eventually leads to strong red-shift of emission. These characteristics in combination with strong orange-red emission (600-700 nm) mean these new DPP-based zinc probes are promising for bioimaging applications.

7. References

1. a) Herschel, J. F. W., *Philos. Trans. R. Soc.,* **1845**, *135*, 143-145; b) Herschel, J. F. W., *Philos. Trans. R. Soc.,* **1845**, *135*, 147-153.
2. Stokes, G. G., *Philos. Trans. R. Soc.,* **1852**, *142*, 463-562.
3. Jabłoński, A., *Z. Physik*, **1935**, *94*, 38-46.
4. de Silva, A. P.; Fox, D. B.; Moody, T. S.; Weir, S. M., *Trends Biotechnol*, **2001**, *19*, 29-34.
5. Rich, R. L.; Myszka, D. G., *J. Mol. Recognit.*, **2002**, *15*, 352-376.
6. Cammann, K., *Phys. Chem. Chem. Phys.*, **2003**, *5*, 5159-5168.
7. Badugu, R., *J. Fluoresc*., **2005**, *15*, 71-83.
8. Wang, X.-D.; Wolfbeis, O. S., *Anal. Chem.,* 2012, 85, 487-508.
9. de Silva, A. P.; Gunaratne, H. Q. N.; Gunnlaugsson, T.; Huxley, A. J. M.; McCoy, C. P.; Rademacher, J. T.; Rice, T. E., *Chem. Rev*., **1997**, *97*, 1515-1566.
10. Nolan, E. M.; Lippard, S. J., *Chem. Rev.*, **2008**, *108*, 3443-3480.
11. Duke, R. M.; Veale, E. B.; Pfeffer, F. M.; Kruger, P. E.; Gunnlaugsson, T., *Chem. Soc. Rev.*, **2010**, *39*, 3936-3953.
12. Chen, X.; Pradhan, T.; Wang, F.; Kim, J. S.; Yoon, J., *Chem. Rev.*, **2011**, *112*, 1910-1956.
13. Hargrove, A. E.; Nieto, S.; Zhang, T.; Sessler, J. L.; Anslyn, E. V., *Chem. Rev.*, **2011**, *111*, 6603-6782.
14. Boens, N.; Leen, V.; Dehaen, W., *Chem. Soc. Rev.*, **2012**, *41*, 1130-1172.
15. Li, X.; Gao, X.; Shi, W.; Ma, H., *Chem. Rev.*, **2013**, *114*, 590-659.
16. a) Yin, J.; Hu, Y.; Yoon, J., *Chem. Rev.*, **2015**, *44*, 4619-4644; b) Wu, D.; Sedgwick, A. C.; Gunnlaugsson, T.; Akkaya, E. U.; Yoon, J.; James, T. D., *Chem. Rev.*, **2017**, *46*, 7105-7123.
17. Shi, W.; Ma, H., *Chem. Commun.*, **2012**, *48*, 8732-8744.
18. a) Pedersen, C. J., *J. Am. Chem. Soc.*, **1967**, *89*, 7017-7036; b) Cram, D., *Science*, **1988**, *240*, 760-767; c) Pedersen, C. J., *Science,* **1988**, *241*, 536-540.
19. a) Tsien, R. Y., *Nature*, **1981**, *290*, 527-528; b) Minta, A.; Kao, J. P.; Tsien, R. Y., *J. Biol. Chem.*, **1989**, *264*, 8171-8178; c) Minta, A.; Tsien, R. Y., *J. Biol. Chem.*, **1989**, *264*, 19449-19457; d) de Silva, A. P.; Gunaratne, H. Q. N.; Gunnlaugsson, T.; Nieuwenhuizen, M., *Chem. Commun.*, **1996**, 1967-1968; e) Miyawaki, A.; Llopis, J.; Heim, R.; McCaffery, J. M.; Adams, J. A.; Ikura, M.; Tsien, R. Y., *Nature*, **1997**, *388*, 882-887; f) He, H.; Mortellaro, M. A.; Leiner, M. J. P.; Young, S. T.; Fraatz, R. J.; Tusa, J. K., *Anal. Chem.*, **2002**, *75*, 549-555; g) He, H.; Mortellaro, M. A.; Leiner, M. J. P.; Fraatz, R. J.; Tusa, J. K., *J. Am. Chem. Soc.*, **2003**, *125*, 1468-1469.
20. a) Obare, S. O.; Murphy, C. J., *Inorg. Chem.*, **2001**, *40*, 6080–6082; b) Citterio, D.; Takeda, J.; Kosugi, M.; Hisamoto, H.; Sasaki, S.; Komatsu, H.; Suzuki, K., *Anal. Chem.*, **2007**, *79*, 1237–1242; c) Heng, S.; Nguyen, M. –C.; Kostecki, R.; Monro, T. M.; Abell, A. D., *RSC Adv.*, **2013**, *3*, 8308-8317; d) Stubing, D. B.; Heng, S.; Abell, A. D., *Org. Biomol. Chem.*, **2016**, *14*, 3752–3757; e) Hangarge, R. V.; La, D. D.; Boguslavsky, M.; Jones, L. A.; Kim, Y. S.; Bhosale, S. V., *ChemistrySelect*, **2017**, *2*, 11487 –11491; f) Li, E.; Kang, J.; Ye, P.; Zhang, W.; Cheng. F.; Yin, C., *J. Mater. Chem. B*, **2019**, *7*, 903-907.
21. a) Martin, V. V.; Rothe, A.; Diwu, Z.; Gee, K. R., *Bioorg. Med. Chem. Lett.*, **2004**, *14*, 5313–5316; b) Martin, V. V.; Rothe, A.; Gee, K. R., *Bioorg. Med. Chem. Lett.*, **2005**, *15*, 1851–1855; c) Domaille, D. W.; Que, E. L.; Chang, C. J., *Nat. Chem. Biol.*, **2008**, *4*, 168–175; d) Gunnlaugsson, T.; Nieuwenhuyzen, M.; Richard, L.; Thoss, V., *Tetrahedron Lett.*, **2001**, *42*, 4725-4728; e) Gokel, G. W.; Leevy, W. M.; Weber, M. E., *Chem. Rev.*, **2004**, *104*, 2723−2750; f) Gao, G.; Cao, Y.; Liu, W.; Li, D.; Zhou, W.; Liu, J., *Anal. Methods*, **2017**, *9*, 5570-5579.

22. a) Martin, V. V.; Rothe, A.; Diwu, Z.; Gee, K. R., *Bioorg. Med. Chem. Lett.*, **2004**, *14*, 5313–5316; b) Kim, M. K.; Lim, C. S.; Hong, J. T.; Han, J. H.; Jang, H.-Y.; Kim, H. M.; Cho, B. R., *Angew. Chem., Int. Ed.*, **2010**, *49*, 364–367; c) Sarkar, A. R.; Heo, C. H.; Park, M. Y.; Lee, H. W.; Kim, H. M., *Chem. Commun.*, **2014**, *50*, 1309–1312; d) Ast, S.; Muller, H.; Flehr, R.; Klamroth, T.; Walz, B.; Holdt, H. –J., *Chem. Commun.*, **2011**, *47*, 4685-4687; e) Ast, S.; Schwarze, T.; Muller, H.; Sukhanov, A.; Michaelis, S.; Wegener, J.; Wolfbeis, O. S.; Korzdorfer, T.; Durkop, A.; Holdt, H. –J., *Chem. Eur. J.*, **2013**, *19*, 14911 –14917; f) Schwarze, T.; Muller, H.; Ast, S.; Steinbruck, D.; Eidner, S.; Geibler, F.; Kumke, M. U.; Holdt, H. –J., *Chem. Commun.*, **2014**, *50*, 14167-14170; g) Schwarze, T.; Muller, H.; Schmidt, D.; Reimer, J.; Holdt, H. –J., *Chem. Eur. J.*, **2017**, *23*, 7255 –7263; h) Schwarze, T.; Reimer, J.; Reimer, J.; John, L.; Holdt, H. –J.; Wessig, P., *Chem. Eur. J.*, **2019**, *25*, 12412–12422.

23. a) He, H.; Mortellaro, M.A.; Leiner, M.J.P.; Fraatz, R.J.; Tusa, J.K., *J. Am. Chem. Soc.,* **2003**, *125*, 1468–1469; b) Padmawar, P.; Yao, X.; Bloch, O.; Manley, G. T.; Verkman, A. S., *Nat. Methods*., **2005**, *2*, 825-827; c) Namkung, W.; Padmawar, P.; Mills, A. D.; Verkman, A. S., *J. Am. Chem. Soc.,* **2008**, *130*, 7794-7795; d) Hirata, T.; Terai, T.; Komatsu, T.; Hanaoka, K.; Nagano, T., *Bioorg. Med. Chem. Lett.*, **2011**, *21*, 6090-6093; e) Zhou, X.; Su, F.; Gao, W.; Tian, Y.; Youngbull, C.; Johnson, R. H.; Meldrum, D. R. *Biomaterials*, **2011**, *32*, 8574-8583; f) Zhou, X.; Su, F.; Tian, Y.; Youngbull, C.; Johnson, R. H.; Meldrum, D. R. *J. Am. Chem. Soc.,* **2011**, *133*, 18530-18533; g) Sui, B.; Yue, X.; Tichy, M.G.; Liu, T.; Belfield, K.D., *Eur. J. Org. Chem.*, **2015**, 1189–1192; h) Kong, X.; Su, F.; Zhang, L.; Yaron, J.; Lee, F.; Shi, Z.; Tian, Y.; Meldrum, D.R., *Angew. Chem. Int. Ed.*, **2015**, *54*, 12053–12057; i) Sui, B.; Yue, X.; Kim, B.; Belfield, K.D., *ACS Appl. Mater. Interfaces*, **2015**, *7*, 17565–17568; j) Müller, B.J.; Borisov, S.M.; Klimant, I., *Adv. Funct. Mater.* **2016**, 26, 7697–7707; k) Hirata, T.; Terai, T.; Yamamura, H.; Shimonishi, M.; Komatsu, T.; Hanaoka, K.; Ueno, T.; Imaizumi, Y.; Nagano, T.; Urano, Y., *Anal. Chem.*, **2016**, *88*, 2693–2700; l) Bandara, H. M. D.; Hua, Z.; Zhang, M.; Pauff, S. M.; Miller, S. C.; Davie, E. A. C.; Kobertz, W. R., *J. Org. Chem.*, **2017**, *82*, 8199–8205; m) Ning, J.; Tian, Y., *Sens. Actuators B*, **2020**, *307*, 127659; n) Song, G.; Jiang, D.; Wang, L.; Ning, J.; Sun, X.; Su, F.; Chen, M.; Tian, Y., *Chem. Commun.*, **2020**, *56*, 5405–5408; o) Ning, J.; Lin, X.; Su, F.; Sun, A.; Liu, H.; Luo, J.; Wang, L.; Tian, Y., *Anal. Bioanal. Chem.*, **2020**, *412*, 6947–6957; p) Wang, Z.; Detomasi, T. C.; Chang, C. J., *Chem. Sci.*, **2021**, *12*, 1720-1729; q) Song, G.; Sun, R.; Du, J.; Chen, M.; Tian, Y., *Chem. Commun.*, **2017**, *53*, 5602–5605.

24. a) Rusakov, D. A.; Fine, A., *Neuron*, **2003**, *37*, 287-297; b) Suzuki, Y.; Komatsu, H.; Ikeda, T.; Saito, N.; Araki, S.; Citterio, D.; Hisamoto, H.; Kitamura, Y.; Kubota, T.; Nakagawa, J.; Oka, K.; Suzuki, K., *Anal. Chem.*, **2002**, *74*, 1423-1428; c) Csordás, G.; Hajnóczky, G., *J. Biol. Chem.*, **2003**, *278*, 42273-42282; d) Leite, M. F.; Thrower, E. C.; Echevarria, W.; Koulen, P.; Hirata, K.; Bennett, A. M.; Ehrlich, B. E.; Nathanson, M. H., *Proc. Natl. Acad. Sci.*, **2003**, *100*, 2975-2980; e) Behanna, H. A.; Stupp, S. I., *Chem. Commun.*, **2005**, 4845-4847; f) Komatsu, H.; Miki, T.; Citterio, D.; Kubota, T.; Shindo, Y.; Kitamura, Y.; Oka, K.; Suzuki, K., *J. Am. Chem. Soc.,* **2005**, *127*, 10798-10799; g) Kim, H. M.; Kim, B. R.; Hong, J. H.; Park, J.-S.; Lee, K. J.; Cho, B. R., *Angew. Chem. Int. Ed.,* **2007**, *46*, 7445-7448; h) Kim, H. M.; Kim, B. R.; An, M. J.; Hong, J. H.; Lee, K. J.; Cho, B. R., *Chem. Eur. J.*, **2008**, *14*, 2075-2083; i) Dong, X.; Yang, Y.; Sun, J.; Liu, Z.; Liu, B.-F. *Chem. Commun.,* **2009**, 3883-3885; j) Kamiya, M.; Johnsson, K., *Anal. Chem.,* **2010**, *82*, 6472-6479; k) Egawa, T.; Hanaoka, K.; Koide, Y.; Ujita, S.; Takahashi, N.; Ikegaya, Y.; Matsuki, N.; Terai, T.; Ueno, T.; Komatsu, T.; Nagano, T., *J. Am. Chem. Soc.,* **2011**, *133*, 14157-14159; l) Matsui, A.; Umezawa, K.; Shindo, Y.; Fujii, T.; Citterio, D.; Oka, K.; Suzuki, K.,

Chem. Commun., **2011**, *47*, 10407-10409; m) Liu, Q.; Bian, W.; Shi, H.; Fan, L.; Shuang, S.; Dong, C.; Choi, M. M. F., *Org. Biomol. Chem.,* **2013**, *11*, 503-508; n) Liu, Z.; Jing, X.; Zhang, S.; Tian, Y., *Anal. Chem.,* **2019**, *19*, 2488-2497.

25. a) Komatsu, H.; Iwasawa, N.; Citterio, D.; Suzuki, Y.; Kubota, T.; Tokuno, K.; Kitamura, Y.; Oka, K.; Suzuki, K., *J. Am. Chem. Soc.,* **2004**, *126*, 16353-16360; b) Farruggia, G.; Iotti, S.; Prodi, L.; Montalti, M.; Zaccheroni, N.; Savage, P. B.;Trapani, V.; Sale, P.; Wolf, F. I., *J. Am. Chem. Soc.,* **2005**, *128*, 344-350; c) Kim, H. M.; Jung, C.; Kim, B. R.; Jung, S.-Y.; Hong, J. H.; Ko, Y.-G.; Lee, K. J.; Cho, B. R., *Angew. Chem. Int. Ed.*, **2007**, *46*, 3460-3463; d) Kim, H. M.; Yang, P. R.; Seo, M. S.; Yi, J.-S.; Hong, J. H.; Jeon, S.-J.; Ko, Y.-G.; Lee, K. J.; Cho, B. R., *J. Org. Chem.*, **2007**, *72*, 2088-2096; e) Jin, J.; Desai, B. N.; Navarro, B.; Donovan, A.; Andrews, N. C.; Clapham, D. E., *Science*, **2008**, *322*, 756-760; f) Marraccini, C.; Farruggia, G.; Lombardo, M.; Prodi, L.; Sgarzi, M.; Trapani, V.; Trombini, C.; Wolf, F. I.; Zaccheroni, N.; Iotti, S., *Chem. Sci.,* **2012**, *3*, 727-734; g) Liu, M.; Yu, X.; Li, M.; Liao, N.; Bi, A.; Jiang, Y.; Liu, S.; Gong, Z.; Zeng, W., *RSC Adv.*, **2018**, *8*, 12573–12587.
26. a) Mao, J.; Wang, L.; Dou, W.; Tang, X.; Yan, Y.; Liu, W., *Org. Lett.,* **2007**, *9*, 4567-4570; b) Huang, K.; Yang, H.; Zhou, Z.; Yu, M.; Li, F.; Gao, X.; Yi, T.; Huang, C., *Org. Lett.,* **2008**, *10*,
2557-2560; c) Zhou, Z.; Yu, M.; Yang, H.; Huang, K.; Li, F.; Yi, T.; Huang, C., *Chem. Commun.,* **2008**, 3387-3389; d) He, X.; Wu, C.; Qian, Y.; Li, Y.; Zhang, L.; Ding, F.; Chen, H.; Shen, J., *Analyst*, **2019**, *144*, 3807-3816.
27. Sahoo, S. K.; Crisponi, G., *Molecules,* **2019**, *24*, 3267.
28. a) Maity, D.; Govindaraju, T., *Inorg. Chem.*, **2011**, *50*, 11282-11284; b) Zhen, S. J.; Guo, F. L.; Chen, L. Q.; Li, Y. F.; Zhang, Q.; Huang, C. Z., *Chem. Commun.,* **2011**, *47*, 2562-2564; c) Shiraishi, Y.; Matsunaga, Y.; Hirai, T., *Chem. Commun.,* **2012**, *48*, 5485-5487
29. a) Dodani, S. C.; He, Q.; Chang, C. J., *J. Am. Chem. Soc.,* **2009**, *131*, 18020-18021; b) Banerjee, A.; Sahana, A.; Guha, S.; Lohar, S.; Hauli, I.; Mukhopadhyay, S. K.;Sanmartín Matalobos, J.; Das, D. *Inorg. Chem.*, **2012**, *51*, 5699-5704; c) Kang, M. Y.; Lim, C. S.; Kim, H. S.; Seo, E. W.; Kim, H. M.; Kwon, O.; Cho, B. R., *Chem. Eur. J.*, **2012**, *18*, 1953-1960; d) Song, Y.; Tao, J.; Wang, Y.; Cai, Z.; Fang, X.; Wang, S.; Xu, H., *Inorg. Chim. Acta*, **2021**, *516*, 120099; e) Wang, X.; Liu, C.; Zhu, H.; Cheng, S.; Zhang, Y.; Su, M.; Rong, X.; Yu, M.; Sheng, W.; Zhu, B., *Sens. Actuators B*, **2022**, *369*, 132300.
30. a) Royzen, M.; Dai, Z.; Canary, J. W., *J. Am. Chem. Soc.,* **2005**, *127*, 1612-1613; b) Xiang, Y.; Tong, A.; Jin, P.; Ju, Y., *Org. Lett.,* **2006**, *8*, 2863-2866; c) Zhao, Y.; Zhang, X.-B.; Han, Z.-X.; Qiao, L.; Li, C.-Y.; Jian, L.-X.; Shen, G.-L.; Yu,R.-Q., *Anal. Chem.*, **2009**, *81*, 7022-7030; d) Goswami, S.; Sen, D.; Das, N. K., *Org. Lett.,* **2010**, *12*, 856-859; e) Li, P.; Duan, X.; Chen, Z.; Liu, Y.; Xie, T.; Fang, L.; Li, X.; Yin, M.; Tang, B., *Chem. Commun.,* **2011**, *47*, 7755-7757.
31. a) Nolan, E. M.; Jaworski, J.; Okamoto, K.-I.; Hayashi, Y.; Sheng, M.; Lippard, S. J., *J. Am. Chem. Soc.,* **2005**, *127*, 16812-16823; b) Atilgan, S.; Ozdemir, T.; Akkaya, E. U., *Org. Lett.,* **2008**, *10*, 4065-4067; c) Sivaraman, G.; Anand, T.; Chellappa, D. *Analyst*, **2012**, *137*, 5881-5884; d) Zhang, Z.; Wang, F.-W.; Wang, S.-Q.; Ge, F.; Zhao, B.-X.; Miao, J.-Y., *Org. Biomol. Chem.,* **2012**, *10*, 8640-8644; e) Xue, L.; Li, G.; Yu, C.; Jiang, H., *Chem. Eur. J.*, **2012**, *18*, 1050-1054; f) Masanta, G.; Lim, C. S.; Kim, H. J.; Han, J. H.; Kim, H. M.; Cho, B. R., *J. Am. Chem. Soc.,* **2011**, *133*, 5698-5700; g) Roopa; Kumar, N.; Bhalla, V.; Kumar, M., *Chem. Commun.*, **2015**, *51*, 15614-15628; h) Zastrow, M. L.; Radford, R. J.; Chyan, W.; Anderson, C. T.; Zhang, D. Y.; Loas, A.; Tzounopoulos, T.; Lippard, S. J., *ACS Sens.,* **2016**, *1*, 32–39; i) Komatsu, K.; Urano, Y.; Kojima, H.; Nagano, T., *J. Am. Chem. Soc.,* **2007**, *129*, 13447–13454; j) Lee, J. H.; Lee, J. H.; Jung, S. H.; Hyun, T. K.; Feng, M.; Kim, J.-Y.; Lee, J.-

H.; Lee, H.; Kim, J. S.; Kang, C.; Kwon, K.-Y.; Jung, J. H., *Chem. Commun.*, **2015**, *51*, 7463–7465.

32. a) Sreenath, K.; Yuan, Z.; Allen, J. R.; Davidson, M. W.; Zhu, L., *Chem. Eur. J.*, **2015**, *21*, 867–874; b) Su, H. Z.; Chen, X. B.; Fang, W. H., *Anal. Chem.*, **2014**, *86*, 891–899; c) Sumalekshmy, S.; Henary, M. M.; Siegel, N.; Lawson, P. V.; Wu, Y. Schmidt, K.; Bredas, J.-L.; Perry, J. W.; Fahrni, C. J., *J. Am. Chem. Soc.*, **2007**, *129*, 11888-11889; d) Chen, X. –Y.; Shi, J.; Li, Y. –M.; Wang, F. –L.; Wu, X.; Guo, Q. –X.; Liu, L., *Org. Lett.*, **2009**, *19*, 4426-4429; e) Fang, L.; Watinkson, M., *Chem. Sci.*, **2020**, *11*, 11366-11379; f) Woodroofe, C. C.; Lippard, S. J., *J. Am. Chem. Soc.*, **2003**, *125*,11458-11459; g) You, Y.; Lee, S.; Kim, T.; Ohkubo, K.; Chae, W.-S.; Fukuzumi, S.; Jhon, G.-J.;Nam, W.; Lippard, S. J., *J. Am. Chem. Soc.*, **2011**, *133*, 18328-18342; h) Wong, B. A.; Friedle, S.; Lippard, S. J., *J. Am. Chem. Soc.*, **2009**, *131*, 7142-7152; i) Du, P.; Lippard, S. J. *Inorg. Chem.*, **2010**, *49*, 10753-10755.
33. Chen, S. –Y.; Li, Z.; Li, K.; Yu, X. –Q., *Coord. Chem. Rev.*, **2021**, *429*, 213691.
34. Callan, J. F.; de Silva, A. P.; Magri, D. C., *Tetrahedron*, **2005**, *61*, 8551-8588.
35. Deng, R.; Wang, J.; Chen, R.; Huang, W.; Liu, X., *J. Am. Chem. Soc.*, **2016**, *138*, 15972-15979.
36. Junager, N. P. L.; Kongsted, J.; Astakhova, K., *Sensors*, **2016**, *16*, 1173.
37. Xu, H.; Zhu, C.; Chen, Y.; Bai, Y.; Han, Z.; Yao, S.; Jiao, Y.; Yuan, H.; He, W.; Guo, Z., *Chem. Sci.*, **2020**,*11*, 11037-11041.
38. a) Valeur, B.; Leray, I., *Coord. Chem. Rev.*, **2000**, *205*, 3-40; b) Grynkiewicz, G.; Poenie, M.; Tsien, R. Y. *J. Biol. Chem.* **1985**, *260*, 3440–3450.
39. a) Grynkiewicz, G.; Poenie, M.; Tsien, R. Y., *J. Biol. Chem.*, **1985**, *260*, 3440-3450; b) Tsien, R. Y., *Trends Neurosci.*, **1988**, *11*, 419-424.
40. a) Nolan, E. M.; Lippard, S. J., *Acc. Chem. Res.*, **2008**, *42*, 193-203; b) Wong, J.K.H.; Todd, M.H.; Rutledge, P.J., *Molecules*, **2017**, *22*, 200.
41. Kong, X.; Su, F.; Zhang, L.; Yaron, J.; Lee, F.; Shi, Z.; Tian, Y.; Meldrum, D.R., *Angew. Chem. Int. Ed.*, **2015**, *54*, 12053–12057.
42. a) Sui, B.; Yue, X.; Kim, B.; Belfield, K. D., *ACS Appl. Mater. Interfaces,* **2015**, *7*, 17565−17568; b) Ning, J.; Tian, Y., *Sens. Actuators B*, **2020**, *307*, 127659; c) Song, G.; Jiang, D.; Wang, L.; Ning, J.; Sun, X.; Su, F.; Chen, M.; Tian, Y., *Chem. Commun.*, **2020**, *56*, 5405–5408.
43. Farnum, D. G.; Mehta, G.; Moore, G. G. I.; Siegal, F. P., *Tetrahedron Lett.*, **1974**, *29*, 2549-2552.
44. A) Rochat, A. C.; Cassar, L.; Iqbal, A., (Ciba-Geigy AG), *Eur. Pat. Appl.* 94911, **1983**; b) Iqbal, A.; Jost, M.; Kirchmayr, R.; Rochat, A. C, *Bull. SOC. Chim. Belg.*, **1988**, *97*, 615-644.
45. Grzybowski, M.; Gryko, D. T., *Adv. Opt. Mater.*, **2015**, *3*, 280–320.
46. a) Liu, Q.; Bottle, S. E.; Sonar, P., *Adv. Mater.*, **2019**, *32*, 1903882; b) Molina, D.; Álvaro-Martins, M. J.; Sastre-Santos, Á., *J. Mater. Chem. C*, **2021**, *9*, 16078-16109; c) Yi, Z.; Wang, S.; Liu, Y., *Adv. Mater.*, **2015**, *27*, 3589-3606; d) Tang, A.; Zhan, C.; Yao, J.; Zhou, E., *Adv. Mater.*, **2017**, *29*, 1600013; e) Liu, Q.; Chavhan, S.; Zhang, H.; Sun, H.; Brock, A. J.; Manzhos, S.; Chen, Y.; Feron, K.; Bottle, S. E.; McMurtrie, J. C.; Jou, J.-H.; Chen, H.-S.; Nagar, M. R.; Hu, W.; Noh, Y.-Y.; Zhen, Y.; Sonar, P., *Adv. Electron. Mater.*, **2021**, *7*, 2000804; f) Shukla, A.; McGregor, S. K. M.; Wawrzinek, R.; Saggar, S.; Moore, E. G.; Lo, S.-C.; Namdas, E. B., *Adv. Funct. Mater.*, **2021**, *31*, 2009817; g) Leventis, A.; Royakkers, J.; Rapidis, A. G.; Goodeal, N.; Corpinot, M. K.; Frost, J. M.; Bucar, D. –K.; Blunt, M. O.; Cacialli, F.; Bronstein, H., *J. Am. Chem. Soc.*, **2018**, *140*, 1622-1626.
47. a) Mauck, C. M.; Hartnett, P. E.; Margulies, E. A.; Ma, L.; Miller, C. E.; Schatz, G. C.; Marks, T. J.; Wasielewski, M. R., *J. Am. Chem. Soc.*, **2016**, *138*, 11749−11761; b) Ye, C.; Mallick,

S.; Hertzog, M.; Kowalewski, M.; Börjesson, K., *J. Am. Chem. Soc.*, **2021**, *143*, 19, 7501–7508; c) Papadopoulos, I.; Álvaro-Martins, M. J.; Molina, D.; McCosker, P. M.; Keller, P. A.; Clark, T.; Sastre-Santos, Á.; Guldi, D. M., *Adv. Energy Mater.*, **2020**, *10*, 2001496; d) Masoomi-Godarzi, S.; Liu, M.; Tachibana, Y.; Goerigk, L.; Ghiggino, K. P.; Smith, T. A.; Jones, D. J., *Adv. Energy Mater.*, **2018**, *8*, 1801720; e) Krishnapriya, K. C.; Roy, P.; Puttaraju, B.; Salzner, U.; Musser, A. J.; Jain, M.; Dasgupta, J.; Patil, S., *Nat. Commun.,* **2019**, *10*, 1-8.

48. Lee, Y.; Oh, J. Y.; Xu, W.; Kim, O.; Kim, T. R.; Kang, J.; Kim, Y.; Son, D.; Tok, J. B.-H.; Park, M. J.; Bao, Z.; Lee, T-W., *Sci. Adv.*, **2018**, *4*, eaat7387.
49. Dhbaibi, K.; Favereau, L.; Srebro-Hooper, M.; Jean, M.; Vanthuyne, N.; Zinna, F.; Jamoussi, B.; Bari, L. D.; Autschbach, J.; Crassous, J., *Chem. Sci.*, **2018**, *9*, 735-742.
50. a) Pfenninger, J.; Iqbal, A.; Rochat, A. C.; Wallquist, O., (Ciba-Geigy AG), *Eur. Pat. Appl.* 184982, **1986**; b) Potrawa, T.; Langhals, H., *Chem. Ber.*, **1987**, *120*, 1075-1078; c) Morton, C. J. H.; Riggs, R. L.; Smith, D. M.; Lightfoot, P.; Slawin, A. M. Z.; MacLean, E. J., *Tetrahedron*, **2002**, *58*, 5547-5565; d) Stas, S.; Balandier, J.-Y.; Lemaur, V.; Fenwick, O.; Tregnago, G.; Quist, F.; Cacialli, F.; Cornil, J.; Geerts, Y. H., *Dyes Pigm.*, **2013**, *97*, 198–208; e) Ding, S.; Ni, Z.; Hu, M.; Qiu, G.; Li, J.; Ye, J.; Zhang, X.; Liu, F.; Dong, H.; Hu, W., *Macromol. Rapid Commun.*, **2018**, *39*, 1800225; f) Jiang, Z.; Ni, Z.; Wang, H.; Wang, Z.; Zhang, J.; Qiu, G.; Fang, J.; Zhang, Y.; Dong, H.; Lu, K.; Hu, W.; Wei, Z., *Polym. Chem.*, **2017**, *8*, 5603–5610; g) Qiu, G.; Jiang, Z.; Ni, Z.; Wang, H.; Dong, H.; Zhang, J.; Zhang, X.; Shu, Z.; Lu, K.; Zhen, Y.; Wei, Z.; Hu, W., *J. Mater. Chem. C*, **2017**, *5*, 566–572; h) Wang, X.; Jiang, B.; Du, C.; Ren, X.; Duan, Z.; Wang, H., *New J. Chem.*, **2019**, *43*, 16411–16420.
51. Pieczykolan, M.; Sadowski, B.; Gryko, D. T., *Angew. Chem. Int. Ed.*, **2020**, *59*, 7528–7535.
52. a) Li, W.; Wang, L.; Tang, H.; Cao, D., *Dyes Pigm.* **2019**, *162*, 934-950; b) Auwalu, M. A.; Cheng, S., *Chemosensors*, **2021**, *9*, 44.
53. Qu, Y.; Hua, J.; Tian, H., *Org. Lett.*, **2010**, *12*, 3320-3323.
54. a) Zhang, G. J.; Li, H. Y.; Bi, S. M.; Song, L. F.; Lu, Y. X.; Zhang, L.; Yua, J. J.; Wang, L. M., *Analyst*, **2013**, *138*, 6163–6170; b) Zhang, G. J.; Bi, S. M.; Song, L. F.; Wang, F.; Yu, J. J.; Wang, L. M., *Dyes Pigm.*, **2013**, *99*, 779–786.
55. a) Du, C. C.; Fu, S. B.; Ren, X. L.; Wang, X. H.; Wang, Z.; Zhou, J.; Wang, H. Y., *New J. Chem.*, **2018**, *42*, 3493–3502; b) Du, C. C.; Fu, S. B.; Wang, X. H.; Sedgwick, A. C.; Zhen, W.; Li, M.; Li, X.; Zhou, J.; Wang, Z.; Wang, H. Y.; Sessler, J. L., *Chem. Sci.*, **2019**, *10*, 5699-5704.
56. Li, J.; Yim, D.; Jang, W. –D.; Yoon, J., *Chem. Soc. Rev.*, **2017**, *46*, 2437-2458.
57. Lee, M. H.; Kim, J. S.; Sessler, J. L., *Chem. Soc. Rev.*, **2015**, *44*, 4185–4191.
58. a) Ning, P.; Jiang, J. C.; Li, L. C.; Wang, S. X.; Yu, H. Z.; Feng, Y.; Zhu, M.Z.; Zhang, B. C.; Yin, H.; Guo, Q. X.; Meng, X. M., *Biosens. Bioelectron.*, **2016**, *77*, 921–927; b) Zastrow, M. L.; Radford, R. J.; Chyan, W.; Anderson, C. T.; Zhang, D. Y.; Loas, A.; Tzounopoulos, T.; Lippard, S. J., *ACS Sens.*, **2016**, *1*, 32–39; c) Komatsu, K.; Urano, Y.; Kojima, H.; Nagano, T., *J. Am. Chem.Soc.*, **2007**, *129*, 13447–13454; d) Lee, J. H.; Lee, J. H.; Jung, S. H.; Hyun, T. K.; Feng, M.; Kim, J.-Y.; Lee, J.-H.; Lee, H.; Kim, J. S.; Kang, C.; Kwon, K.-Y.; Jung, J. H., *Chem. Commun.*, **2015**, *51*,7463–7465; e) Sreenath, K.; Yuan, Z.; Allen, J. R.; Davidson, M. W.; Zhu, L., *Chem. Eur. J.*, **2015**, *21*, 867–874; f) Su, H.Z.; Chen, X. B.; Fang, W. H.; *Anal. Chem.*, **2014**, *86*, 891–899.
59. a) Zhu, S.; Zhang, J.; Janjanam, J.; Vegesna, G.; Luo, F.-T.; Tiwari, A.; Liu, H., *J. Mater. Chem. B*, **2013**, *1*, 1722–1728; b) Xue, L.; Li, G.; Yu, C.; Jiang, H., *Chem. Eur. J.*, **2012**, *18*, 1050-1054; c) Masanta, G.; Lim, C. S.; Kim, H. J.; Han, J. H.; Kim, H. M.; Cho, B. R., *J. Am. Chem. Soc.*, **2011**, *133*, 5698-5700; d) Peng, S.; He, Q.; Vargas-Zúñiga, G. I.; Qin, L.;

Hwang, I.; Kim, S. K.; Heo, N. J.; Lee, C.-H.; Dutta, R.; Sessler, J. L., *Chem. Soc. Rev.*, **2020**, *49*, 865-907; e) Kanegae, A.; Takata, Y.; Takashima, I.; Uchinomiya, S.; Kawagoe, R.; Usui, K.; Yamashita, A.; Wongkongkatep, J.; Sugimoto, M.; Ojida, A., *Commun. Chem.*, **2021**, *4*, 104; f) Lim, N. C.; Brückner, C., *Chem. Commun.*, **2004**, 1094–1095.

60. Obare, S. O.; Murphy, C. J., *Inorg. Chem.*, **2001**, *40*, 6080–6082.
61. Citterio, D.; Takeda, J.; Kosugi, M.; Hisamoto, H.; Sasaki, S.; Komatsu, H.; Suzuki, K., *Anal. Chem.*, **2007**, *79*, 1237-1242.
62. Gupta, V. K.; Singh, A. K.; Kumawat, L. K.; Mergu, N., *Sens. Actuators B*, **2016**, 468-482.
63. Jiao, S. –Y.; Peng, L. –L.; Li, K.; Xie, Y. –M.; Ao, M. –Z.; Wang, X.; Yu, X. –Q., *Analyst*, **2013**, *138*, 5762-5768.
64. Stubing, D. B.; Heng, S.; Abell, A. D., *Org. Biomol. Chem.*, **2016**, *14*, 3752-3757.

7. Original publications

DOI: 10.1002/asia.202001376

CHEMISTRY AN ASIAN JOURNAL Full Paper

Switch-On Diketopyrrolopyrrole-Based Chemosensors for Cations Possessing Lewis Acid Character

G. Dinesh Kumar,[a] Marzena Banasiewicz,[b] Denis Jacquemin,*[c] and Daniel T. Gryko*[a]

Abstract: For the first time diketopyrrolopyrroles (DPPs) have been synthesized directly from nitriles possessing (aza)crown ethers leading to macrocycle-dye hybrids. Depending on the nature of the linkage between DPP and macrocyclic ring, various coordination effects are found. The strong interaction of the cations possessing Lewis acid character such as Li^+, Mg^{2+} and Zn^{2+} with 2-aminopyridin-4-yl-DPPs, leading to a bathochromic shift of both emission and absorption, as well as to strong enhancement of fluorescence was rationalized in terms of strong binding of these cations to the N=C–NR_2 functionality. The same effect has been observed for protonation. Depending on the size and the structure of the macrocyclic ring the complexation of cations by aza-crown ethers plays an important but secondary role. The interaction of Na^+ and K^+ with 2-aminopyridin-4-yl-DPPs leads to moderate enhancement of fluorescence due to the aza-crown ethers binding. The very weak fluorescence of DPP bearing 2-dialkylamino-pyridine-4-yl substituent is due to the closely lying T_2 state and the resulting intersystem crossing.

CHEMISTRY
AN ASIAN JOURNAL

Supporting Information

Switch-On Diketopyrrolopyrrole-Based Chemosensors for Cations Possessing Lewis Acid Character

G. Dinesh Kumar, Marzena Banasiewicz, Denis Jacquemin,* and Daniel T. Gryko*

Author Contributions

D.K. Investigation:Lead; Visualization:Supporting; Writing – original draft:Equal; Writing – review & editing:Supporting
M.B. Data curation:Equal; Investigation:Lead; Writing – original draft:Supporting; Writing – review & editing:Supporting
D.J. Investigation:Lead; Visualization:Equal; Writing – original draft:Equal; Writing – review & editing:Equal

Table of contents

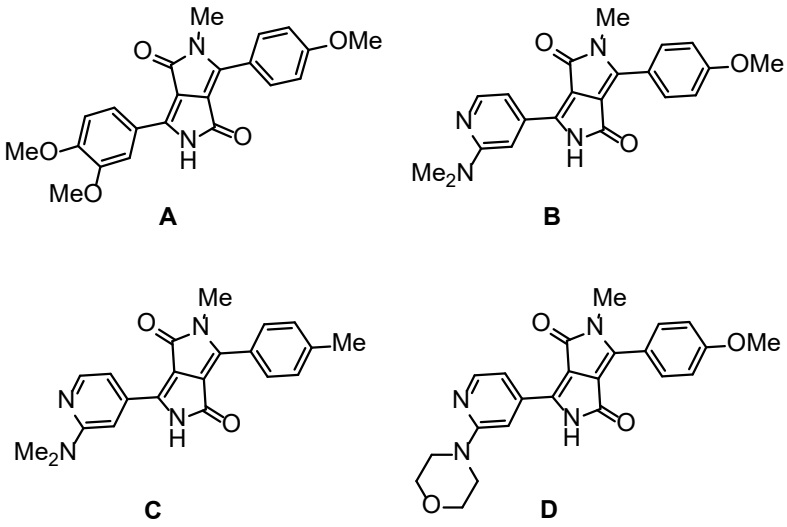

Fig S1. Structures used in computational studies.

Section S1: General Information

All chemicals are from commercial sources and were used as received, unless otherwise noted. All reported NMR spectra were recorded on Bruker 500 MHz and Varian 500 MHz spectrometers. Chemical shifts (δ; ppm) for ^{1}H and ^{13}C NMR spectra were determined with TMS or residual solvent signals as the internal reference. J values are given in Hz. Spectroscopic-grade solvents were used in all fluorescence/absorption-spectroscopy measurements. Mass spectra were obtained with EI ion source and the EBE double focusing geometry mass analyzer or spectrometer equipped with electro-spray ion source with Q-TOF type mass analyzer. The synthesis of compounds 2a, 2b, 2c [1] and 2g [2] have been described previously.

Section S2: Experimental Procedures

1,4,7,10,13-Pentaoxa-16-azacyclooctadecane, 16-(2-pyridine)-4-nitrile (2d)

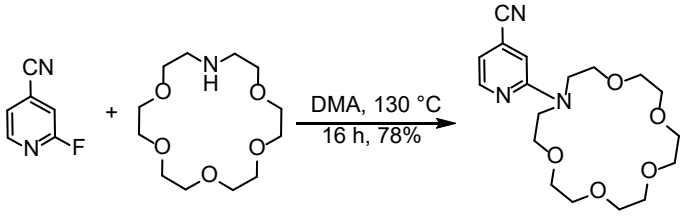

2d

A mixture commercially available 2-fluoro-4-cyanopyridine (500 mg, 4 mmol), 1-Aza-18-crown-6 (1.1 g, 4 mmol) in 5 ml of deoxygenated N,N-dimethylacetamide was heated (130 °C) under argon for overnight. Then reaction mixture was cooled to room temperature, diluted with water (100 mL) and extracted with EtOAc (2x100 mL). The organic phase dried over anhydrous Na_2SO_4 and filtered. The solvent was removed under reduced pressure and the resulting colorless oil was chromatographed on silica gel (hexane/EtOAc = 1: 1) to obtain 78 % yield, 1.17 g. ^{1}H NMR (500 MHz, $CDCl_3$) δ 8.15 (d, *J* = 2.4 Hz, 1H), 6.80 (s, 1H), 6.66 (d, *J* = 2.3 Hz, 1H), 3.79 (t, *J* = 8.0 Hz, 4H), 3.72 (t, *J* = 12.0 Hz, 4H), 3.66 (s, 16H). ^{13}C NMR (126 MHz, $CDCl_3$) δ 157.7, 148.9, 120.7, 117.6, 111.6, 108.3, 70.7, 70.6, 68.9, 49.5. HRMS (ESI, m/z): [M+H]+ Calcd. for $C_{18}H_{27}N_3O_5$: 366.4300; found, 388.4300[M+Na].

1,4,10,13-Tetraoxa-7,16-diazacyclooctadecane, 16-(2-pyridine)-4-nitrile (2e)

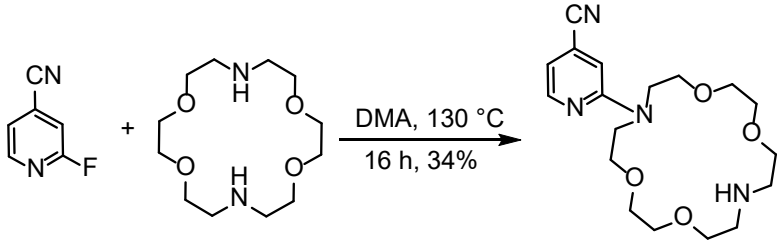

2e

A mixture commercially available 2-fluoro-4-cyanopyridine (500 mg, 4mmol), 1, 10-Diaza-18-crown-6 (1.08 g, 4mmol) in 5 ml of deoxygenated N,N-dimethylacetamide was heated (130 °C) under argon for overnight. Then reaction mixture was cooled to room temperature, diluted with water (100 mL) and extracted with EtOAc (2x100 mL). The organic phase dried over anhydrous Na_2SO_4 and filtered. The solvent was removed under reduced pressure and the resulting colorless oil was chromatographed on silica gel (hexane/EtOAc = 1: 1) to obtain 34 % yield, 500 mg. ^{1}H NMR (500 MHz, $CDCl_3$) δ 8.09 (d, *J* = 4.8 Hz, 1H), 6.61 (s, 1H), 6.57 (d, *J* = 4.8 Hz, 1H), 3.85 (m, 8H), 3.73 (t, *J* = 10.8 Hz, 4H), 3.67 (s, 8H), 3.18 (t, *J* = 8 Hz, 4H). ^{13}C NMR (126 MHz, $CDCl_3$) δ 157.4, 149.0, 120.7, 117.3, 111.8, 107.5, 69.9, 69.4, 68.8, 65.3, 48.6, 47.3 HRMS (ESI, m/z): [M+H]+ Calcd. for $C_{18}H_{28}N_4O_4$: 365.4460; found, 387.4360[M+Na].

1,4,7,10-Tetraoxa-13-azacyclopentadecane, 13-(2-pyridine)-4-nitrile (2f)

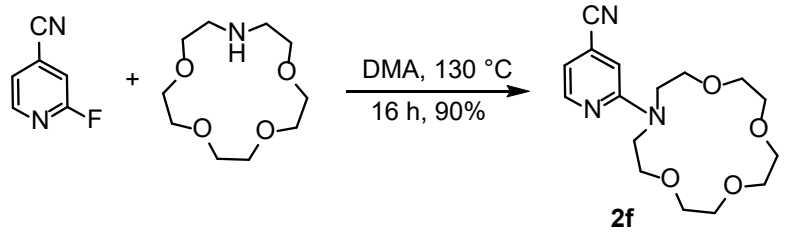

2f

A mixture commercially available 2-fluoro-4-cyanopyridine (500 mg, 4mmol), 1-Aza-15-crown-5 (900 mg, 4mmol) in 5 ml of deoxygenated N,N-dimethylacetamide was heated (130 °C) under argon for overnight. Then reaction mixture was cooled to room temperature, diluted with water (100 mL) and extracted with EtOAc (2x100 mL). The organic phase dried over anhydrous Na_2SO_4 and filtered. The solvent was removed under reduced pressure and the resulting colorless oil was chromatographed on silica gel (hexane/EtOAc = 1: 1) to obtain 90 % yield, 1.2 g. ^{1}H NMR (500 MHz, $CDCl_3$) δ 8.15 (d, *J* = 2.4 Hz, 1H), 6.84 (s, 1H), 6.66 (d, *J* = 2.3 Hz, 1H), 3.79 (t, *J* = 8.0 Hz, 4H), 3.72 (t, *J* = 12.0 Hz, 4H), 3.66 (s, 12H). ^{13}C NMR (126 MHz, $CDCl_3$) δ 157.7, 148.9, 120.7, 117.6, 111.6, 108.3, 70.1, 69.8, 51.2. HRMS (ESI, m/z): [M+H]+ Calcd. for $C_{16}H_{23}N_3O_4$: 322.3770; found, 344.3770[M+Na].

1,4,7-Trioxa-10-azacyclododecane, 10-(2-pyridine)-4-nitrile (2h)

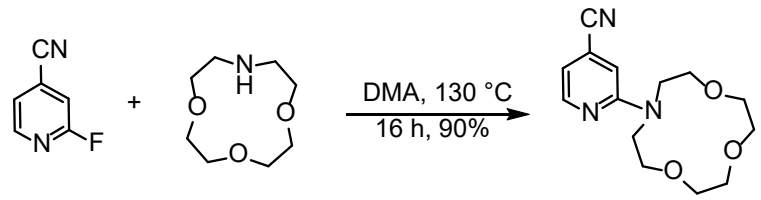

2h

A mixture commercially available 2-fluoro-4-cyanopyridine (500 mg, 4 mmol), 1-Aza-12-crown-4 (700 mg, 4 mmol) in 5 ml of deoxygenated N,N-dimethylacetamide was heated (130 °C) under argon for overnight. Then reaction mixture was cooled to room temperature, diluted with water (100 mL) and extracted with EtOAc (2x100 mL). The organic phase dried over anhydrous Na_2SO_4 and filtered. The solvent was removed under reduced pressure and the resulting colorless oil was chromatographed on silica gel (hexane/EtOAc = 1: 1) to obtain 90 % yield, 1.17 g. ^{1}H NMR (600 MHz, $CDCl_3$) δ 8.19 (dd, *J* = 5.8 Hz, 1H), 6.94 (s, 1H), 6.66 (dd, *J* = 6.1 Hz, 1H), 3.89 (t, *J* = 9.9 Hz, 4H), 3.70 (t, *J* = 9.80 Hz, 4H), 3.66 (m, 8H). ^{13}C NMR (126 MHz, $CDCl_3$) δ 158.5, 148.6, 120.7, 117.8, 111.9, 109.6, 71.3, 69.7, 69.5, 51.2. HRMS (ESI, m/z): [M+H]+ Calcd. for $C_{14}H_{19}N_3O_3$: 277.3240; found, 278.1540[M+H].

Section S3: Absorption and emission spectra

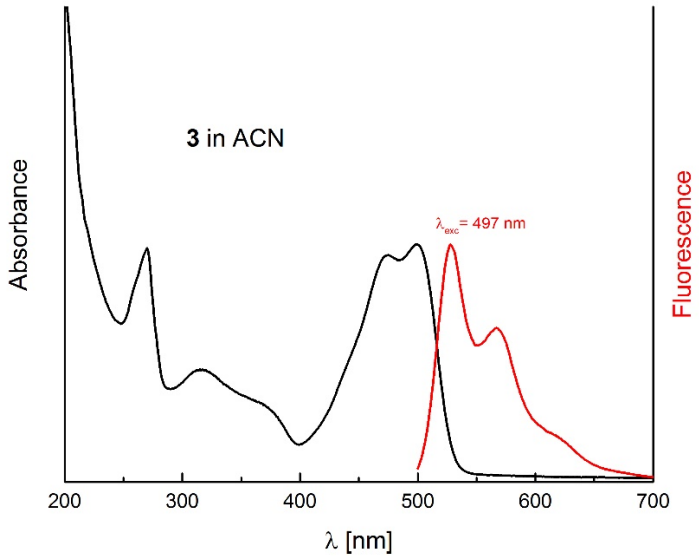

Fig. S2. The absorption and emission spectra of DPP **3** in acetonitrile.

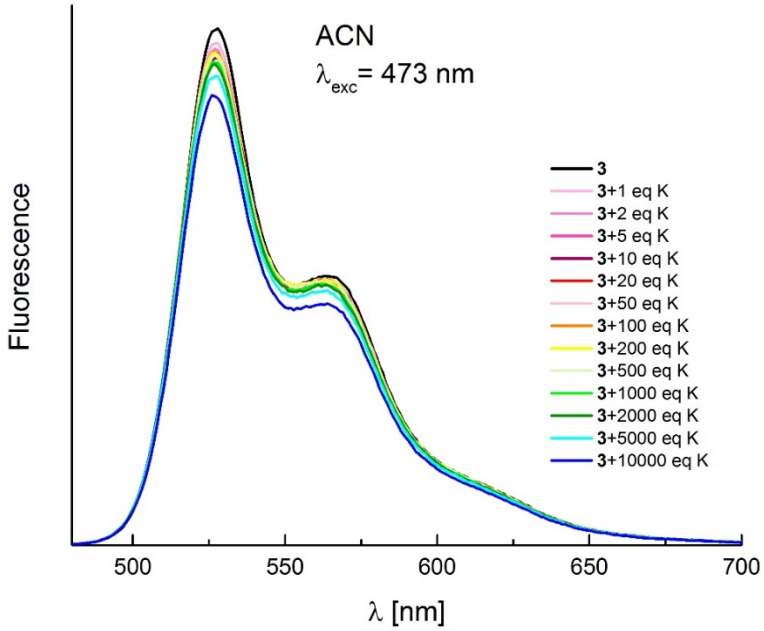

Fig. S3. The effect of KBF_4 addition on the emission spectra of DPP **3** measured in ACN.

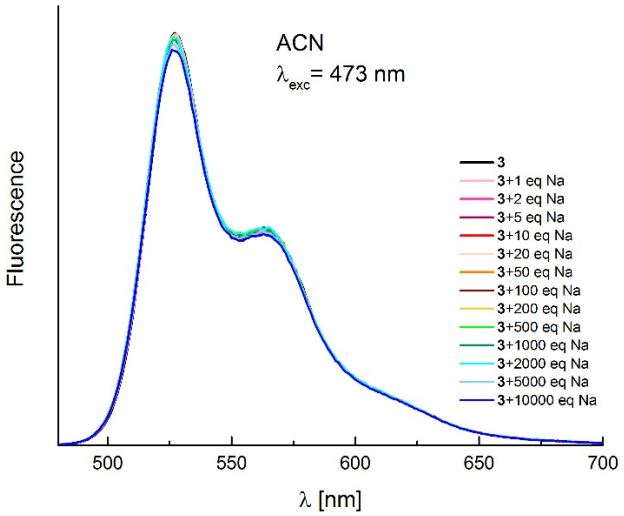

Fig. S4. The effect of $NaClO_4$ addition on the emission spectra of DPP **3** measured in ACN.

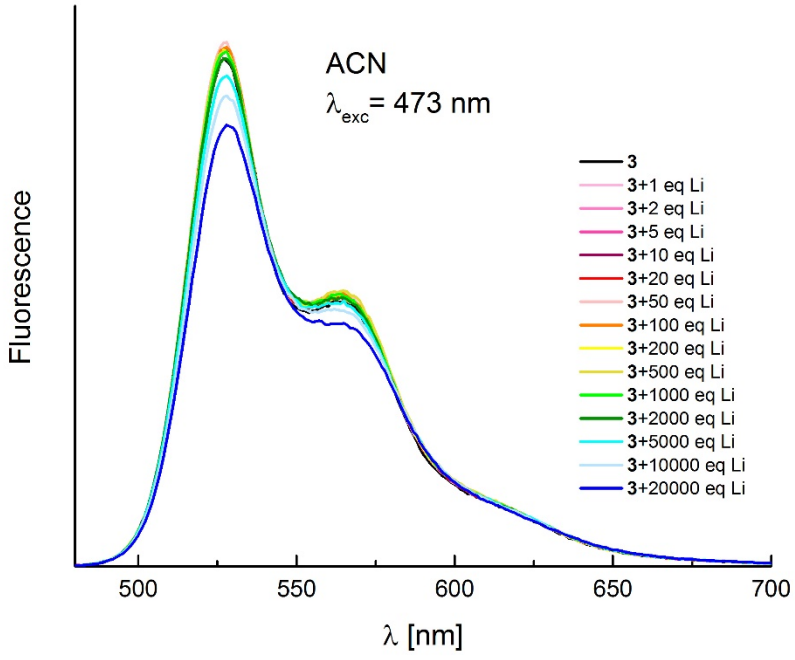

Fig. S5. The effect of $LiClO_4$ addition on the emission spectra of DPP **3** measured in ACN.

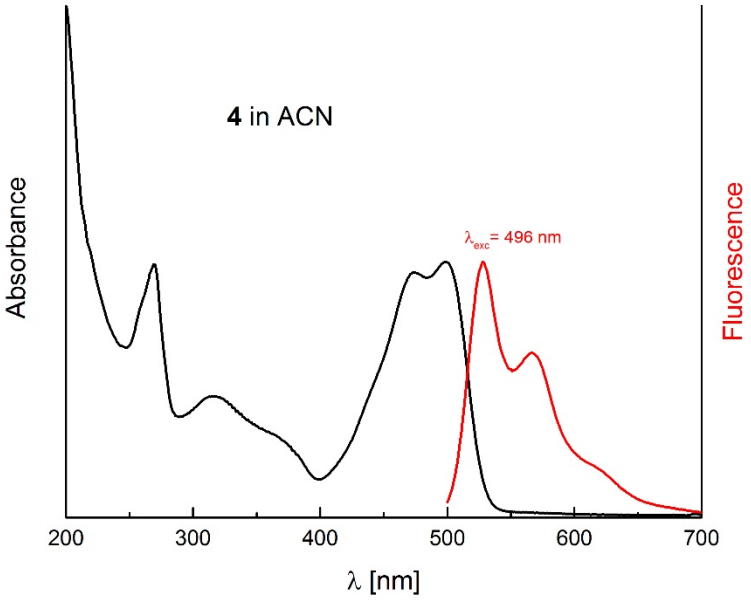

Fig. S6. The absorption and emission spectra of DPP **4** in acetonitrile.

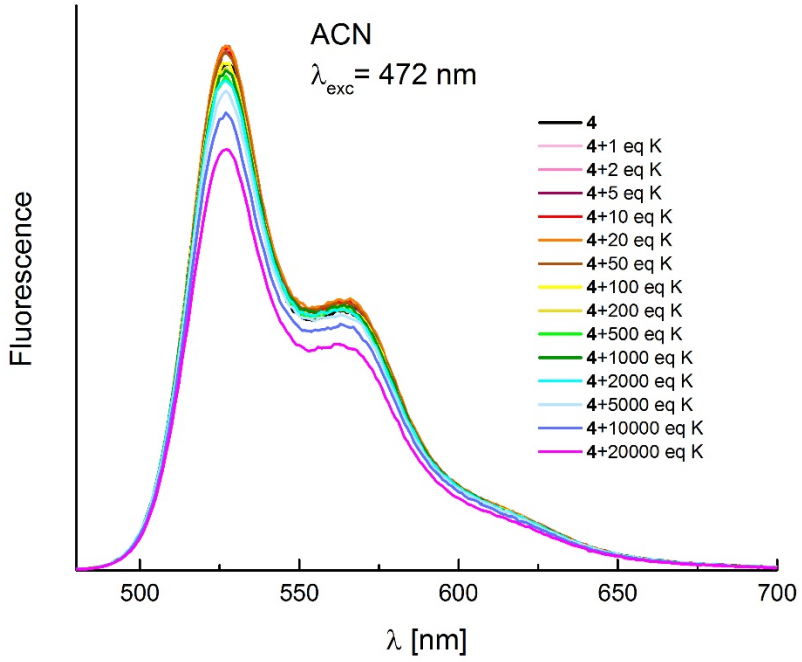

Fig. S7. The effect of KBF_4 addition on the emission spectra of DPP **4** measured in ACN.

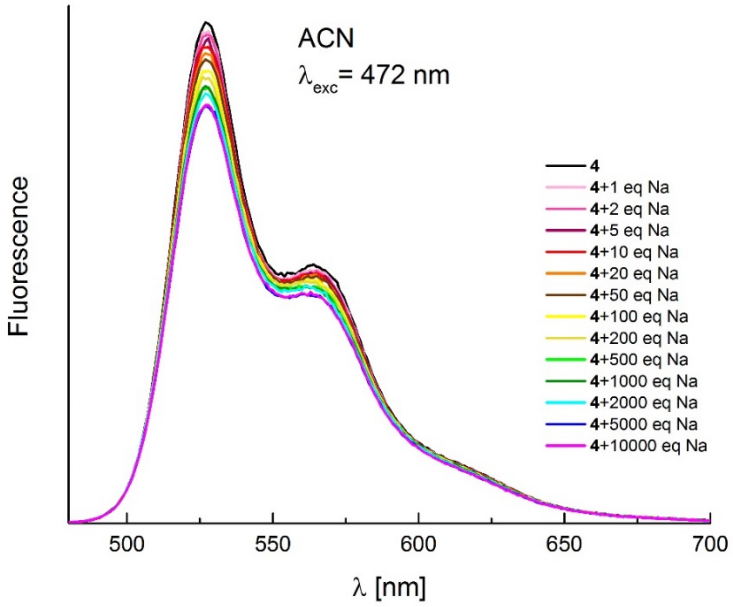

Fig. S8. The effect of $NaClO_4$ addition on the emission spectra of DPP **4** measured in ACN.

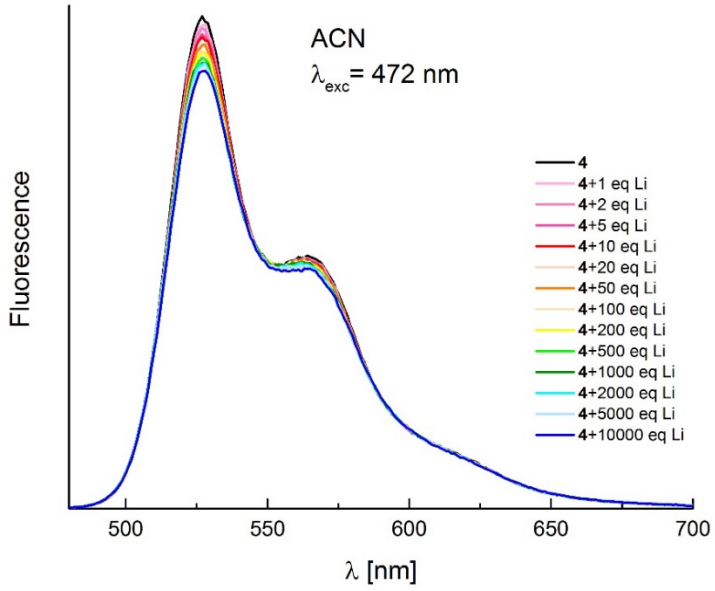

Fig. S9. The effect of $LiClO_4$ addition on the emission spectra of DPP **4** measured in ACN.

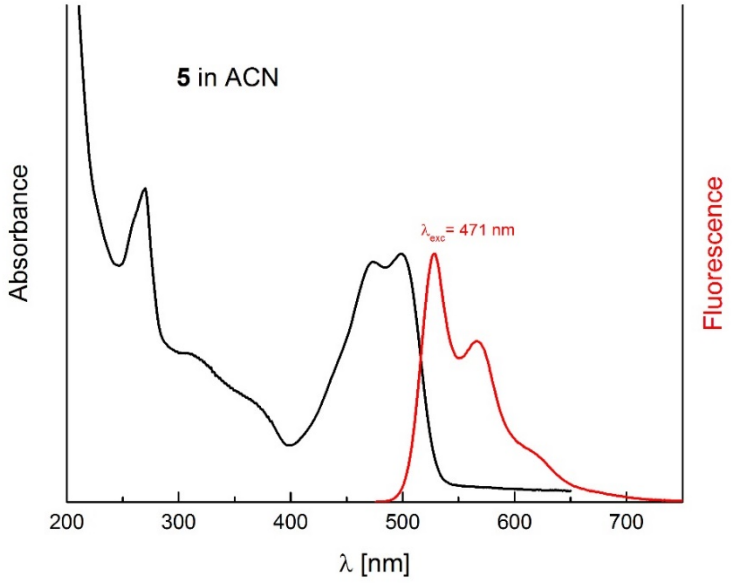

Fig. S10. The absorption and emission spectra of DPP **5** in acetonitrile.

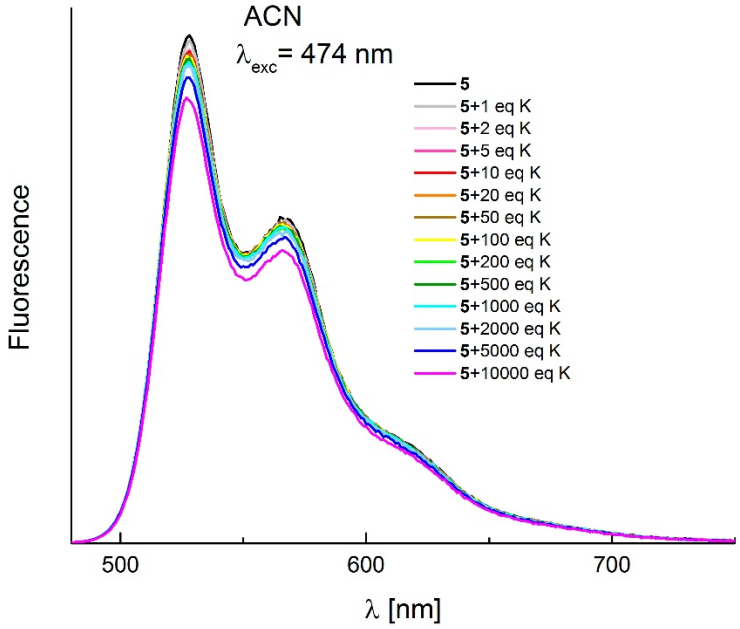

Fig. S11. The effect of KBF_4 addition on the emission spectra of DPP **5** measured in ACN.

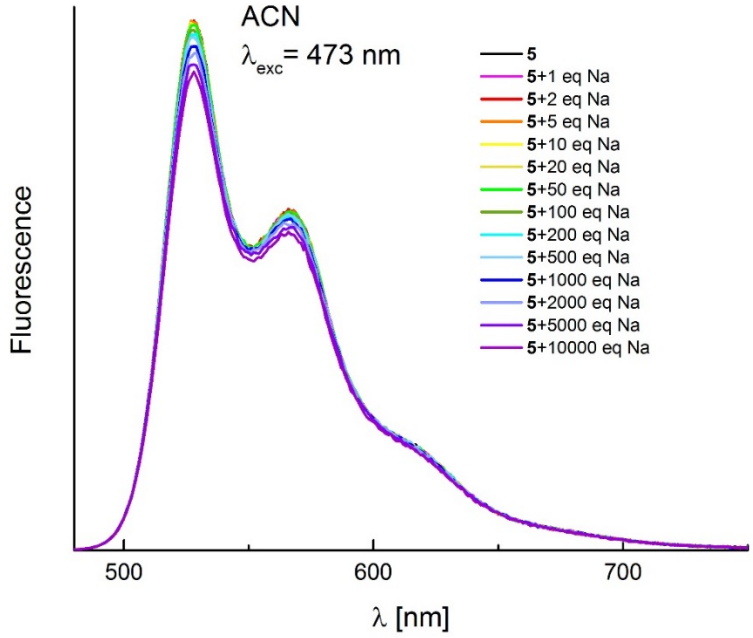

Fig. S12. The effect of $NaClO_4$ addition on the emission spectra of DPP **5** measured in ACN.

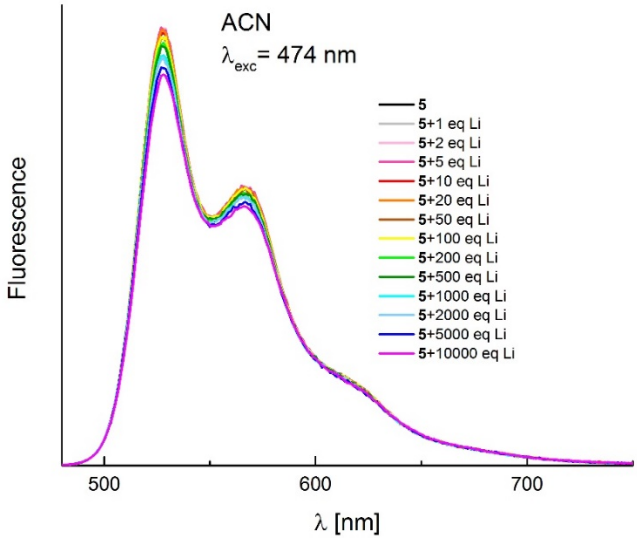

Fig. S13. The effect of $LiClO_4$ addition on the emission spectra of DPP **5** measured in ACN.

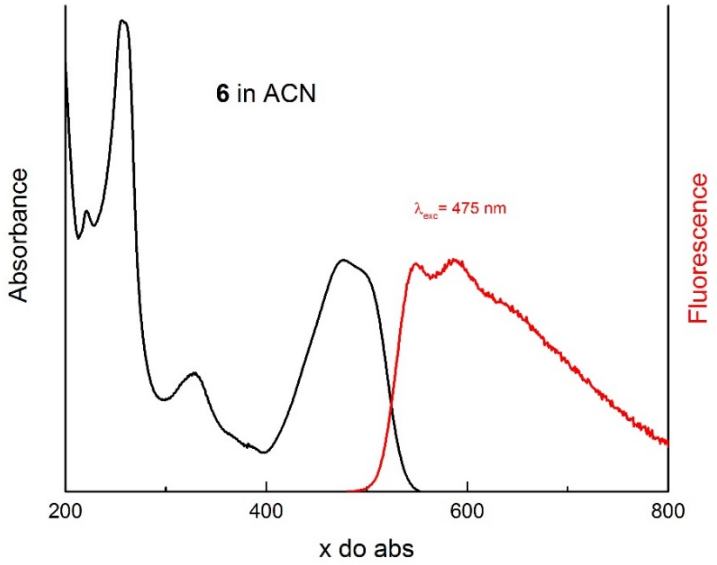

Fig. S14. The absorption and emission spectra of DPP **6** in acetonitrile.

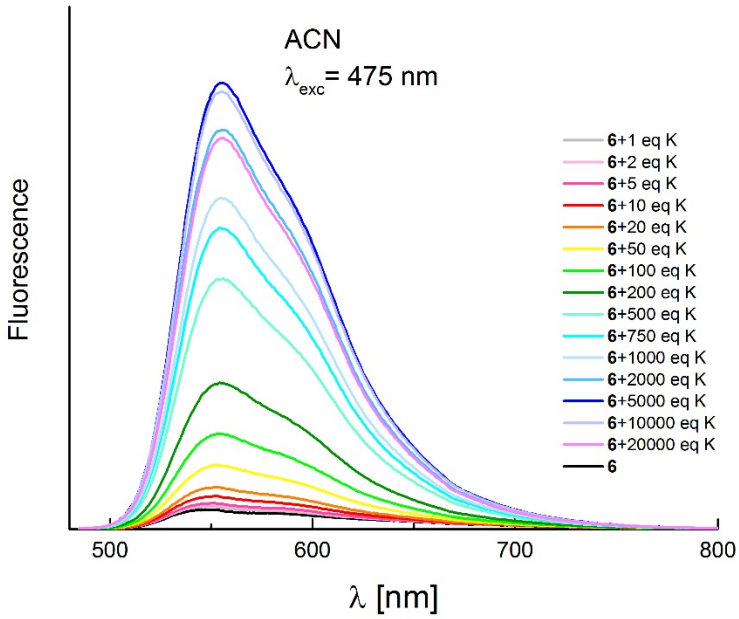

Fig. S15. The effect of KBF_4 addition on the emission spectra of DPP **6** measured in ACN.

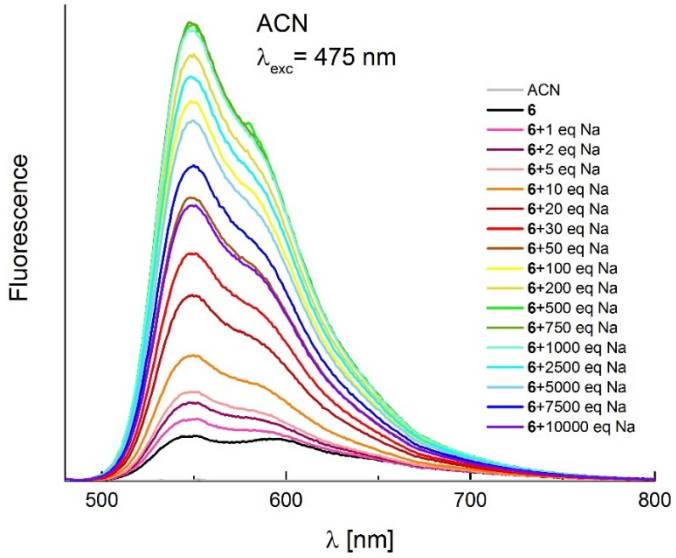

Fig. S16. The effect of $NaClO_4$ addition on the emission spectra of DPP **6** measured in ACN.

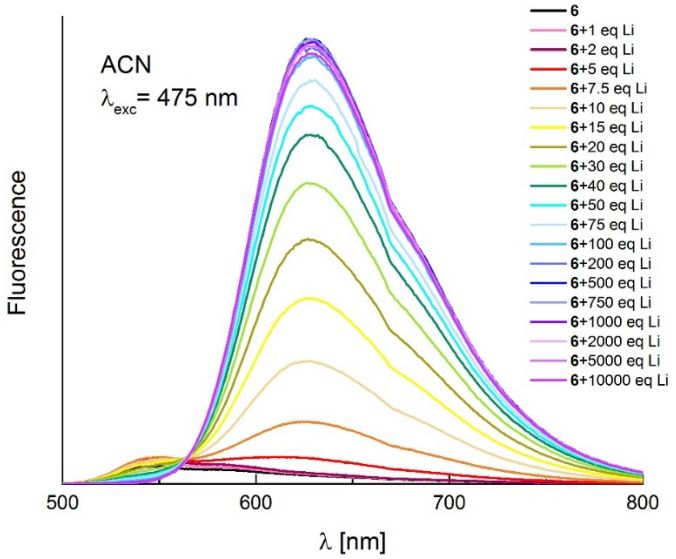

Fig. S17. The effect of $LiClO_4$ addition on the emission spectra of DPP **6** measured in ACN.

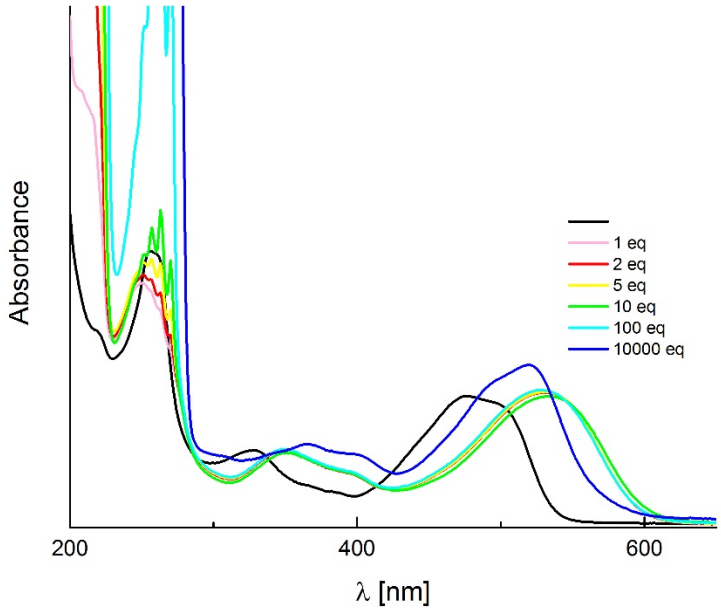

Fig. S18. The effect of $PhSO_3H$ addition on the absorption spectra of DPP **6** measured in ACN.

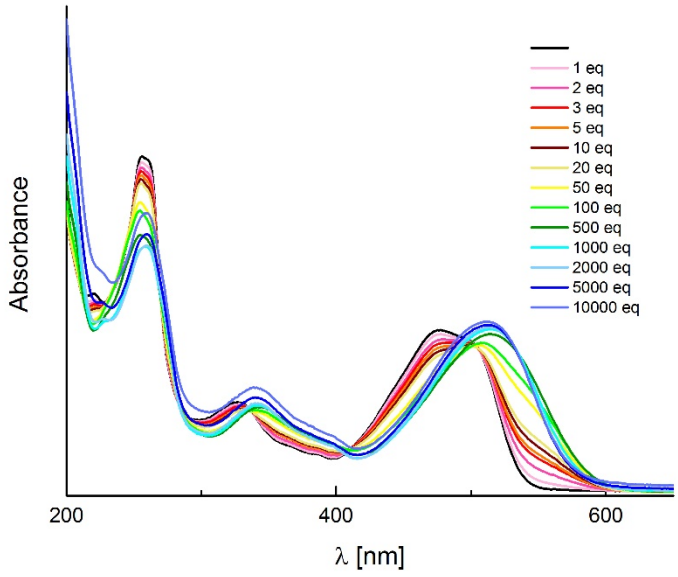

Fig. S19. The effect of $Mg(ClO_4)_2$ addition on the absorption spectra of DPP **6** measured in ACN.

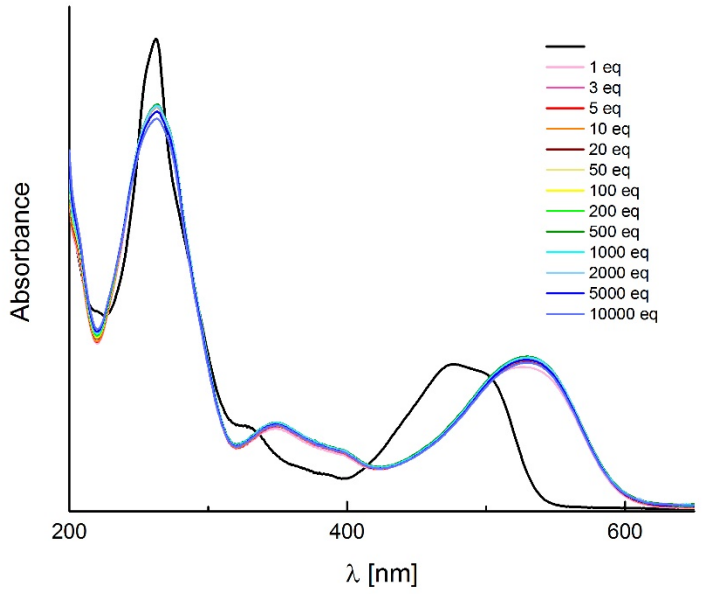

Fig. S20. The effect of $Zn(ClO_4)_2$ addition on the absorption spectra of DPP **6** measured in ACN.

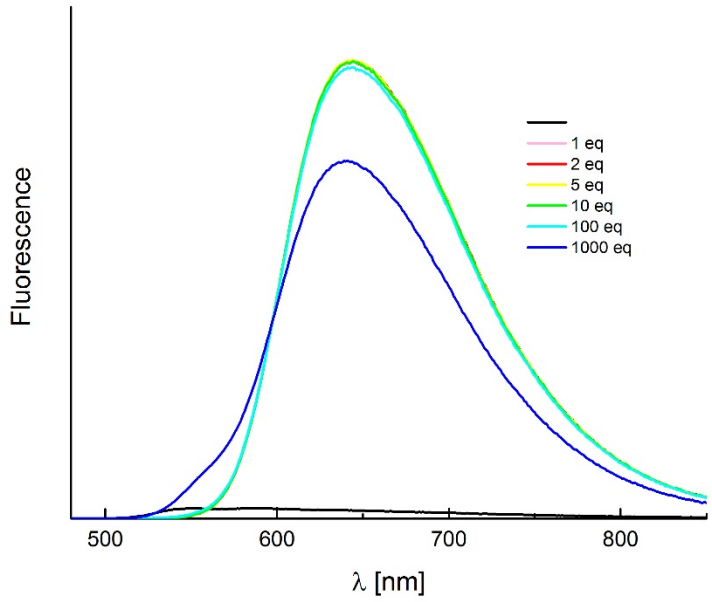

Fig. S21. The effect of $PhSO_3H$ addition on the emission spectra of DPP **6** measured in ACN.

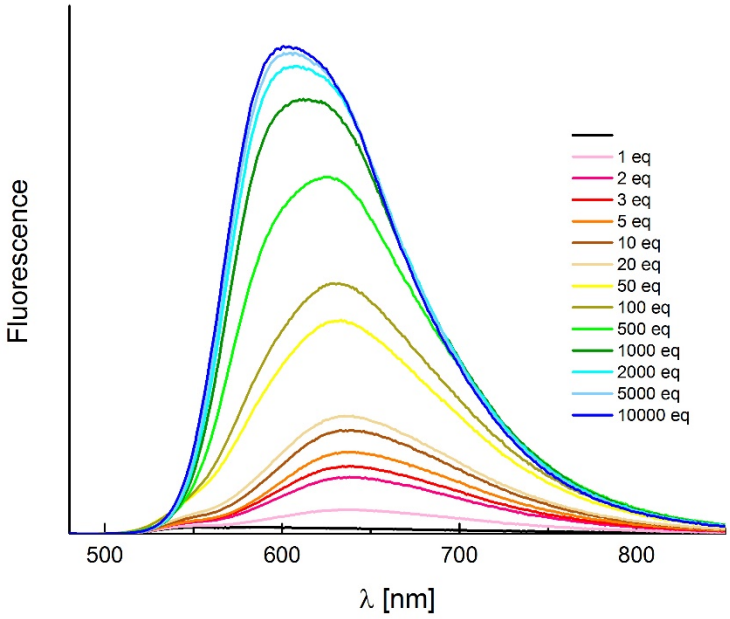

Fig. S22. The effect of $Mg(ClO_4)_2$ addition on the emission spectra of DPP **6** measured in ACN.

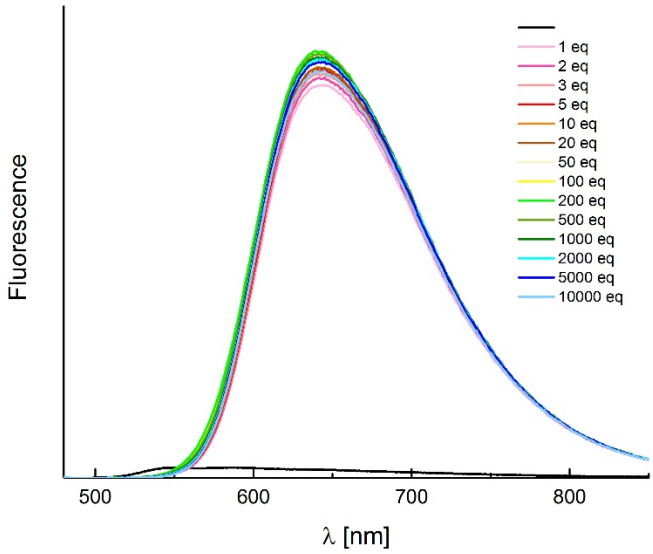

Fig. S23. The effect of $Zn(ClO_4)_2$ addition on the emission spectra of DPP **6** measured in ACN.

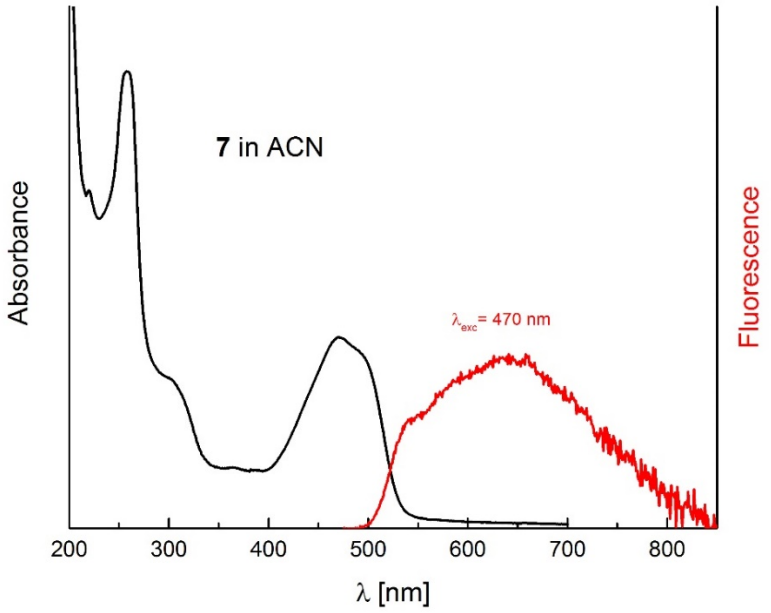

Fig. S24. The absorption and emission spectra of DPP **7** in acetonitrile.

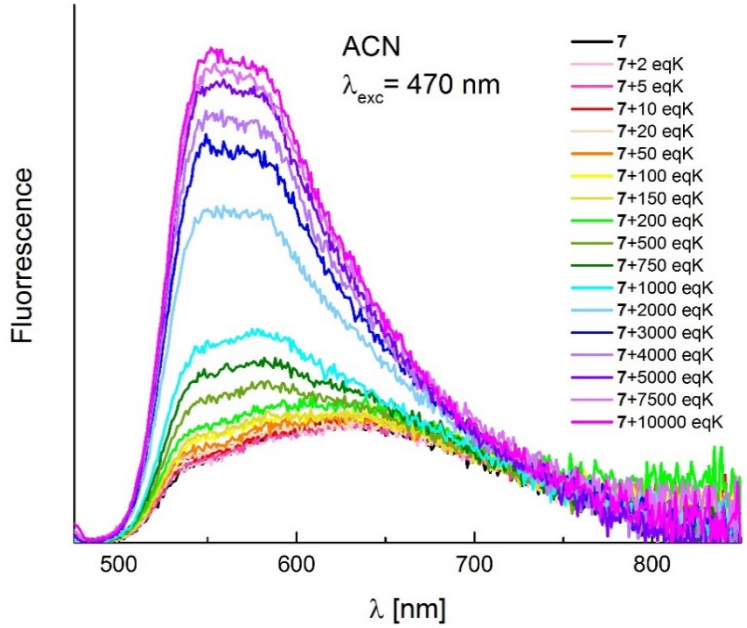

Fig. S25. The effect of KBF_4 addition on the emission spectra of DPP **7** measured in ACN.

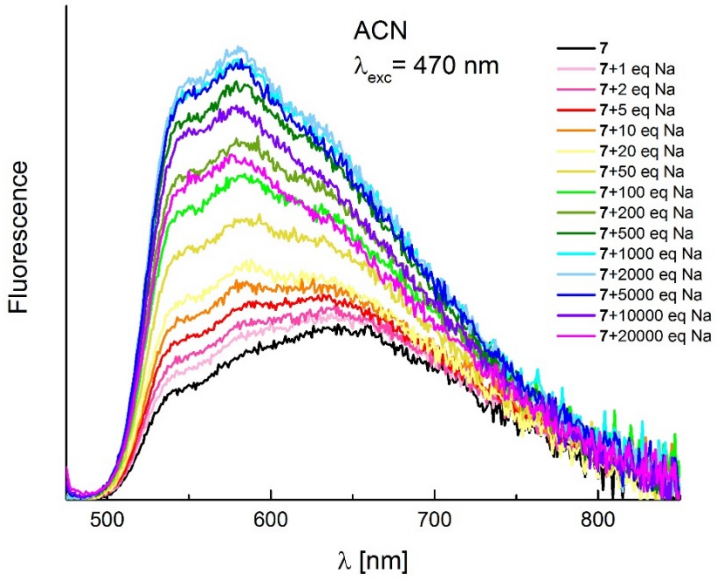

Fig. S26. The effect of $NaClO_4$ addition on the emission spectra of DPP **7** measured in ACN.

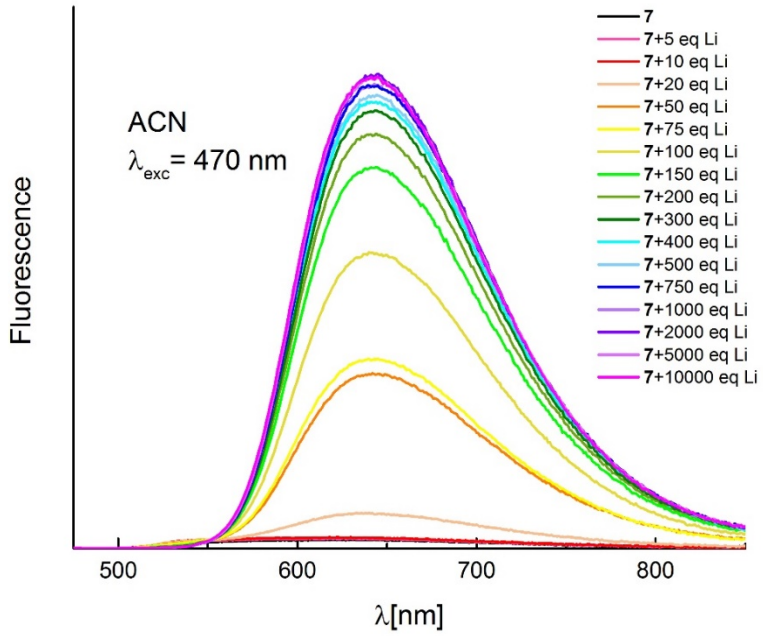

Fig. S27. The effect of $LiClO_4$ addition on the emission spectra of DPP **7** measured in ACN.

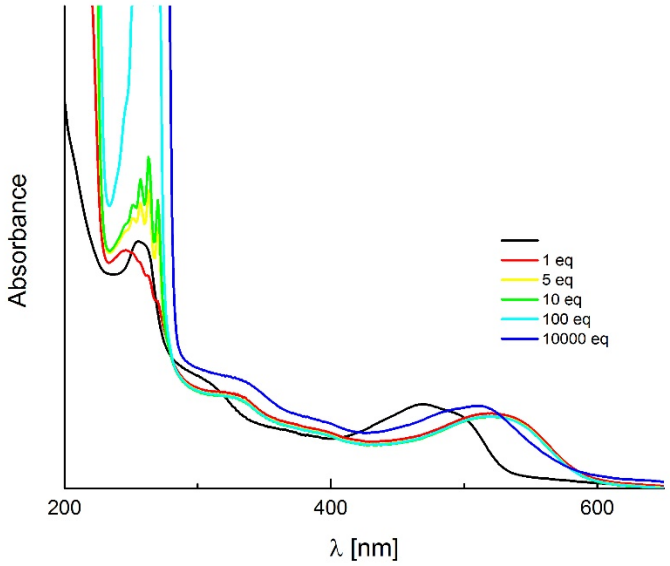

Fig. S28. The effect of $PhSO_3H$ addition on the absorption spectra of DPP **7** measured in ACN.

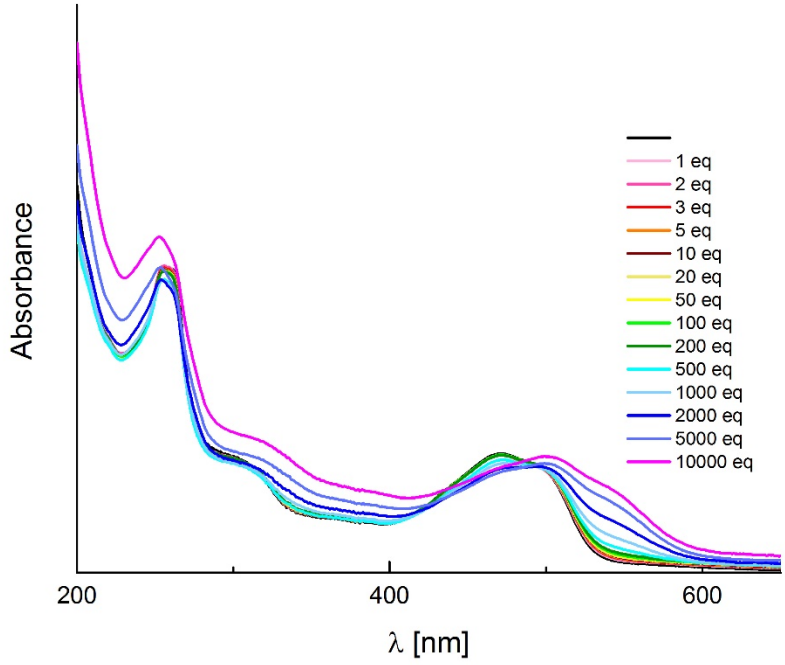

Fig. S29. The effect of $Mg(ClO_4)_2$ addition on the absorption spectra of DPP **7** measured in ACN.

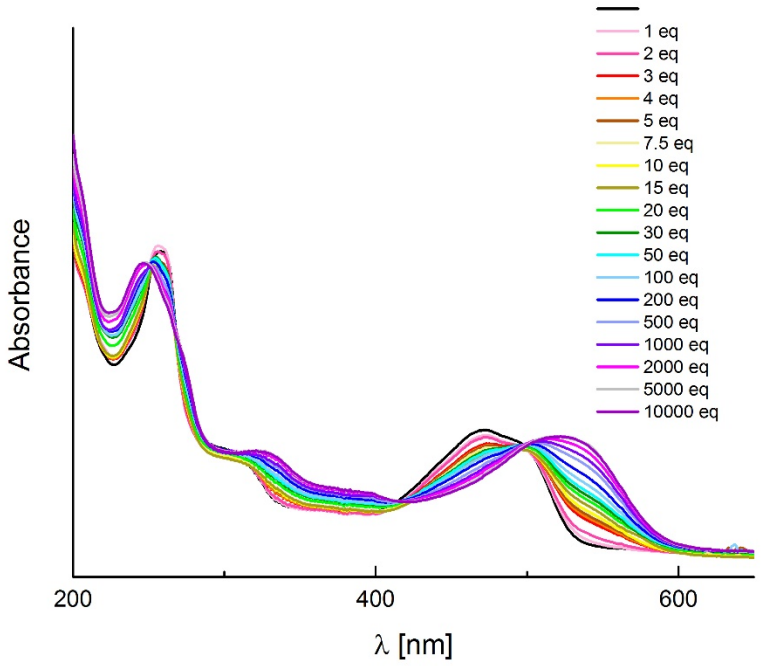

Fig. S30. The effect of $Zn(ClO_4)_2$ addition on the absorption spectra of DPP **7** measured in ACN.

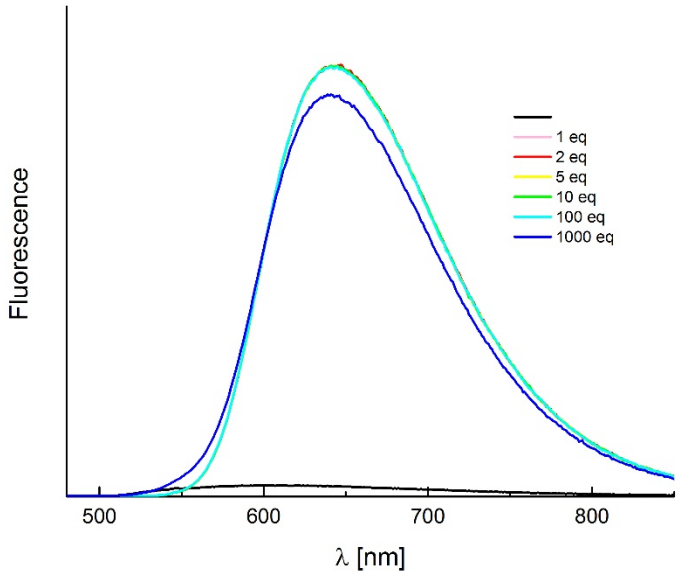

Fig. S31. The effect of $PhSO_3H$ addition on the emission spectra of DPP **7** measured in ACN.

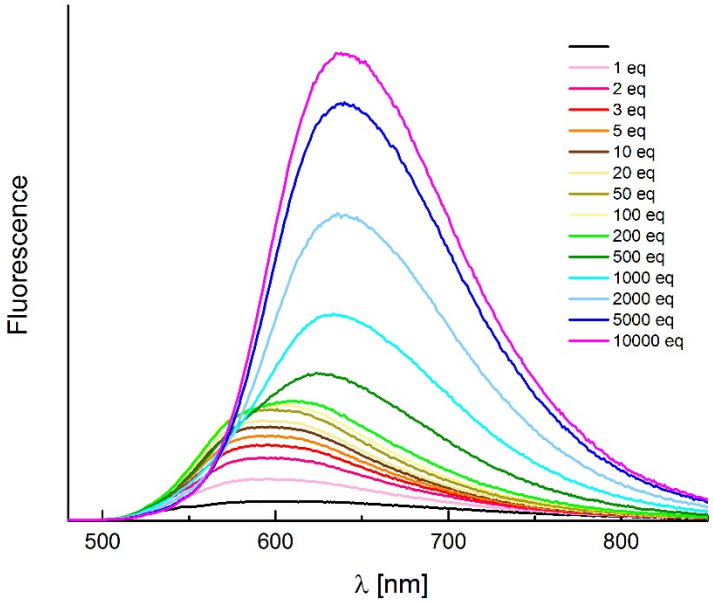

Fig. S32. The effect of $Mg(ClO_4)_2$ addition on the emission spectra of DPP **7** measured in ACN.

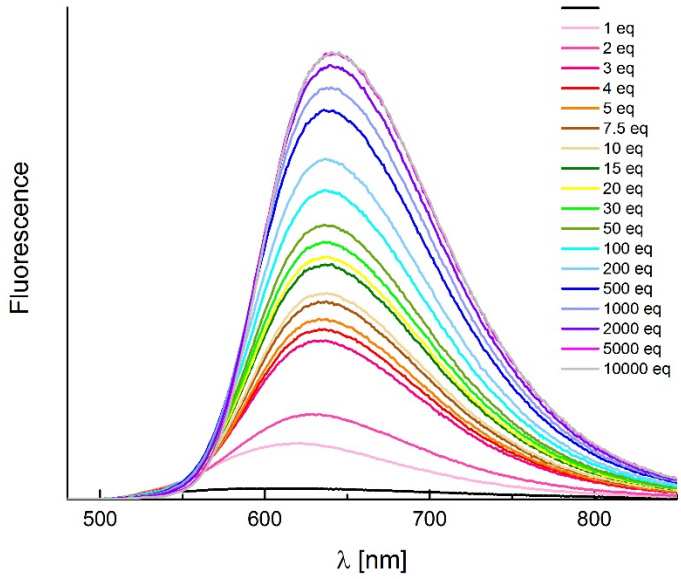

Fig. S33. The effect of $Zn(ClO_4)_2$ addition on the emission spectra of DPP **7** measured in ACN.

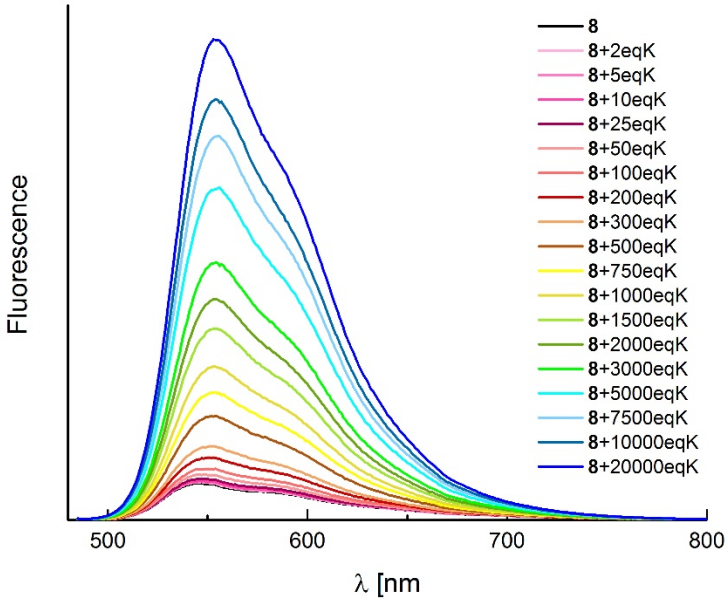

Fig. S34. The effect of KBF_4 addition on the emission spectra of DPP **8** measured in ACN.

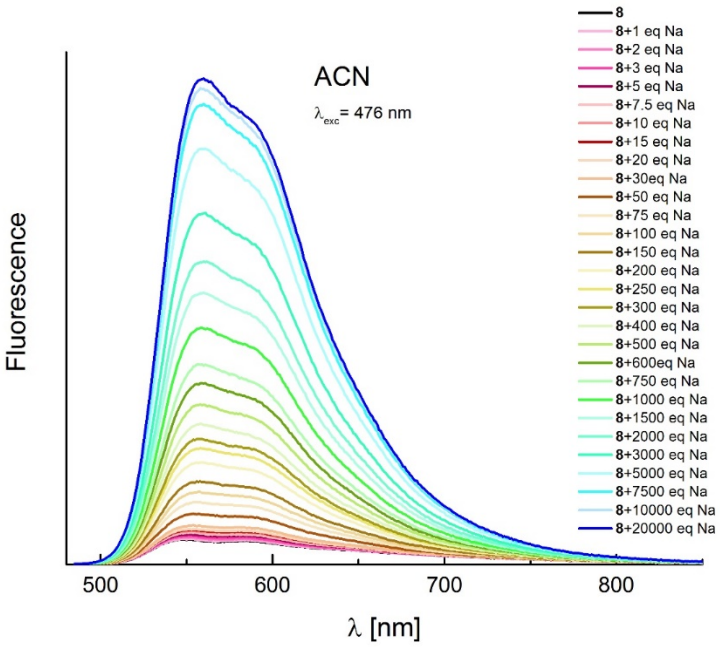

Fig. S35. The effect of $NaClO_4$ addition on the emission spectra of DPP **8** measured in ACN.

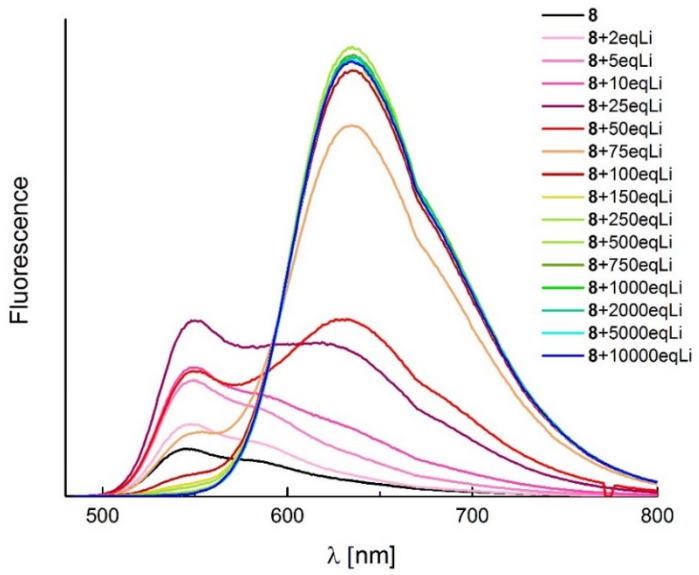

Fig. S36. The effect of $LiClO_4$ addition on the emission spectra of DPP **8** measured in ACN.

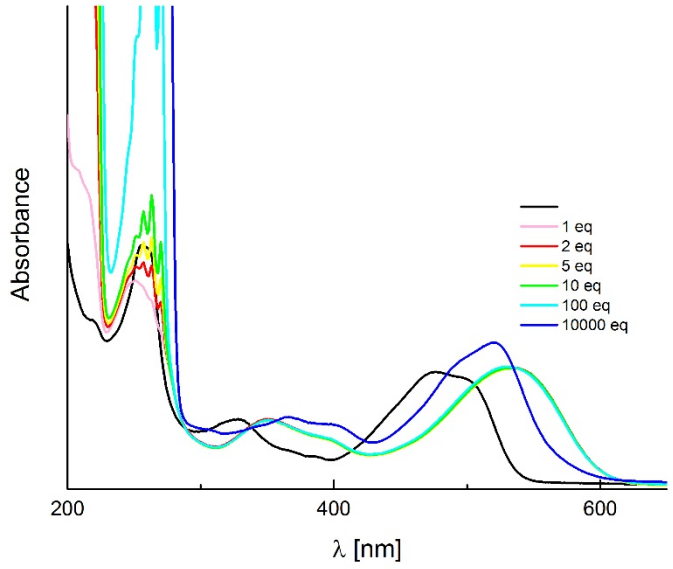

Fig. S37. The effect of $PhSO_3H$ addition on the absorption spectra of DPP **8** measured in ACN.

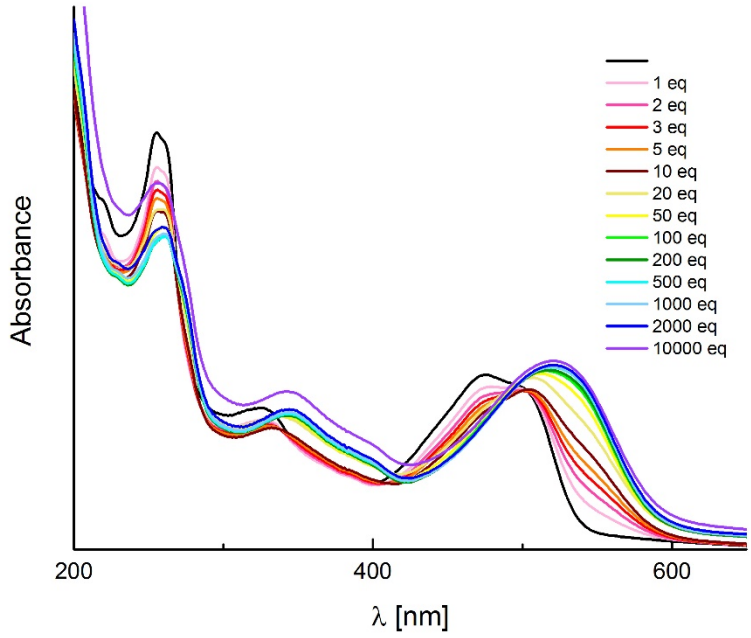

Fig. S38. The effect of $Mg(ClO_4)_2$ addition on the absorption spectra of DPP **8** measured in ACN.

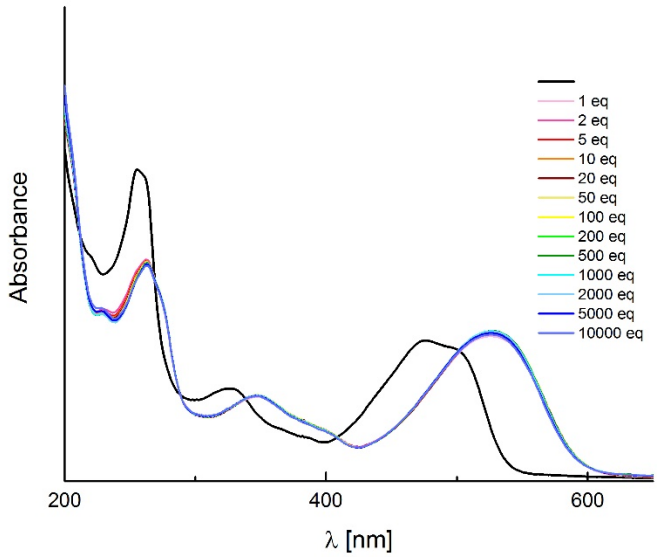

Fig. S39. The effect of $Zn(ClO_4)_2$ addition on the absorption spectra of DPP **8** measured in ACN.

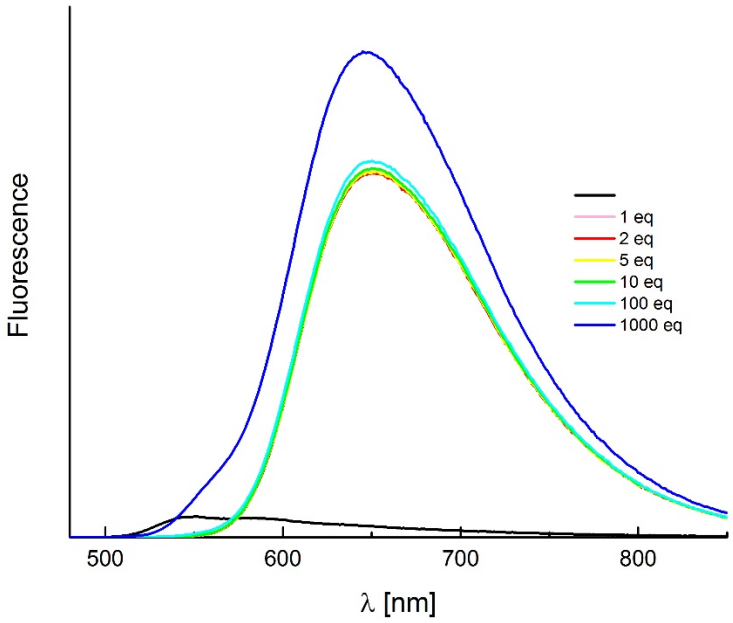

Fig. S40. The effect of $PhSO_3H$ addition on the emission spectra of DPP **8** measured in ACN.

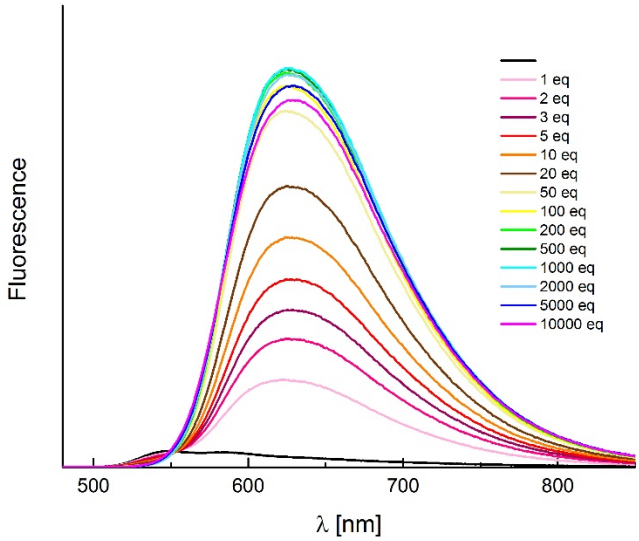

Fig. S42. The effect of $Mg(ClO_4)_2$ addition on the emission spectra of DPP **8** measured in ACN.

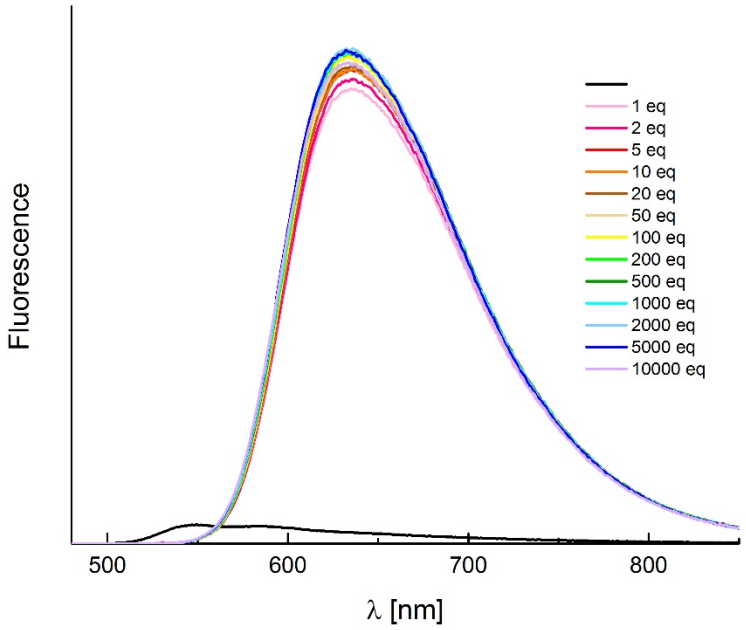

Fig. S43. The effect of $Zn(ClO_4)_2$ addition on the emission spectra of DPP **8** measured in ACN.

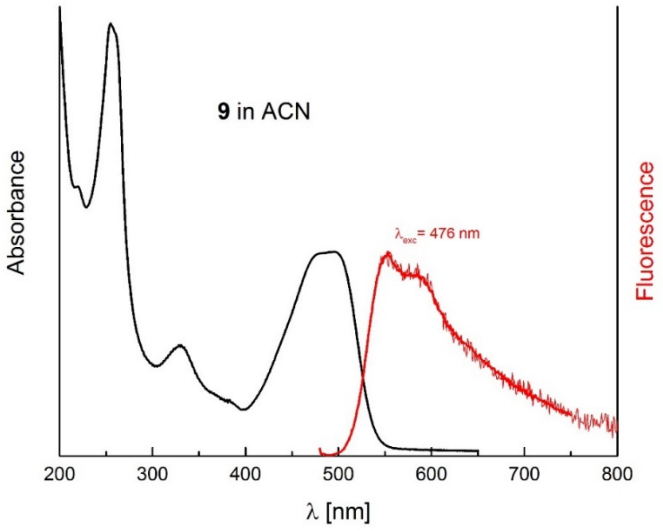

Fig. S44. The absorption and emission spectra of DPP **9** in acetonitrile.

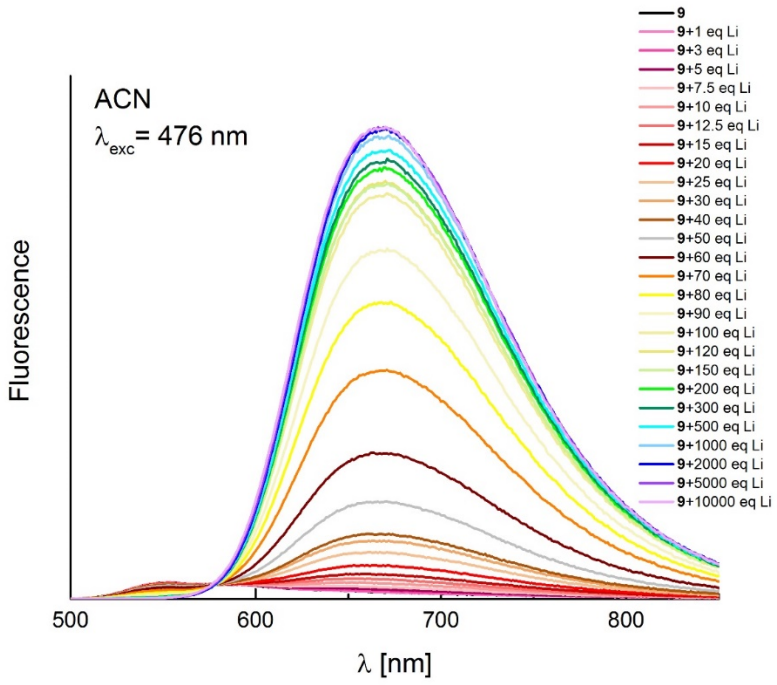

Fig. S45. The effect of $LiClO_4$ addition on the emission spectra of DPP **9** measured in ACN.

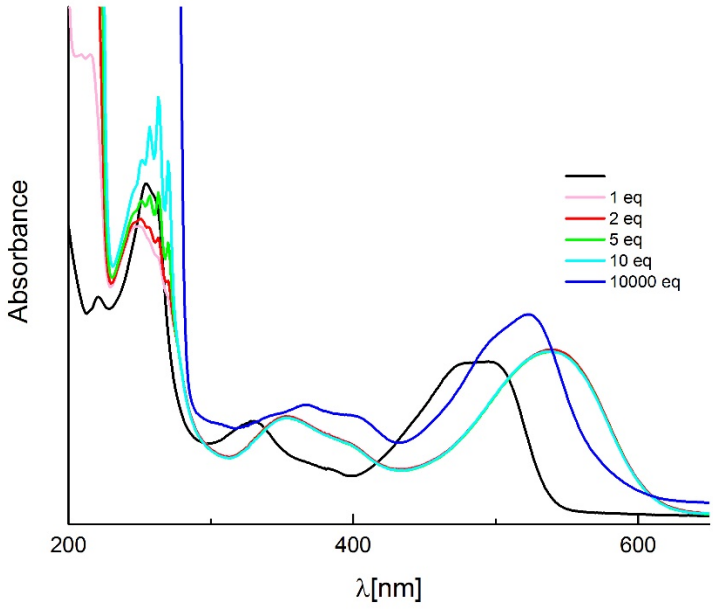

Fig. S46. The effect of $PhSO_3H$ addition on the absorption spectra of DPP **9** measured in ACN.

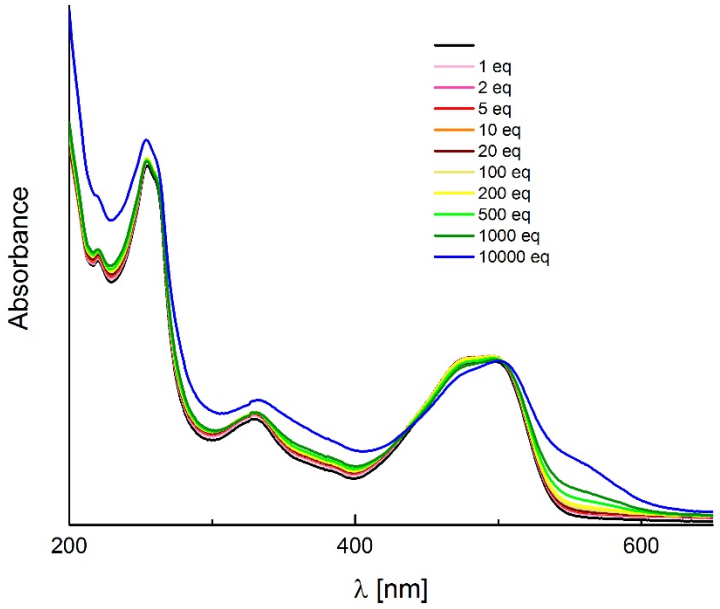

Fig. S47. The effect of $Mg(ClO_4)_2$ addition on the absorption spectra of DPP **9** measured in ACN.

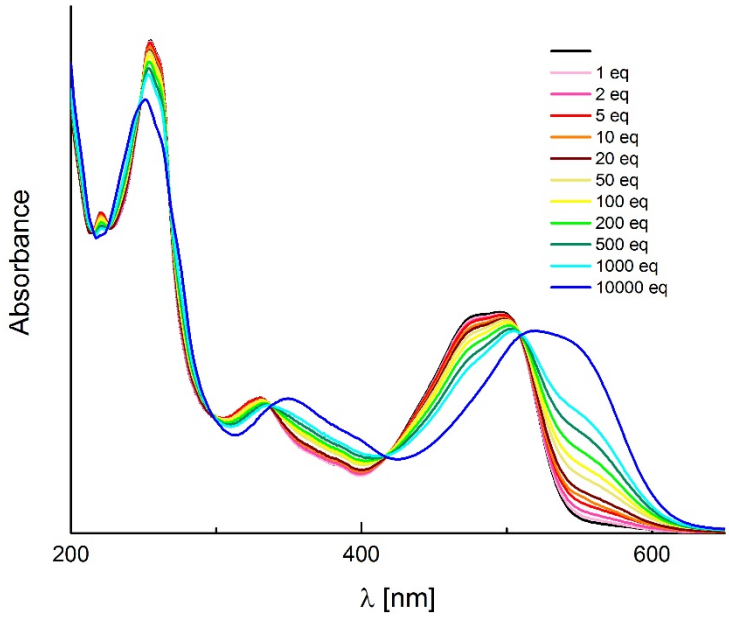

Fig. S48. The effect of $Zn(ClO_4)_2$ addition on the absorption spectra of DPP **9** measured in ACN.

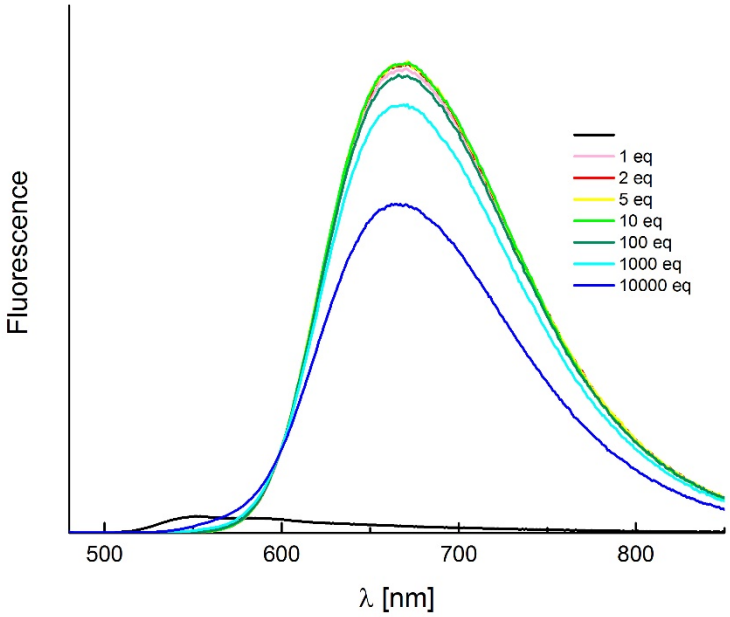

Fig. S49. The effect of $PhSO_3H$ addition on the emission spectra of DPP **9** measured in ACN.

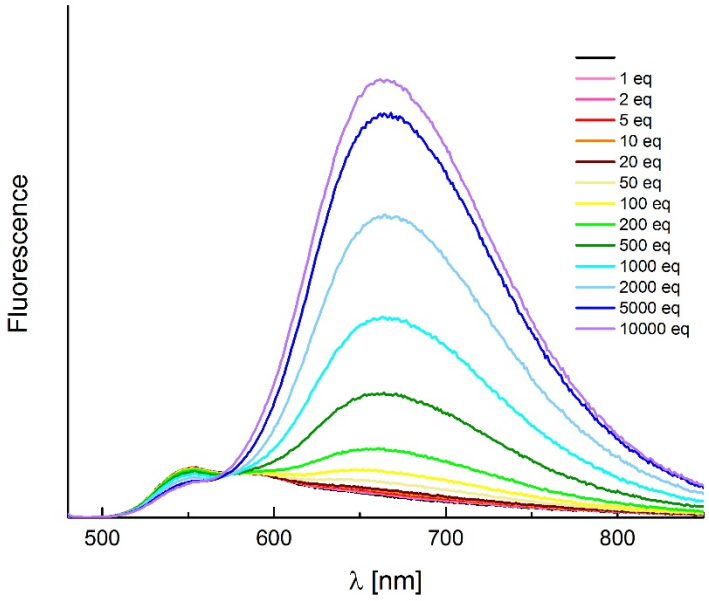

Fig. S50. The effect of $Mg(ClO_4)_2$ addition on the emission spectra of DPP **9** measured in ACN.

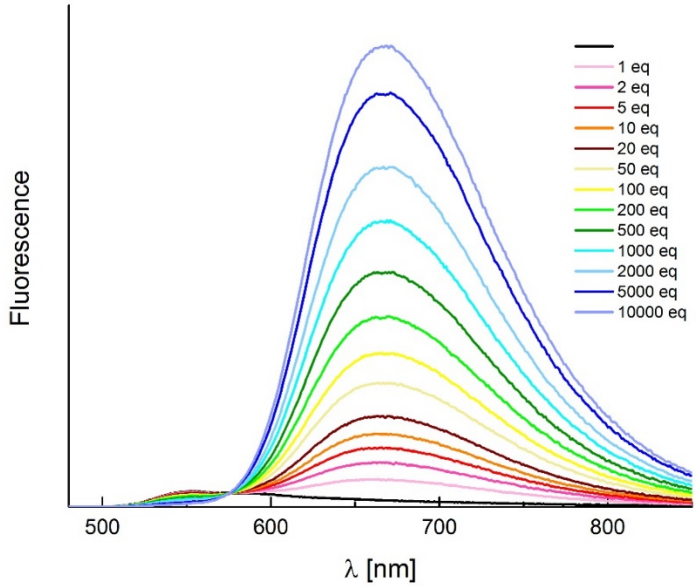

Fig. S51. The effect of $Zn(ClO_4)_2$ addition on the emission spectra of DPP **9** measured in ACN.

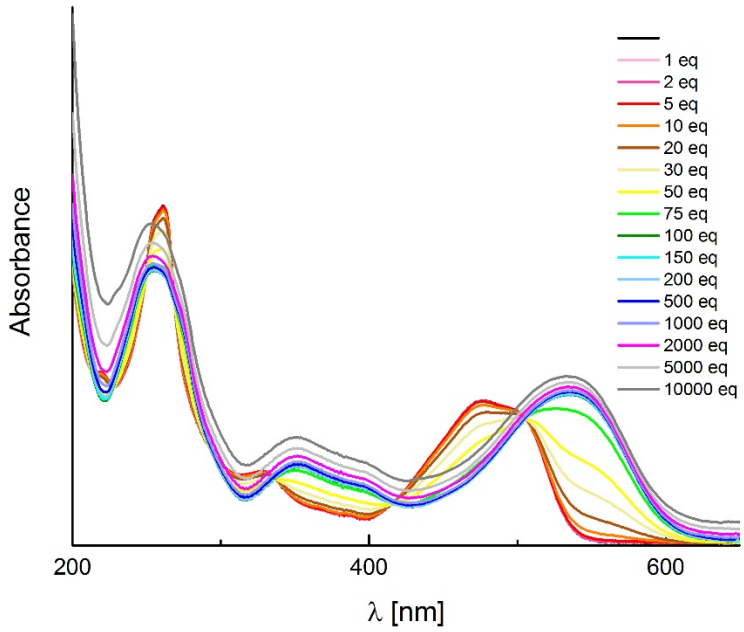

Fig. S52. The effect of $LiClO_4$ addition on the emission spectra of DPP **10** measured in ACN.

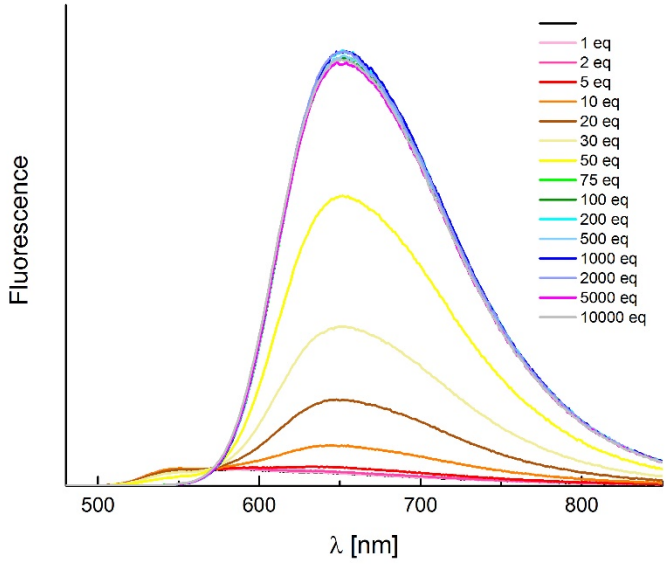

Fig. S53. The effect of $LiClO_4$ addition on the emission spectra of DPP **10** measured in ACN.

Section S4: ^{1}H NMR and ^{13}C NMR Spectra

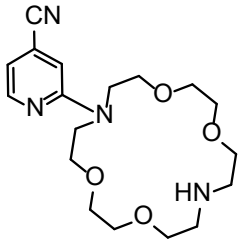

2e

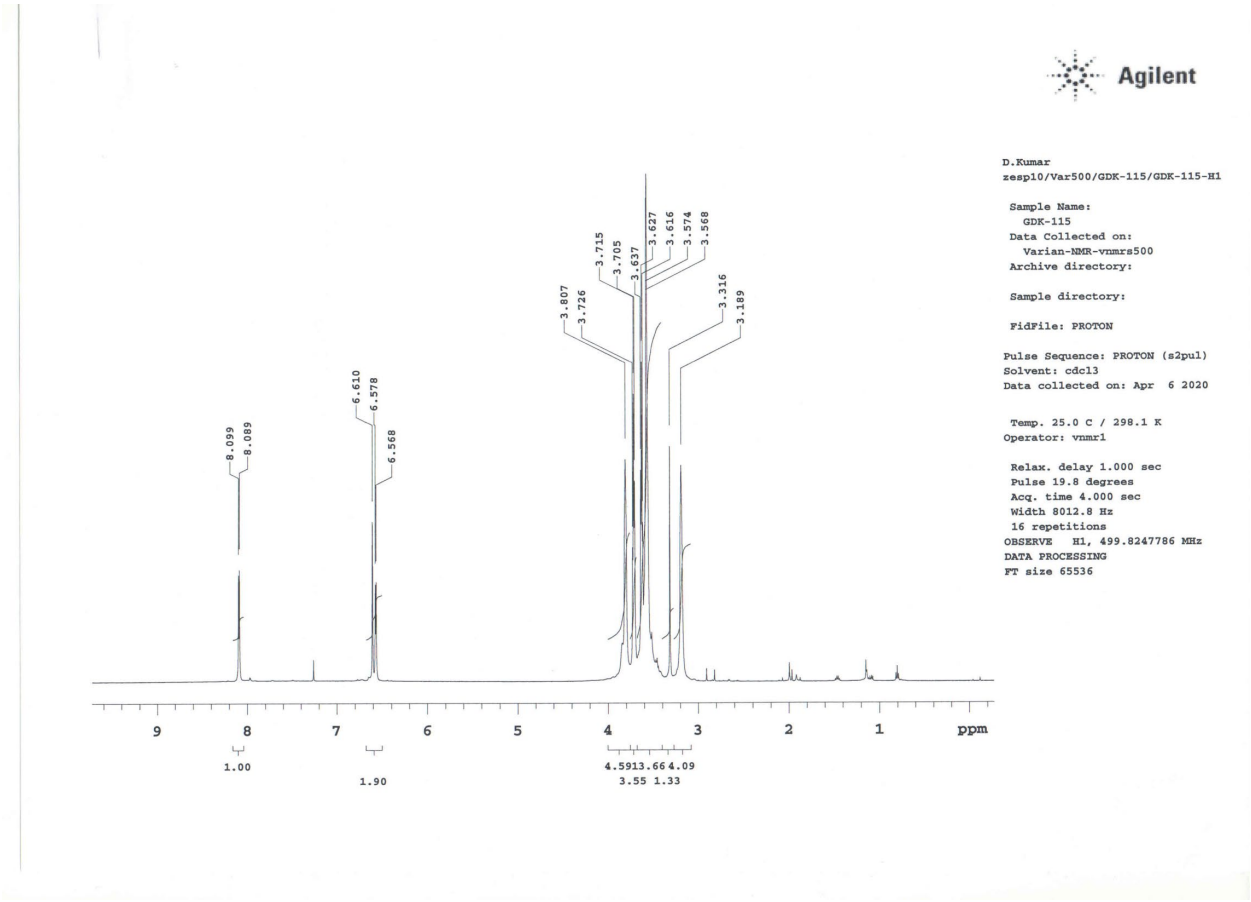

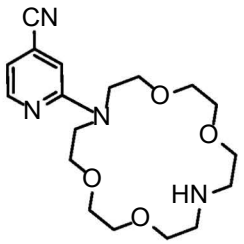

2e

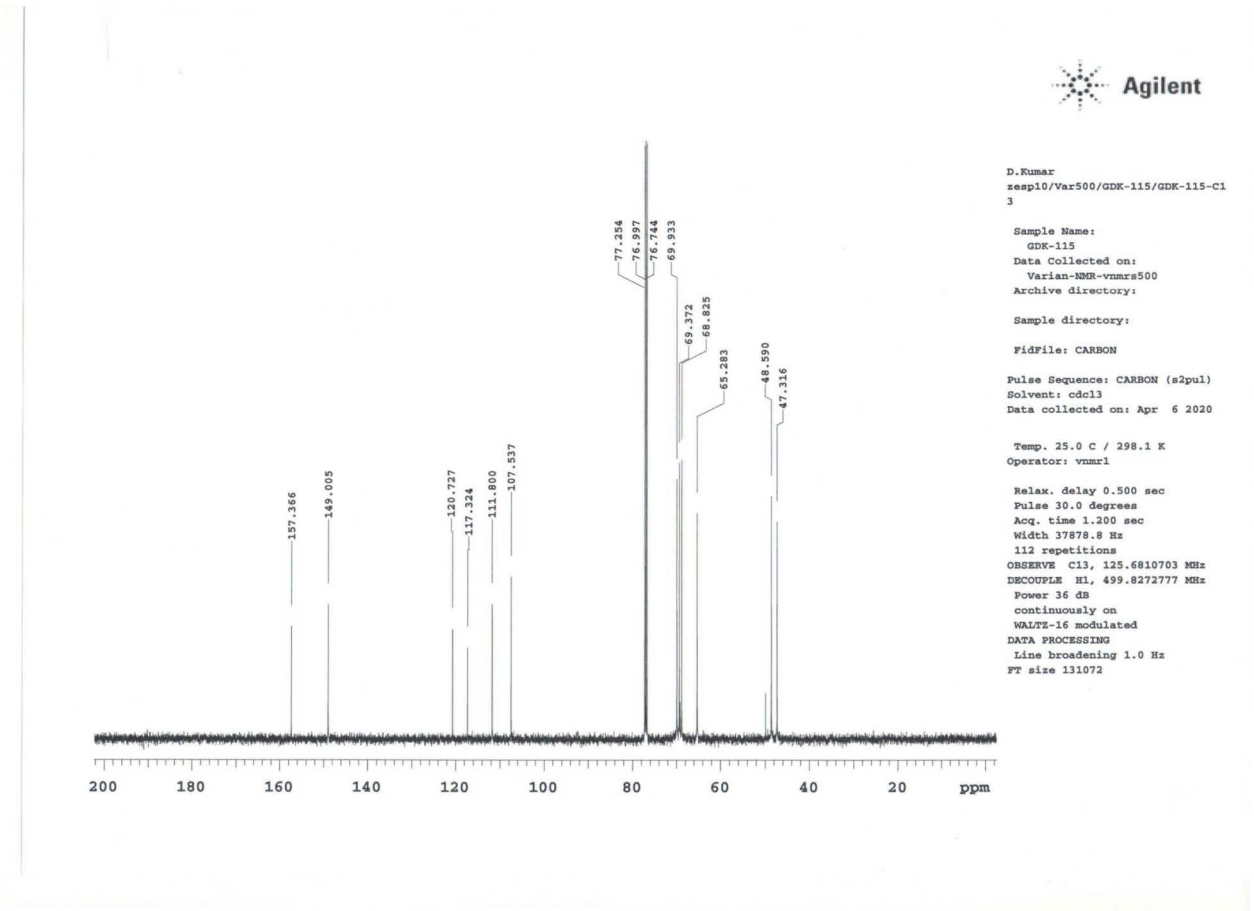

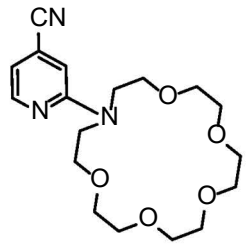

2d

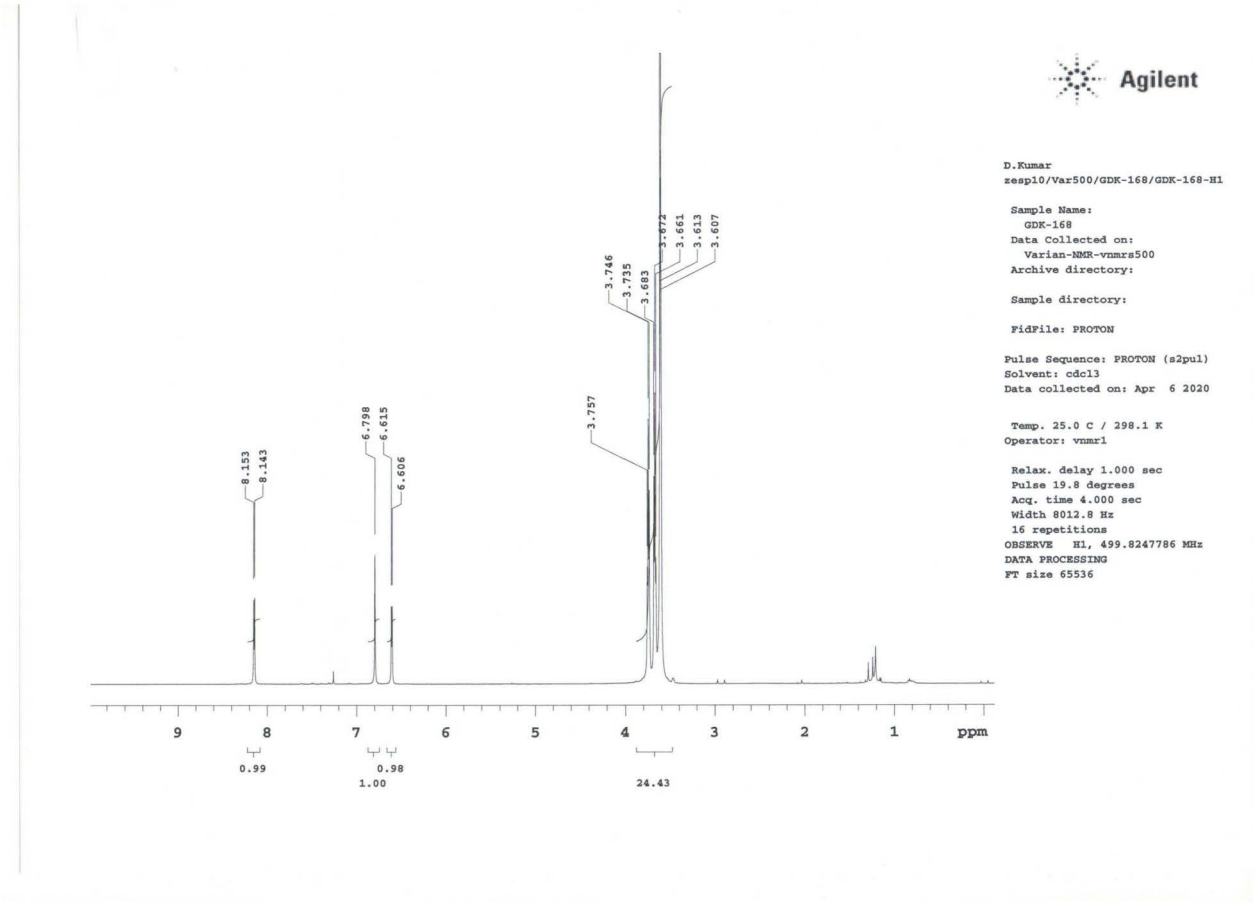

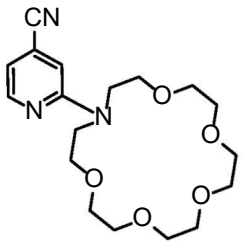

2d

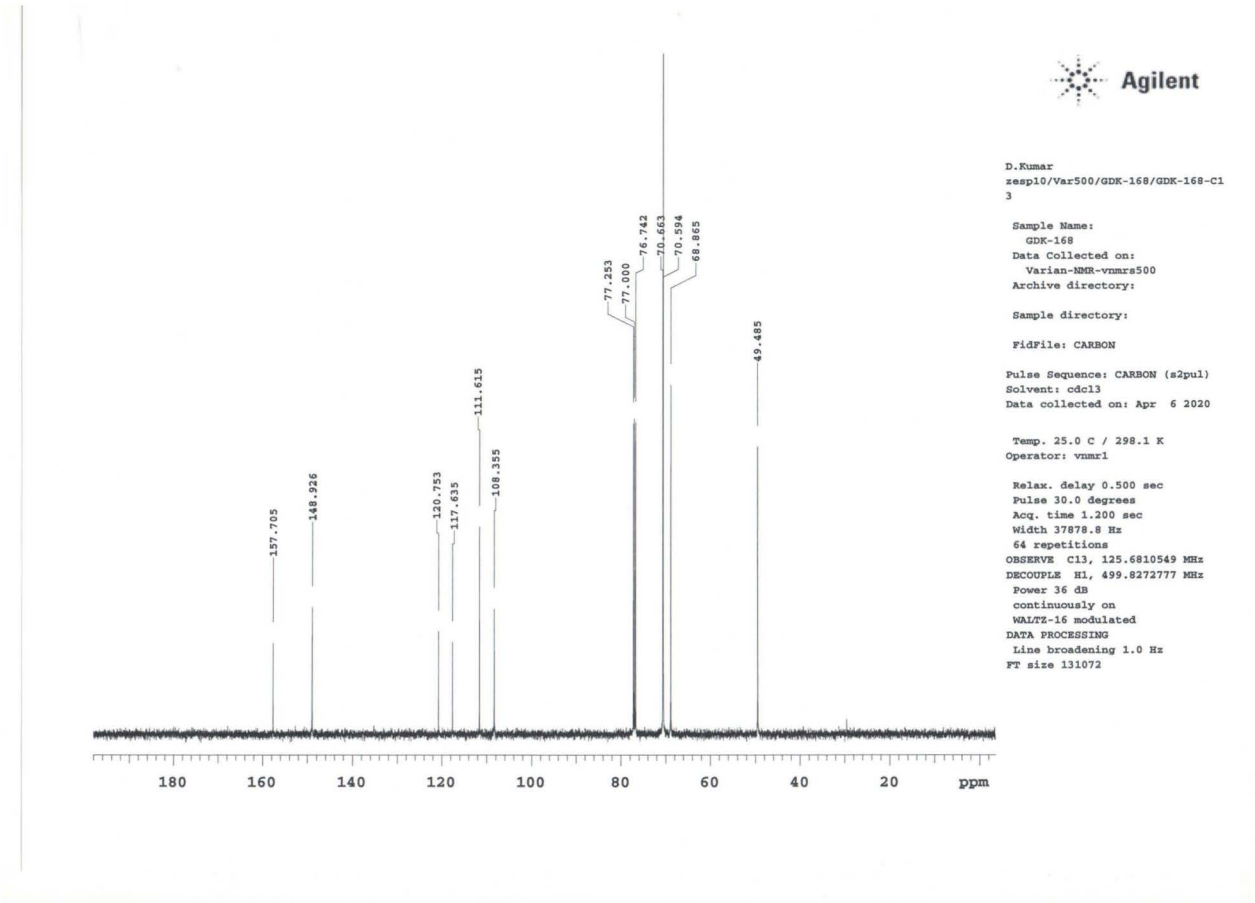

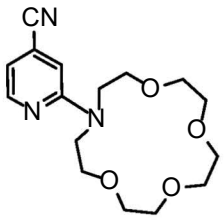

2f

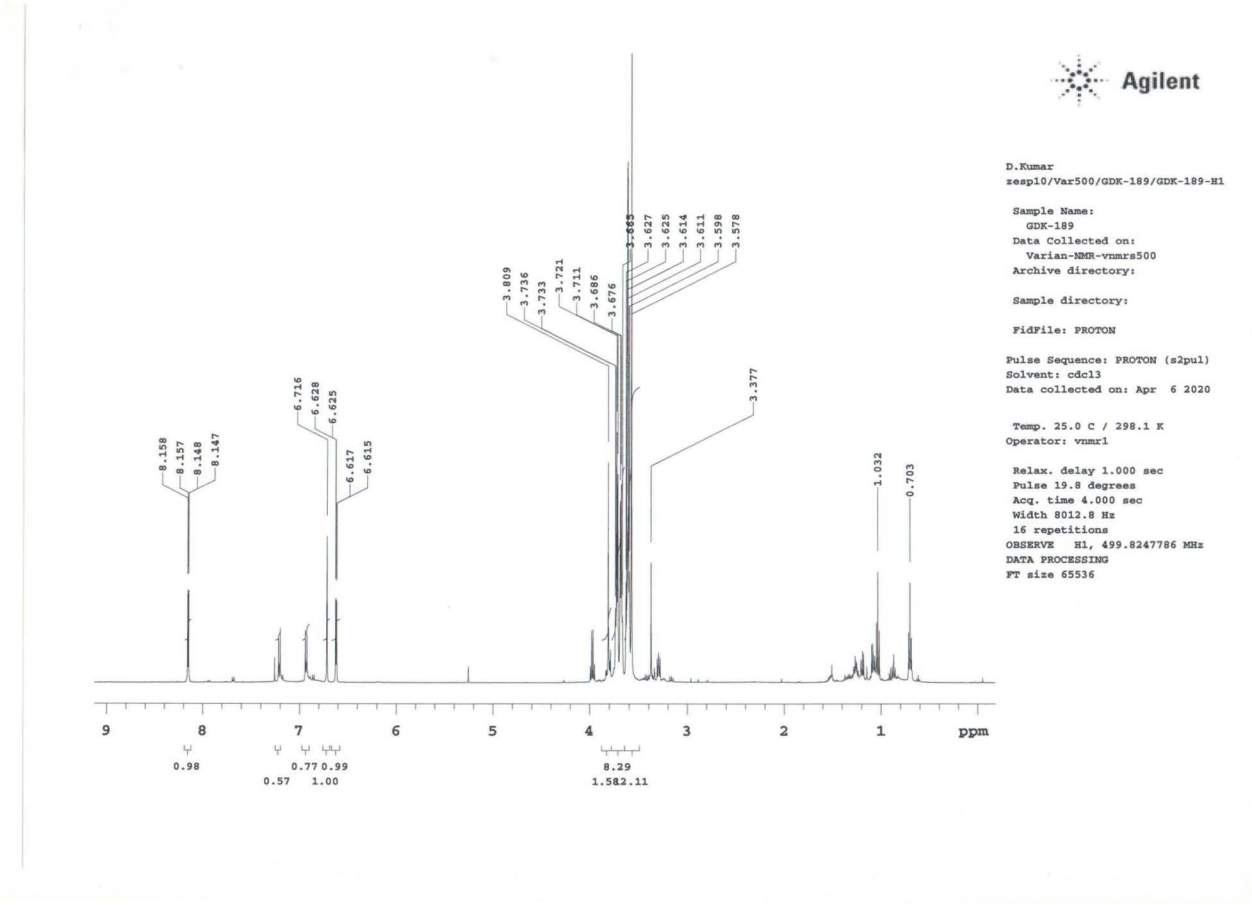

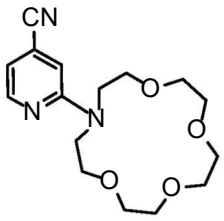

2f

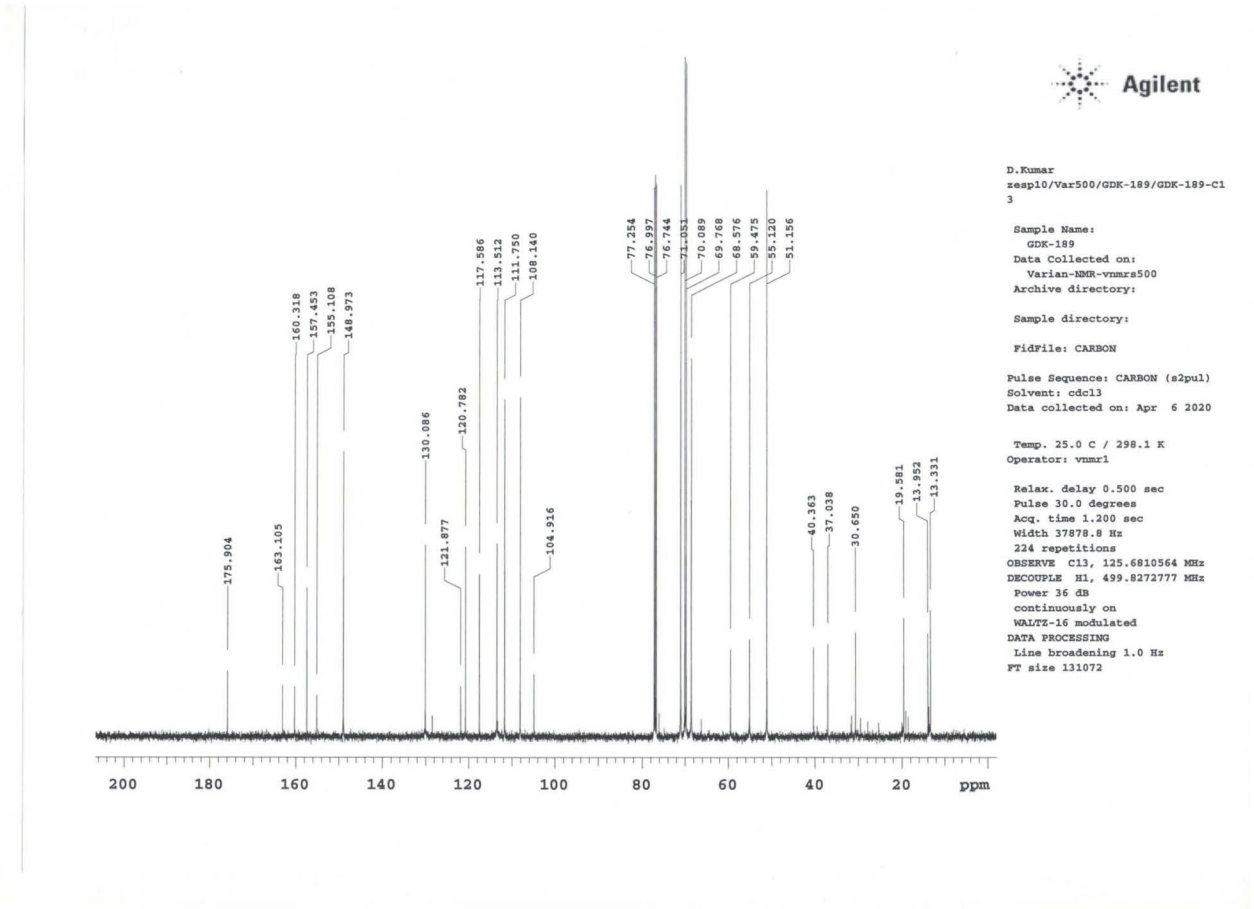

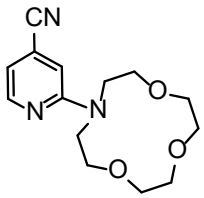

2h

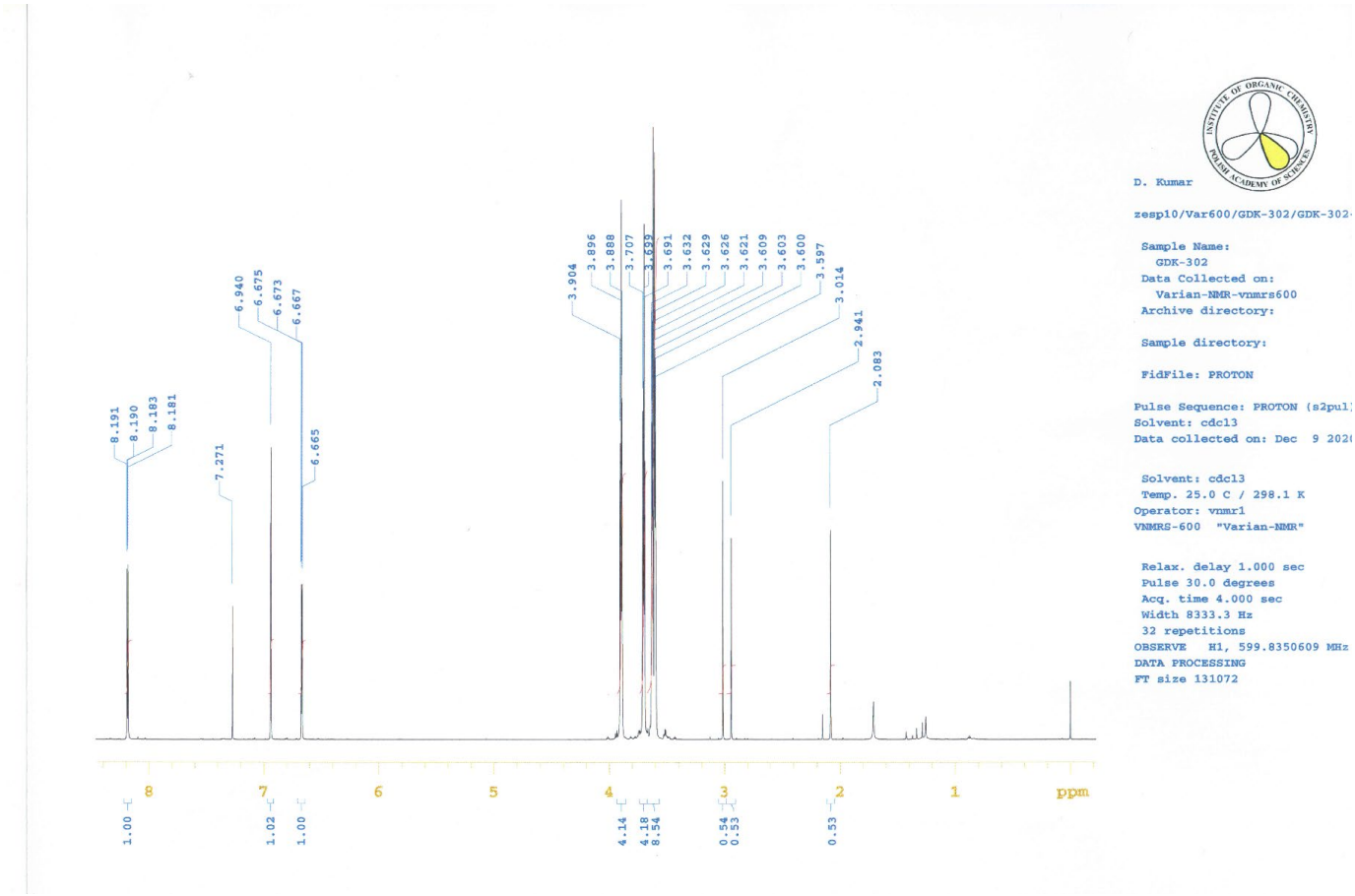

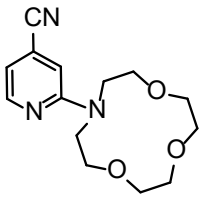

2h

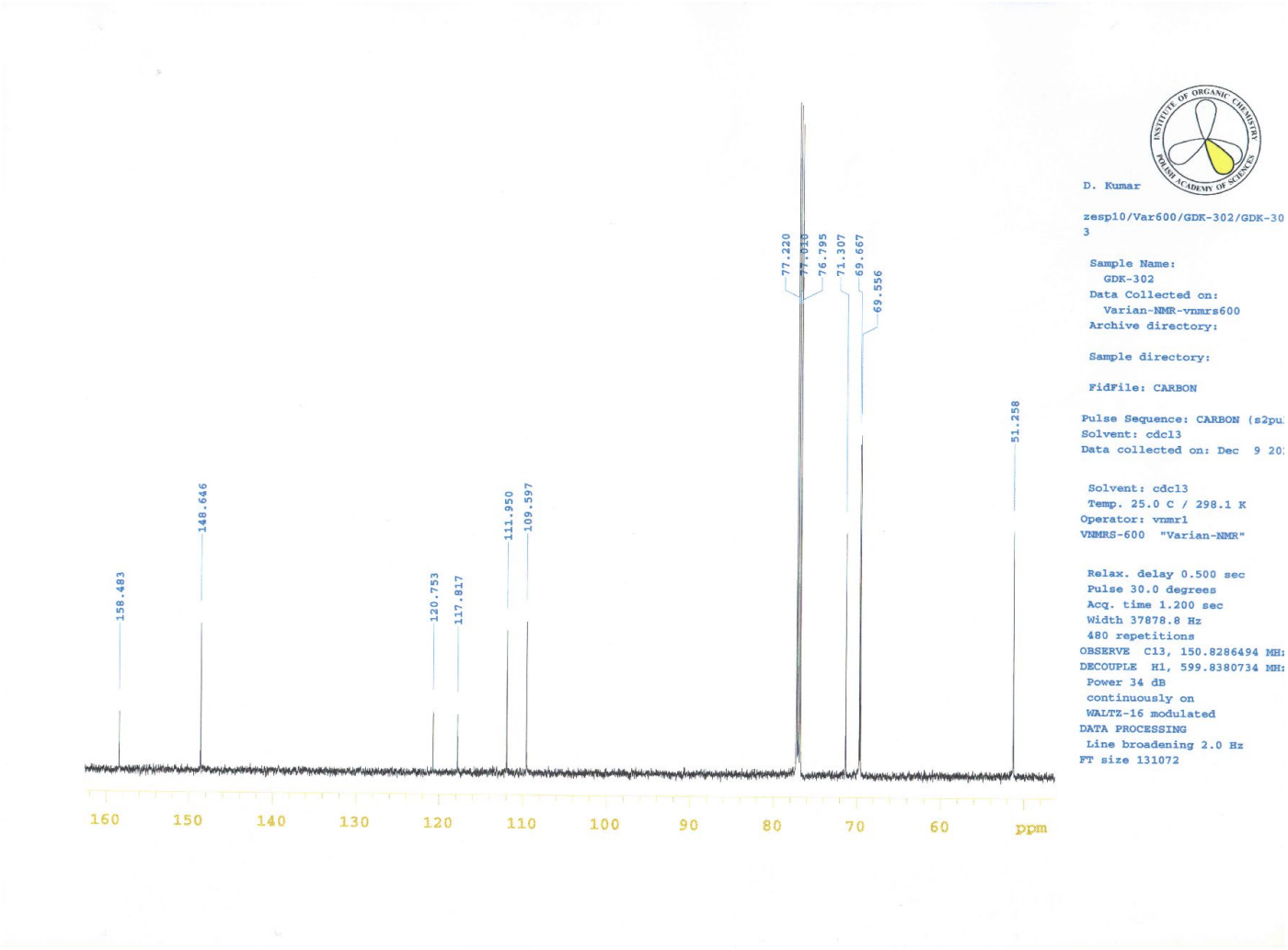

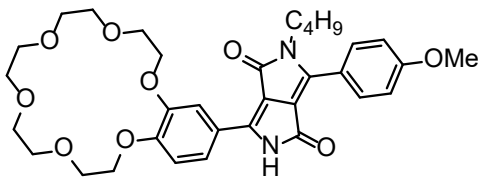

3

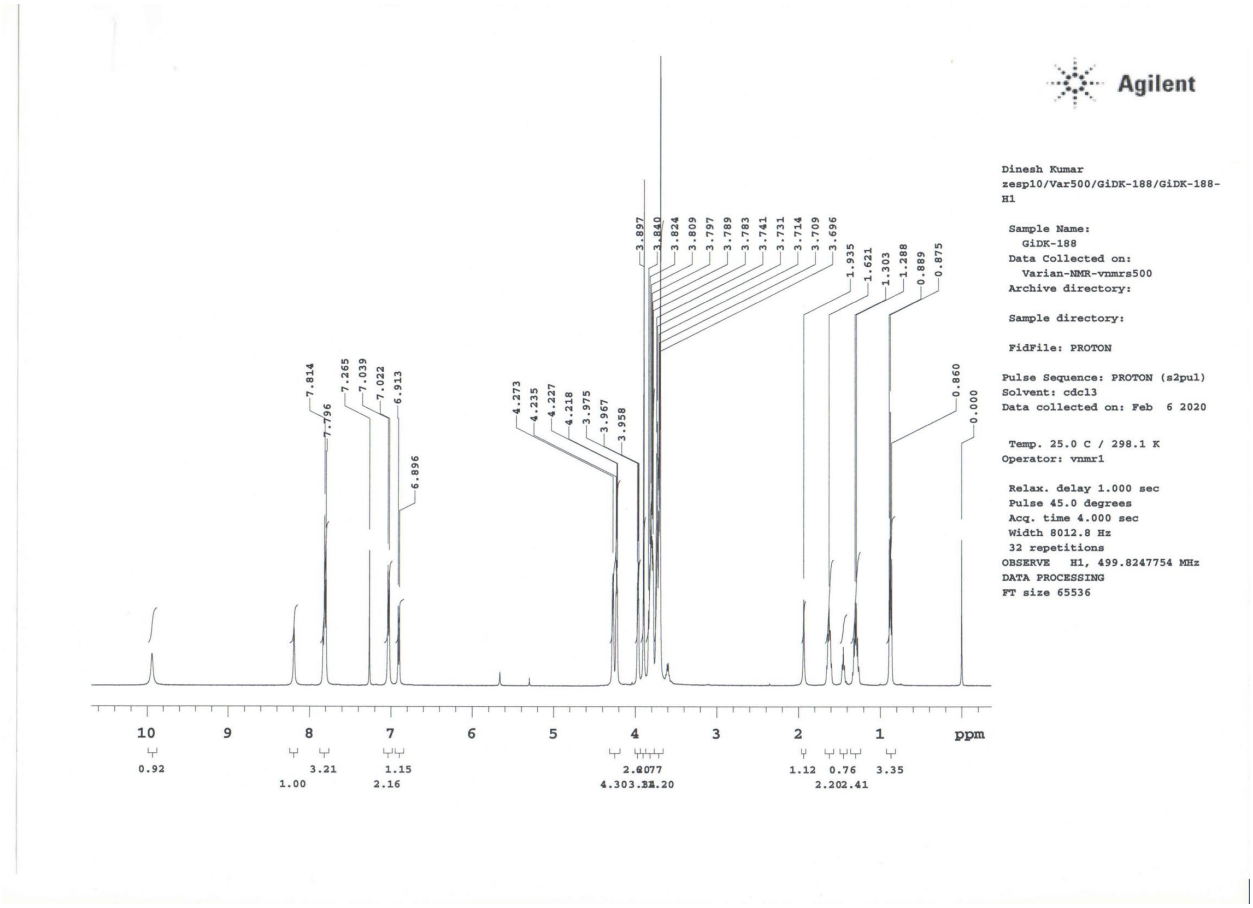

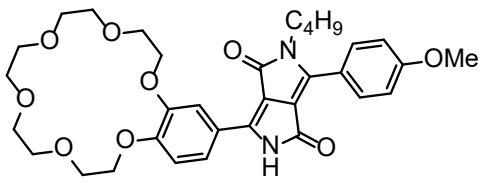

3

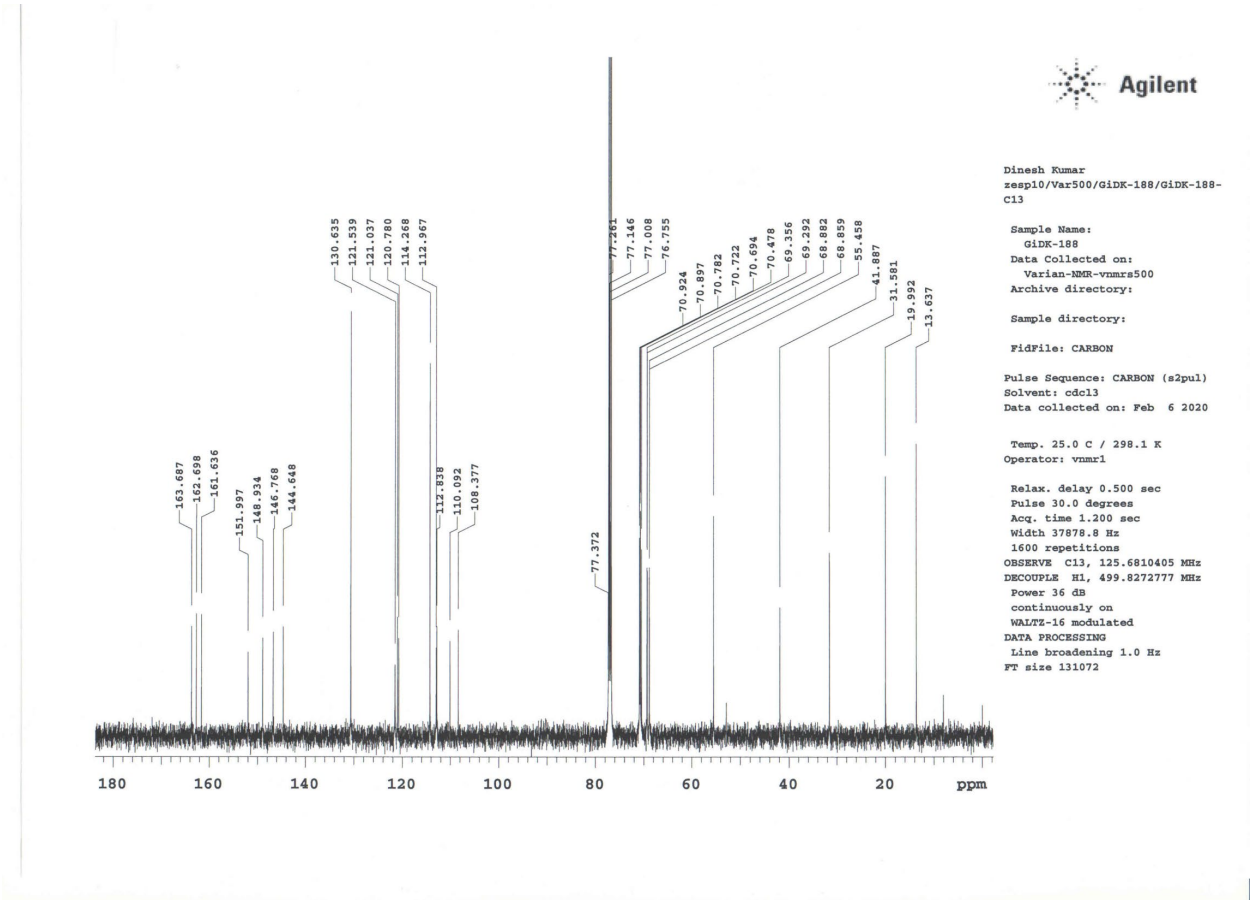

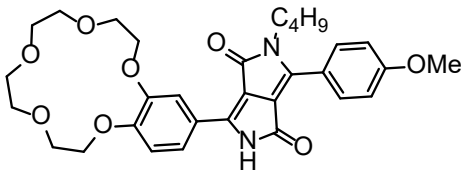

4

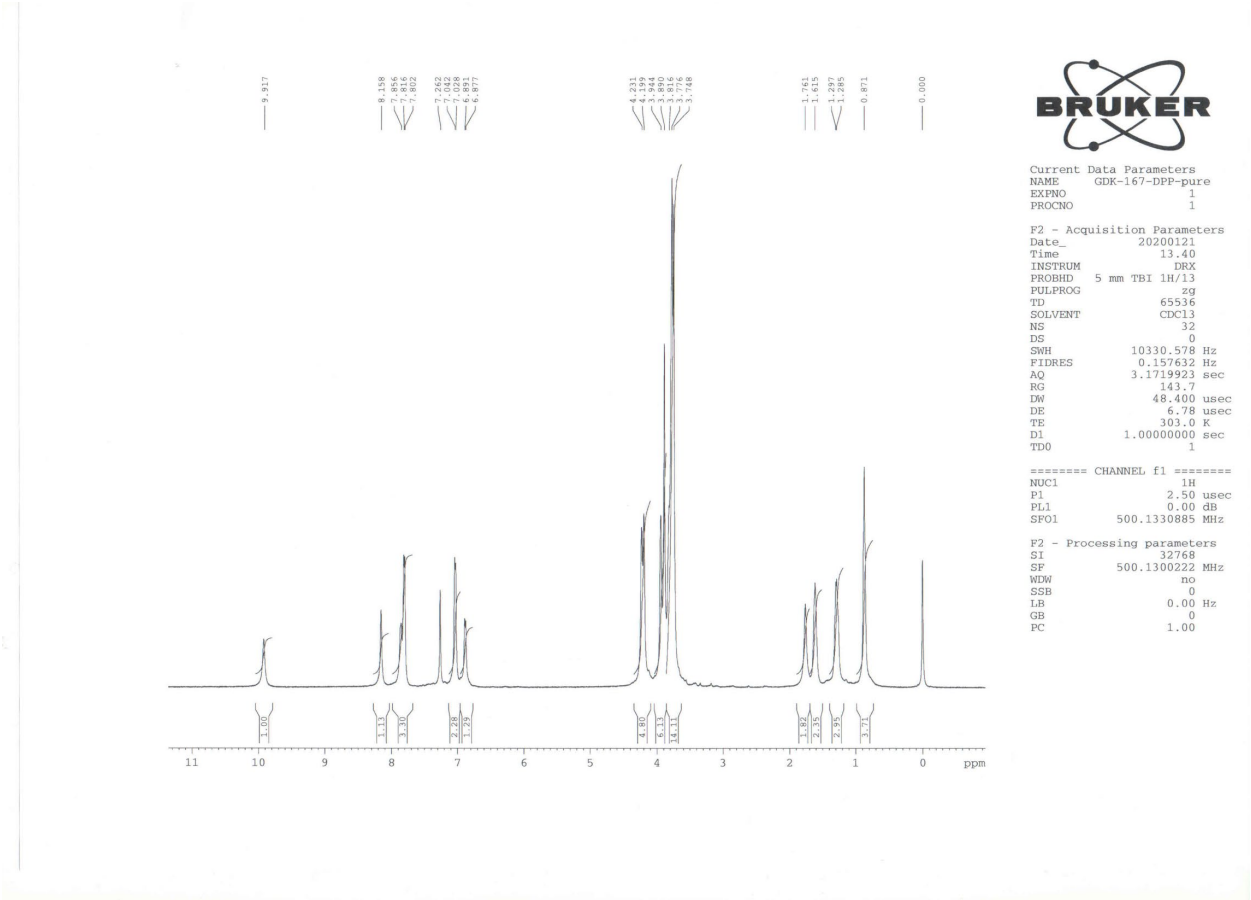

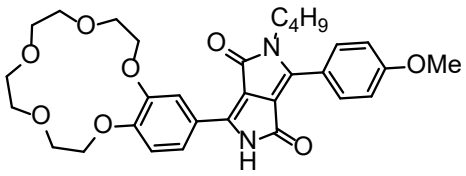

4

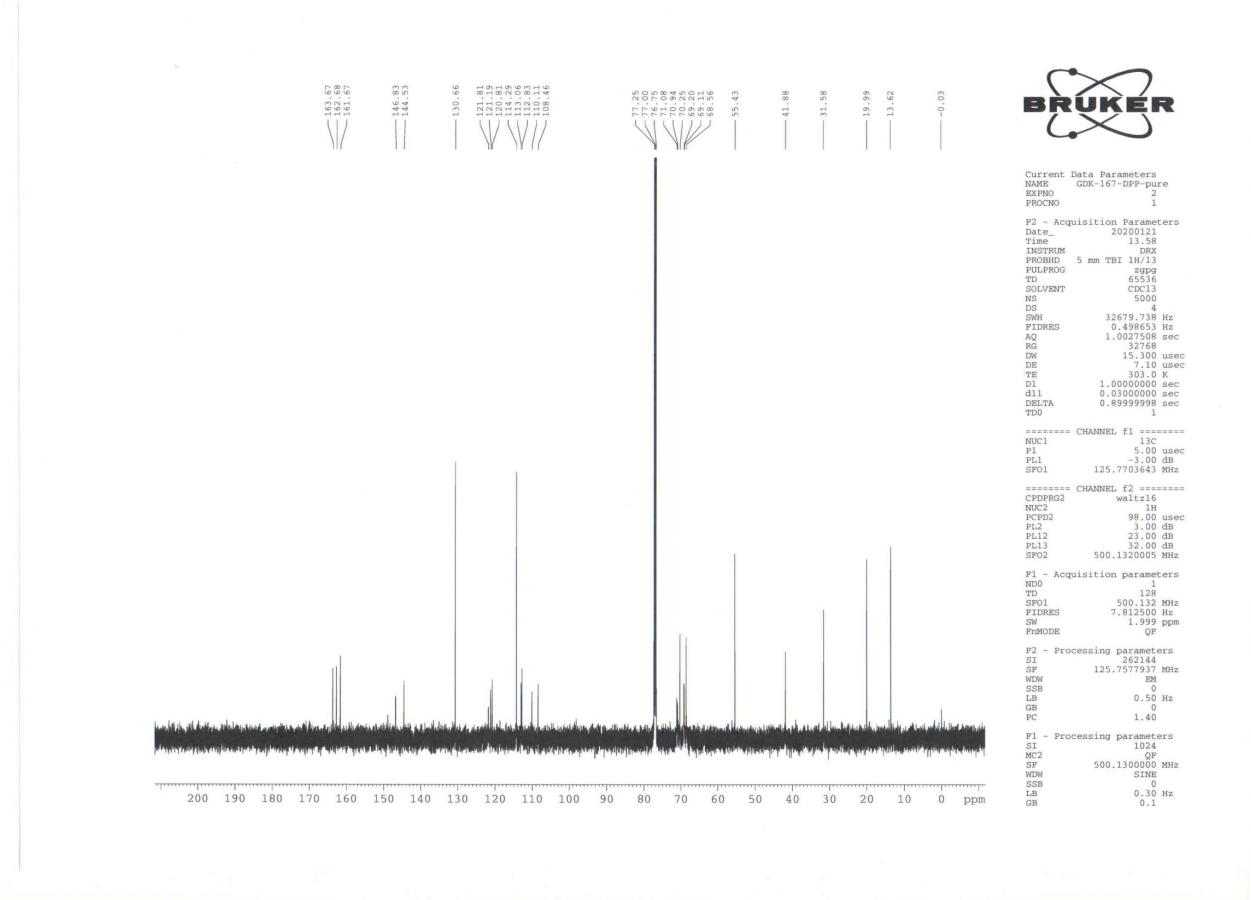

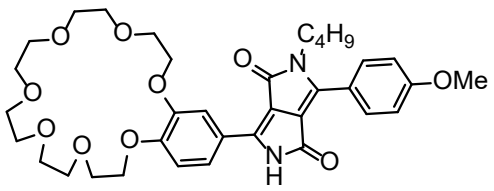

5

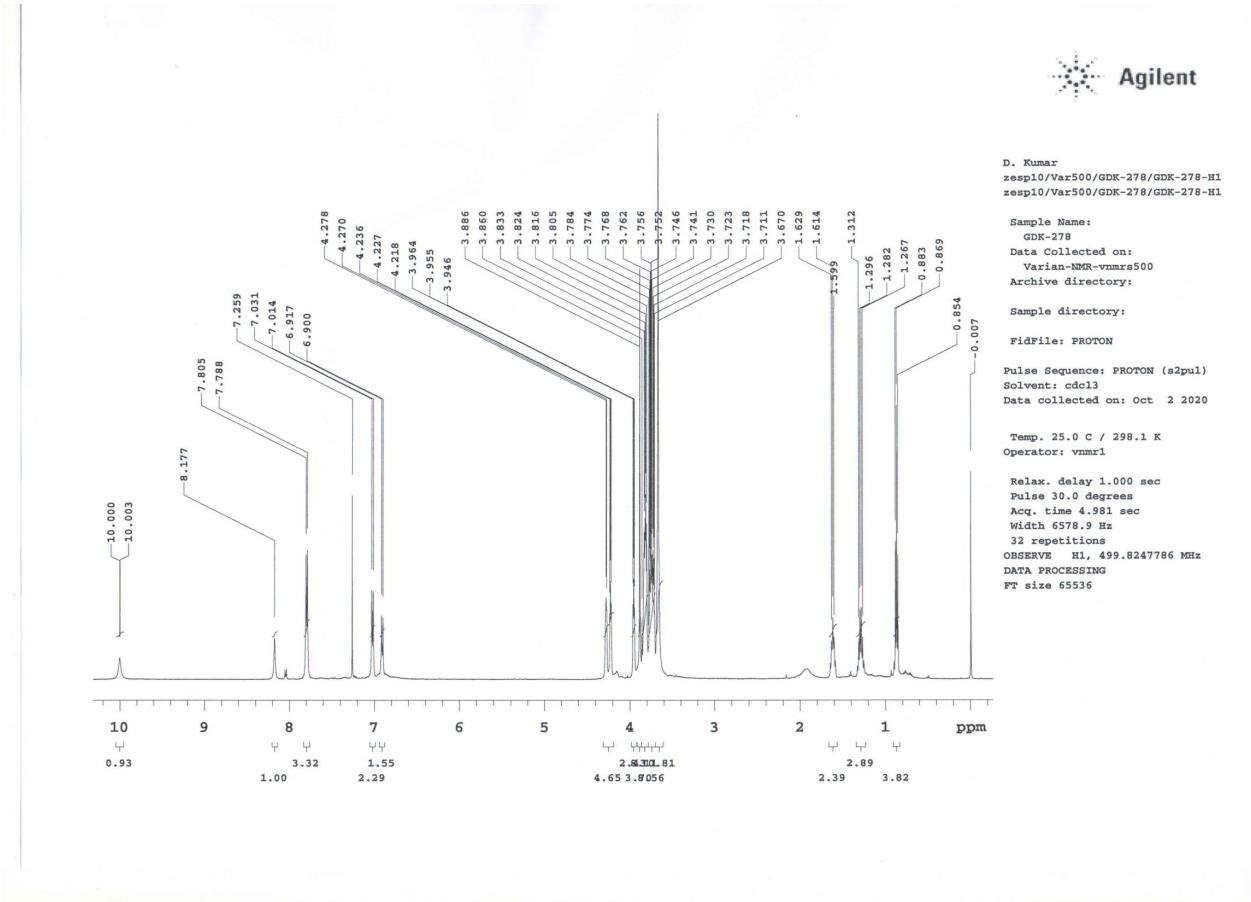

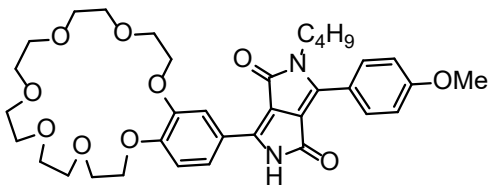

5

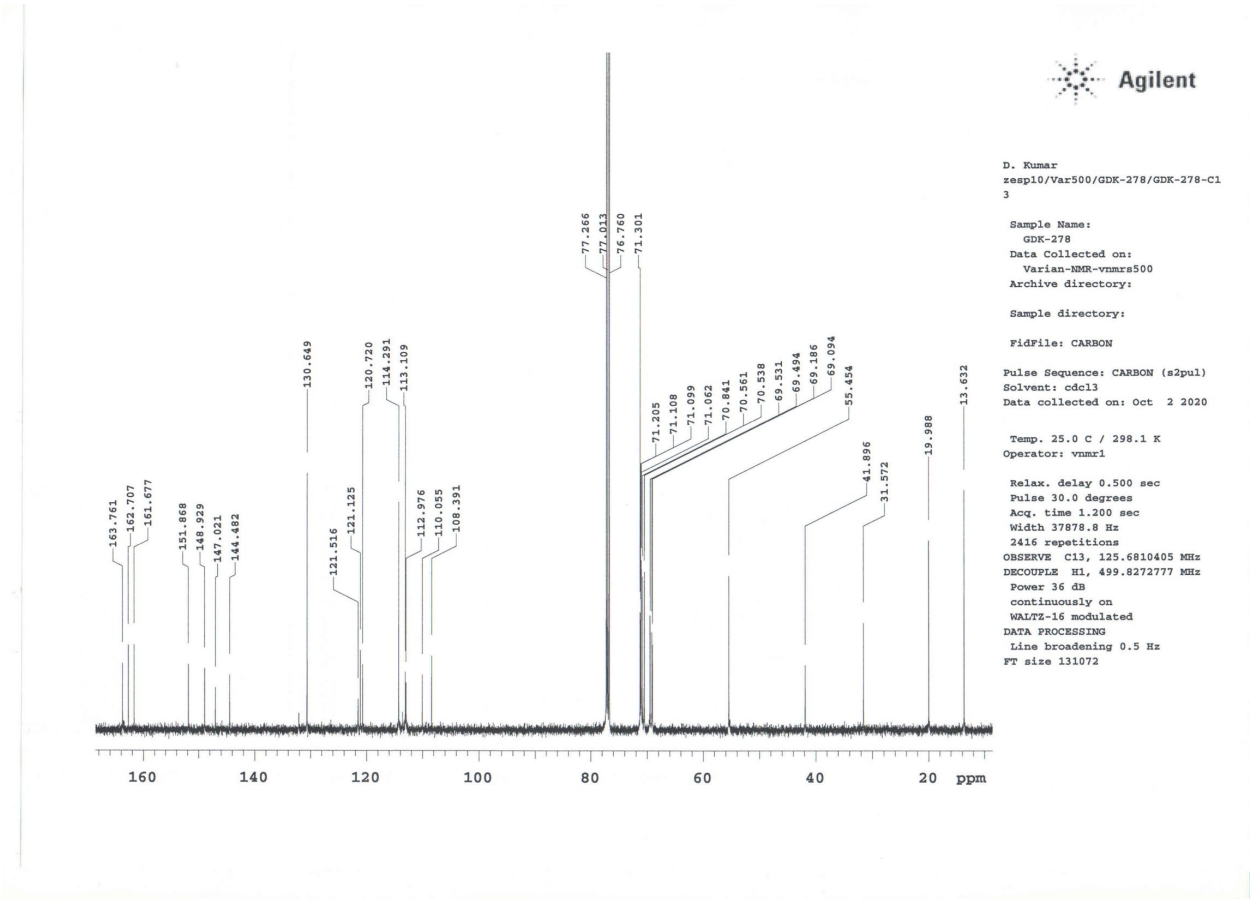

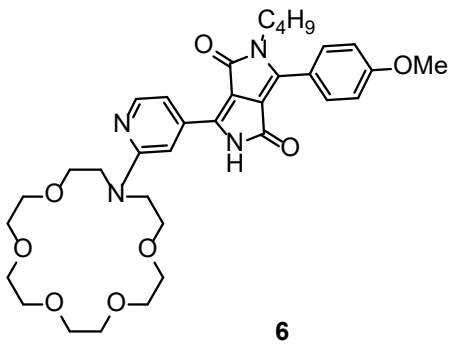

6

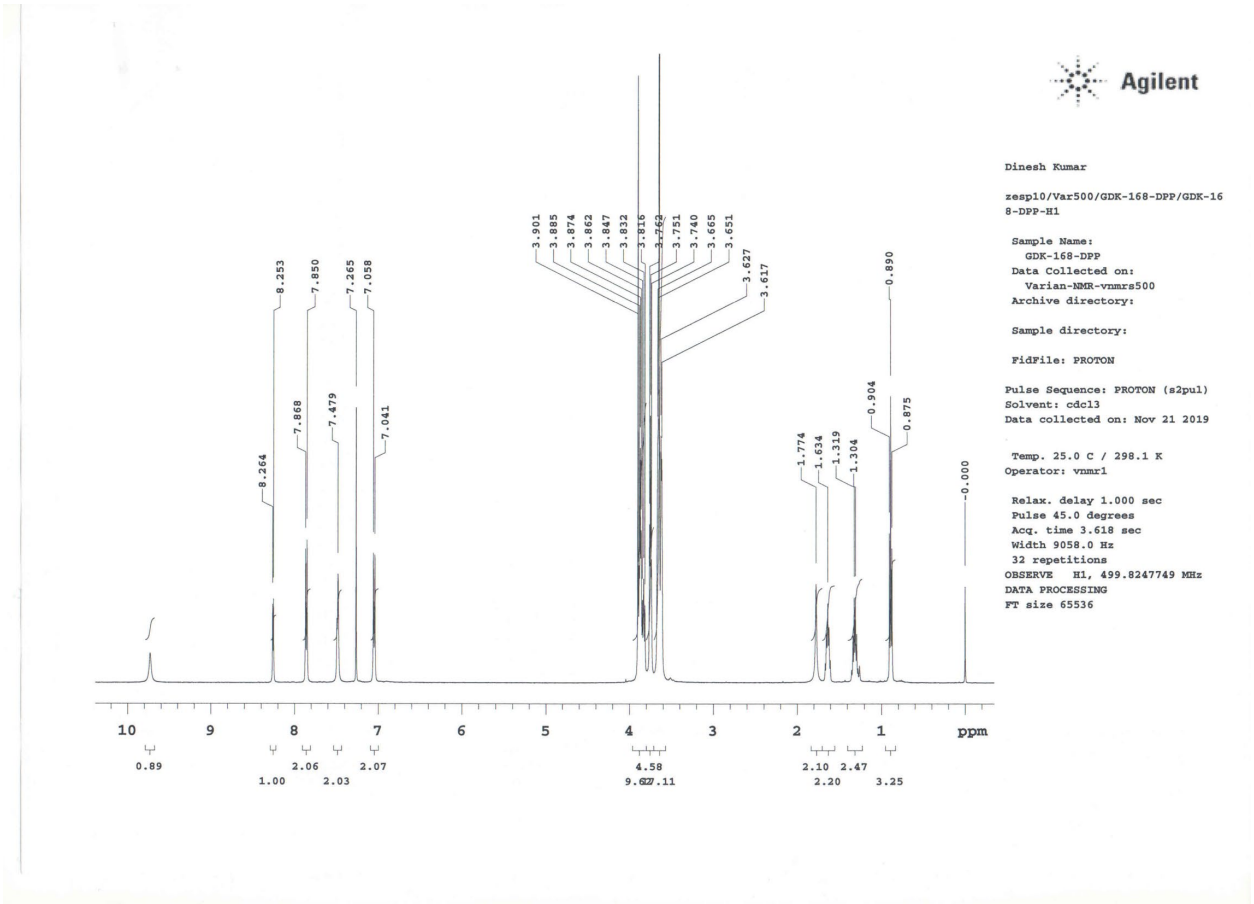

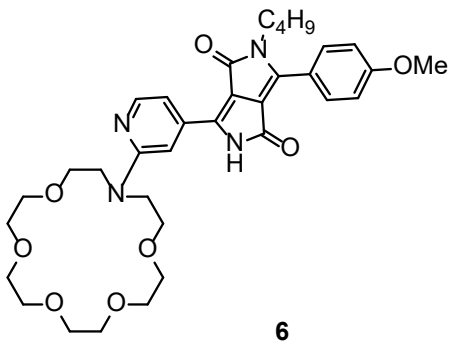

6

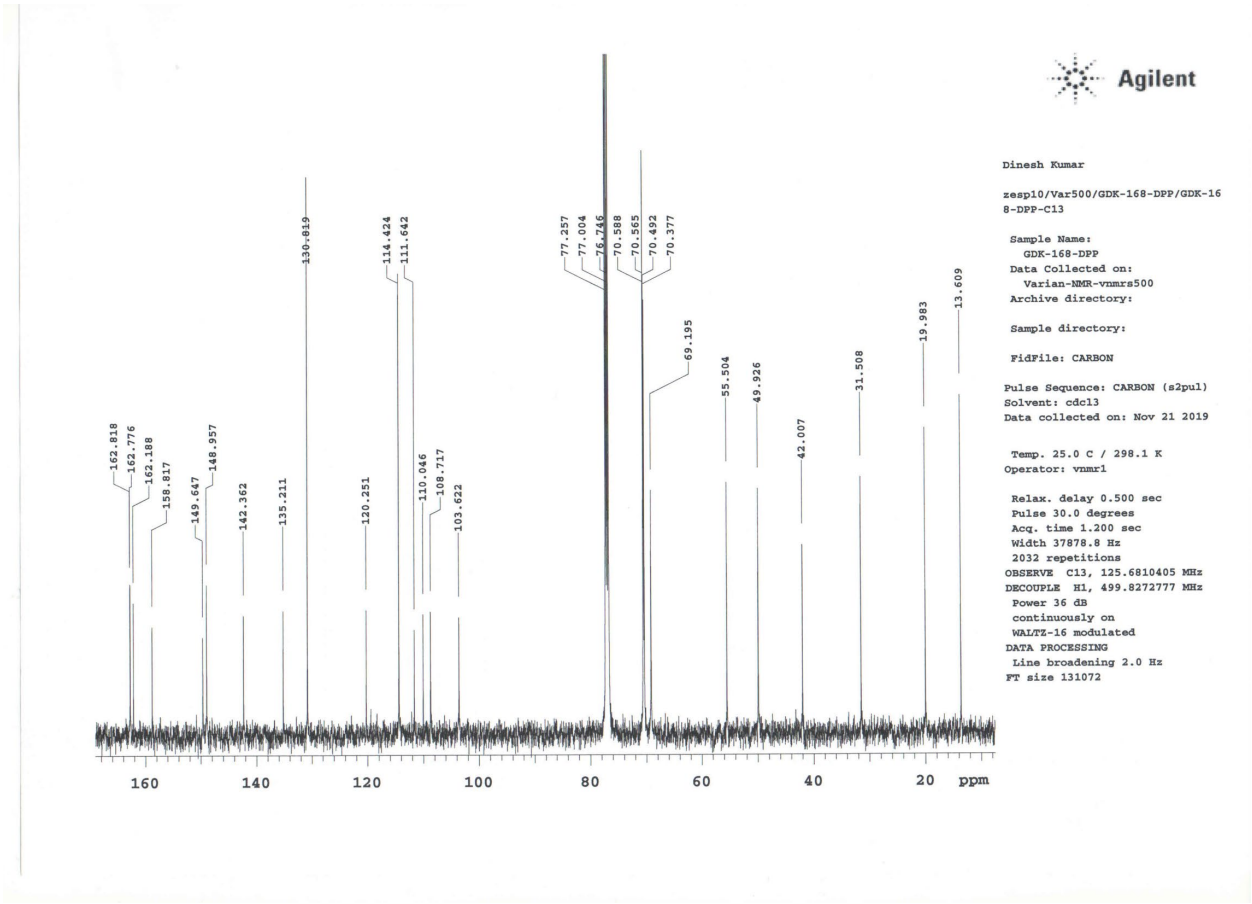

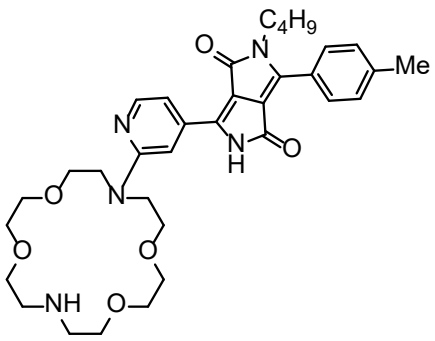

7

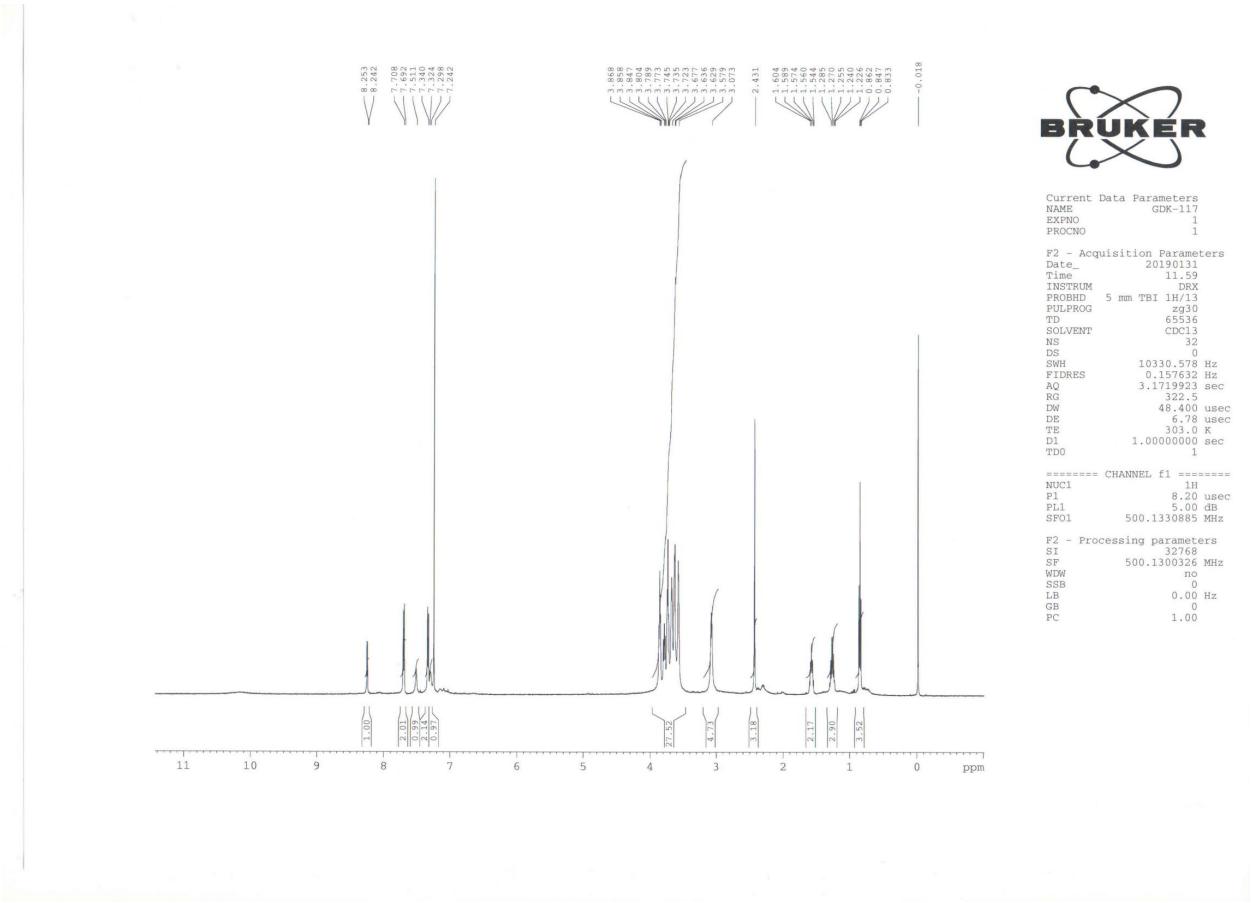

BRUKER

Current Data Parameters
NAME GDK-117
EXPNO 1
PROCNO 1

F2 - Acquisition Parameters
Date_ 20190131
Time 11.59
INSTRUM DRX
PROBHD 5 mm TBI 1H/13
PULPROG zg30
TD 65536
SOLVENT CDCl3
NS 32
DS 0
SWH 10330.578 Hz
FIDRES 0.157632 Hz
AQ 3.1719923 sec
RG 322.5
DW 48.400 usec
DE 6.78 usec
TE 303.0 K
D1 1.00000000 sec
TD0 1

======== CHANNEL f1 ========
NUC1 1H
P1 8.20 usec
PL1 5.00 dB
SFO1 500.1330885 MHz

F2 - Processing parameters
SI 32768
SF 500.1300326 MHz
WDW no
SSB 0
LB 0.00 Hz
GB 0
PC 1.00

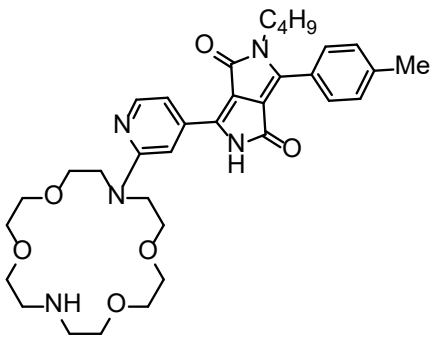

7

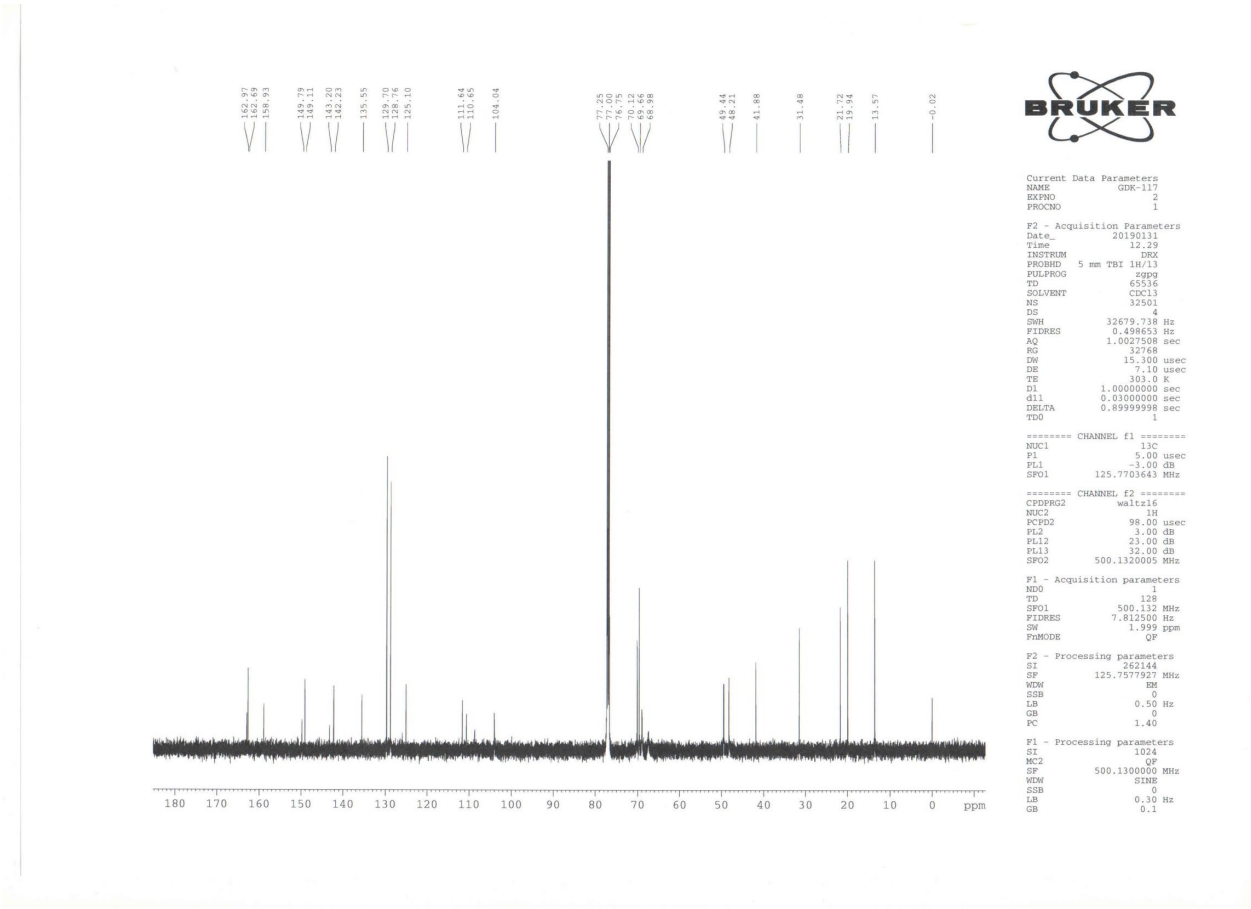

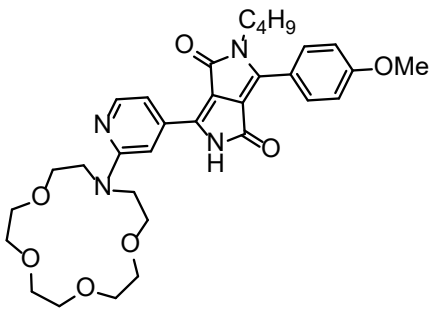

8

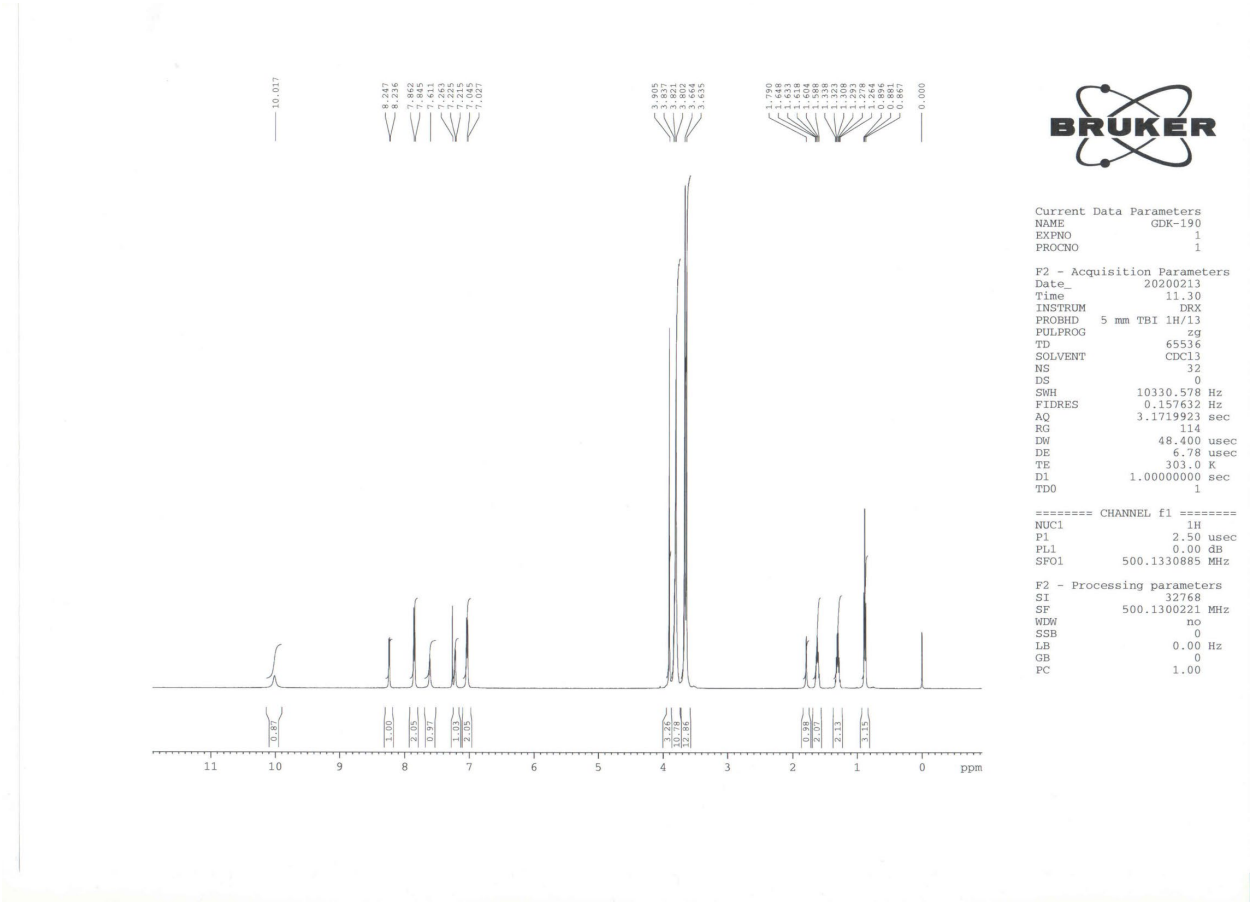

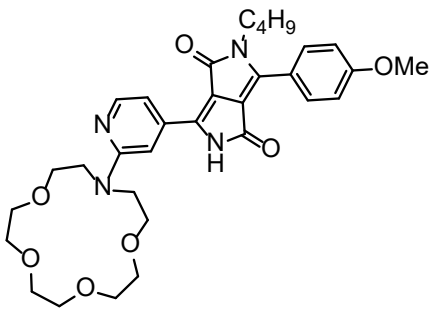

8

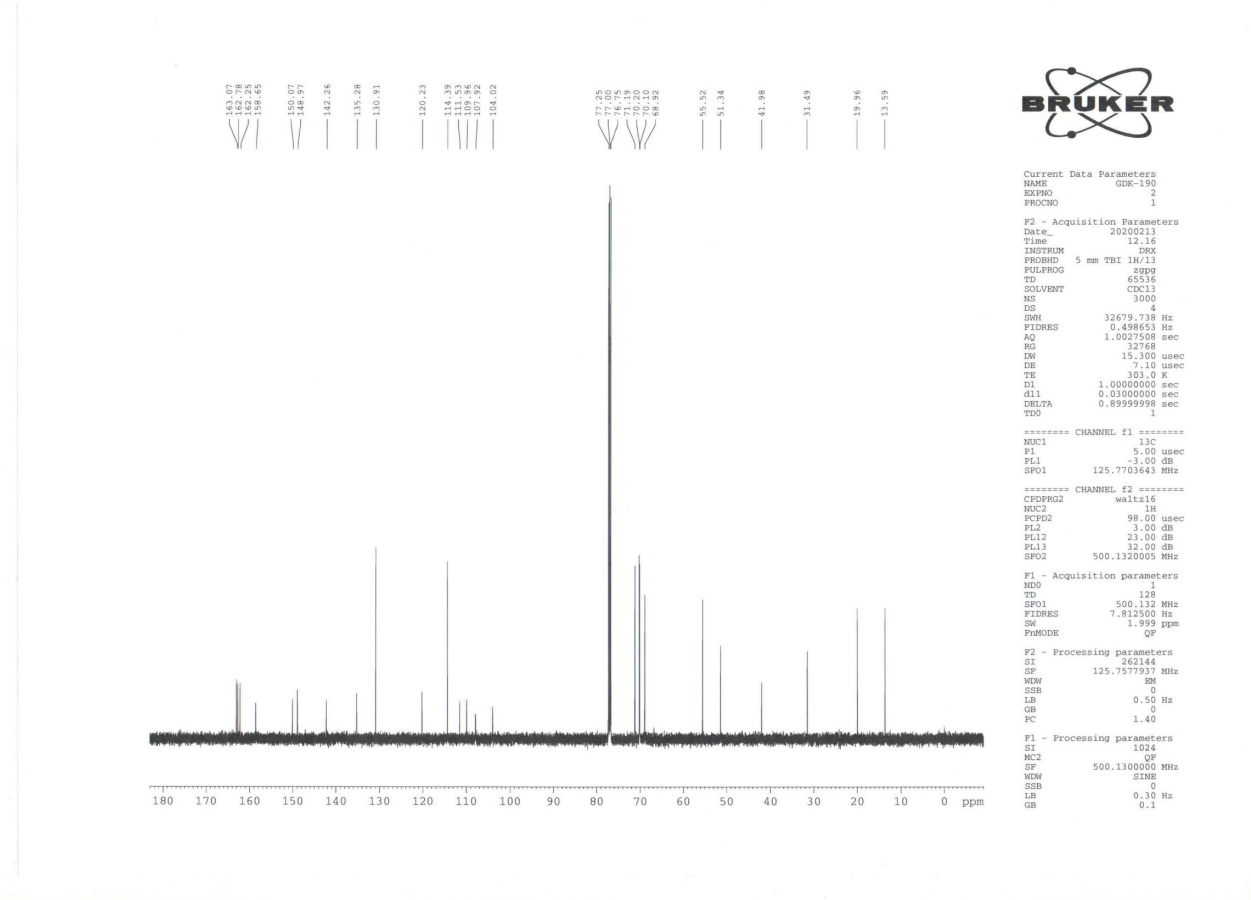

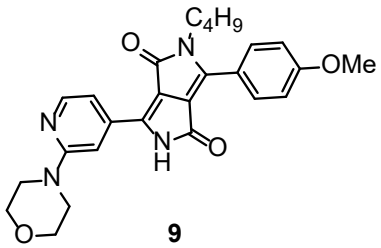

9

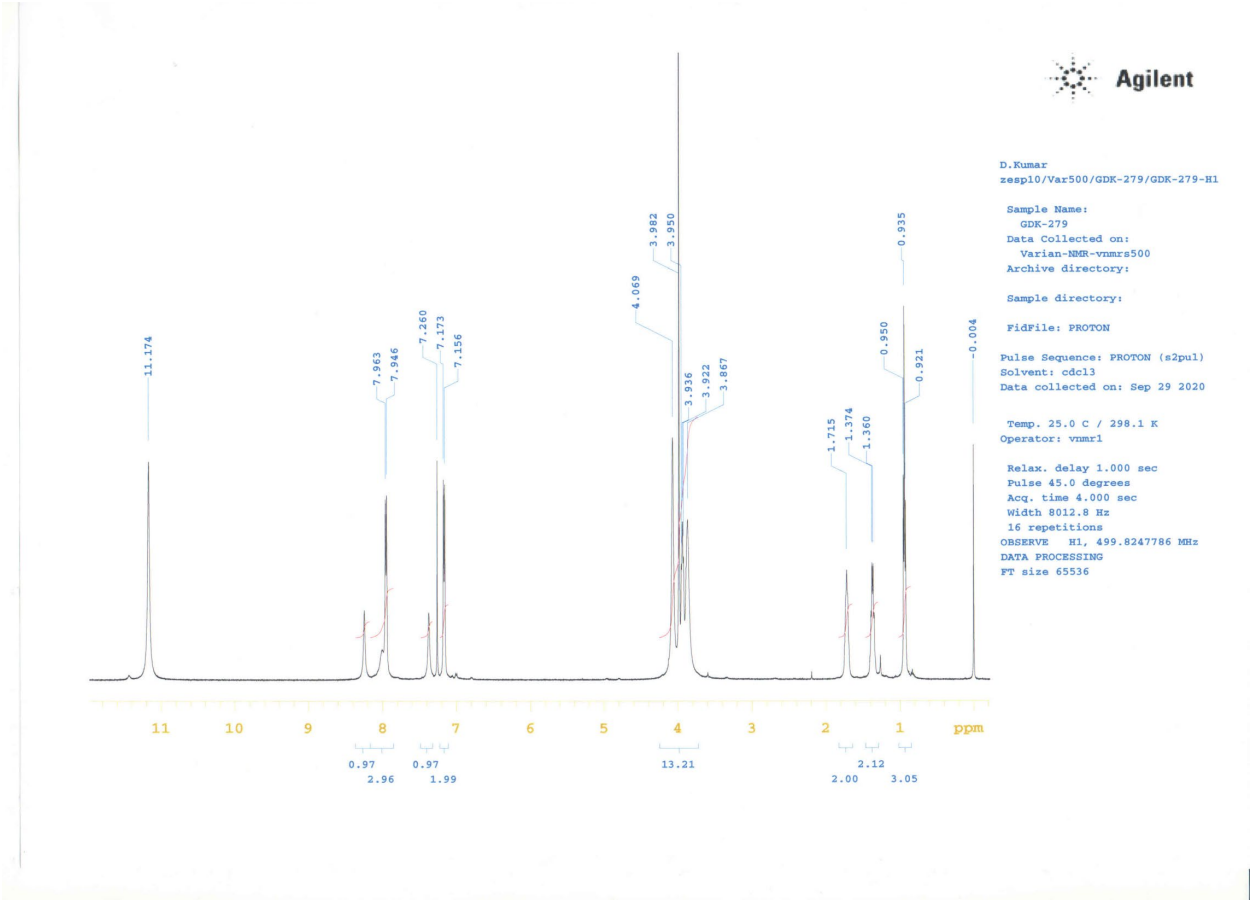

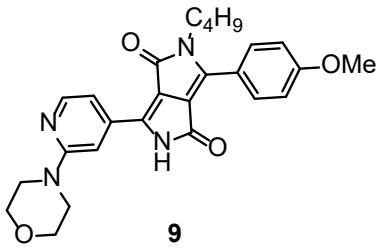

9

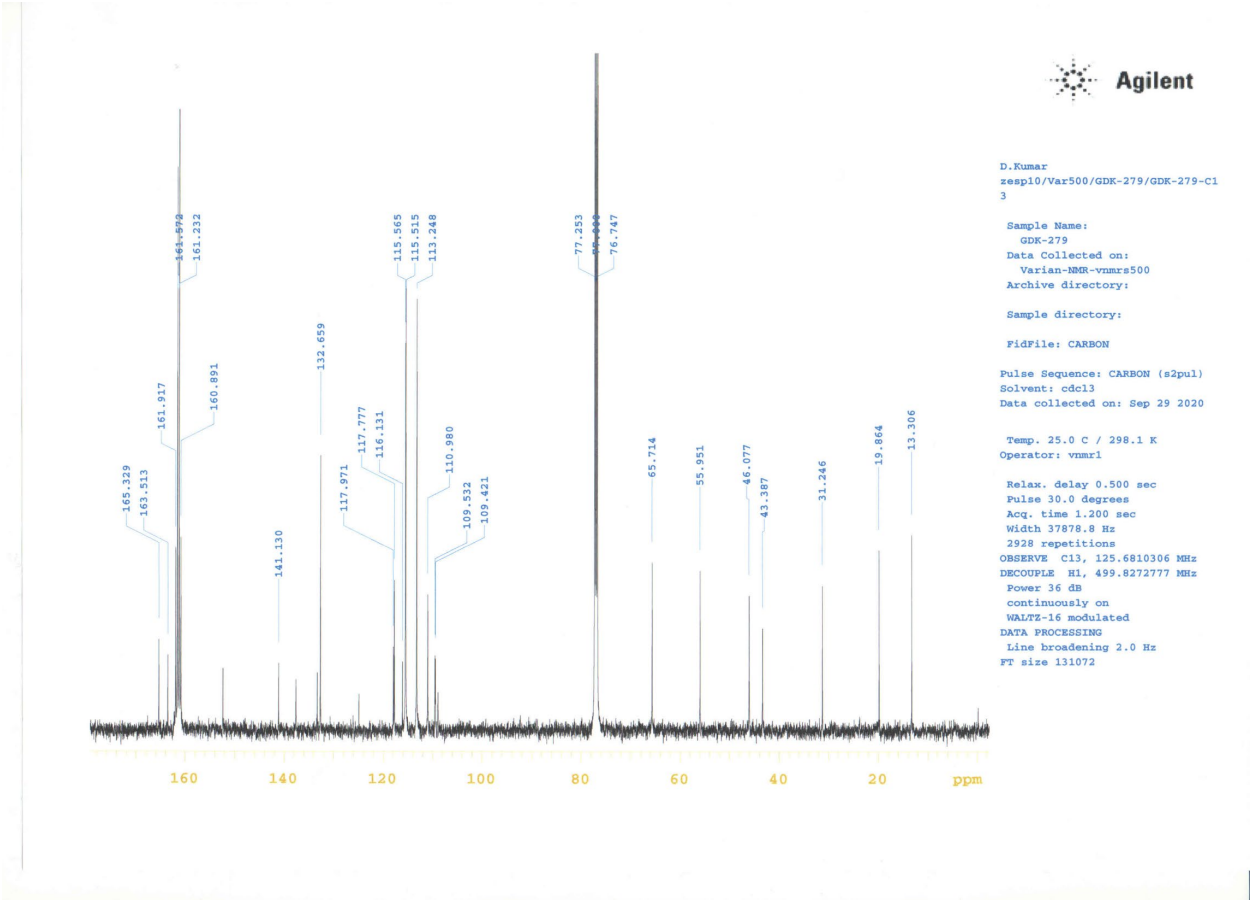

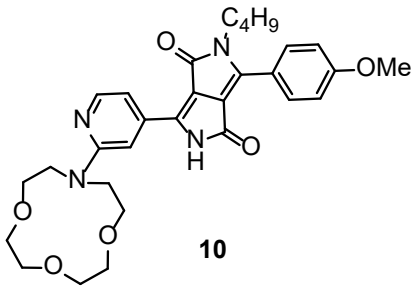

10

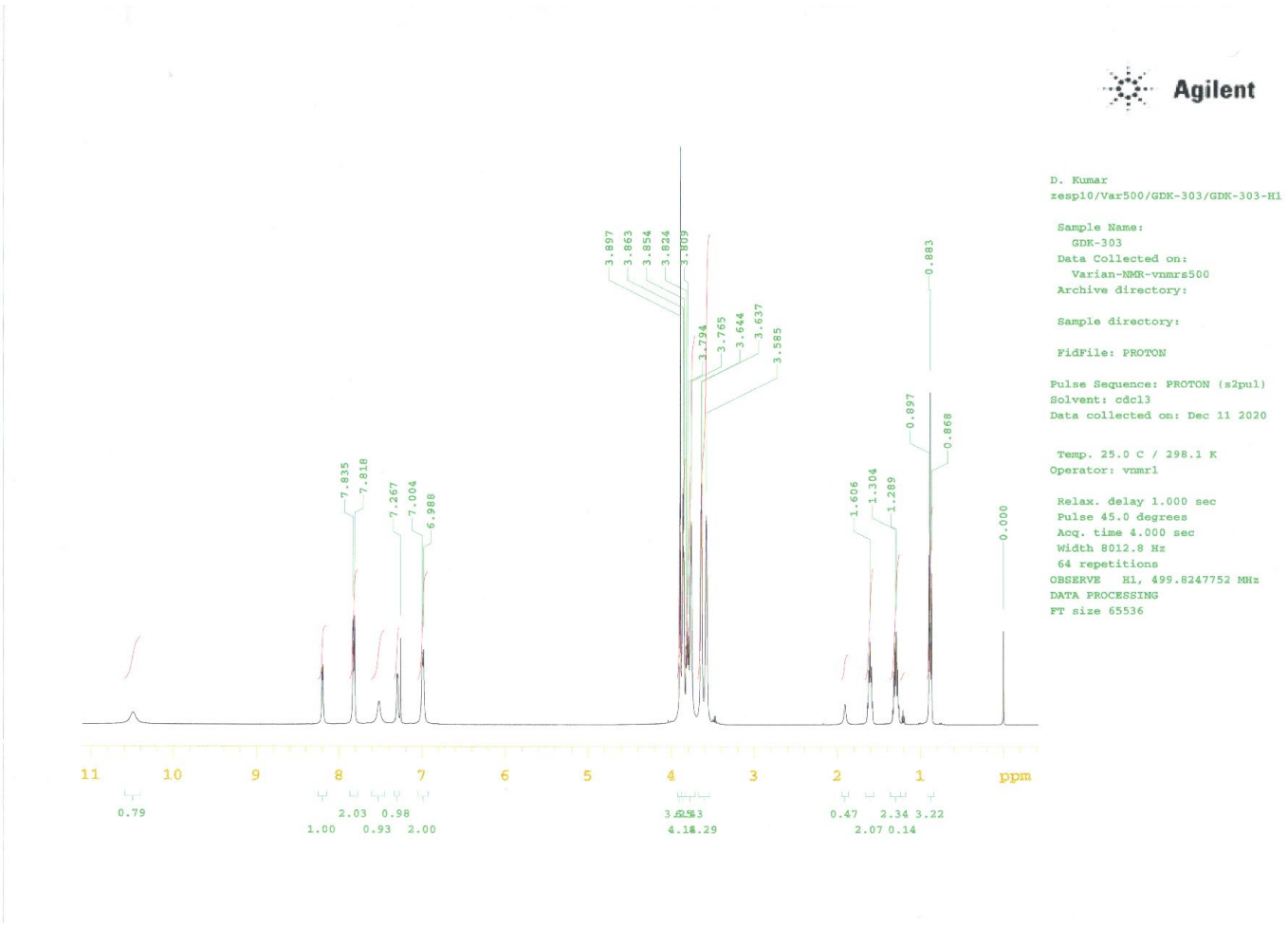

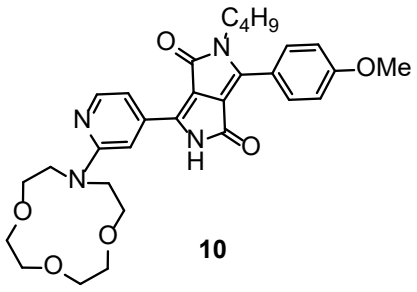

10

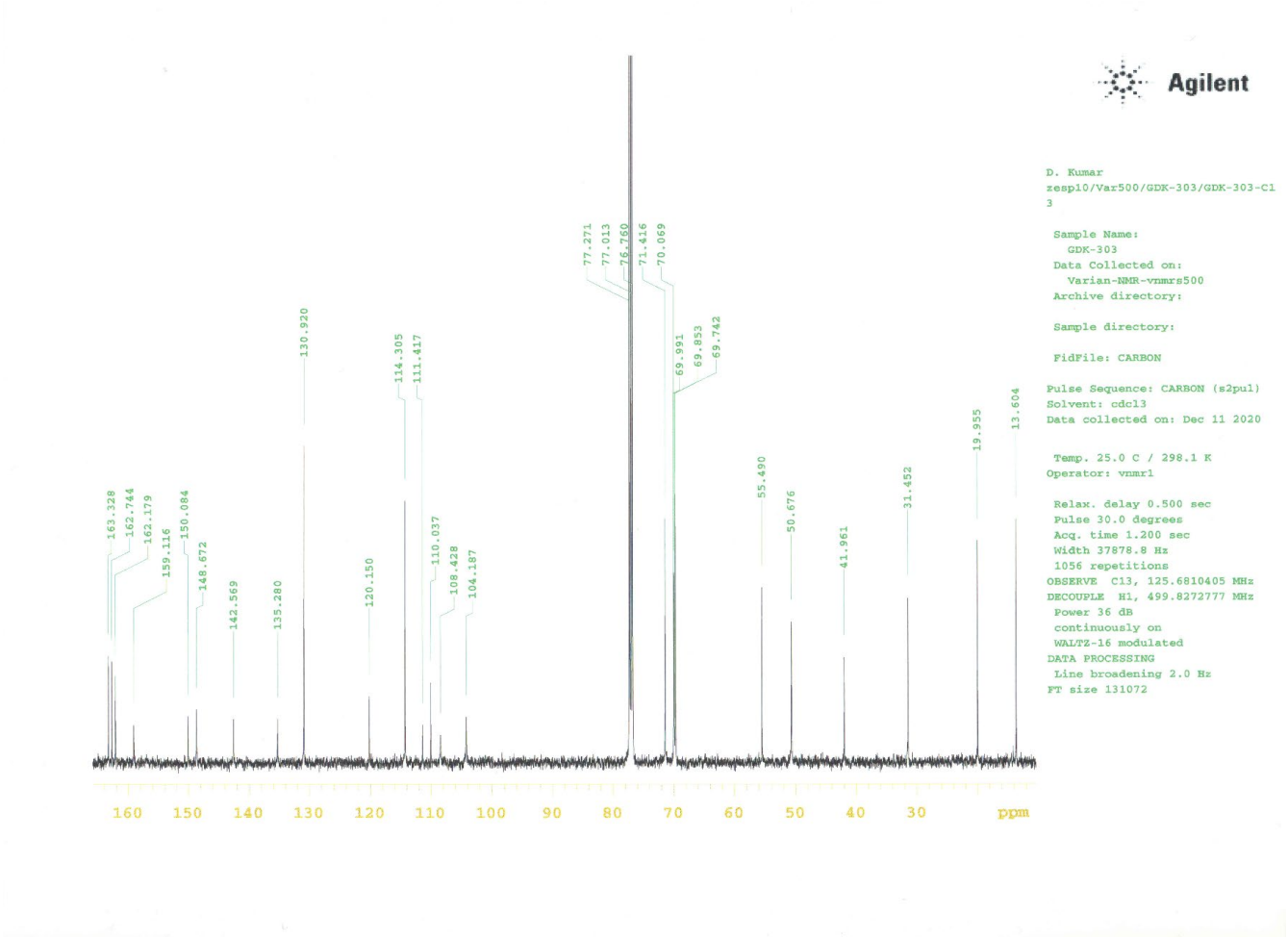

Section S5: References

1. Y. Zhang, Y. Ouyang, Z. Luo, S. Dong. *Eur. J. Org. Chem.* **2019**, 4741-4744.
2. A. Purc, M. Banasiewicz, E. Glodkowska-Mrowka, D. T.Gryko, *J. Mater. Chem. C*, **2016**, 4, 2877 – 2885.

ChemComm

ROYAL SOCIETY OF CHEMISTRY

COMMUNICATION

View Article Online
View Journal | View Issue

Cite this: *Chem. Commun.*, 2022, **58**, 4500

Received 17th January 2022,
Accepted 9th March 2022

DOI: 10.1039/d2cc00324d

rsc.li/chemcomm

Probing the flux of mitochondrial potassium using an azacrown-diketopyrrolopyrrole based highly sensitive probe†

G. Dinesh Kumar,[a] Marzena Banasiewicz,[b] Antoni Wrzosek,[c] Rafał P. Kempa,[c] Manon H. E. Bousquet,[d] Damian Kusy,[a] Denis Jacquemin,*[d] Adam Szewczyk*[c] and Daniel T. Gryko*[a]

Supporting Information

Probing flux of mitochondrial potassium using an azacrown-diketopyrrolopyrrole based highly sensitive probe

G. Dinesh Kumar,[a] Marzena Banasiewicz,[b] Antoni Wrzosek,[c] Rafal P. Kampa,[c] Manon H. E. Bousquet,[d] Damian Kusy,[a] Denis Jacquemin,*[d] Adam Szewczyk,*[c] and Daniel T. Gryko*[a]

[a] Institute of Organic Chemistry, Polish Academy of Sciences, Kasprzaka 44/52, 01-224 Warsaw, Poland. E-mail: dtgryko@icho.edu.pl

[b] Institute of Physics, Polish Academy of Sciences, Al. Lotników 32/46, 02-668 Warsaw, Poland.

[c] Nencki Institute of Experimental Biology of Polish Academy of Sciences, Pasteur 3, 02-093 Warsaw, Poland. E-mail: a.szewczyk@nencki.gov.pl.

[d] CEISAM UMR 6230, CNRS, Université de Nantes, 44000 Nantes, France. E-mail :Denis.Jacquemin@univ-nantes.fr

Table of contents

Section S1: General Information

All reagents and solvents were purchased from commercial sources and were used as received unless otherwise noted. Reagent grade solvents (CH_2Cl_2, hexanes) were distilled prior to use. Transformations with moisture- and oxygen-sensitive compounds were performed under a stream of argon. The reaction progress was monitored by means of thin-layer chromatography (TLC), which was performed on Kieselgel 60. The identity and purity of prepared compounds were proved by ^{1}H NMR and ^{13}C NMR as well as by mass spectrometry (via EI-MS or ESI-MS). HRMS (ESI-TOF) and HRMS (EI): double-focusing magnetic sector instruments with EBE geometry were utilized. NMR spectra were measured on 400 or 500 or 600 MHz instruments. Chemical shifts (δ, ppm) were determined with tetramethylsilane (TMS) as the internal reference; J values are given in Hz. All melting points for crystalline products were measured with an automated melting point apparatus and are given without correction.

UV/Vis absorption spectra were recorded on a PerkinElmer Lambda 35 Spectrometer. Fluorescence spectra were recorded on a FLS1000 of Edinburgh Instruments. All linear optical studies were performed with freshly prepared air-equilibrated solutions at room temperature (298 K). Acetonitrile was spectrophotometric grade and was used without further purification. Quartz cells (10 mm) were used for the measurements of absorption and emission spectra. As a standard, Rh6G (Φ_{fl} = 0.94 in EtOH) was used to determine fluorescence quantum yields.

Section S2: Synthesis

The synthetic strategy used to prepare DPP-based probes is based on the synthesis of asymmetrical DPPs incorporating a single bromoaryl substituent followed by Buchwald-Hartwig amination with a corresponding azacrown ether. Hence, DPP **S5** was prepared from 4-bromobenzonitrile (**S2**) and pyrrolidin-2-one **S1** following our previously developed strategy in 48% yield (Scheme S1). Subsequently the desired crown-DPP **S9** was obtained by Buchwald-Hartwig amination with 1-aza-18-crown-6 (**S8**) in 23 % yield (Scheme S2).

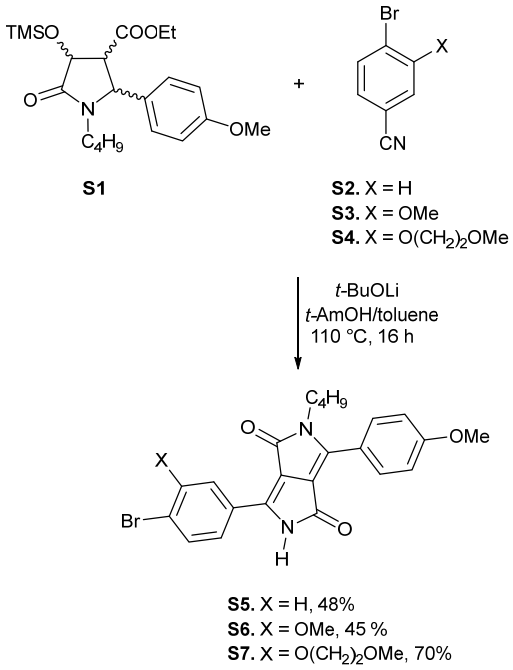

Scheme S1. The synthesis of diketopyrrolopyrroles **S5**-S**7**.

It is well known that the presence of an additional alkoxy group at an ortho position relative to an 18-azacrown-6 moiety increases the binding constant with K^+ as well as its selectivity versus this cation. In order to exploit this beneficial property, following similar synthetic procedures we designed DPPs **S10** and **S12** possessing MeO and $MeOCH_2CH_2O$ groups, respectively. We also designed DPP **S11** possessing a 15-azacrown-5 macrocycle as a model. The synthesis of these three DPPs was achieved following the aforementioned pathway, i.e., synthesis of unsymmetrical bromophenyl-DPPs **S6** and **S7** followed by optimized Buchwald-Hartwig amination with 1-aza-18-crown-6 or 1-aza-15-crown-5 to provide crown DPPs **S10** and **S11** in 15% and 50% yield respectively (Scheme S1, Fig. S1). Nitrile **S4**, obtained in two steps from 4-bromo-3-methoxy benzonitrile, was reacted with pyrrolidin-2-one **S1** forming DPP **S7** in high yield (70%). The latter dye was used for amination with 1-aza-18-crown-6 (**S8**) to afford DPP **1** in 18% yield (Scheme S1, Fig. S1).

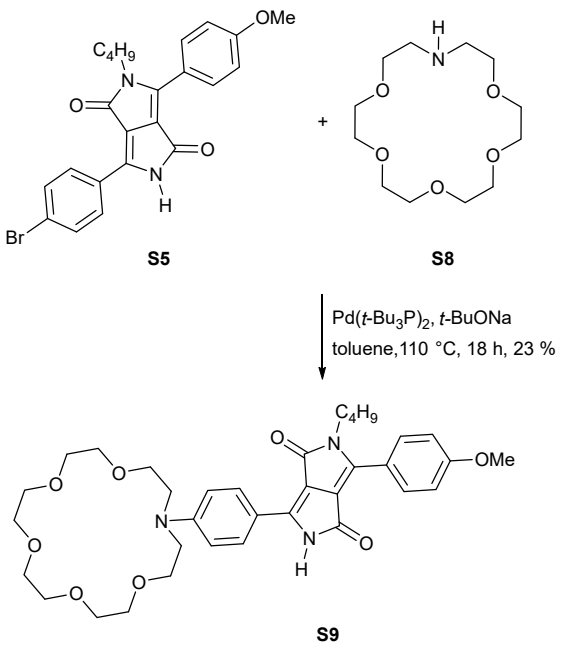

Scheme S2. The synthesis of DPP **S9** via Buchwald-Hartwig amination.

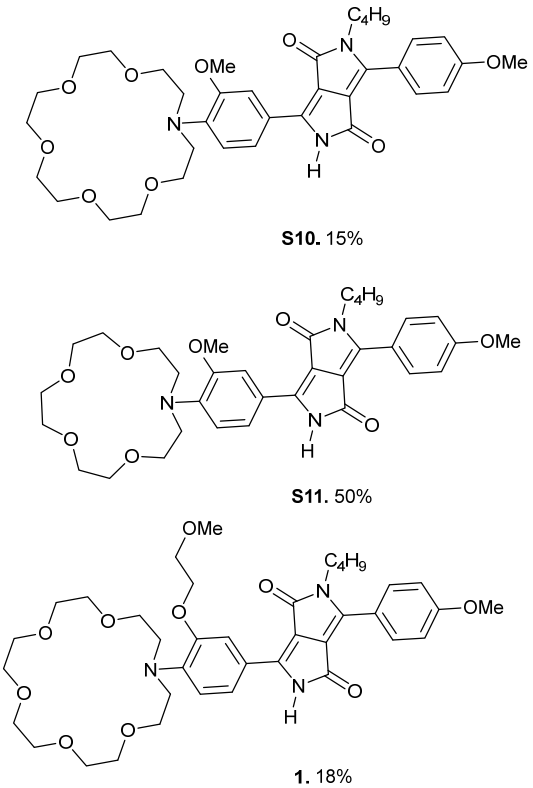

Fig. S1. The structures of crown-DPPs **S10**-**S11** and **1**.

The photophysical properties of unsymmetrically substituted DPPs strongly depend on the nature of both aryl substituents. Previously, it was found that the replacement of 4-$MeOC_6H_4$ with 4-$CF_3C_6H_4$ can render DPPs' fluorescence inert to changes in solvent polarity. This provided us with motivation to prepare analogues of DPPs **S9**-**S11** and **1** possessing 4-trifluoromethylphenyl substituents at position 2. The 4-trifluoromethylphenyl pyrrolidin-2-one **S15** was synthesized following the general procedure developed by us. The multicomponent reaction of 4-trifluoromethylbenzaldehyde with butylamine and diethyl oxalacetate afforded pyrrolidone **S13** (Scheme S3). Subsequent reduction gave lactam **S14** which was finally protected with TMS to give **S15** in 62% overall yield. The condensation of pyrrolidone **S15** with 4-bromobenzonitrile followed by Buchwald-Hartwig amination with 1-aza-18-crown-6 (**S8**) led to the formation of DPP **S17** in 29% yield.

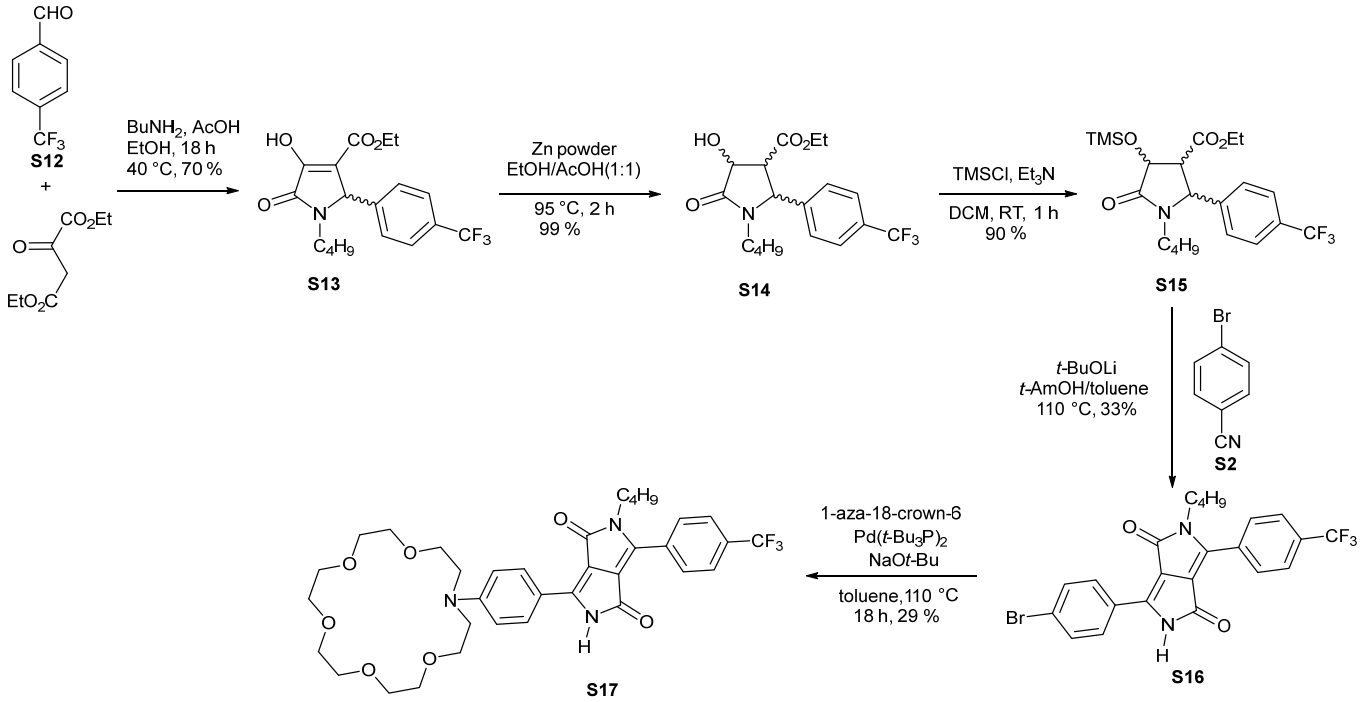

Scheme S3. Synthesis of diketopyrrolopyrrole **17**.

Finally DPP **1** was transformed into DPP **2** possessing a triphenylphosphonium salt using standard procedures (Scheme S4).

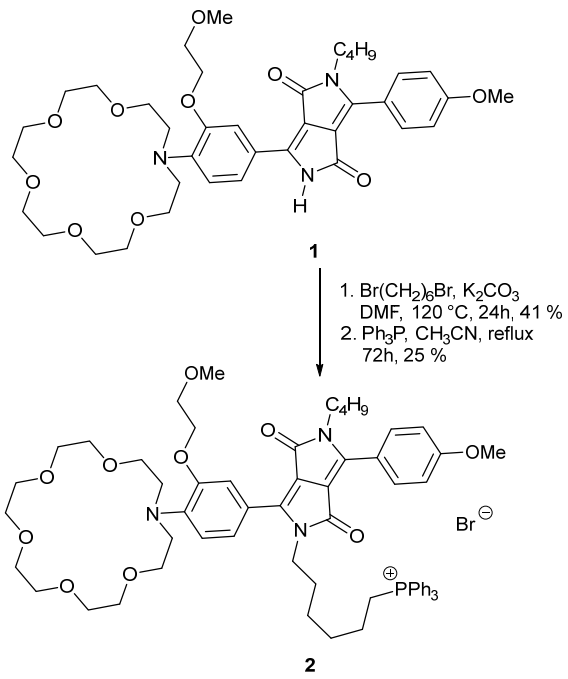

Scheme S4. The transformation of DPP **1** into mitochondrion probe **2**.

Section S3: Experimental Procedure

All reagents and solvents were purchased from commercial sources and were used as received unless otherwise noted. Reagent grade solvents (DCM, hexanes) were distilled prior to use. Transformations with moisture- and oxygen-sensitive compounds were performed under a stream of argon. The reaction progress was monitored by means of thin-layer chromatography (TLC), which was performed on Kieselgel 60. The identity and purity of prepared compounds were proved by 1H NMR and 13C NMR, 19F NMR as well as by mass spectrometry (via EI-MS or ESI-MS). HRMS (ESI-TOF) and HRMS (EI): double-focusing magnetic sector instruments with EBE geometry were utilized. NMR spectra were measured on 400 or 500 or 600 MHz instruments. Chemical shifts (δ, ppm) were determined with tetramethylsilane (TMS) as the internal reference; J values are given in Hz. All melting points for crystalline products were measured with an automated melting point apparatus and are given without correction. Pyrrolidone **S1** was obtained following the literature procedure.[1]

Synthesis of 4-bromo-3-(2-methoxyethoxy)benzonitrile (S4)

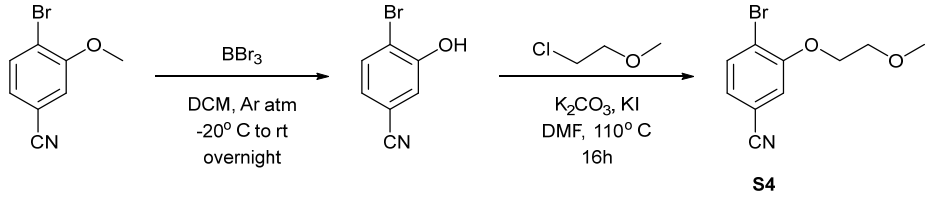

S4

4-bromo-3-hydroxybenzonitrile was synthesized according to following known literature procedure.[2]

A suspension of 4-bromo-3-hydroxybenzonitrile (0.8 g, 4 mmol), chloroethyl methyl ether(0.37mL, 4 mmol), KI (0.33g, 2 mmol) and K_2CO_3 (0.84g, 6 mmol) in 20 mL DMF was heated at 110 °C for 16 h. Then reaction mixture was cooled to room temperature and dissolved in 100 mL ethyl acetate and 50 mL water. Organic phase was separated and washed with 50 mL sat. NaCl, dried over Na_2SO_4. The solvent was evaporated to afford as brown solid in 97 % yield, 1.0 g. m.p. = 184 °C. ^{1}H NMR (500 MHz, $CDCl_3$) δ 7.65 (d, *J* = 8.1 Hz, 1H), 7.14 (m, 2H), 4.21 (t, *J* = 4.9 Hz, 2H), 3.82 (t, *J* = 4.6 Hz, 2H), 3.48(s, 3H). ^{13}C NMR (126 MHz, $CDCl_3$) δ 155.8, 134.3, 125.5, 118.5, 118.1, 116.0, 112.1, 70.6, 69.4, 59.5. HRMS (EI, m/z): [$M^{+\bullet}$] Calcd. for $C_{10}H_{10}BrNO_2$: 254.9895; found, 254.9904.

General procedure for the synthesis of DPP derivatives S5-S7:

In flame dried Schlenk flask, a mixture of appropriate nitrile (1 eq.) and lithium *tert*-butoxide (4 eq.) was heated to 110 °C under argon. To this solid mixture, *tert*-amyl alcohol (5 mL) was added in one portion followed by dropwise addition of pyrrolidone **S1** (1 eq.) dissolved in dry toluene (3 mL). The resulting dark solution was left to stir at this temperature for overnight. After cooling to room temperature reaction mixture was diluted with water (100 mL) and extracted with DCM

(100 mL), water phase was one more time washed with DCM (50 mL). The combined organic phases were dried over Na2SO4, filtered and concentrated in vacuum. The resulting crude compound was chromatographed on silica gel (DCM/MeOH = 9: 1) and crystallization from DCM/n-hexanes allowed to obtain the desired DPP product.

2-Butyl-3-(4-methoxyphenyl)-6-(4-bromophenyl)-2,5-dihydropyrrolo[3,4-*c*]pyrrole-1,4-dione (S5).

4-Bromobenzonitrile (**S2**, 1.0 g, 5.5 mmol), lithium *tert*-butoxide (1.8 g, 22 mmol) and pyrrolidone **S1** (2.2 g, 5.5 mmol) in combined solvent were used to obtain **S5** as red crystals in 48 % yield, 1.2 g. m.p. = 290 °C. ^{1}H NMR (500 MHz, $CDCl_3$) δ 10.68 (s, 1H), 8.15 (d, *J* = 8.0 Hz, 2H), 7.82 (d, *J* = 8.5 Hz, 2H), 7.47 (d, *J* = 8.1 Hz, 2H), 6.95 (d, *J* = 8.5 Hz, 2H), 3.92 (s, 3H), 3.78 (t, *J* = 7.6 Hz, 2H), 1.65 (quint, *J* = 7.1 Hz, 2H), 1.32 (m, 2H), 0.90 (t, *J* = 7.3 Hz, 3H). ^{13}C NMR (126 MHz, $CDCl_3$) δ 163.5, 162.7, 162.1, 148.9, 142.6, 132.1, 131.0, 129.4, 126.8, 125.8, 120.2, 114.1, 55.5, 42.2, 31.5, 20.05, 13.6. HRMS (ESI, m/z): $[M+Na]^+$ Calcd. for $C_{23}H_{21}BrN_2O_3Na$: 475.3360; found, 475.3380.

2-Butyl-3-(4-methoxyphenyl)-6-(4-bromo-3-methoxyphenyl)-2,5-dihydropyrrolo[3,4-*c*]pyrrole-1,4-dione (S6).

4-Bromo-3-methoxybenzonitrile (**S3**, 1.0 g, 4.7 mmol), lithium *tert*-butoxide (1.5 g, 18.8 mmol) and pyrrolidone **S1** (1.92 g, 4.7 mmol) in combined solvent were used to obtain **S6** as orange-red crystals in 45 % yield, 1.0 g. m.p. = 292 °C. ^{1}H NMR (600 MHz, $CDCl_3$) δ 10.87 (s, 1H), 8.07 (s, 1H), 7.80 (d, *J* = 8.8 Hz, 2H), 7.69 (d, *J* = 8.2 Hz, 1H), 7.18 (d, *J* = 7.3 Hz, 1H), 7.08 (d, *J* = 8.8 Hz, 2H), 4.04 (s, 3H), 3.94 (s, 3H), 3.85 (t, *J* = 7.9 Hz, 2H), 1.65 (quint, *J* = 7.5 Hz, 2H), 1.32 (m, 2H), 0.90 (t, *J* = 7.3 Hz, 3H). ^{13}C NMR (150 MHz, $CDCl_3$) δ 163.3, 163.2, 159.9, 159.6, 156.7, 154.0, 134.2, 131.3, 127.3, 119.9, 119.1, 116.9, 115.5, 114.9, 113.6, 111.1, 56.5, 55.6, 42.6, 31.3, 19.8, 13.4. HRMS (ESI, m/z): $[M+Na]^+$ Calcd. For $C_{24}H_{23}BrN_2O_4Na$: 505.0739; found, 505.0726.

2-Butyl-3-(4-methoxyphenyl)-6-(4-bromo-3-methoxyethoxyphenyl)-2,5-dihydropyrrolo[3,4-*c*]pyrrole-1,4-dione (S7).

4-Bromo-3-methoxyethoxybenzonitrile (**S4**, 1.0 g, 3.9 mmol), lithium *tert*-butoxide (1.25 g, 15.6 mmol) and pyrrolidone **S1** (1.6 g, 3.9 mmol) in combined solvent were used to obtain **S7** as orange-red crystals in 70 % yield, 1.4 g. m.p. = 284 °C. ^{1}H NMR (600 MHz, $CDCl_3$) δ 8.12 (s, 1H), 7.80 (d, *J* = 9.0 Hz, 2H), 7.69 (d, *J* = 8.2 Hz, 1H), 7.38 (d, *J* = 9.9 Hz, 1H), 7.08 (d, *J* = 8.8 Hz, 2H), 4.40 (t, *J* = 4.5 Hz, 2H), 4.02 (t, *J* = 4.4 Hz, 2H), 3.92(s, 3H), 3.86 (t, *J* = 7.8 Hz, 2H), 3.62 (s, 3H), 3.57 (s, 1H), 1.65 (quint, *J* = 7.5 Hz, 2H), 1.32 (m, 2H), 0.90 (t, *J* = 7.4 Hz, 3H). ^{13}C NMR (150 MHz, $CDCl_3$) δ 163.3, 159.9, 159.7, 155.7, 153.7, 134.3, 131.3, 127.3, 119.9, 119.2, 117.0, 115.5, 114.8, 113.6, 112.1, 108.8, 70.7, 68.4, 59.3, 55.6, 42.5, 31.3, 19.8, 13.4. HRMS (ESI, m/z): $[M+H]^+$ Calcd. for $C_{26}H_{26}BrN_2O_5$: 525.1025; found, 525.1008.

2-Butyl-3-(4-trifluoromethylphenyl)-6-(4-bromophenyl)-2,5-dihydropyrrolo[3,4-*c*]pyrrole-1, 4-dione (S16).

4-Bromobenzonitrile (**S2**, 1.0 g, 5.5 mmol), lithium *tert*-butoxide (1.75 g, 22 mmol) and pyrrolidone **S15** (2.5 g, 5.5 mmol) in combined solvent were used to obtain **S16** as red crystals in 33 % yield, 900 mg. m.p. = 283 ˚C. ^{1}H NMR (500 MHz, $CDCl_3$) δ 9.27 (s, 1H), 8.16 (d, *J* = 8.7 Hz, 2H), 7.92 (d, *J* = 8.1 Hz, 2H), 7.82 (d, *J* = 8.4 Hz, 2H), 7.64 (d, *J* = 8.7 Hz, 2H), 3.82 (t, *J* = 7.7 Hz, 2H), 1.60 (quint, *J* = 7.6 Hz, 2H), 1.28 (m, 2H), 0.88 (t, *J* = 7.4 Hz, 3H). ^{13}C NMR (126 MHz, CDCl3) δ 162.7, 162.2, 146.2, 144.5, 132.6, 131.3, 129.2, 129.1, 129.0, 127.2, 126.1, 125.9, 125.9, 111.7, 110.0, 42.0, 31.6, 20.0, 13.6. HRMS (ESI, m/z): $[M+H]^+$ Calcd. for $C_{23}H_{17}BrF_3N_2O_2$: 489.0426; found, 489.0413.

General procedure for Buchwald-Hartwig amination of DPP derivatives S9-S11 and 1:

A mixture of appropriate DPP (1 eq.), 1-aza-18-crown-6 (2 eq.), sodium *tert*-butoxide (4 eq.) and bis(tri-*tert*-butylphosphine)palladium(0) (0.05 eq.) were placed in a dried Schenk flask under argon atmosphere followed by 10 mL dry toluene were added. The reaction mixture was stirred at 110 ˚C for 18 h. After cooling to room temperature, reaction mixture was diluted with water (100 mL) and extracted with DCM (100 mL), aqueous phase was one more time washed with DCM (50 mL). The combined organic phases were dried over Na_2SO_4, filtered and concentrated in vacuum. The crude product was purified by column chromatography over silica gel using a step gradient of MeOH in DCM as eluent (from 0% to 10%). Crystallization from DCM/hexanes allowed to obtain desired product.

2-Butyl-3-(4-methoxyphenyl)-6-(1,4,7,10,13-pentaoxa-16-azacyclooctadecane,16-(4-phenyl)-2,5-dihydropyrrolo[3,4-*c*]pyrrole-1, 4-dione (S9).

DPP (**S5**, 0.25 g, 0.55 mmol), 1-aza-18-crown-6 (**S8**, 0.29 g, 1.1 mmol), sodium *tert*-butoxide (0.21 g, 2.2 mmol), and bis(tri-*tert*-butylphosphine)palladium(0) (15 mg, 0.05 mmol) in 10 mL of dry toluene were used to obtain product **S9** as a red crystals in 23 % yield, 80 mg. m.p. = 208 ˚C. ^{1}H NMR (500 MHz, $CDCl_3$) δ 9.35 (s, 1H), 8.27 (d, *J* =7.8 Hz, 2H), 7.8 (s, 2H), 7.03 (d, *J* = 8.6 Hz, 2H), 6.80 (s, 2H), 3.87 (s, 3H), 3.73-3.65 (m, 26H), 1.63 (quint, *J* =7.3 Hz, 2H), 1.3 (m, 2H), 0.88 (t, *J* = 7.3 Hz, 3H). ^{13}C NMR (126 MHz, $CDCl_3$) δ 163.7, 162.4, 161.3, 161.2, 150.8, 145.2, 144.4, 144.3, 130.5, 130.2, 121.2, 115.3, 114.2, 111.6, 110.0, 106.5, 70.9, 70.8, 70.7, 68.5, 55.4, 51.5, 41.9, 31.7, 20.0, 13.7. HRMS (ESI, m/z): $[M+Na]^+$ Calcd. for $C_{35}H_{45}N_3O_8Na$: 658.3104; found, 658.3085.

2-Butyl-3-(4-methoxyphenyl)-6-(1,4,7,10,13-pentaoxa-16-azacyclooctadecane,16-(2-methoxyphenyl-4-yl)-2,5-dihydropyrrolo[3,4-*c*]pyrrole-1, 4-dione (S10).

DPP (**S6**, 0.25 g, 0.51 mmol), 1-aza-18-crown-6 (**S8**, 0.22 g, 1.03 mmol), sodium *tert*-butoxide (0.16 g, 2.06 mmol), and bis(tri-*tert*-butylphosphine)palladium(0) (20 mg, 0.05 mmol) in 10 mL of dry toluene were used to obtain **S10** as red crystals in 15 % yield, 50 mg. m.p. = 188 ˚C. ^{1}H NMR (500 MHz, $CDCl_3$) δ 9.46 (s, 1H), 8.17 (s, 1H), 7.79 (d, *J* =8.2 Hz, 2H), 7.7 (s, 1H), 7.05 (d, *J* = 8.6 Hz, 2H), 6.99 (s, 1H), 3.89 (s, 6H), 3.7-3.61 (m, 26H), 1.63 (quint, *J* =7.0 Hz, 2H), 1.3 (m, 2H), 0.88 (t, *J* = 7.4 Hz, 3H). ^{13}C NMR (126 MHz, $CDCl_3$) δ 163.7, 162.6, 161.5, 151.0, 145.6, 144.8, 143.7, 130.5,

121.0, 117.7, 114.3, 112.0, 110.1, 70.7, 70.2, 69.9, 69.2, 55.9, 52.6, 41.8, 31.6, 20.0, 13.7. HRMS (EI, m/z): [$M^{+\bullet}$] Calcd. for $C_{36}H_{47}N_3O_9$: 665.3312; found, 665.3304.

2-Butyl-3-(4-methoxyphenyl)-6-(1,4,7,10-tetraoxa-13-azacyclopentadecane,16-(2-methoxyphenyl-4-yl)-2,5-dihydropyrrolo[3,4-*c*]pyrrole-1, 4-dione (S11).

DPP (**S6**, 0.25 g, 5.1 mmol), 1-aza-15-crown-5 (0.23 g, 10.3 mmol), sodium *tert*-butoxide (0.2 g, 20.4 mmol), and bis(tri-*tert*-butylphosphine)palladium(0) (15 mg, 0.05 mmol) in 10 mL of dry toluene were used to obtain **S11** as red crystals in 50 % yield, 160 mg. m.p. = 210 ˚C. ^{1}H NMR (600 MHz, $CDCl_3$) δ 9.82 (s, 1H), 8.17 (s, 1H), 7.79 (s, 1H), 7.77 (d, *J* = 8.3 Hz, 2H), 7.03 (d, *J* = 8.6 Hz, 2H), 6.99 (d, *J* = 8.2 Hz, 1H), 3.92 (m, 6H), 3.89-3.80 (s, 6H), 3.73-3.64 (m, 13H), 3.2 (t, *J* = 8.9 Hz, 2H), 1.61 (quint, *J* = 7.0 Hz, 2H), 1.3 (m, 2H), 0.86 (t, *J* = 7.2 Hz, 3H). ^{13}C NMR (150 MHz, $CDCl_3$) δ 163.9, 162.5, 161.4, 150.7, 145.2, 143.6, 130.5, 130.4, 121.7, 121.1, 119.1, 117.1, 114.2, 112.0, 110.2, 107.4, 71.0, 70.4, 70.0, 69.7, 69.6, 69.1, 65.2, 55.9, 55.4, 53.5, 47.7, 41.7, 31.6, 20.0, 13.6. HRMS (ESI, m/z): $[M+Na]^+$ Calcd. for $C_{34}H_{43}N_3O_8Na$: 644.2948; found, 644.2941.

2-Butyl-3-(4-methoxyphenyl)-6-(1,4,7,10,13-Pentaoxa-16-azacyclooctadecane,16-(2-methoxyethoxyphenyl-4-yl)-2,5-dihydropyrrolo[3,4-*c*]pyrrole-1, 4-dione (1).

DPP (**S7**, 0.5 g, 0.94 mmol), 1-aza-18-crown-6 (**S8**, 0.5 g, 1.9 mmol), sodium *tert*-butoxide (0.37 g, 3.8 mmol), and bis(tri-*tert*-butylphosphine)palladium(0) (25 mg, 0.05 mmol) in 10 mL of dry toluene were used to obtain **1** as red crystals in 18 % yield, 120 mg. m.p. = 182 ˚C. ^{1}H NMR (500 MHz, $CDCl_3$) δ 8.19 (s, 1H), 7.79 (d, *J* = 8.6 Hz, 2H), 7.03 (d, *J* = 8.8 Hz, 4H), 3.82 (t, *J* =7.8 Hz, 2H), 3.68-3.59 (m, 29H), 3.38(s, 6H), 1.63 (quint, *J* =7.2 Hz, 2H), 1.3 (m, 2H), 0.88 (t, *J* = 7.2 Hz, 3H). ^{13}C NMR (126 MHz, $CDCl_3$) δ 163.7, 162.7, 161.6, 149.6, 145.3, 144.8, 130.6, 129.4, 121.7, 121.6, 120.9, 115.6, 114.5, 114.3, 114.1, 113.0, 110.2, 71.1, 70.8, 70.2, 69.6, 69.4, 69.3, 69.2, 69.1, 69.0, 68.9, 67.5, 58.9, 55.5, 52.8, 41.8, 31.6, 20.0, 13.7. HRMS (ESI, m/z): $[M+H]^+$ Calcd. for $C_{38}H_{52}N_3O_{10}$: 710.3653; found, 710.3666.

2-Butyl-3-(4-trifluoromethylphenyl)-6-(1,4,7,10,13-pentaoxa-16-azacyclooctadecane,16-(4-phenyl)-2,5-dihydropyrrolo[3,4-*c*]pyrrole-1,4-dione (S17).

DPP (**S16**, 0.1 g, 0.2 mmol), 1-aza-18-crown-6 (**S8**, 0.11 g, 0.4 mmol), sodium *tert*-butoxide (0.08 g, 0.8 mmol), and bis(tri-*tert*-butylphosphine)palladium(0) (5 mg, 0.05 mmol) in 10 mL of dry toluene were used to obtain **S17** as red crystals in 29 % yield, 50 mg. m.p. = 205 ˚C. ^{1}H NMR (500 MHz, $CDCl_3$) δ 10.05 (s, 1H), 8.32 (s, 2H), 7.92 (d, *J* =8.0 Hz, 2H), 7.75 (d, *J* = 8.5 Hz, 2H), 6.76 (d, *J* = 9.0 Hz, 2H), 3.83 (t, *J* =7.0 Hz, 2H), 3.73-3.65 (m, 24H), 1.63 (quint, *J* = 7.5 Hz, 2H), 1.3 (m, 2H), 0.88 (t, *J* = 7.5 Hz, 3H). ^{13}C NMR (126 MHz, $CDCl_3$) δ 164.3, 161.9, 151.5, 147.6, 141.0, 132.3, 131.5, 131.2, 131.1, 130.9, 130.8, 129.0, 128.9, 128.8, 125.6, 125.5, 125.0, 124.8, 122.8, 114.9, 112.4, 111.8, 111.7, 106.2, 70.8, 70.7, 68.5, 51.5, 41.9, 31.7, 20.0, 13.7. HRMS (ESI, m/z): $[M+Na]^+$ Calcd. for $C_{35}H_{42}F_3N_3O_7Na$: 696.2873; found, 696.2889.

Preparation of mitochondrial probe (2):

A suspension of unsymmetrical DPP **1** (100 mg, 0.14 mmol) and K_2CO_3 (40 mg, 0.28 mmol) in dry DMF (5 mL) was stirred at 120˚C under argon atmosphere for 5 min. Then 1, 6-dibromohexane (0.22 mL, 1.4 mmol) was added and the mixture was stirred at 120 ˚C under argon for 24 h. Thereafter, the mixture was cooled down to room temperature and water (50 mL) was added. The product was extracted with DCM three times. The combined organic layers were dried over anhydrous Na_2SO_4, filtered and the solvent was evaporated under reduced pressure. The product was purified by column chromatography over silica gel using a step gradient of MeOH in DCM as eluent (from 0% to 10%). Compound was obtained as an orange red semi solid in 41% yield, 50 mg. HRMS (ESI, m/z): $[M+Na]^+$ Calcd.for $C_{44}H_{62}BrN_3O_{10}Na$: 894.3516; found, 894.3496.

Alkylated crude compound of **1** (50 mg, 0.06 mmol) and triphenylphosphine (0.15 g, 0.57 mmol) were added into a flask containing 5 mL of acetonitrile. The mixture was refluxed for 72 h. After removal of solvent in vacuo, the remaining solid was purified by column chromatography with gradient solvent from CH_2Cl_2 to CH_2Cl_2/MeOH (v/v = 9/1). Compound **2** was obtained as orange-red crystals by recrystallization from diethyl ether in 25% yield, 15 mg. m.p. = 94 ˚C. ^{1}H NMR (600 MHz, CD_3CN): δ 7.86-7.62 (m, 15H), 7.46 (dd, *J* = 6.6 Hz, 2H), 7.24 (dd, *J* = 8.4 Hz, 2H), 7.09 (d, *J* = 9.0 Hz, 1H), 6.99 (d, *J* = 8.4 Hz, 2H), 4.01 (t, *J* = 6.6 Hz, 2H), 3.85-3.40 (m, 28H), 2.81 (t, *J* = 7.8 Hz, 2H), 2.54 (t, *J* = 7.2 Hz, 2H), 1.39-1.27 (m, 19H), 0.88 (t, *J* = 6.6 Hz, 3H). ^{13}C NMR (126 MHz, $CDCl_3$) δ 173.8, 163.4, 162.9, 153.0, 148.7, 139.6, 138.2, 136.1, 135.8, 134.7, 134.6, 133.2, 132.9, 131.7, 131.2, 130.6, 125.8, 125.1, 119.8, 116.2, 115.2, 114.8, 70.5, 70.1, 65.1, 59.3, 56.3, 42.1, 36.9, 35.6, 35.2, 35.1, 34.4, 32.6, 32.1, 31.8, 31.6, 30.6, 30.5, 30.3, 30.2, 30.1, 29.9, 29.6, 29.4, 26.6, 26.3, 23.4, 22.7, 22.3, 20.5, 14.4, 13.9.; HRMS (ESI, m/z): $[M+H]^+$ Calcd. for $C_{62}H_{78}N_3O_{10}P^+$: 1055.5425; found, 1055.5405.

Ethyl-1-butyl-4-hydroxy-5-oxo-2-(4-Trifluoromethylphenyl)-2,5-dihydro-1H-pyrrole-3-carboxylate (S13).

A 250 mL round-bottom flask equipped with a magnetic stirring bar, was charged with ethanol (100 mL), 4-trifluoromethyl benzaldehyde **S12** (7.3 mL, 53 mmol) and *n*-butylamine (5.25 mL, 53 mmol), reaction mixture was kept at room temperature, with constant stirring for 15 minutes. Next diethyl oxalacetate (10.0 g, 53 mmol) was added in one portion, followed by dropwise addition of acetic acid (6.1 mL, 106 mmol). Reaction mixture was heat up to 40 ˚C, and vigorously stirred overnight. Then reaction mixture was cooled to room temperature and diluted with water (200 mL), and extracted with DCM (200mL×2). Organic phase was dried over anhydrous Na_2SO_4, filtered and concentrated in vacuo. Yellowish solid was recrystallized from EtOAc to obtain product **S13** as white crystals 70 %, 14.0 g. m.p. = 198-199 ˚C. ^{1}H NMR (600 MHz, $CDCl_3$) δ 9.02 (s, 1H), 7.61 (d, *J* = 8.2 Hz, 2H), 7.30 (d, *J* = 8.0 Hz, 2H), 5.14 (s, 1H), 4.13 (q, *J* = 7.1 Hz, 2H), 3.78 (m, 1H), 2.63 (m, 1H), 1.48 – 1.41 (m, 2H), 1.28 – 1.22 (m, 2H), 1.12 (t, *J* = 7.1 Hz, 3H), 0.86 (t, *J* = 7.4 Hz, 3H); ^{13}C NMR (151 MHz, $CDCl_3$) δ 164.8, 163.6, 157.7, 139.3, 131.2, 128.1, 125.8, 122.9, 112.4, 61.2, 60.0, 40.3, 30.3, 19.9, 13.9, 13.6. ^{19}F NMR (470 MHz, $CDCl_3$) δ -62.71. HRMS (ESI, m/z): $[M+Na]^+$ Calcd. for $C_{18}H_{20}F_3NO_4Na$: 394.3562; found, 394.3520.

Ethyl-1-butyl-4-hydroxy-2-(4-Trifluoromethylphenyl)-5-oxopyrrolidine-3-carboxylate (S14).

Compound **S13** (14.0 g, 37.7 mmol) was dissolved in 150 mL mixture of EtOH/AcOH (1:1) and zinc powder (15.0 g, 226.2 mmol) was added and reaction mixture vigorously stirred at 95 °C for 1h. A second portion of zinc powder (15.0 g, 226.2 mmol) was added and stirring was continued at 95 °C until completion of the reaction. After cooling to room temperature reaction mixture was diluted with EtOAc (100 mL) the excess of zinc and the inorganic salts were filtered off. The filtrate was then diluted with water (150 mL). The aqueous layer was extracted with EtOAc (100 mL), and the combined organic phases were washed with saturated $NaHCO_3$ solution until neutral and finally dried over Na_2SO_4, filtered and concentrated in vacuo to obtain liquid product **S14** as mixture of diastereoisomers in 85% yield, 11.9 g. Careful analysis of ^{1}H NMR spectra of crude **S14** showed the ratio 2:1 of major isomer **S14** with the all-trans configuration in relation to the rest three minor compounds.

Crude compound (11.9 g, 31.9 mmol) was dissolved in dry EtOH (75 mL), freshly powdered K_2CO_3 (11.2 g, 68.5 mmol) was added in one portion. Reaction mixture was stirred at room temperature for 30 minutes. Next reaction mixture was diluted with EtOAc (100 mL) the excess of inorganic salts were filtered off. The filtrate was then washed with water (100 mL x 2), organic phase was dried over Na_2SO_4, filtered and concentrated in vacuum to obtain yellowish liquid product in 99.5 %, 11.8 g. ^{1}H NMR spectra showed 10:1 ratio of major isomer **S14a** with the all-trans configuration in relation to the rest two minor compounds. ^{1}H NMR (500 MHz, $CDCl_3$) δ 7.63 (d, *J* = 8.0 Hz, 2H), 7.44 (d, *J* = 8.0 Hz, 2H), 4.75 (d, *J* = 7.5 Hz, 1H), 4.65 (d, *J* = 8.0 Hz, 1H), 4.15 (m, 2H), 3.7-3.65 (m, 1H), 3.03 (t, *J* = 8.5 Hz, 1H), 2.45 (quint, *J* = 7.5 Hz, 1H), 1.32-1.11 (m, 8H), 0.79 (t, *J* = 7.5 Hz, 3H); ^{13}C NMR (126 MHz, $CDCl_3$) δ 173.6, 171.1, 142.3, 131.1, 129.4, 129.0, 126.1, 125.3, 72.1, 61.6, 55.9, 40.6, 28.5, 19.9, 13.9, 13.6. HRMS (EI, m/z): [$M^{+\bullet}$] Calcd. for $C_{18}H_{22}F_3NO_4$: 373.3722; found, 373.1507.

Ethyl-1-butyl-2-(4-trifluoromethylphenyl)-5-oxo-4-((trimethylsilyl)oxy)pyrrolidine-3-carboxylate (S15).

To cooled to ~0 °C solution of **S14a** (11.8 g, 31.6 mmol) in dry DCM (100 mL), dry Et_3N (8.0 mL, 56.8 mmol) was added, next TMSCl (6.0 mL, 47.4 mmol) was added drop wise. After addition cooling bath was removed, and reaction mixture was allowed to reach room temperature and stirring was continued at room temperature for 1.5 h. Next reaction mixture was diluted with water (100 mL), phases were separated and organic phase was dried over anhydrous Na_2SO_4, filtered and concentrated in vacuo gives 90% yield, 12.8 g of product **S15** without chromatographic purification. ^{1}H NMR spectra showed 10:1 ratio of major isomer **S15** with the all-trans configuration in relation to the rest two minor compounds, used for next reaction without further purification. ^{1}H NMR (500 MHz, $CDCl_3$) δ 7.63 (d, *J* = 8.0 Hz, 2H), 7.40 (d, *J* = 8.0 Hz, 2H), 4.70 (d, *J* = 7.5 Hz, 1H), 4.56 (d, *J* = 8.0 Hz, 1H), 4.16 (m, 2H), 3.69-3.63 (m, 1H), 2.91 (t, *J*

= 7.5 Hz, 1H), 2.52 (m, 1H), 1.39 – 1.31 (m, 4H), 1.24-1.17 (m, 3H), 0.81 (t, *J* = 11.5 Hz, 3H), 0.21 (s, 9H). ^{13}C NMR (101 MHz, $CDCl_3$) δ 171.6, 171.1, 142.5, 131.0, 130.7, 129.3, 127.7, 125.9, 73.1, 61.5, 60.5, 56.6, 45.7, 40.6, 28.6, 19.8, 14.0, 13.6, 0.1. HRMS (EI m/z): [$M^{+\bullet}$] Calcd. for $C_{21}H_{30}F_3NO_4Si$: 445.5542; found, 445.5510.

Section S4: Photophysical studies

The photophysical properties of DPPs **S7**, **S9-S11** and **S17** were studied in toluene and MeCN as prototypical non-polar and polar solvents (Table S1, Figures in ESI). From a structural point of view these DPPs represent D-A-D' systems where the azacrownphenyl is a strongly electron-donating group, the 4-$MeOC_6H_4$ is a weakly electron-donating substituent, and the DPP core is electron-deficient. DPPs **S7**, **S9-S11** and **S17** absorb at approx. 530 nm and emit at 540-580 nm in toluene. There is a small but noticeable hypsochromic shift of absorption in CH_3CN as compared to toluene (506-525 nm). Simultaneously emission shifts bathochromically to ~580 nm. Replacing $MeOC_6H_4$ with 4-$CF_3C_6H_4$ effectively increases the strength of the acceptor in the donor-acceptor system, by going from a quadrupolar-like D-A-D' structure to a dipolar like D-A-A' architecture. This should lead to a bathochromic shift of absorption and emission which is indeed observed experimentally (**S17** vs. **S9**: abs. 540 nm vs. 530 nm, em. 578 nm vs. 555 nm in toluene, Table S1). Solvatochromic trends are the same as for DPPs **S9**-**S11**. Interestingly, adding a triphenylphosphonium moiety strongly affects the photophysical properties shifting absorption hypsochromically and emission bathochromically to 590 nm. At the same time, the emission maxima does not show any solvent polarity effects (Table S1).

In all cases the fluorescence quantum yields are very high (80-90%) and the difference between toluene and CH_3CN is trifling in spite of the nature of the considered transitions. This observation is in strong contrast to solvatochromic behavior of 6-(3,5-bis(trifluoromethyl)phenyl)-2-butyl-3-(4-(dimethylamino)phenyl)-2,5-dihydropyrrolo[3,4-*c*]pyrrole-1,4-dione which showed very bright emission in toluene that almost totally quenched in CH_3CN.

Table 1. Photophysical properties of DPPs in toluene and CH_3CN.

Compound	solvent	$^{max}\lambda_{abs}$ [nm]	$^{max}\lambda_{ems}$ [nm]	Stokes shift [cm^{-1}]	Φ_{fl}[a]
S7	toluene	508	540	1200	0.77
	CH_3CN	498	538	1400	0.66
S9	toluene	529	555	900	0.78
	CH_3CN	525	563	1300	0.87
S10	toluene	528	566	1300	0.88
	CH_3CN	506	581	2500	0.84
S11	toluene	531	564	1100	0.85
	CH_3CN	519	582	2100	0.86
1	toluene	530	569	1300	0.77
	CH_3CN	514	583	2300	0.81
S17	toluene	540	578	1200	0.88
	CH_3CN	530	599	2200	0.87
2	toluene	519	592	2400	0.80
	CH_3CN	499	591	3100	0.48

[a]Determined using Rhodamine 6G in EtOH.

Table S2. Changes of fluorescence of DPPs **S7**, **S9-S11** and **S17** in the presence of 5 eq. KPF_6 and $PhSO_3H$ in CH_3CN.

DPP	KPF_6 (5 eq.)		$PhSO_3H$ (5 eq.)	
	Enhancement of fluorescence	λ_{em} (nm)	Enhancement of fluorescence	λ_{em} (nm)
S7	1.02	536	1.01	537
S9	0.99	564	0.55	550
S10	0.80	536	0.83	550
S11	0.96	582/536	0.65	551
S17	1.02	596	0.49	536

Having the fundamental photophysical properties measured, we moved on to investigation of the influence of both K^+ cations and protonation on the absorption and emission of DPPs **S7**, **S9-S11** and **S17** (Table S2). The influence of KPF_6 addition on the fluorescence of these DPPs strongly depends on the presence of the additional alkoxy substituents. In their absence (DPPs **S9** and **S17**) there is essentially no effect even in the presence of a huge excess of KPF_6 (Fig. S9 & S34). In contrast, for DPP **S10** which bears MeO substituent that assist coordination, the effect is spectacular and the addition of just one equivalent of K^+ shifts emission hypsochromically from 580 to 525 nm (Fig. 3). Decreasing the size of macrocycle to 15-crown-5 (DPP **S11**, too small to accommodate K^+) makes the response a very weak one, and hundreds of equivalents of KPF_6 are necessary to induce comparable changes (Fig. 4). The addition of benzenesulfonic acid yields the same trend, however, there is no difference in strength of the bathochromic shift between

DPPs bearing differently sized crowns (Figs. S3, S5, S10, S13, S16, S19, S21, S26, S30, S33, S35, S38, S40). The presence of auxiliary alkoxy groups does not help in obtaining a more marked response to benzenesulfonic acid either.

Section S5: Absorption and emission spectra

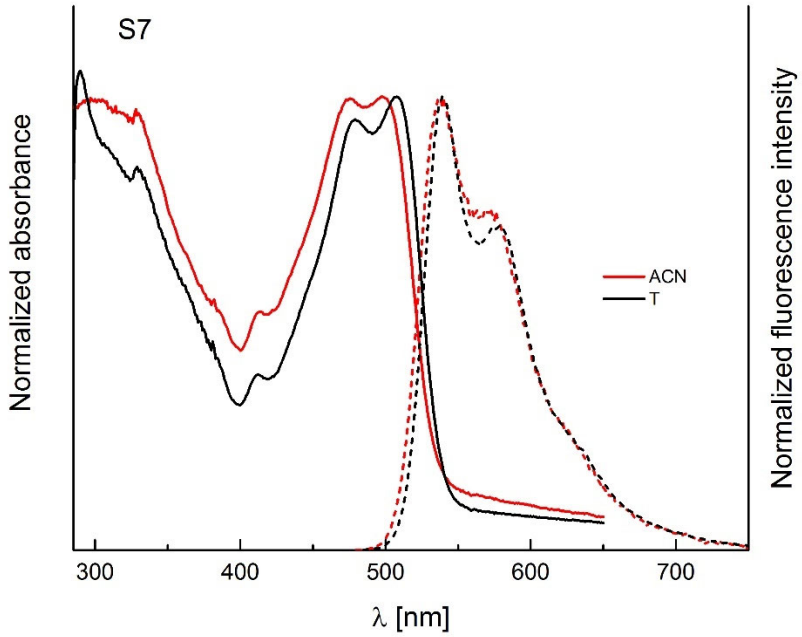

Fig. S1. The absorption and emission spectra of DPP **S7** in acetonitrile and in toluene.

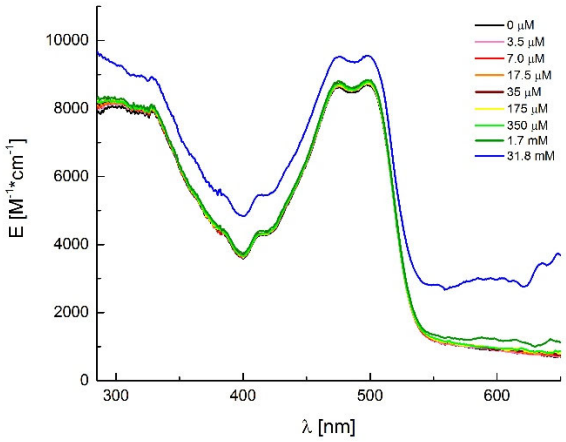

Fig. S2. The effect of KPF_6 addition on the absorption spectra of DPP **S7** measured in CH_3CN.

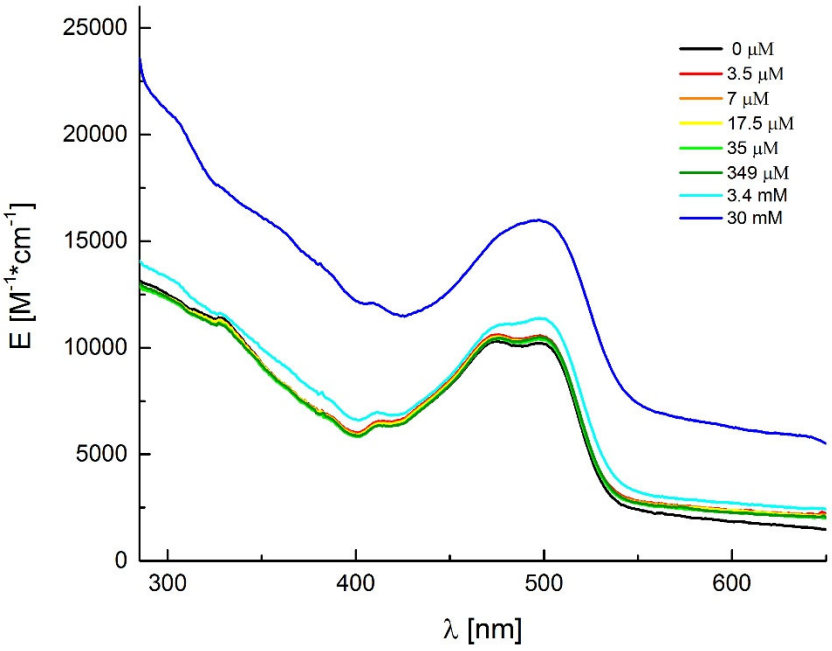

Fig. S3. The effect of BENZENESULFONIC ACID addition on the absorption spectra of DPP **S7** measured in CH_3CN.

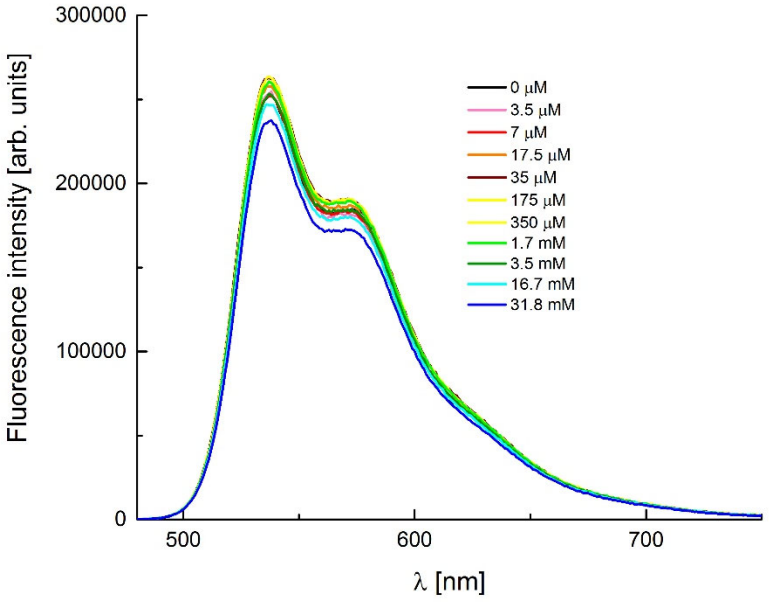

Fig. S4. The effect of KPF_6 addition on the emission spectra of DPP **S7** measured in CH_3CN.

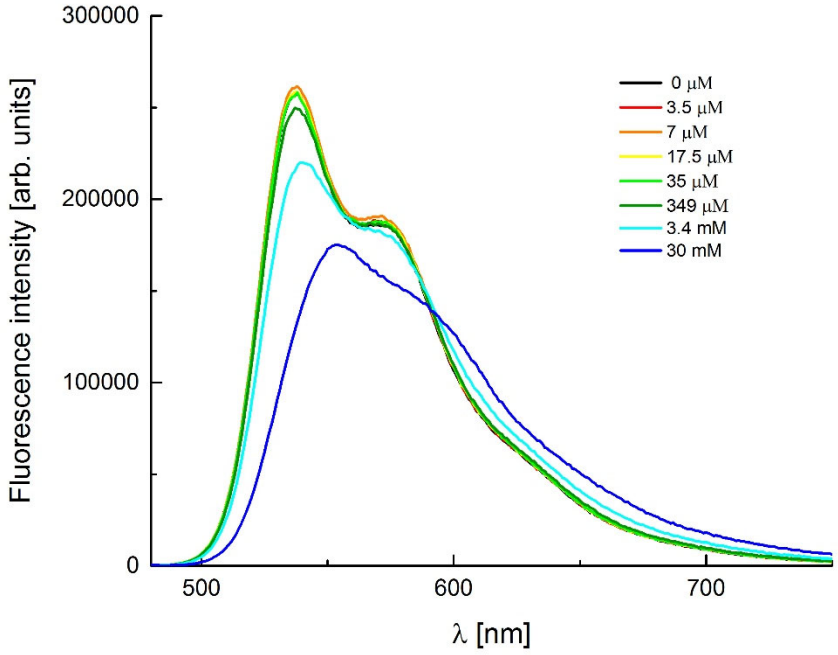

Fig. S5. The effect of BENZENESULFONIC ACID addition on the emission spectra of DPP **S7** measured in CH_3CN.

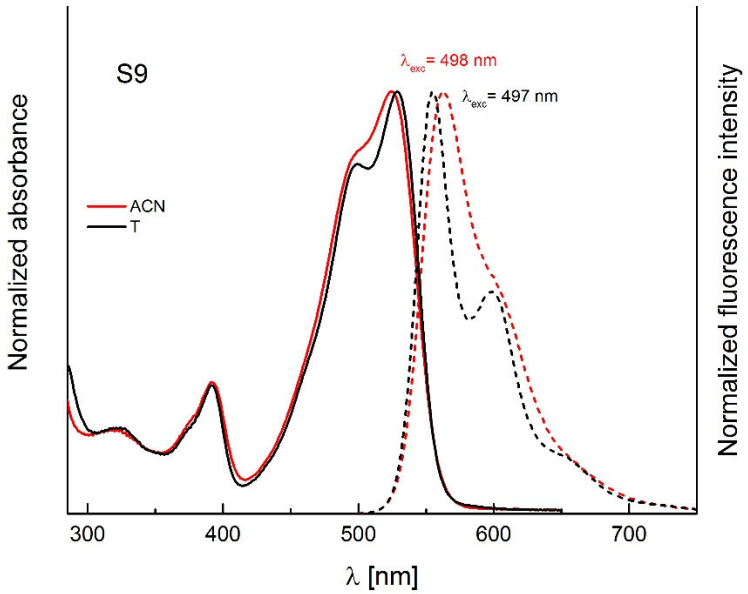

Fig. S6. The absorption and emission spectra of DPP **S9** in acetonitrile and in toluene.

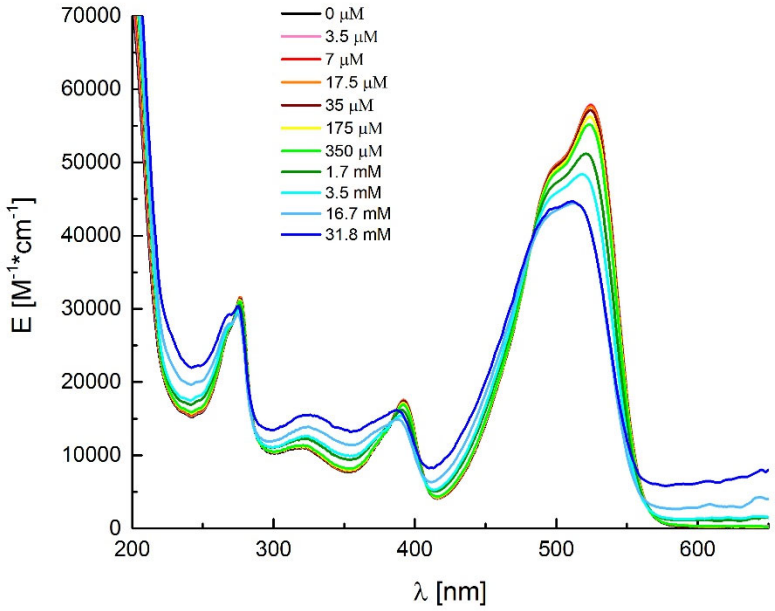

Fig. S7. The effect of KPF_6 addition on the absorption spectra of DPP **S9** measured in CH_3CN.

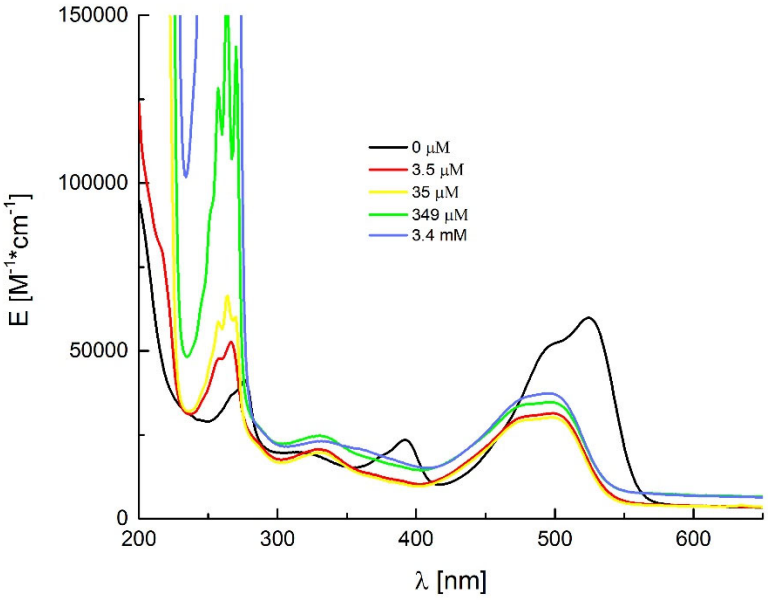

Fig. S8. The effect of BENZENESULFONIC ACID addition on the absorption spectra of DPP **S9** measured in CH_3CN.

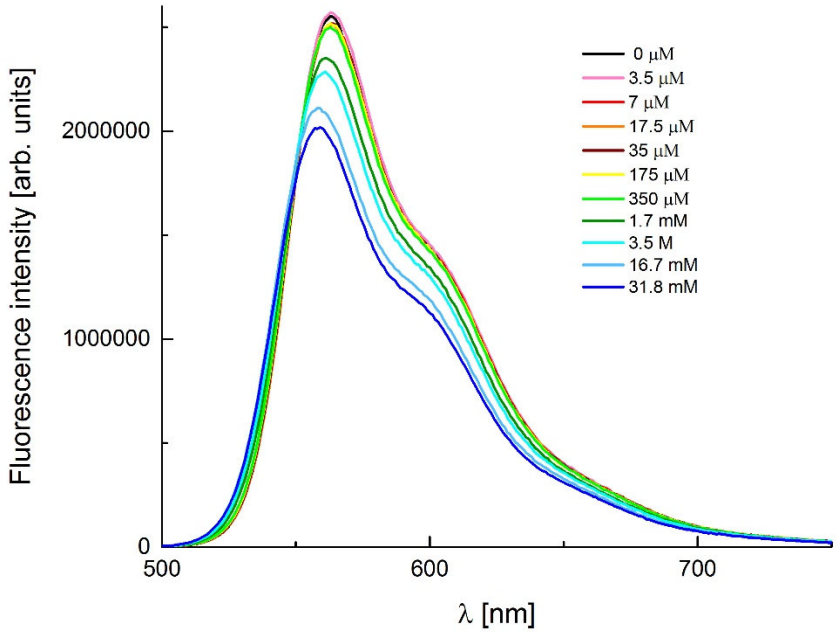

Fig. S9. The effect of KPF_6 addition on the emission spectra of DPP **S9** measured in CH_3CN.

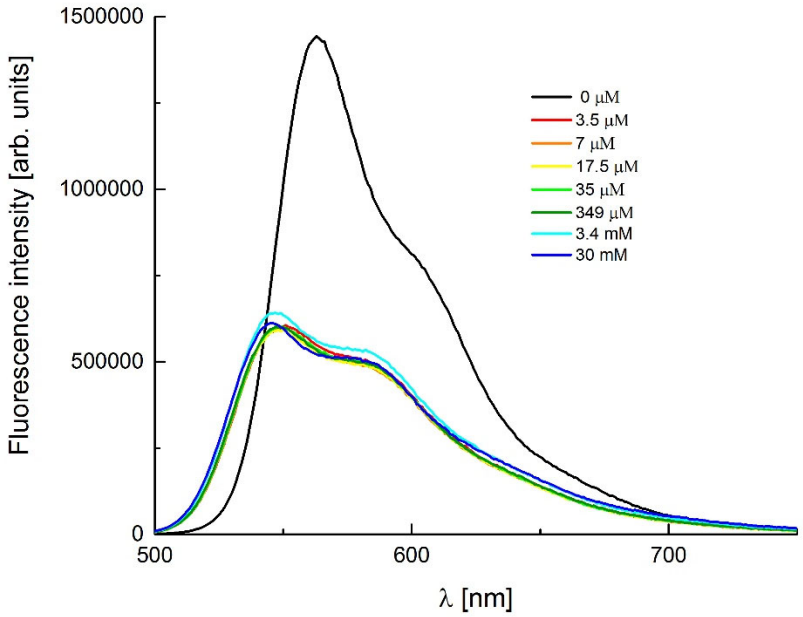

Fig. S10. The effect of BENZENESULFONIC ACID addition on the emission spectra of DPP **S9** measured in CH_3CN.

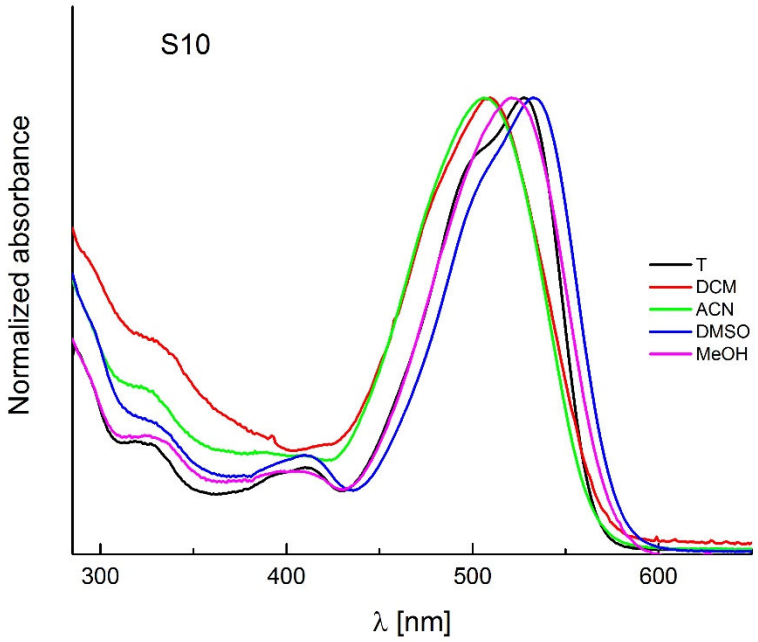

Fig. S11. The absorption and emission spectra of DPP **S10** in various solvents.

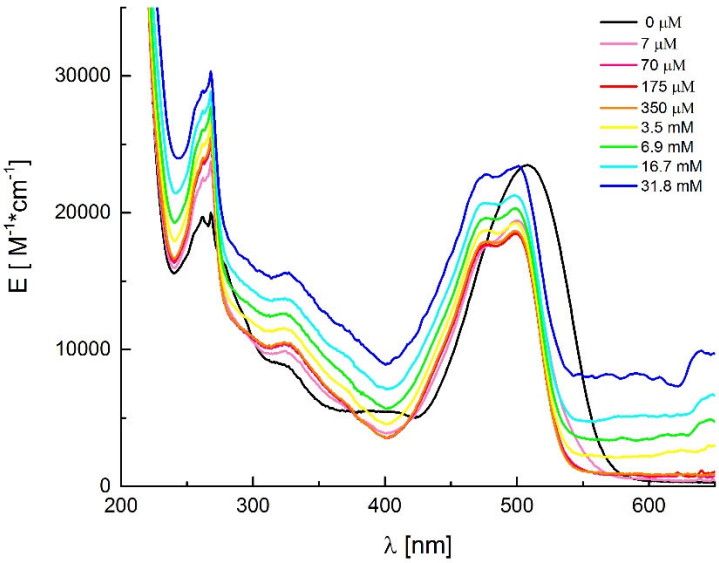

Fig. S12. The effect of KPF_6 addition on the absorption spectra of DPP **S10** measured in CH_3CN.

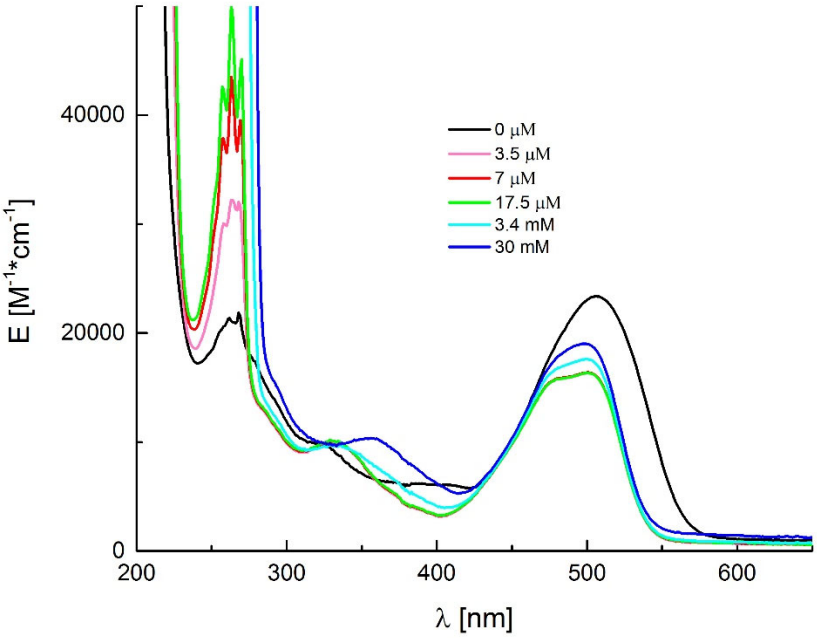

Fig. S13. The effect of BENZENESULFONIC ACID addition on the absorption spectra of DPP **S10** measured in CH_3CN.

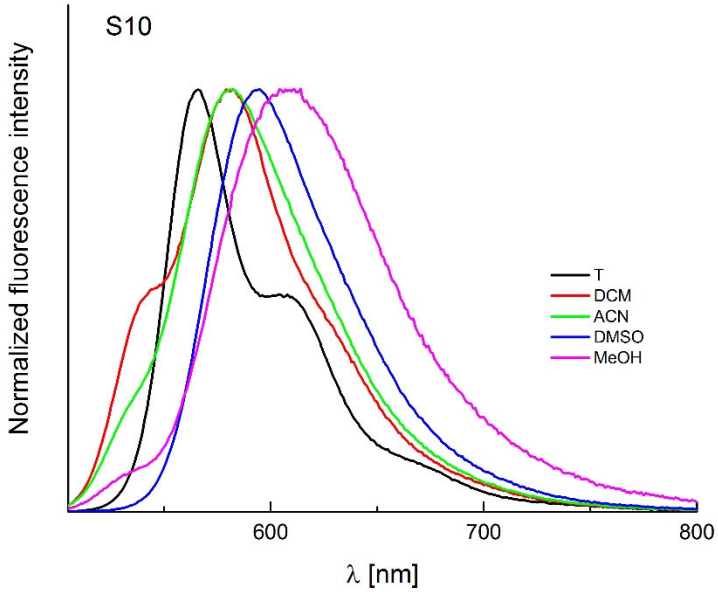

Fig. S14. The emission spectra of DPP **S10** in various solvents.

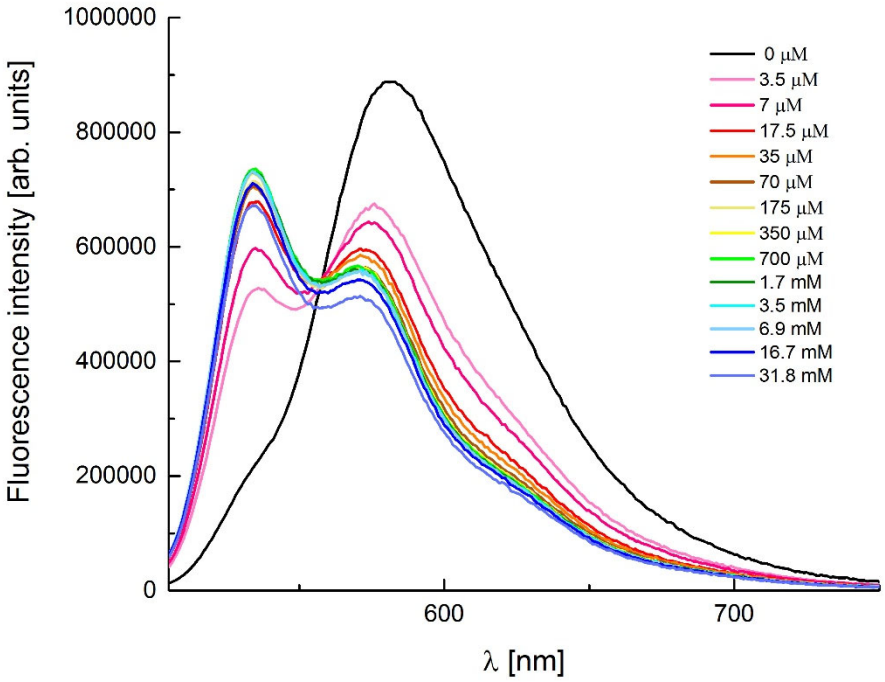

Fig. S15. The effect of KPF_6 addition on the emission spectra of DPP **S10** measured in CH_3CN.

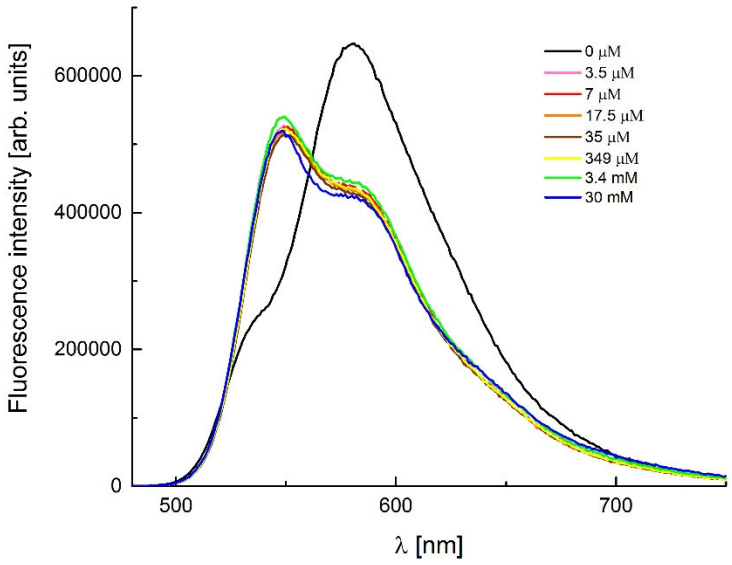

Fig. S16. The effect of BENZENESULFONIC ACID addition on the emission spectra of DPP **S10** measured in CH_3CN.

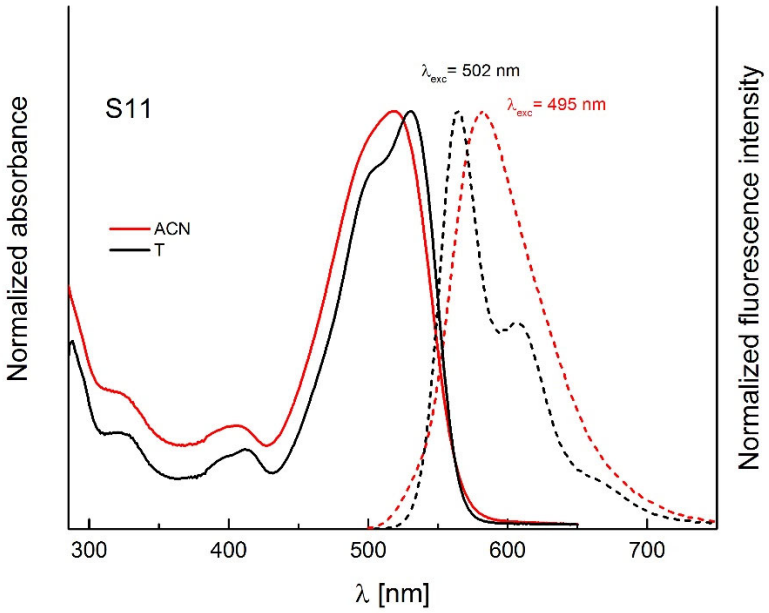

Fig. S17. The absorption and emission spectra of DPP **S11** in acetonitrile and in toluene.

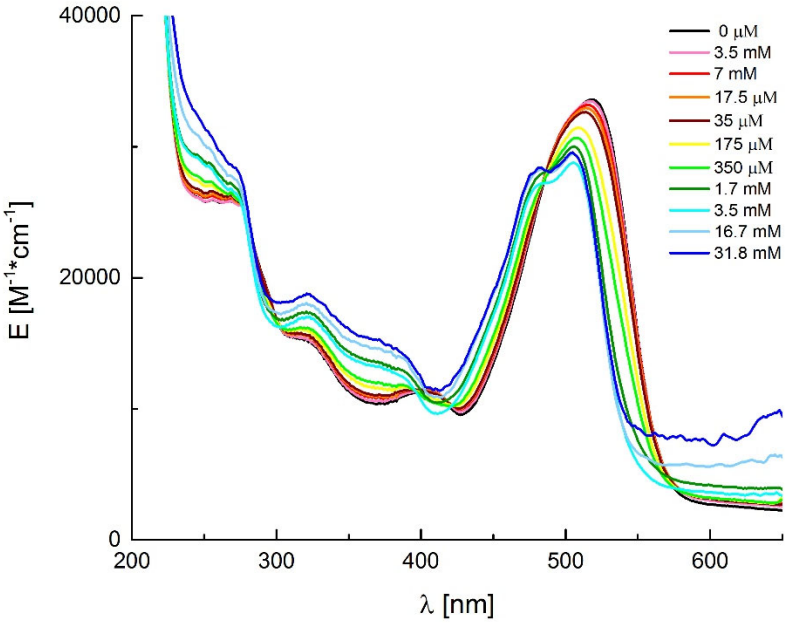

Fig. S18. The effect of KPF_6 addition on the absorption spectra of DPP **S11** measured in CH_3CN.

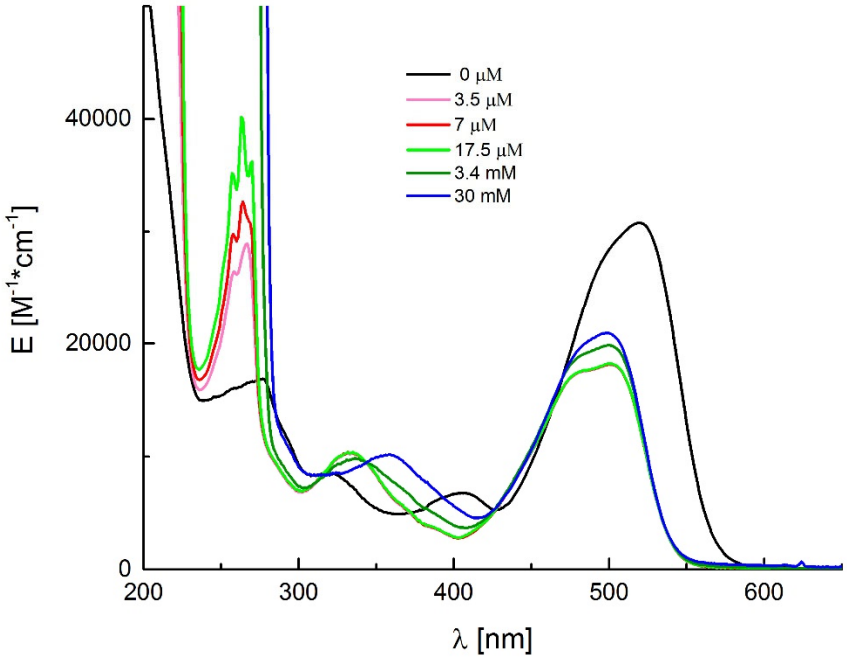

Fig. S19. The effect of BENZENESULFONIC ACID addition on the absorption spectra of DPP **S11** measured in CH_3CN.

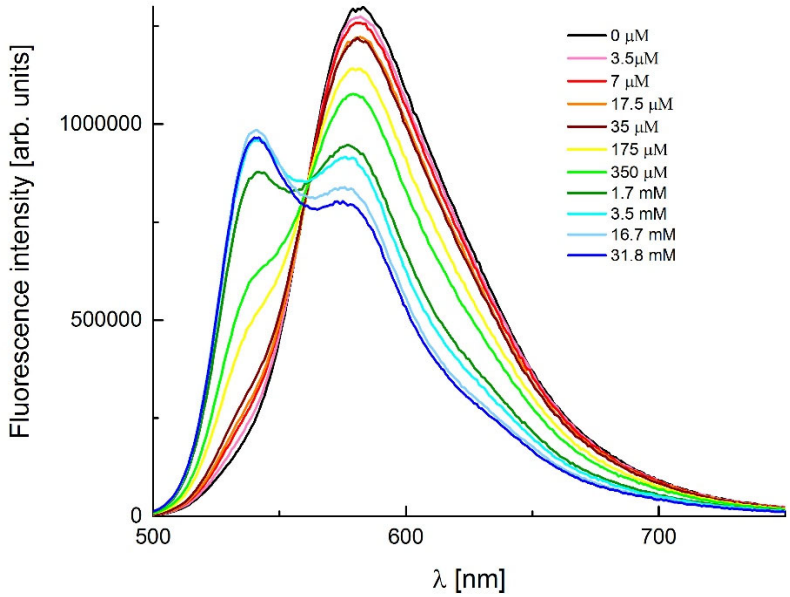

Fig. S20. The effect of KPF_6 addition on the emission spectra of DPP **S11** measured in CH_3CN.

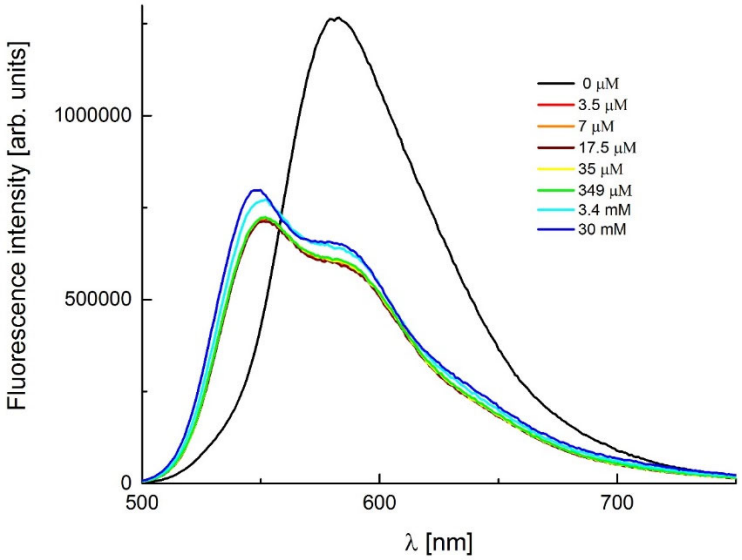

Fig. S21. The effect of BENZENESULFONIC ACID addition on the emission spectra of DPP **S11** measured in CH_3CN.

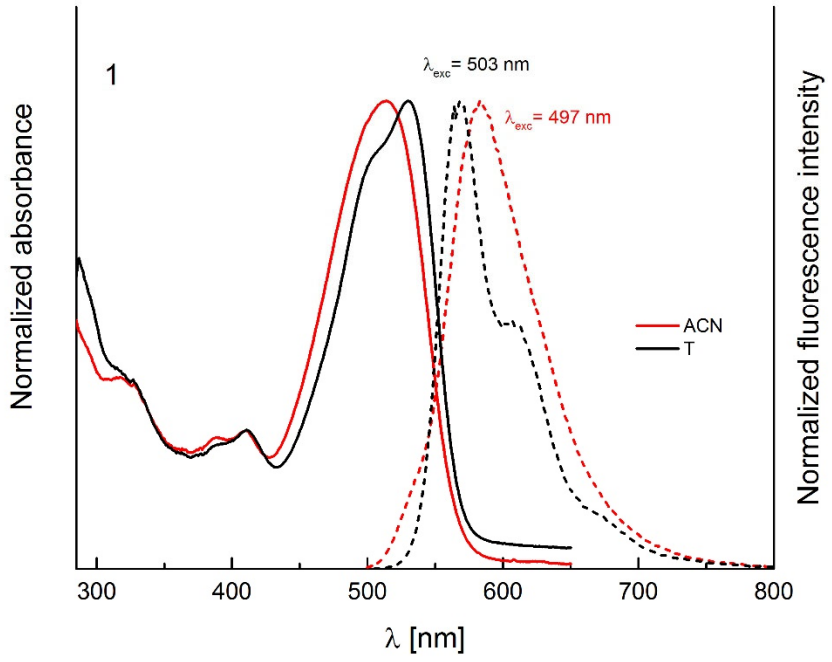

Fig. S22. The absorption and emission spectra of DPP **1** in acetonitrile and in toluene.

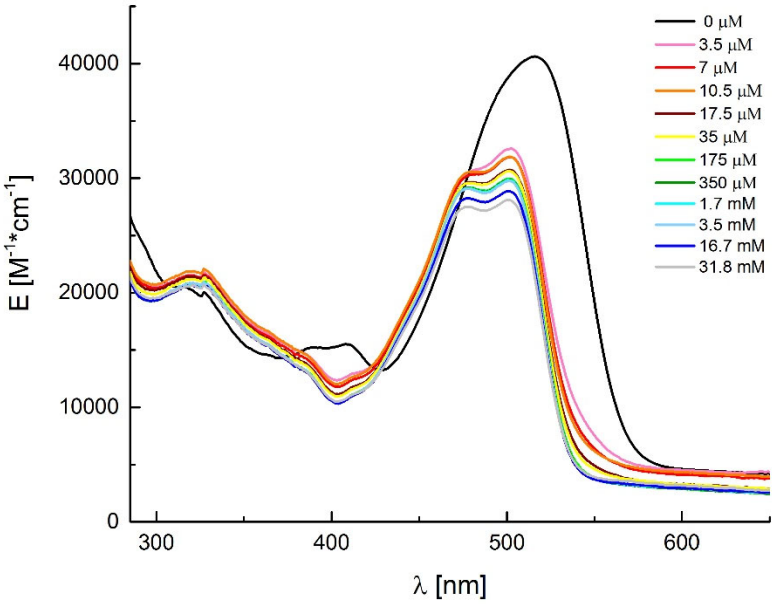

Fig. S23. The effect of KPF_6 addition on the absorption spectra of DPP **1** measured in CH_3CN.

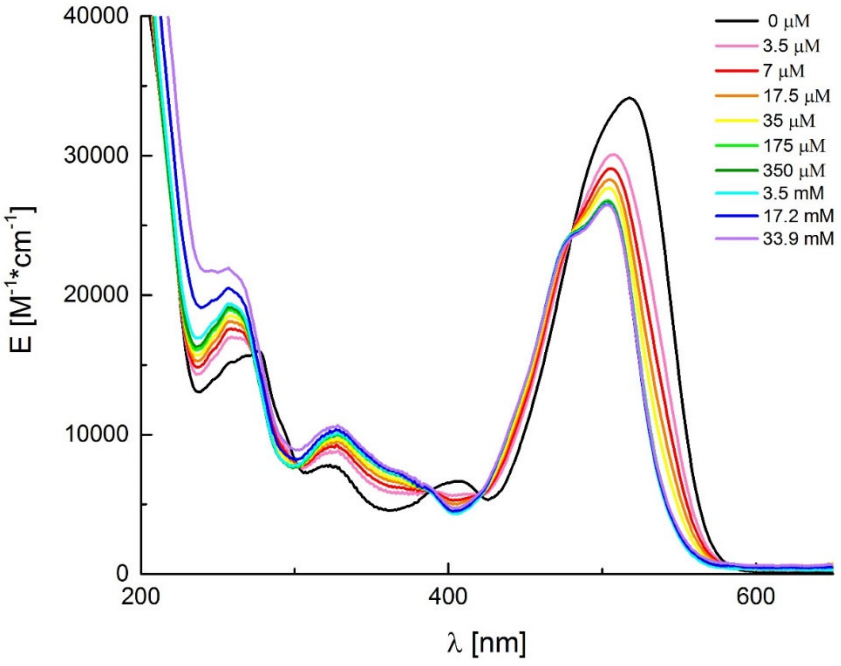

Fig. S24. The effect of sodium perchlorate addition on the absorption spectra of DPP **1** measured in CH_3CN.

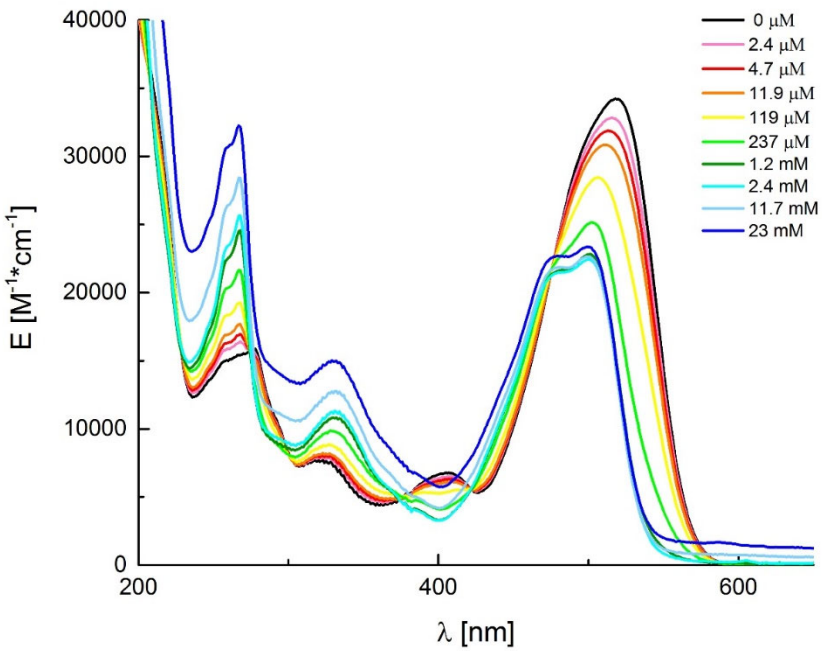

Fig. S25. The effect of magnesium perchlorate addition on the absorption spectra of DPP **1** measured in CH_3CN.

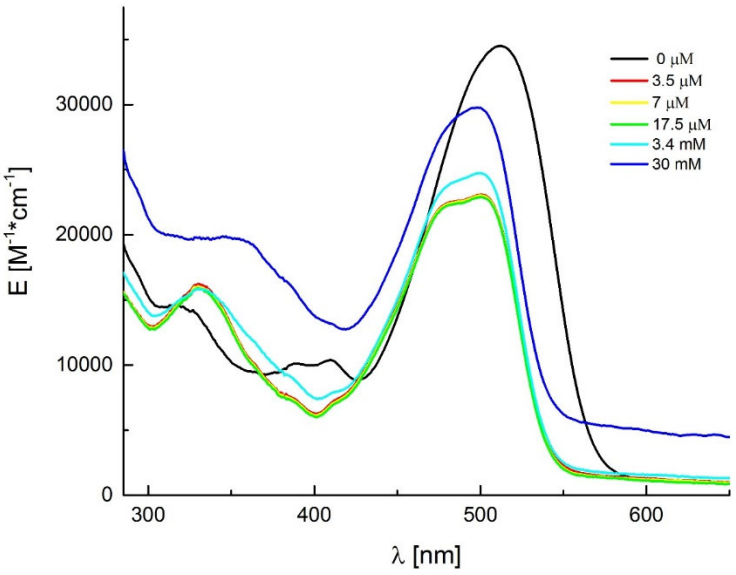

Fig. S26. The effect of benzenesulfonic acid addition on the absorption spectra of DPP **1** measured in CH_3CN.

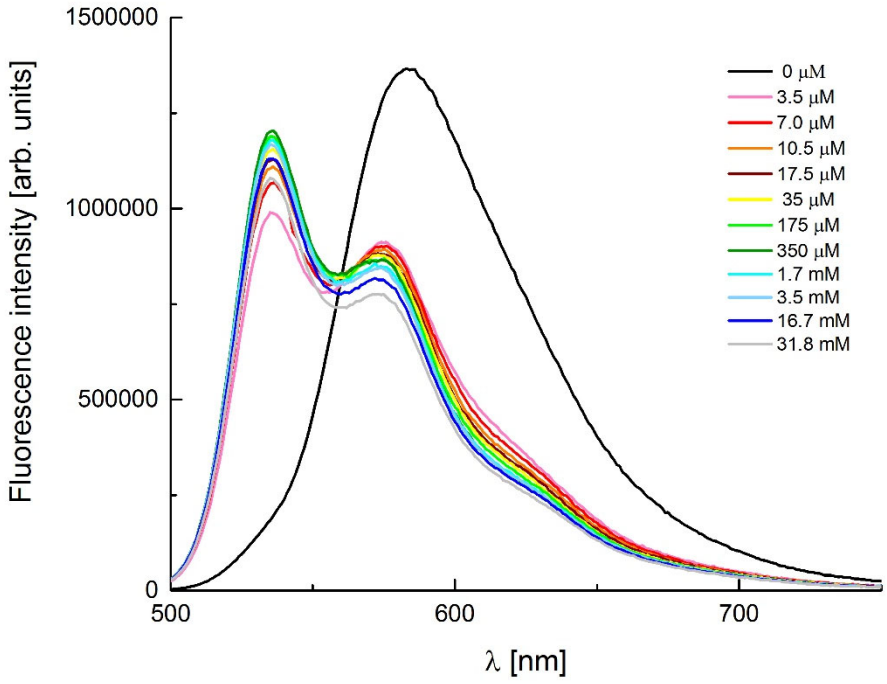

Fig. S27. The effect of KPF_6 addition on the emission spectra of DPP **1** measured in CH_3CN.

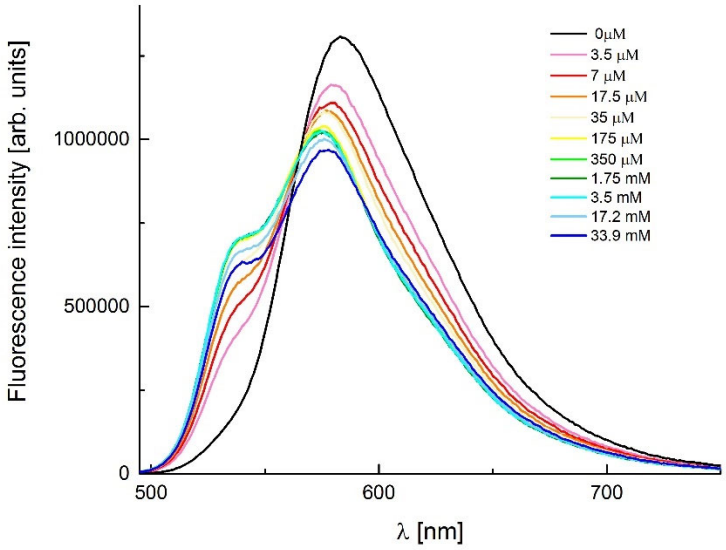

Fig. S28. The effect of sodium perchlorate addition on the emission spectra of DPP **1** measured in CH_3CN.

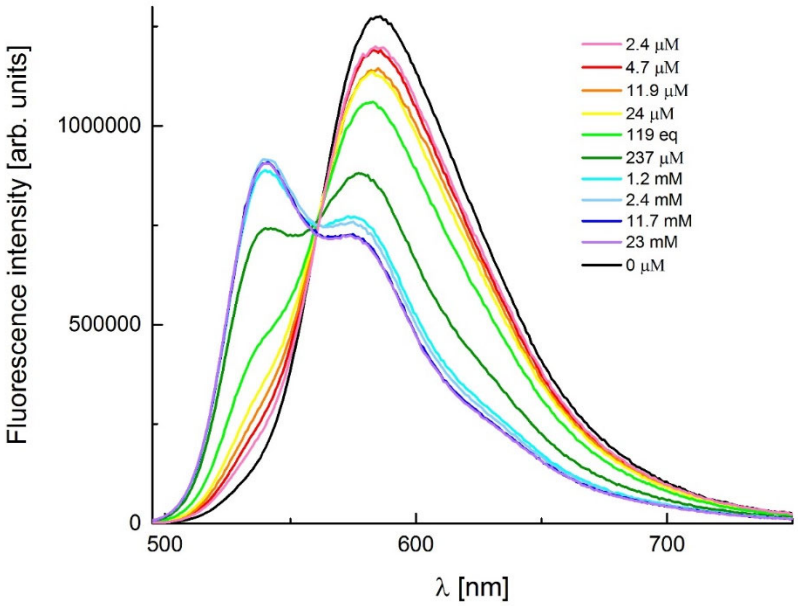

Fig. S29. The effect of magnesium perchlorate addition on the emission spectra of DPP **1** measured in CH_3CN.

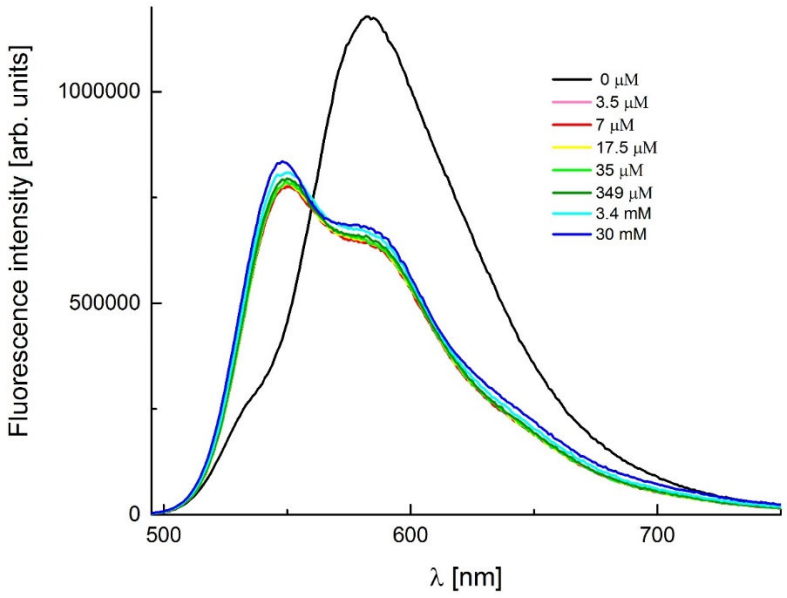

Fig. S30. The effect of BENZENESULFONIC ACID addition on the emission spectra of DPP **1** measured in CH_3CN.

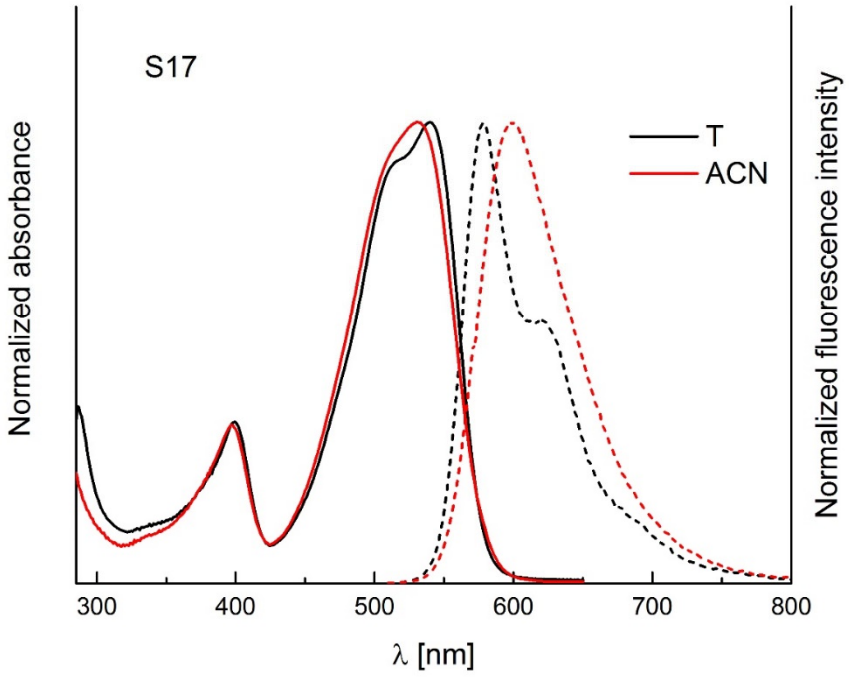

Fig. S31. The absorption and emission spectra of DPP **S17** in acetonitrile and in toluene.

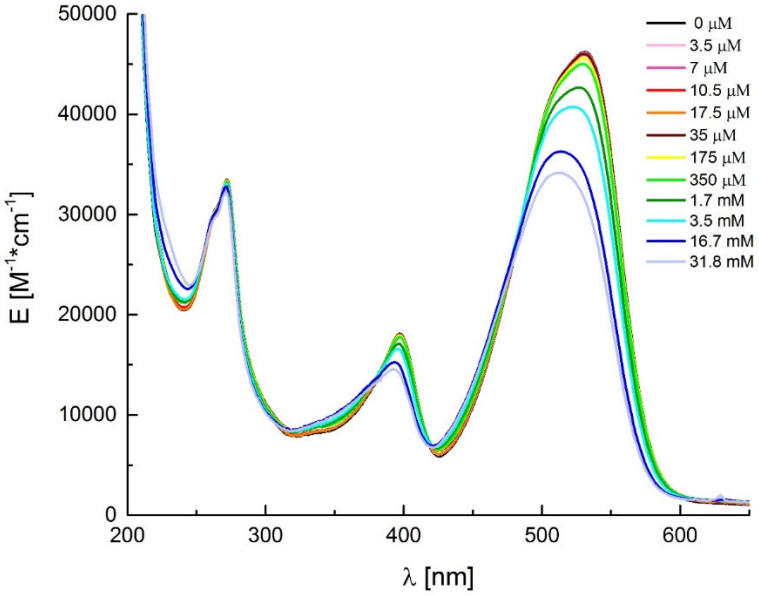

Fig. S32. The effect of KPF_6 addition on the absorption spectra of DPP **S17** measured in CH_3CN.

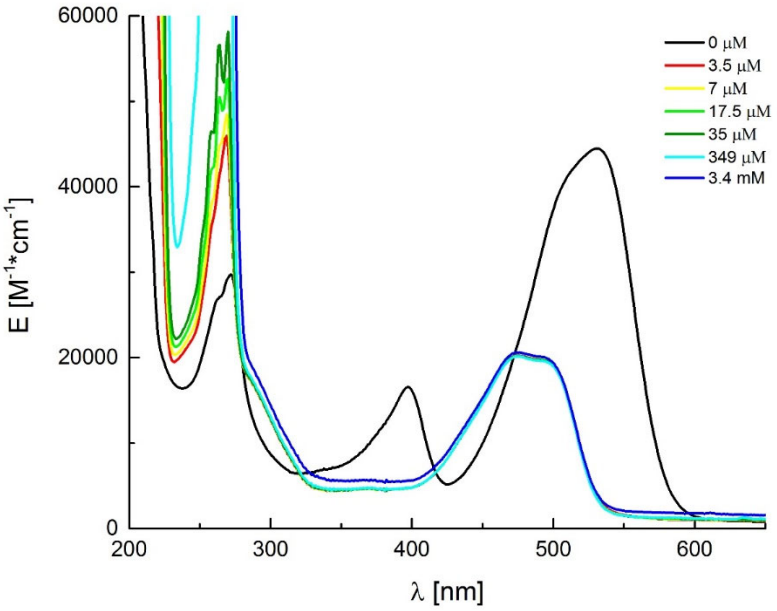

Fig. S33. The effect of BENZENESULFONIC ACID addition on the absorption spectra of DPP **S17** measured in CH_3CN.

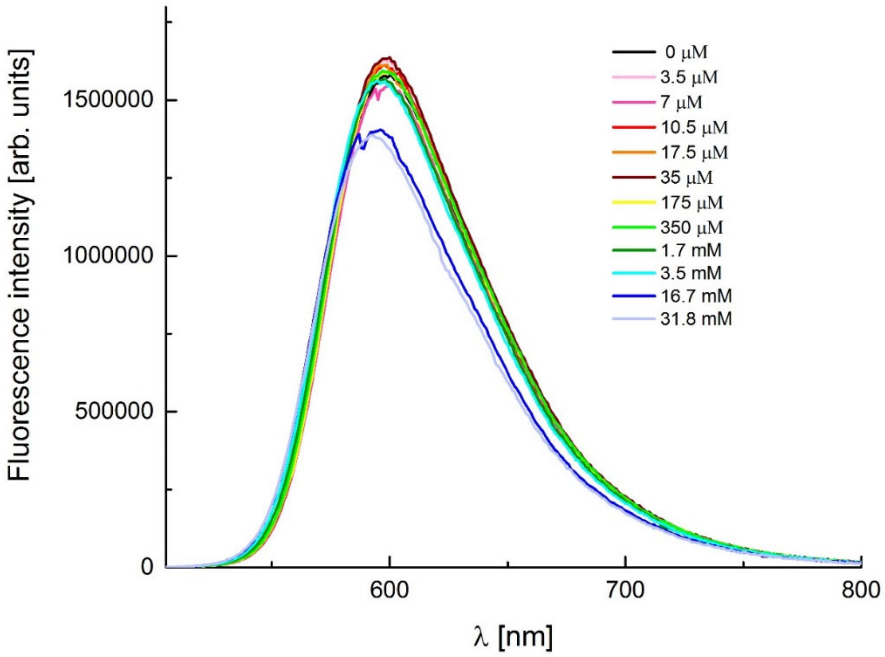

Fig. S34. The effect of KPF_6 addition on the emission spectra of DPP **S17** measured in CH_3CN.

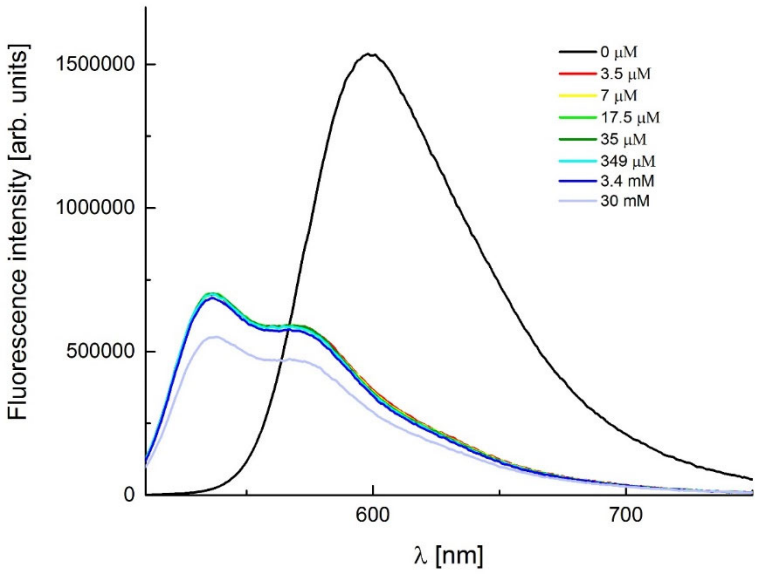

Fig. S35. The effect of BENZENESULFONIC ACID addition on the emission spectra of DPP **S17** measured in CH_3CN.

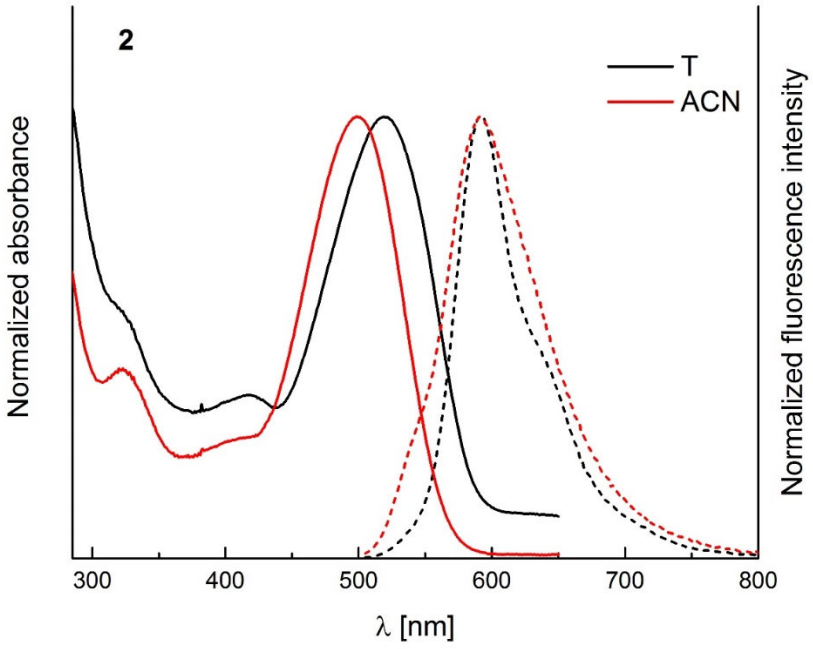

Fig. S36. The absorption and emission spectra of DPP **2** in acetonitrile and in toluene.

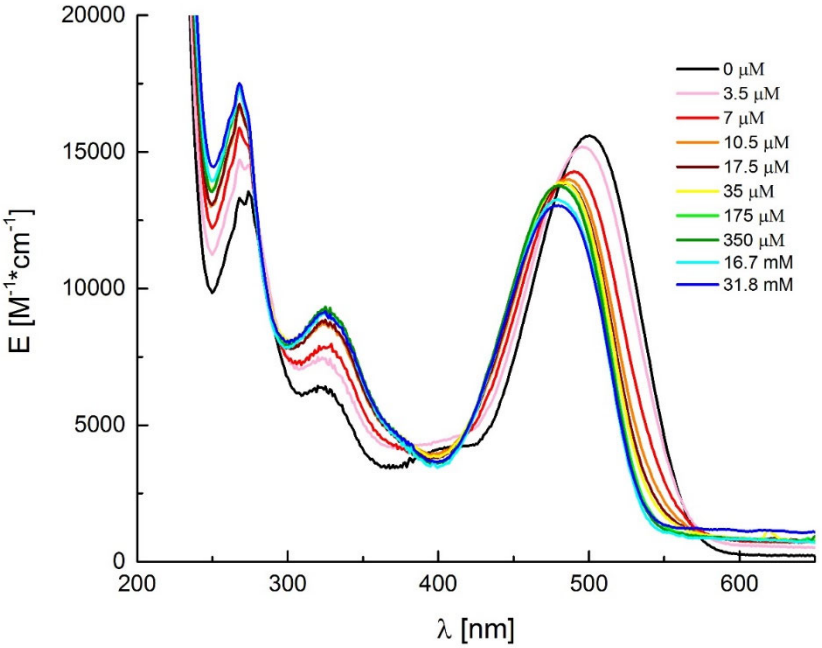

Fig. S37. The effect of KPF_6 addition on the absorption spectra of DPP **2** measured in CH_3CN.

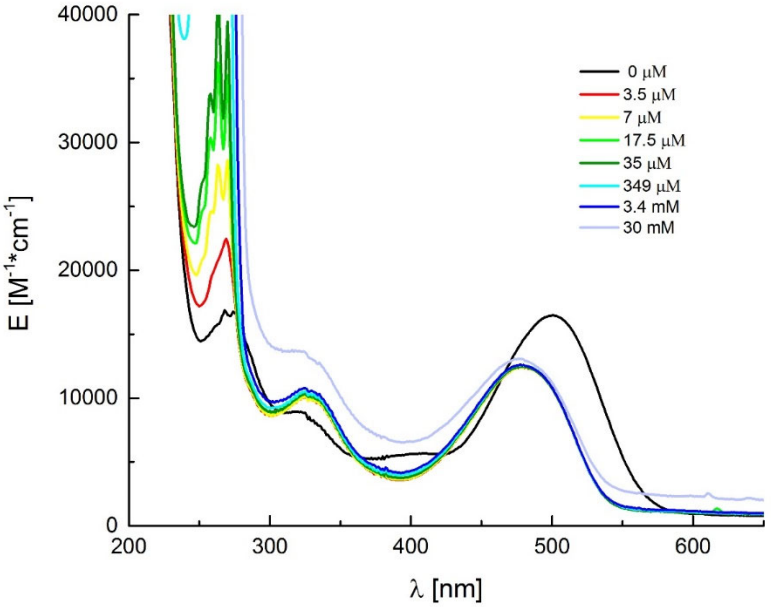

Fig. S38. The effect of BENZENESULFONIC ACID addition on the absorption spectra of DPP **2** measured in CH_3CN.

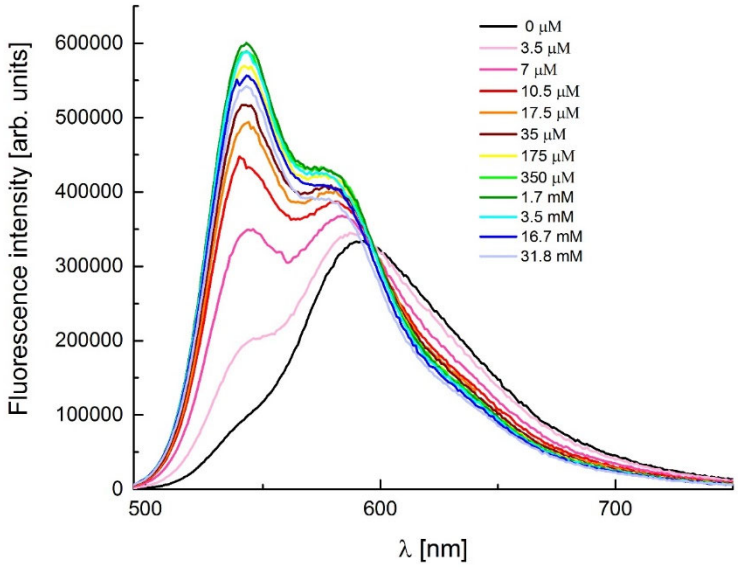

Fig. S39. The effect of KPF_6 addition on the emission spectra of DPP **2** measured in CH_3CN.

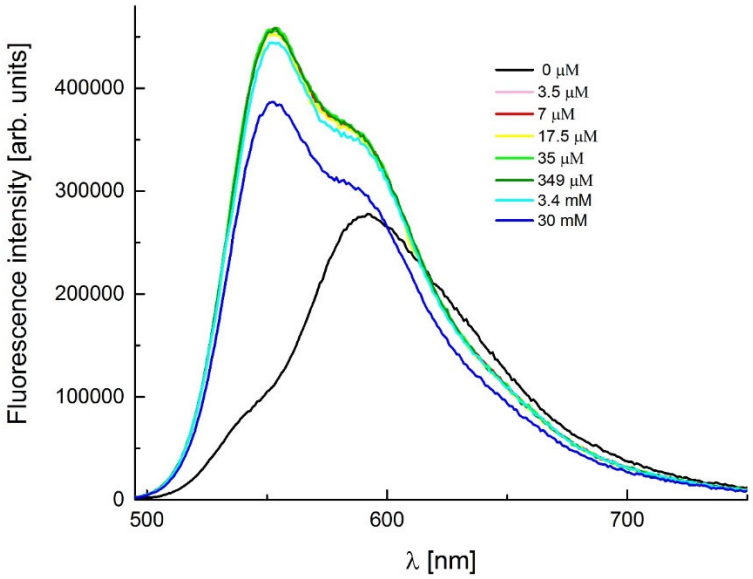

Fig. S40. The effect of BENZENESULFONIC ACID addition on the emission spectra of DPP **2** measured in CH_3CN.

Photostability measurements

Photostability of DPP **2** was determined through the variation in absorption of each sample at the appropriate absorption maximum wavelength (λ_{abs}) with respect to irradiation time. Toluene was selected as the solvent. Concentrations giving similar optical densities (A ≈ 1) were used. Quartz cells of samples were irradiated with a 300 W Xe lamp (Asahi spectra MAX-350, light power: 0.115 W/cm^2) for 180 min at 25 °C equipped with a UV/vis mirror module through a glass fiber. The absorption spectra were measured at appropriate times during the irradiation. BODIPY (difluoro{2-[1-(3,5-dimethyl-2*H*-pyrrol-2-ylidene-*N*)ethyl]-3,5-dimethyl-1*H*-pyrrolato-*N*}boron), DPP (2,5-dimethyl-3,6-bis(3,4-dimethoxyphenyl)pyrrolo[3,4-*c*]pyrrole-1,4(2*H*,5*H*)-dione) and Alexa Fluor 555 were used as references.

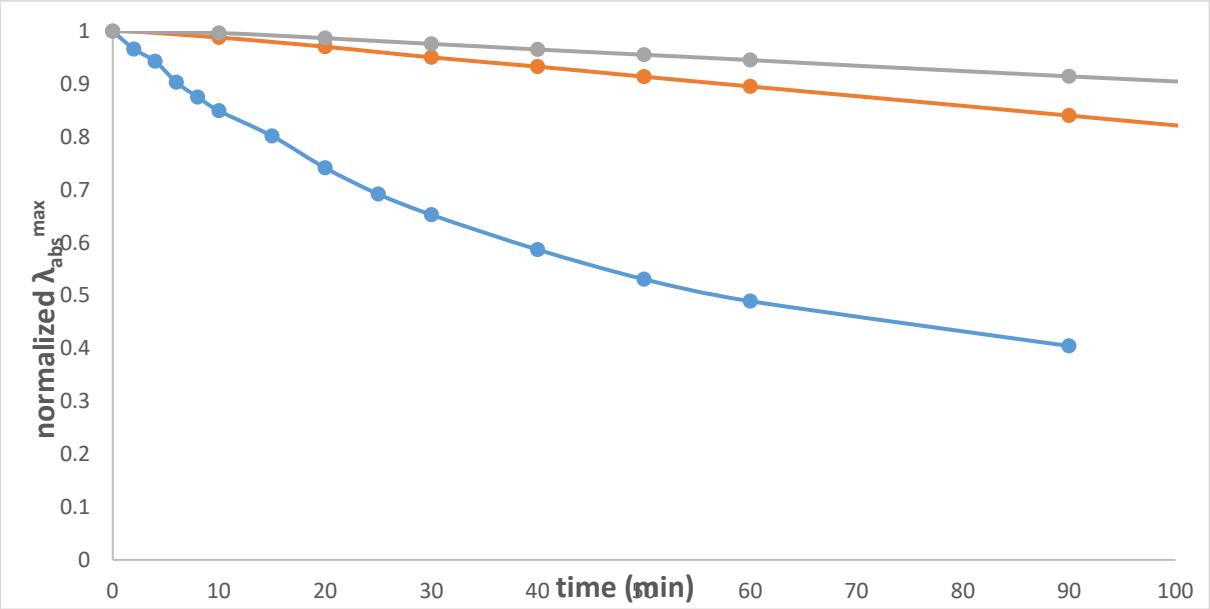

Fig. S41. Photostability of DPP **2** measured in CH_3CN (DPP **2** – blue line, BODIPY 493/503 – gray line, DPP (2,5-dioctyl-3,6-bis(3,4,5-trimethoxyphenyl)pyrrolo[3,4-c]pyrrole-1,4(2H,5H)-dione – orange line).

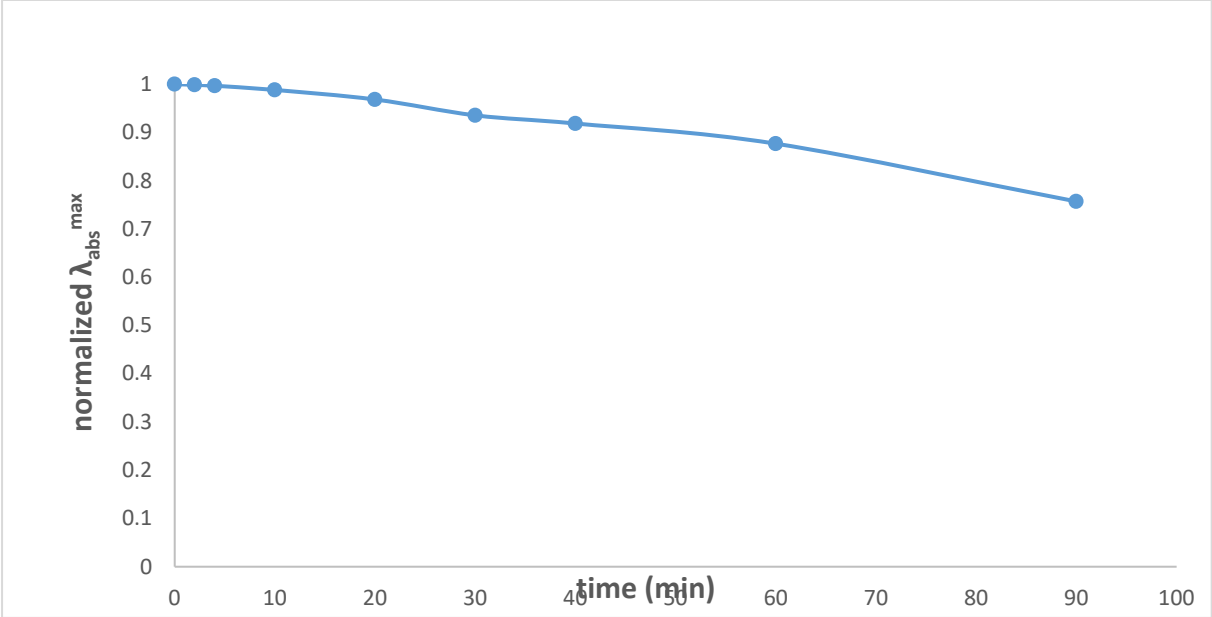

Fig. S42. Photostability of DPP **2** measured in water (containing 10% of DMSO).

Section S6: IMAGING

Cell culture conditions. The rat embryonic cardiomyoblast-derived H9C2 and endothelial EA.hy 926 cell lines were cultured at 37 ˚C in a humidified atmosphere containing 5% CO_2 in DMEM supplemented with 10% foetal bovine serum, 2 mM glutamine, 100 U/ml penicillin, and 100 µg/ml streptomycin.

Fluorescence localization of crown-diketopyrrolopyrroles within the cells. The cardiac H9C2 cells were loaded with fluorophores in DMEM medium supplemented with 10% foetal bovine serum, 2 mM glutamine, 100 U/ml penicillin, and 100 µg/ml streptomycin at 37 ˚C in a humidified atmosphere containing 5% CO_2 for 15 to 30 minutes with the crown-diketopyrrolopyrroles compounds at the final concentration ranging from 200 to 500 nM. The final concentration of the MitoTracker™ Green FM was 150 nM. Both fluorophores were dissolved in DMSO. Before measurements, the incubation medium was replaced with FluoroBrite™ DMEM. The measurements were performed with use of Olympus IX83 confocal microscope with the water objective 60x UPLSAPO 60XW. Registered data were transferred to the ImageJ and analyzed for presentation.

The research was carried out on "live" unfixed cells. The given run of the experiment, the control, the administration of valinomycin and naringenin, and the change of the incubation medium to 200 mM KCl were performed on the same cells. The research was carried out on "live" unfixed cells. The given run of the experiment, the control, the administration of valinomycin and

naringenin, and the change of the incubation medium to 200 mM KCl were performed on the same Petri dish.

H9C2 cells, which had been incubated for 30 minutes with DPP **2** at 37°C at 5% CO_2, were washed with incubation medium (FloroBrite) and measurements were made under control conditions Fig A. Then valinomycin and nigericin were added to the control medium to a final concentration of 30 µM and 10 uM respectively and after 5 min of incubation the measurements were performed for 5 mM KCl conditions. After that, the incubation medium was changed to a medium containing 200 mM KCl with appropriate concentrations of valinomycin and nigericin. And the fluorescence intensity was measured for 200 mM KCl conditions. Measurements performed only in the presence of valinomycin transport only potassium ions, which in the case of the cell membrane would do the job. However, in the case of mitochondria, the process is more complicated. Administration of valinomycin alone would change only the electrical potential ΔΨ of the inner mitochondrial membrane which would lead to activation of the respiratory chain and an increase in pH. The addition of nigericin reduces the transmembrane ΔpH (Kang, Chen et al. 2017).

Kang, P. T., C. L. Chen, P. Lin, W. M. Chilian and Y. R. Chen (2017). "Impairment of pH gradient and membrane potential mediates redox dysfunction in the mitochondria of the post-ischemic heart." Basic Res Cardiol 112(4): 36.

The number of cells used for the measurement is usually 100,000 if we take into account their volume (assuming that they are a sphere) $4/3\pi r^3$ (radius of the cell 50 µm) then compared to the volume of 2 ml of incubation medium, if the concentration on both sides of the biological membrane is equalized, the concentration will be close to the value of 5 mM as it is in incubation medium.

mean from both samples	B3-A	YG2-A	B3-A/YG2-A
Probe	5,77E+05	1,57E+05	3,81E+00
Probe_valinomycin_nigeri	4,44E+05	1,72E+05	2,56E+00
Probe_valinomycin_nigeri	6,14E+05	1,09E+05	5,65E+00
Control	18052	4170	4,32901679
Pearson r (B3 vs YG2):	-0,82		

In response to this comment the measurements were performed using a flow cytometer and the results confirmed those obtained for the confocal microscopy measurements. Only the extreme values of potassium ions were used to define the limit of changes in the value of the fluorescence intensity ratio for green and red colors. Further studies with potassium titration are planned, but require a separate approach to demonstrate the biological usefulness of a given fluorescent probe.

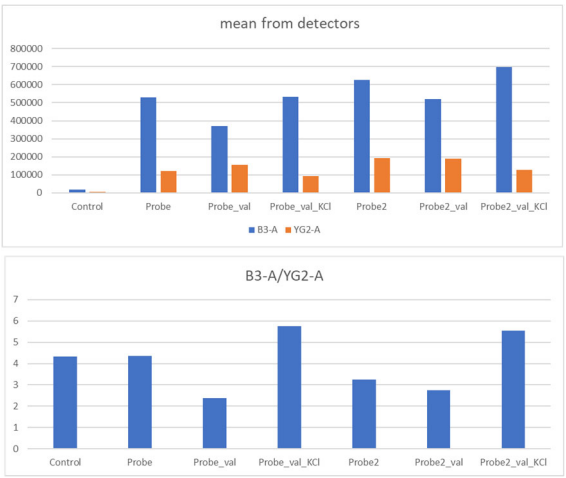

Figure 43. Measurements made using flow cytometry for different KCl concentrations. Probe_val is for valinomycin and nigericin. Data from two experiments.

In order to determine the viability of cells under the influence of the tested crown-diketopyrrolopyrroles, an annexin V-based apoptosis and necrosis test (RealTime-Glo ™ Annexin V Apoptosis and Necrosis Assay, Promega) was performed, allowing the simultaneous examination of the effect of the substances on the induction of apoptotic and necrotic cell death.

Section S7: Confocal fluorescence microscopy images

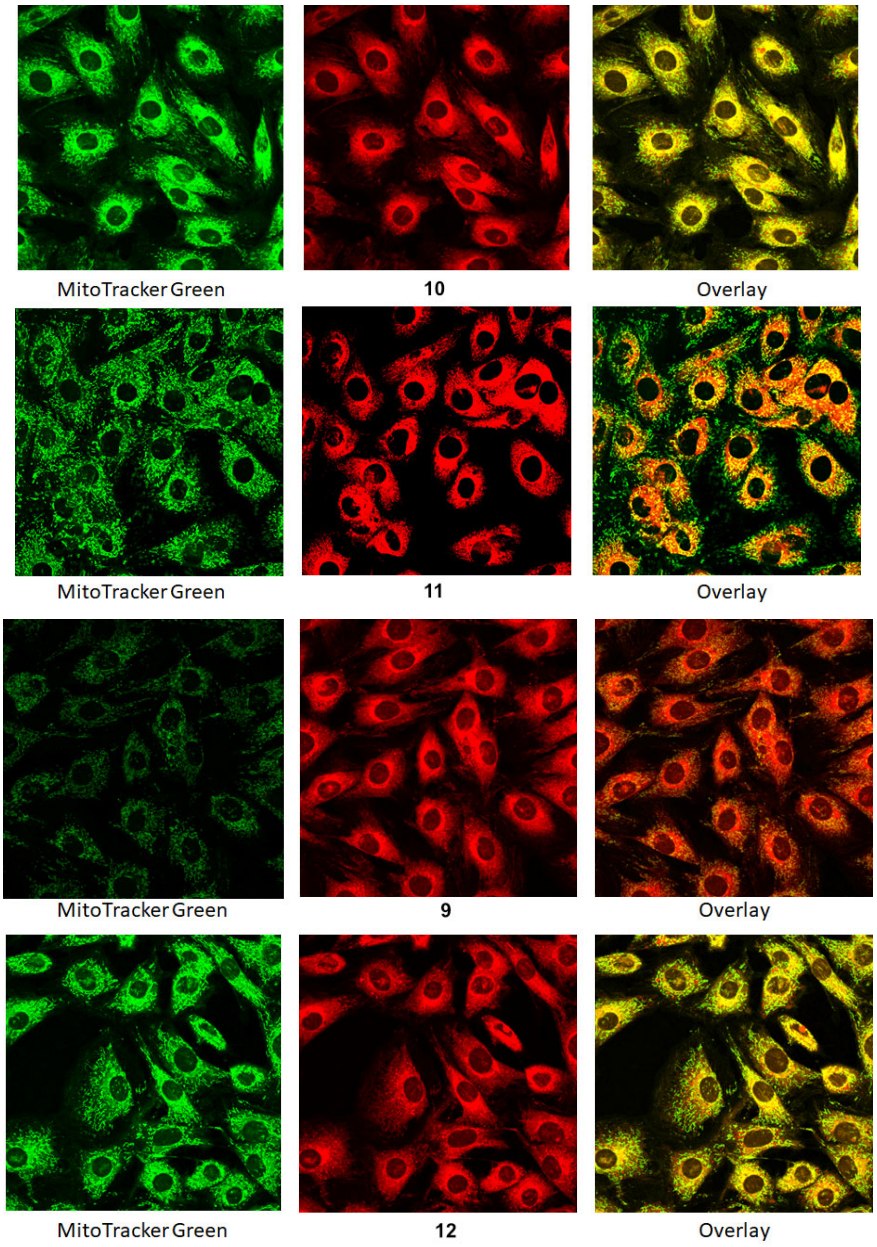

Fig. S44. Intracellular localization of **S10, S11, S9** and **1** compounds as detected using confocal fluorescence microscopy.

The fluorescence of MitoTracker™ Green (green) as a well-established marker for mitochondria, and the fluorescence of the **S10**, **S11**, **S9** and **S12** (red) compounds were recorded with 559 nm excitation wavelength and emission range 610–750 nm. Overlay picture recorded simultaneously for two fluorophore in living H9C2 cells line.

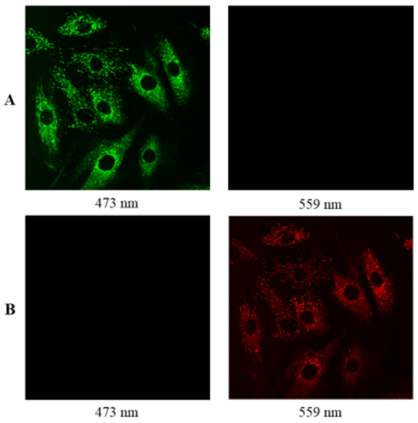

Fig. S45. Separation of the fluorescence emission wavelength with excitation with laser line 473 nm (A) and 559 nm (B). Detection channels were set for fluorescence green and red light respectively.

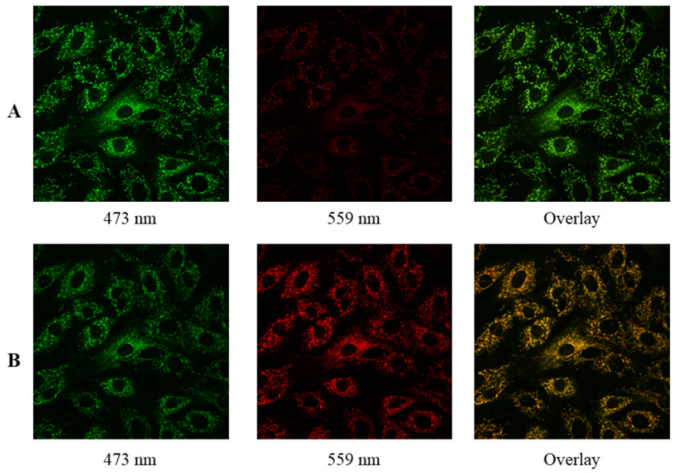

Fig. S46. Changes in the fluorescence of the **2** compound in the different intracellular K^+ concentration caused by nigericin. A control condition. B in the presence of nigericin (10 µM).

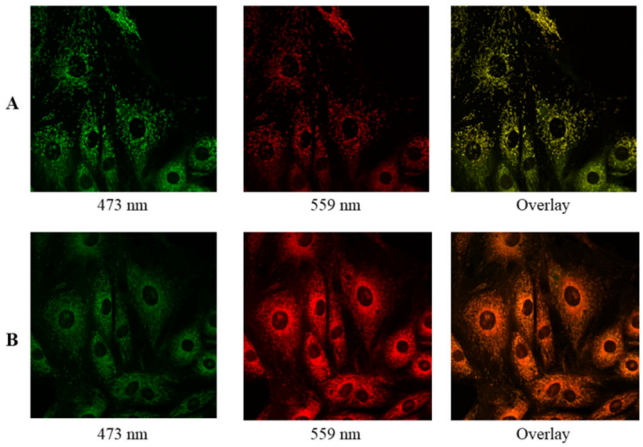

Fig. S47. Changes in the fluorescence of the **2** compound in the different intracellular K^+ concentration caused by valinomycin. A control condition. B in the presence of valinomycin (30 μM).

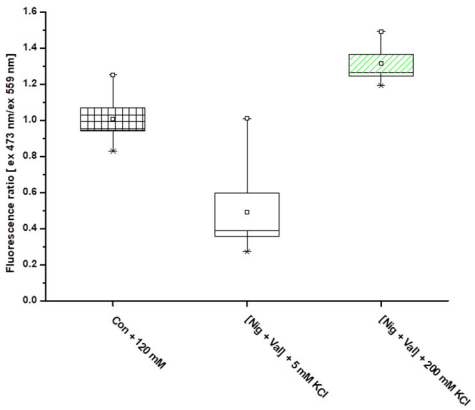

Fig. S48. Changes in the ratio (473 nm/559 nm) of the fluorescence intensity at the different excitation wavelength as measured with use of ImageJ. The ratio is statistically different for each conditions as measured in paired sample t Test at the level 0.05.

Penetration into the cell depends on a number of factors and under our conditions, after many trials, we decided to load the cells with the dye in the presence of Pluronic 127 detergent and FBS in the incubation medium. This is due to the fact that research on living cells is taken into account and the dye entering the cell accumulates in the inner mitochondrial membrane and

mitochondria. Too rapid accumulation could damage the performance of the mitochondrial activity system and produce undesirable results. It turned out that the penetration of the dye into the cell without FBS in the environment is extremely fast, but it is easier to control the charge level of the cell in the presence of FBS by changing the time of loading. In our opinion, it is more important to obtain a stable dye balance. In the ratiometric measurements of fluorescence the level of dyes loading is less important.

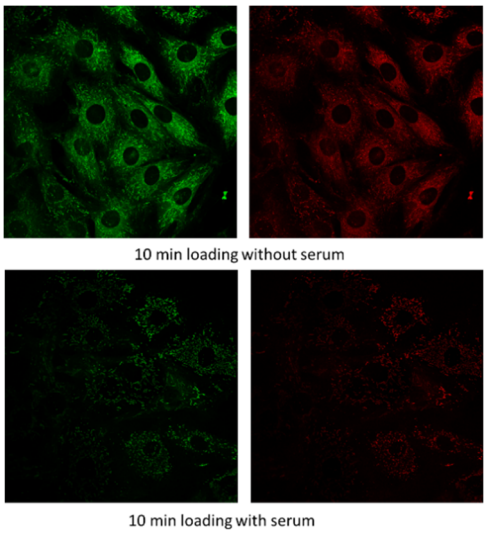

Figure 49. Different level loading of dye **6** in the presence and absence of serum.

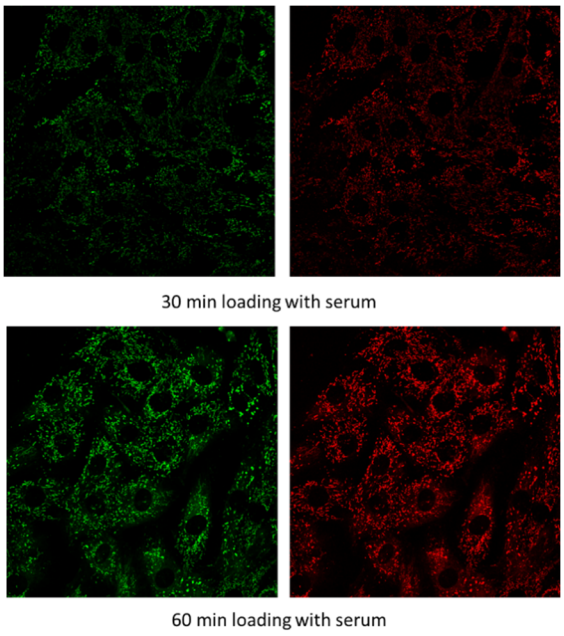

Figure 50. Different time loading of dye **6** in the presence of serum in incubation medium.

Pearson's correlation coefficient and Mander's overlap coefficient (MOC).

For pair of two signal channels Mitotracker Green and DPP **1** Pearson's Coefficient: r=0.597, Manders' Coefficients (original): M1=0.997 (fraction of Mitotracker Green overlapping DPP **1**), M2=0.763 (fraction of DPP **1** overlapping Mitotracker Green).

For pair of two signal channels Mitotracker Green and DPP **2** Pearson's Coefficient: r=0.793, Manders' Coefficients (original): M1=0.888 (fraction of Mitotracker Green overlapping DPP **2**) M2=0.993 (fraction of DPP **2** overlapping Mitotracker Green).

For pair of two signal channels: Mitotracker Green and DPP **2** (B) Pearson's Coefficient: r=0.788, Manders' Coefficients (original): M1=0.944 (fraction of Mitotracker Green overlapping DPP **2**), M2=0.968 (fraction of DPP **2** overlapping Mitotracker Green).

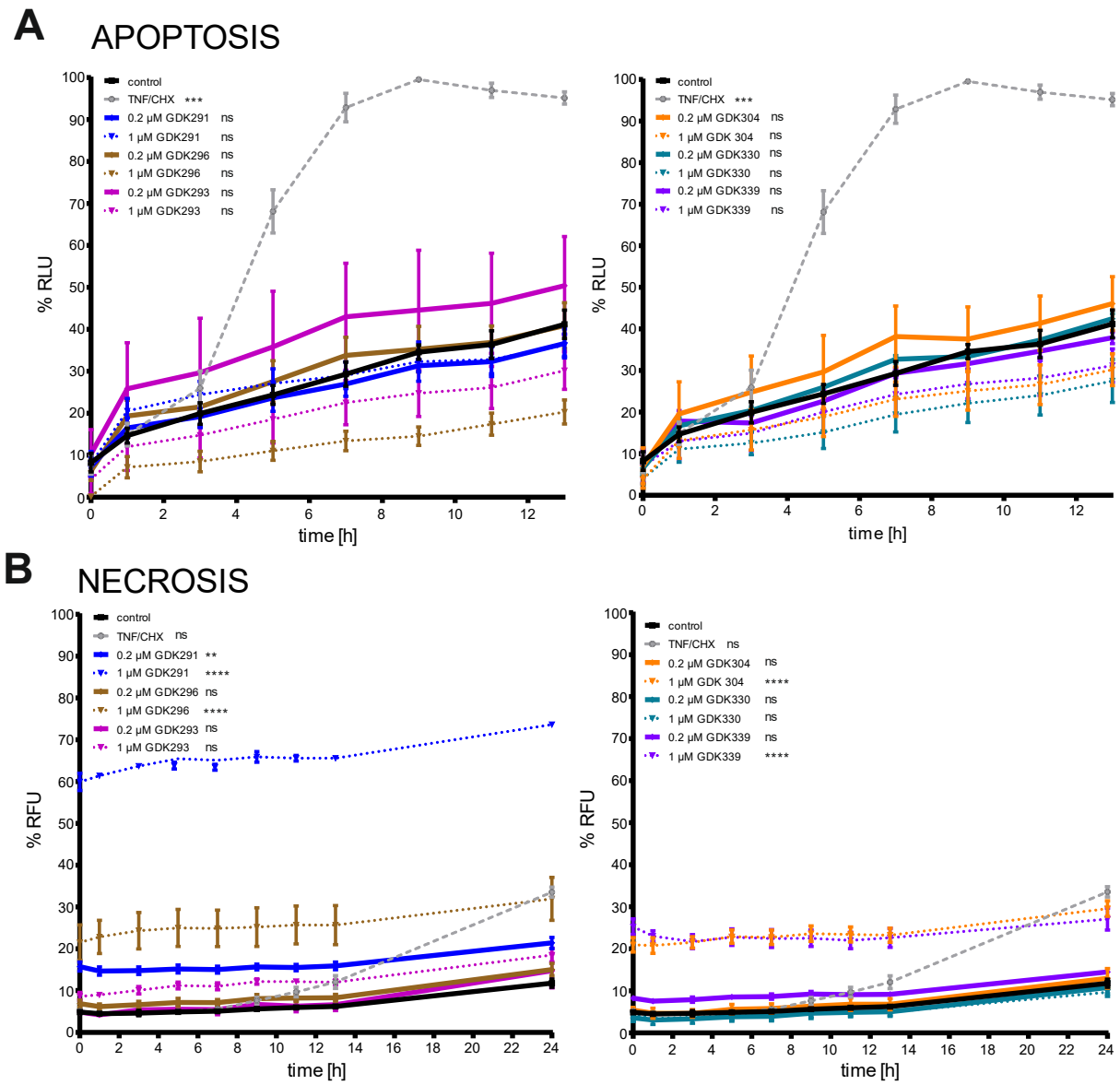

Fig. S51. Effect of crown-diketopyrrolopyrroles on apoptosis and necrosis of the EA.hy 926 cells.

Change in luminescence as a measure of apoptosis (A) and fluorescence (B) over the time. Statistical significance relative to the control was determined by two-way ANOVA with Tukey's test for n = 3 ($p < 0.0001$ (****); $p > 0.05$ (ns).

Section S8: Theoretical calculations

Methods

For the calculations, the selected protocol follows one that has been extensively described and tested before,[3] and is only briefly outlined below. In this approach, the ground and excited state geometries are optimized at the PCM[4]-(TD-)M06-2X[5] 6-31+G(d) level, the vibrational frequencies are obtained at the exact sale level of theory, the total and transition energies are determined at CC2/*aug*-cc-pVTZ level, and the solvent corrections (here acetonitrile) on these CC2 energies are included at the PCM(LR+cLR[6])-TD-M06-2X/6-311+G(2d,p) level. All (TD-)DFT calculations have been performed with the Gaussian16.A03 program,[7] whereas the CC2 calculations have been achieved with Turbomole 7.3,[8] applying the RI density fitting approach. This approach allows to obtain 0-0 energies that correspond to the crossing point between the measured absorption and emission curves. Finally, the vibronic calculations shown in the ESI was performed with the FCClasses code within the TD approach and the vertical-gradient vibronic model. Temperature effects were considered (298 K) and a broadening function was used (Gaussian, HWMH: 200 cm^{-1}).[9]

Studies

To gain further insights into the photophysics of these DPPs, we conducted a computational study. In the performed computations, we used model compounds (denoted with an added **M**, Fig. S20) in which the crown ether groups were replaced by NMe_2 moieties. This decision was justified by computational savings as well as the non-conjugated nature of the crown ether. We computed the 0-0 energies to be 2.24, 2.24, and 2.17 eV for **9M**, **10M**, and **17M** respectively. These values can be rightfully compared to the experimental absorption-fluorescence crossing point, which has the values 2.28, 2.28, and 2.20 eV. Naturally, the selected level of theory can restore the experimental values with high accuracy. In addition, as can be seen in Fig. 48 for **9M**, the shape of the absorption spectrum with the presence of two maxima is globally reproduced when vibronic calculations are made.

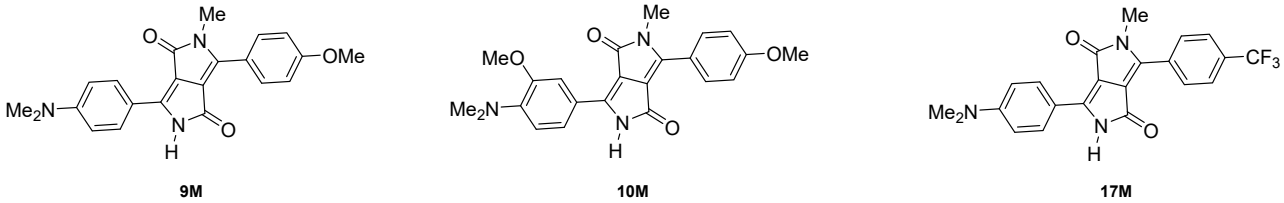

Fig. S52. Structures used in computational studies

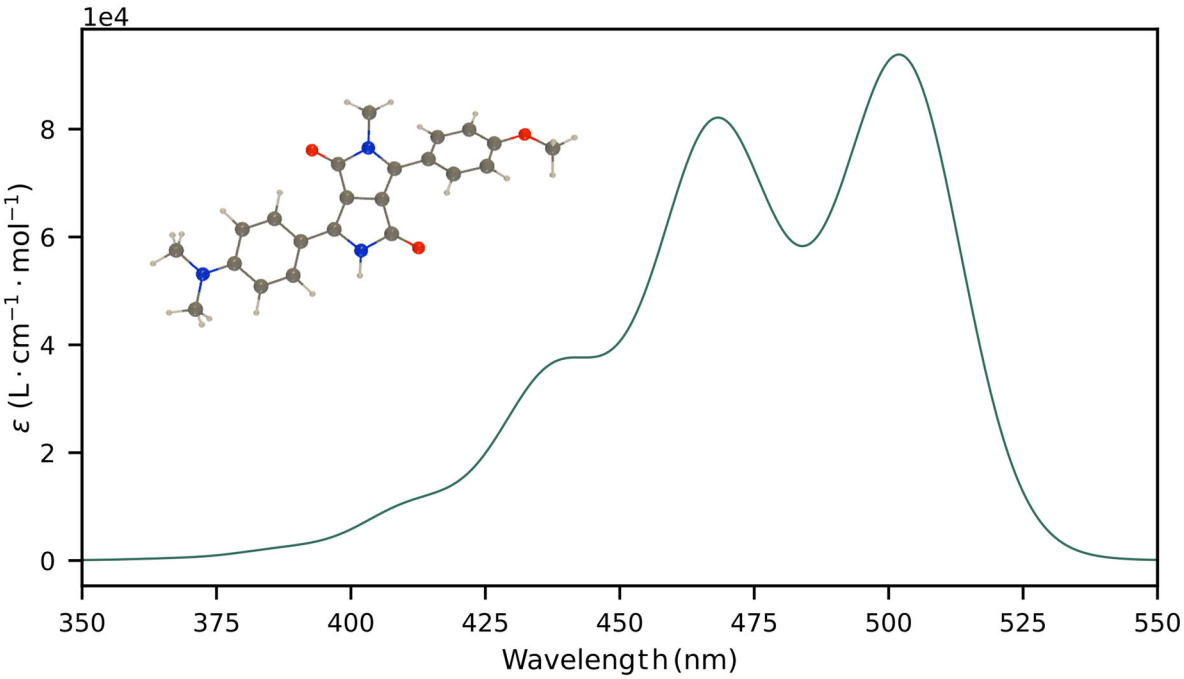

Fig. S53. Vibrationally-resolved absorption spectrum of **9M** calculated with PCM-TD-M06-2X/6-31+G(d), using the TD-VG vibronic model.

Plots displaying density differences for the three dyes are presented in Figure S22. In **9M**, the 4-$Me_2NC_6H_4$ is nearly coplanar with the DPP with a twist of only 6° as compared to a value of 33° for the 4-$MeOC_6H_4$. As can be further seen in Figure 5, the amino group, which is perfectly coplanar in both ground and excited states with the benzene ring, acts as the main donor. The DPP unit acts as the acceptor, while the methoxy group has a weak impact. When adding the secondary OMe (in **10M**), the steric clash between the two donating groups induces a twist of the NMe_2 as compared to the phenyl (40° in the ground, and 35° in the excited state). The latter however remains coplanar with the DPP as in **9M**. Nevertheless, the twist of the NMe_2 in **10M** makes it slightly less donating than in **9M**, though the topologies remain vastly similar, as consistent with the D-A-D' architecture. We note that the non-planarity of NMe_2 in **10M** hints at a more flexible structure, thus likely able to accommodate complexation. When one turns to **17M**, the pattern significantly changes with a clearer charge-transfer character, as well as the CF_3-bearing ring acting as the acceptor in a D-A-A' structure. The above noted differences are reflected in the excited-state dipole moments that attain 7.8, 6.4, and 16.5 D in **9M**, **10M**, and **17M**, respectively. It is noted experimentally that these series of dyes are especially emissive. To explain this, let us first note that TD-DFT yields very large oscillator strengths for the $S_1 \rightarrow S_0$ transition (ca. 1.0 for all three compounds), which is indicative of a very large radiative constant. At the same time TD-DFT reveals that, at the optimal S_1 geometry, there is only a triplet available

below the S_1, but the gap is hugged between the singlet and triplet (> 1.2 eV), which is clearly detrimental for ISC to occur. These two facts are consistent with a bright emission.

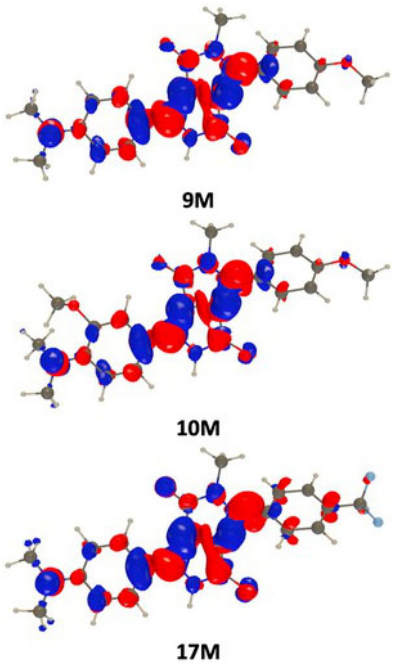

Fig. S54. Density difference plot for the model dyes of **9M**, **10M**, and **17M**. The blueberry and crimson lobed indicate regions of decreased and increase of density upon absorption. Contour threshold $1x10^{-3}$.

As a simple way to model complexation, we have used a structure in which **10M** has been protonated. In this case, the CT character is lost (see Figure S23), consistent with the blueshift and the stronger vibrationally resolved character of the experimental band after complexation (Figure 4).

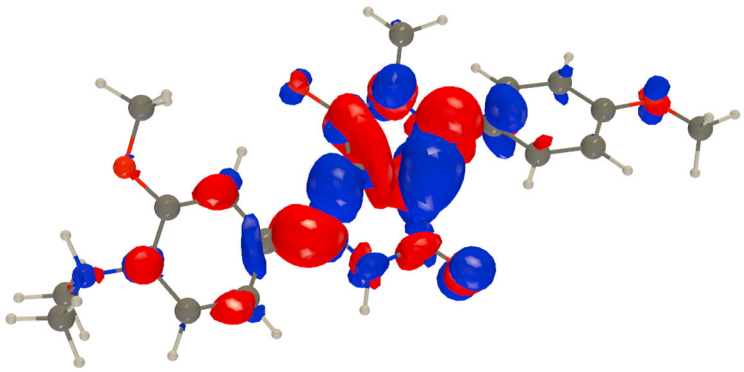

Fig. S55. Density difference plot for the model dyes of **10M+H$^+$** Contour threshold $1x10^{-3}$.

Section S9: ^{1}H NMR and ^{13}C NMR Spectra

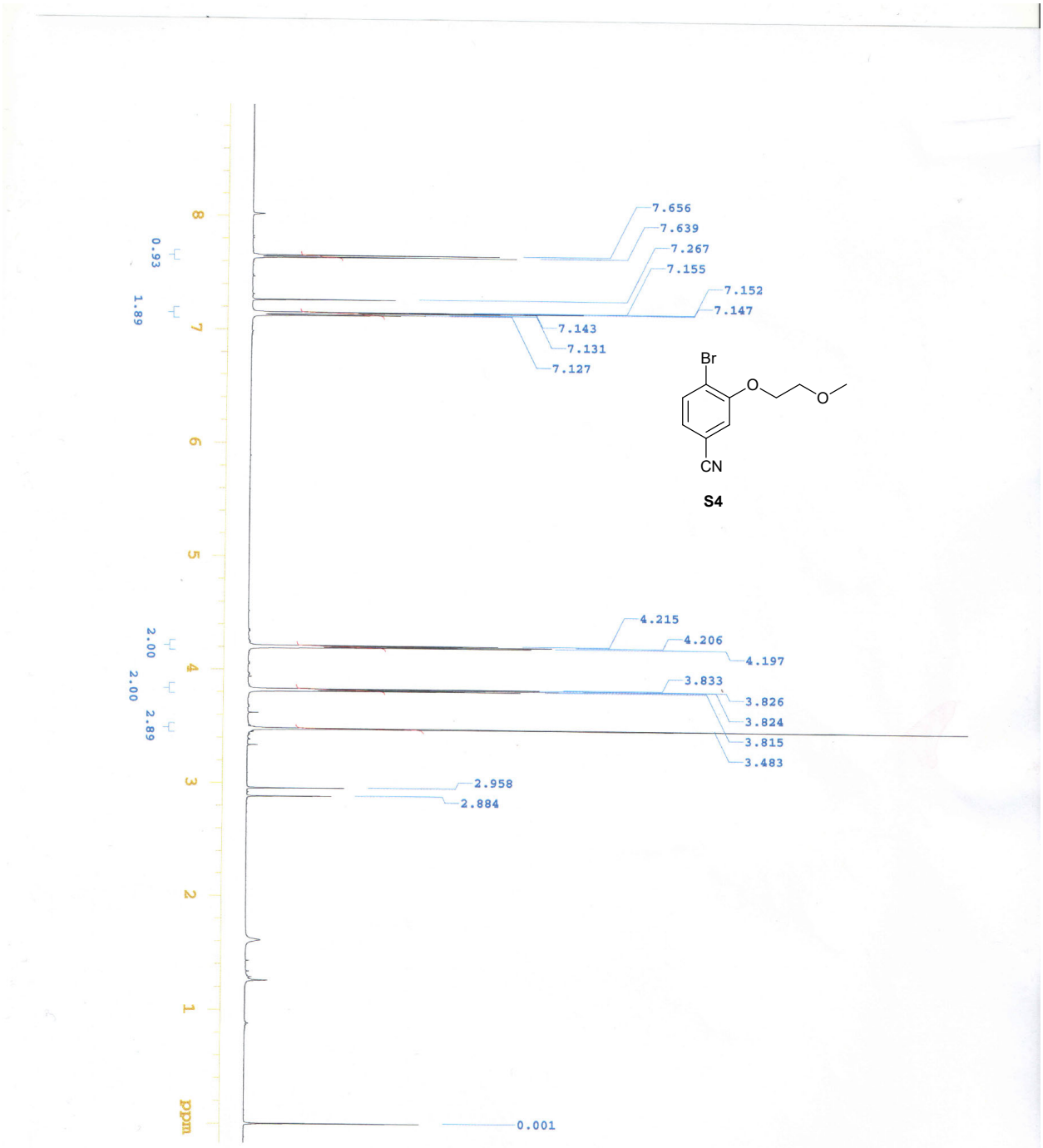

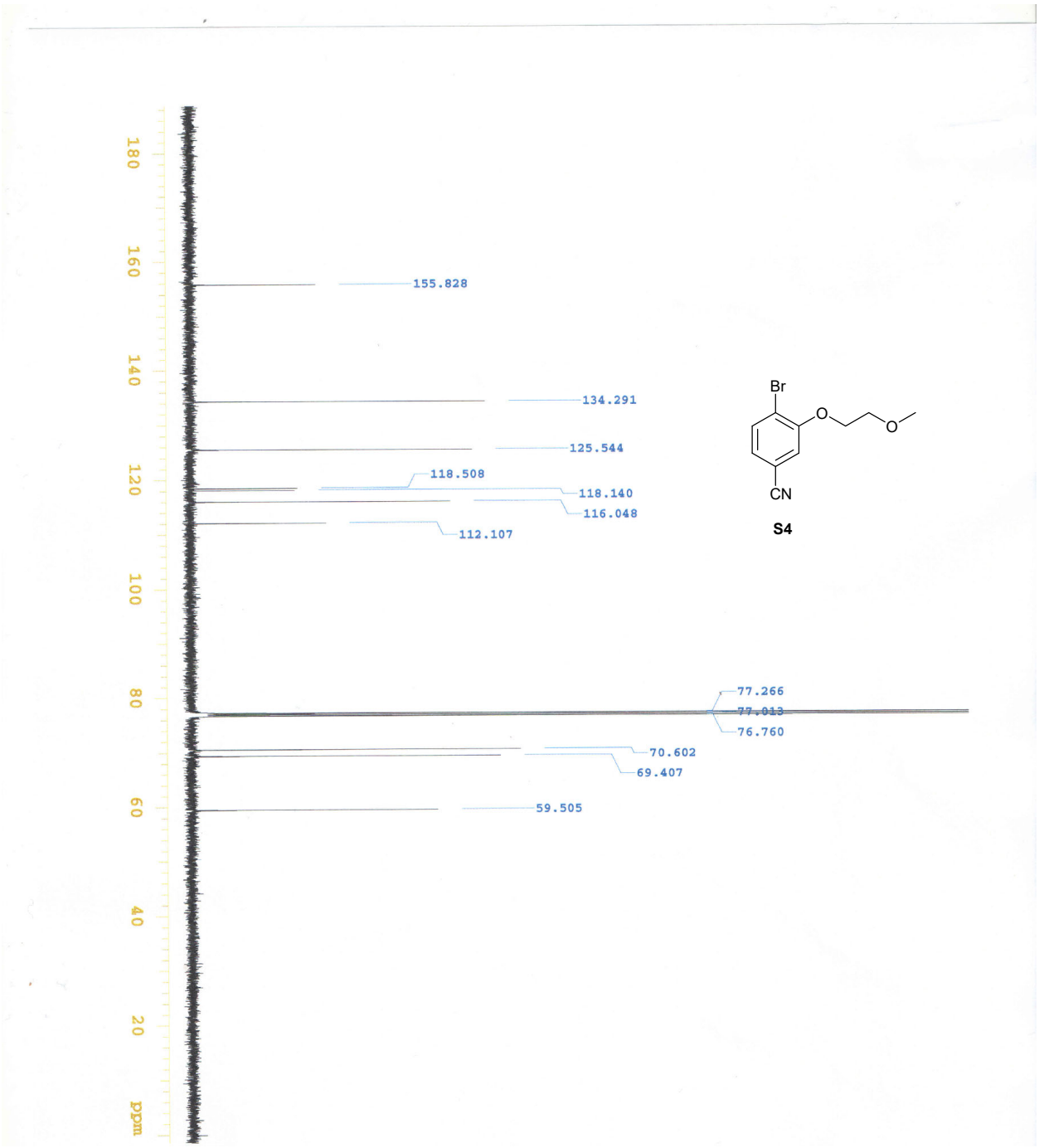

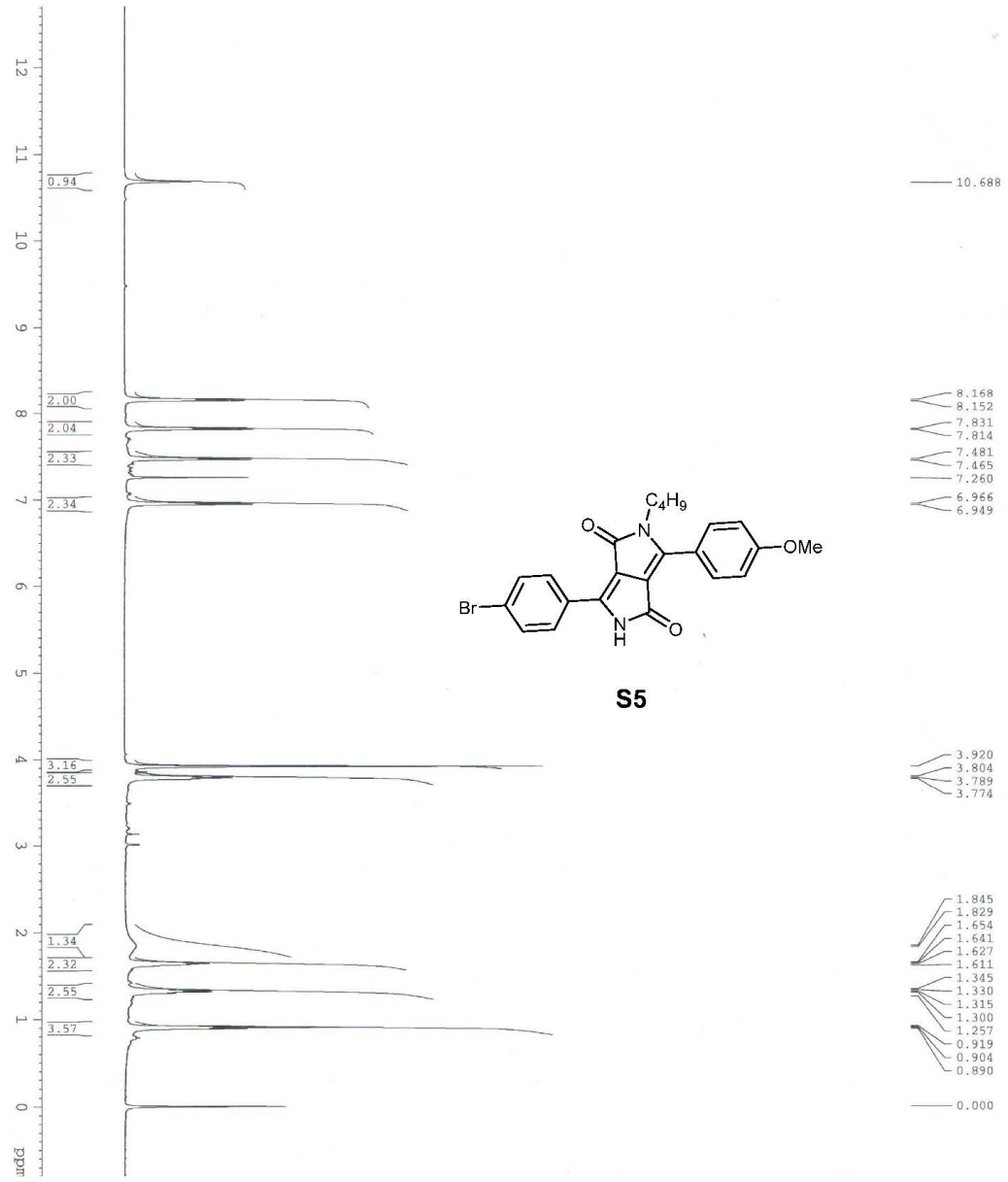

S5

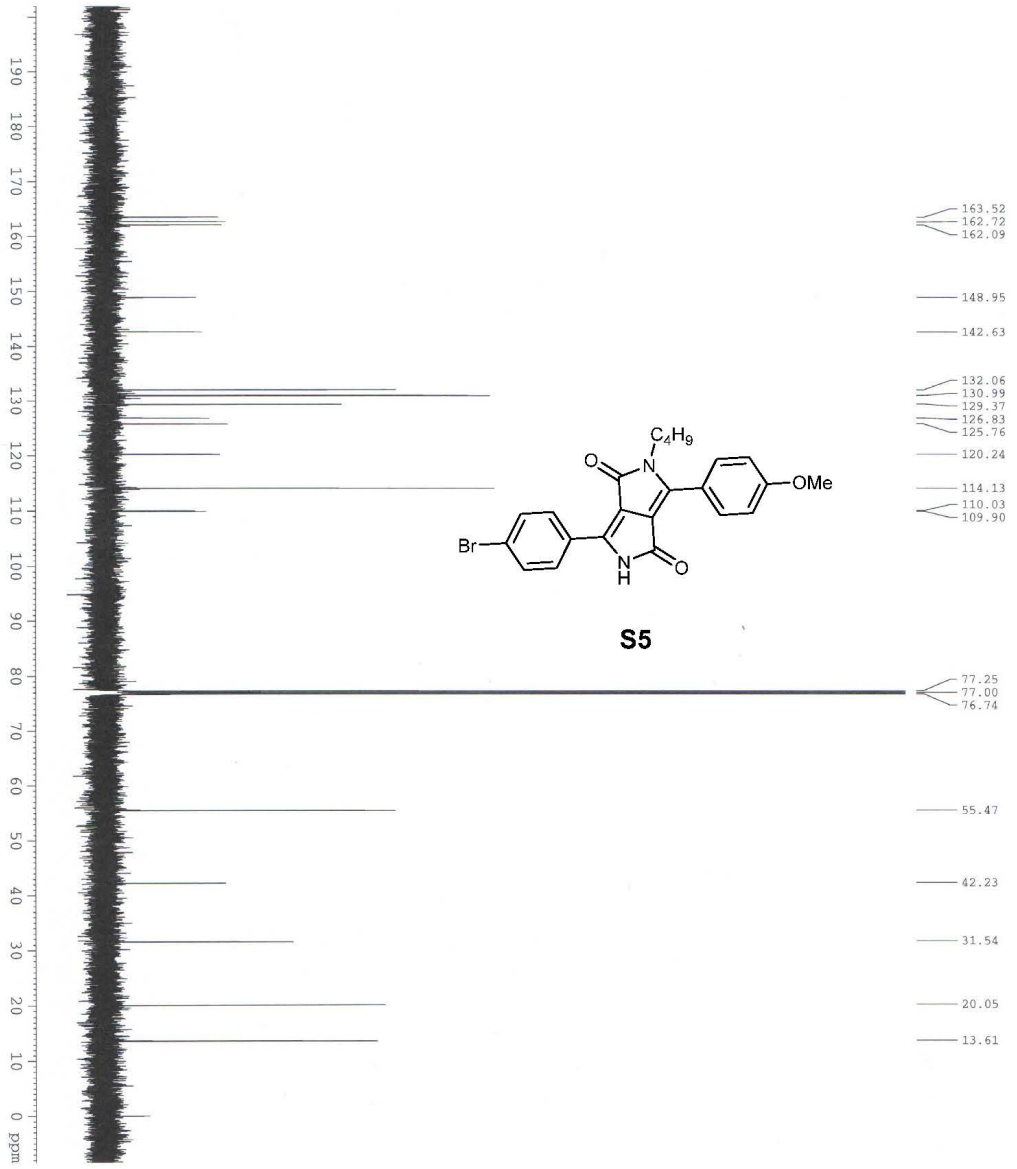

S5

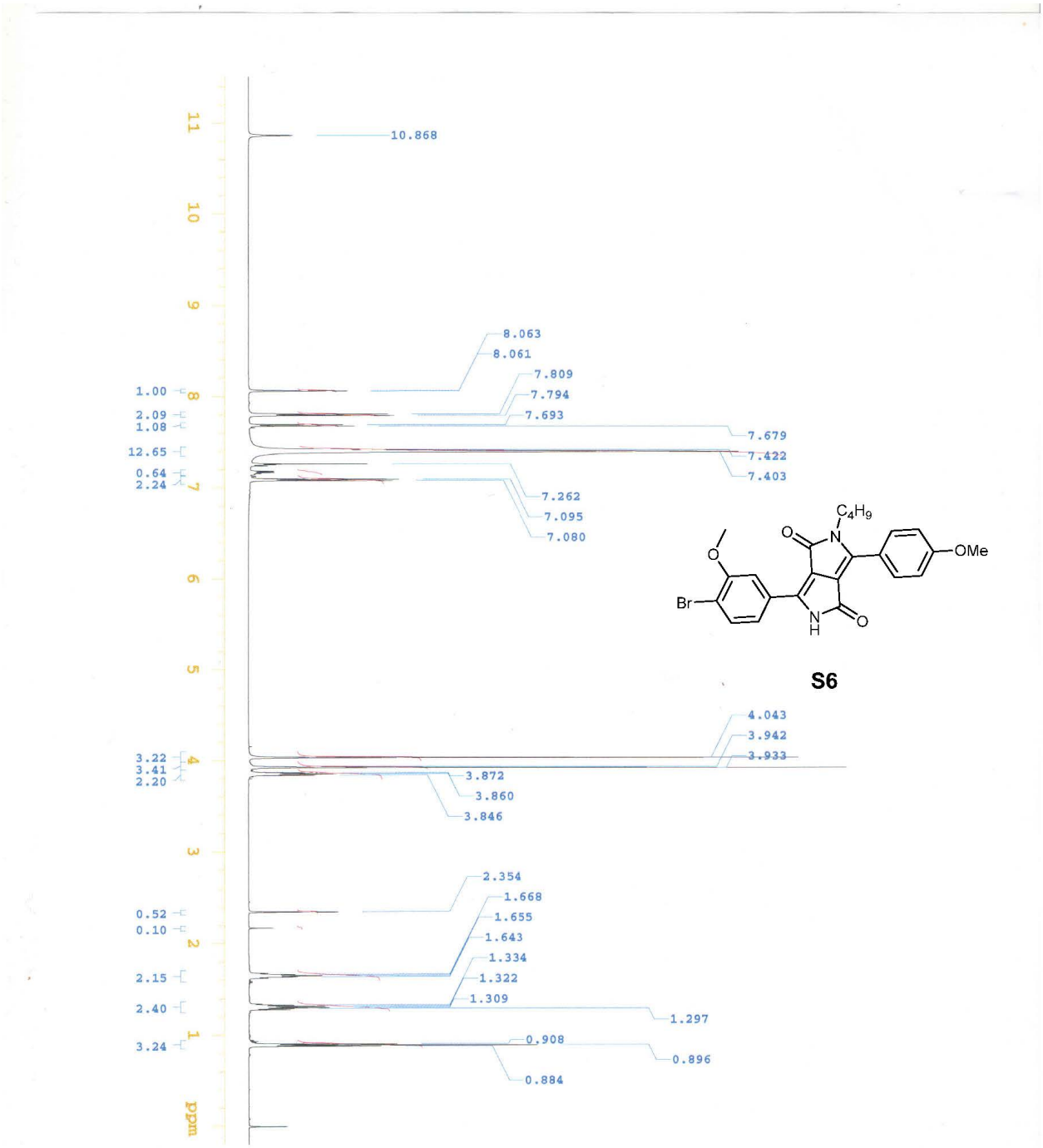

S6

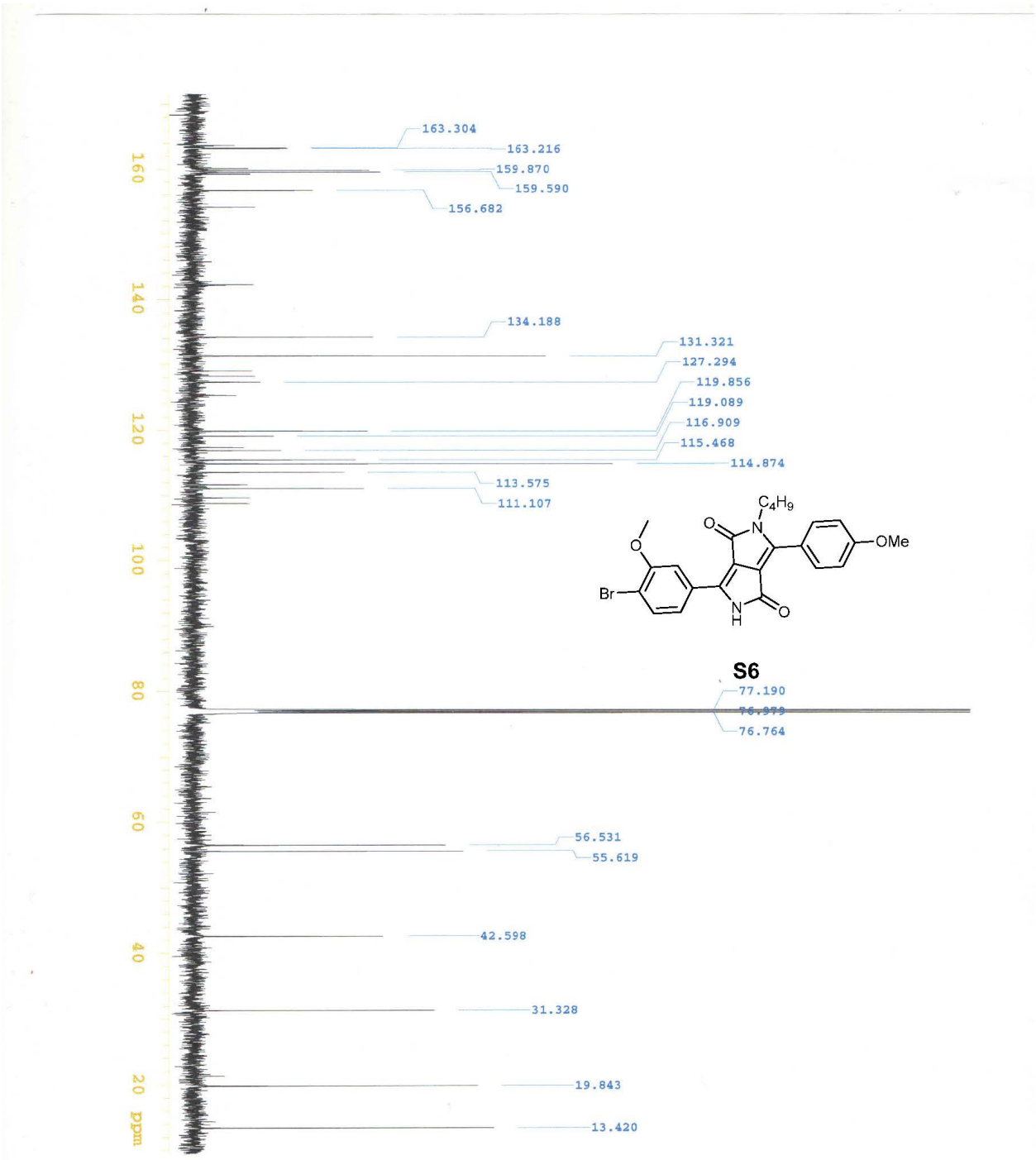

S6

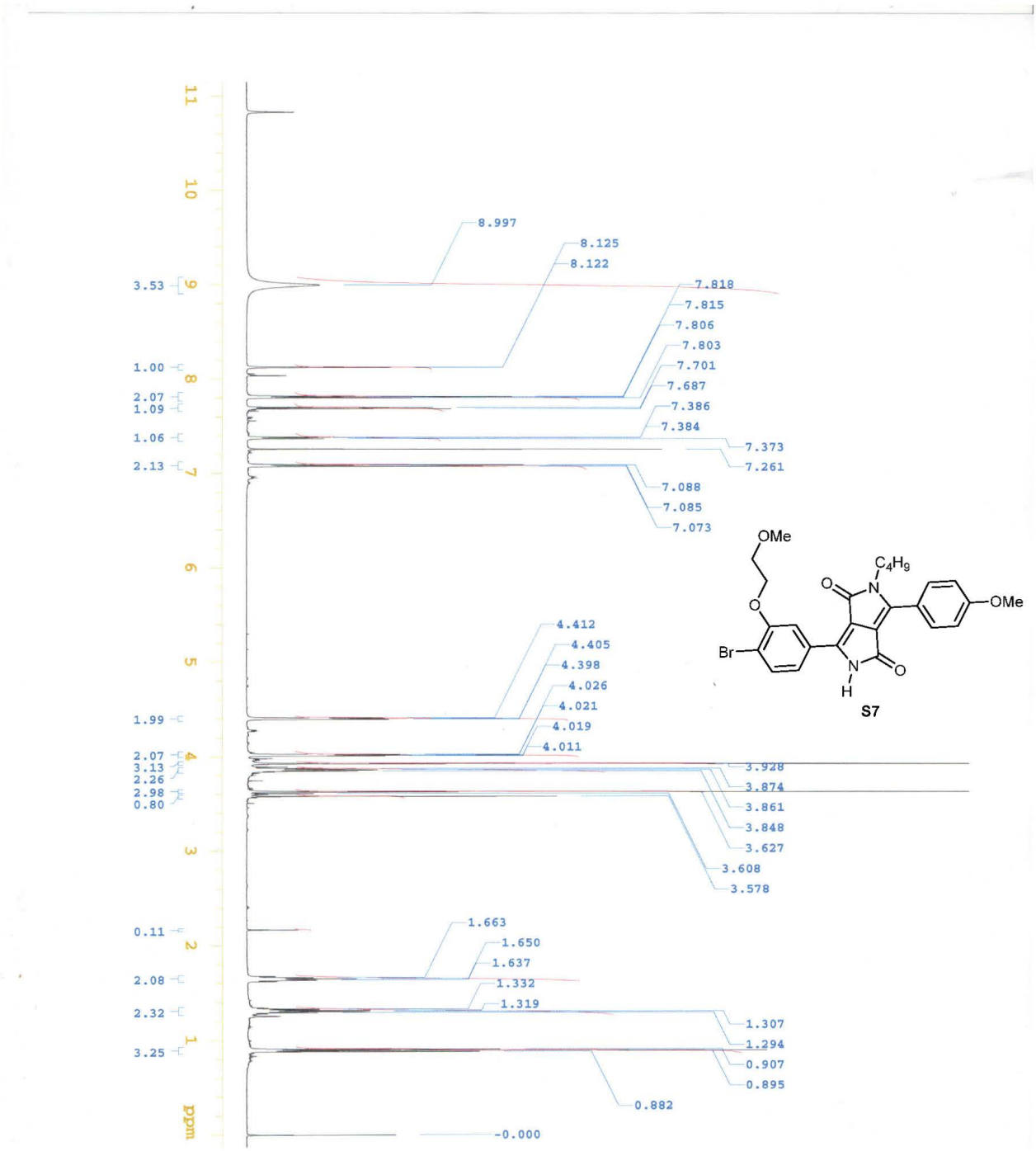

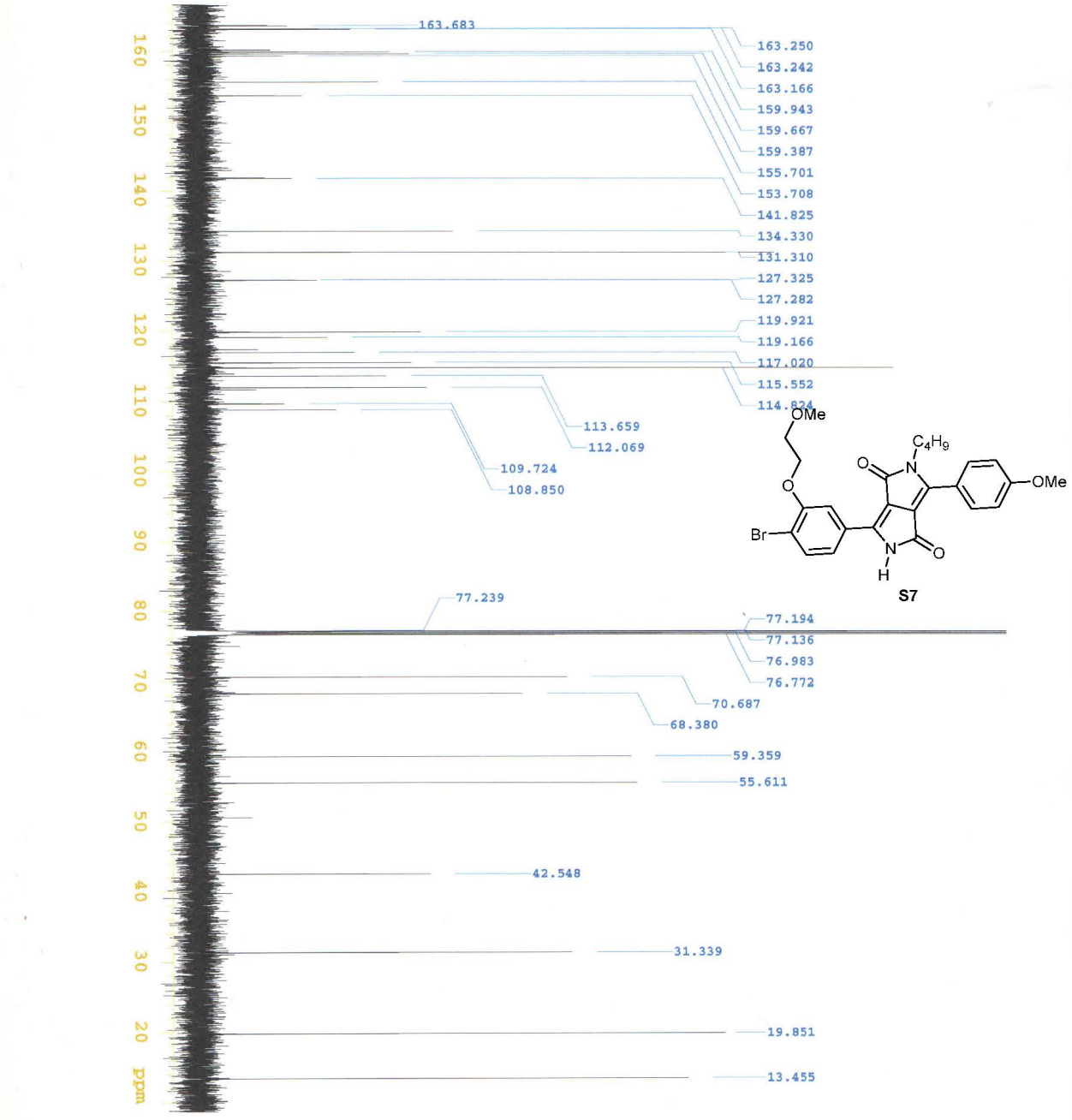

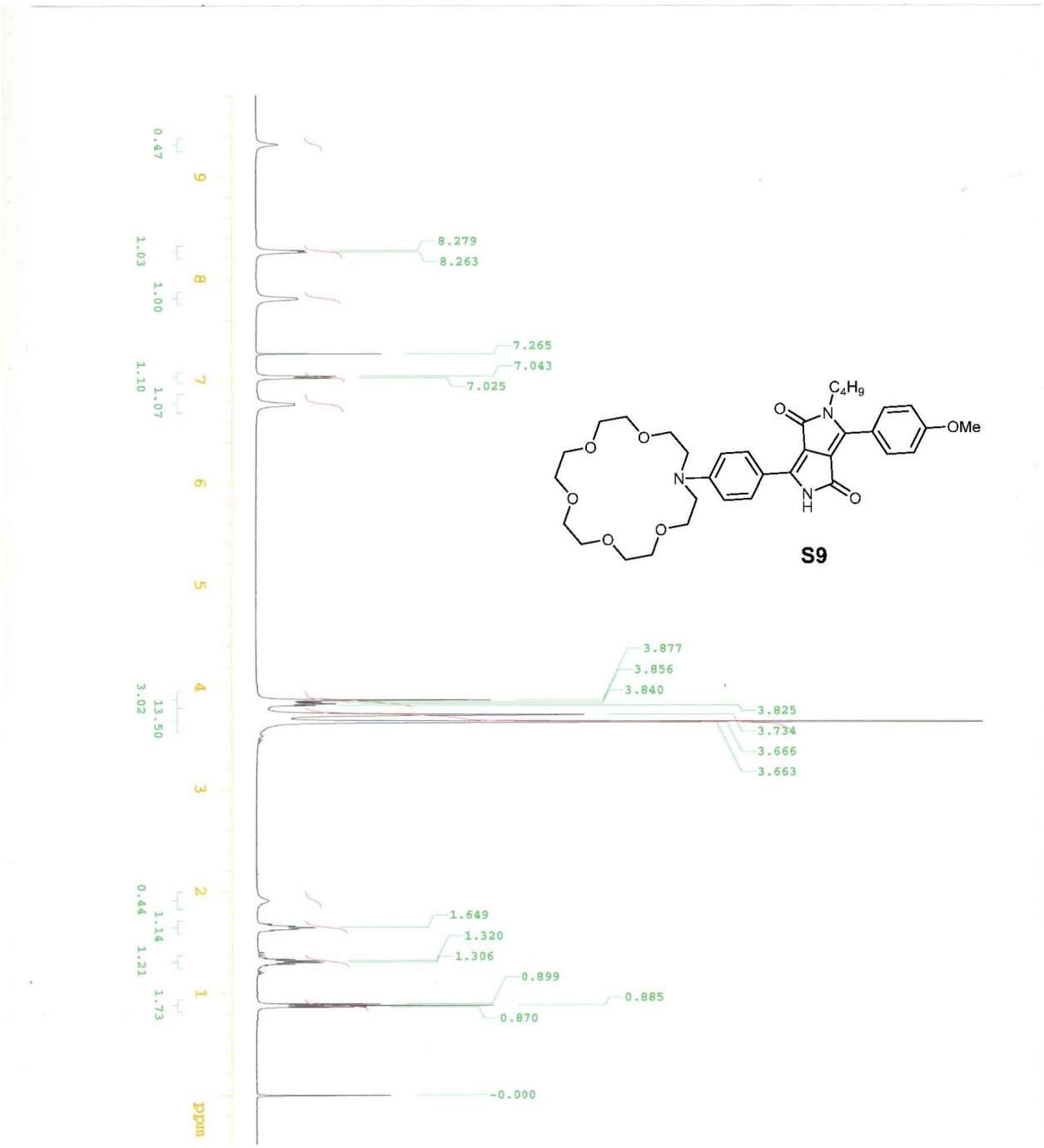

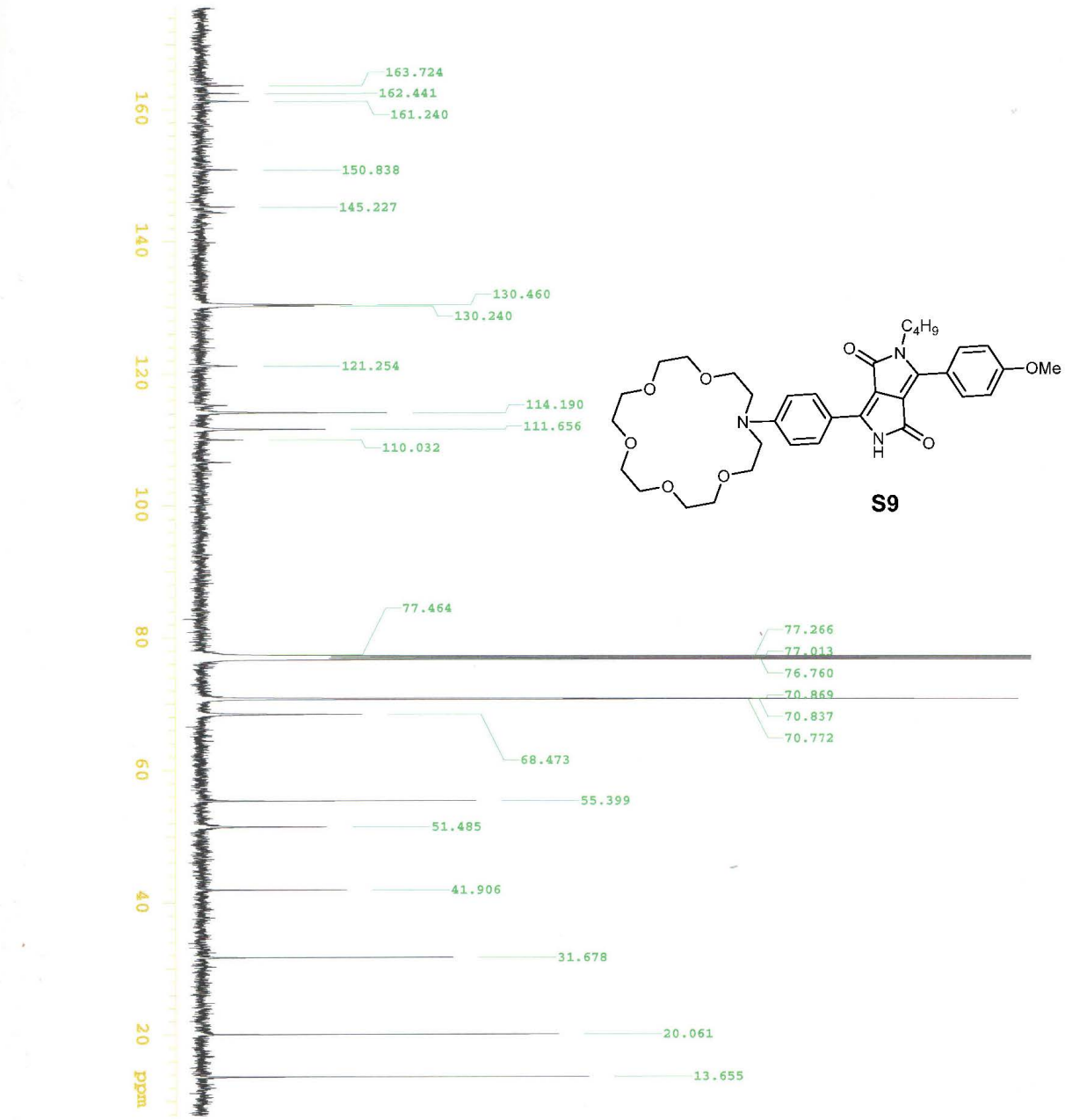

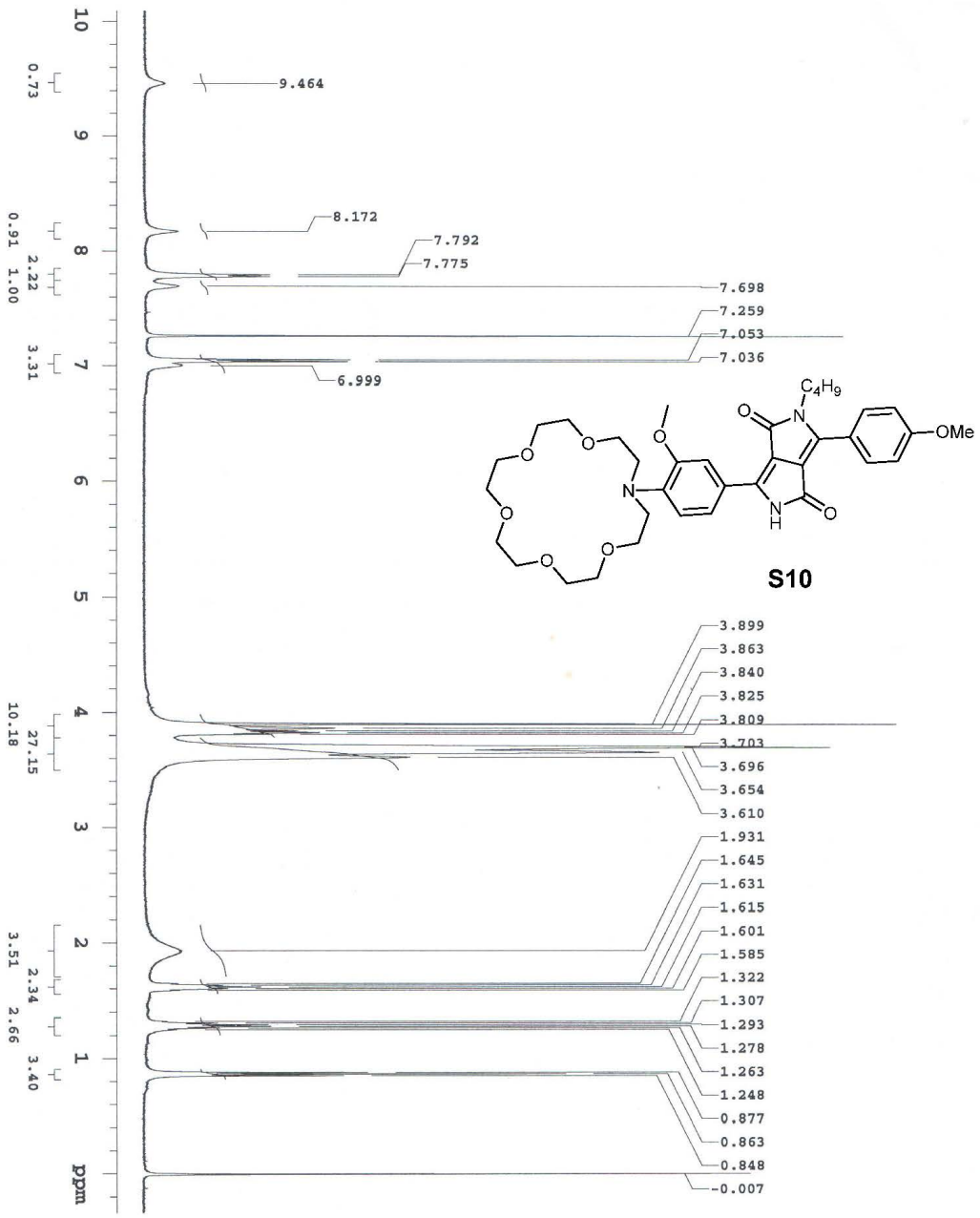

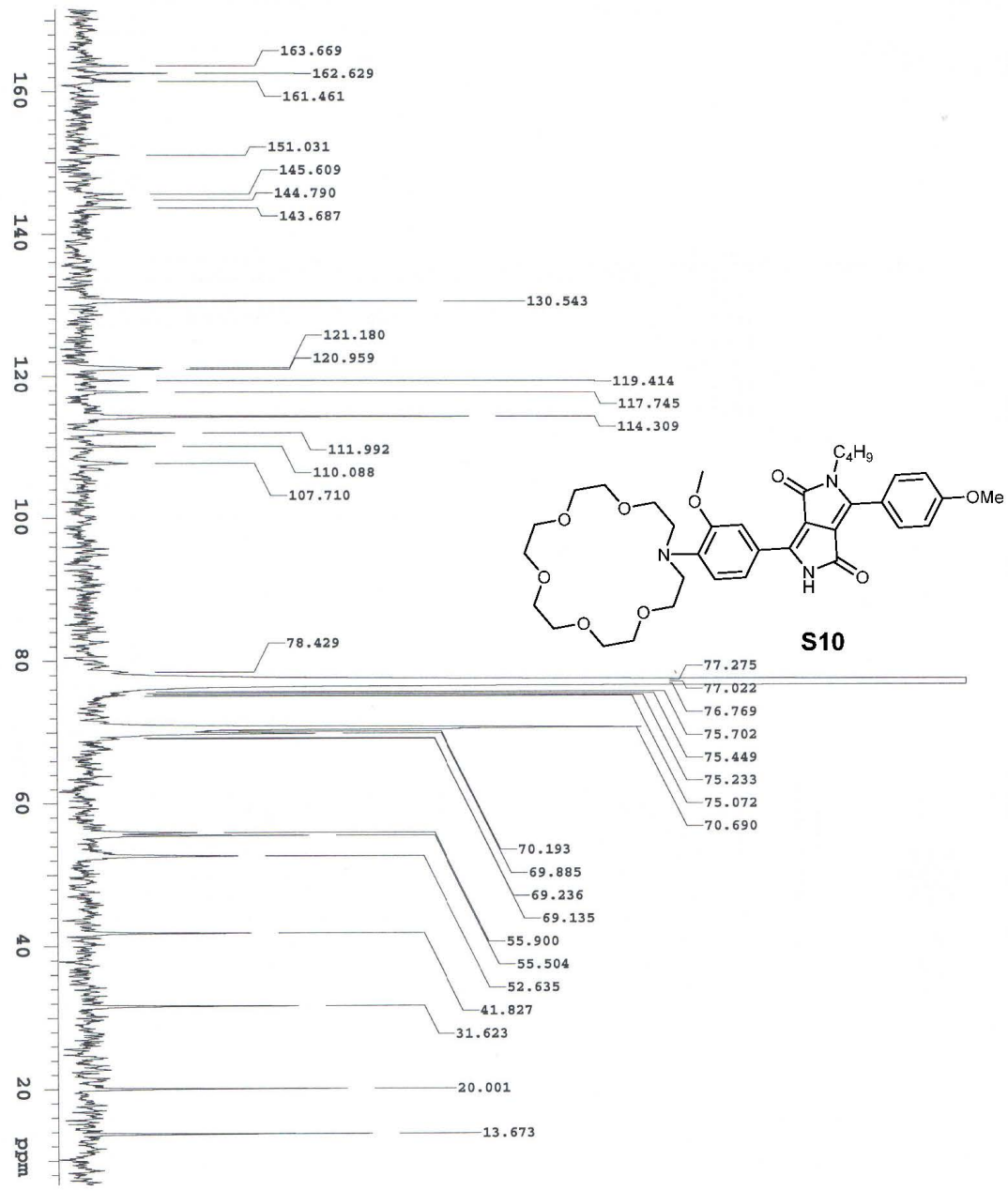

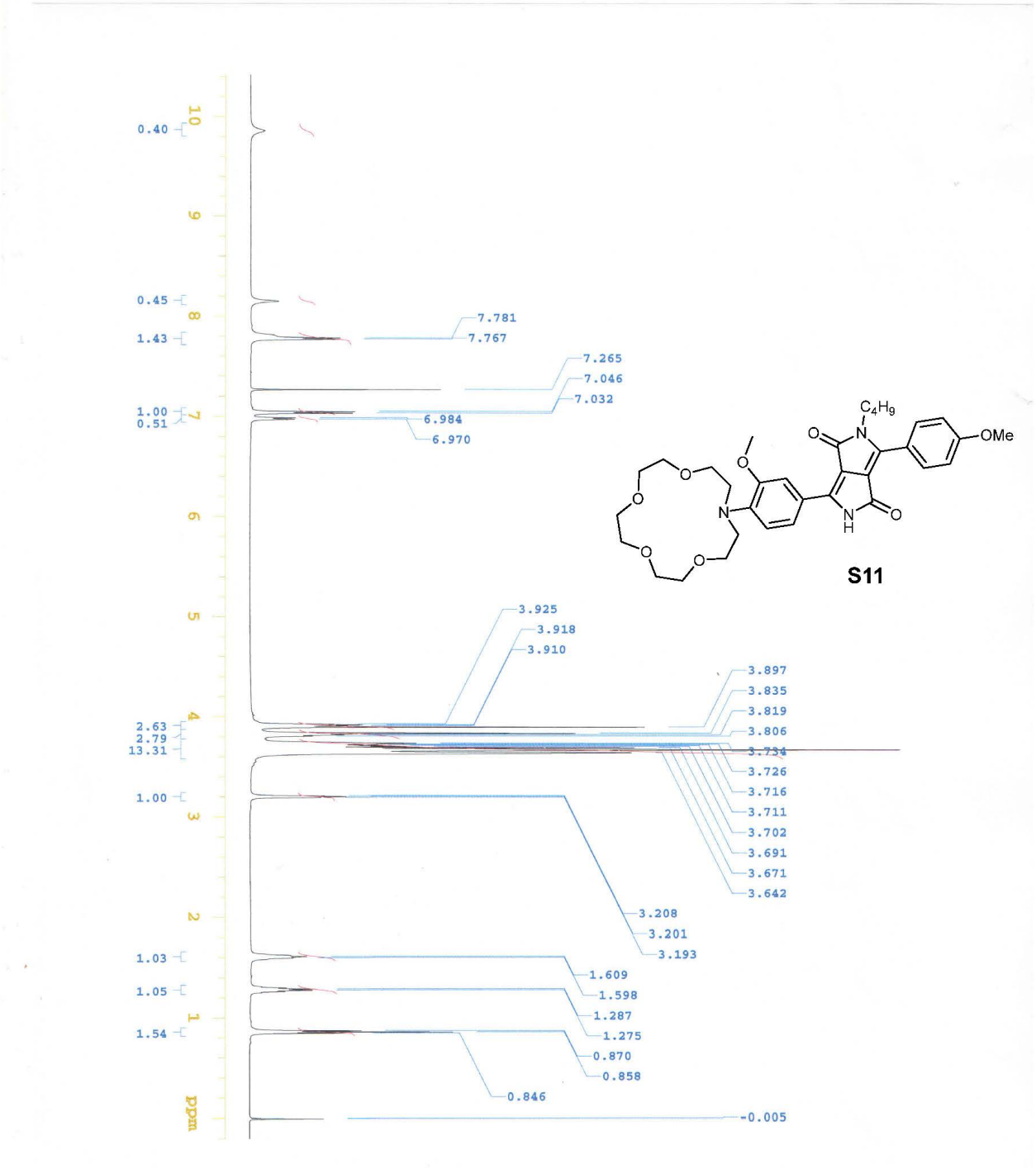

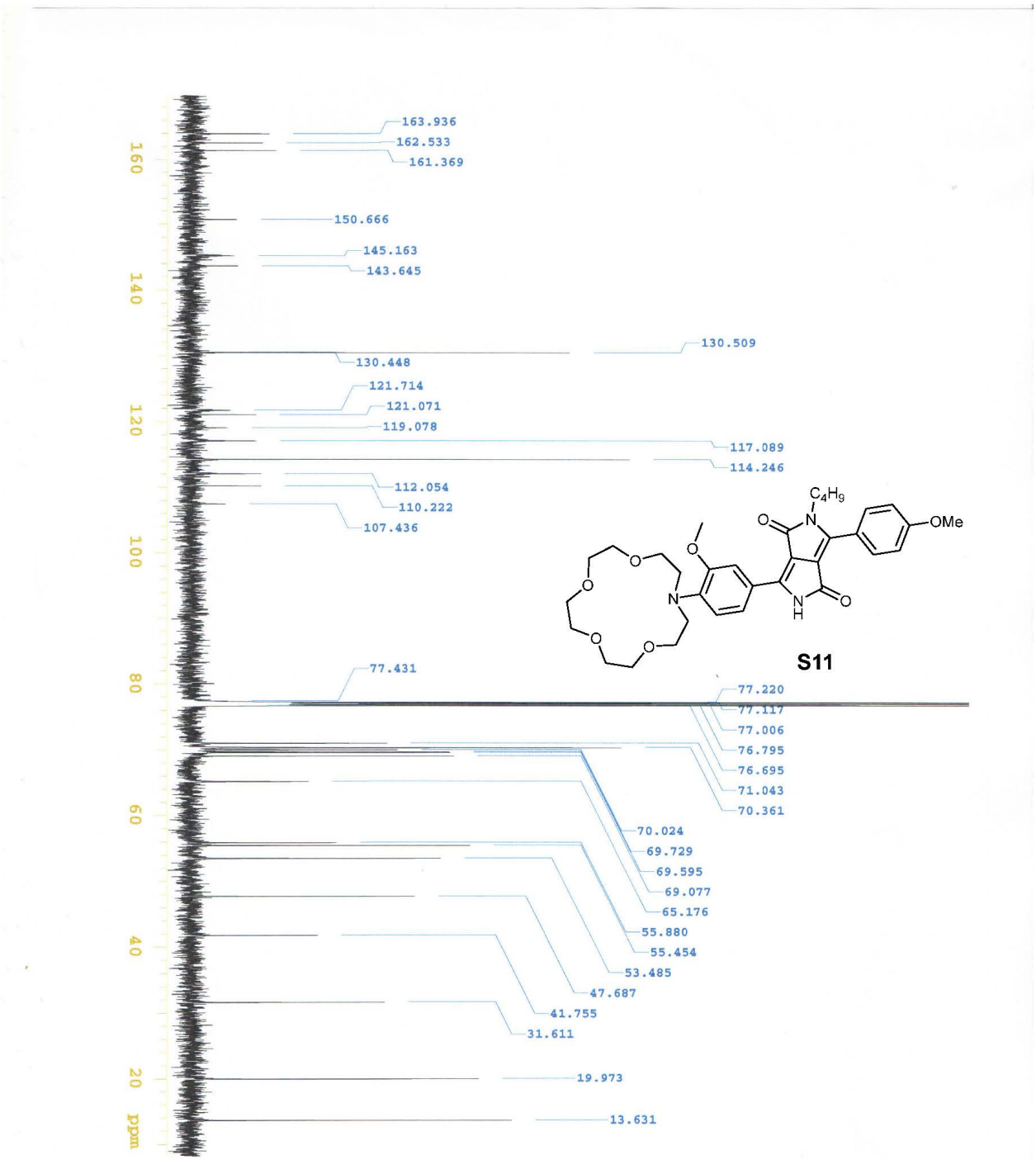

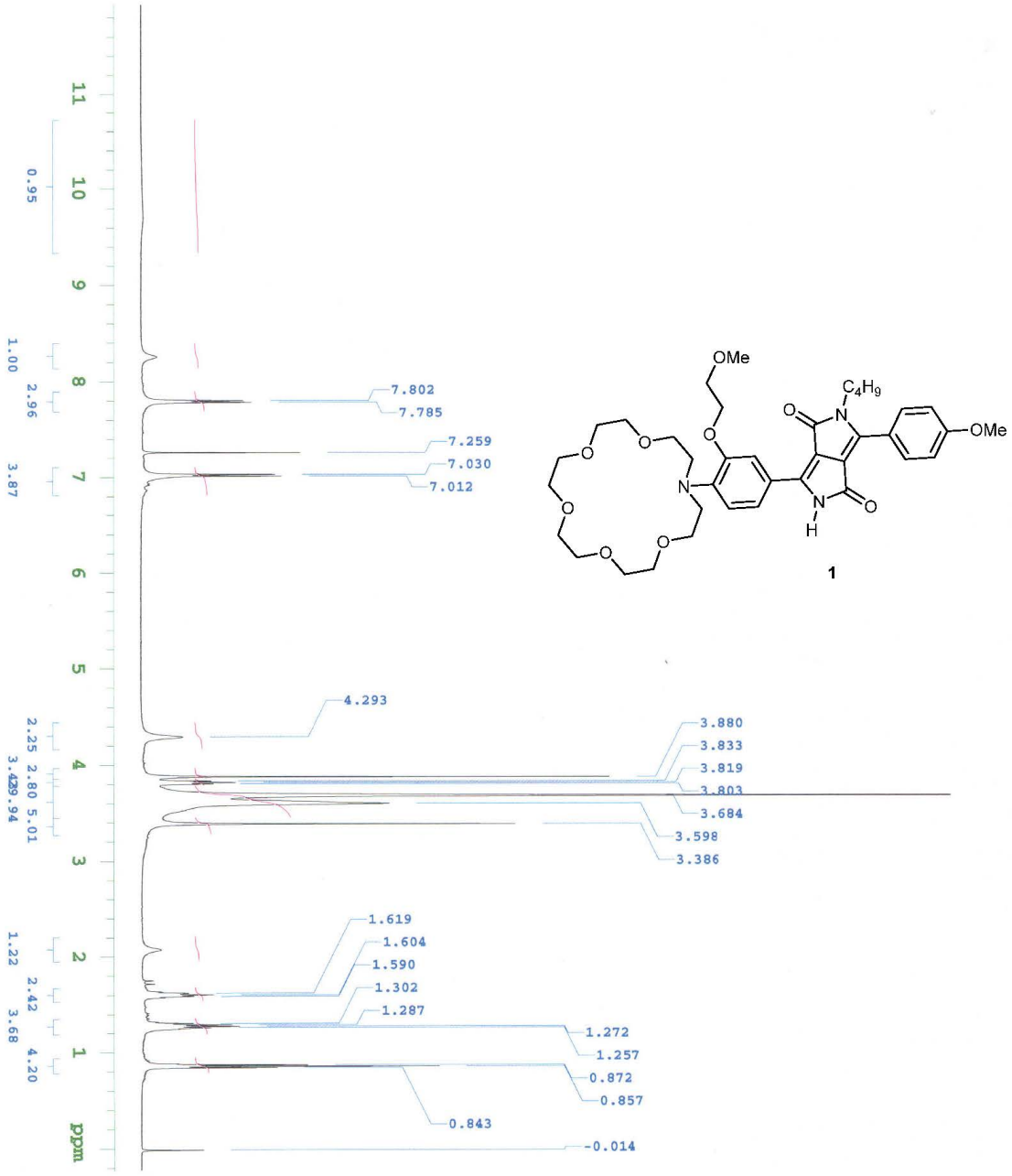

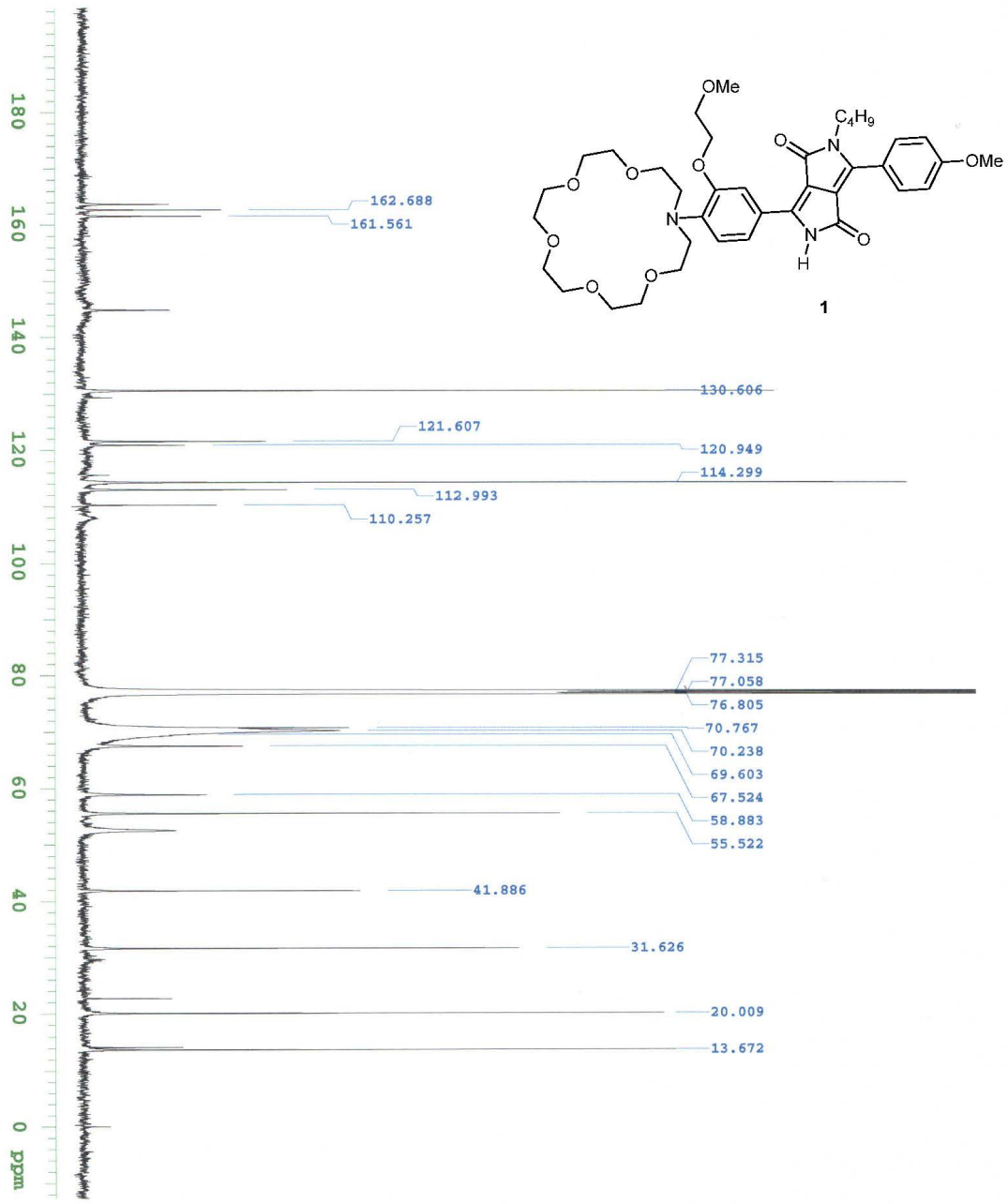

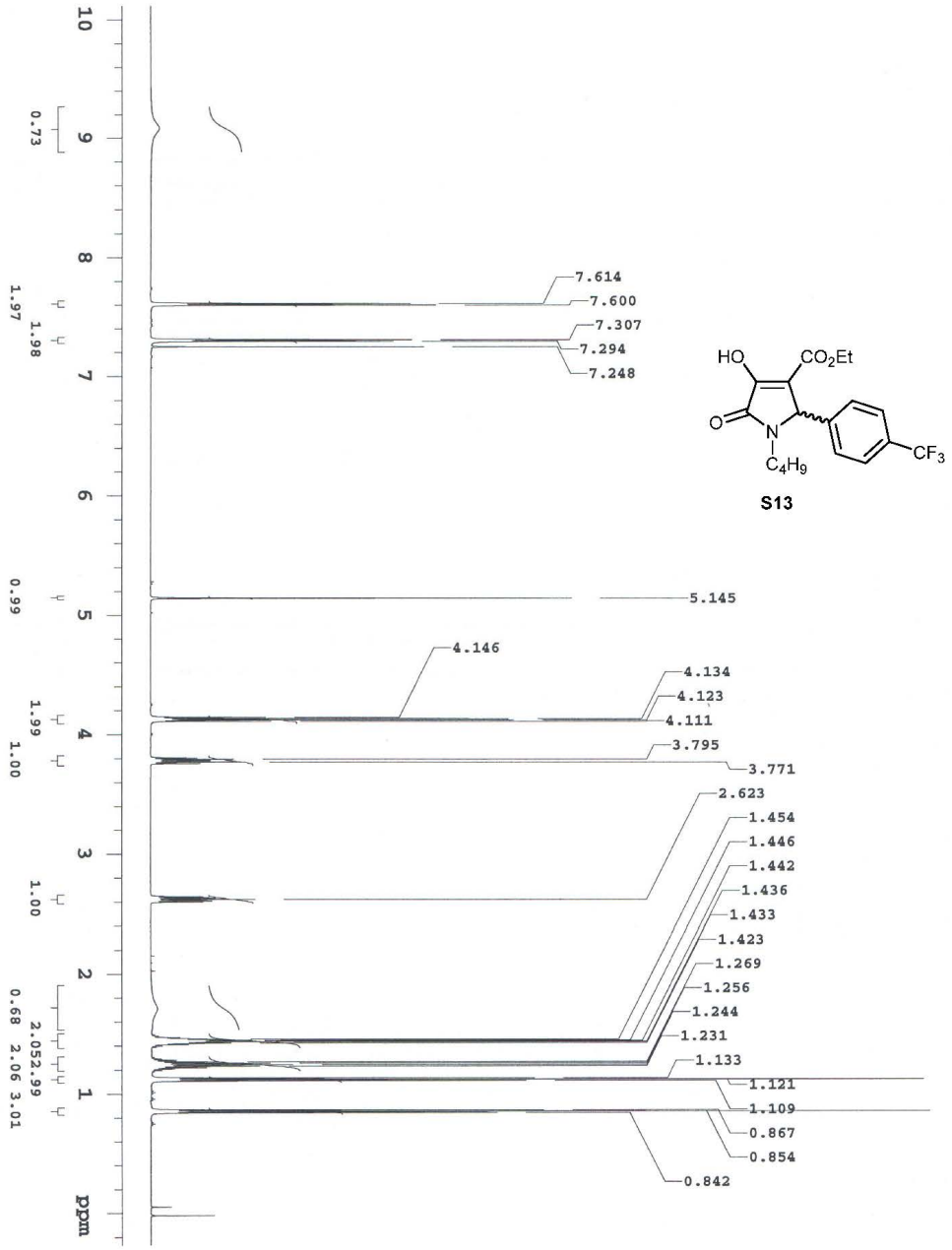

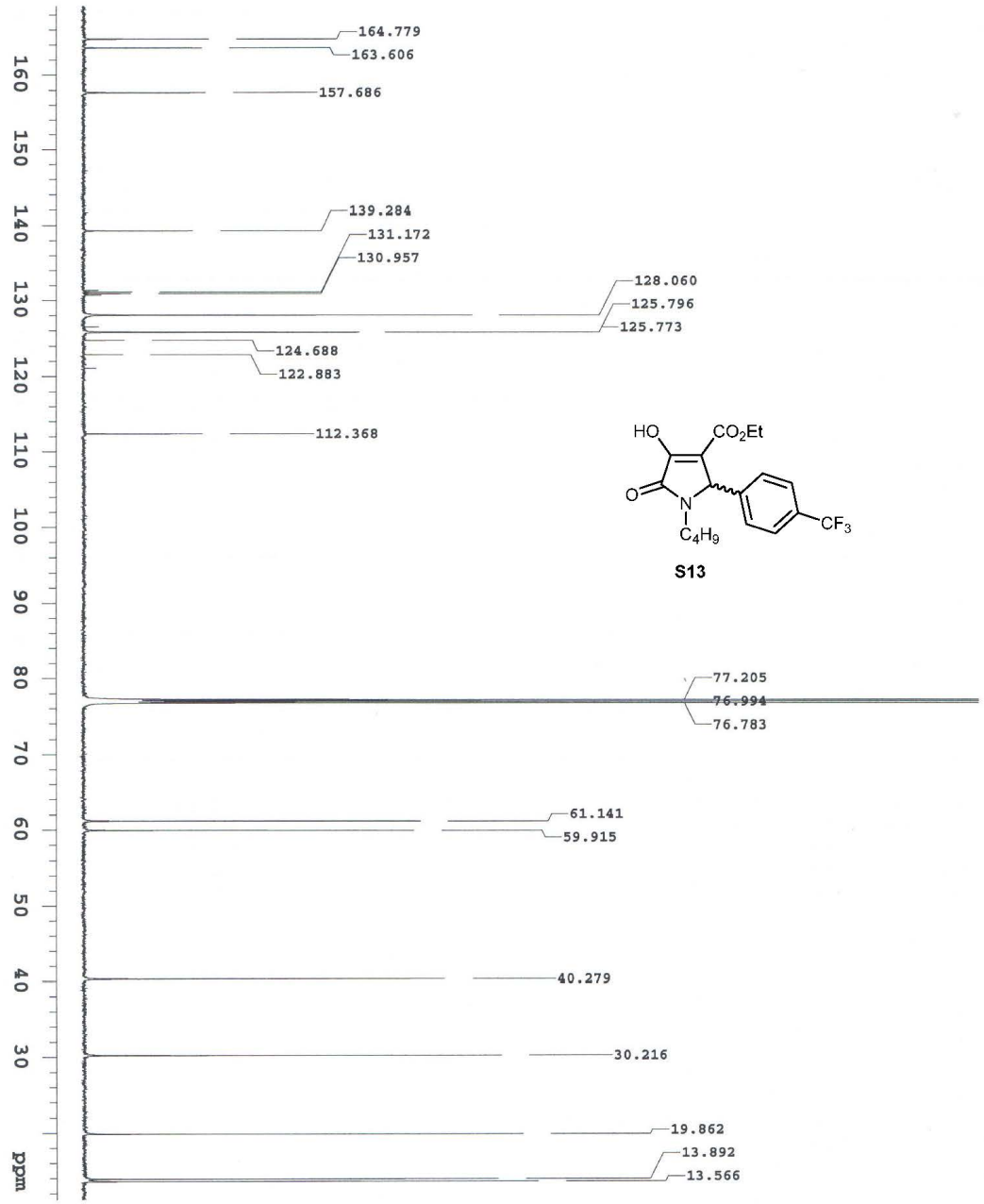

S13

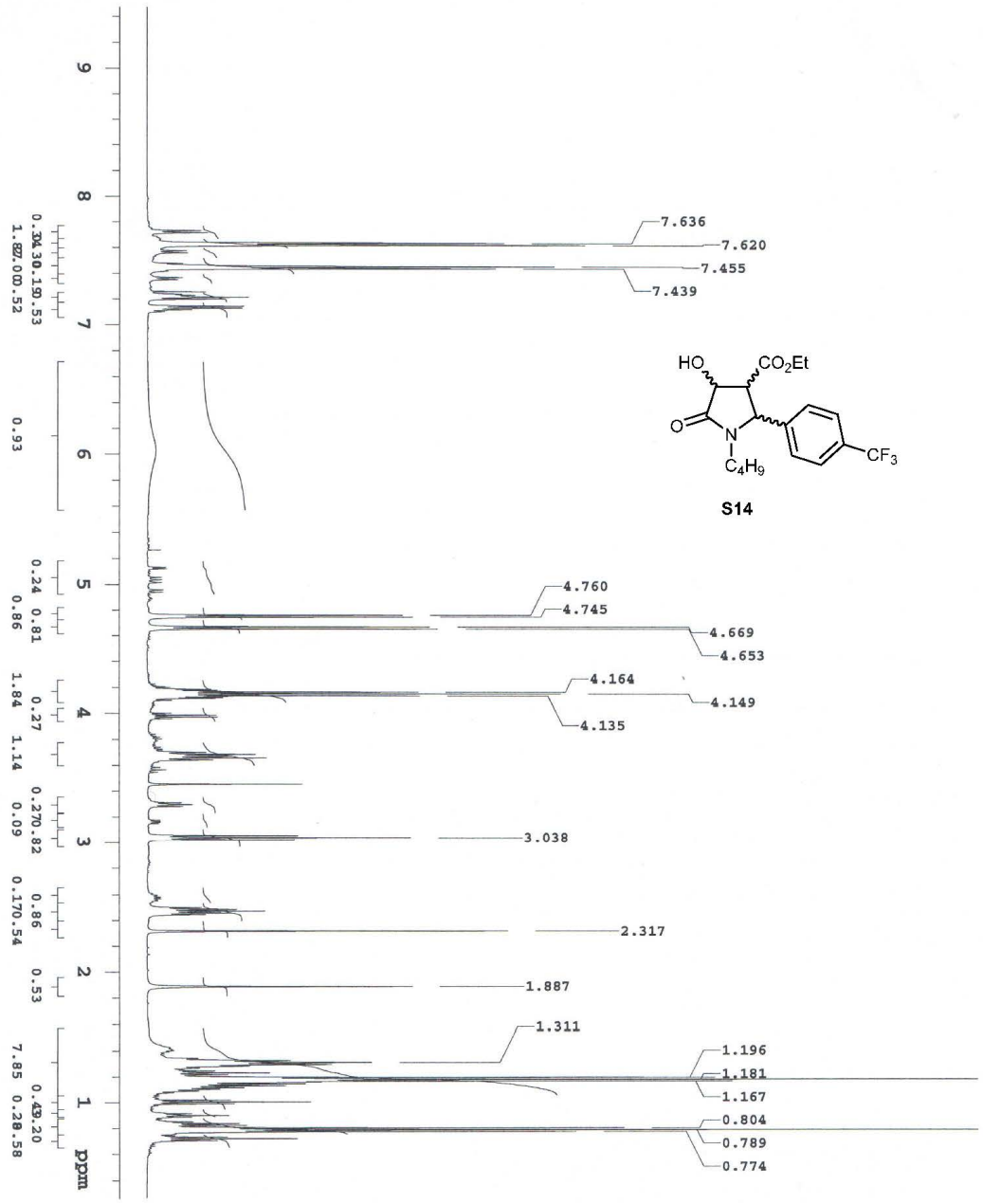

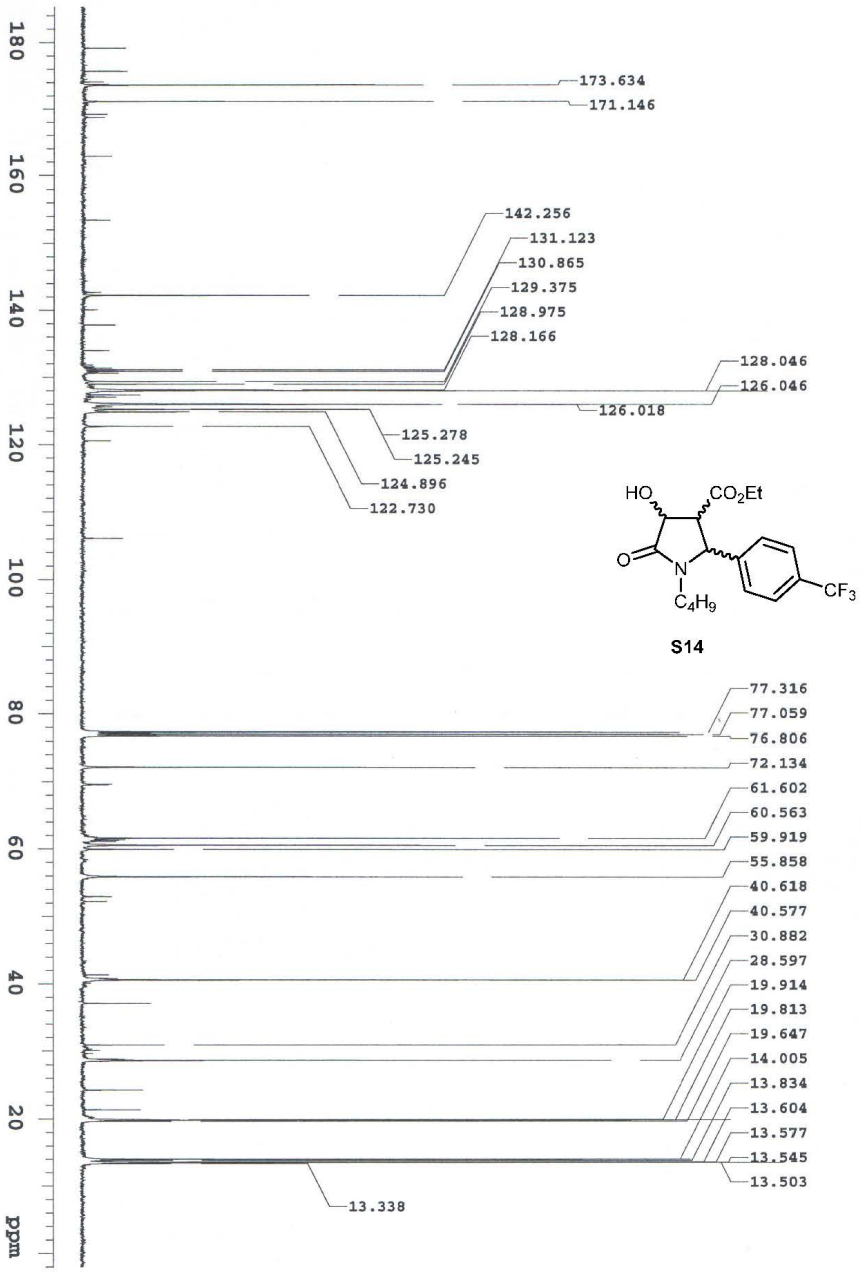

S14

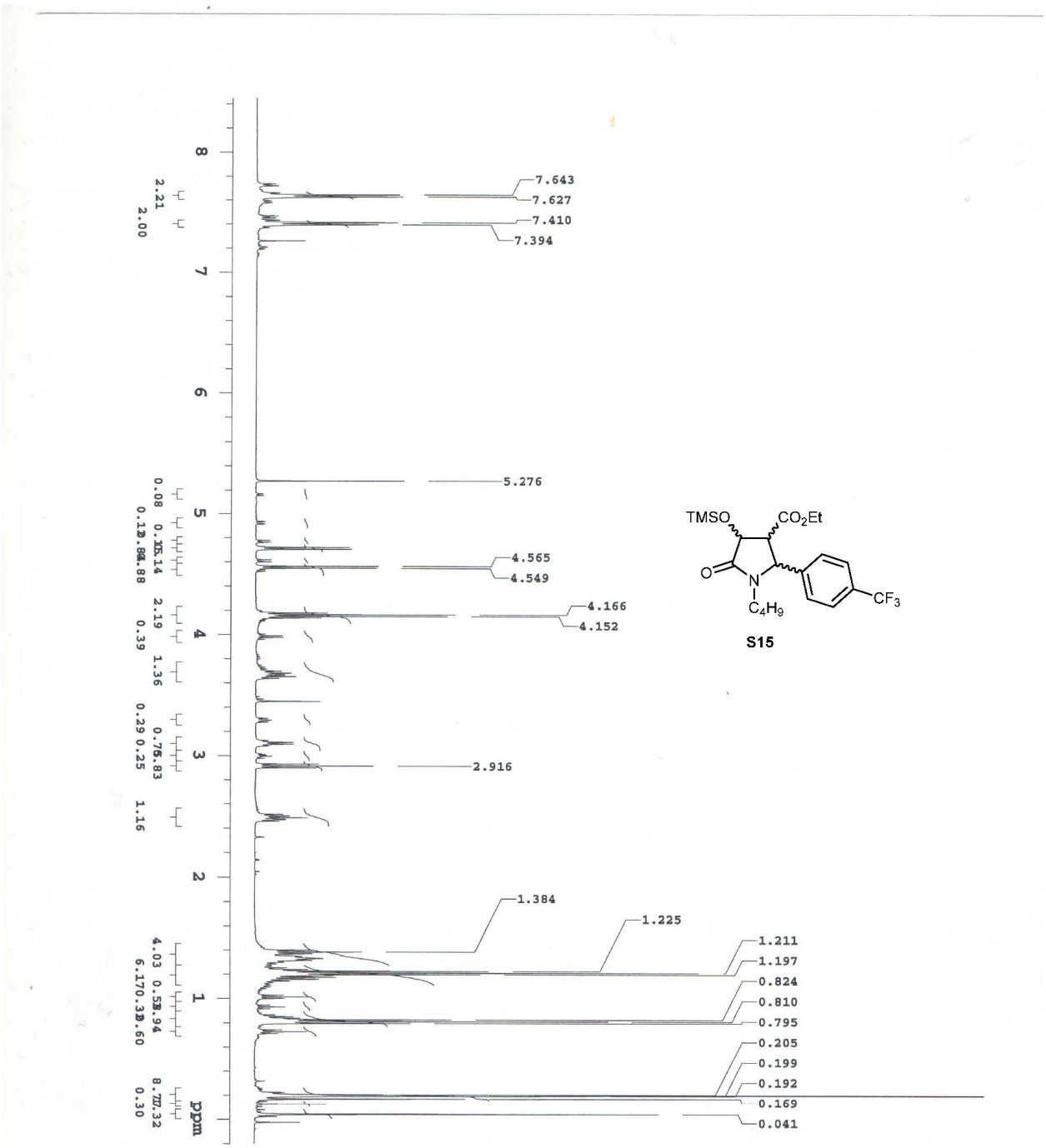

S15

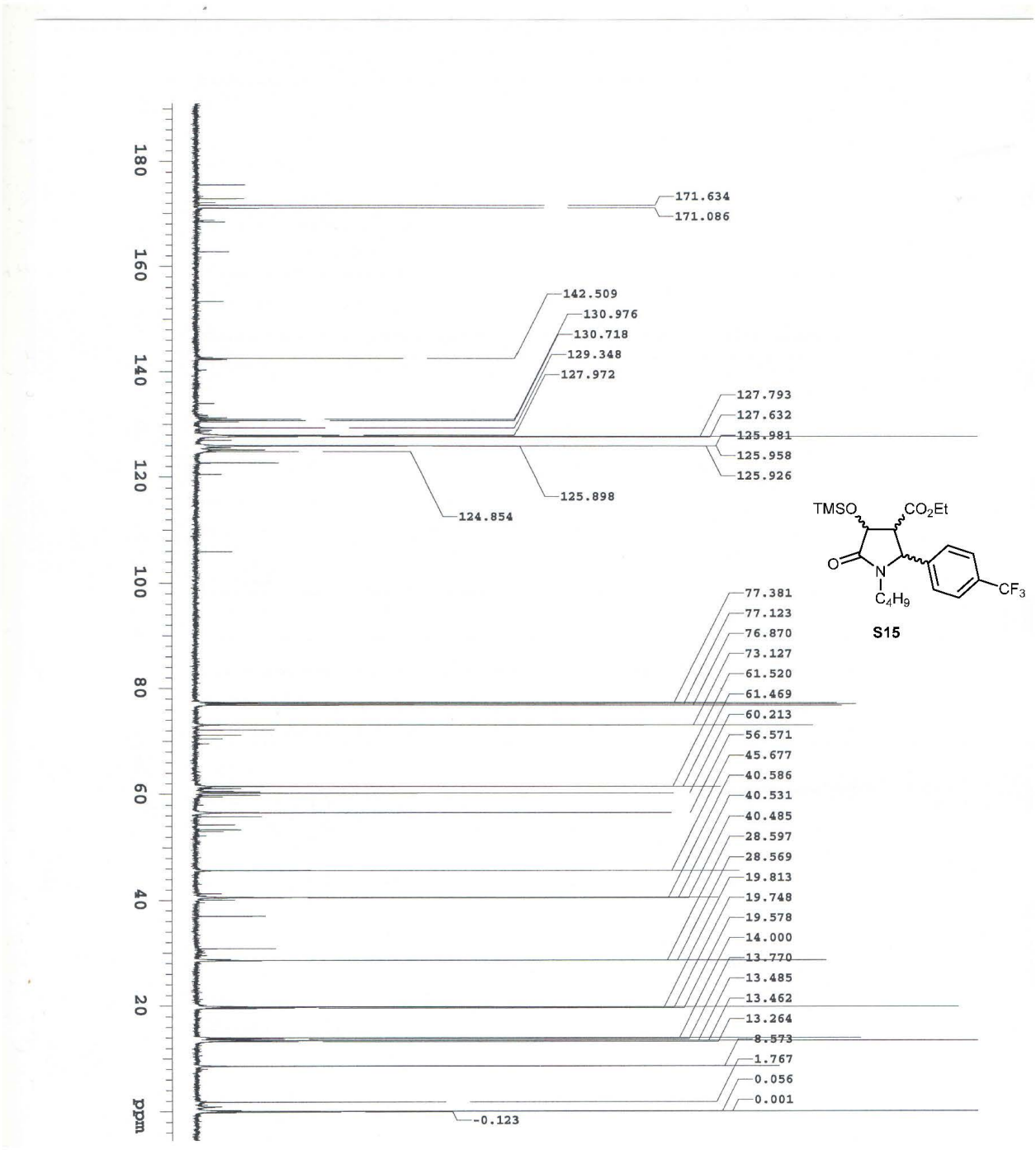

S15

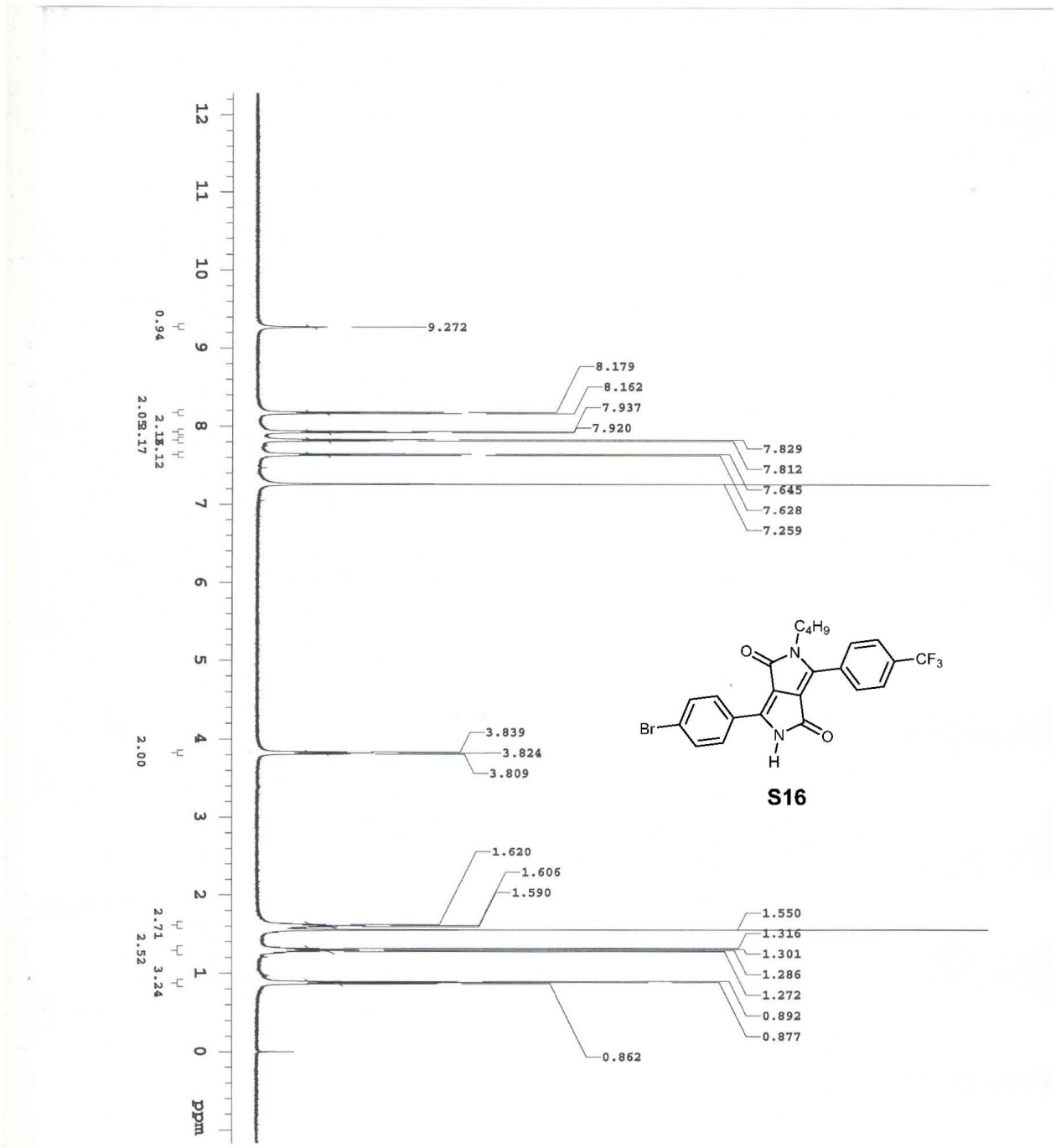

S16

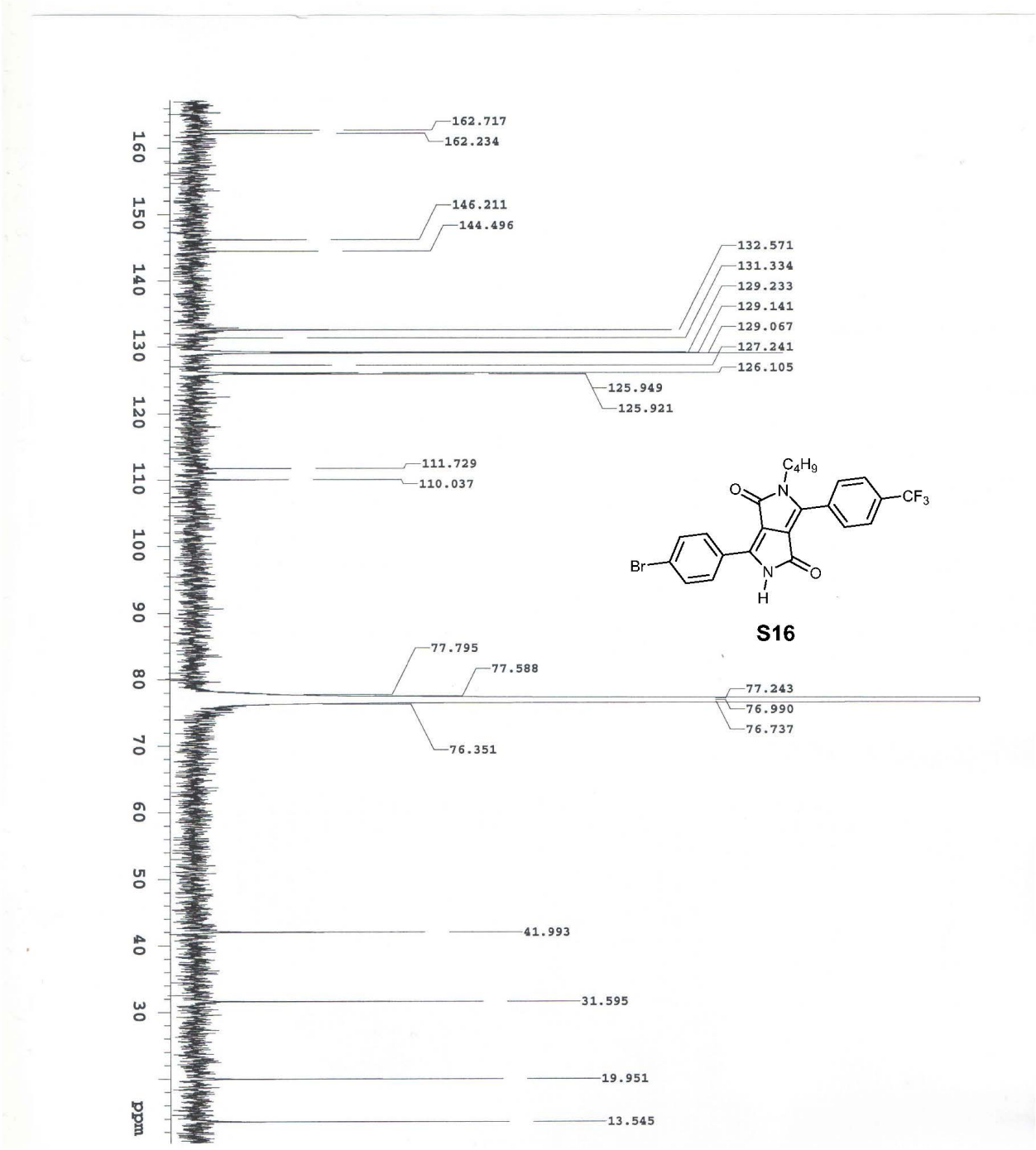

S16

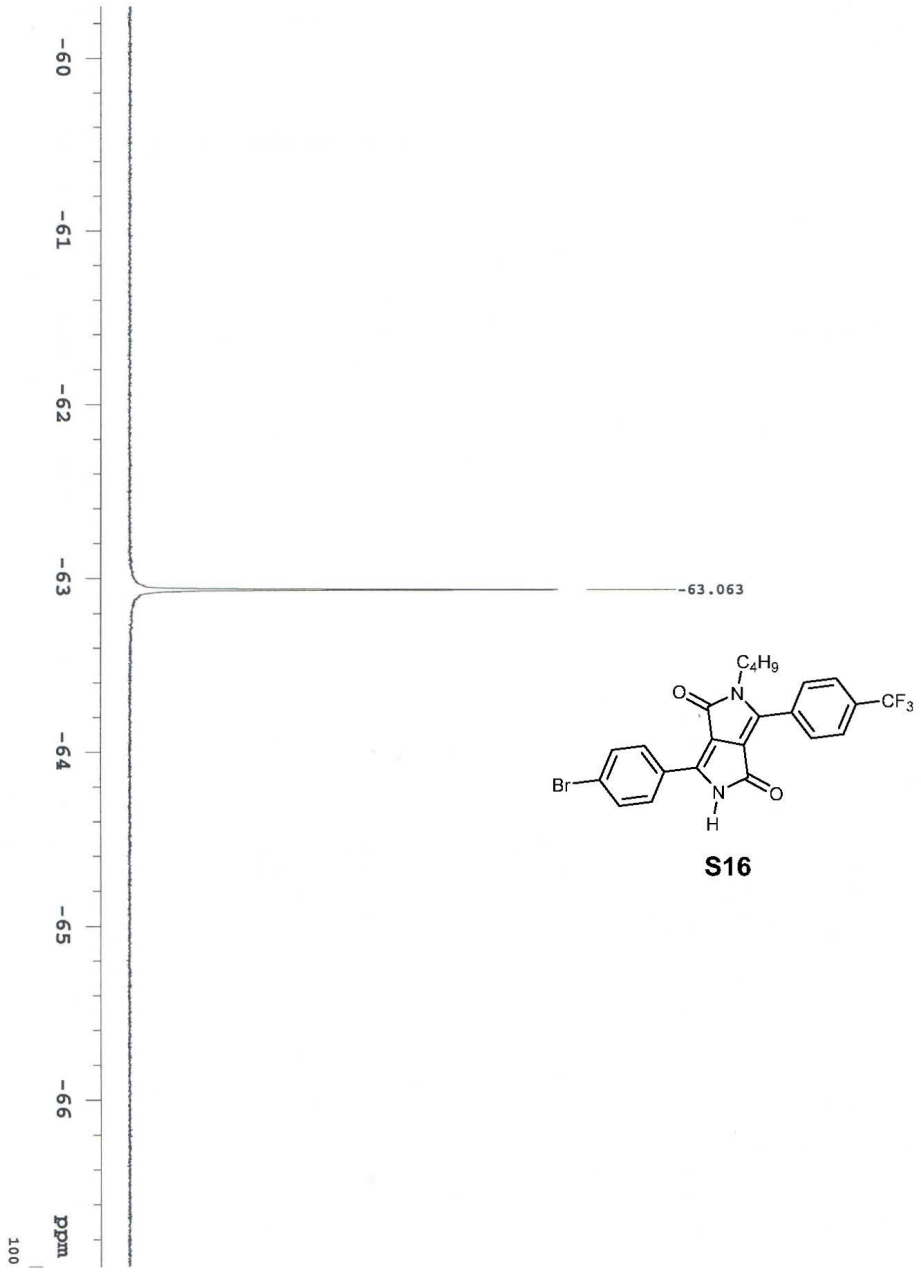

S16

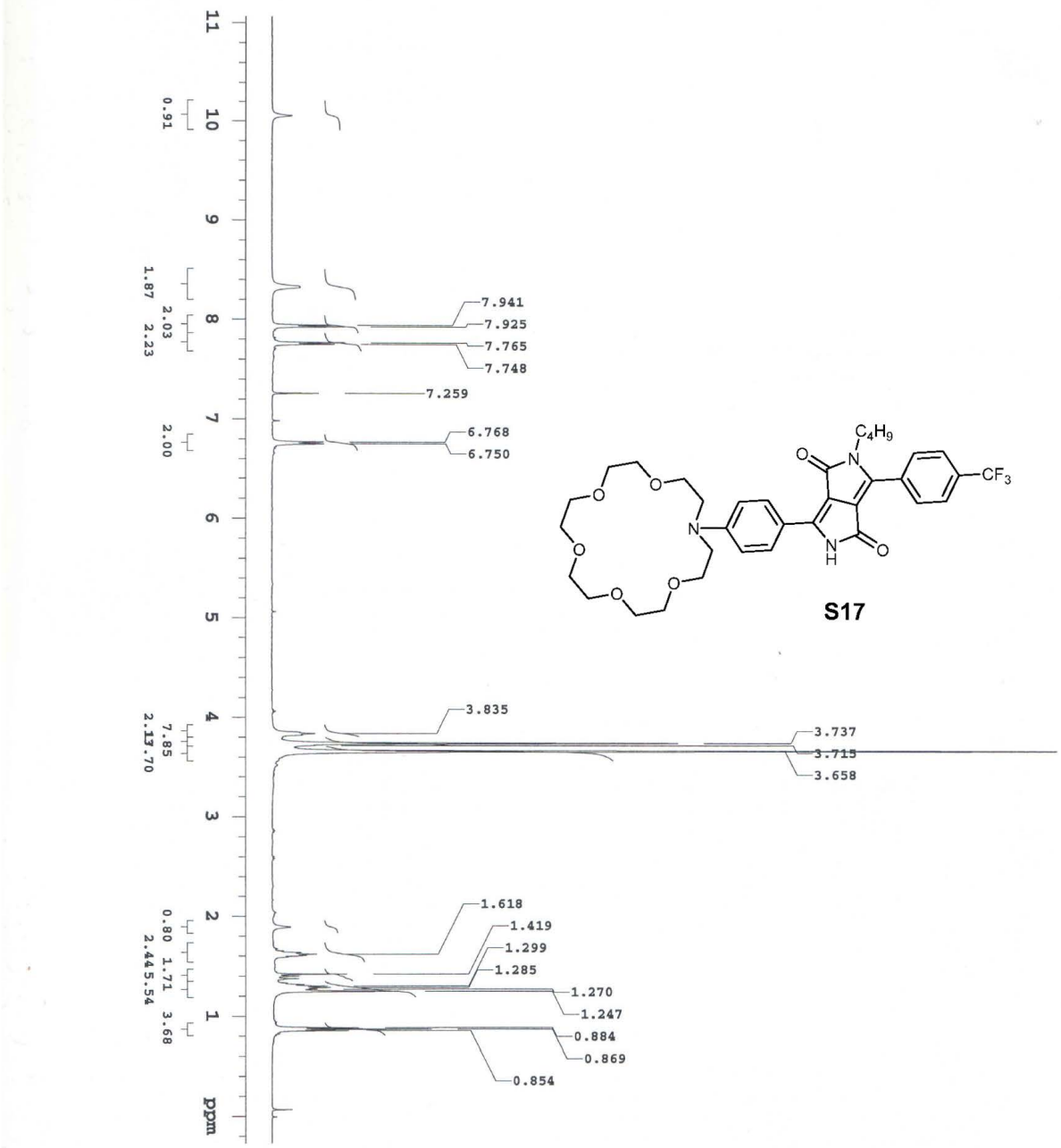

S17

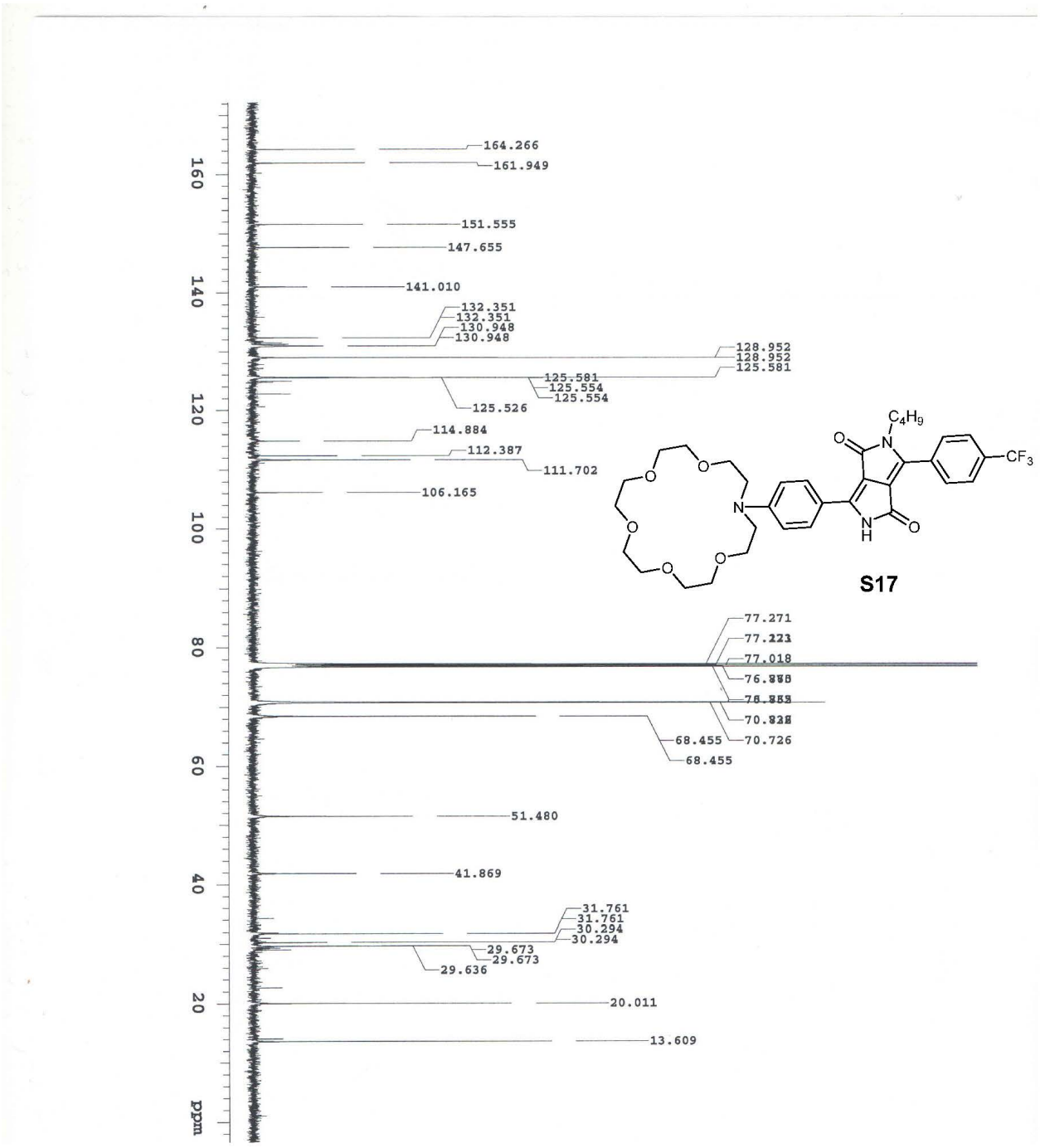

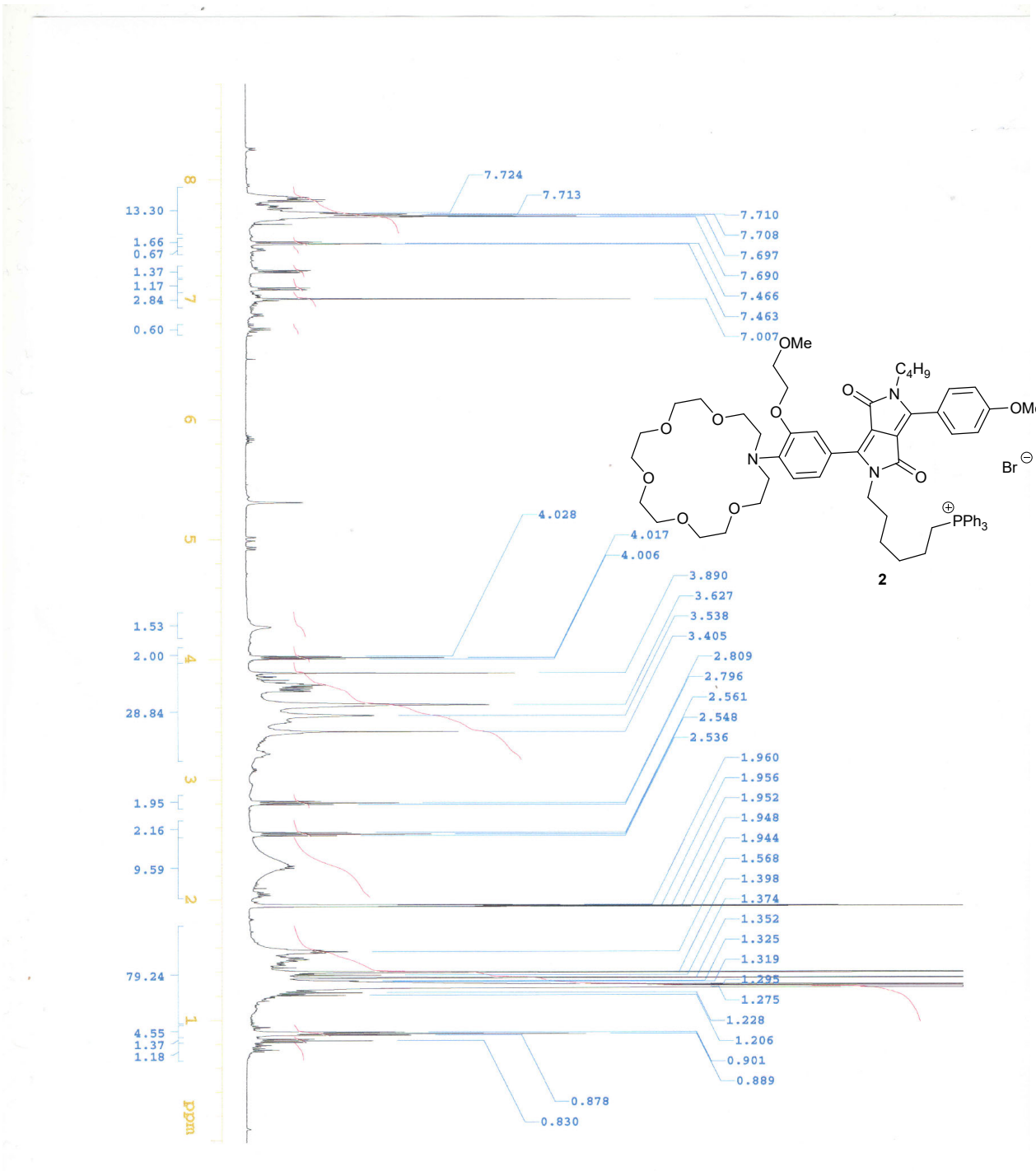

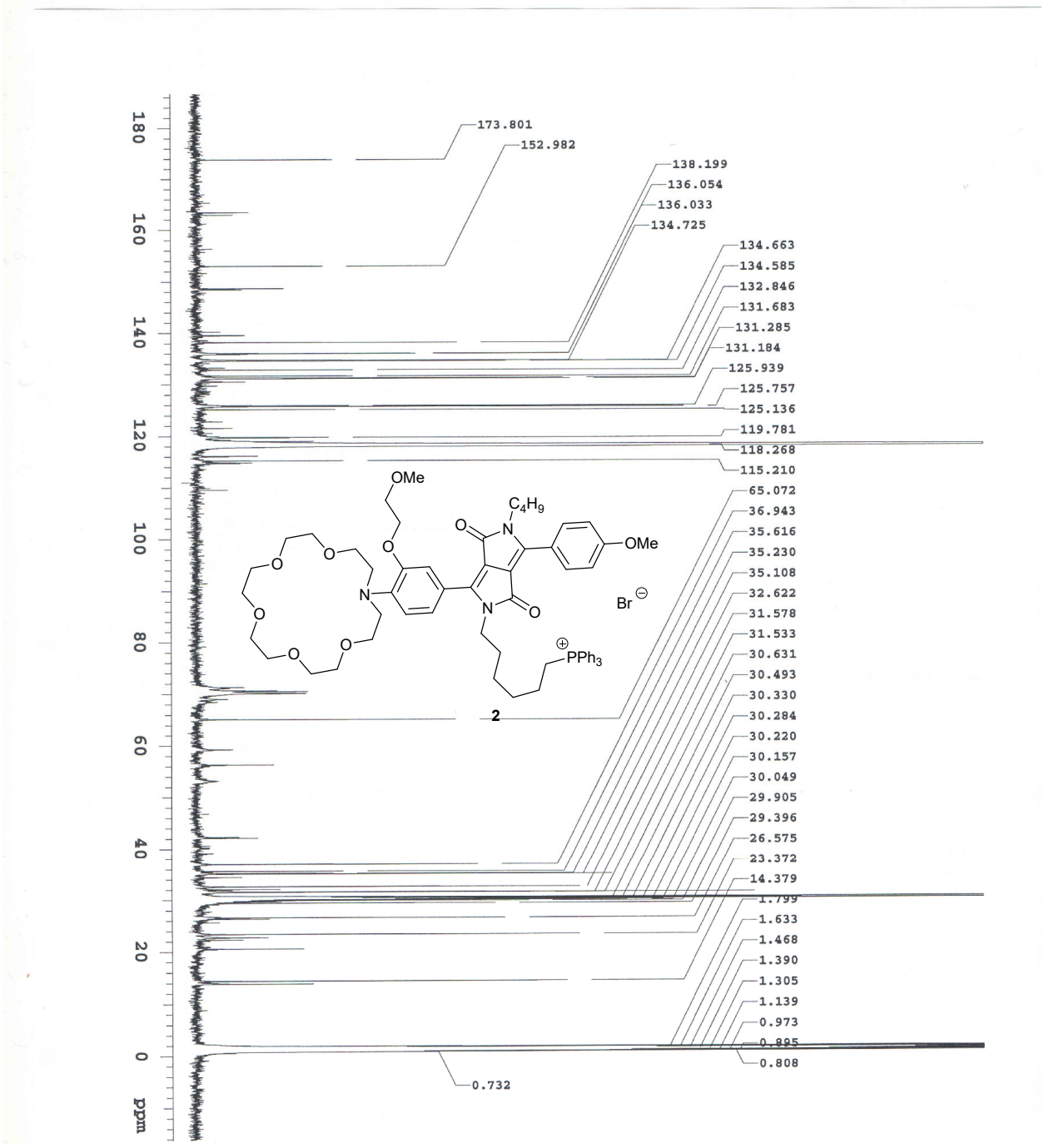

MS spectra

Elemental Composition Report

Page 1

Single Mass Analysis
Tolerance = 20.0 PPM / DBE: min = -1.5, max = 50.0
Selected filters: None

Monoisotopic Mass, Odd and Even Electron Ions
31 formula(e) evaluated with 1 results within limits (up to 50 best isotopic matches for each mass)
Elements Used:
C: 0-70 H: 0-100 N: 0-2 O: 0-3 Br: 1-1

D. Kumar
GDK-300
z10_dk2286 97 (3.700) Cm (82:99)

AUTOSPEC

04-Dec-2020 11:48:06
Operator: Malgorzata Grela
Voltage EI+
5.99e4

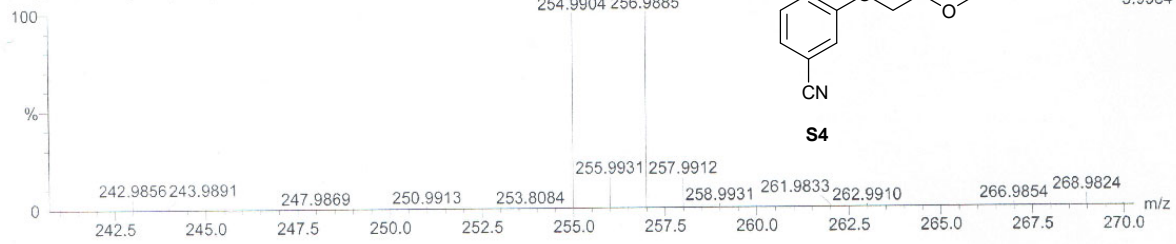

S4

Minimum:				-1.5		
Maximum:		5.0	20.0	50.0		
Mass	Calc. Mass	mDa	PPM	DBE	i-FIT	Formula
254.9904	254.9895	0.9	3.5	6.0	248.2	C10 H10 N O2 Br

C: 0-200 H: 0-200 N: 0-2 O: 0-4 Na: 0-1 Br: 0-2

Mass	Calc. Mass	mDa	PPM	DBE	Formula	i-FIT	i-FIT Norm	Fit Conf %	C	H	N	O	Na	Br
505.0726	505.0742	-1.6	-3.2	33.5	C37 H10 N2 Na	416.0	13.734	0.00	37	10	2		1	
	505.0742	-1.6	-3.2	9.5	C25 H31 O Br2	402.5	0.218	80.43	25	31		1		2
	505.0739	-1.3	-2.6	13.5	C24 H23 N2 O4 Na Br	403.9	1.634	19.52	24	23	2	4	1	1
	505.0718	0.8	1.6	6.5	C23 H32 O Na Br2	409.9	7.635	0.05	23	32		1	1	2

OV-959

z10_dk716 11 (0.243) Cm (8:20-(2:4+40:47))

1: TOF MS ES+
2.03e5

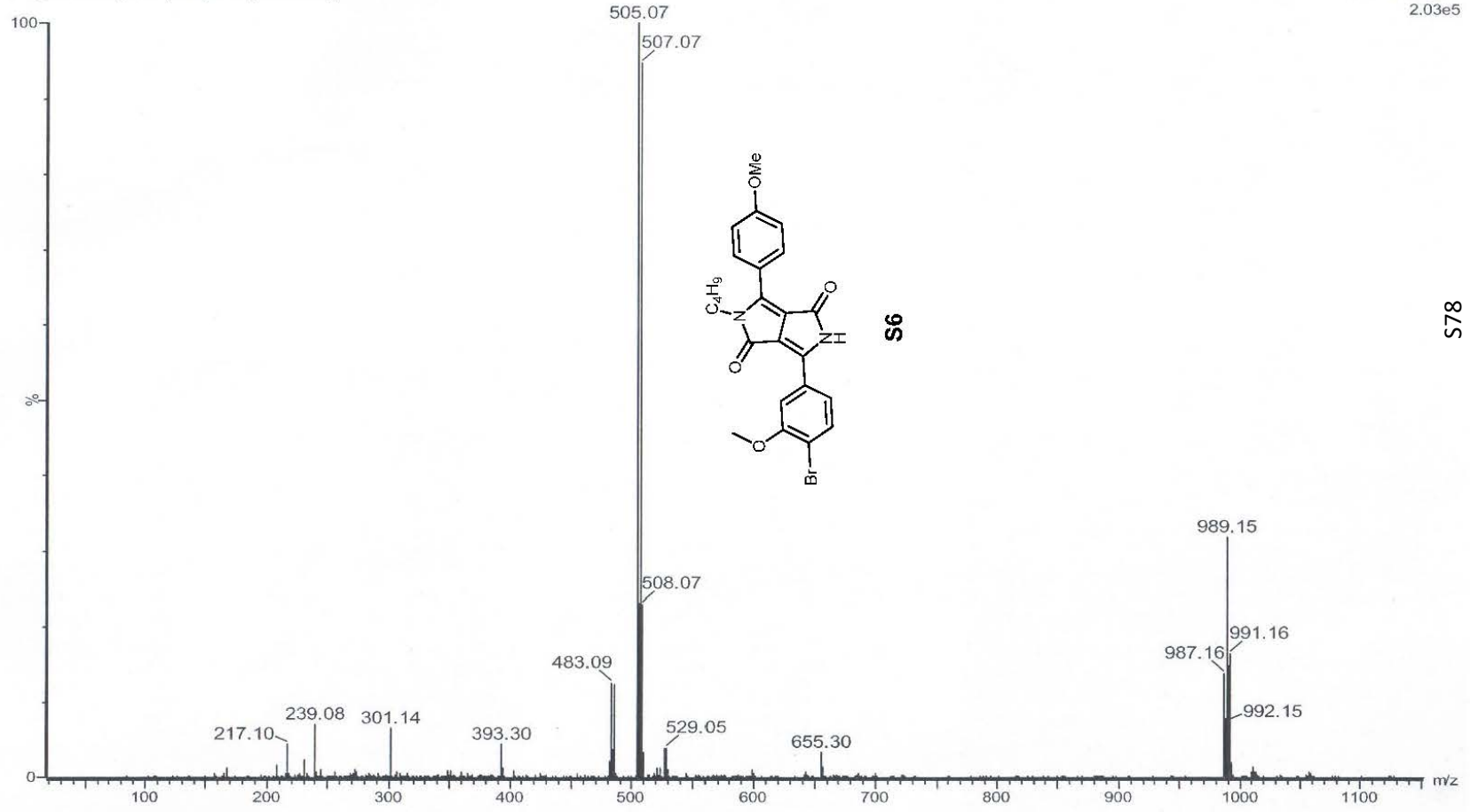

S6

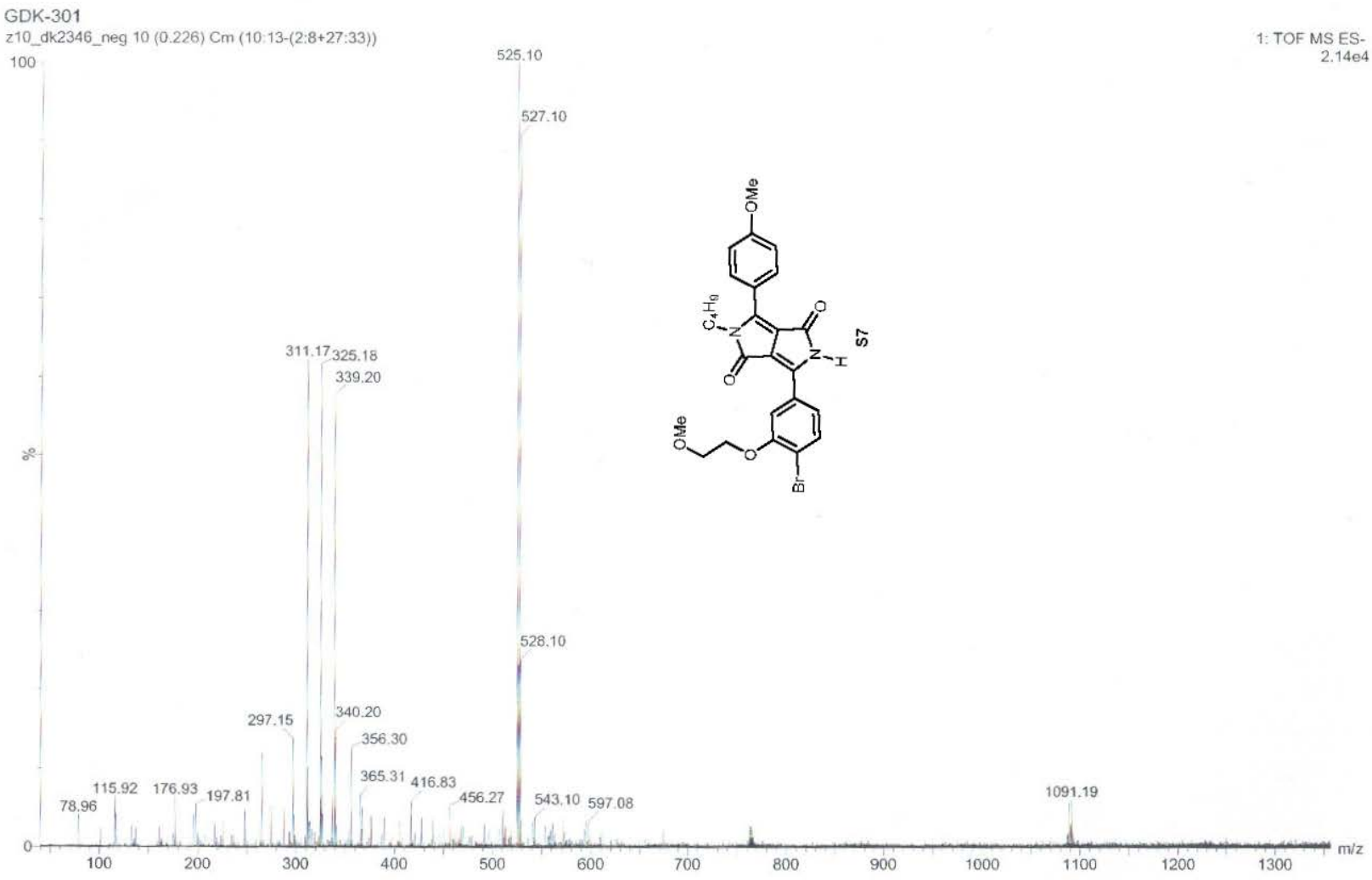

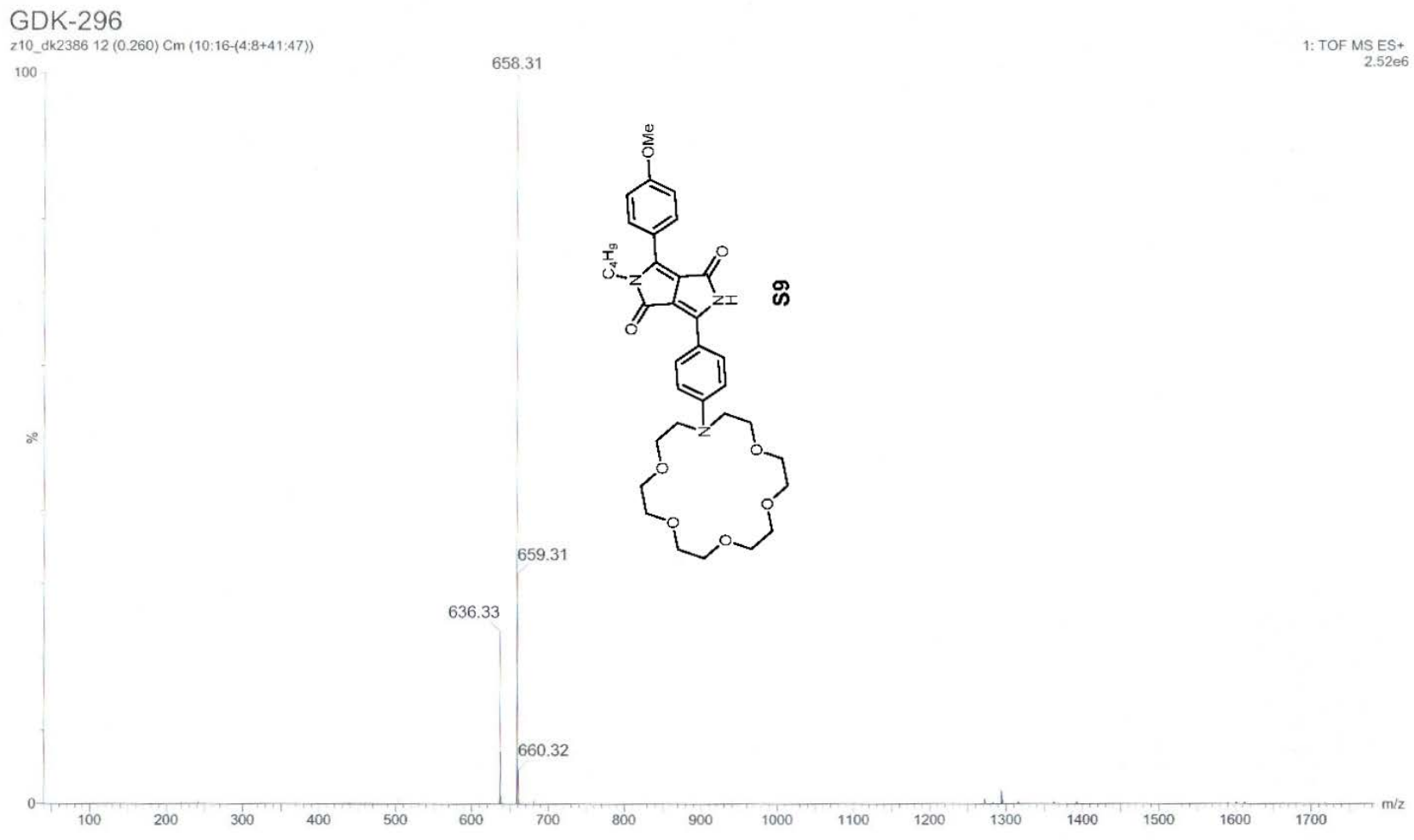

Elemental Composition Report **Page 1**

Single Mass Analysis
Tolerance = 15.0 PPM / DBE: min = -1.5, max = 50.0
Selected filters: None

Monoisotopic Mass, Odd and Even Electron Ions
28 formula(e) evaluated with 1 results within limits (up to 50 best isotopic matches for each mass)
Elements Used:
C: 0-70 H: 0-100 N: 0-3 O: 9-9

D. Kumar
GDK-273
z10_dk1498h 93 (3.547) Cm (93:113)

AUTOSPEC

17-Sep-2020 11:42:39
Operator: Malgorzata Grela
Voltage EI+
3.68e3

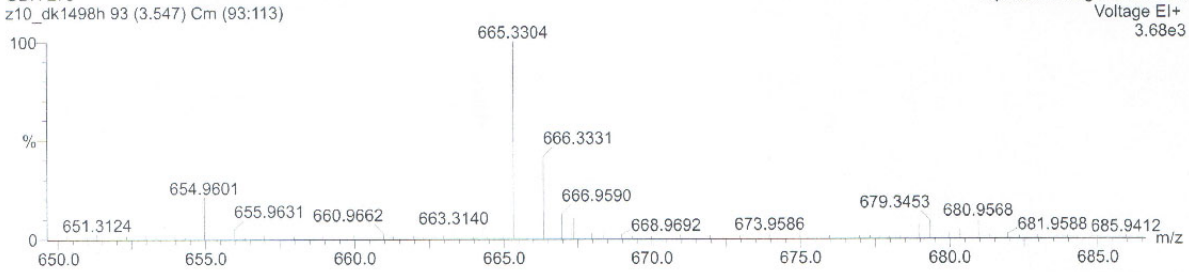

Minimum:				-1.5		
Maximum:		5.0	15.0	50.0		
Mass	Calc. Mass	mDa	PPM	DBE	i-FIT	Formula
665.3304	665.3312	-0.8	-1.2	15.0	1.2	C36 H47 N3 O9

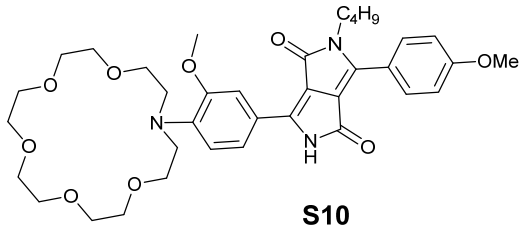

S10

GDK-293

z10_dk2345 12 (0.260) Cm (9:20-(2:8+32:40))

1: TOF MS ES+
2.38e5

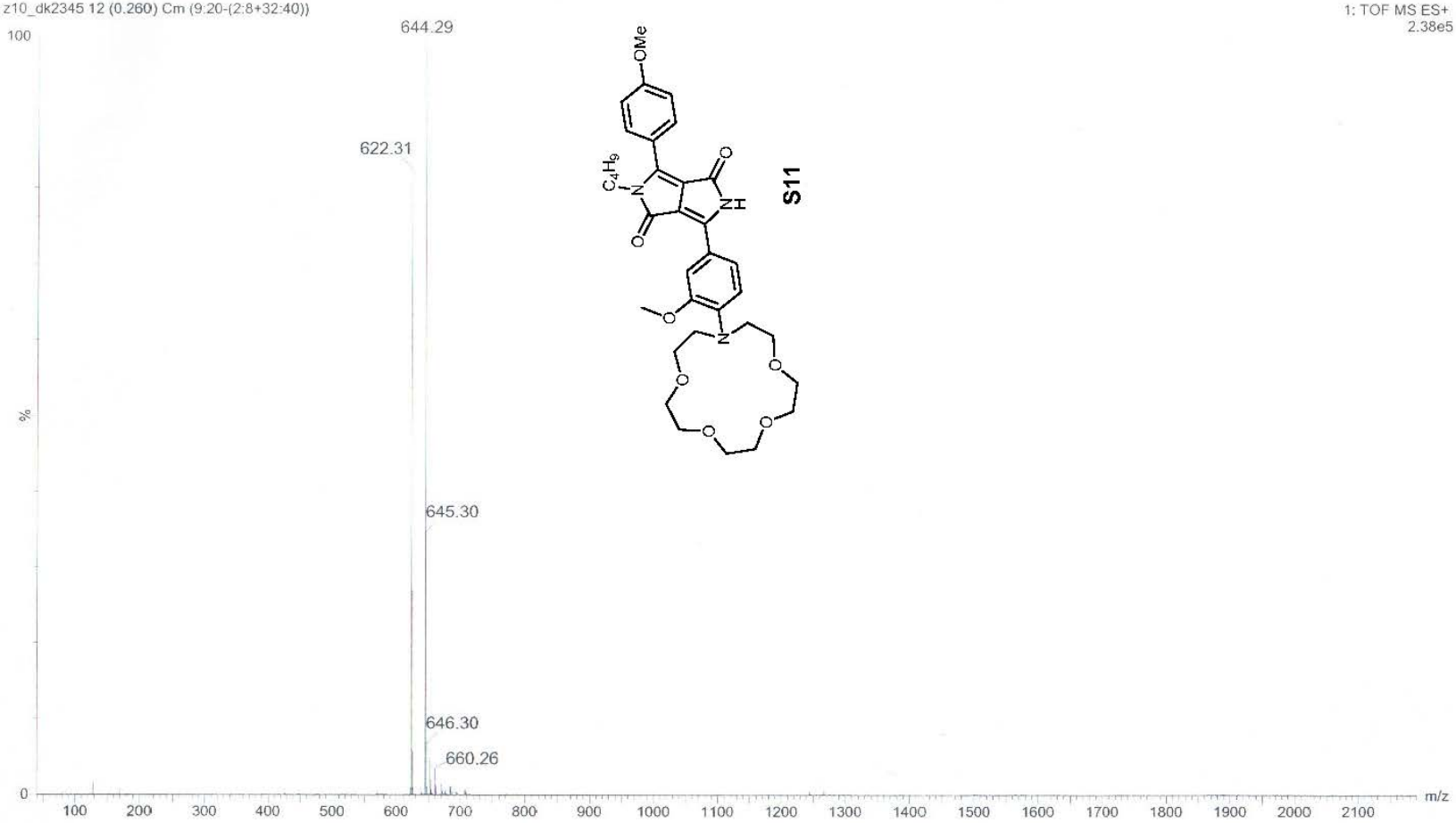

S11

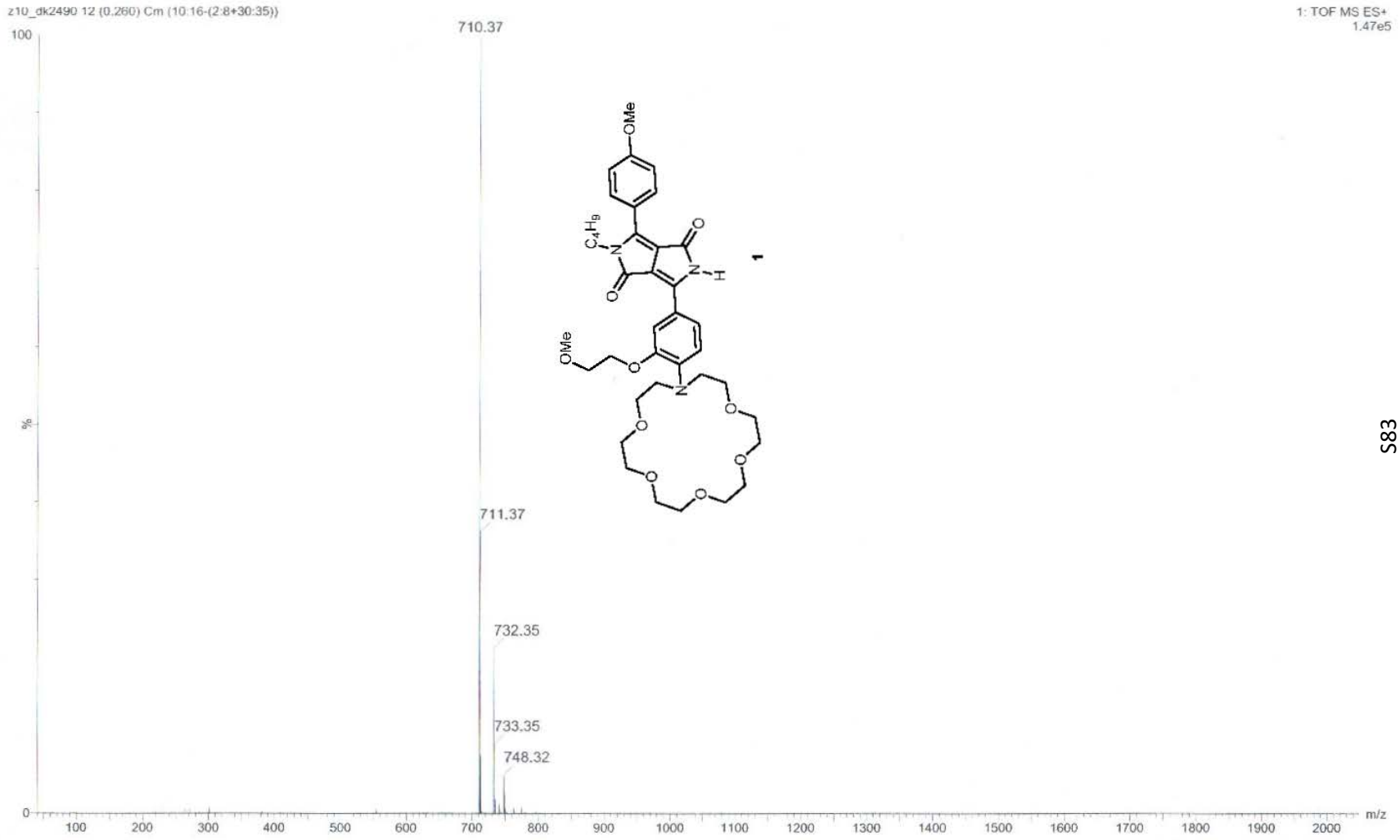

Single Mass Analysis

Tolerance = 15.0 PPM / DBE: min = -1.5, max = 50.0
Selected filters: None

Monoisotopic Mass, Odd and Even Electron Ions
42 formula(e) evaluated with 1 results within limits (up to 50 best isotopic matches for each mass)
Elements Used:
C: 0-70 H: 0-100 N: 0-1 O: 0-4 F: 3-3

K. Dinesh
GDK0344-10
z10_kd0708h 142 (5.415) Cm (136:142)

AUTOSPEC

31-Mar-2021 15:06:39
Operator: Marian Olejnik
Voltage EI+
625

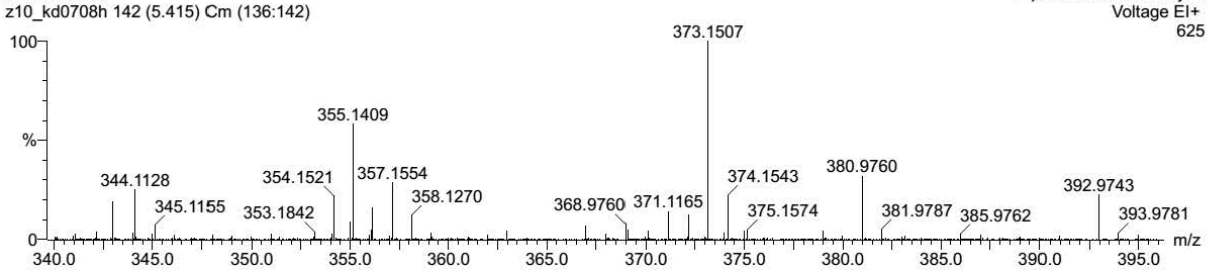

Minimum:				-1.5		
Maximum:		5.0	15.0	50.0		
Mass	Calc. Mass	mDa	PPM	DBE	i-FIT	Formula
373.1507	373.1501	0.6	1.6	7.0	2.9	C18 H22 N O4 F3

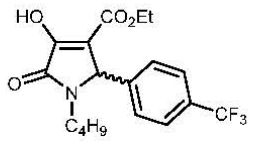

S13

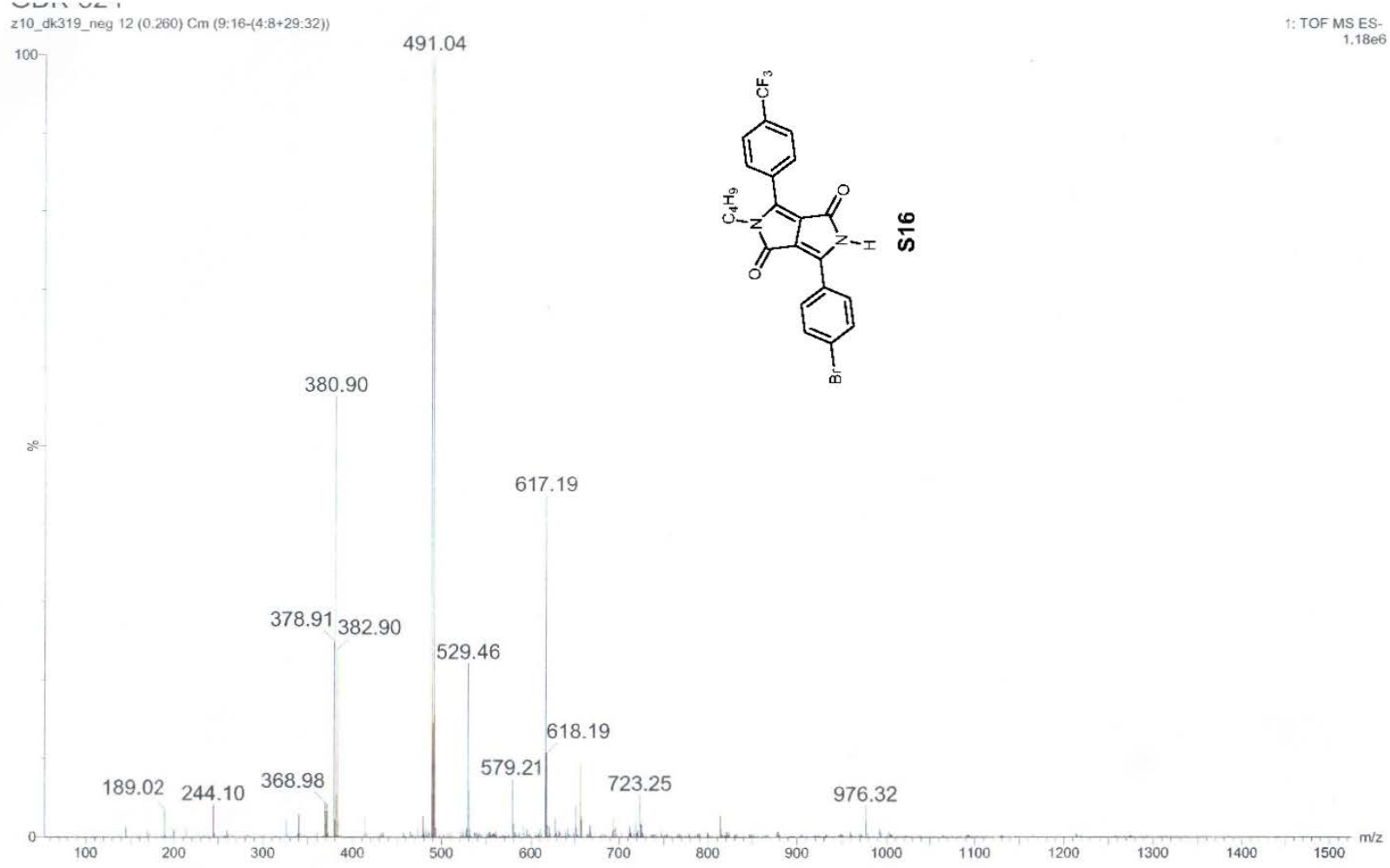

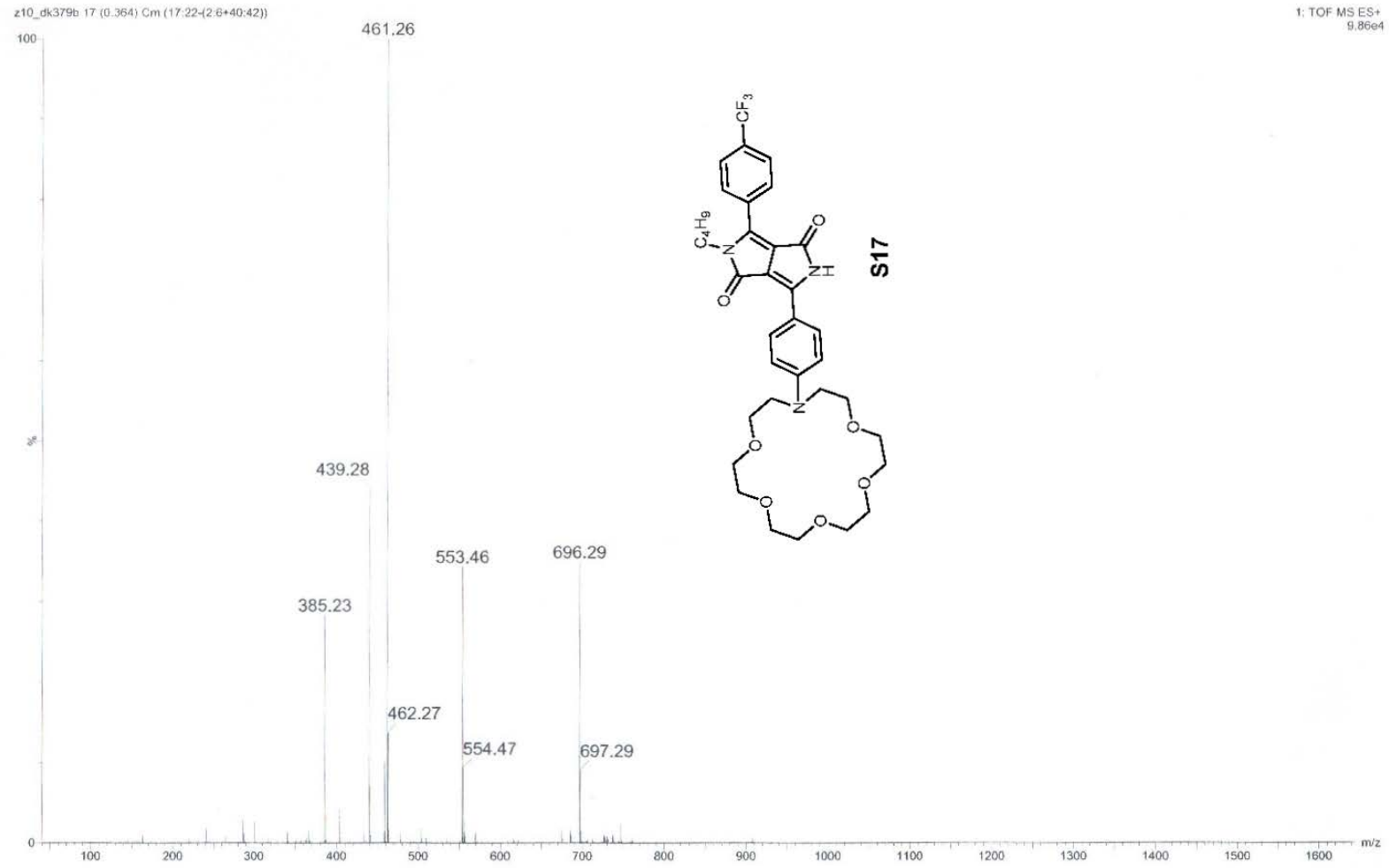

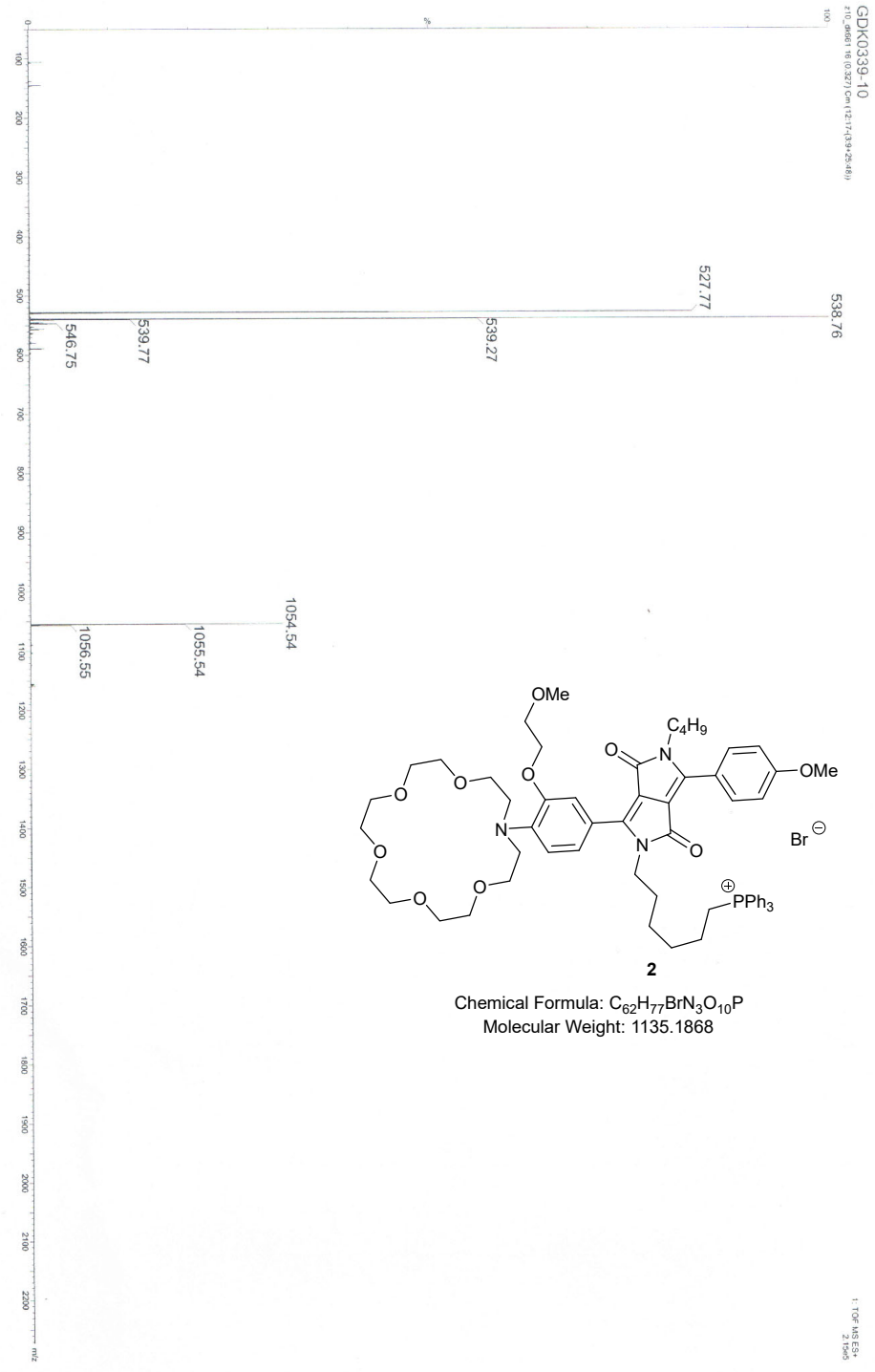

2

Chemical Formula: $C_{62}H_{77}BrN_3O_{10}P$
Molecular Weight: 1135.1868

Section S7: References

1. M. Pieczykolan, B. Sadowski and D. T. Gryko, *Angew. Chem. Int. Ed*., 2020, **59**, 7528-7535.
2. Q. Hu, J. Kunde, N. Hanke and R. W. Hartmann, *Eur. J. Med. Chem.,* 2015, **96**, 139-150.
3. D. Jacquemin, I. Duchemin, X. Blasé, *J. Chem. Theory Comput.* **2015**, *11*, 5340-5359.
4. J. Tomasi, B. Mennucci, R. Cammi, *Chem. Rev.* **2005**, *105*, 2999-3094.
5. Y. Zhao, D. G. Truhlar, *Theor. Chem. Acc.* **2008**, *120*, 215-241.
6. P. M. Vérité, C. A. Guido, D. Jacquemin, *Phys. Chem. Chem. Phys*. **2019**, *21*, 2307-2317.
7. M. J. Frisch, G. W. Trucks, H. B. Schlegel, G. E. Scuseria, M. A. Robb, J. R. Cheeseman, G. Scalmani, V. Barone, G. A. Petersson, H. Nakatsuji, X. Li, M. Caricato, A. V. Marenich, J. Bloino, B. G. Janesko, R. Gomperts, B. Mennucci, H. P. Hratchian, J. V. Ortiz, A. F. Izmaylov, J. L. Sonnenberg, Williams, F. Ding, F. Lipparini, F. Egidi, J. Goings, B. Peng, A. Petrone, T. Henderson, D. Ranasinghe, V. G. Zakrzewski, J. Gao, N. Rega, G. Zheng, W. Liang, M. Hada, M. Ehara, K. Toyota, R. Fukuda, J. Hasegawa, M. Ishida, T. Nakajima, Y. Honda, O. Kitao, H. Nakai, T. Vreven, K. Throssell, J. A. Montgomery Jr., J. E. Peralta, F. Ogliaro, M. J. Bearpark, J. J. Heyd, E. N. Brothers, K. N. Kudin, V. N. Staroverov, T. A. Keith, R. Kobayashi, J. Normand, K. Raghavachari, A. P. Rendell, J. C. Burant, S. S. Iyengar, J. Tomasi, M. Cossi, J. M. Millam, M. Klene, C. Adamo, R. Cammi, J. W. Ochterski, R. L. Martin, K. Morokuma, O. Farkas, J. B. Foresman, D. J. Fox, *Gaussian 16 Rev. B.01*, Wallingford, CT, **2016**.
8. TURBOMOLE V6.2 2010, a development of University of Karlsruhe and Forschungszentrum Karlsruhe GmbH, 1989-2007, TURBOMOLE GmbH, since 2007; available from http://www.turbomole.com.
9. a) J. Cerezo, F. Santoro, FCClasses 3.0, http://www.pi.iccom.cnr.it/fcclasses; b) F. Santoro, R. Improta, A. Lami, J. Bloino, V. Barone, *J. Chem. Phys.* **2007**, *126*, 084509; c) F. Santoro, D. Jacquemin, *Wires Comput. Mol. Sci*. **2016**, *6*, 460–486.
1.

Organic & Biomolecular Chemistry

PAPER

View Article Online
View Journal

Cite this: DOI: 10.1039/d2ob01296k

A sensitive zinc probe operating *via* enhancement of excited-state intramolecular charge transfer†

G. Dinesh Kumar,[a] Marzena Banasiewicz,[b] Antoni Wrzosek,[c] Omar O'Mari,[d] Monika Zochowska,[c] Valentine I. Vullev,*[d] Denis Jacquemin,[e] Adam Szewczyk*[c] and Daniel T. Gryko*[a]

Novel highly sensitive fluorescent probes for zinc cations based on the dikethienopyrrolopyrrole scaffold were designed and synthesized. Large bathochromic shifts (≈80 nm) of fluorescence are observed when the Zn^{2+}-recognition unit (di-(2-picolyl)amine) is bridged with the fluorophore possessing an additional pyridine unit able to participate in the coordination process. This effect originates from the dipolar architecture and the increasing electron-withdrawing properties of the diketopyrrolopyrrole core upon addition of the cation. The new, greenish-yellow emitting probes, which operate *via* modulation of intramolecular charge transfer, are very sensitive to the presence of Zn^{2+}. Introduction of a morpholine unit in the diketopyrrolopyrrole structure induces a selective six-fold increase of the emission intensity upon zinc coordination. Importantly, the presence of other divalent biologically relevant metal cations has negligible effects and typically even at a 100-fold higher concentration of Mg^{2+}/Zn^{2+}, the effect is comparable. Computational studies rationalize the strong bathochromic shift upon Zn^{2+}-complexation. Decorating the probes with the triphenylphosphonium cation and morpholine unit enables selective localization in the mitochondria and the lysosome of cardiac H9C2 cells, respectively.

Received 19th July 2022,
Accepted 1st September 2022

DOI: 10.1039/d2ob01296k

rsc.li/obc

Supporting Information

A sensitive zinc probe operating via enhancement of excited-state intramolecular charge transfer

G. Dinesh Kumar,[a] Marzena Banasiewicz,[b] Antoni Wrzosek,[c] Omar O'Mari,[d] Monika Zochowska,[c] Valentine I. Vullev,*[d] Denis Jacquemin,*[e] Adam Szewczyk,*[c] and Daniel T. Gryko*[a]

[a] Institute of Organic Chemistry, Polish Academy of Sciences, Kasprzaka 44/52, 01-224 Warsaw, Poland. E-mail: dtgryko@icho.edu.pl

[b] Institute of Physics, Polish Academy of Sciences, Al. Lotników 32/46, 02-668 Warsaw, Poland.

[c] Nencki Institute of Experimental Biology of Polish Academy of Sciences, Pasteur 3, 02-093 Warsaw, Poland. E-mail: a.szewczyk@nencki.gov.pl.

[d] Department of Bioengineering, University of California, Riverside, 900 University Ave., Riverside, CA 92521, USA. Email: vullev@ucr.edu

[e] CEISAM UMR 6230, CNRS, Université de Nantes, 44000 Nantes, France. E-mail: denis.Jacquemin@univ-nantes.fr

Table of contents

Section S1: General Information

All reagents and solvents were purchased from commercial sources and were used as received unless otherwise noted. Reagent grade solvents (CH_2Cl_2, hexanes) were distilled prior to use. Transformations with moisture- and oxygen-sensitive compounds were performed under a stream of argon. The reaction progress was monitored by means of thin-layer chromatography (TLC), which was performed on Kieselgel 60. The identity and purity of prepared compounds were proved by ^{1}H NMR and ^{13}C NMR as well as by mass spectrometry (via EI-MS or ESI-MS). HRMS (ESI-TOF) and HRMS (EI): double-focusing magnetic sector instruments with EBE geometry were utilized. NMR spectra were measured on 400 or 500 or 600 MHz instruments. Chemical shifts (δ, ppm) were determined with tetramethylsilane (TMS) as the internal reference; J values are given in Hz. All melting points for crystalline products were measured with an automated melting point apparatus and are given without correction.

UV/Vis absorption spectra were recorded on a PerkinElmer Lambda 35 Spectrometer. Fluorescence spectra were recorded on a FLS1000 of Edinburgh Instruments. All linear optical studies were performed with freshly prepared air-equilibrated solutions at room temperature (298 K). Acetonitrile was spectrophotometric grade and was used without further purification. Quartz cells (10 mm) were used for the measurements of absorption and emission spectra. As a standard, Rh6G (Φ_{fl} = 0.94 in EtOH) was used to determine fluorescence quantum yields.

Section S2: Experimental Procedure

All reagents and solvents were purchased from commercial sources and were used as received unless otherwise noted. Reagent grade solvents (DCM, hexanes) were distilled prior to use. Transformations with moisture- and oxygen-sensitive compounds were performed under a stream of argon. The reaction progress was monitored by means of thin-layer chromatography (TLC), which was performed on Kieselgel 60. The identity and purity of prepared compounds were proved by ^{1}H NMR and ^{13}C NMR as well as by mass spectrometry (via EI-MS or ESI-MS). HRMS (ESI-TOF) and HRMS (EI): double-focusing magnetic sector instruments with EBE geometry were utilized. NMR spectra were measured on 400 or 500 or 600 MHz instruments. Chemical shifts (δ, ppm) were determined with tetramethylsilane (TMS) as the internal reference; J values are given in Hz. All melting points for crystalline products were measured with an automated melting point apparatus and are given without correction. Pyrrolidone **1** was obtained following the literature procedure.[1]

Synthesis of nitriles:

2-(bis(pyridin-2-ylmethyl)amino)isonicotinonitrile (2a)

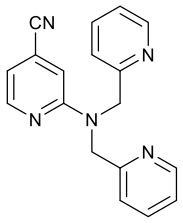

2a

A mixture commercially available 2-fluoro-4-cyanopyridine (0.5 g, 4 mmol), di-(2-picolyl)amine (0.82 g, 4 mmol) in 5 ml of deoxygenated N,N-dimethylacetamide was heated to 130 °C under argon for overnight. Then reaction mixture was cooled to room temperature, diluted with water (100 mL) and extracted with EtOAc (2×100 mL). The organic phase dried over anhydrous Na_2SO_4 and filtered. The solvent was removed under reduced pressure and the resulting colorless oil was chromatographed on silica gel (hexane/EtOAc = 1: 1) to obtain desired product as colorless oil (1.06 g, 86%). ^{1}H NMR (500 MHz, $CDCl_3$) δ 8.56 (dd, *J* = 9.6 Hz, 2H), 8.27 (d, *J* = 11.2 Hz, 1H), 7.62 (dt, *J* = 3.4 Hz, 2H), 7.22-7.17 (m, 4H), 6.7 (dd, *J* = 8.0 Hz, 2H), 4.98 (s, 4H). ^{13}C NMR (126 MHz, $CDCl_3$) δ 158.2, 157.4, 149.6, 149.3, 136.8, 122.4, 121.4, 121.3, 117.4, 113.3, 108.5, 54.1. HRMS (ESI, *m/z*): $[M+Na]^+$ Calcd. for $C_{18}H_{15}N_5Na$: 324.3530; found, 324.3460.

2-((bis(pyridin-2-ylmethyl)amino)methyl)isonicotinonitrile (2b)

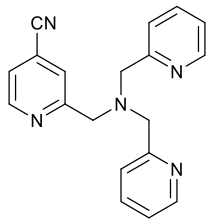

2b

To a mixture of 2-Formylpyridine-4-carbonitrile (1 g, 7.5 mmol) and di-2-picolylamine (1.4 mL, 7.5 mmol) in 1,2-dicloroethane (20 mL), then $NaBH(OAc)_3$ (2.1 g, 9.8 mmol) was added in portions. Then the reaction was stirred at room temperature for overnight, then reaction mixture was first acidified with 1N HCl to pH 4-5, followed by neutralized with 1N NaOH to pH 7-8. The organic phase was separated, and aqueous phase was extracted with DCM (2×100mL). The organic phases were combined and dried over Na_2SO_4 and the solvent was evaporated to give crude product which was purified by column chromatography using DCM/CH3OH (10:1) to obtain the desired product **2b** as a brown liquid (1.94 g, 82%). ^{1}H NMR (500 MHz, $CDCl_3$) δ 8.65 (d, *J* = 5.1 Hz, 1H), 8.52 (m, 2H), 7.85 (s, 1H), 7.65 (dt, *J* = 7.6 Hz, 2H), 7.49 (d, *J* = 7.8 Hz, 2H), 7.32 (dd, *J* = 5.1 Hz, 1H), 7.14 (m, 2H), 3.9 (s, 2H), 3.8(s, 4H). ^{13}C NMR (126 MHz, $CDCl_3$) δ 161.8, 158.6, 149.8, 149.3, 136.5, 124.6, 123.2, 123.1, 122.2, 120.1, 116.8, 60.5, 59.6. HRMS (ESI, *m/z*): $[M+Na]^+$ Calcd. for $C_{19}H_{17}N_5Na$: 338.1382; found, 338.1380.

ethyl 4-hydroxy-2-(4-methoxyphenyl)-1-(3-morpholinopropyl)-5-oxo-2,5-dihydro-1H-pyrrole-3-carboxylate (5)

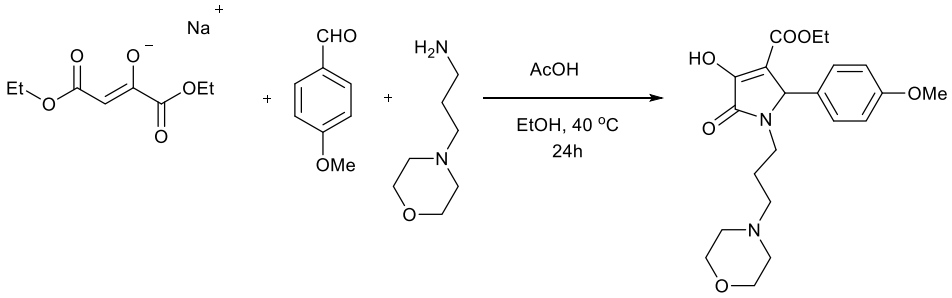

5

A 250 mL round bottom flask equipped with a magnetic stirring bar, was charged with ethanol (100 mL), 4-methoxy benzaldehyde (6.5 mL, 53 mmol) and (3-Aminopropyl)morpholine (7.8 mL, 53 mmol), reaction mixture was kept at room temperature, with constant stirring for 15 minutes. Next diethyl oxalacetate (10.0 g, 53 mmol) was added in one portion, followed by dropwise addition of acetic acid (6.1 mL, 106 mmol). Reaction mixture was heat up to 40 °C, and vigorously stirred overnight. Then reaction mixture was cooled to room temperature and diluted with water (200 mL), and extracted with DCM (200mL×2). Organic phase were dried over anhydrous Na_2SO_4, filtered and concentrated in vacuo. Yellowish solid was recrystallized from EtOAc to obtain product **5** as white crystals (15.6 g, 72%); mp 171-172 °C.^{1}H NMR (600 MHz, $CDCl_3$) δ 7.10 (d, *J* = 8.6 Hz, 2H), 6.86 (d, *J* = 8.7 Hz, 2H), 5.07 (s, 1H), 4.65 (bs, 2H), 4.14 (q, *J* = 6.3 Hz, 2H), 3.8 (s, 3H), 3.73-3.65 (m, 5H), 2.84-2.79 (m, 1H), 2.49 (s, 3H), 2.46-2.34 (m, 2H), 1.77 – 1.64 (m, 2H), 1.12 (t, *J* = 7.1 Hz, 3H); ^{13}C NMR (151 MHz, $CDCl_3$) δ 166.1, 165.1, 164.8, 159.8, 158.6, 128.9, 127.3, 114.1,

111.6, 66.4, 60.5, 55.7, 55.3, 53.2, 38.6, 24.4, 14.0. HRMS (ESI, *m/z*): $[M+H]^+$ Calcd. for $C_{21}H_{29}N_2O_6$: 405.2026; found, 405.2024.

ethyl 4-hydroxy-2-(4-methoxyphenyl)-1-(3-morpholinopropyl)-5-oxopyrrolidine-3-carboxylate (6)

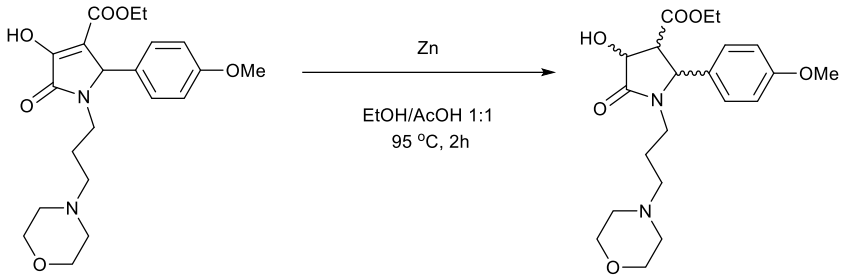

6

Compound **5** (15.0 g, 37.1 mmol) was dissolved in 150 mL mixture of EtOH/AcOH (1:1) and zinc powder (14.6 g, 222.5 mmol) was added and reaction mixture vigorously stirred at 95 °C for 1h. A second portion of zinc powder (14.6 g, 222.5 mmol) was added and stirring was continued at 95 °C until completion of the reaction. After cooling to room temperature reaction mixture was diluted with EtOAc (100 mL) the excess of zinc and the inorganic salts were filtered off. The filtrate was then diluted with water (150 mL). The aqueous layer was extracted with EtOAc (100 mL), and the combined organic phases were washed with saturated $NaHCO_3$ solution until neutral and finally dried over Na_2SO_4, filtered and concentrated in vacuo to obtain liquid product **6** as mixture of diastereoisomers (10.8 g, 72%). Careful analysis of ^1H NMR spectra of crude **6** showed the ratio 2:1 of major isomer **6** with the all-trans configuration in relation to the rest three minor compounds.

Crude compound (10.8 g, 31.9 mmol) was dissolved in dry EtOH (75 mL), freshly powdered K_2CO_3 (8.0 g, 79.7 mmol) was added in one portion. Reaction mixture was stirred at room temperature for 30 minutes. Next reaction mixture was diluted with EtOAc (100 mL) the excess of inorganic salts were filtered off. The filtrate was then washed with water (100 mL x 2), organic phase was dried over Na_2SO_4, filtered and concentrated in vacuum to obtain yellowish liquid product (10.8 g, 99.5 %). ^1H NMR spectra showed 10:1 ratio of major isomer **6a** with the all-trans configuration in relation to the rest two minor compounds.

^1H NMR (500 MHz, $CDCl_3$) δ 7.22 (d, *J* = 8.7 Hz, 2H), 7.03 (bs, 4H), 6.91 (d, *J* = 8.7 Hz, 2H), 4.66 (dd, *J* = 8.4, 7.9 Hz, 2H), 4.14 (q, *J* = 4.8 Hz, 2H), 3.8 (s, 3H), 3.73-3.65 (m, 5H), 3.58-3.50 (m, 1H), 2.75-2.60 (m, 2H), 2.44 – 2.35 (m, 2H), 1.66-1.56 (m, 2H), 1.22 (t, *J* = 7.1 Hz, 3H); ^{13}C NMR (101 MHz, $CDCl_3$) δ 175.6, 173.5, 171.2, 160.0, 129.0, 114.4, 72.2, 65.9, 61.4, 60.9, 55.2, 52.6, 49.2, 38.7, 22.7, 21.4, 14.0. HRMS (ESI, *m/z*): $[M+H]^+$ Calcd. for $C_{21}H_{31}N_2O_6$: 407.2182; found, 407.2183.

ethyl 2-(4-methoxyphenyl)-1-(3-morpholinopropyl)-5-oxo-4-((trimethylsilyl)oxy)pyrrolidine-3-carboxylate (7)

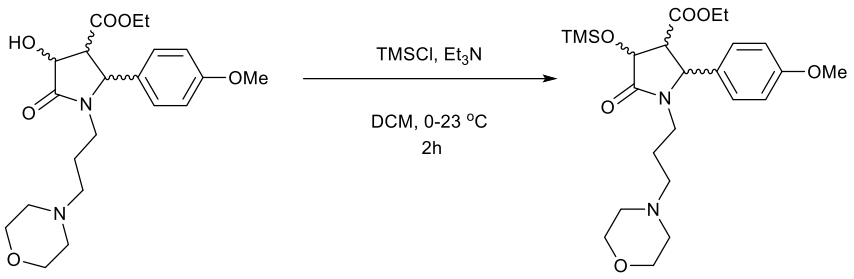

7

To cooled to ~0 °C solution of **6a** (7.0 g, 17.2 mmol) in dry DCM (100 mL), dry Et_3N (4.4 mL, 30.9 mmol) was added, next TMSCl (3.3 mL, 25.8 mmol) was added drop wise. After addition cooling bath was removed, and reaction mixture was allowed to reach room temperature and stirring was continued at room temperature for 1.5 h. Next reaction mixture was diluted with water (100 mL), phases were separated and organic phase was dried over anhydrous Na_2SO_4, filtered and concentrated in vacuo gives brownish oil (6.8 g, 82%) of product **7** without chromatographic purification. ^{1}H NMR spectra showed 10:1 ratio of major isomer **7** with the all-trans configuration in relation to the rest two minor compounds, used for next reaction without further purification.

^{1}H NMR (600 MHz, $CDCl_3$) δ 7.13 (d, *J* = 8.5 Hz, 2H), 6.84 (d, *J* = 8.7 Hz, 2H), 4.55-4.49 (m, 2H), 4.10-4.06 (m, 2H), 3.75 (s, 3H), 3.56 (m, 6H), 2.91 (m, 1H), 2.62-2.58 (m, 1H), 2.22 (bs, 4H), 1.57-1.51 (m, 2H), 1.46-1.4 (m, 1H), 1.15 (t, *J* = 7.2 Hz, 3H), 0.15 (s, 9H). ^{13}C NMR (151 MHz, $CDCl_3$) δ 171.7, 171.6, 159.8, 129.7, 128.8, 114.3, 73.4, 66.8, 61.3, 60.5, 57.1, 55.9, 55.3, 53.5, 39.1, 23.5, 14.1, 1.9, 0.1. HRMS (ESI, *m/z*): $[M+H]^+$ Calcd. for $C_{24}H_{39}N_2O_6Si$: 479.2577; found, 479.2588.

General procedure for the synthesis of DPP derivatives

In flame dried Schlenk flask, a mixture of appropriate nitrile (1 eq.) and lithium *tert*-butoxide (4 eq.) was heated to 110 °C under argon. To this solid mixture, *tert*-amyl alcohol (5 mL) was added in one portion followed by dropwise addition of pyrrolidone **1** or **7** (1 eq.) dissolved in dry toluene (3 mL). The resulting dark solution was left to stir at this temperature for overnight. After cooling to room temperature reaction mixture was diluted with water (100 mL) and extracted with DCM (100 mL), water phase was one more time washed with DCM (50 mL). The combined organic phases were dried over Na_2SO_4, filtered and concentrated in vacuum. The resulting crude compound was chromatographed on silica gel (DCM/MeOH = 9: 1) and crystallization from DCM/n-hexanes allowed to obtain the desired DPP product.

6-(2-(bis(pyridin-2-ylmethyl)amino)pyridin-4-yl)-2-butyl-3-(4-methoxyphenyl)-2,5-dihydropyrrolo[3,4-*c*]pyrrole-1,4-dione (3)

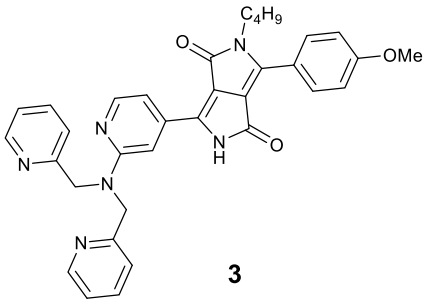

3

2-(bis(pyridin-2-ylmethyl)amino)isonicotinonitrile **2a** (1.5 g, 4.4 mmol), lithium *tert*-butoxide (1.42 g, 17.8mmol) and pyrrolidone **1** (1.82 g, 4.4 mmol) in combined solvent were used to obtain **3** as shiny red crystals (0.4 g, 21%); mp 217 °C. ^{1}H NMR (500 MHz, $CDCl_3$) δ 10.01 (s, 1H), 8.52 (s, 2H), 8.26 (d, *J* = 4.8 Hz, 1H), 7.80 (d, *J* = 7.8 Hz, 2H), 7.59-7.49 (m, 4H), 7.27 (s, 2H), 7.18 (s, 2H), 6.98 (d, *J* = 8.2 Hz, 2H), 5.03 (s, 4H), 3.82 (s, 3H), 3.77 (t, *J* = 7.5 Hz, 2H), 2.66 (br s, 2H), 1.57 (t, *J* = 6.8 Hz, 2H), 1.28 (q, *J* = 7.3 Hz, 2H), 0.87 (t, *J* = 7.3 Hz, 3H). ^{13}C NMR (126 MHz, $CDCl_3$) δ 162.8, 162.7, 162.2, 158.7, 158.1, 150.3, 149.0, 148.9, 141.7, 136.9, 136.0, 130.9, 122.2, 121.7, 120.1, 114.4, 112.0, 110.1, 110.0, 103.3, 55.4, 53.6, 42.0, 31.4, 19.9, 13.6. HRMS (ESI, *m/z*): $[M+H]^+$ Calcd. for $C_{34}H_{33}N_6O_3$: 573.2614; found, 573.2628.

6-(2-((bis(pyridin-2-ylmethyl)amino)methyl)pyridin-4-yl)-2-butyl-3-(4-methoxyphenyl)-2,5-dihydropyrrolo[3,4-*c*]pyrrole-1,4-dione (4)

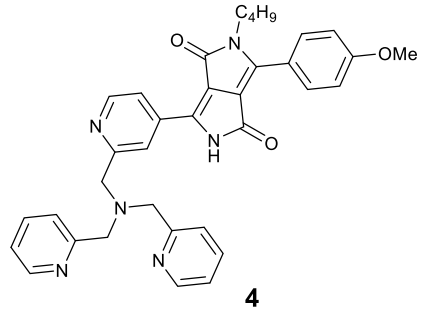

4

2-((bis(pyridin-2-ylmethyl)amino)methyl)isonicotinonitrile **2b** (0.5 g, 1.6 mmol), lithium *tert*-butoxide (0.5 g, 6.3 mmol) and pyrrolidone **1** (0.65 g, 1.6 mmol) in combined solvent were used to obtain **4** as shiny red crystals (0.19 g, 21%); mp 204 °C. ^{1}H NMR (600 MHz, $CDCl_3$) δ 10.3 (s, 1H), 8.99 (s, 1H), 8.78 (d, *J* = 4.0 Hz, 2H), 8.68 (d, *J* = 5.2 Hz, 1H), 8.40 (d, *J* = 4.3 Hz, 1H), 7.9 (d, *J* = 8.9 Hz, 2H), 7.59 (dt, *J* = 7.7 Hz, 2H), 7.41 (d, *J* = 7.7 Hz, 2H), 7.17 (dt, *J* = 5.7 Hz, 6.7 Hz, 2H), 7.09 (d, *J* = 8.8 Hz, 2H), 3.98 (s, 3H), 3.91 (d, *J* = 4.2 Hz, 6H), 3.87 (t, *J* = 7.8 Hz, 2H), 2.66 (br s, 1H), 1.67 (quint, *J* = 7.8 Hz, 2H), 1.33 (m, 2H), 0.91 (t, *J* = 7.0 Hz, 3H). ^{13}C NMR (151 MHz, $CDCl_3$) δ 162.9, 162.4, 162.3, 160.9, 158.6, 150.5, 150.1, 149.5, 141.3, 136.6, 135.0, 130.9, 123.8, 122.5, 120.2, 119.9, 119.2, 114.5, 112.4, 110.3, 59.6, 59.4, 55.5, 42.1, 31.5, 20.0, 13.6. HRMS (ESI, *m/z*): $[M+H]^+$ Calcd. for $C_{35}H_{35}N_6O_3$: 587.2757; found, 587.2781.

6-(2-(bis(pyridin-2-ylmethyl)amino)pyridin-4-yl)-3-(4-methoxyphenyl)-2-(3-morpholinopropyl)-2,5-dihydropyrrolo[3,4-*c*]pyrrole-1,4-dione (8)

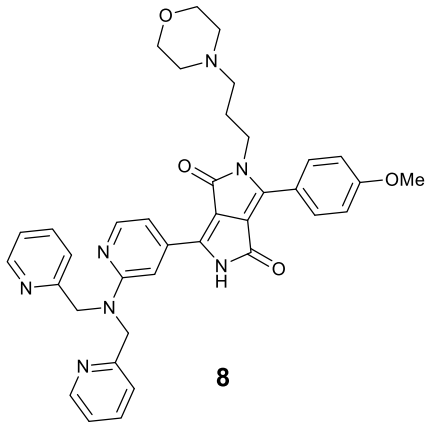

8

2-(bis(pyridin-2-ylmethyl)amino)isonicotinonitrile **2a** (1.0 g, 3.3 mmol), lithium *tert*-butoxide (1.06 g, 13.2 mmol) and pyrrolidone **7** (1.58 g, 3.3 mmol) in combined solvent were used to obtain **8** as shiny red crystals (0.31 g, 15%); mp 230 °C. ^{1}H NMR (500 MHz, $CDCl_3$) δ 10.02 (s, 1H), 8.51 (d, *J* = 3.7 Hz, 2H), 8.29 (d, *J* = 5.2 Hz, 1H), 7.81 (d, *J* = 8.0 Hz, 2H), 7.57 (d, *J* = 7.2 Hz, 2H), 7.50 (d, *J* = 5.0 Hz, 2H), 7.23 (d, *J* = 7.7 Hz, 2H), 7.12 (d, *J* = 6.0 Hz, 2H), 6.98 (d, *J* = 8.5 Hz, 2H), 5.01 (s, 4H), 3.88 (d, *J* = 7.4 Hz ,2H), 3.81 (s, 3H), 3.58 (t, *J* = 4.0 Hz ,4H), 2.28 (bs, 6H), 1.75 (m, 2H). ^{13}C NMR (126 MHz, $CDCl_3$) δ 162.8, 162.2, 159.0, 158.3, 150.0, 149.3, 149.2, 141.9, 136.6, 135.9, 130.9, 122.0, 121.4, 120.1, 114.4, 111.9, 110.1, 109.1, 103.1, 66.9, 59.9, 55.4, 53.6, 40.5, 26.9, 25.9. HRMS (ESI, *m/z*): $[M+H]^+$ Calcd. for $C_{37}H_{38}N_7O_4$: 644.2985; found, 644.2988.

6-(2-((bis(pyridin-2-ylmethyl)amino)methyl)pyridin-4-yl)-3-(4-methoxyphenyl)-2-(3-morpholinopropyl)-2,5-dihydropyrrolo[3,4-*c*]pyrrole-1,4-dione (9)

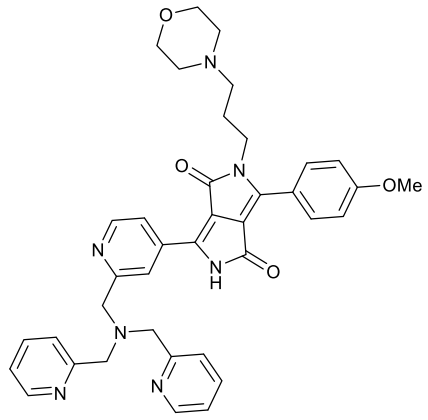

9

2-((bis(pyridin-2-ylmethyl)amino)methyl)isonicotinonitrile **2b** (0.5 g, 1.6 mmol), lithium *tert*-butoxide (0.5 g, 6.3 mmol) and pyrrolidone **7** (0.76 g, 1.6 mmol) in combined solvent were used to obtain **9** as shiny red crystals (0.14 g, 14%); mp 194 °C. ^{1}H NMR (500 MHz, $CDCl_3$) δ 10.34 (s, 1H), 8.96 (s, 1H), 8.74 (d, *J* = 4.0 Hz, 2H), 8.66 (d, *J* = 5.0 Hz, 1H), 8.35 (d, *J* = 4.4 Hz, 1H), 7.88 (d, *J* = 8.9 Hz, 2H), 7.58 (td, *J* = 7.6,

2H), 7.40 (d, *J* = 7.7 Hz, 2H), 7.15 (td, *J* = 5.5, 5.0, 6.6 Hz, 2H), 7.03 (d, *J* = 8.8 Hz, 2H), 3.96 (m, 4H), 3.88 (d, *J* = 7.9 Hz ,7H), 3.61 (bs, 4H), 2.34 (bs, 6H), 1.84 (bs, 2H). ^{13}C NMR (126 MHz, $CDCl_3$) δ 162.9, 162.4, 162.3, 160.9, 158.6, 150.5, 149.9, 149.5, 141.5, 136.6, 134.9, 130.9, 123.8, 122.5, 120.1, 119.8, 119.3, 114.5, 112.3, 110.5, 66.7, 59.6, 59.4, 55.9, 55.5, 53.5, 45.8, 40.6, 25.9, 8.6. HRMS (ESI, *m/z*): $[M+H]^+$ Calcd. for $C_{38}H_{40}N_7O_4$: 658.3142; found, 658.3164.

Preparation of mitochondrial probe 10:

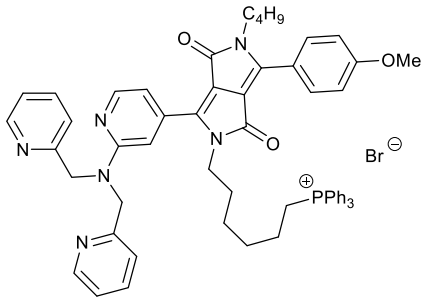

10

A suspension of DPP **3** (0.3 g, 0.52 mmol) and *t*-BuOK (0.15 g, 1.3 mmol) in dry NMP (10 mL) was stirred at 75 °C under argon atmosphere for 15 min. then 1,6-dibromohexane (0.25 mL, 1.6 mmol) was added and the mixture was stirred at 75 °C under argon for 3 h. After cooling to room temperature reaction mixture was diluted with water (100 mL) and extracted with DCM (100 mL), water phase was one more time washed with DCM (50 mL). The combined organic phases were dried over Na_2SO_4, filtered and concentrated in vacuum. The product was purified by column chromatography over silica gel using a step gradient of MeOH in DCM as eluent (from 0% to 10%). Compound was obtained as an orange red semi solid (300 mg, 78%); HRMS (ESI, m/z): $[M+Na]^+$Calcd.for $C_{40}H_{43}BrN_6O_3Na$: 757.2478; found, 757.2467.

Alkylated crude compound of **3** (300 mg, 0.41 mmol) and triphenylphosphine (1.06 g, 4.1 mmol) were added into a flask containing 5 mL of acetonitrile. The mixture was refluxed for 72 h. After removal of solvent in vacuo, the remaining solid was purified by column chromatography with gradient solvent from CH_2Cl_2 to CH_2Cl_2/MeOH (v/v = 9/1). Compound **10** was obtained as orange-red crystals by recrystallization from diethyl ether (130 mg, 35%); mp 105 °C. ^{1}H NMR (600 MHz, CD_3CN): δ 8.9 (s, 2H), 8.8 (s, 1H), 8.35-8.26 (m, 4H), 8.03 (d, *J* = 6.0 Hz, 2H), 7.79-7.65 (m, 17H), 7.20 (d, *J* = 9.6 Hz, 2H), 6.99 (d, *J* = 9.6 Hz, 2H), 5.53 (s, 4H), 3.86 (s, 3H), 3.64 (t, *J* = 7.8 Hz, 4H), 3.4-3.2 (m, 6H), 1.39-1.27 (m, 8H), 0.88 (t, *J* = 9.0 Hz, 3H). ^{13}C NMR (126 MHz, $CDCl_3$) δ 162.2, 161.7, 158.6, 149.4, 148.7, 144.3, 137.0, 135.0, 133.7, 130.9, 130.3, 130.2, 122.2, 121.3, 118.8, 117.3, 114.3, 111.1, 108.2, 104.8, 65.3, 55.4, 54.5, 54.3, 41.2, 40.8, 31.0, 29.7, 28.5, 27.8, 25.2, 24.8, 21.9, 21.4, 19.5, 14.6, 12.9; HRMS (ESI, *m/z*): $[M+H]^+$ Calcd. for $C_{58}H_{58}N_6O_3P$: 917.4308; found, 917.4303.

Section S3: Absorption and emission spectra

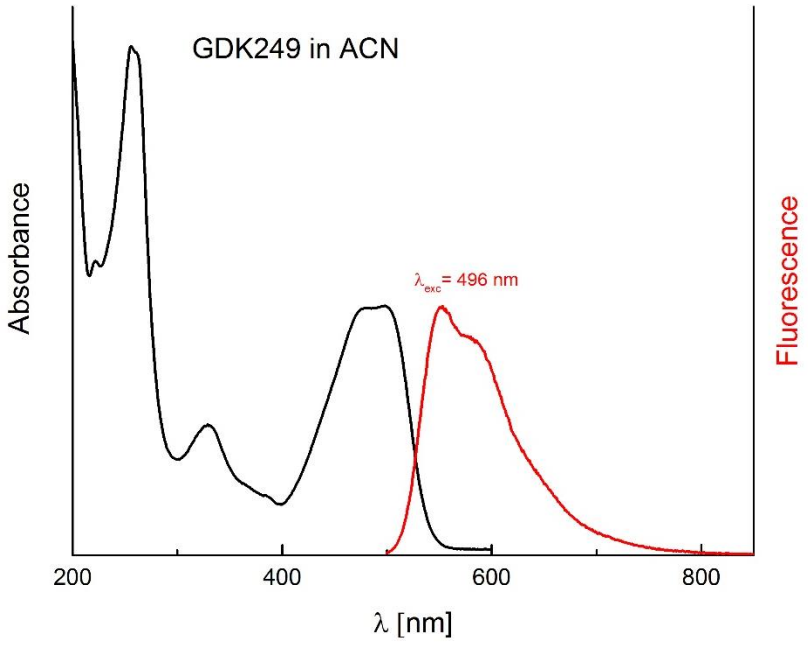

Fig. S1. The absorption and emission spectra of DPP **3** in CH_3CN.

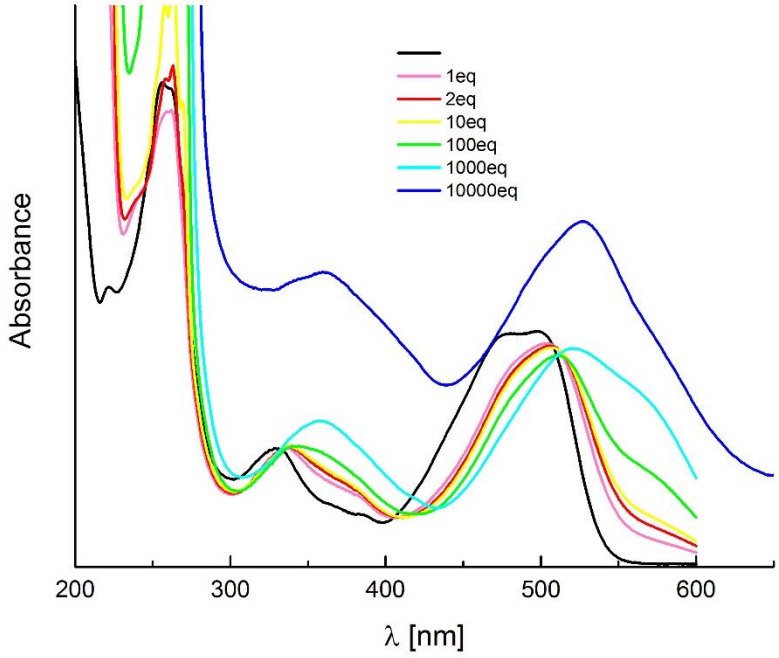

Fig. S2.The effect of $PhSO_3H$ addition on the absorption spectra of DPP **3** measured in CH_3CN.

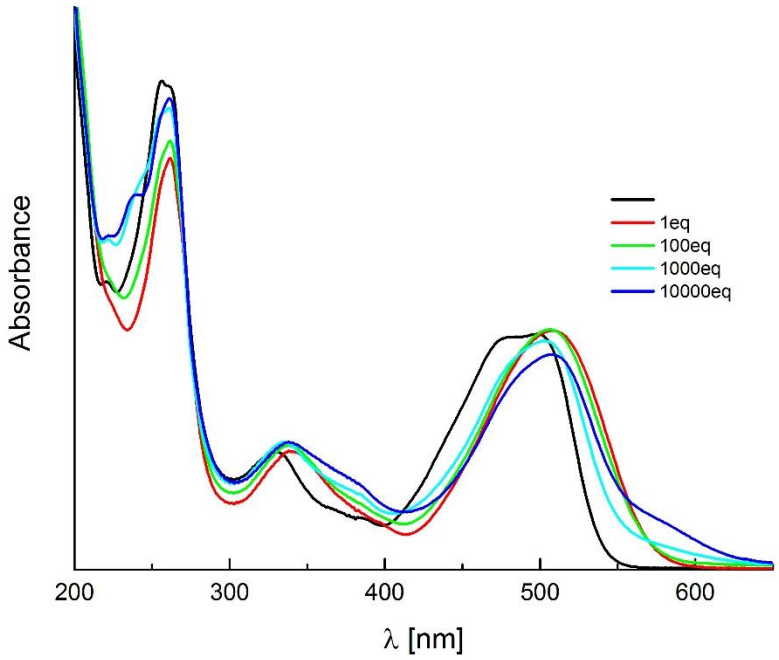

Fig. S3.The effect of cadmium perchlorate addition on the absorption spectra of DPP **3** measured in CH_3CN.

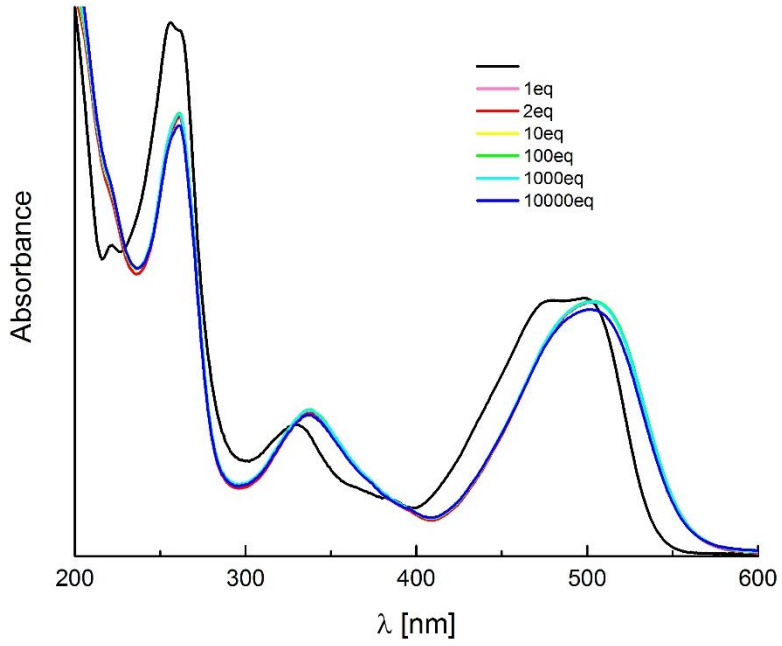

Fig. S4.The effect of zinc perchlorate addition on the absorption spectra of DPP **3** measured in CH_3CN.

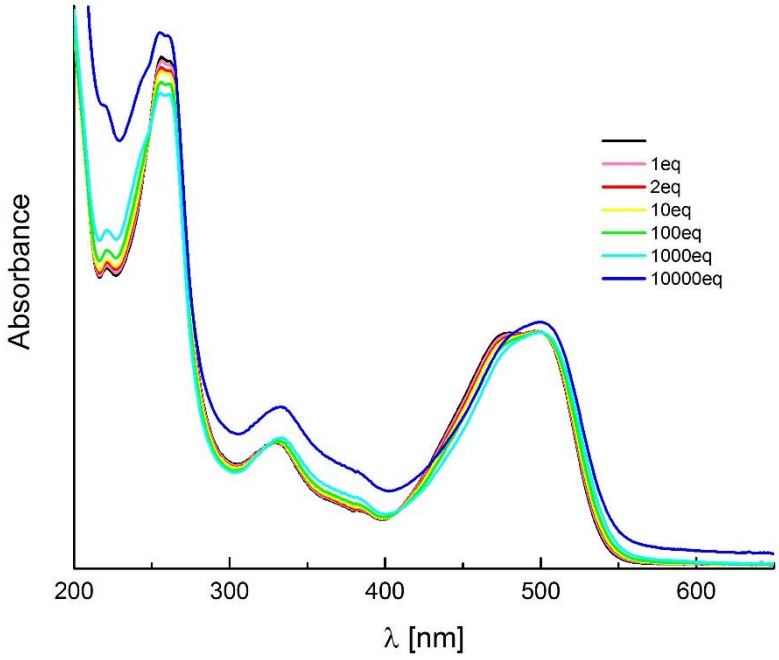

Fig. S5.The effect of magnesium perchlorate addition on the absorption spectra of DPP **3** measured in CH_3CN.

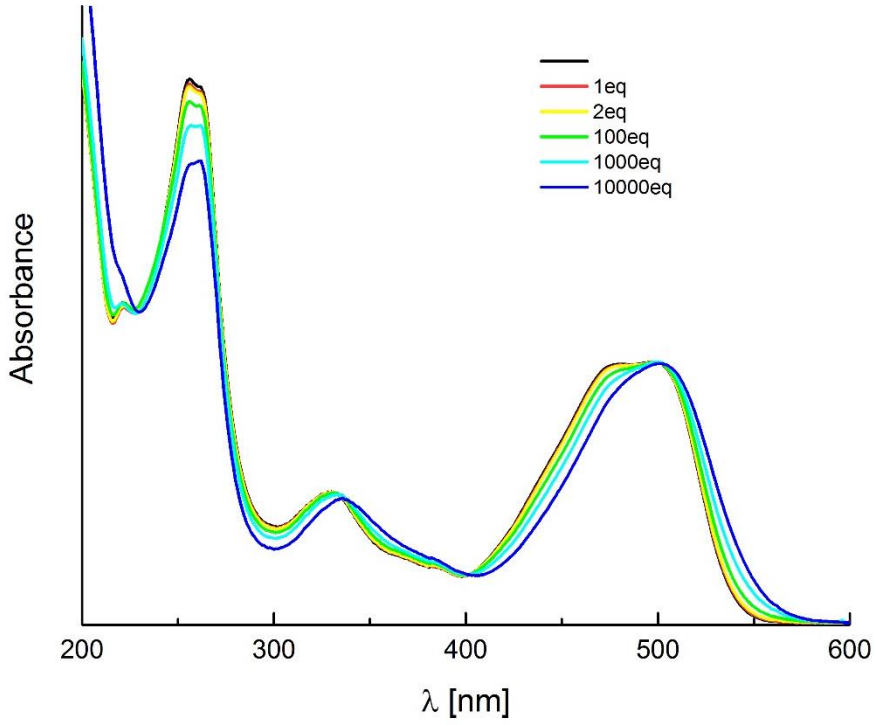

Fig. S6.The effect of calcium perchlorate addition on the absorption spectra of DPP **3** measured in CH_3CN.

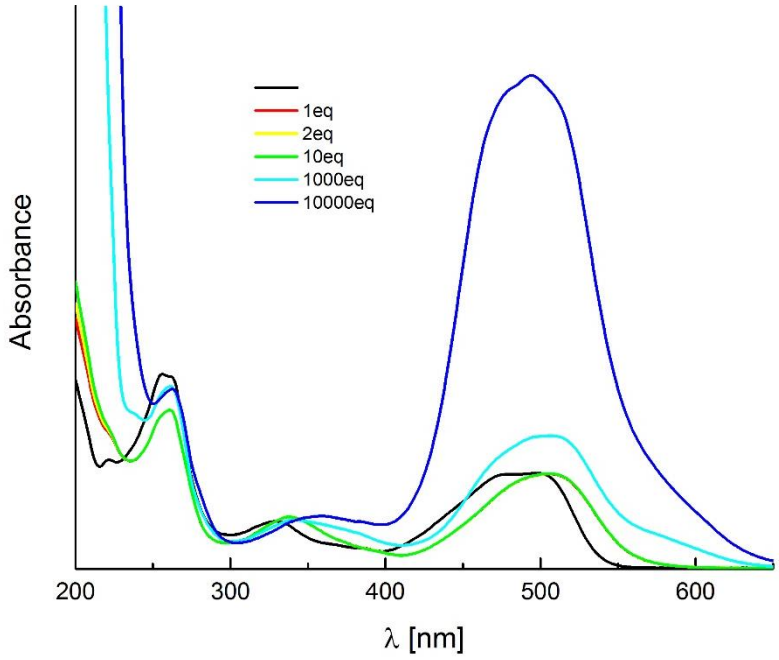

Fig. S7.The effect of cobalt perchlorate addition on the absorption spectra of DPP **3** measured in CH_3CN.

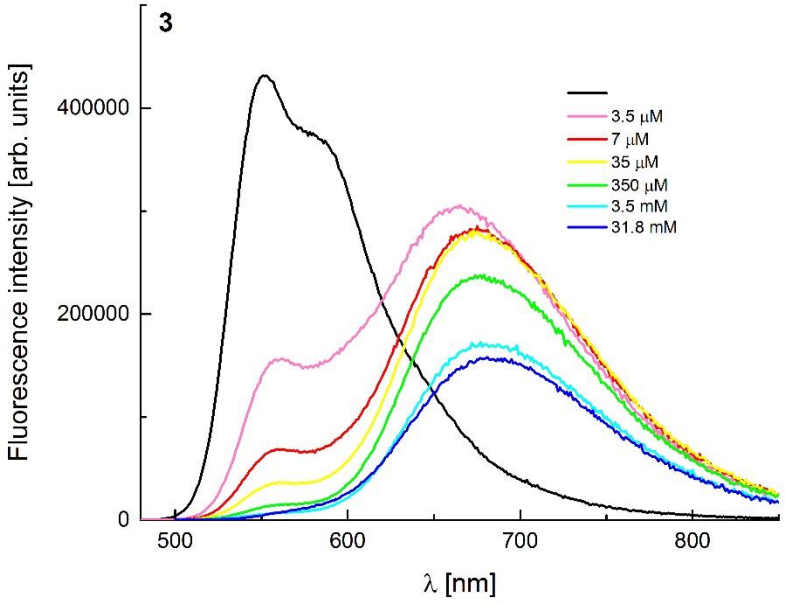

Fig. S8. The effect of $PhSO_3H$ addition on the emission spectra of DPP **3** measured in CH_3CN.

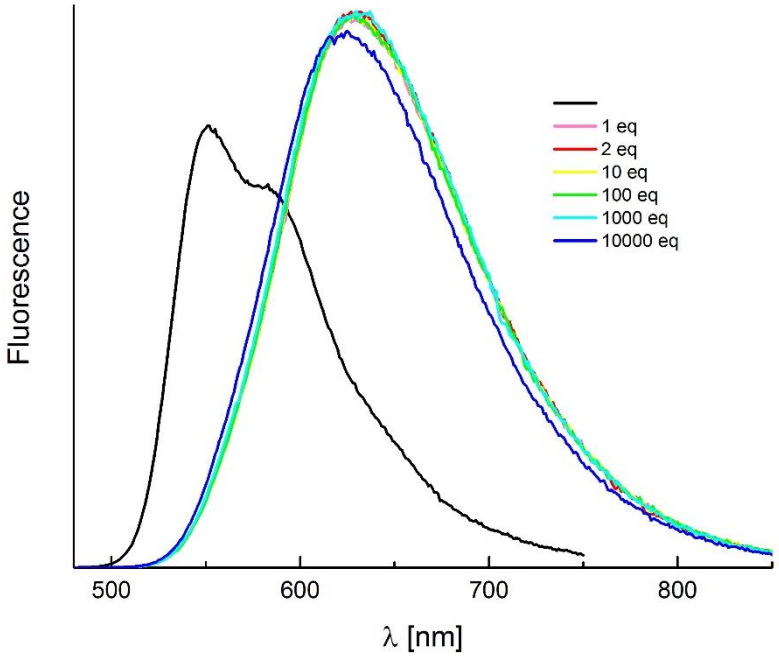

Fig. S9. The effect of zinc perchlorate addition on the emission spectra of DPP **3** measured in CH_3CN.

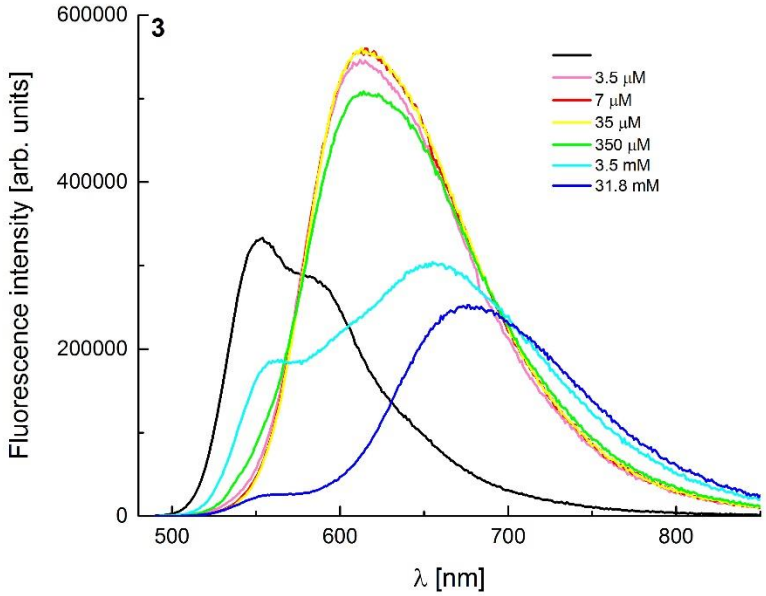

Fig. S10. The effect of cadmium perchlorate addition on the emission spectra of DPP **3** measured in CH_3CN.

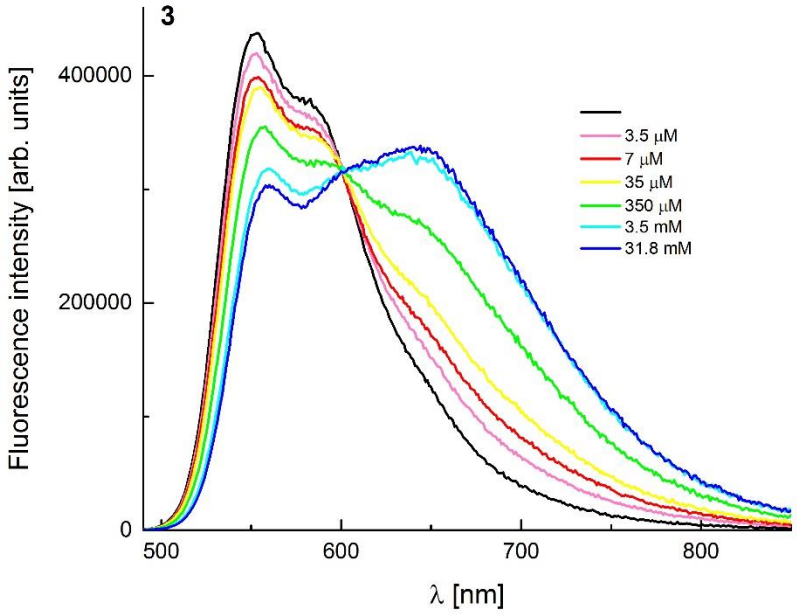

Fig. S11. The effect of magnesium perchlorate addition on the emission spectra of DPP **3** measured in CH_3CN.

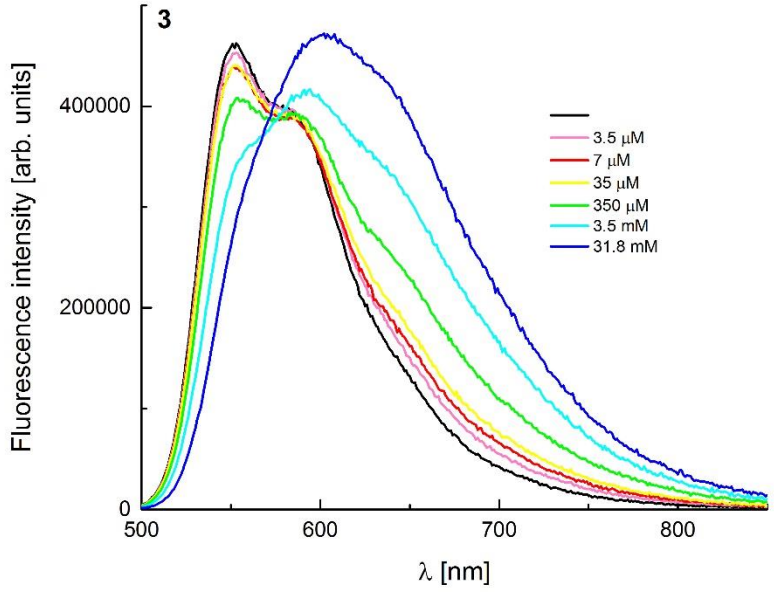

Fig. S12. The effect of calcium perchlorate addition on the emission spectra of DPP **3** measured in CH_3CN.

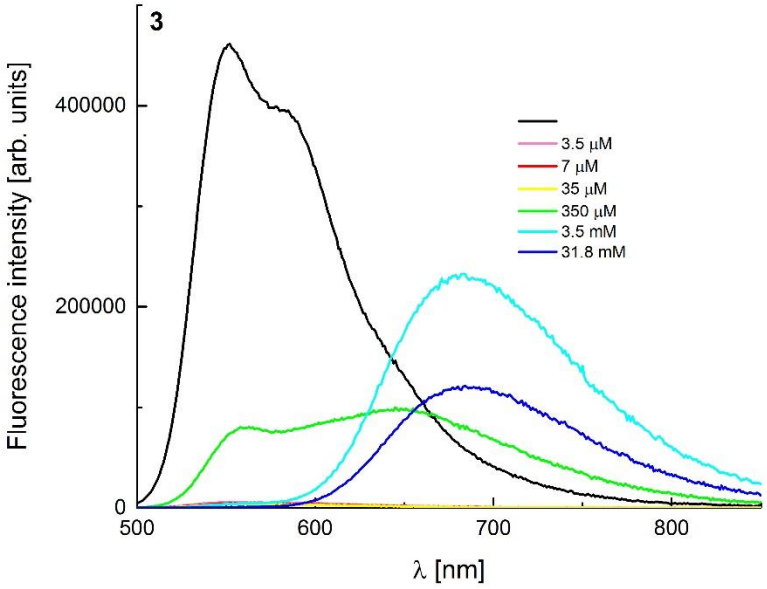

Fig. S13. The effect of cobalt perchlorate addition on the emission spectra of DPP **3** measured in CH_3CN.

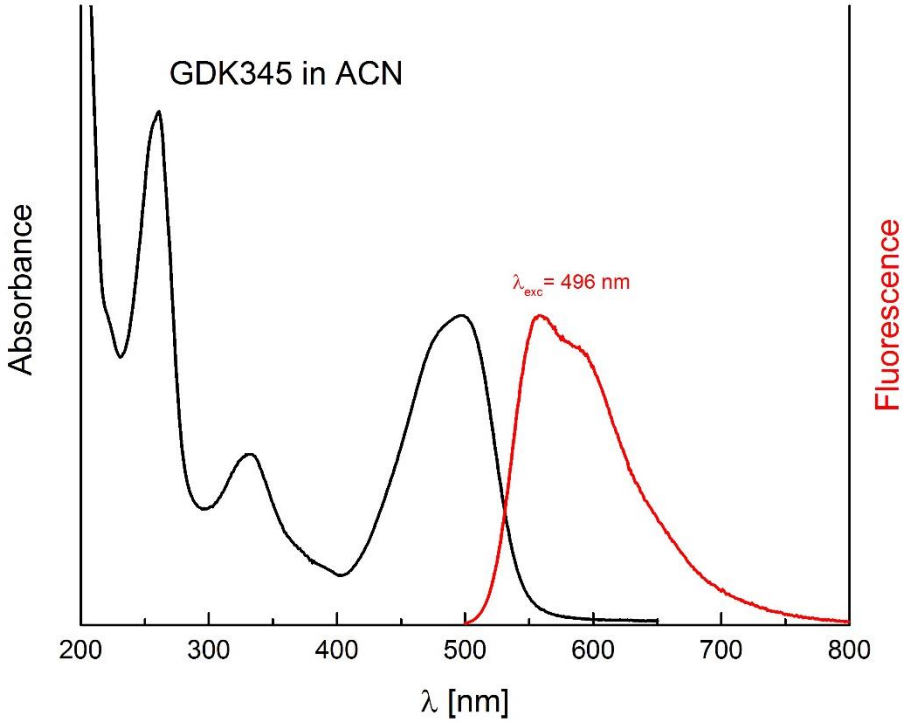

Fig. S14. The absorption and emission spectra of DPP **4** in CH_3CN.

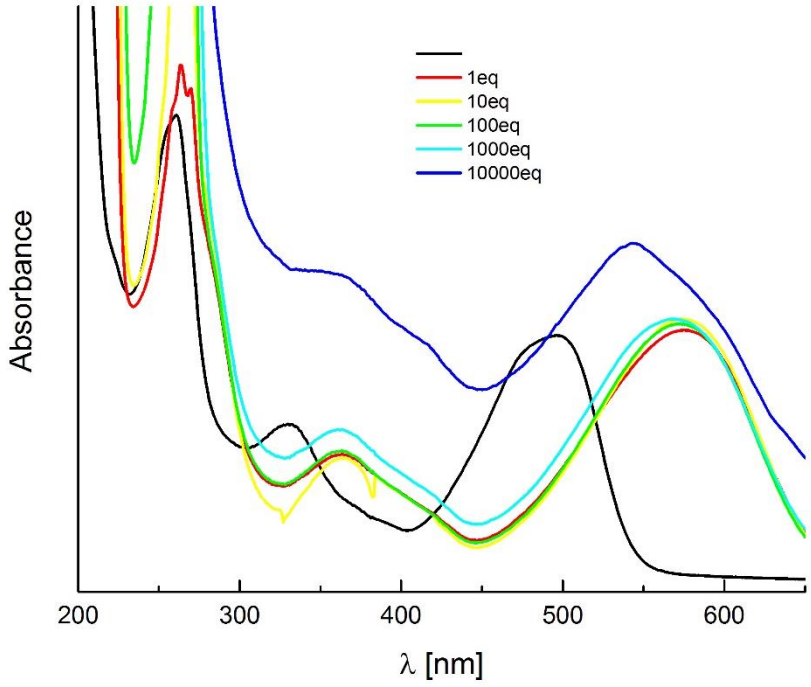

Fig. S15.The effect of $PhSO_3H$ addition on the absorption spectra of DPP **4** measured in CH_3CN.

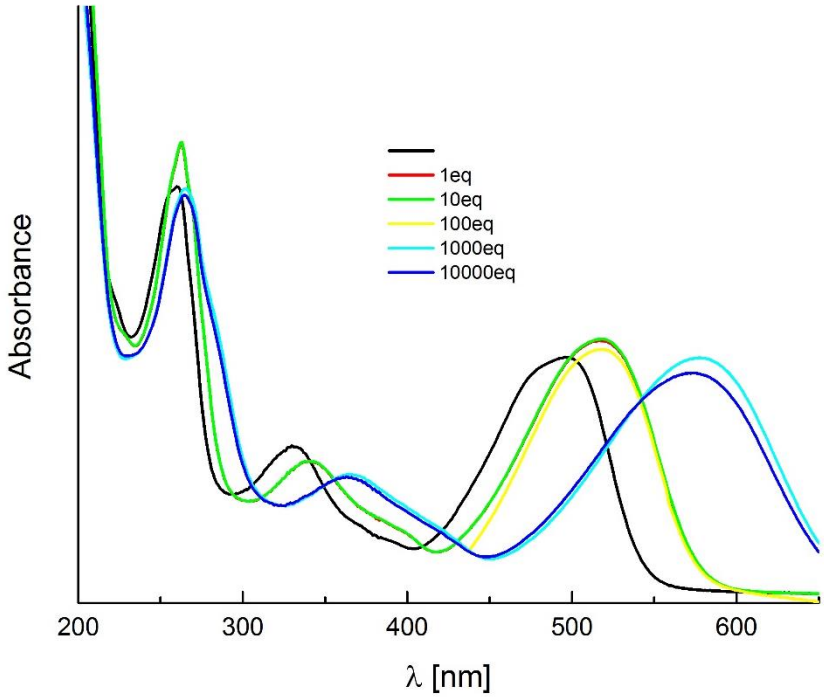

Fig. S16.The effect of cadmium perchlorate addition on the absorption spectra of DPP **4** measured in CH_3CN.

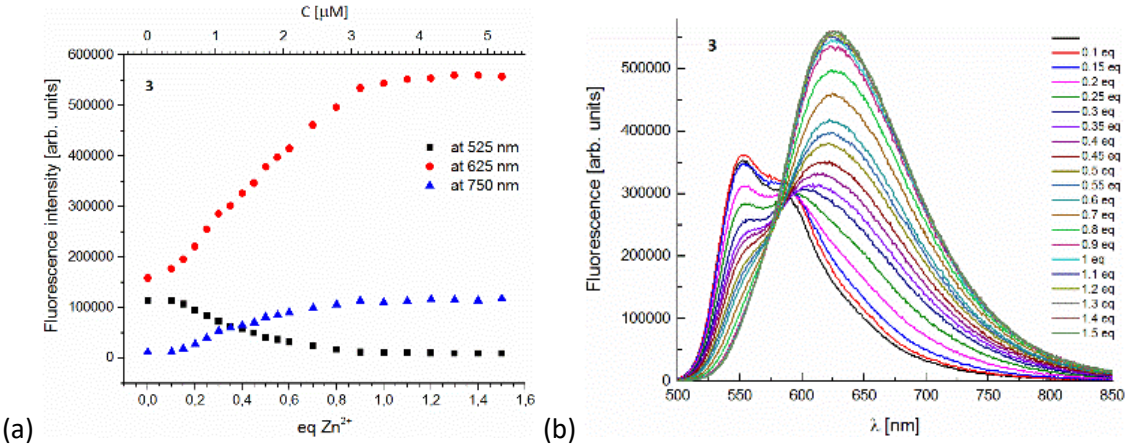

Fig S17. Fluorescence titration for compound **3**. a: Titration curve; b: Fluorescence spectrum

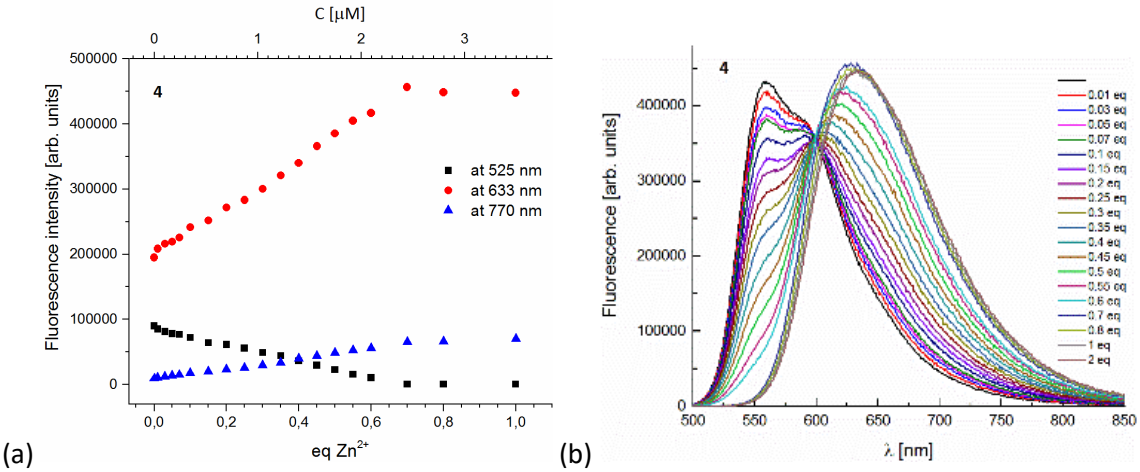

Fig S18. Fluorescence titration for compound **4**. a: Titration curve; b: Fluorescence spectrum

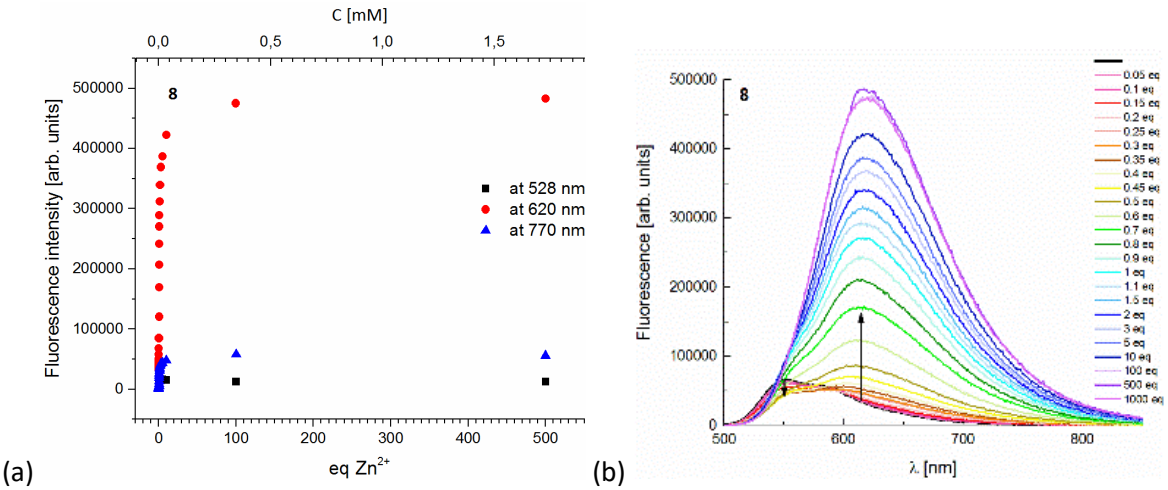

Fig S19. Fluorescence titration for compound **8**. a: Titration curve; b: Fluorescence spectrum

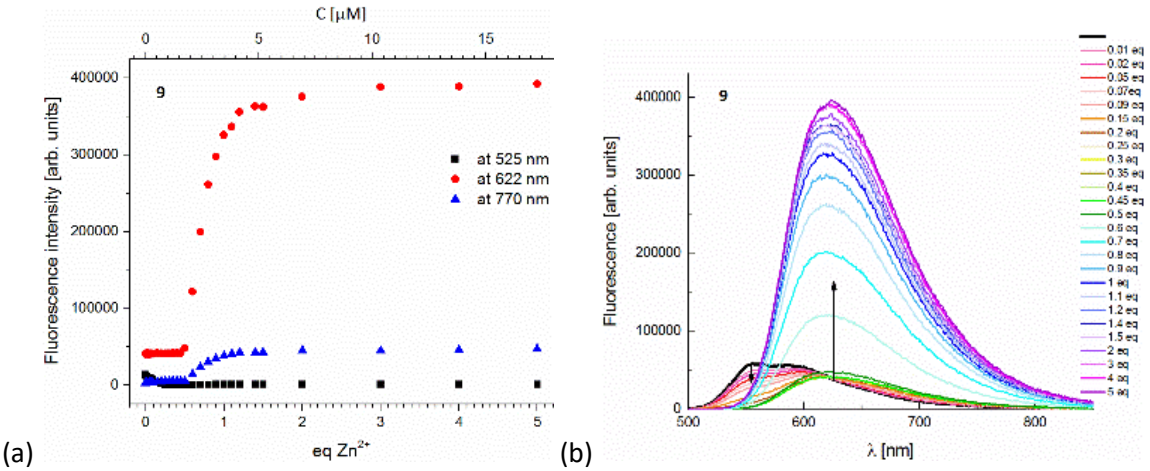

Fig S20. Fluorescence titration for compound **9**. a: Titration curve; b: Fluorescence spectrum

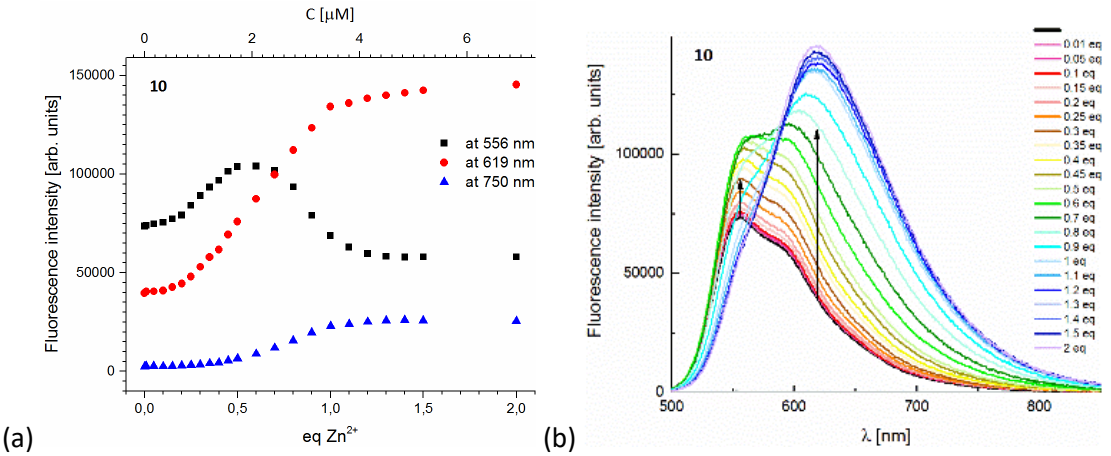

Fig S21. Fluorescence titration for compound **10**. a: Titration curve; b: Fluorescence spectrum

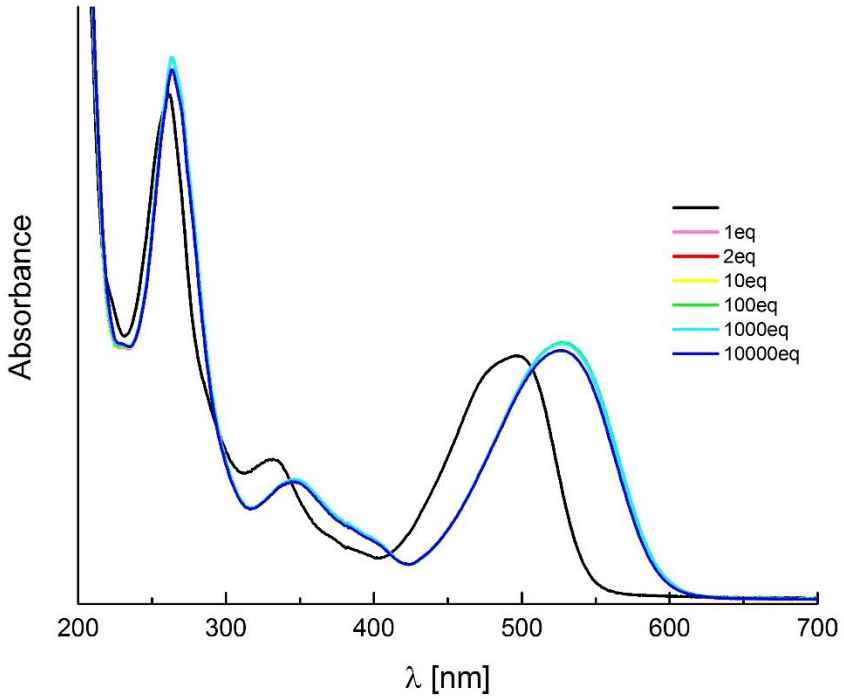

Fig. S22.The effect of zinc perchlorate addition on the absorption spectra of DPP **4** measured in CH_3CN.

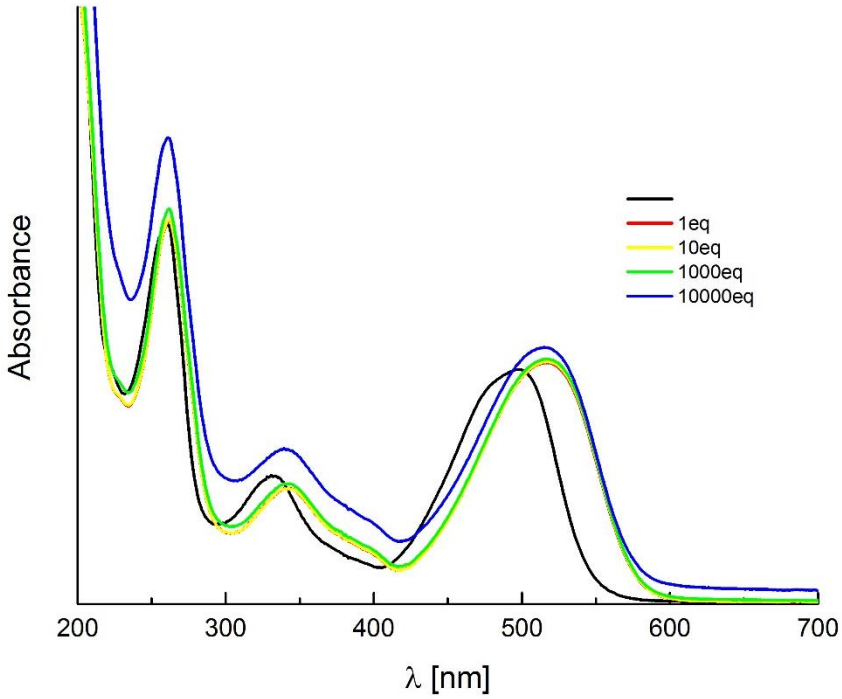

Fig. S23.The effect of magnesium perchlorate addition on the absorption spectra of DPP **4** measured in CH_3CN.

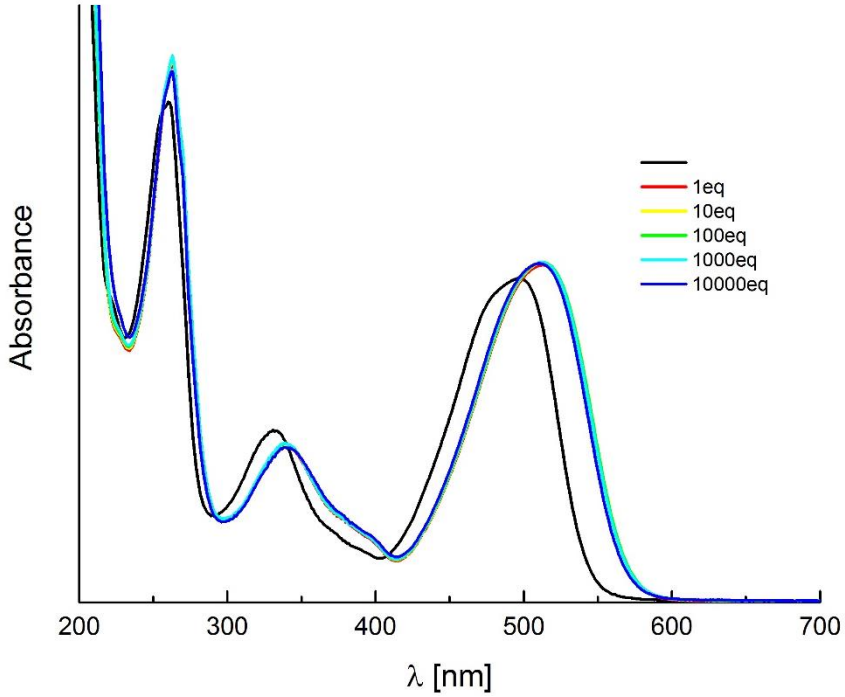

Fig. S24.The effect of calcium perchlorate addition on the absorption spectra of DPP **4** measured in CH_3CN.

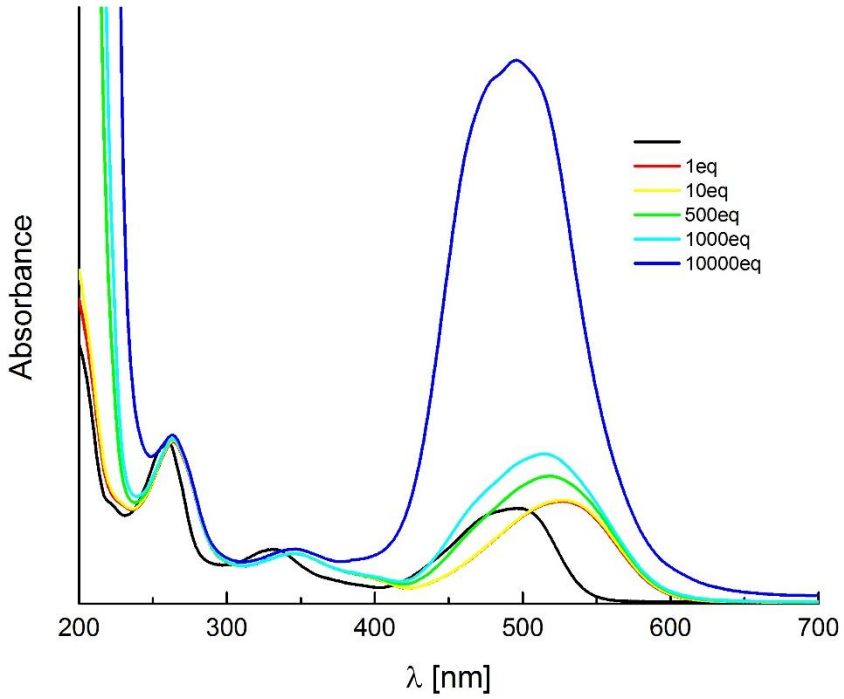

Fig. S25.The effect of cobalt perchlorate addition on the absorption spectra of DPP **4** measured in CH_3CN.

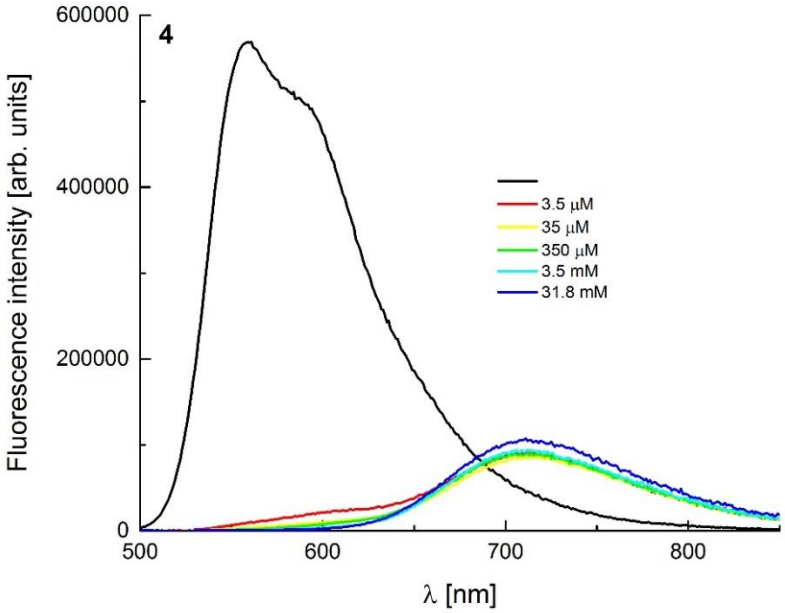

Fig. S26. The effect of $PhSO_3H$ addition on the emission spectra of DPP **4** measured in CH_3CN.

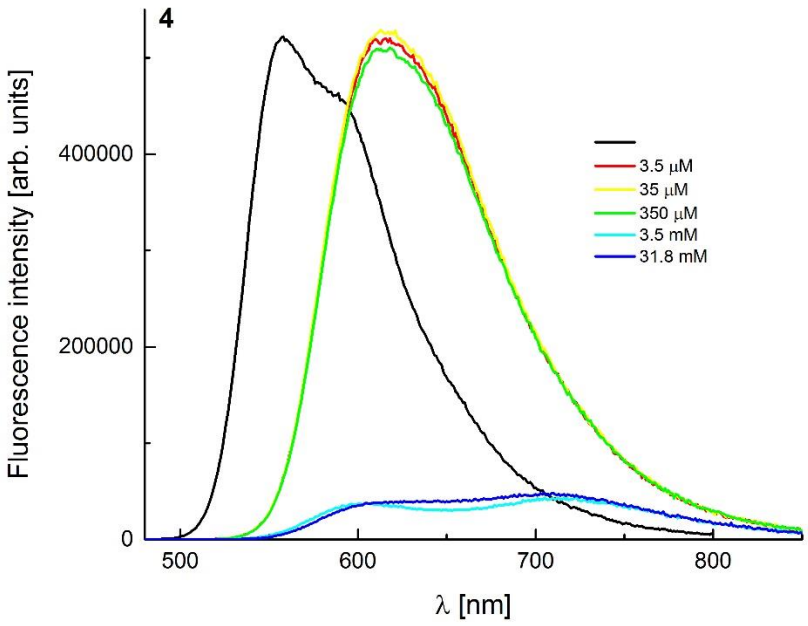

Fig. S27. The effect of cadmium perchlorate addition on the emission spectra of DPP **4** measured in CH_3CN.

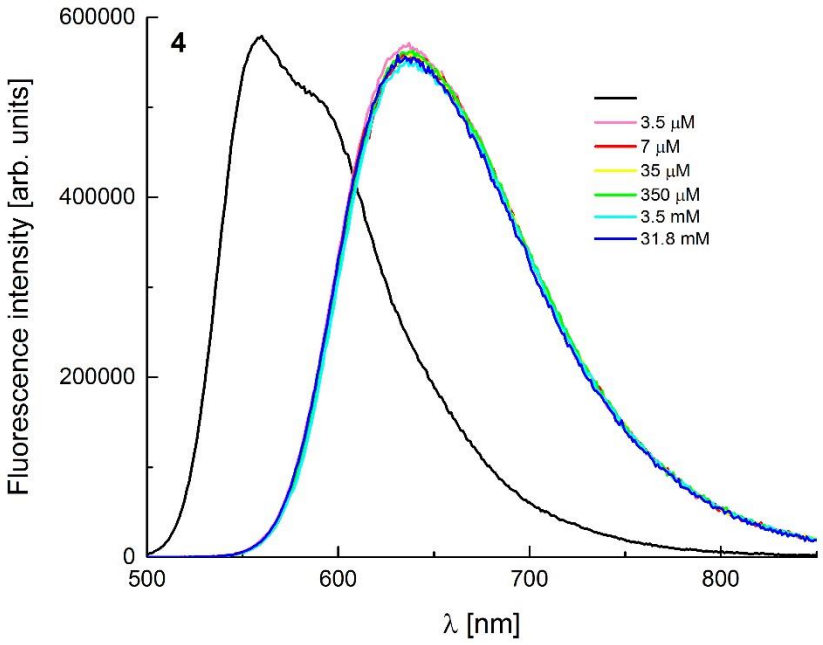

Fig. S28. The effect of zinc perchlorate addition on the emission spectra of DPP **4** measured in CH_3CN.

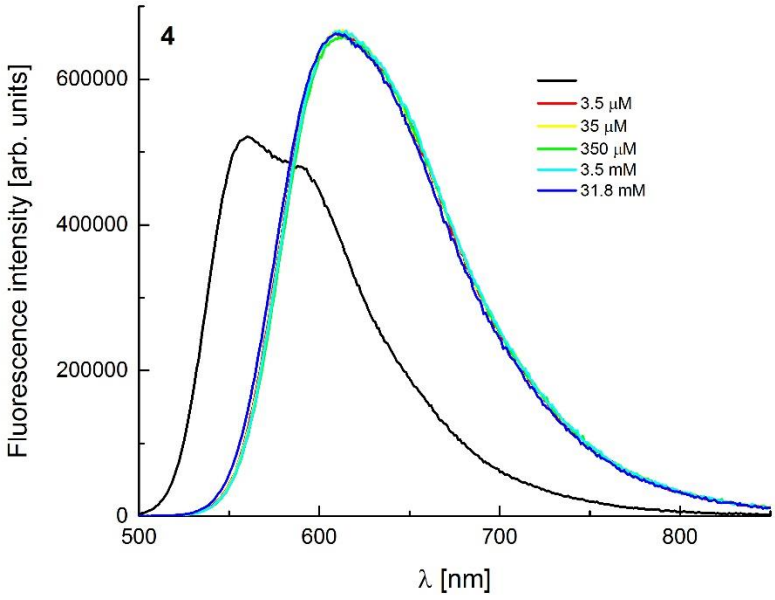

Fig. S29. The effect of magnesium perchlorate addition on the emission spectra of DPP **4** measured in CH_3CN.

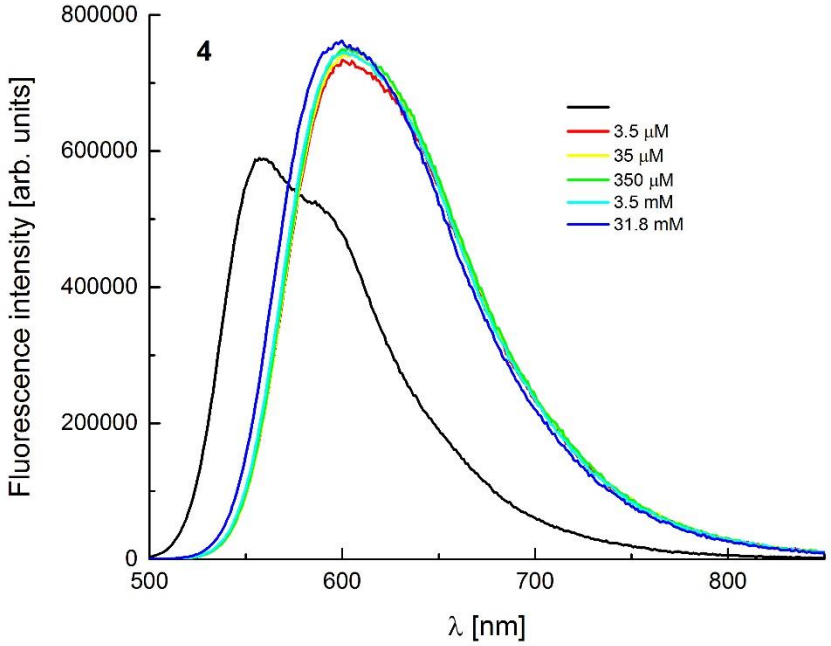

Fig. S30. The effect of calcium perchlorate addition on the emission spectra of DPP **4** measured in CH_3CN.

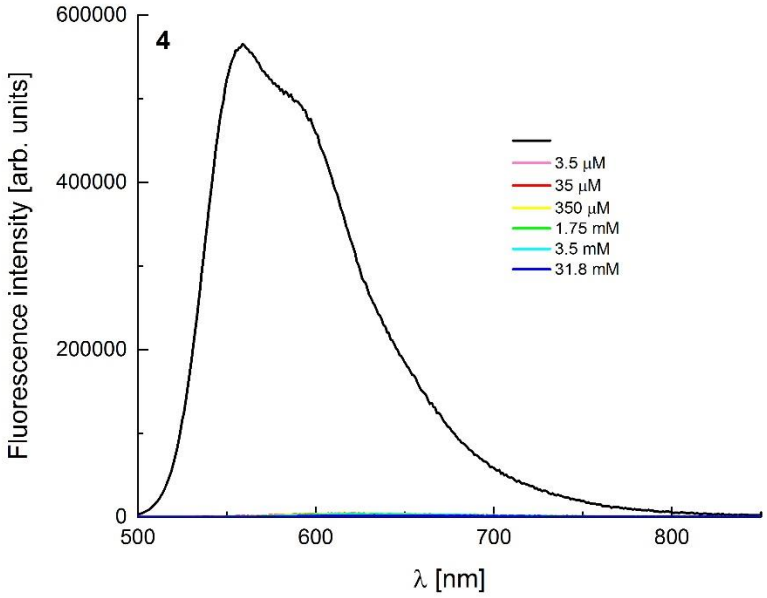

Fig. S31. The effect of cobalt perchlorate addition on the emission spectra of DPP **4** measured in CH_3CN.

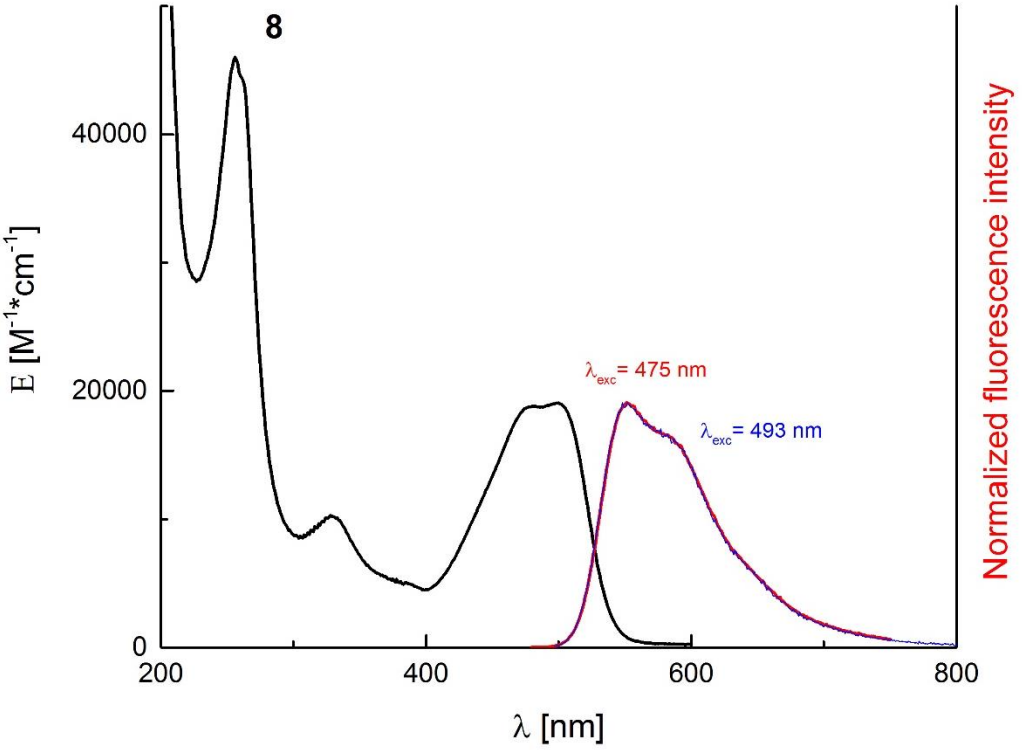

Fig. S32. The absorption and emission spectra of DPP **8** in CH_3CN.

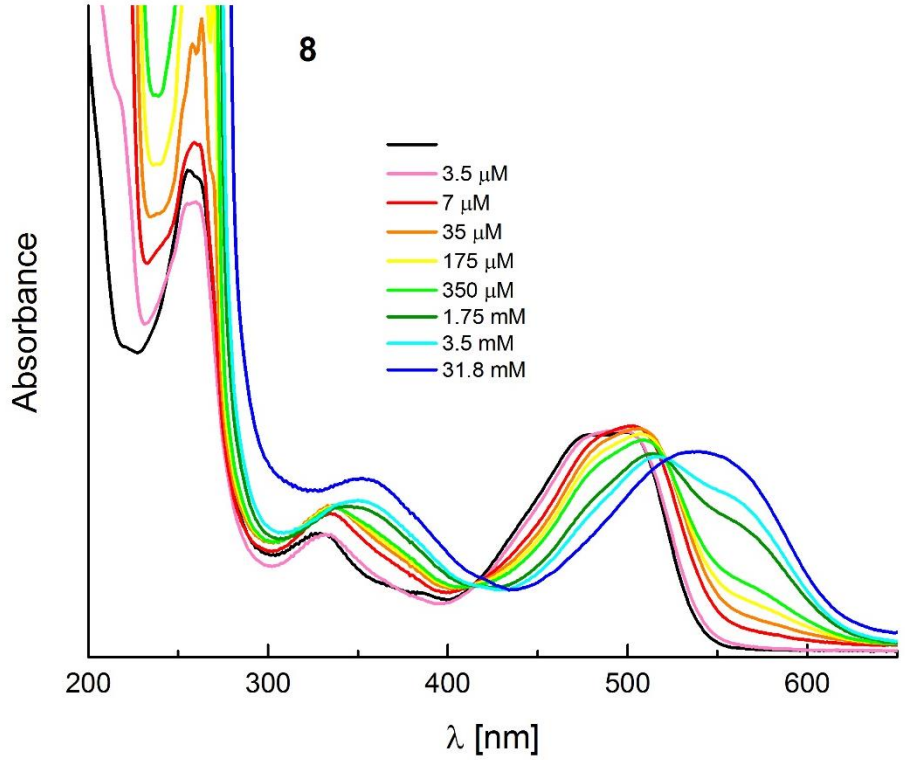

Fig. S33.The effect of $PhSO_3H$ addition on the absorption spectra of DPP **8** measured in CH_3CN.

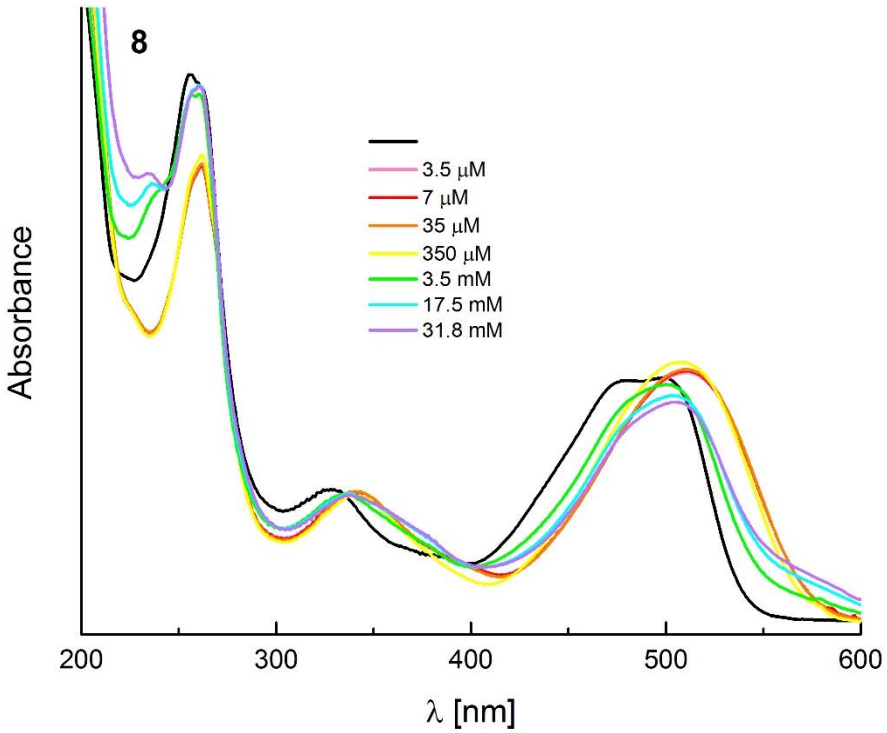

Fig. S34.The effect of cadmium perchlorate addition on the absorption spectra of DPP **8** measured in CH_3CN.

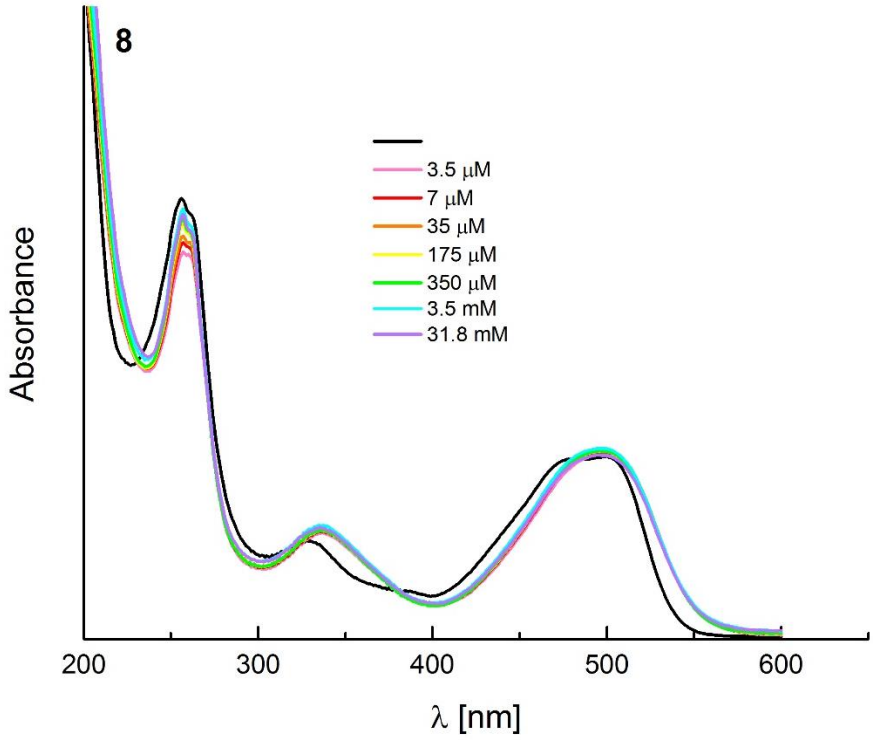

Fig. S35.The effect of zinc perchlorate addition on the absorption spectra of DPP **8** measured in CH_3CN.

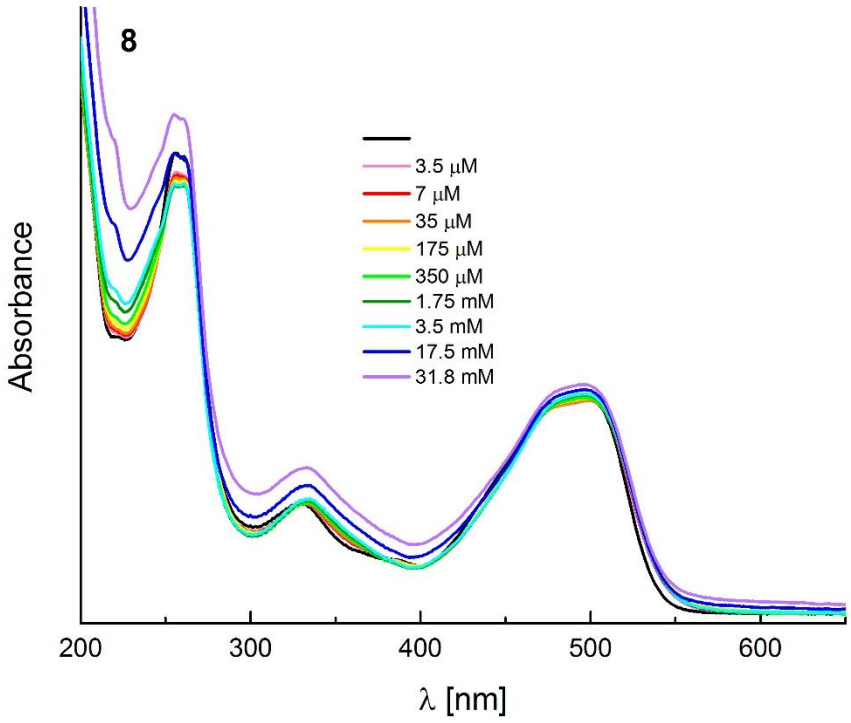

Fig. S36.The effect of magnesium perchlorate addition on the absorption spectra of DPP **8** measured in ACN.

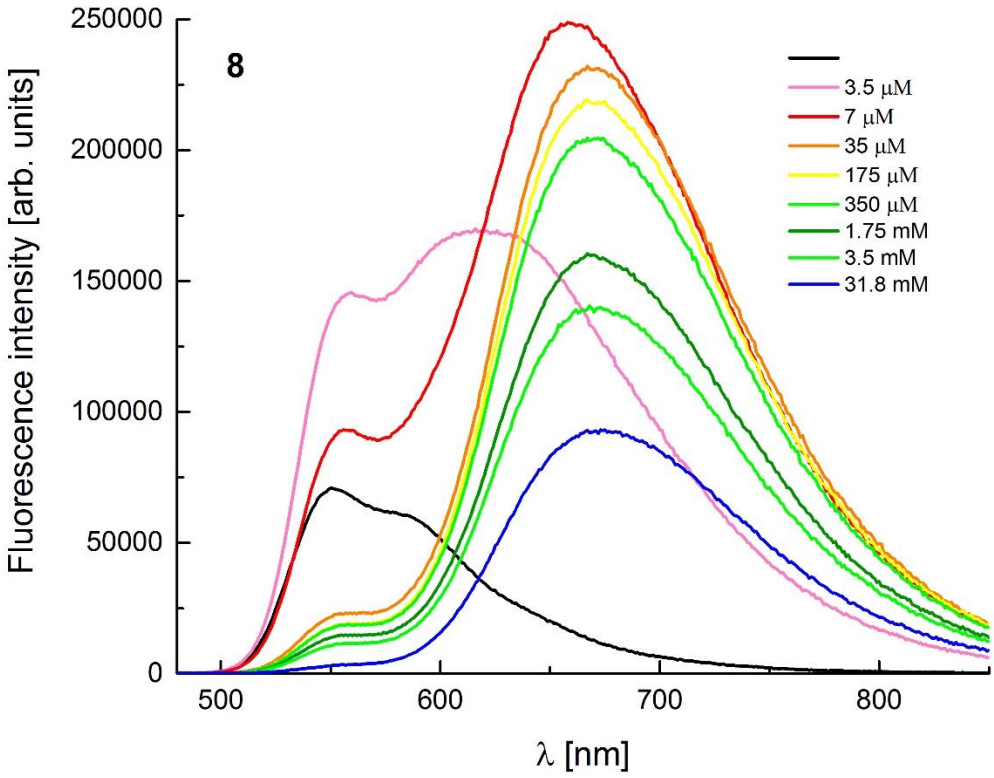

Fig. S37. The effect of $PhSO_3H$ addition on the emission spectra of DPP **8** measured in CH_3CN.

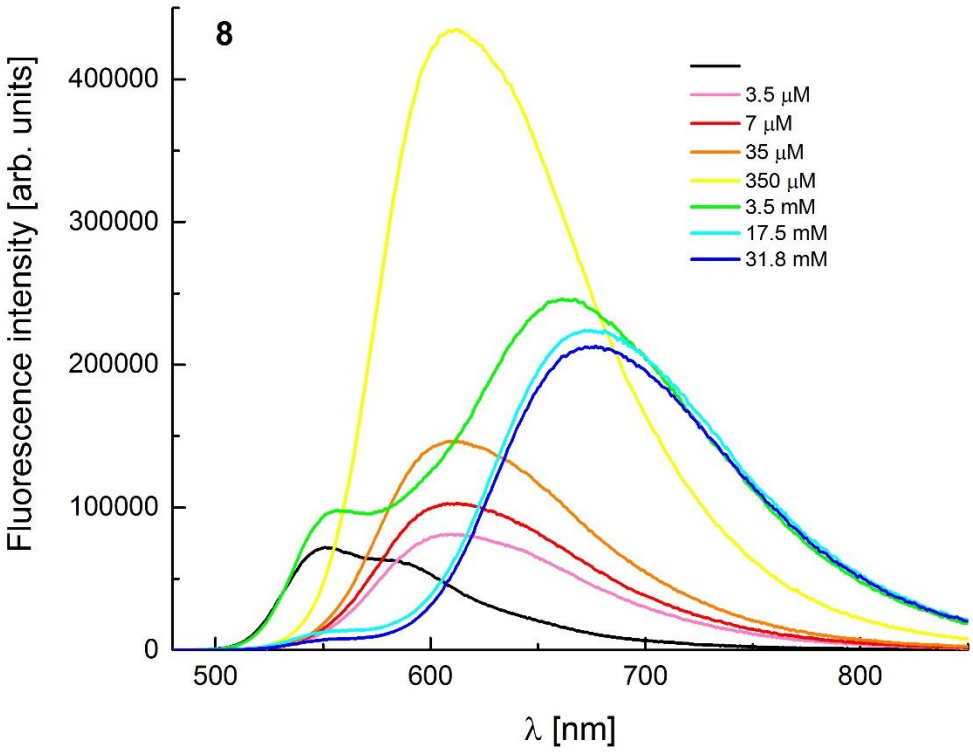

Fig. S38. The effect of cadmium perchlorate addition on the emission spectra of DPP **8** measured in CH_3CN.

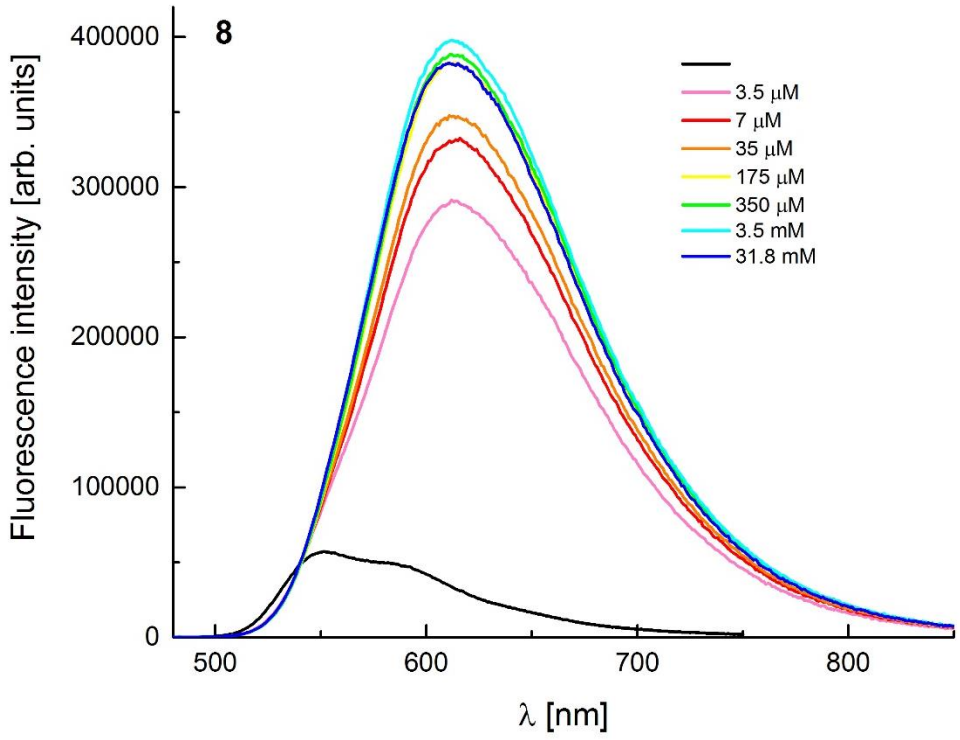

Fig. S39. The effect of zinc perchlorate addition on the emission spectra of DPP **8** measured in CH_3CN.

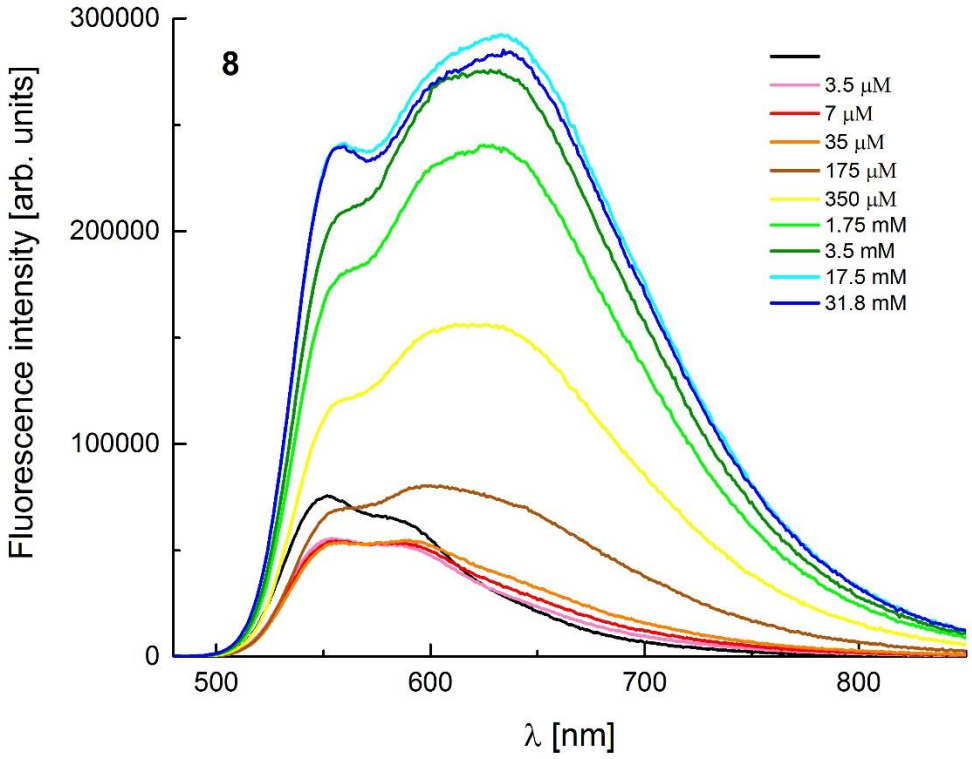

Fig. S40. The effect of magnesium perchlorate addition on the emission spectra of DPP **8** measured in CH_3CN.

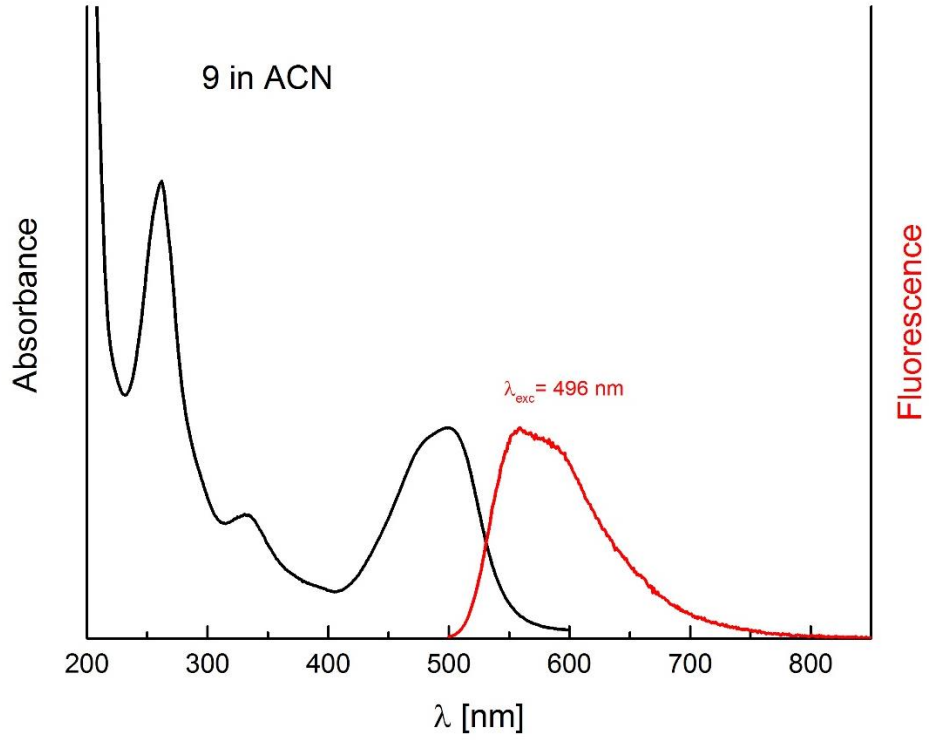

Fig. S41. The absorption and emission spectra of DPP **9** in CH_3CN.

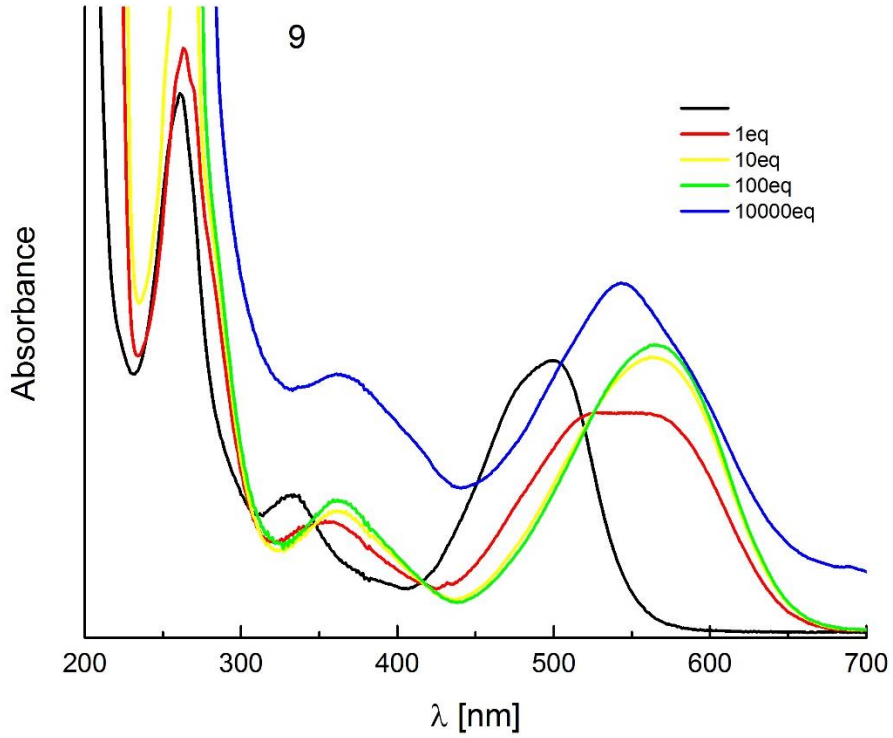

Fig. S42.The effect of $PhSO_3H$ addition on the absorption spectra of DPP **9** measured in CH_3CN.

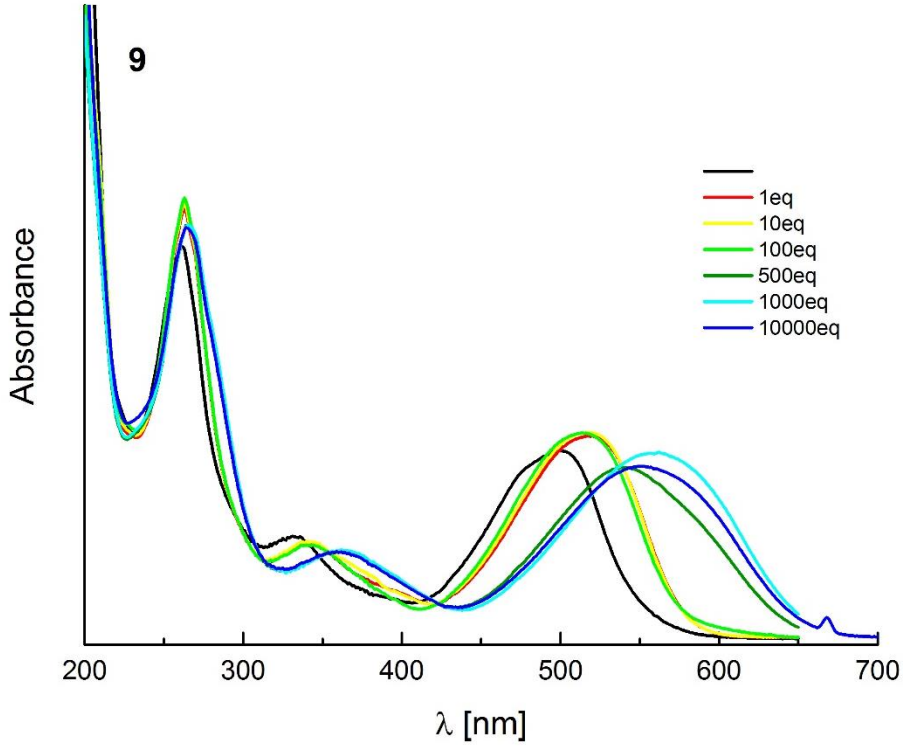

Fig. S43.The effect of cadmium perchlorate addition on the absorption spectra of DPP **9** measured in CH_3CN.

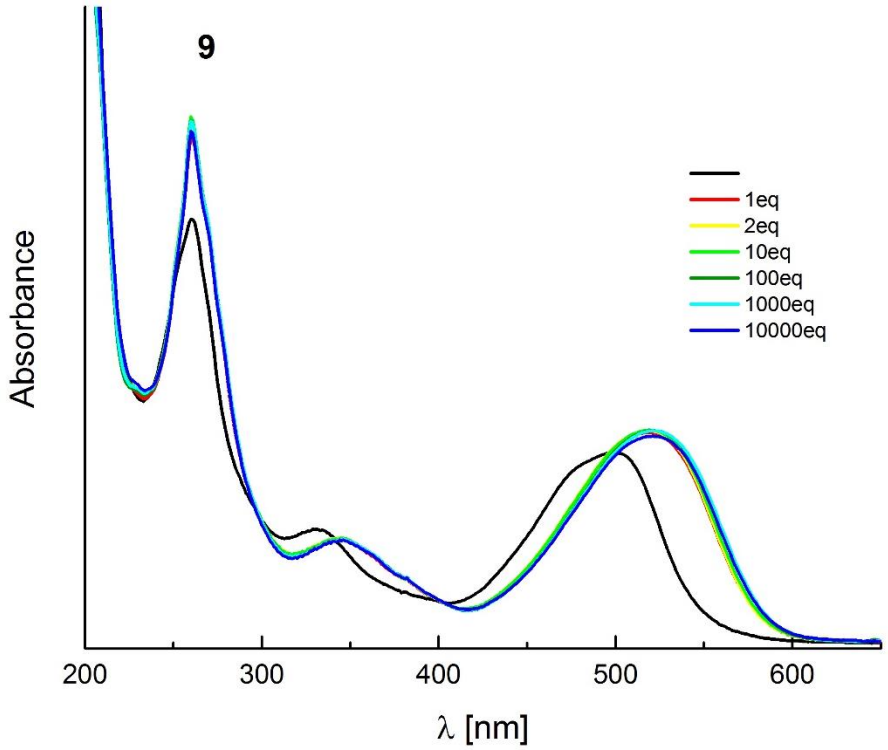

Fig. S44.The effect of zinc perchlorate addition on the absorption spectra of DPP **9** measured in CH_3CN.

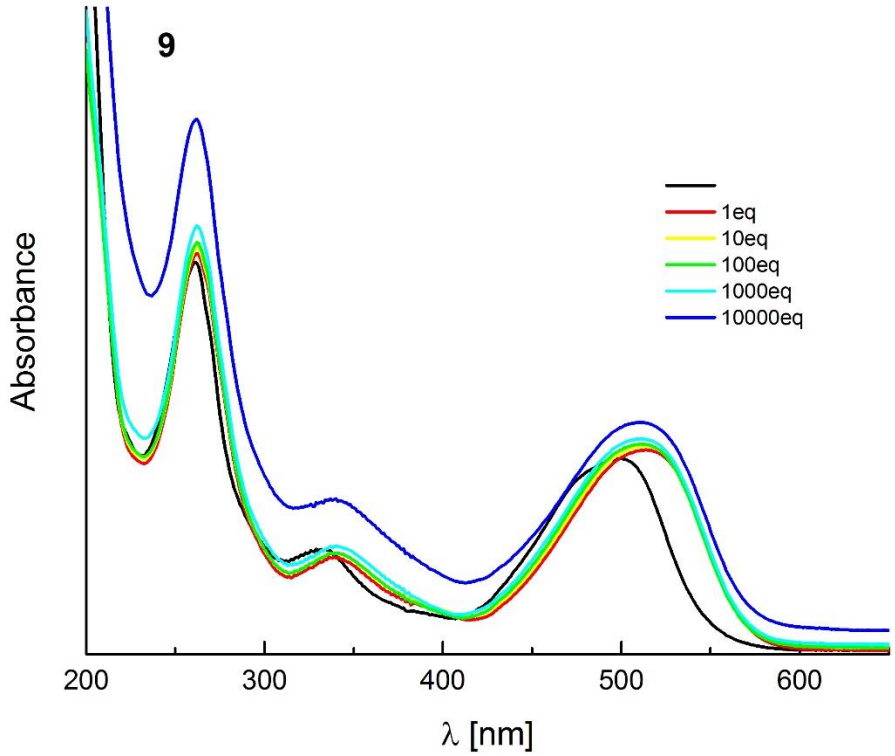

Fig. S45.The effect of magnesium perchlorate addition on the absorption spectra of DPP **9** measured in CH_3CN.

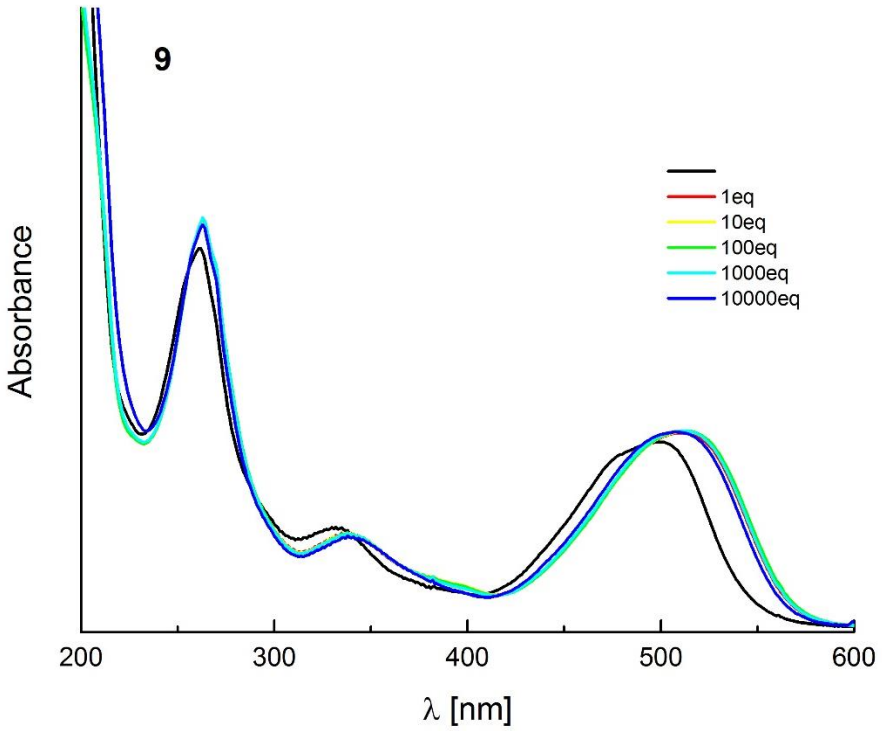

Fig. S46.The effect of calcium perchlorate addition on the absorption spectra of DPP **9** measured in CH_3CN.

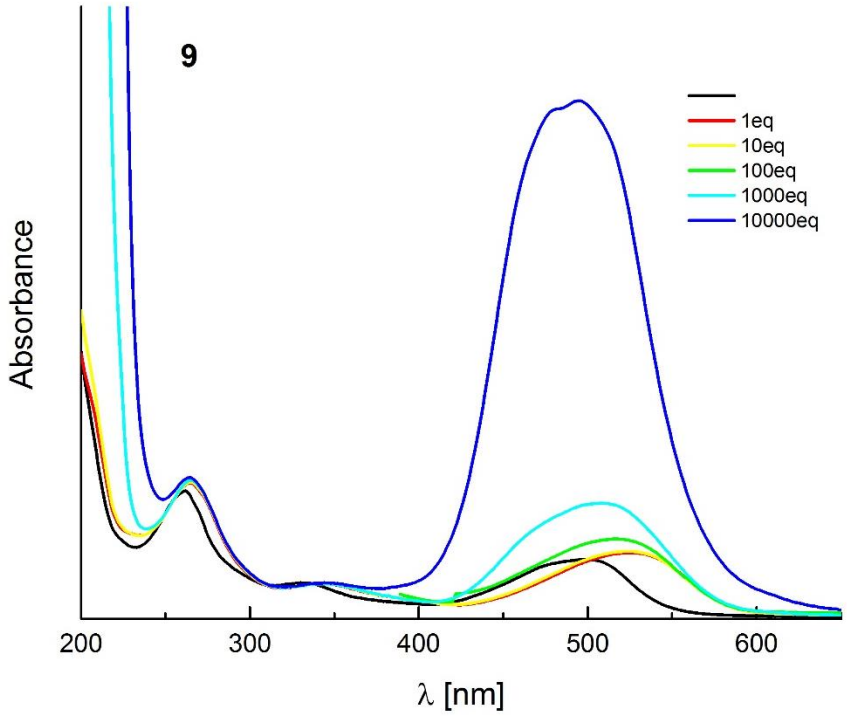

Fig. S47.The effect of cobalt perchlorate addition on the absorption spectra of DPP **9** measured in CH_3CN.

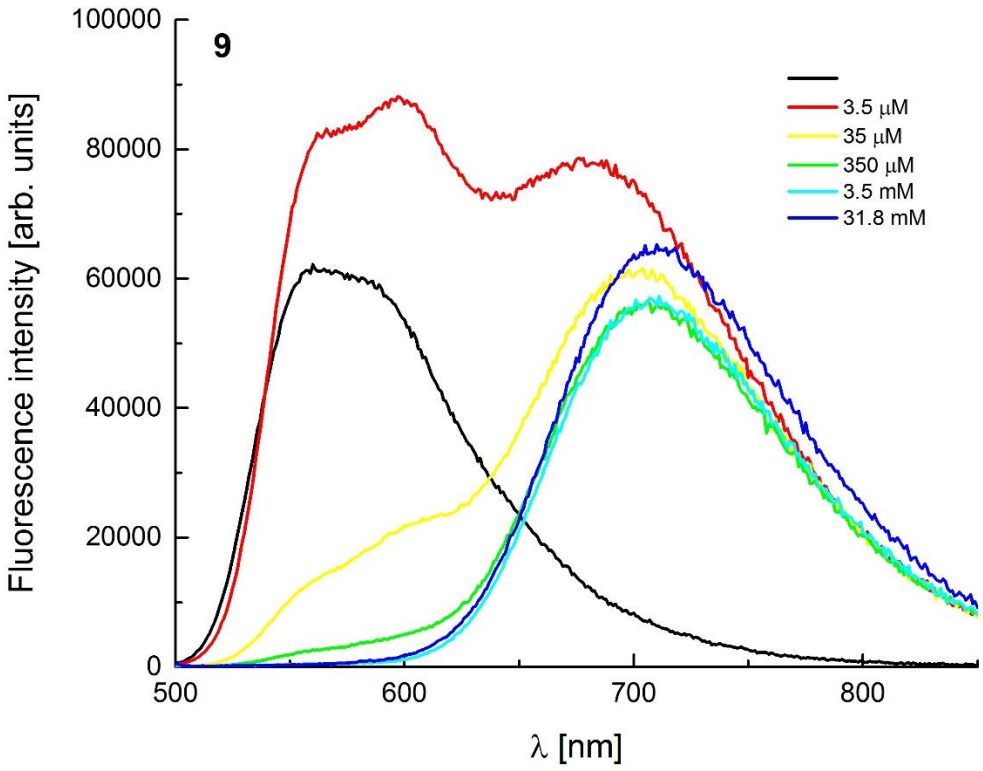

Fig. S48. The effect of $PhSO_3H$ addition on the emission spectra of DPP **9** measured in CH_3CN.

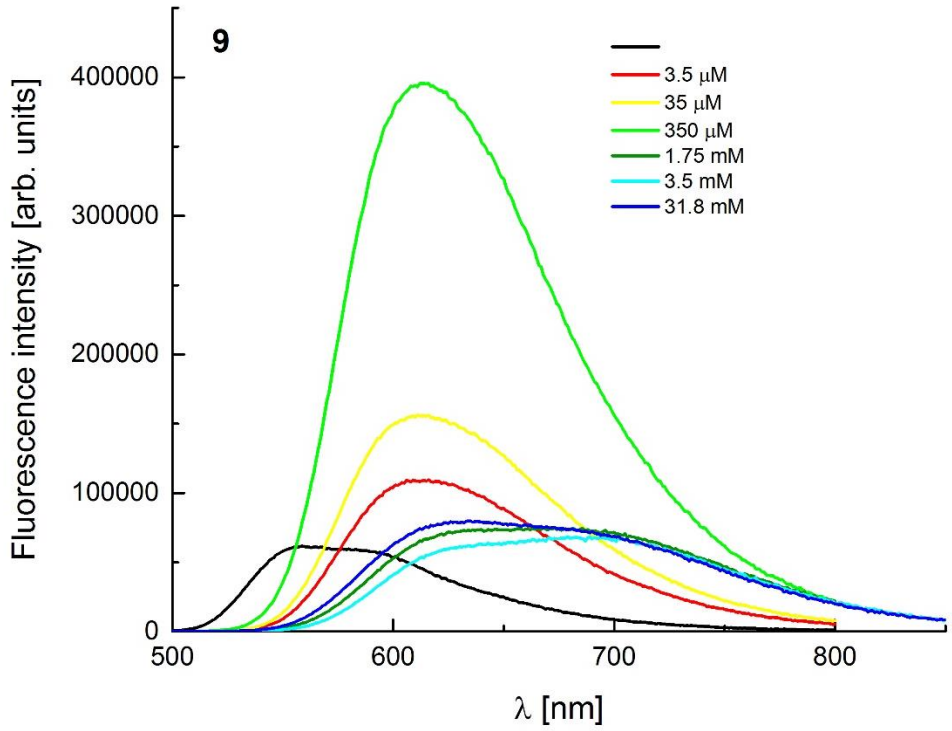

Fig. S49. The effect of cadmium perchlorate addition on the emission spectra of DPP **9** measured in CH_3CN.

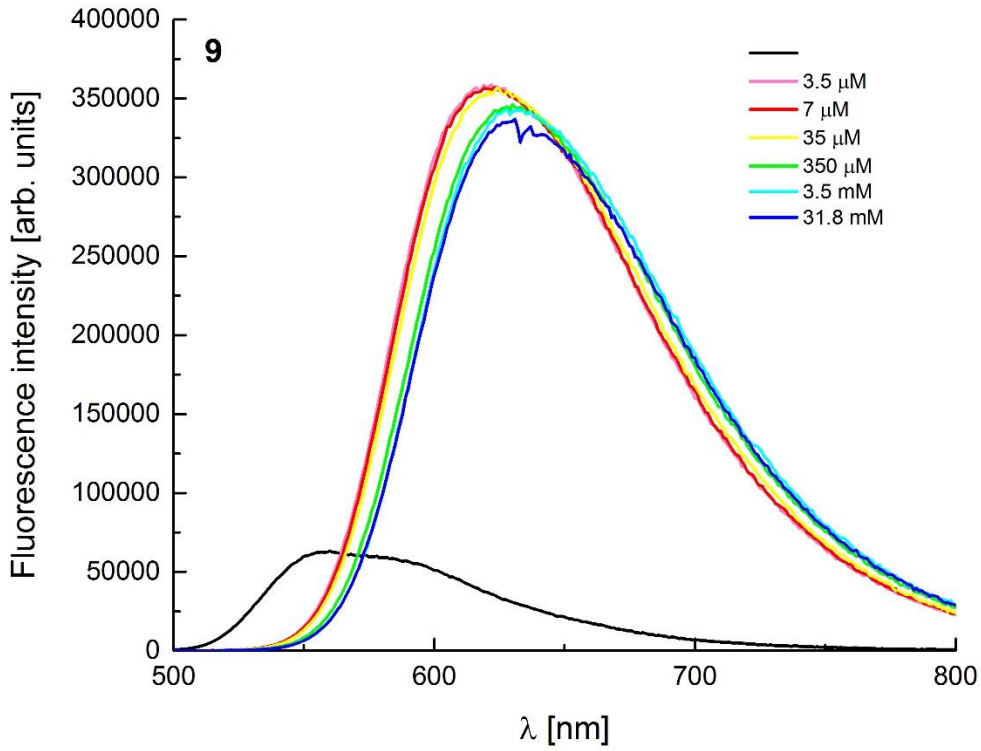

Fig. S50. The effect of zinc perchlorate addition on the emission spectra of DPP **9** measured in CH_3CN.

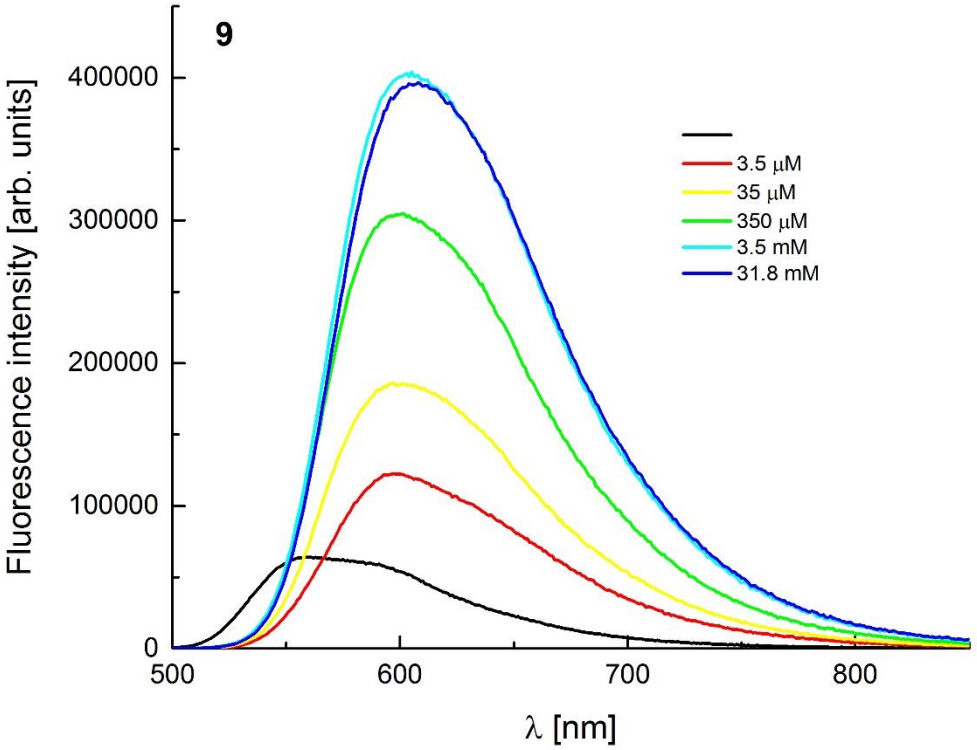

Fig. S51. The effect of magnesium perchlorate addition on the emission spectra of DPP **9** measured in CH_3CN.

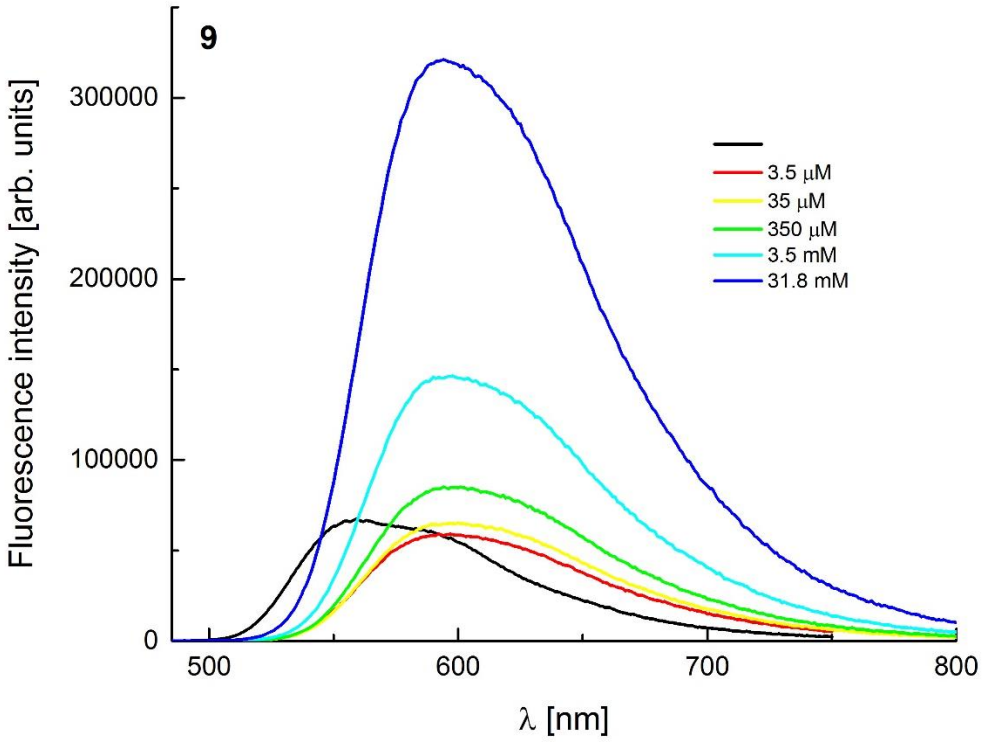

Fig. S52. The effect of calcium perchlorate addition on the emission spectra of DPP **9** measured in CH_3CN.

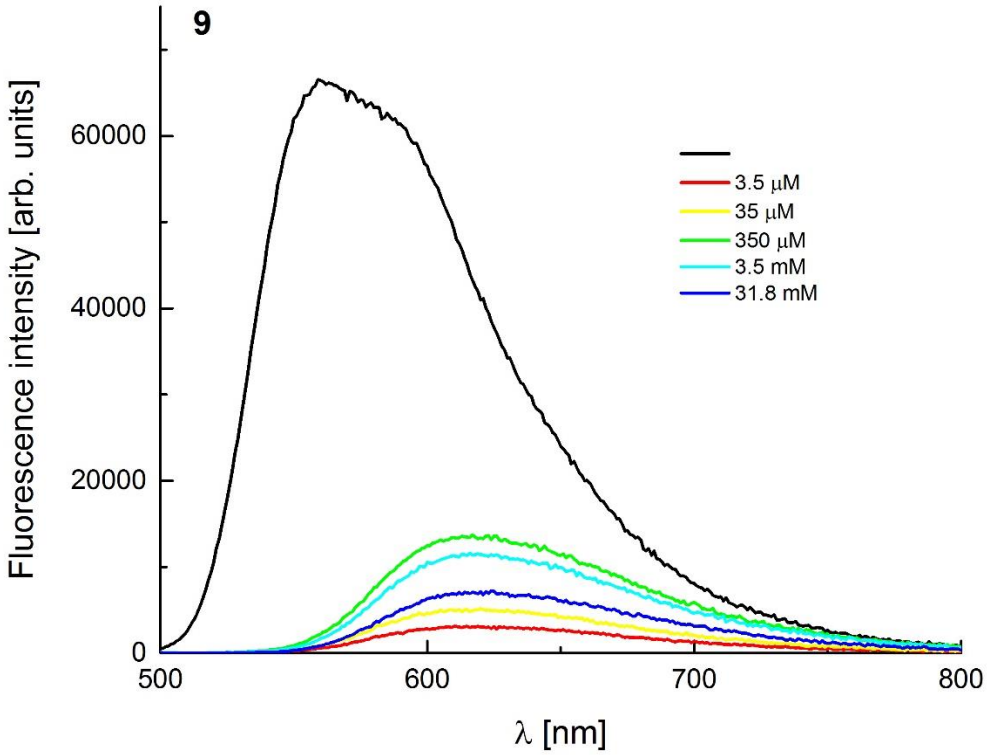

Fig. S53. The effect of cobalt perchlorate addition on the emission spectra of DPP **9** measured in CH_3CN.

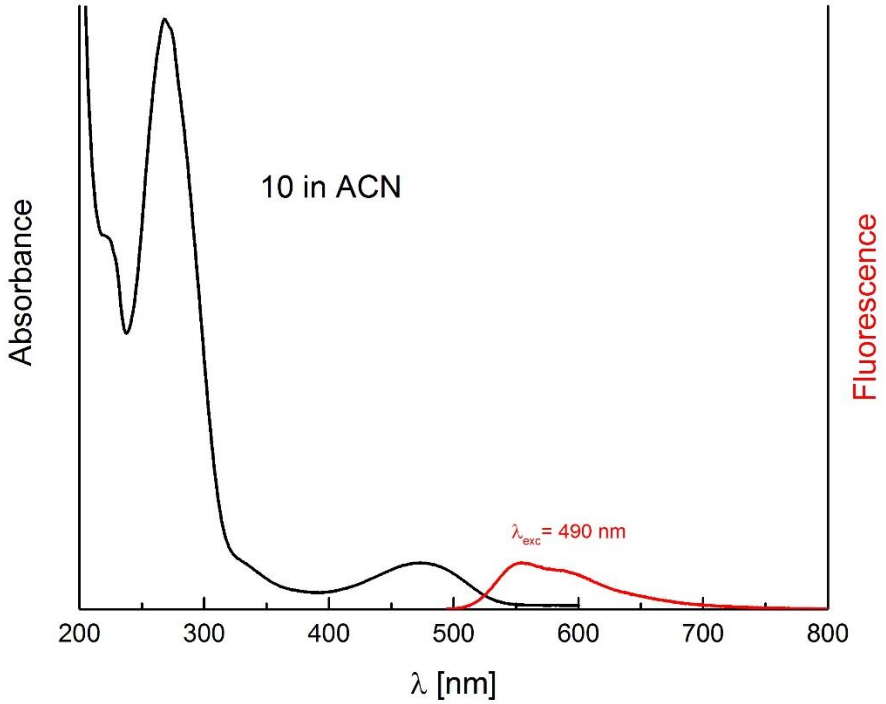

Fig. S54. The absorption and emission spectra of DPP **10** in CH_3CN.

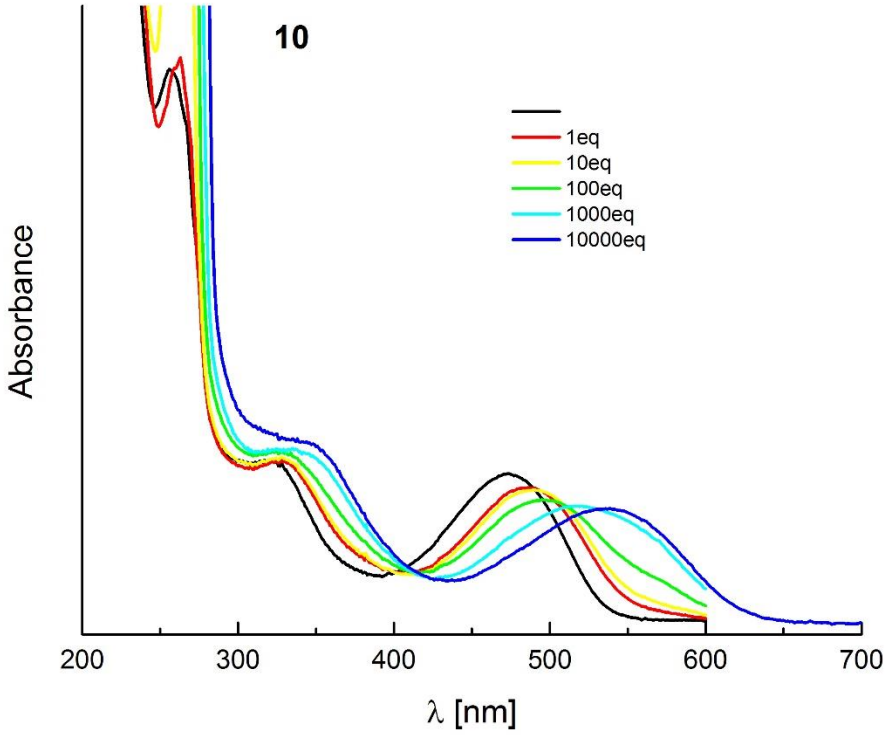

Fig. S55.The effect of $PhSO_3H$ addition on the absorption spectra of DPP **10** measured in CH_3CN.

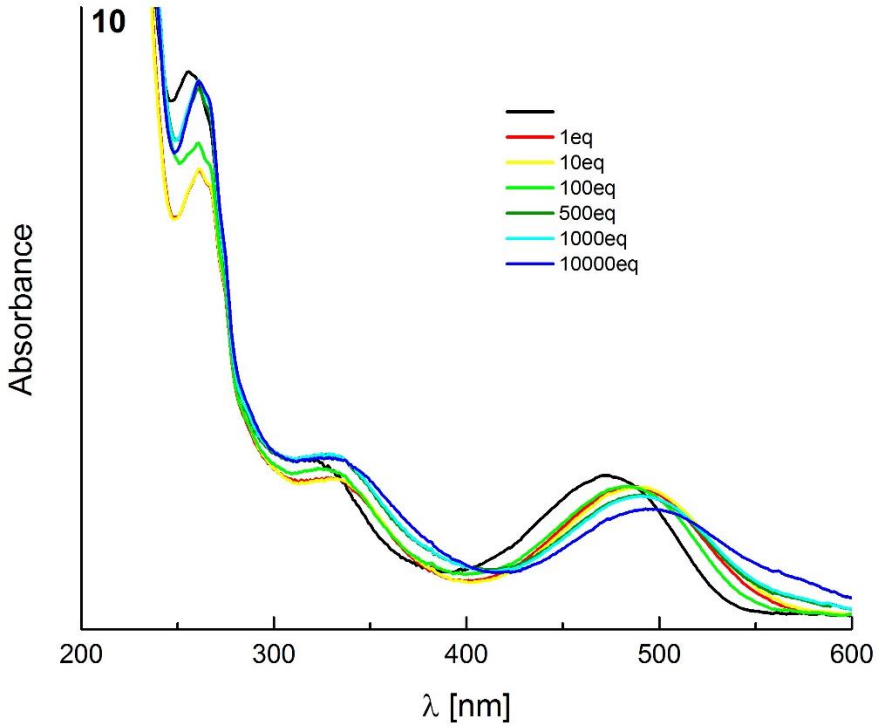

Fig. S56.The effect of cadmium perchlorate addition on the absorption spectra of DPP **10** measured in CH_3CN.

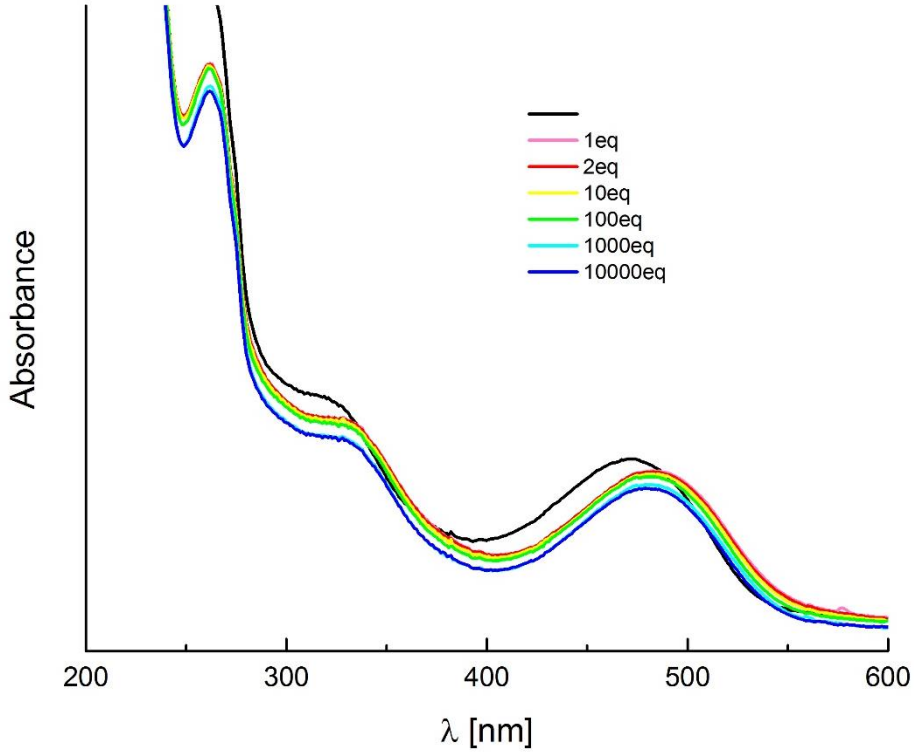

Fig. S57.The effect of zinc perchlorate addition on the absorption spectra of DPP **10** measured in CH_3CN.

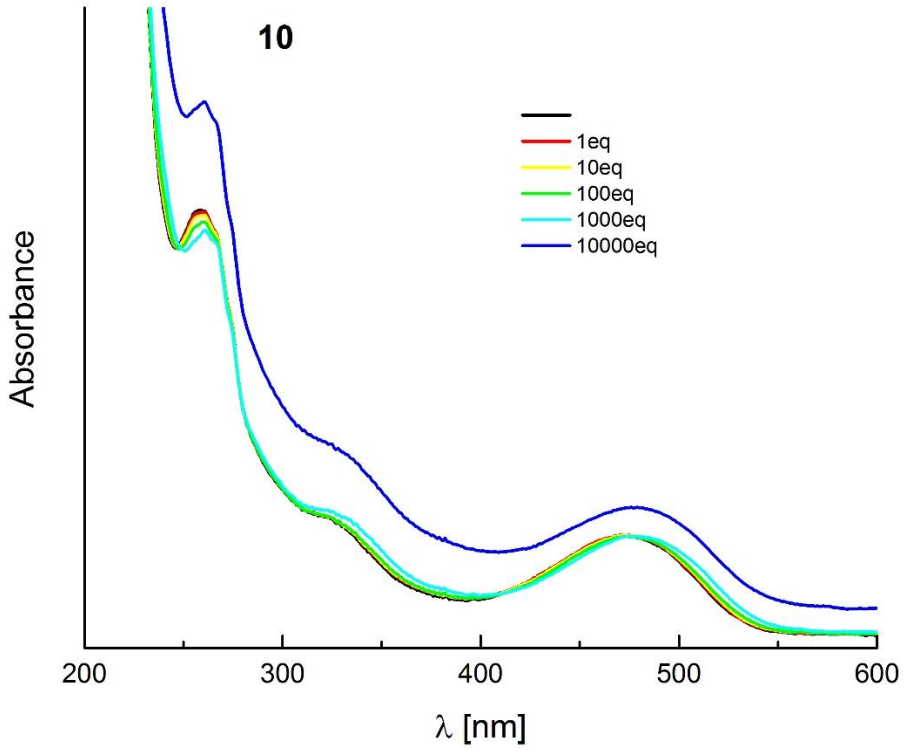

Fig. S58.The effect of magnesium perchlorate addition on the absorption spectra of DPP **10** measured in CH_3CN.

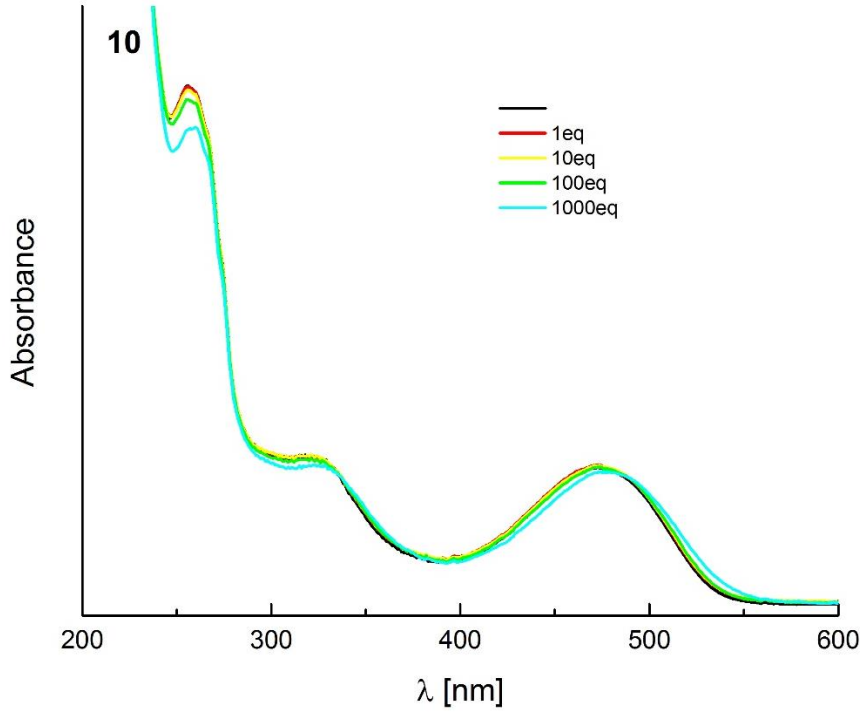

Fig. S59.The effect of calcium perchlorate addition on the absorption spectra of DPP **10** measured in CH_3CN.

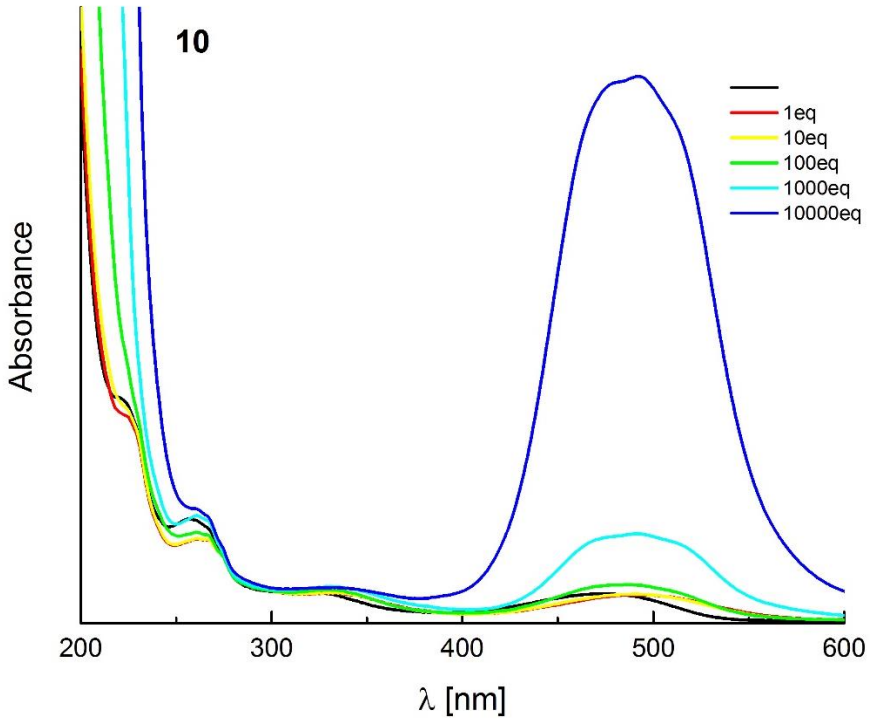

Fig. S60.The effect of cobalt perchlorate addition on the absorption spectra of DPP **10** measured in CH_3CN.

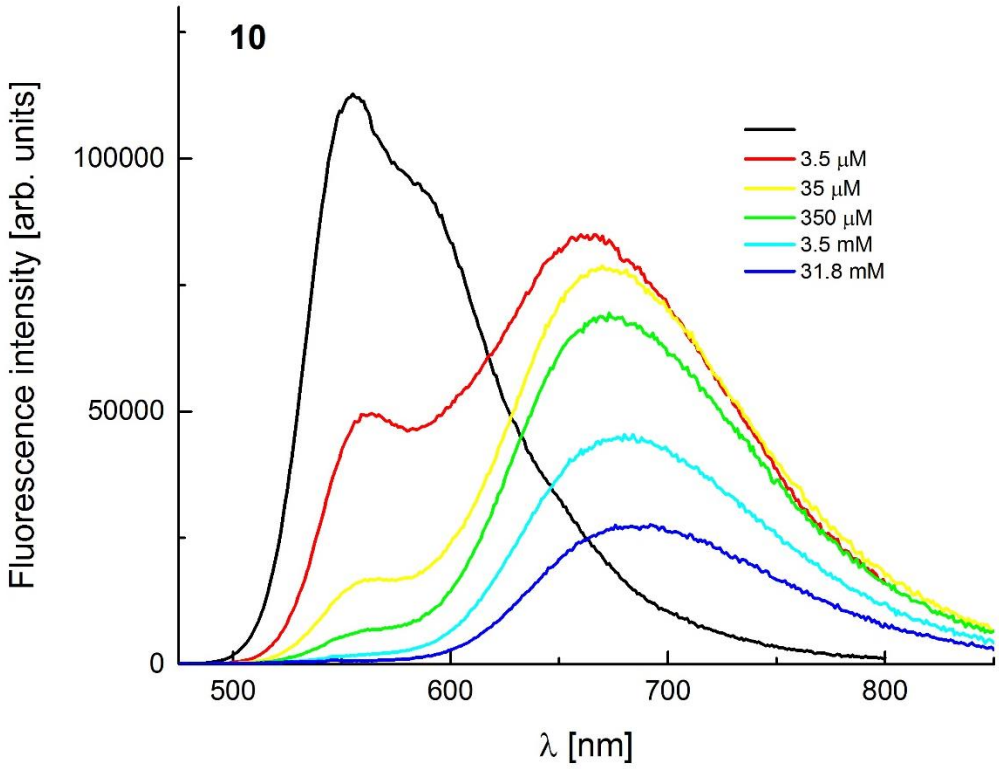

Fig. S61. The effect of $PhSO_3H$ addition on the emission spectra of DPP **10** measured in CH_3CN.

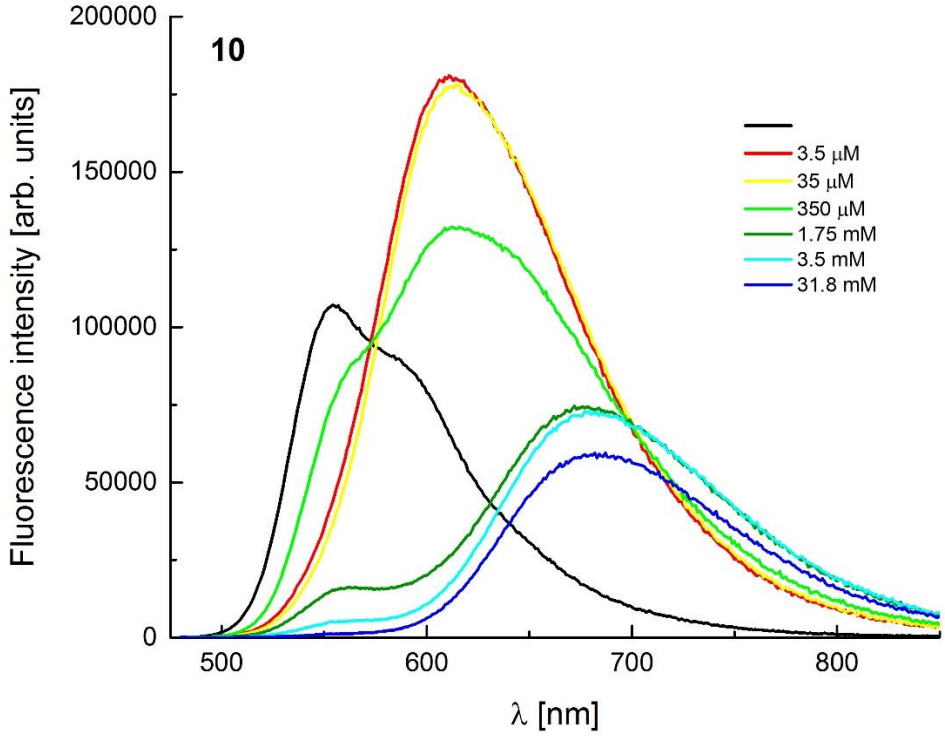

Fig. S62. The effect of cadmium perchlorate addition on the emission spectra of DPP **10** measured in CH_3CN.

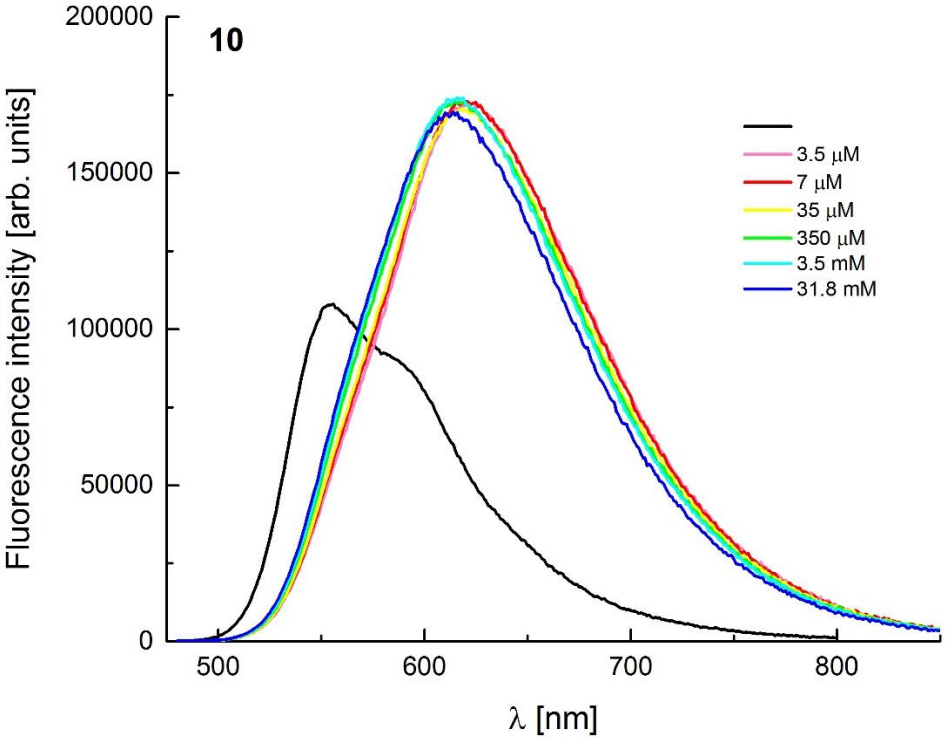

Fig. S63. The effect of zinc perchlorate addition on the emission spectra of DPP **10** measured in CH_3CN.

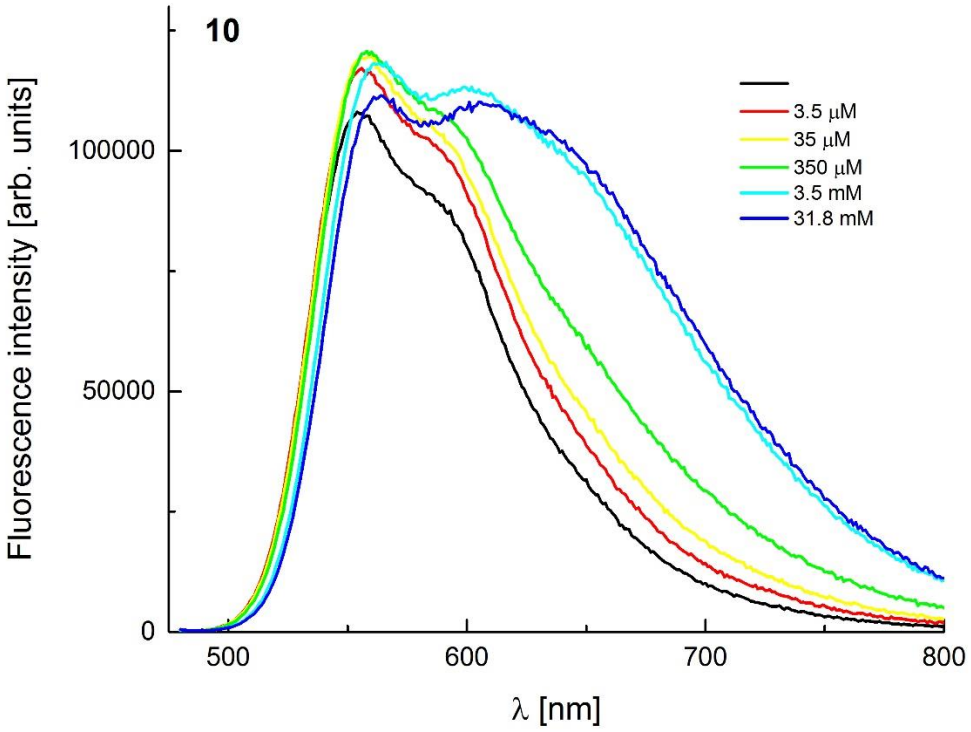

Fig. S64. The effect of magnesium perchlorate addition on the emission spectra of DPP **10** measured in CH_3CN.

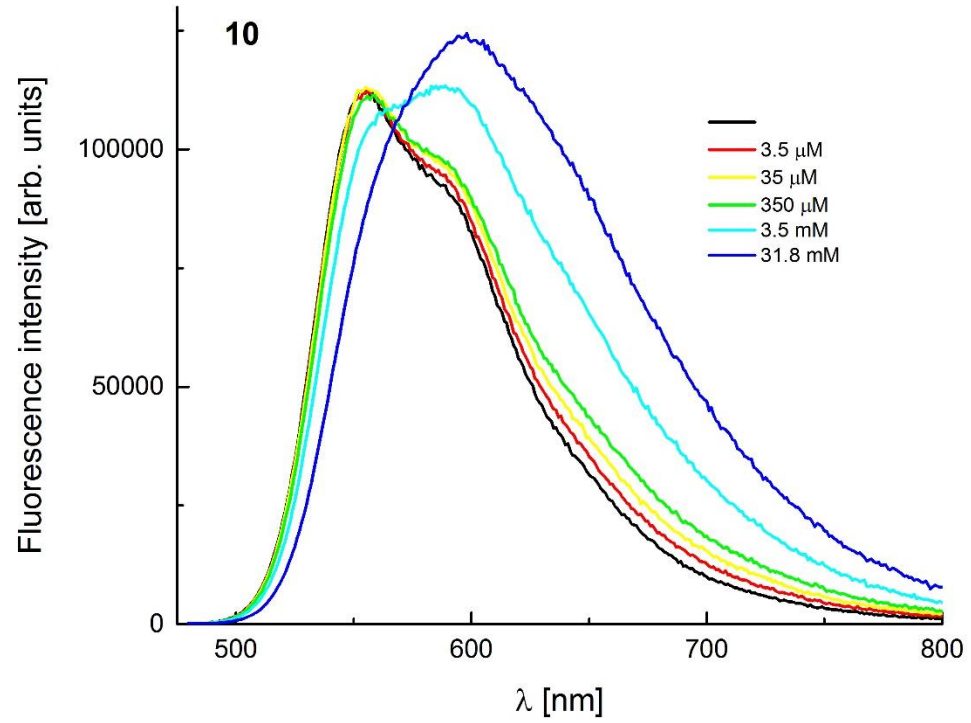

Fig. S65. The effect of calcium perchlorate addition on the emission spectra of DPP **10** measured in CH_3CN.

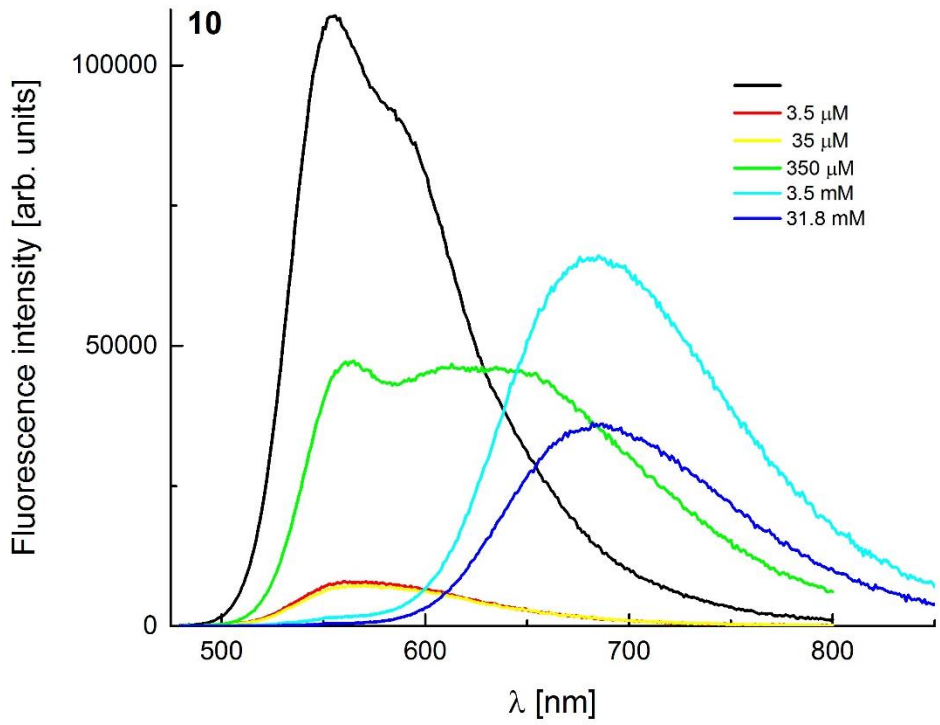

Fig. S66. The effect of cobalt perchlorate addition on the emission spectra of DPP **10** measured in CH_3CN.

Section S4: Water solubility and binding constants

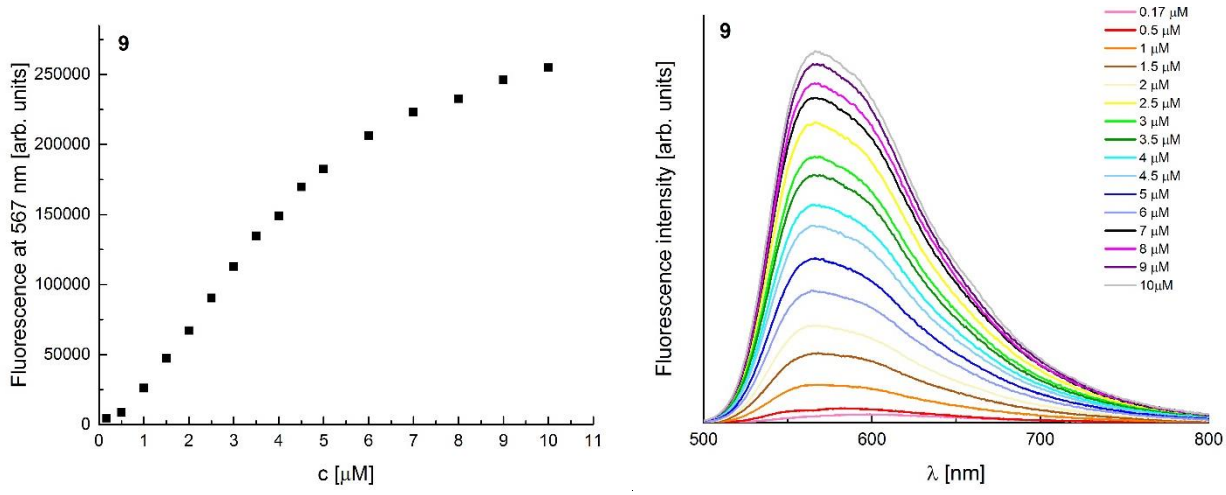

Fig. S67. Plot of fluorescence intensity against concentration of DPP **9** in water.

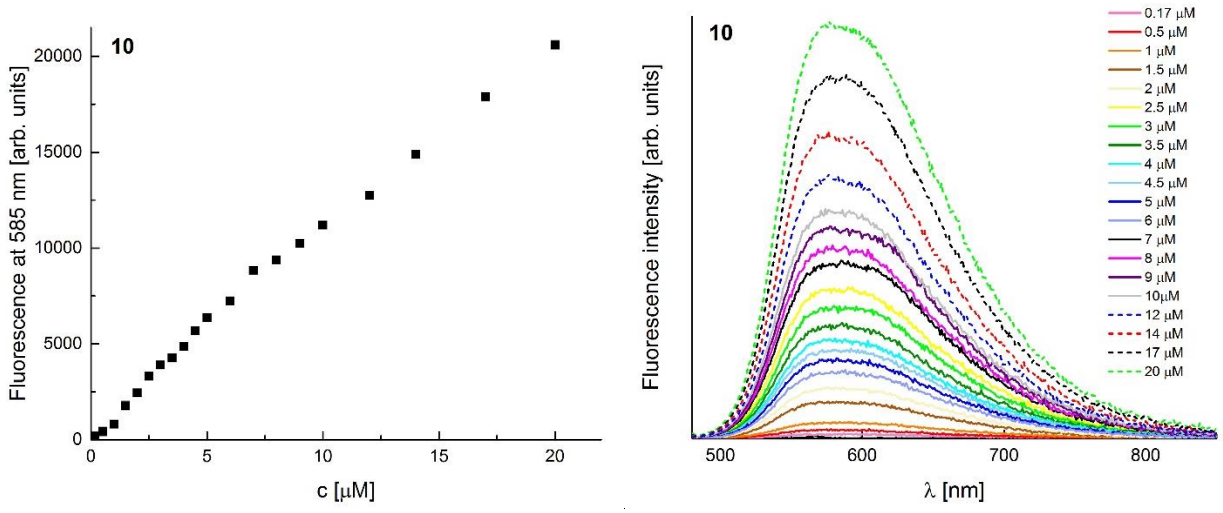

Fig. S68. Plot of fluorescence intensity against concentration of DPP **10** in water.

Section S5: Imaging

Cell culture conditions. The rat embryonic cardiomyoblast-derived H9C2 cell lines were cultured at 37°C in a humidified atmosphere containing 5% CO_2 in DMEM supplemented with 10% foetal bovine serum (FBS), 2 mM glutamine, 100 U/ml penicillin, and 100 µg/ml streptomycin.

Fluorescence localization of diketopyrrolopyrrole-based zinc probes within the cells. The cardiac H9C2 cells were loaded with fluorophores in DMEM medium supplemented with 10% FBS, 2 mM glutamine, 100 U/ml penicillin, and 100 µg/ml streptomycin at 37°C in a humidified atmosphere containing 5% CO_2 for 15 to 30 minutes with the diketopyrrolopyrrole-based zinc probe at the final concentration ranging from 200 to 500 nM. The final concentration of the MitoTracker™ Green FM was 150 nM, and Lysosyme probe was 100 nM. The fluorophores were dissolved in DMSO. Before measurements, the incubation medium was replaced with FluoroBrite™ DMEM. The measurements were performed with use of Olympus IX83 confocal microscope with the water objective 60x UPLSAPO 60XW. Registered data were transferred to the ImageJ and analyzed for presentation.

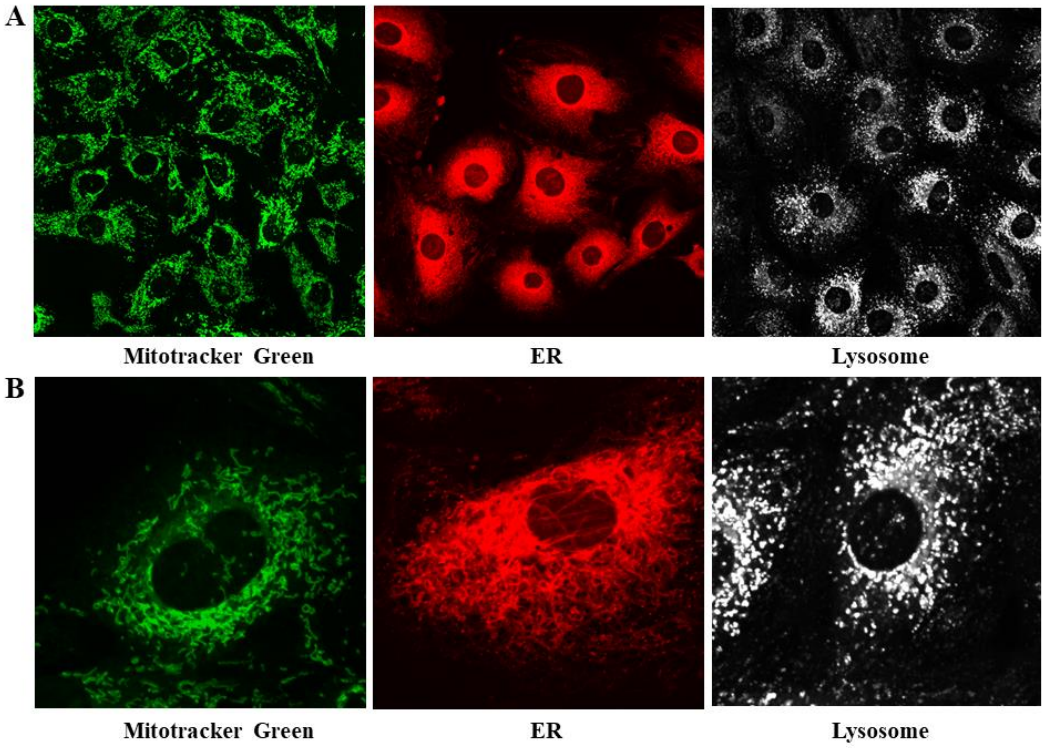

Fig. S69. Confocal imaging of the location of organellar fluorescent markers in H9C2 cells line. A. Localization of fluorescent markers for mitochondria (Mitotracker Green), endoplasmic reticulum (ER), and lysosomes, respectively, in H9C2 cells. B. Three-fold magnification of the selected Region of Interest (ROI), respectively for the individual fluorescent markers.

Section S6: Additional computational results

To ascertain the quality of the TD-DFT results, we have considered three smaller models of the investigated probes, denoted **M3**, and **M4** (see Fig. **S64**) for which CC2/*aug-cc*-pVTZ single point calculations were achievable.

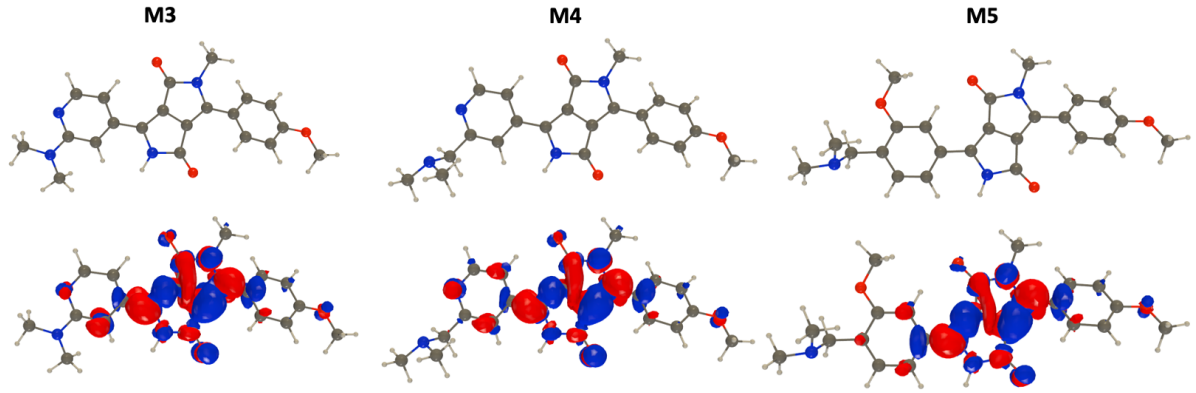

Fig. S70: Representation of the model probes used to test the reliability of the TD-DFT approach. We also provide the density difference plots (contour threshold: 0.001 au).

The cLR^2-PCM-TD-DFT protocol returns vertical absorption at 452, 461, and 453 nm for **M3**, and **M4** respectively. When adding the difference between CC2/*aug*-cc-pVTZ and TD-DFT results computed in gas phase, the values are increases slightly to 464, 473, and 463 nm, respectively. For vertical fluorescence, the cLR^2-PCM-TD-DFT values are 549, 557, and 542 nm, for for **M3**, and **M4**, respectively, whereas the CC2-corrected results are 552, 562, and 541 nm. Again, the values are very close and this hints that the selected functional is well suited for the systems under investigation.

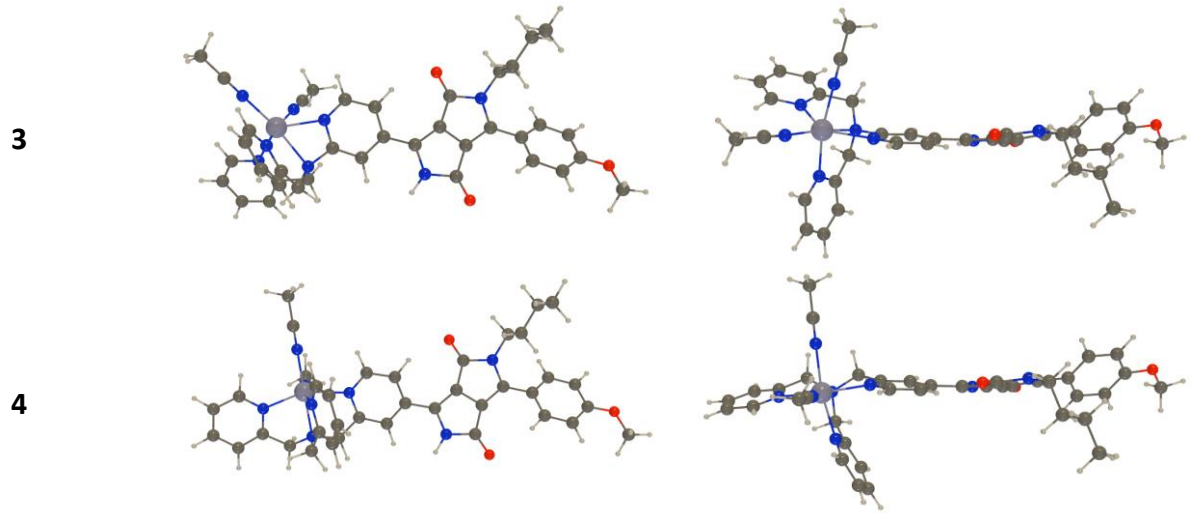

Fig. S71: Optimal geometries of the molecules **3**, **4** with a Zn^{++} ion complexed and explicit ACN molecules added to complete the coordination sphere of the cation. Side (left) and top (right) views.

Section S7: ^{1}H, ^{13}C and HRMS spectra

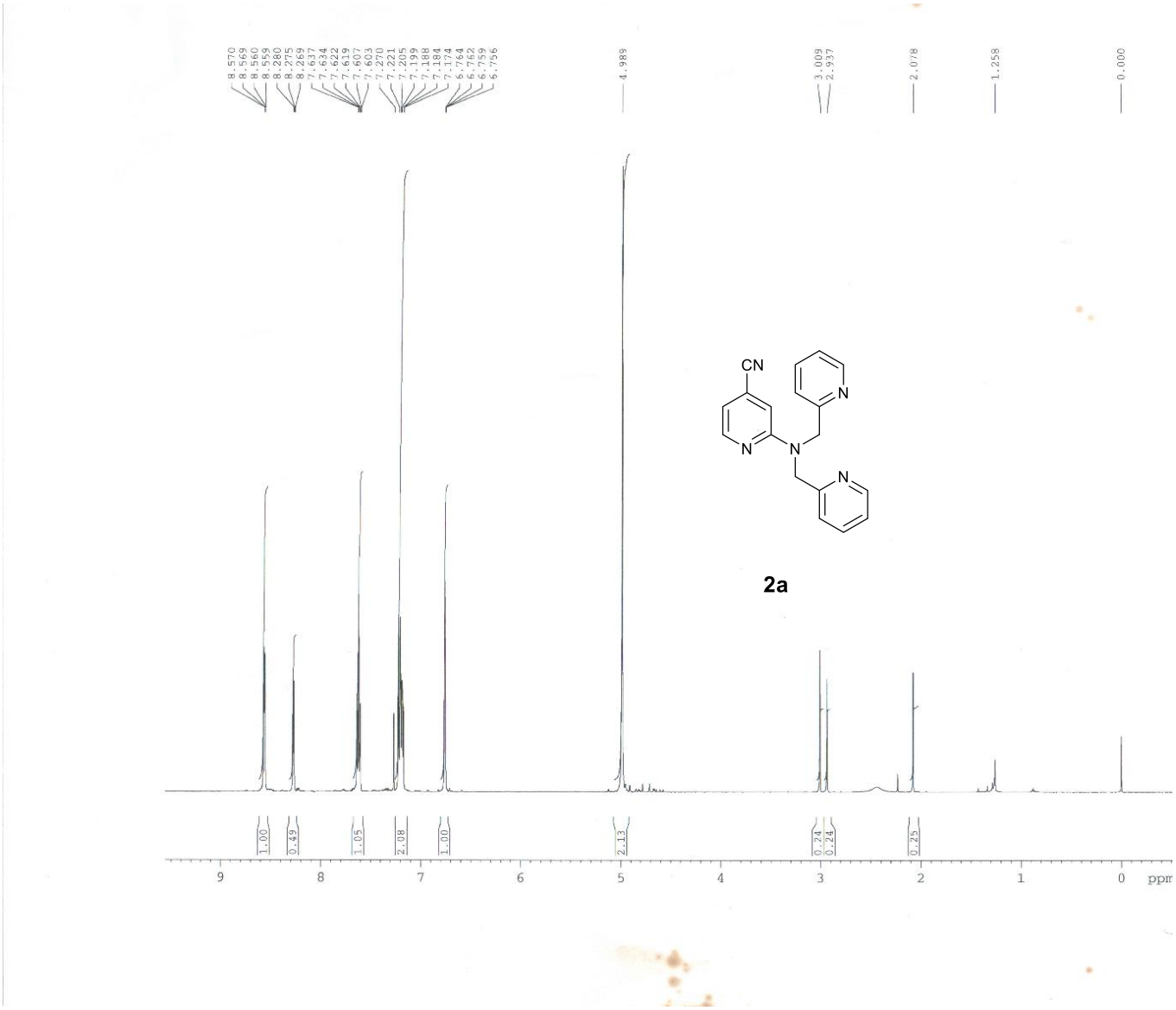

^{1}H-NMR spectra of **2a** in $CDCl_3$

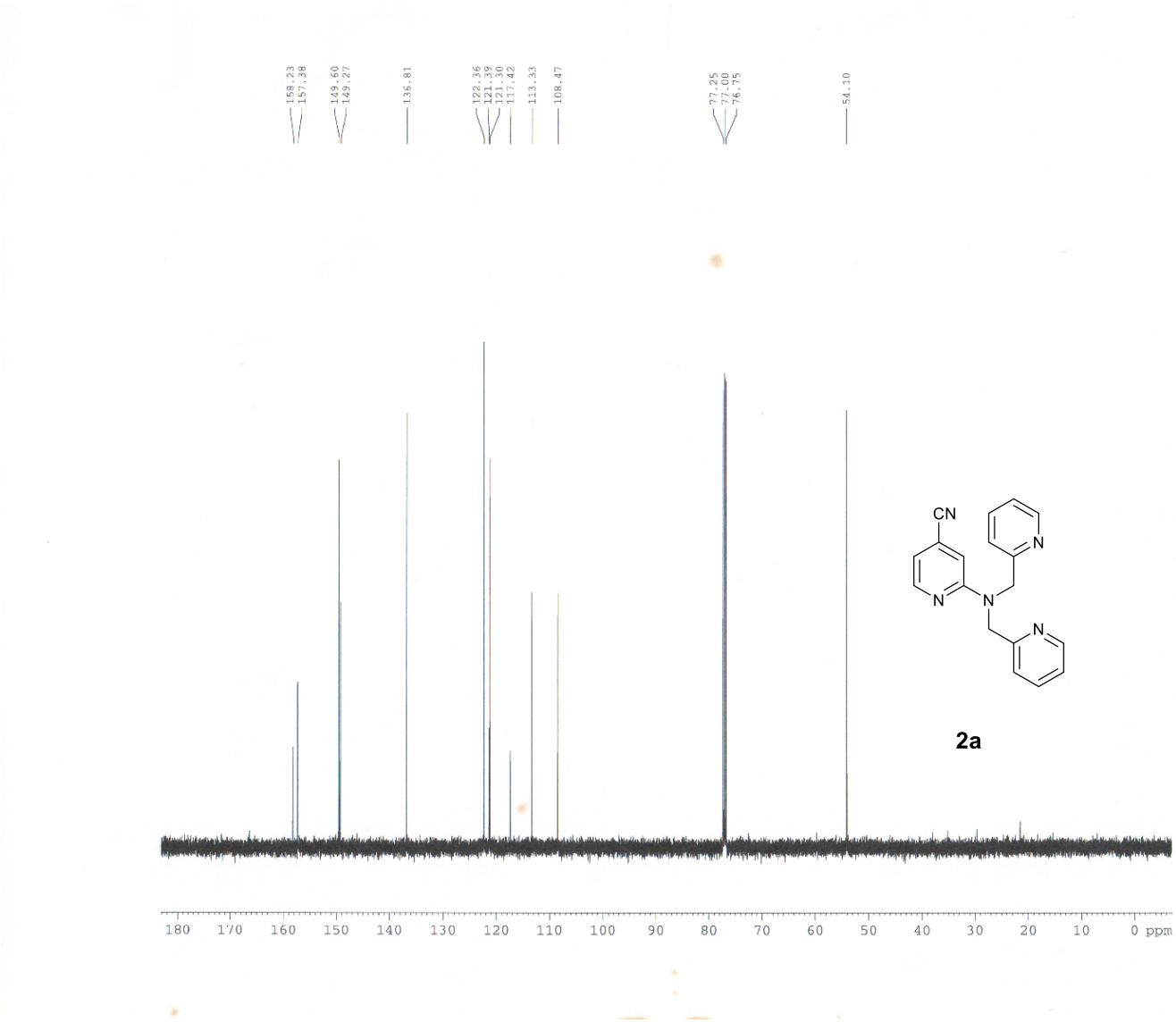

^{13}C-NMR spectra of **2a** in $CDCl_3$

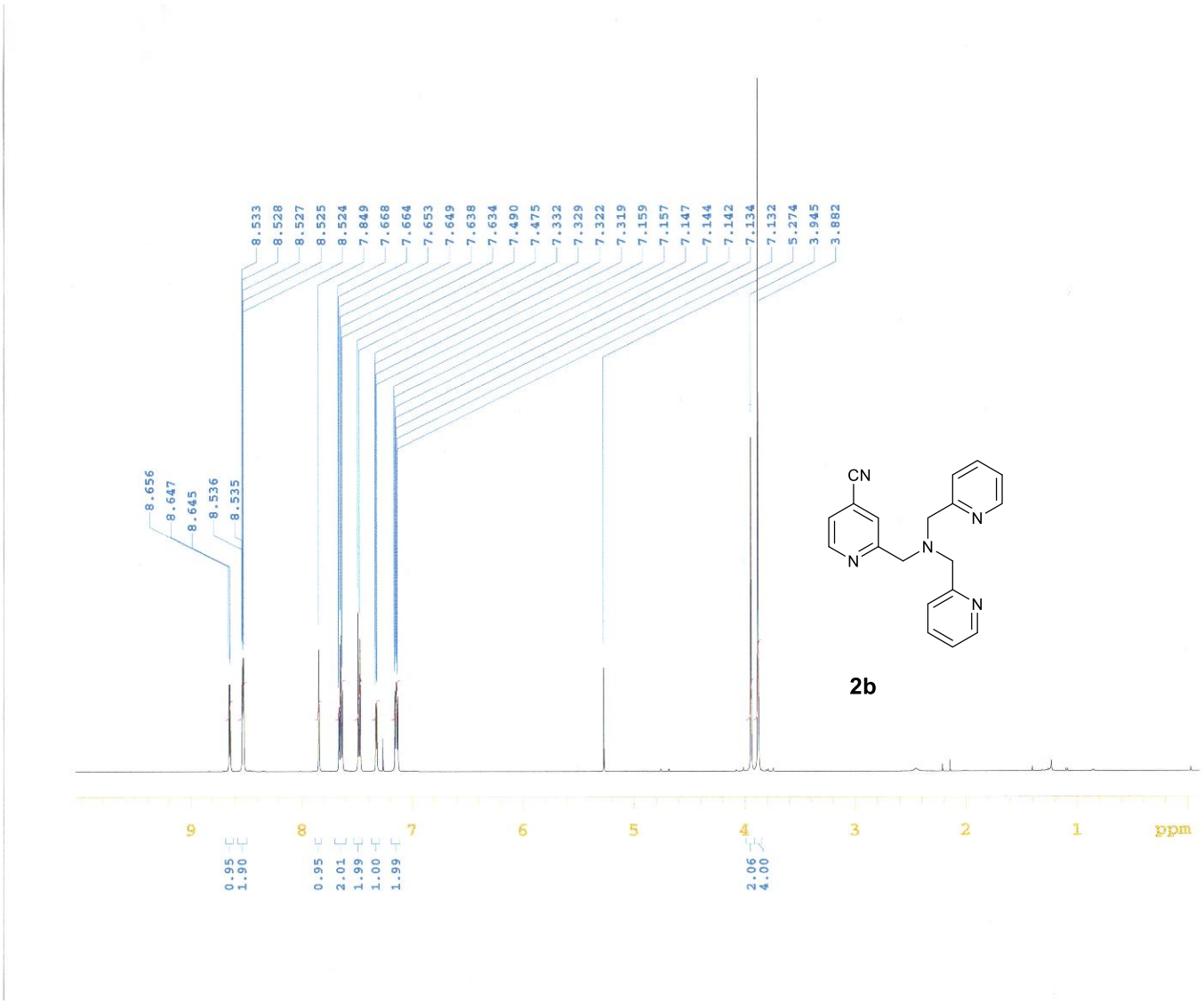

^{1}H-NMR spectra of **2b** in $CDCl_3$

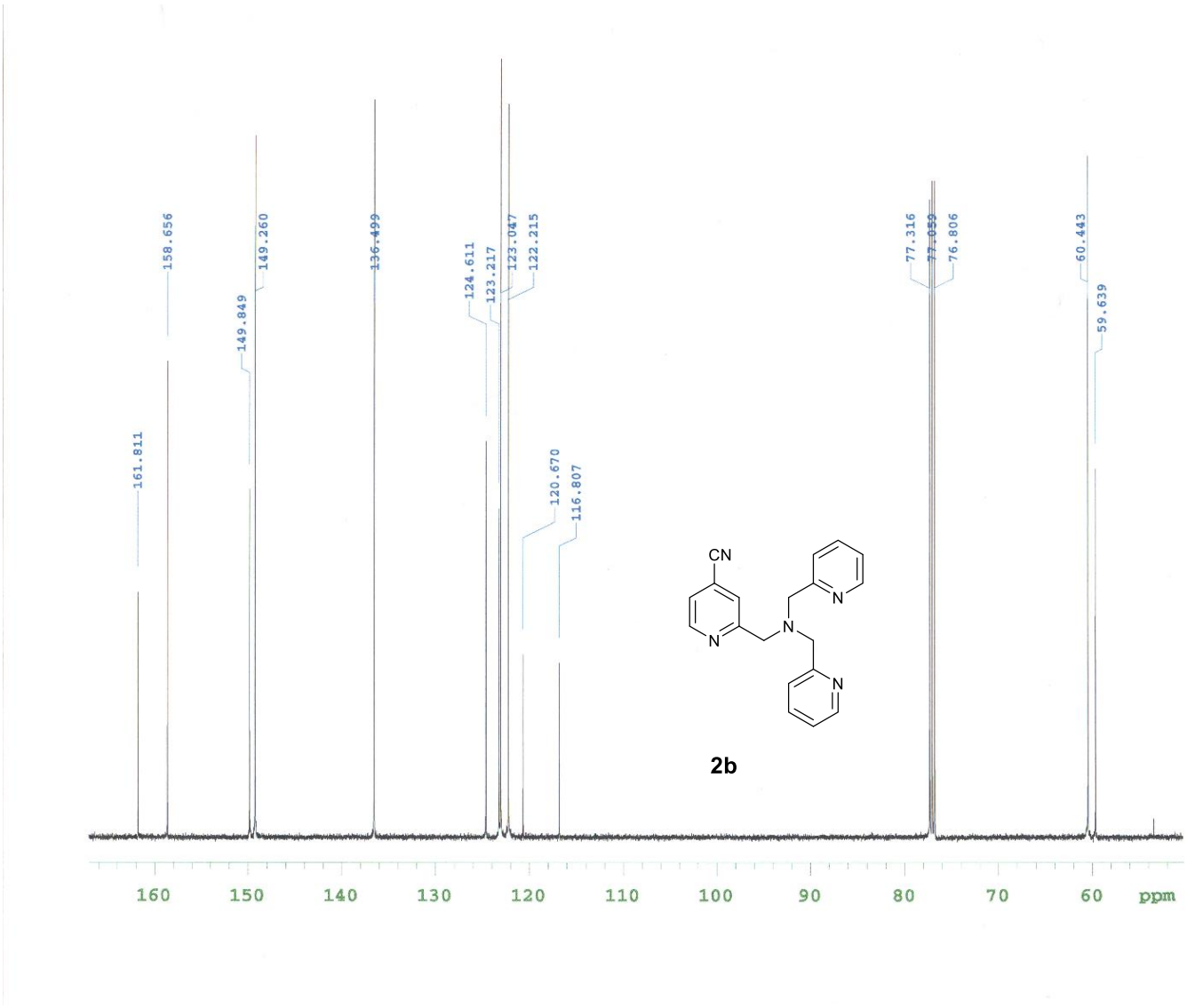

^{13}C-NMR spectra of **2b** in $CDCl_3$

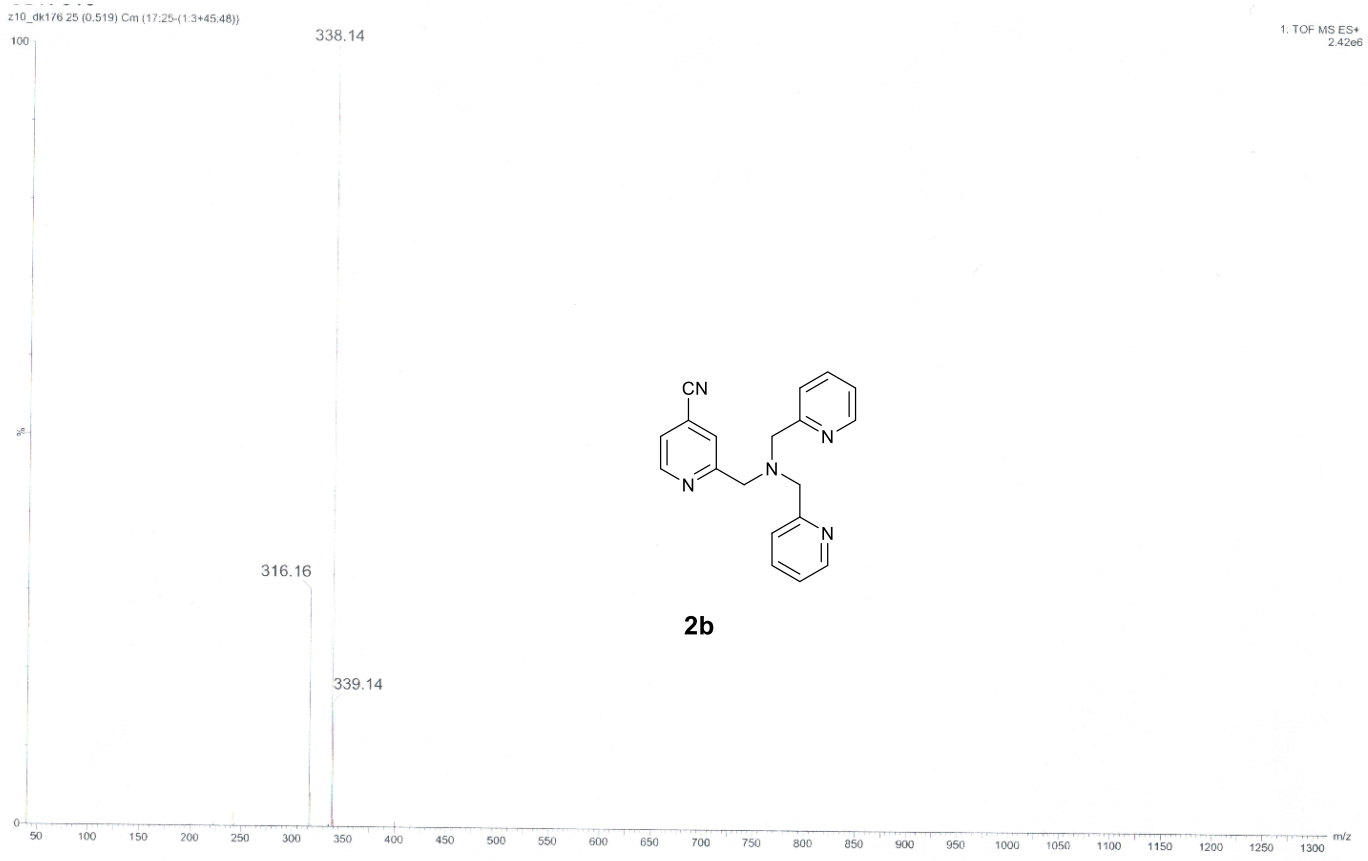

HRMS (ESI, m/z) spectra of **2b**

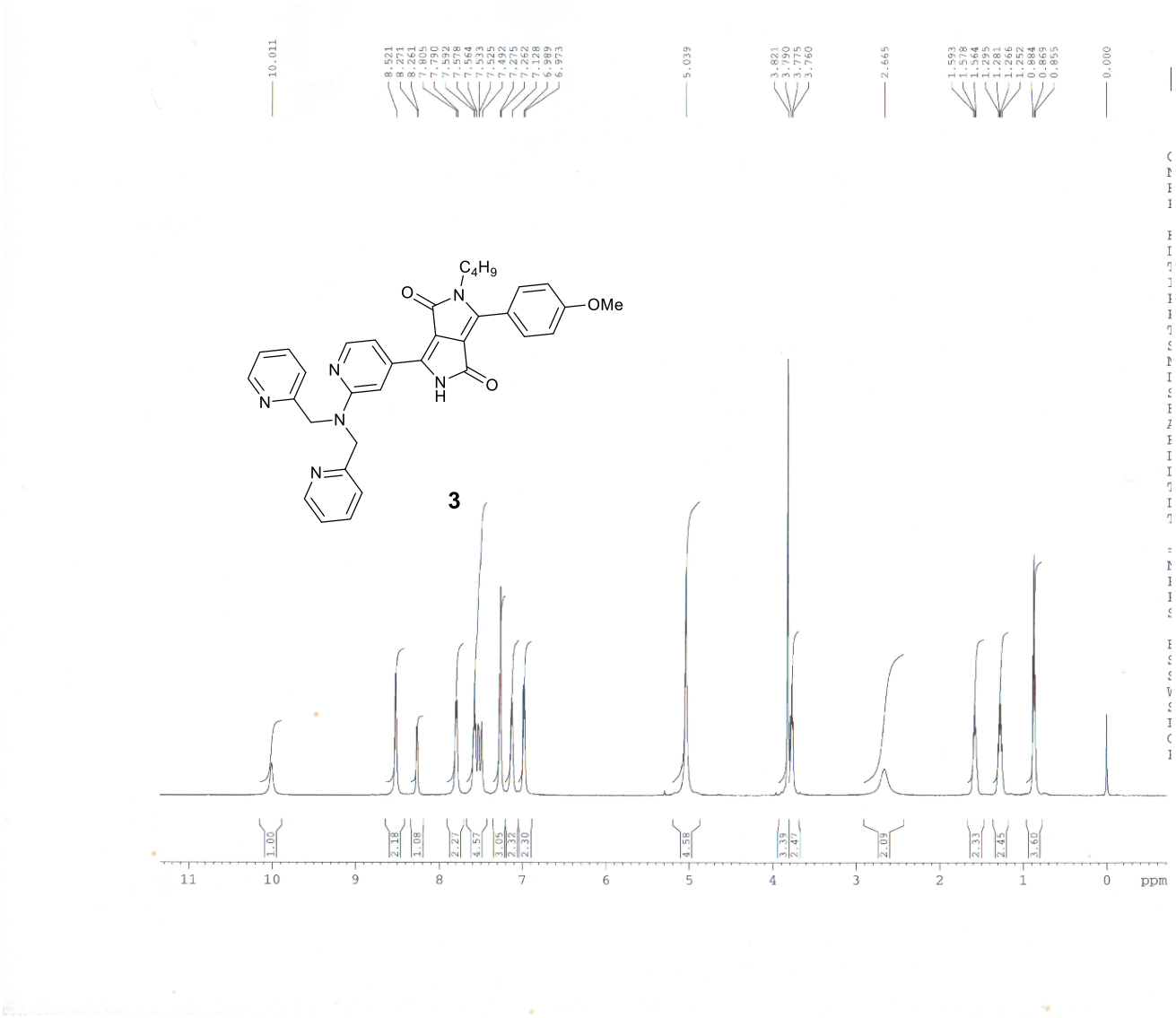

^{1}H-NMR spectra of **3** in $CDCl_3$

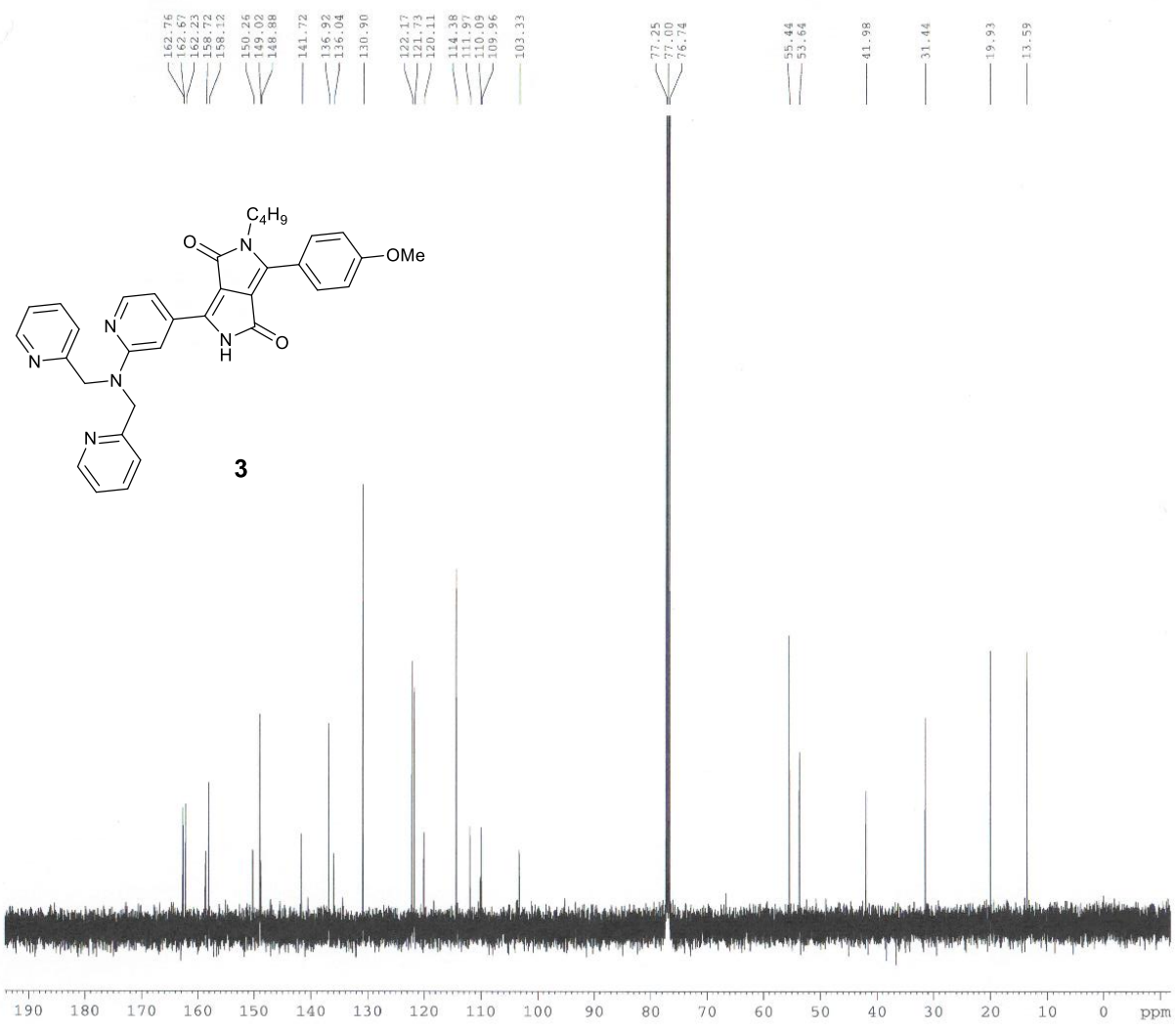

^{13}C-NMR spectra of **3** in $CDCl_3$

Elements Used:
C: 0-150 H: 0-150 N: 0-6 O: 0-3

Mass	Calc. Mass	mDa	PPM	DBE	Formula	i-FIT	i-FIT Norm	Fit Conf %	C	H	N	O
573.2628	573.2614	1.4	2.4	21.5	C34 H33 N6 O3	583.7	0.013	98.75	34	33	6	3
	573.2654	-2.6	-4.5	25.5	C39 H33 N4 O	588.1	4.384	1.25	39	33	4	1

HRMS (ESI, m/z) spectra of **3**

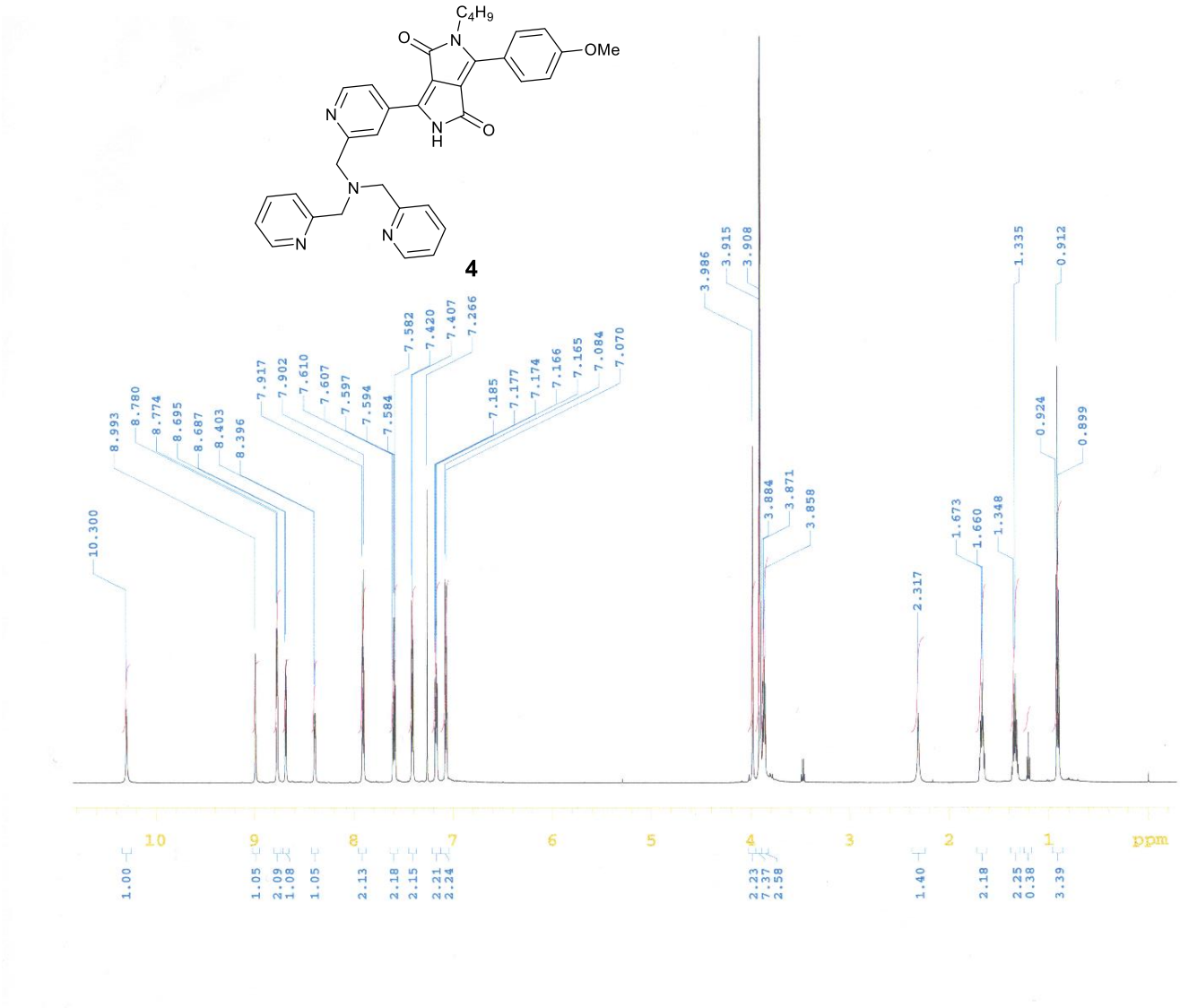

^{1}H-NMR spectra of **4** in $CDCl_3$

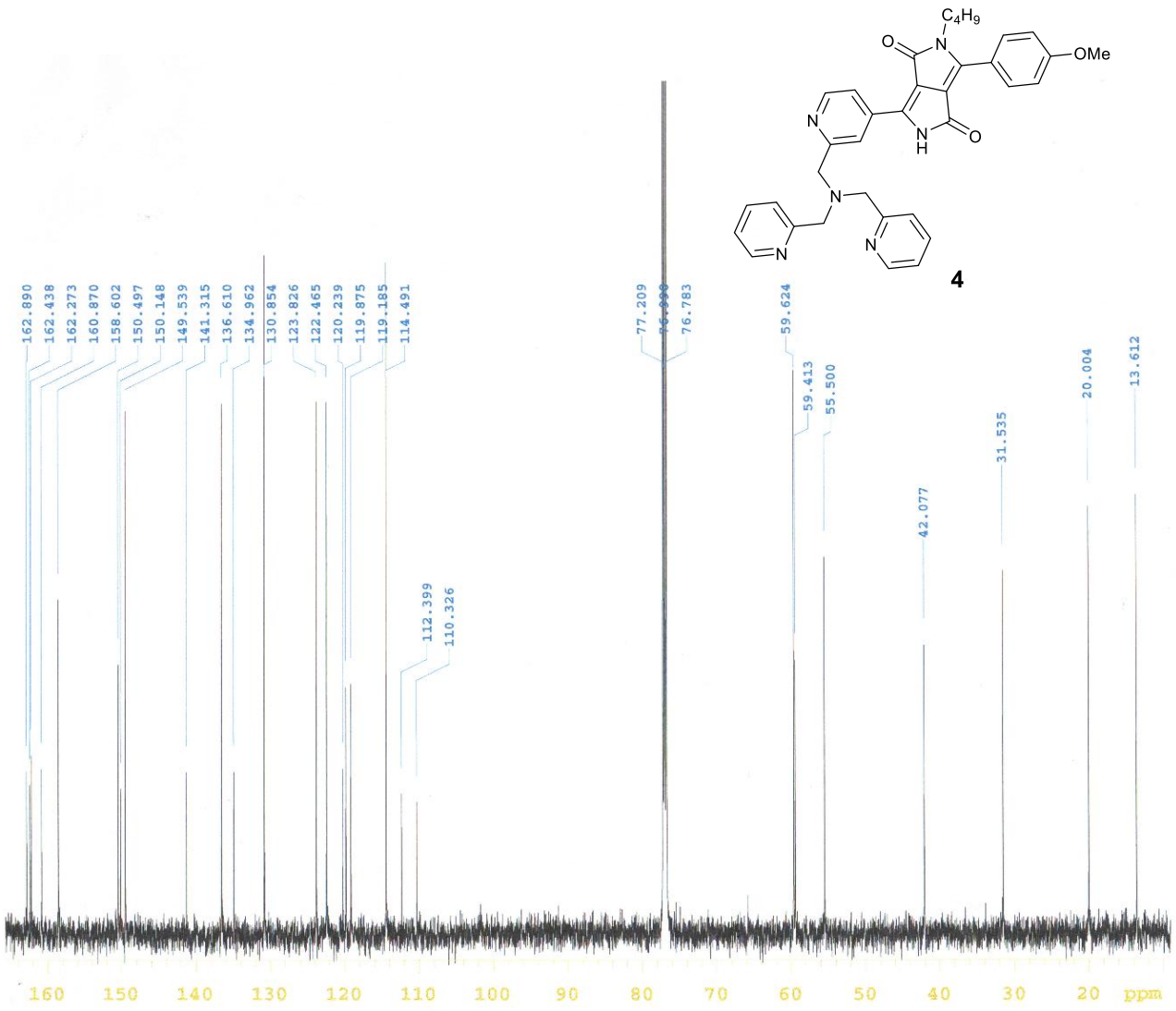

^{13}C-NMR spectra of **4** in $CDCl_3$

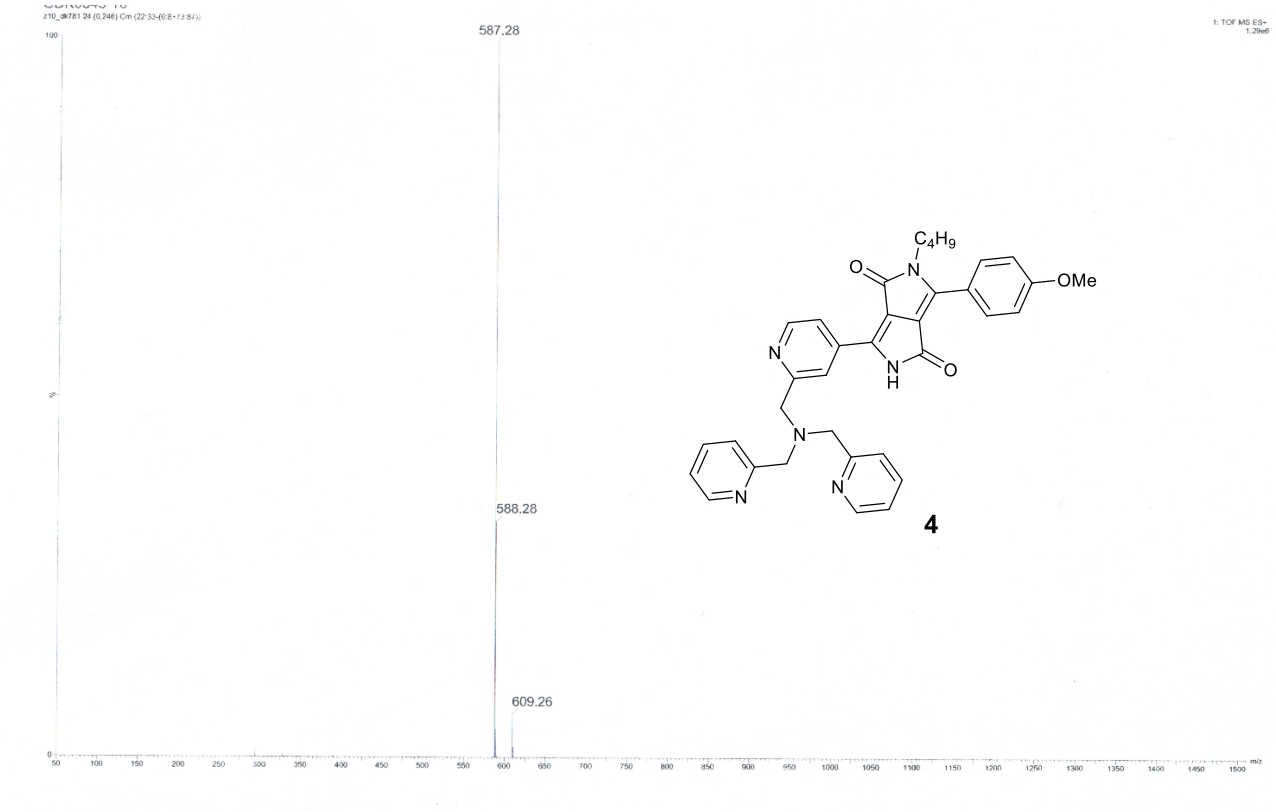

HRMS (ESI, m/z) spectra of **4**

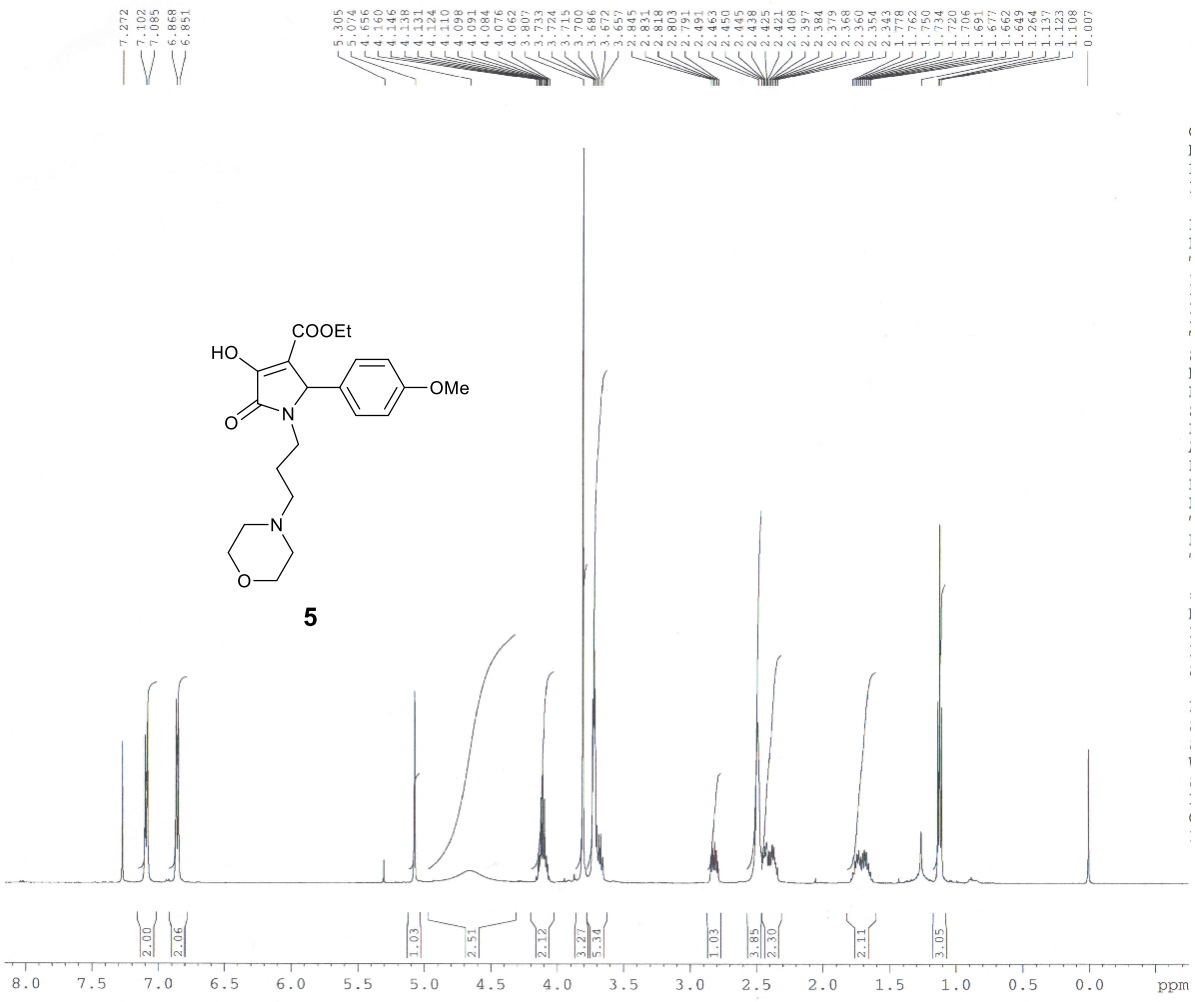

^{1}H-NMR spectra of **5** in $CDCl_3$

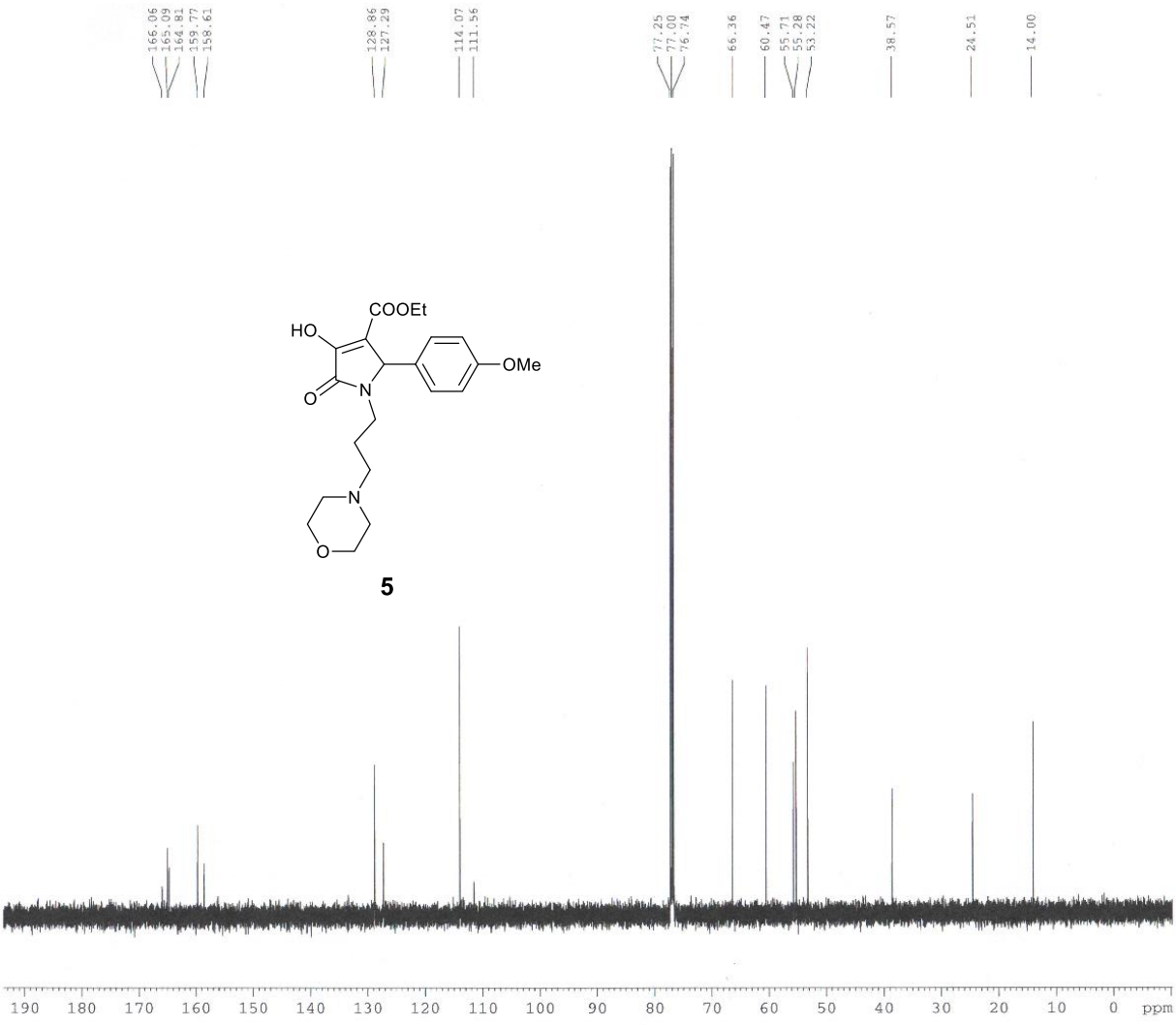

5

^{13}C-NMR spectra of **5** in $CDCl_3$

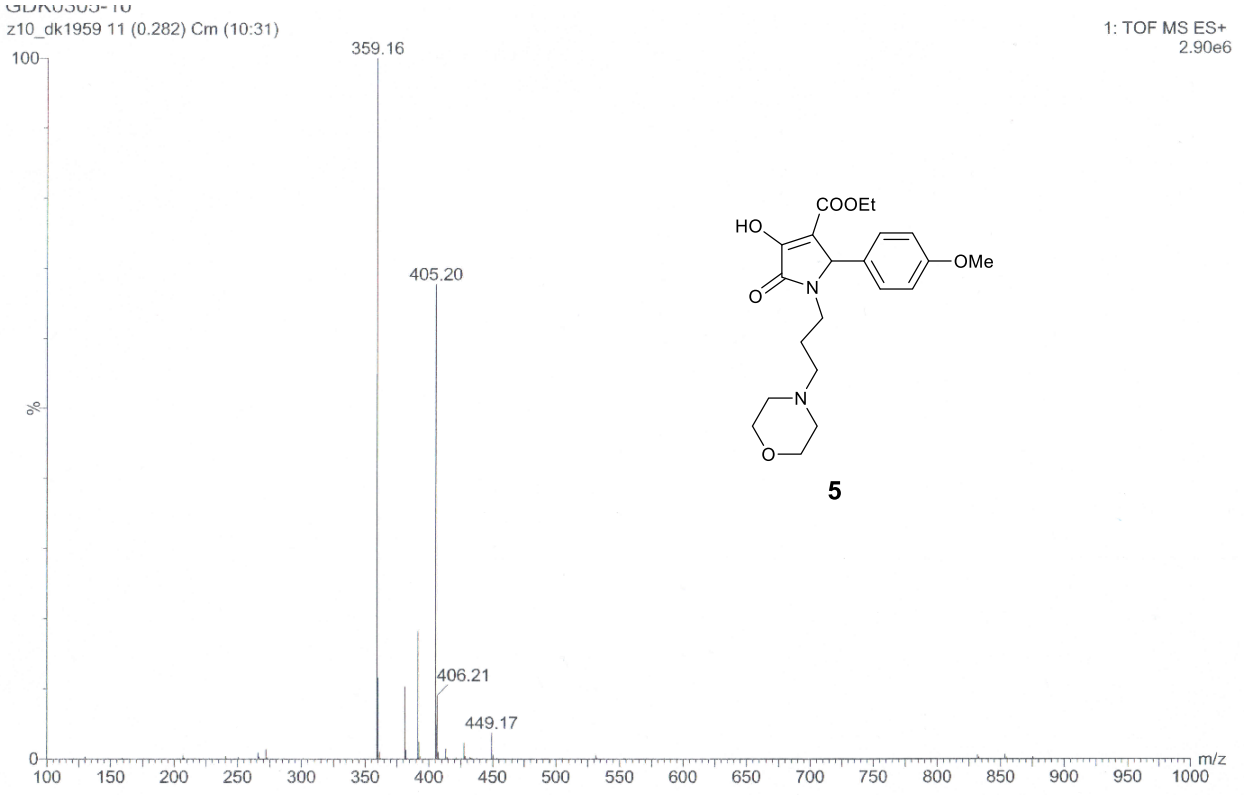

5

HRMS(ESI, m/z) spectra of **5**

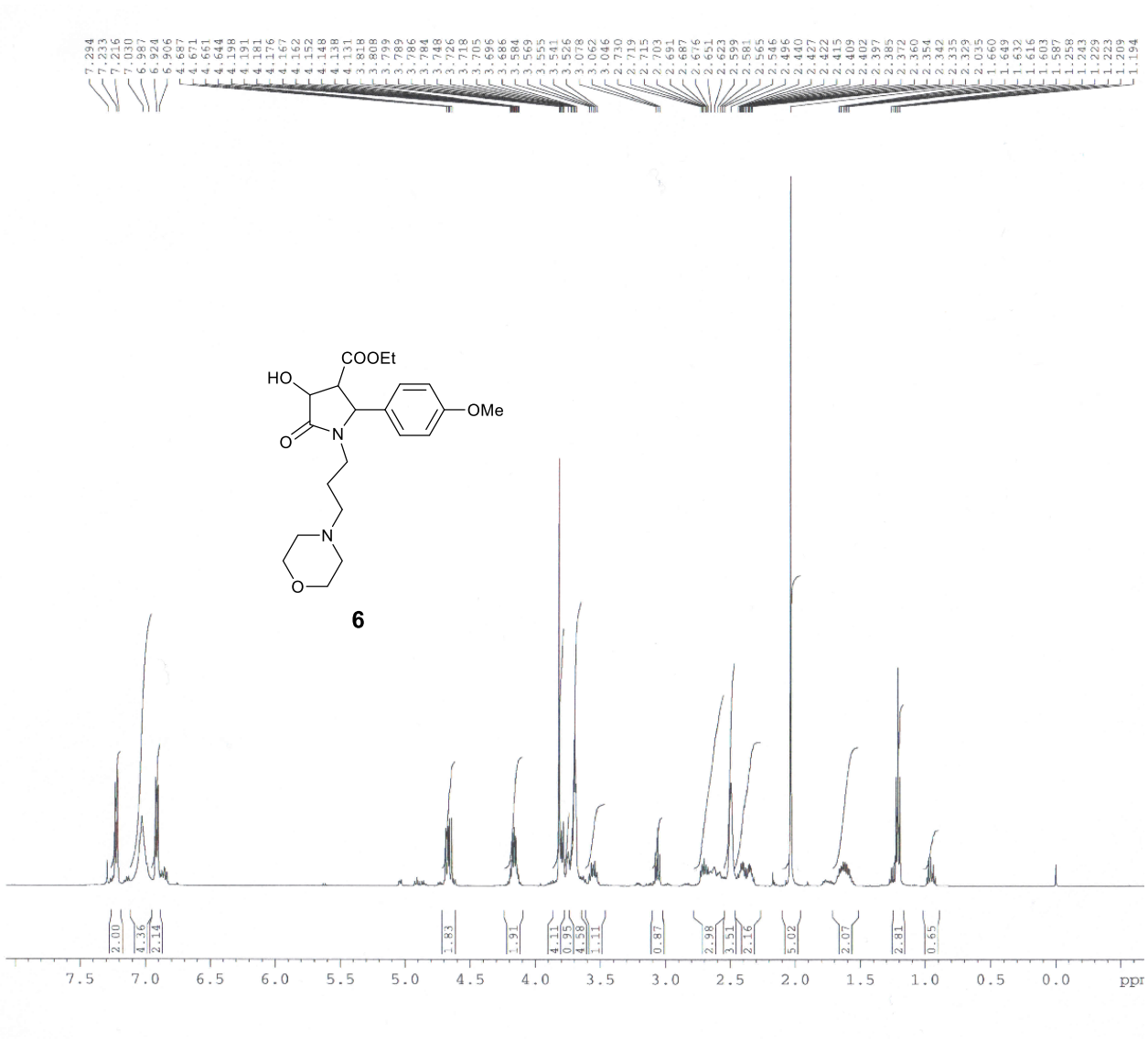

^{1}H-NMR spectra of **6** in $CDCl_3$

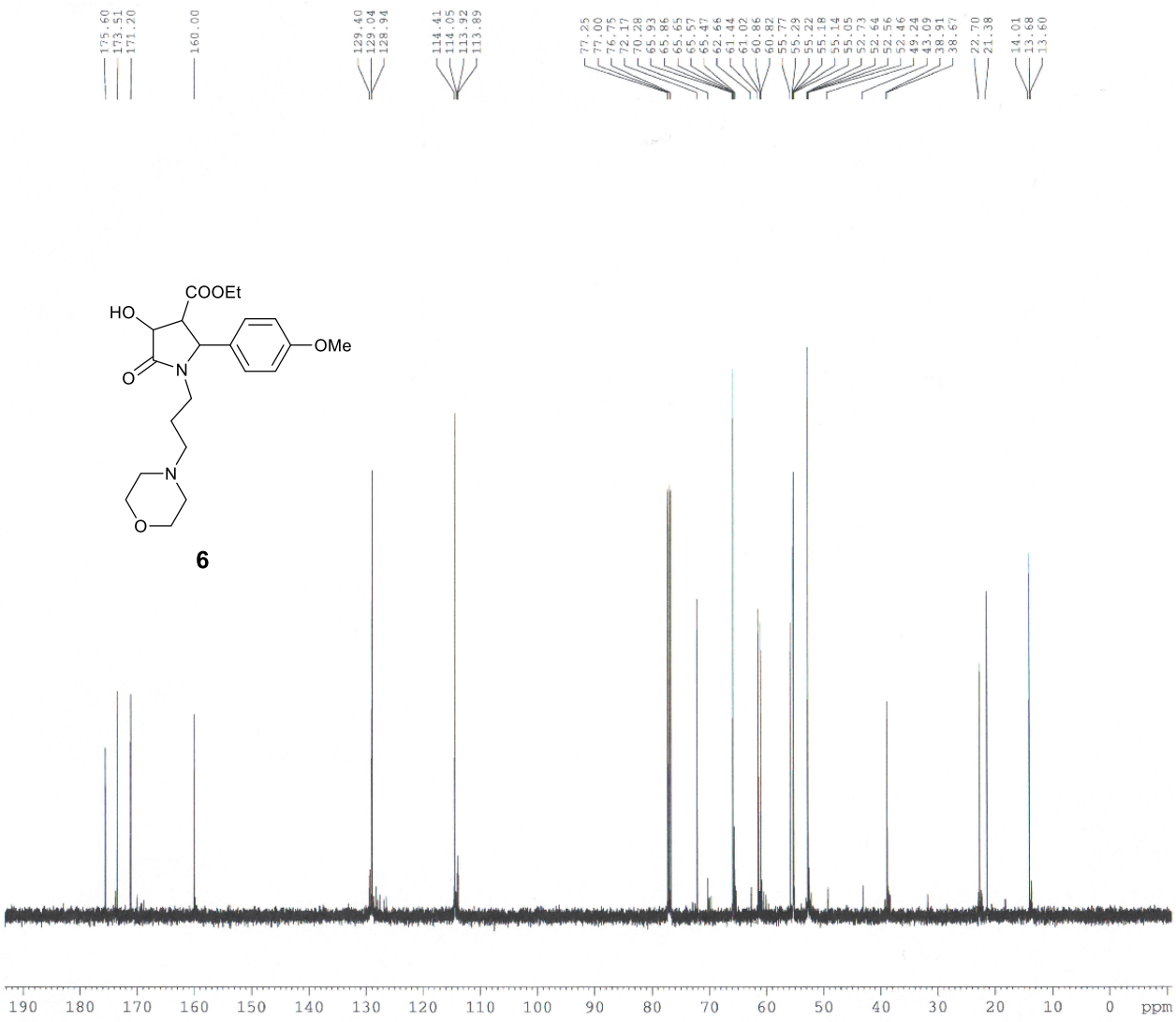

^{13}C-NMR spectra of **6** in $CDCl_3$

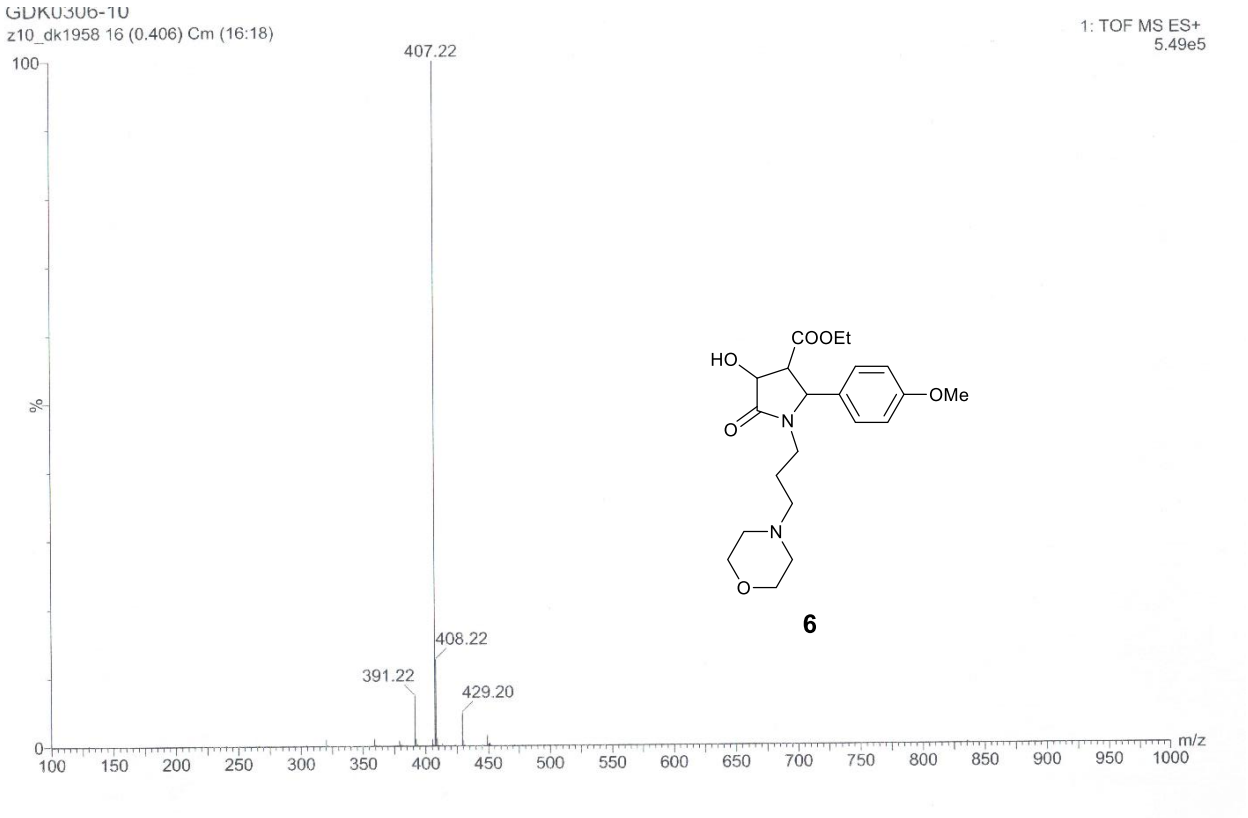

HRMS (ESI, m/z) spectra of **6**

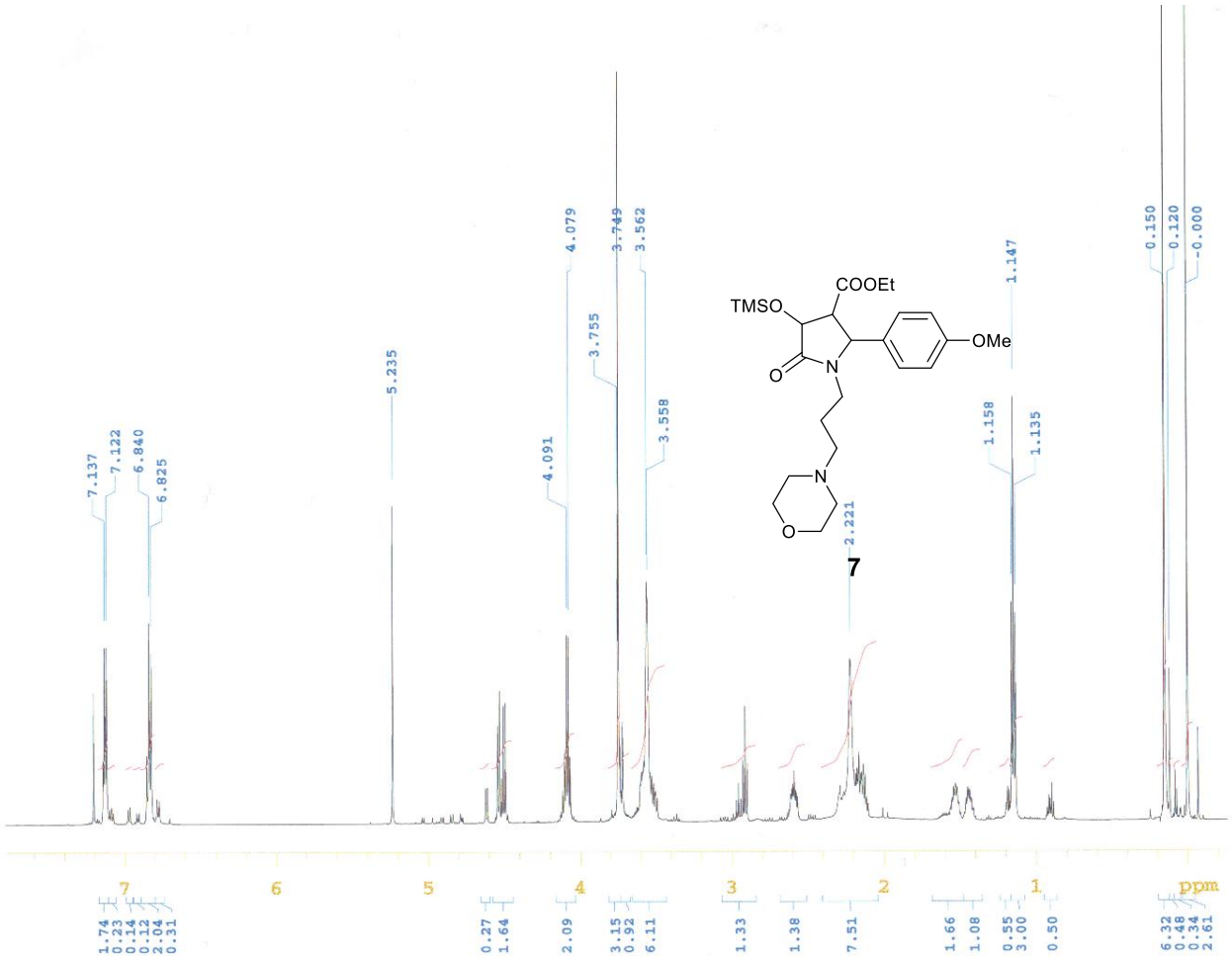

^{1}H-NMR spectra of **7** in $CDCl_3$

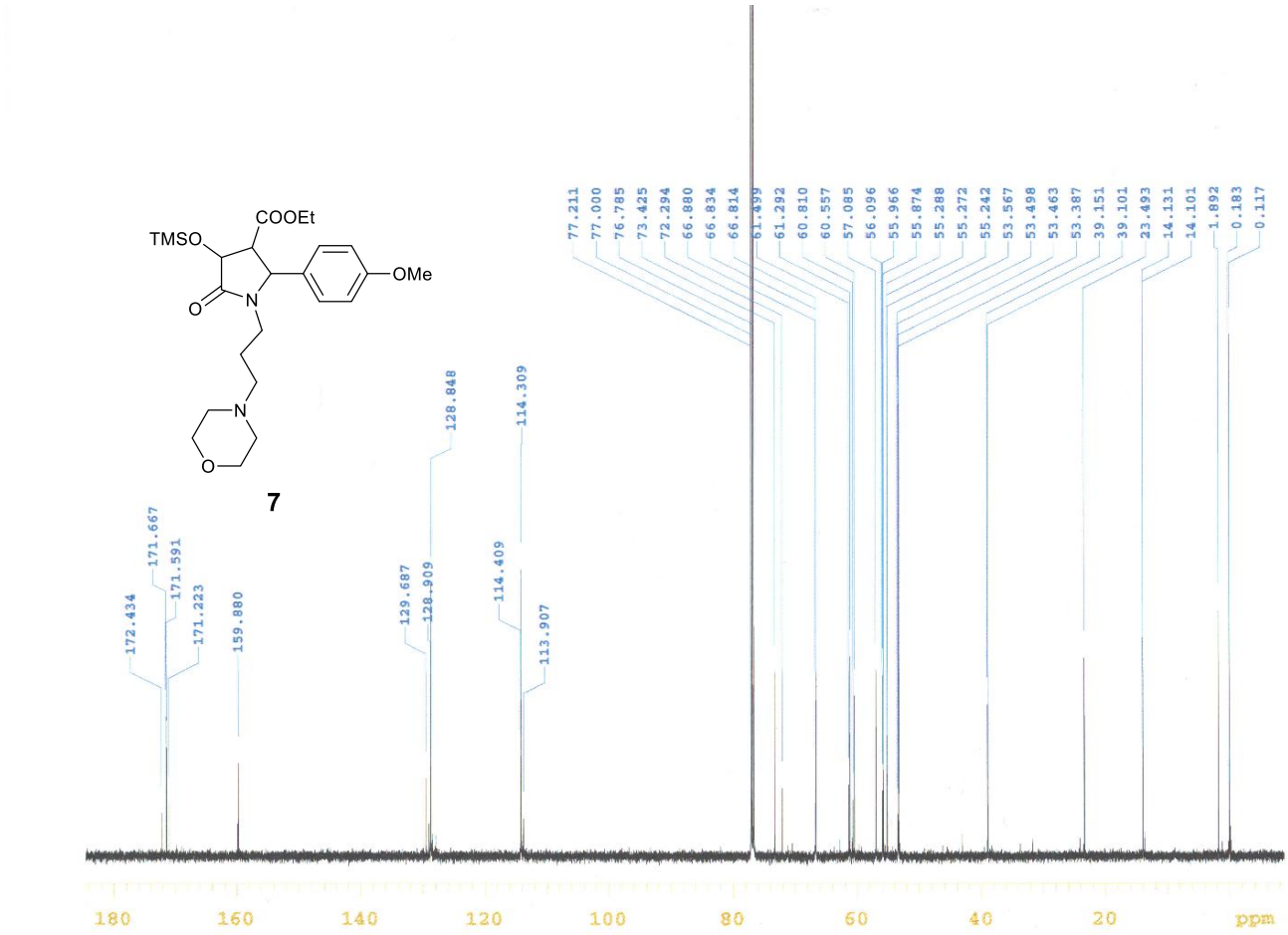

^{13}C-NMR spectra of **7** in $CDCl_3$

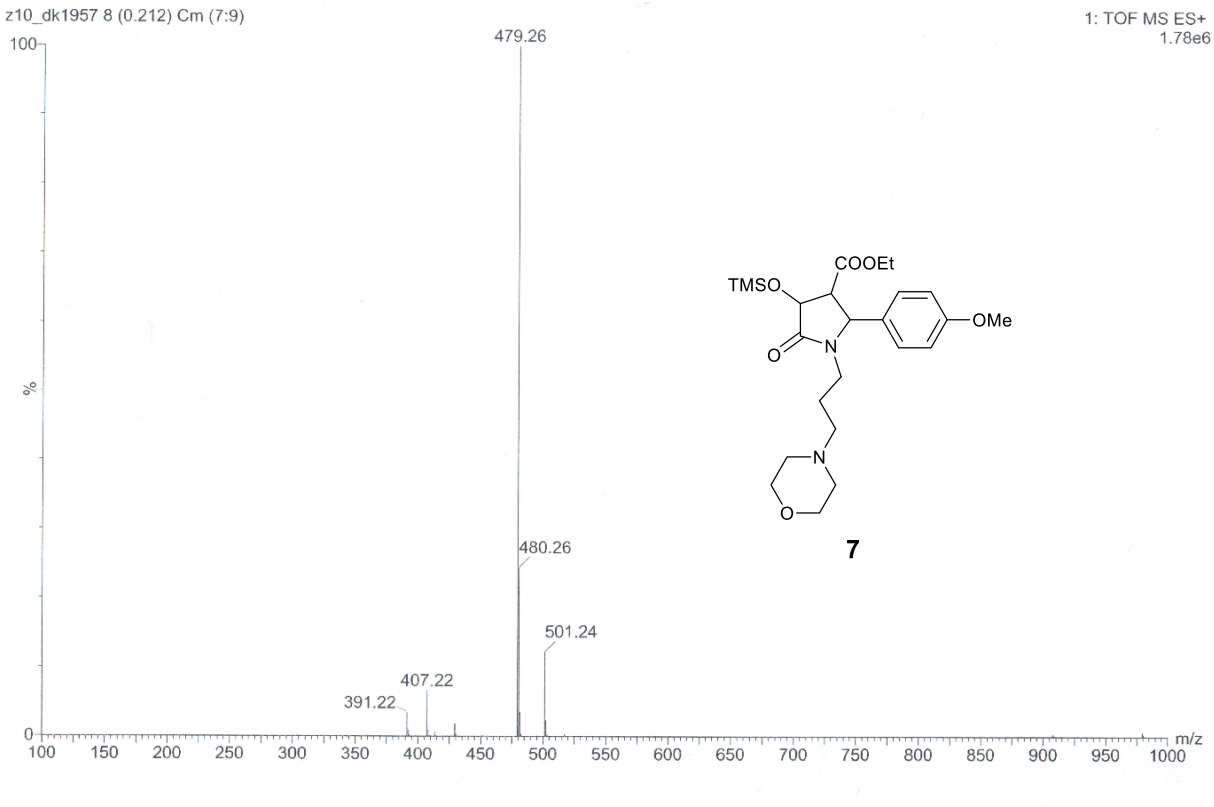

7

HRMS (ESI, m/z) spectra of **7**

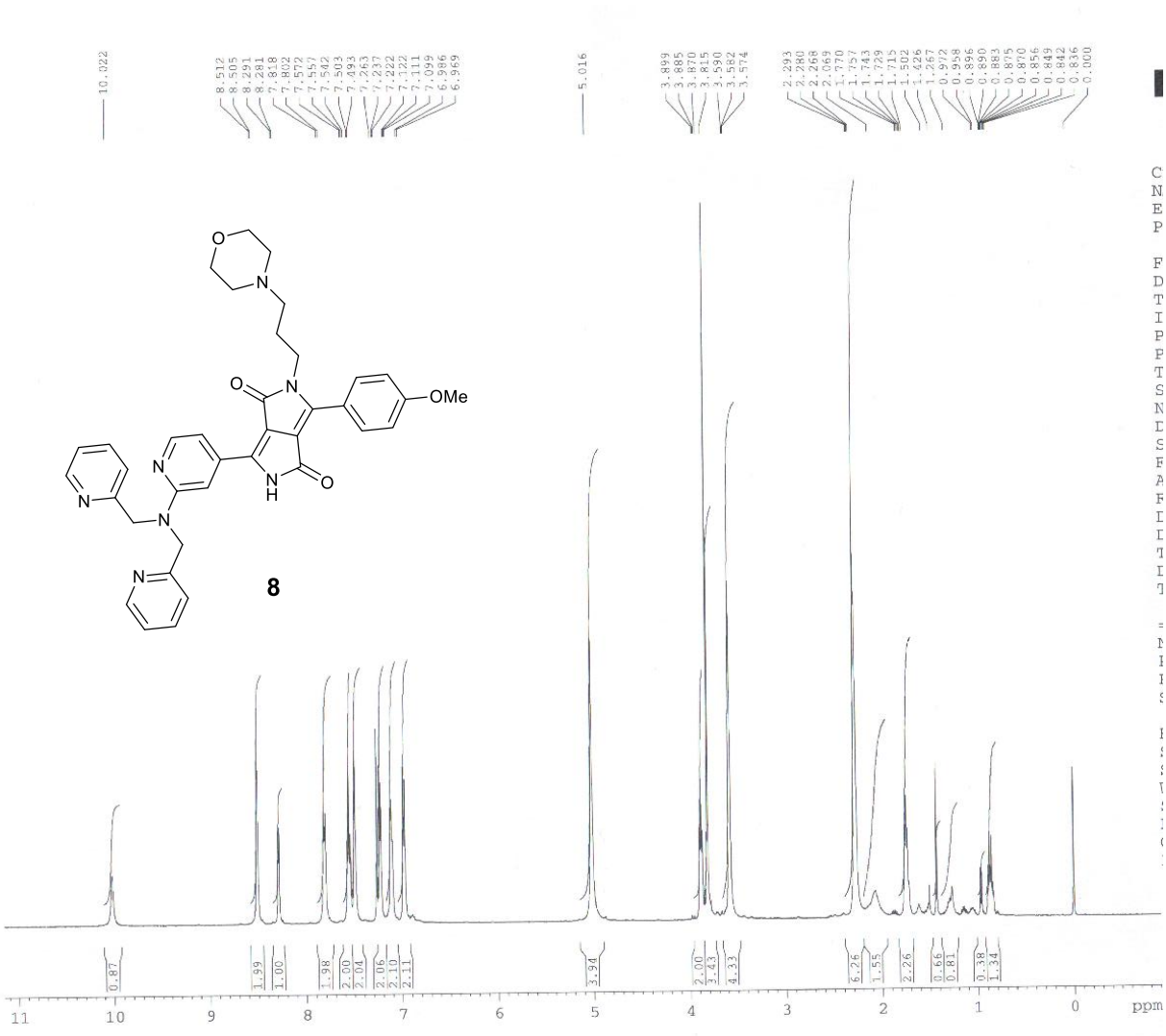

^{1}H-NMR spectra of **8** in $CDCl_3$

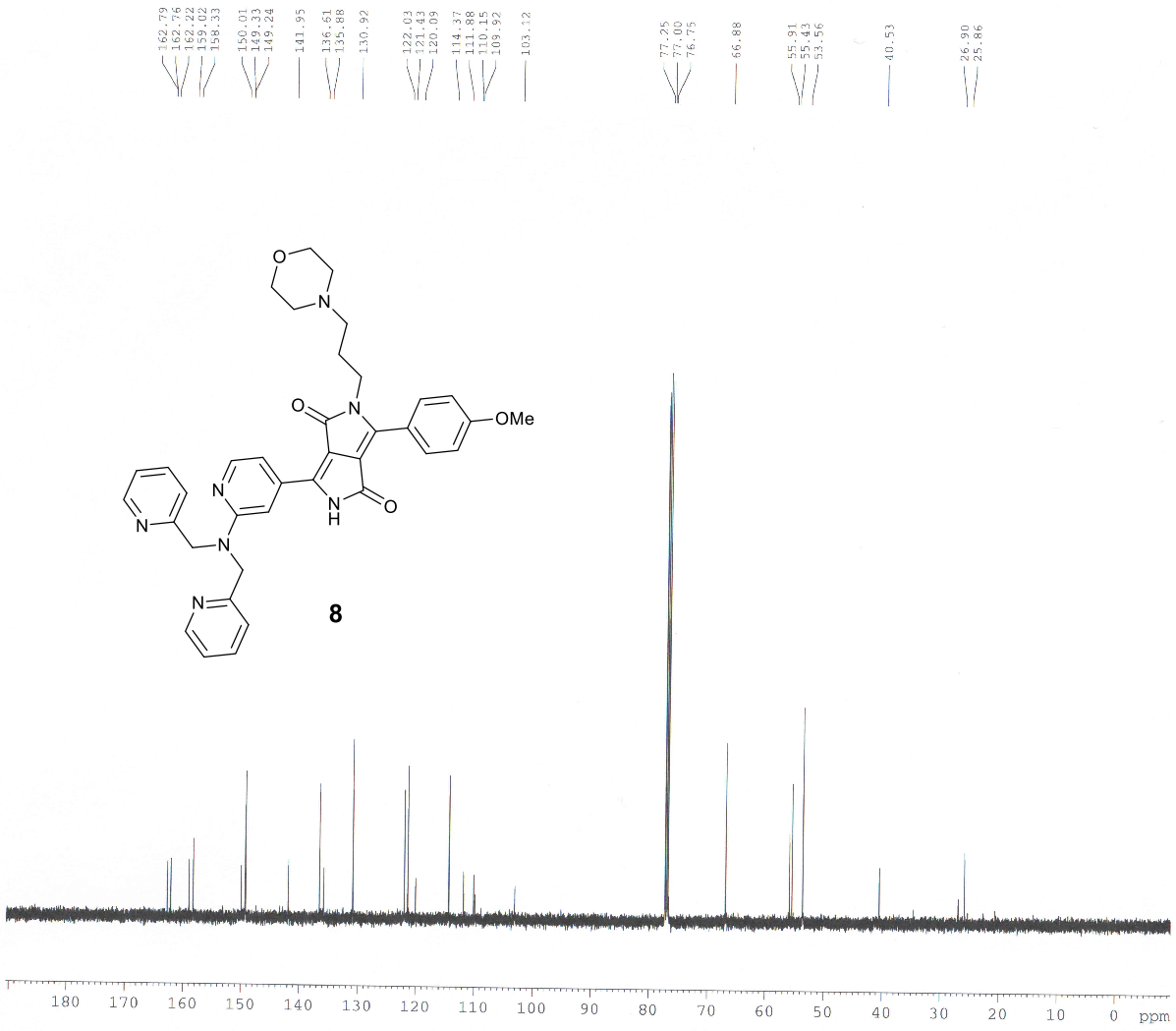

^{13}C-NMR spectra of **8** in $CDCl_3$

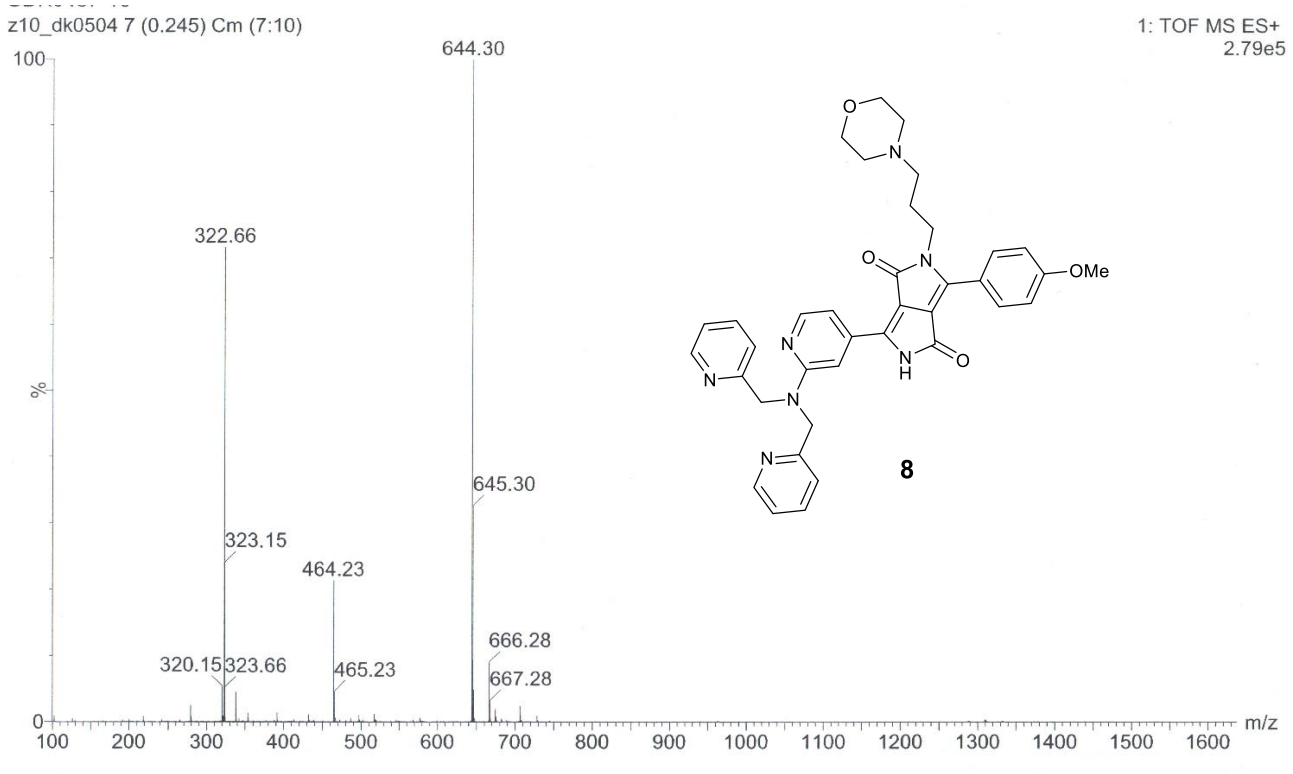

HRMS (ESI, m/z) spectra of **8**

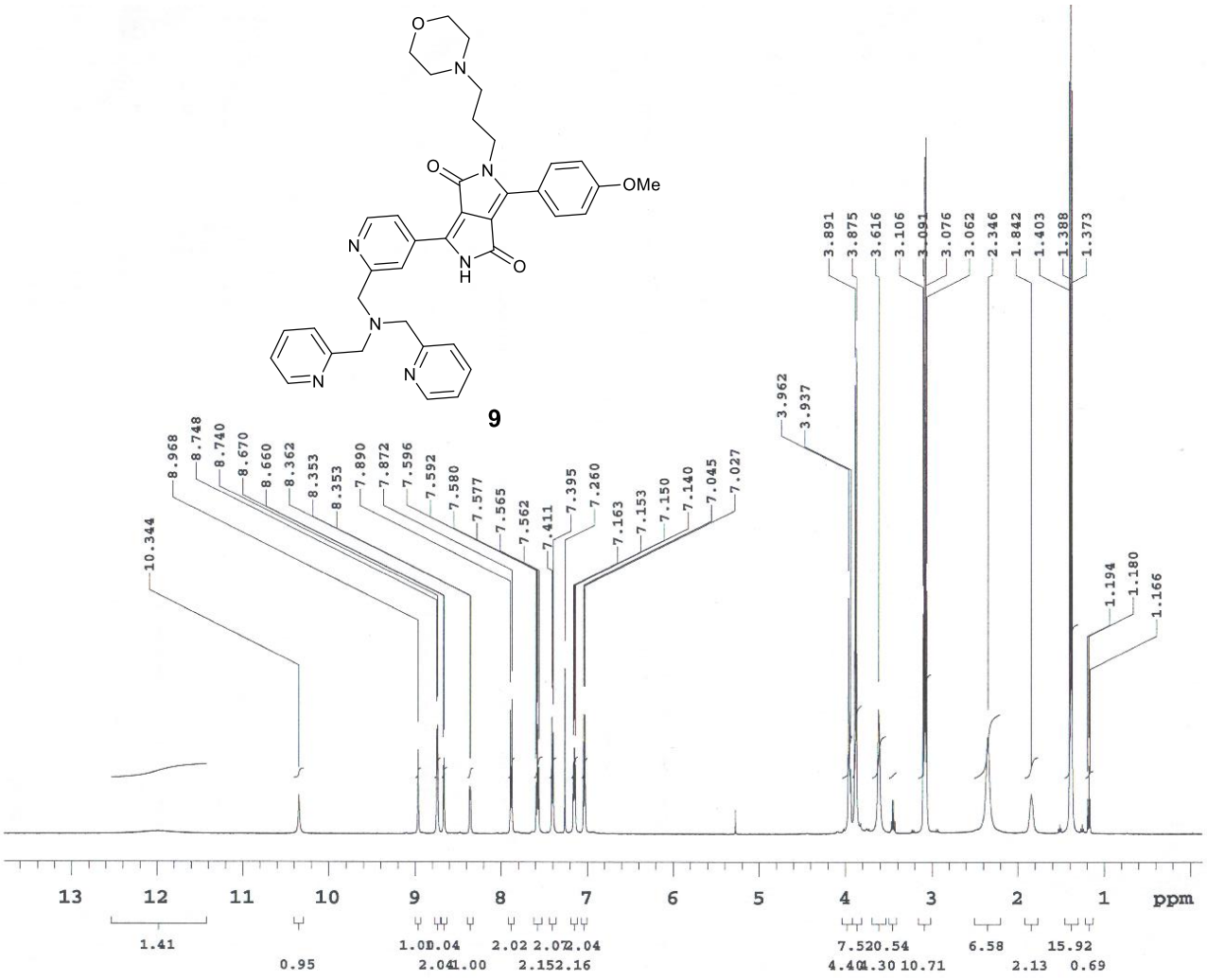

^{1}H-NMR spectra of **9** in $CDCl_3$

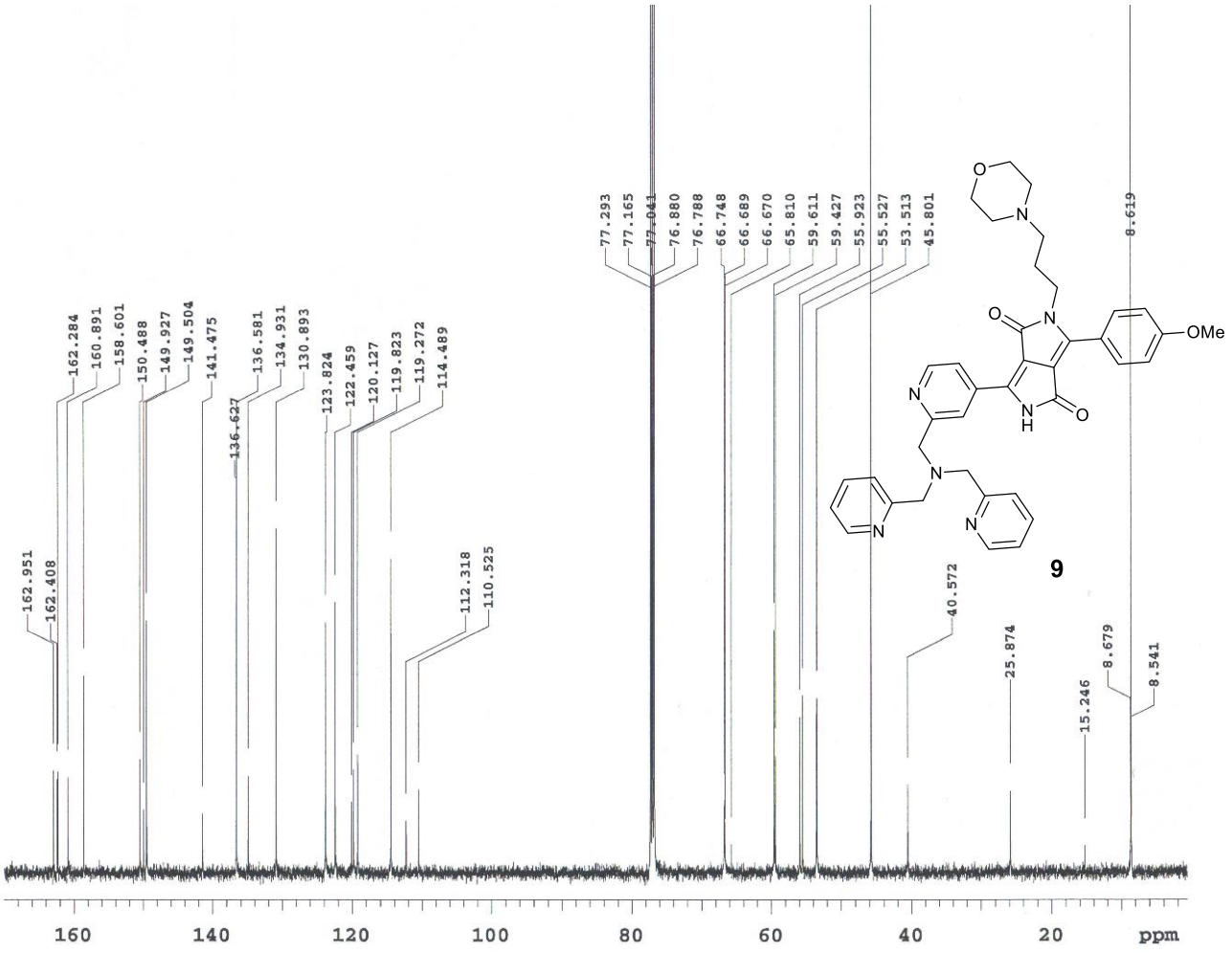

^{13}C-NMR spectra of **9** in $CDCl_3$

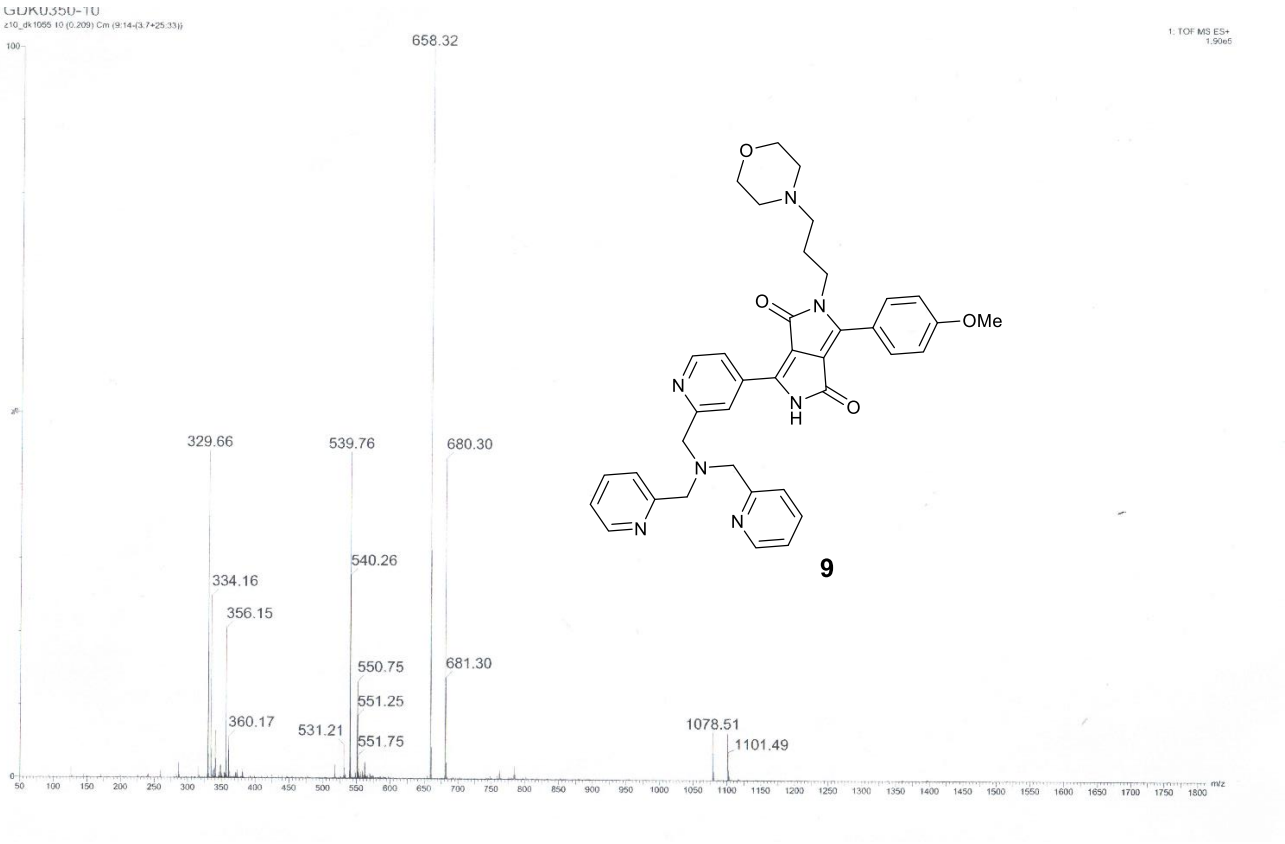

HRMS (ESI, m/z) spectra of **9**

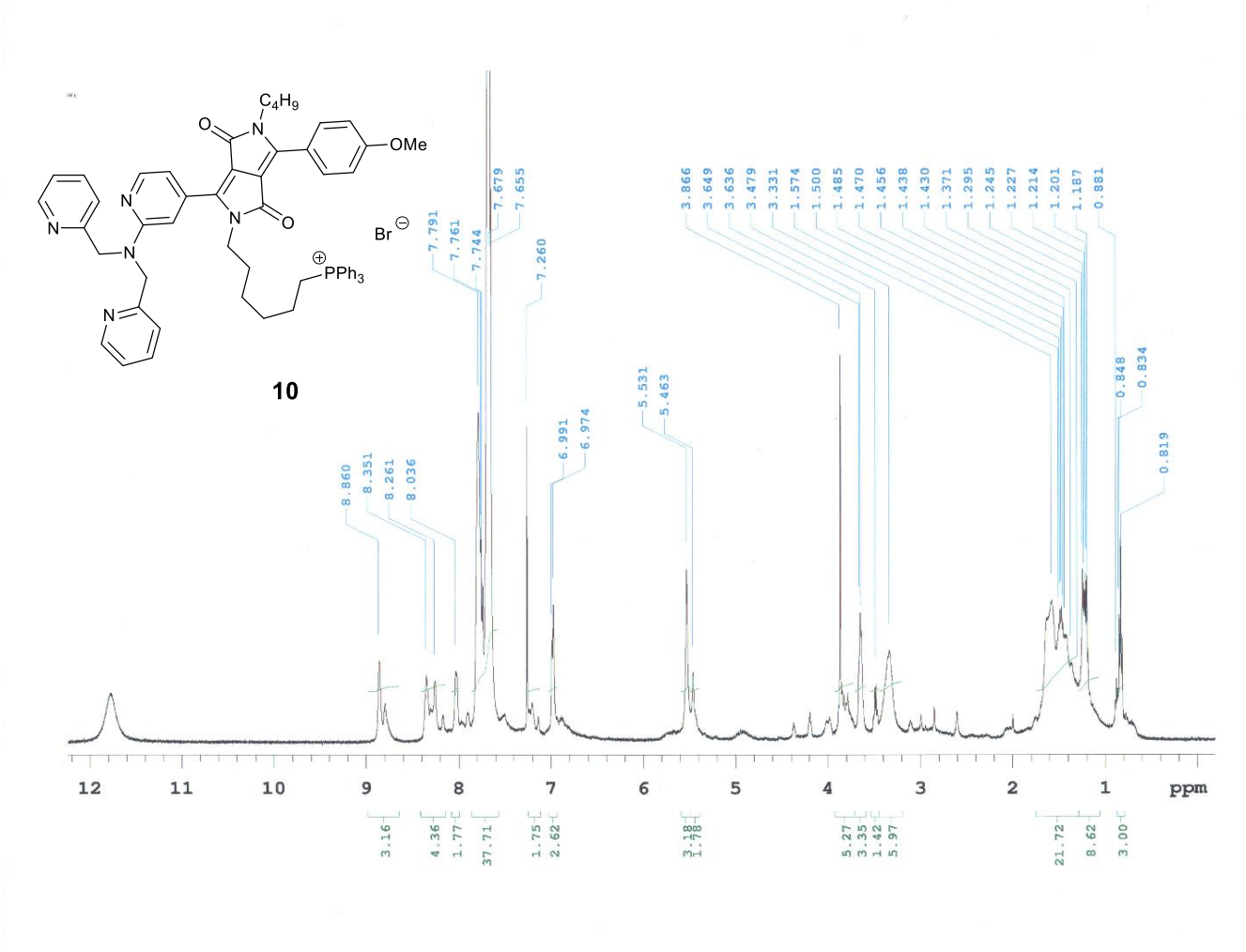

^{1}H-NMR spectra of **10** in $CDCl_3$

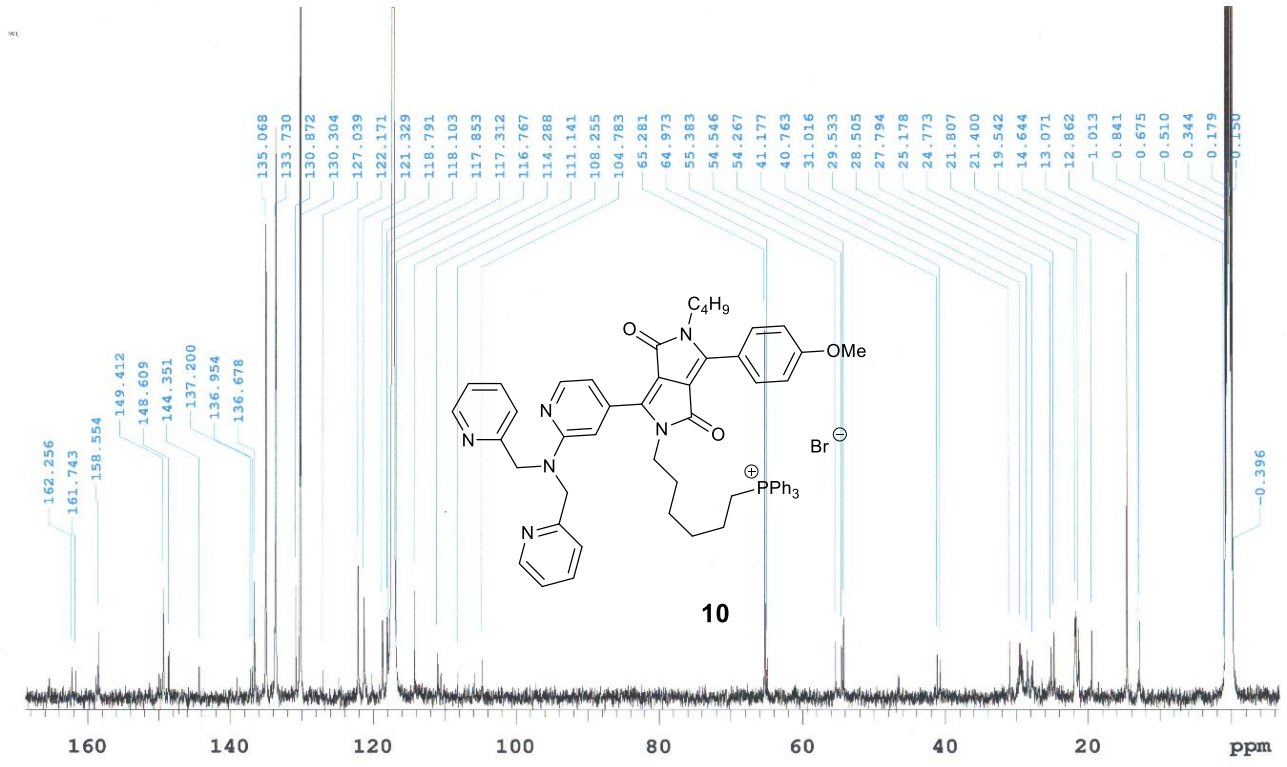

^{13}C-NMR spectra of **10** in $CDCl_3$

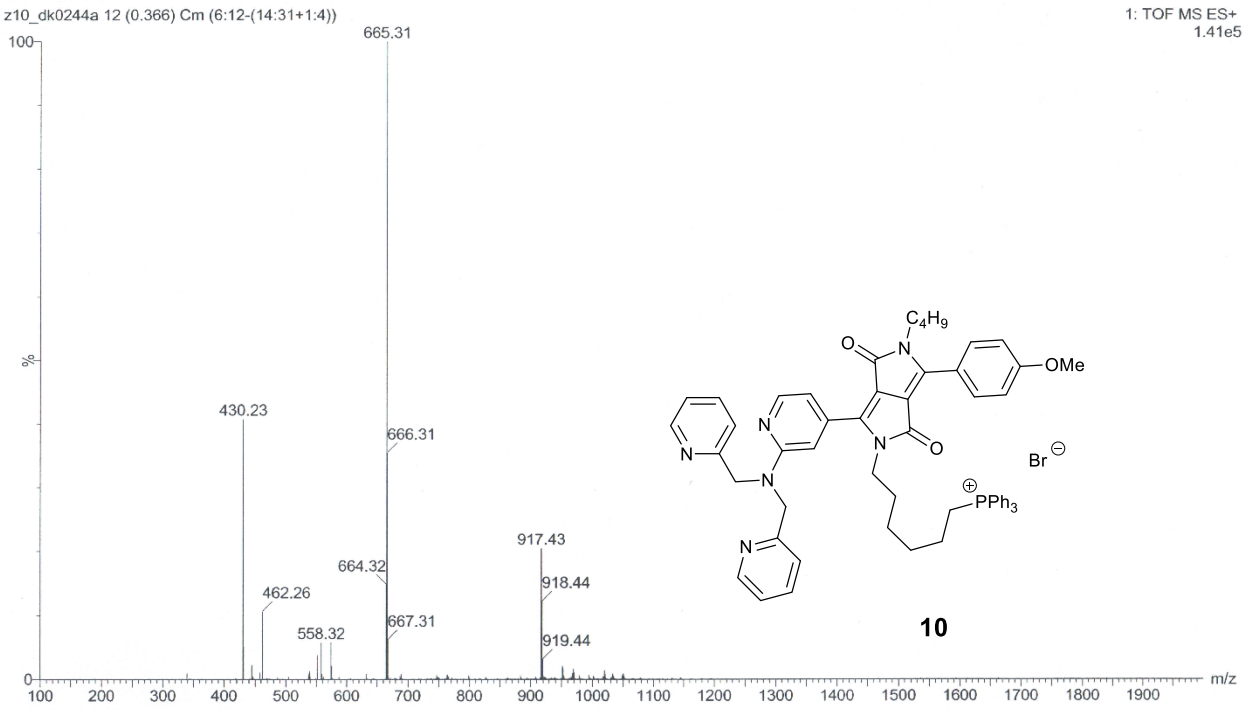

HRMS (ESI, m/z) spectra of **10**

Section S8: References

1. M. Pieczykolan, B. Sadowski and D. T. Gryko, *Angew. Chem. Int. Ed*., 2020, **59**, 7528-7535.

7. Declarations of the authors of publications

Instytut Chemii Organicznej
Polskiej Akademii Nauk

mgr Dinesh Kumar Ganga Reddy
+48 739-696-439
kdinesh@icho.edu.pl

Instytut Chemii Organicznej, PAN
ul. Kasprzaka 44/52
01-224 Warszawa
Polska

Warszawa, 30.11.2022r.

I declare that my contribution to the following publications consisted of:

- G. Dinesh Kumar, M. Banasiewicz, D. Jacquemin, D. T. Gryko, *Chem. Asian J.* **2021**, *16*, 355–362. *„Switch-on Diketopyrrolopyrrole-Based Chemosensors for Cations Possessing Lewis Acid Character".*

  Co-development of research concepts and interpretation of results. I developed and carried out the synthesis of nitrile substrates 2a-2h and transformed into final compounds 3-10 under developed conditions, which I subjected to a full chemical analysis. I participated in analyzing the photophysical properties and preparation of the manuscript.

- G. Dinesh Kumar, M. Banasiewicz, A. Wrzosek, R. P. Kampa, M. H. E. Bousquet, D. Kusy, D. Jacquemin, A. Szewczyk, D. T. Gryko, *Chem. Commun.*, **2022**, *58*, 4500–4503. *„Probing the flux of mitochondrial potassium using an azacrown-diketopyrrolopyrrole based highly sensitive probe".*

  Co-development of research concepts and interpretation of results. I developed and carried out the synthesis of substrates S4, S5-7, and S13-16, used them for synthesis of final compounds S9-S11, S17, 1 and 2 under optimized Buchwald-Hartwig amination reaction conditions, which I subjected to a full chemical analysis. I wrote the first draft of the manuscript. I participated in analyzing the photophysical properties, biological imaging experiments and preparation of the final version of the manuscript.

- G. Dinesh Kumar, M. Banasiewicz, A. Wrzosek, O. O'Mari, M. Zochowska, V. I. Vullev, D. Jacquemin, A. Szewczyk, D. T. Gryko, *Org. Biomol. Chem.*, **2022**, *20*, 7439–7447. *„A sensitive zinc probe operating via enhancement of excited-state intramolecular charge transfer".*

  Co-development of research concepts and interpretation of results. I developed and carried out the synthesis of substrates 2a-2b and 5-7, used them for synthesis of final compounds 3-4 and 8-10 under optimized conditions, which I subjected to a full chemical analysis I wrote the first draft of the manuscript. I participated in analyzing the photophysical properties, biological imaging experiments and preparation of the final version of the manuscript.

.....

Institute of Organic Chemistry
Polish Academy of Sciences

Professor Daniel Gryko
Director

+48 22 343 23 21
daniel.gryko@icho.edu.pl

Warsaw 24th November 2022.

I declare that my contribution to the following publications consisted of:

- G. Dinesh Kumar, M. Banasiewicz, D. Jacquemin, D. T. Gryko, *Chem. Asian J.* **2021**, *16*, 355–362. *„Switch-on Diketopyrrolopyrrole-Based Chemosensors for Cations Possessing Lewis Acid Character".*

  Co-development of research concepts, interpretation of results and preparation of the final version of the manuscript.

- G. Dinesh Kumar, M. Banasiewicz, A. Wrzosek, R. P. Kampa, M. H. E. Bousquet, D. Kusy, D. Jacquemin, A. Szewczyk, D. T. Gryko, *Chem. Commun.*, **2022**, *58*, 4500–4503. *„Probing the flux of mitochondrial potassium using an azacrown-diketopyrrolopyrrole based highly sensitive probe".*

  Co-development of research concepts, interpretation of results and preparation of the final version of the manuscript.

- G. Dinesh Kumar, M. Banasiewicz, A. Wrzosek, O. O'Mari, M. Zochowska, V. I. Vullev, D. Jacquemin, A. Szewczyk, D. T. Gryko, *Org. Biomol. Chem.*, **2022**, *20*, 7439–7447. *„A sensitive zinc probe operating via enhancement of excited-state intramolecular charge transfer".*

  Co-development of research concepts, interpretation of results and preparation of the final version of the manuscript.

Yours sincerely,

INSTYTUT FIZYKI
POLSKIEJ AKADEMII NAUK

Dr Marzena Banasiewicz
mbanas@ifpan.edu.pl
Instytut Fizyki PAN
Al. Lotników 32/46
02-668 Warsaw
Poland

Warsaw 26.09.2022

STATEMENT

I hereby declare that my contribution to the publications listed below is as follows:

1. G. Dinesh Kumar, M. Banasiewicz, D. Jacquemin, D. T. Gryko, *Chem. Asian J.* **2021**, *16*, 355–362. *„Switch-on Diketopyrrolopyrrole-Based Chemosensors for Cations Possessing Lewis Acid Character"*
2. G. Dinesh Kumar, M. Banasiewicz, A. Wrzosek, R. P. Kampa, M. H. E. Bousquet, D. Kusy, D. Jacquemin, A. Szewczyk, D. T. Gryko, *Chem. Commun.*, **2022**, *58*, 4500–4503. *„Probing the flux of mitochandrial potassium using on azacrown-diketopyrrolopyrrole based highly sensitive probe"*
3. G. Dinesh Kumar, M. Banasiewicz, A. Wrzosek, O. O'Mari, M. Zochowska, V. I. Vullev, D. Jacquemin, A. Szewczyk, D. T. Gryko, *Org. Biomol. Chem.*, **2022**, DOI: 10.1039/d2ob01296k. *„A sensitive zinc probe operating via enhancement of excited-stote intromolecular charge transfer"*

I measured absorption and fluorescence spectra in solution of the studied compounds. I worked out these results in form of Tables and Figures. I was involved in editing process of the Manuscript.

Marzena Banasiewicz

nencki institute
of experimental biology

Dr Rafał P. Kampa

Laboratory of Intracellular Ion Channels

Nencki Institute of Experimental Biology PAS

3 Pasteur St., 02-093 Warsaw, Poland

Warsaw, 19.09.2022

Hereby I would like to declare that my contribution to the publications:

1. **G. Dinesh Kumar**, M. Banasiewicz, A. Wrzosek, R. P. Kampa, M. H. E. Bousquet, D. Kusy, D. Jacquemin, A. Szewczyk, D. T. Gryko, *Chem. Commun.*, **2022**, *58*, 4500–4503. *„Probing the flux of mitochondrial potassium using an azacrown-diketopyrrolopyrrole based highly sensitive probe"*

   I participated in the measurement of cell survival in the presence of the studied dyes.

Rafał P. Kampa

nencki institute
of experimental biology

Dr Monika Żochowska

Laboratory of Intracellular Ion Channels

Nencki Institute of Experimental Biology PAS

3 Pasteur St., 02-093 Warsaw, Poland

Warsaw, 19.09.2022

Hereby I would like to declare that my contribution to the publication:

G. Dinesh Kumar, M. Banasiewicz, A. Wrzosek, O. O'Mari, M. Zochowska, V. I. Vullev, D. Jacquemin, A. Szewczyk, D. T. Gryko, *Org. Biomol. Chem.*, **2022**, DOI: 10.1039/d2ob01296k. *„A sensitive zinc probe operating via enhancement of excited-state intramolecular charge transfer"*

I participated in the H9C2 cell culture for the confocal microscopy.

Monika Żochowska

Monika Żochowska

Nencki Institute of Experimental Biology, Polish Academy of Sciences
3 Pasteur St., 02-093 Warsaw, Poland
phone: +48 22 58 92 207, email: dyrekcja@nencki.edu.pl
www.nencki.edu.pl

Prof. dr hab. Adam Szewczyk

Laboratory of Intracellular Ion Channels

Nencki Institute of Experimental Biology PAS

3 Pasteur St., 02-093 Warsaw, Poland

Warsaw, 19.09.2022

Hereby I would like to declare that my contribution to the publications:

1. **G. Dinesh Kumar**, M. Banasiewicz, A. Wrzosek, R. P. Kampa, M. H. E. Bousquet, D. Kusy, D. Jacquemin, A. Szewczyk, D. T. Gryko, *Chem. Commun.*, **2022**, *58*, 4500–4503. *„Probing the flux of mitochondrial potassium using an azacrown-diketopyrrolopyrrole based highly sensitive probe"*
2. **G. Dinesh Kumar**, M. Banasiewicz, A. Wrzosek, O. O'Mari, M. Zochowska, V. I. Vullev, D. Jacquemin, A. Szewczyk, D. T. Gryko, *Org. Biomol. Chem.*, **2022**, DOI: 10.1039/d2ob01296k. *„A sensitive zinc probe operating via enhancement of excited-state intramolecular charge transfer"*

I participated in the supervision, interpretation, and the discussion of confocal microscopy results..

A. Szewczyk

Adam Szewczyk

Nencki Institute of Experimental Biology, Polish Academy of Sciences
3 Pasteur St., 02-093 Warsaw, Poland
phone: +48 22 58 92 207, email: dyrekcja@nencki.edu.pl
www.nencki.edu.pl

nencki institute
of experimental biology

Dr Antoni Wrzosek

Laboratory of Intracellular Ion Channels

Nencki Institute of Experimental Biology PAS

3 Pasteur St., 02-093 Warsaw, Poland

Warsaw, 19.09.2022

Hereby I would like to declare that my contribution to the publications:

1. **G. Dinesh Kumar**, M. Banasiewicz, A. Wrzosek, R. P. Kampa, M. H. E. Bousquet, D. Kusy, D. Jacquemin, A. Szewczyk, D. T. Gryko, *Chem. Commun.*, **2022**, *58*, 4500–4503. *„Probing the flux of mitochondrial potassium using an azacrown-diketopyrrolopyrrole based highly sensitive probe"*
2. **G. Dinesh Kumar**, M. Banasiewicz, A. Wrzosek, O. O'Mari, M. Zochowska, V. I. Vullev, D. Jacquemin, A. Szewczyk, D. T. Gryko, *Org. Biomol. Chem.*, **2022**, DOI: 10.1039/d2ob01296k. *„A sensitive zinc probe operating via enhancement of excited-state intramolecular charge transfer"*

I participated in the measurement of confocal microscopy and the interpretation of the results.

Antoni Wrzosek

Antoni Wrzosek

Prof. Denis Jacquemin
Denis.Jacquemin@univ-nantes.fr

Ref. **Contribution Letter**

Nantes, 19/09/2022

To whom it may concern,

I hereby declare that my contribution to the publications below:

1. G. Dinesh Kumar, M. Banasiewicz, D. Jacquemin, D. T. Gryko, *Chem. Asian J.* 2021, *16*, 355–362. *„Switch-on Diketopyrrolopyrrole-Based Chemosensors for Cations Possessing Lewis Acid Character"*
2. G. Dinesh Kumar, M. Banasiewicz, A. Wrzosek, R. P. Kampa, M. H. E. Bousquet, D. Kusy, D. Jacquemin, A. Szewczyk, D. T. Gryko, *Chem. Commun.,* 2022, *58*, 4500–4503. *„Probing the flux of mitochondrial potassium using an azacrown-diketopyrrolopyrrole based highly sensitive probe"*
3. G. Dinesh Kumar, M. Banasiewicz, A. Wrzosek, O. O'Mari, M. Zochowska, V. I. Vullev, D. Jacquemin, A. Szewczyk, D. T. Gryko, *Org. Biomol. Chem.,* 2022, DOI: 10.1039/d2ob01296k. *„A sensitive zinc probe operating via enhancement of excited-state intramolecular charge transfer"*

I supervised the theoretical parts of this work and wrote the theoretical section of all manuscripts. For publications 1 and 3, I also performed all the DFT and TD-DFT calculations. In all contributions, I was involved in the proof checking of the full manuscript.

With best regards

Prof. Denis Jacquemin

CEISAM
www.ceisam.sciences.univ-nantes.fr
UMR CNRS 6230
Faculté des Sciences et Techniques
Université de Nantes
2 Rue de la Houssinière,
Nantes, France

Manon H.E. Bousquet
Manon.bousquet@unit-nantes.fr

Ref. **Contribution Letter**

Nantes, 19/09/2022

To whom it may concern,

I hereby declare that my contribution to the publications below:

1. G. Dinesh Kumar, M. Banasiewicz, A. Wrzosek, R. P. Kampa, M. H. E. Bousquet, D. Kusy, D. Jacquemin, A. Szewczyk, D. T. Gryko, *Chem. Commun.,* 2022, *58*, 4500–4503. *„Probing the flux of mitochondrial potassium using an azacrown-diketopyrrolopyrrole based highly sensitive probe"*

I performed all theoretical calculations and contributed to analyze the related data.

With best regards

Manon H. E. Bousquet

CEISAM
www.ceisam.sciences.univ-nantes.fr
UMR CNRS 6230
Faculté des Sciences et Techniques
Université de Nantes
2 Rue de la Houssinière,
Nantes, France

Instytut Chemii Organicznej
Polskiej Akademii Nauk

Dr Damian Kusy
d.kusy@icho.edu.pl
Instytut Chemii Organicznej PAN
ul. Kasprzaka 44/52
01-224 Warszawa

Warszawa 25.11.2022r.

Oświadczenie

Oświadczam, że mój wkład w powstanie poniższej publikacji polegał na wykonaniu pomiarów fotostabilności badanych związków.

G. Dinesh Kumar, M. Banasiewicz, A. Wrzosek, R. P. Kampa, M. H. E. Bousquet, D. Kusy, D. Jacquemin, A. Szewczyk, D. T. Gryko, *Chem. Commun.*, **2022**, *58*, 4500–4503. *„Probing the flux of mitochondrial potassium using an azacrown-diketopyrrolopyrrole based highly sensitive probe"*

Damian Kusy

Omar O'Mari
ooma001@ucr.edu

Ref. **Contribution Letter**

O'Mari, 11/04/2022

To whom it may concern,

I hereby declare that my contribution to the publications below:

1. **G. Dinesh Kumar**, M. Banasiewicz, A. Wrzosek, O. O'Mari, M. Zochowska, V. I. Vullev, D. Jacquemin, A. Szewczyk, D. T. Gryko, *Org. Biomol. Chem.*, **2022**, DOI: 10.1039/d2ob01296k. "*A sensitive zinc probe operating via enhancement of excited-state intramolecular charge transfer"*

I performed the initial "classic'' charge transfer analysis.

With best regards

Omar O'Mari

University of California, Riverside
900 University Ave
Riverside , 92521
Ca, U.S.A.

UNIVERSITY OF CALIFORNIA, RIVERSIDE

BERKELEY • DAVIS • IRVINE • LOS ANGELES • MERCED • RIVERSIDE • SAN DIEGO • SAN FRANCISCO

SANTA BARBARA • SANTA CRUZ

THE MARLAN AND ROSEMARY BOURNS
COLLEGE OF ENGINEERING

DEPARTMENT OF BIOENGINEERING
RIVERSIDE, CALIFORNIA 92521

phone: (951) 827-6239
fax: (951) 827-6416
e-mail: vullev@ucr.edu

November 10, 2022

To: Whom it may concern
From: Valentine I. Vullev
Re: Contribution to a publication in *Org. Biomol. Chem.*

Hereby I declare my contribution to the following publication:

G. Dinesh Kumar, M. Banasiewicz, A. Wrzosek, O. O'Mari, M. Zochowska, V. I. Vullev, D. Jacquemin, A. Szewczyk, D. T. Gryko, "A sensitive zinc probe operating via enhancement of excited-state intramolecular charge transfer," *Org. Biomol. Chem.* **2022**, *20*, 7439–7447.

My principal contribution involved supervising the charge-transfer studies for this project.

Sincerely yours,

Valentine I. Vullev
Professor of Bioengineering, Chemistry,
Biochemistry, and Materials Science and Engineering
Fulbright U.S. Scholar Fellow (2018 – 2019)